Acta Physica Hungarica

VOLUME 73 · NUMBER 1, 1993

Akadémiai Kiadó, Budapest
ACTA PHYS. HUNG. APAHAQ 73 (1) 1-122 (1993) HU ISSN 0231-4428

ACTA PHYSICA HUNGARICA

A JOURNAL OF THE HUNGARIAN ACADEMY OF SCIENCES

EDITED BY
I. KOVÁCS

Acta Physica publishes original papers on subjects in physics. Papers are accepted in English, French, German and Russian.

Acta Physica is published in one volume per year (4 issues) by

AKADÉMIAI KIADÓ
Publishing House of the Hungarian Academy of Sciences
H–1117 Budapest, Prielle Kornélia u. 19–35.

Subscription information

Orders should be addressed to

AKADÉMIAI KIADÓ
H–1519 Budapest, P.O. Box 245

Subscription price for Volume 73 (1993) in 4 issues US$ 84, including normal postage, airmail delivery US$ 20.00.

Acta Physica Hungarica is abstracted/indexed in Chemical Abstracts, Mathematical Reviews, Science Abstracts, Physics Briefs, Risk Abstracts, Engineering Information, Inc. EI Page One Database

CONTENTS

Acta Physica Hungarica 73 (1), pp. 3–16 (1993)

DEEP HEAT MUSCLE TREATMENT A MATHEMATICAL MODEL – I

A. OGULU*

International Centre for Theoretical Physics
Trieste, Italy

and

A. R. BESTMAN**

Mathematics Department, University of Port Harcourt
Port Harcourt, Nigeria

(Received 10 September 1992)

The flow of blood during deep heat muscle treatment is studied. We model the blood vessel as a long tube of circular section whose radius varied slowly. Under the Boussinesq approximation, we seek asymptotic series expansions for the velocity components, temperature and pressure about a small parameter, ε, characterizing the radius variation. The study reveals mathematically why physicians recommend a hot bath for cuts and physiotherapists use ice packs for bruises.

1. Introduction

The principle question around which the study of physiological fluid dynamics is centered concerns the range of validity of the assumptions of the Newtonian nature of blood in large blood vessels. In a previous analysis, Bestman [1] studied the unsteady low Reynolds number flow in a heated tube of slowly varying section. In that analysis the effect of forced and free convection heat transfer on flow in an axisymmetric tube whose radius varied slowly in the axial direction was addressed.

The temperature of the body, that is the temperature in the interior, called the core temperature is fairly well regulated, normally varying from the mean by not more that 1 °C. Hence the walls of the blood vessels which travel deep inside the body will not show much variation in temperature.

On the other hand, the surface temperature of the body rises and falls with the temperature of the surroundings, within a certain limit. In such a case, the wall temperature of the blood vessels which start from the core and travel to the surface will exhibit variation with axial distance. Examples of such blood vessels abound

*Permanent address: Department of Physics. R/S University of Science and Technology, Port Harcourt, Nigeria.

**Regretfully, Professor A. R. Bestman passed away before the publication of this report.

but one which readily comes to mind is the subclavian artery which branches from the aorta and bifurcates further into the brachial artery that subsequently travels to the near surface of the body. In this study, Bestman [1] incorporated a heat source/sink term to simulate abnormalities of body temperature regulation in a pathological situation.

In this study we want to look at the behaviour of blood and blood vessels during deep heat treatment in which thermal radiation is prevalent. Here we assume blood to be a constant viscosity fluid and the differential approximation for the radiative heat transfer for an optically thin medium. In a later study we hope to consider the case of a variable viscosity fluid.

The problem is formulated in Section 2 and the leading approximations and solutions are presented in Section 3. Higher approximations are obtained in Section 4. Quantitative results and discussion are given in Section 5.

2. Formulation

The flow of blood in blood vessels during deep heat muscle treatment is governed by the equations of continuity, momentum and energy which can be written in cylindrical polar coordinates (r', o, z') with velocity components (u', v', w').

We consider viscous flow with heat source term q in a heated long tube of circular section whose radius varies slowly as

$$r' = a_0 s\left(\frac{\varepsilon z'}{a_0}\right). \tag{2.1}$$

s is an arbitrary function and prime denotes dimensional quantities.

Assume Boussinesq approximation is valid, so that if ρ designates fluid density, and subscript ∞ denotes a reference density then the equation of state for a Boussinesq fluid, Bestman [2] is

$$\rho_\infty - \rho = \rho_\infty \beta(T - T_\infty), \tag{2.2}$$

where β is the coefficient of volume expansion. Let μ designate the fluid viscosity, k the thermal conductivity and c_p the specific heat at constant pressure.

Generally, the radiative flux satisfies the differential equation, Cheng [3]

$$\nabla^2 q_R - 3\alpha^2 q_R^3 - 16\alpha\sigma T^3 \nabla T = 0, \tag{2.3}$$

where α is the absorption coefficient and σ is the Stefan–Boltzmann constant. We only consider the optically thin limit of Eq. (2.3) since blood can be regarded as an optically thin medium ($\alpha \ldots 1$). Bestman [4] showed that the optically thin limit of Eq. (2.3) in suitable non-dimensional variables is

$$\frac{dq}{dr} = \frac{3}{4} R_\alpha(\theta^4 - 1). \tag{2.4}$$

Hence the governing non-dimensional equations of continuity, momentum and energy incorporating the radiative flux term can be written as

$$\frac{1}{r}\frac{\partial}{\partial r}(ru) + \frac{1}{r}\frac{\partial v}{\partial \phi} + \epsilon\frac{\partial w}{\partial z} = 0,$$

$$R\epsilon^2\left(u\frac{\partial u}{\partial r} + \frac{v}{r}\frac{\partial u}{\partial \phi} + \frac{u^2}{r} + w\frac{\partial u}{\partial z}\right) = -\frac{\partial p}{\partial r} + \epsilon\left[\frac{\partial}{\partial r}\left(\frac{1}{r}\frac{\partial}{\partial r}(ru)\right) + \right.$$

$$\left. + \frac{1}{r^2}\frac{\partial^2 u}{\partial^2 \phi} - \frac{2}{r^2}\frac{\partial v}{\partial \phi} + \epsilon^2\frac{\partial^2}{\partial z^2}\right] - G_r(\theta - 1)\cos\phi,$$

$$R\epsilon^2\left(u\frac{\partial u}{\partial r} + \frac{v}{r}\frac{\partial u}{\partial \phi} + \frac{uv2}{r} + w\frac{\partial v}{\partial z}\right) = -\frac{1}{r}\frac{\partial p}{\partial \phi} + \epsilon\left[\frac{\partial}{\partial r}\left(\frac{1}{r}\frac{\partial}{\partial r}(ru)\right) + \right.$$

$$\left. + \frac{1}{r^2}\frac{\partial^2 v}{\partial \phi^2} - \frac{2}{r^2}\frac{\partial u}{\partial \phi} + \epsilon^2\frac{\partial^2 v}{\partial z^2}\right] - G_r(\theta - 1)\sin\phi,$$

$$R\epsilon^2\left(u\frac{\partial w}{\partial r} + \frac{v}{r}\frac{\partial w}{\partial \phi} + w\frac{\partial w}{\partial z}\right) = -\epsilon\frac{\partial p}{\partial z} + \frac{1}{r}\frac{\partial}{\partial r}\left(r\frac{\partial w}{\partial r}\right) + \frac{1}{r^2}\frac{\partial^2 w}{\partial \phi^2} + \epsilon^2\frac{\partial^2 w}{\partial z^2}$$

$$R.P_r.\epsilon\left(u\frac{\partial \theta}{\partial r} + \frac{v}{r}\frac{\partial \theta}{\partial \phi} + w\frac{\partial \theta}{\partial z}\right) = \frac{1}{r}\frac{\partial}{\partial r}\left(r\frac{\partial \theta}{\partial r}\right) + \frac{1}{r^2}\frac{\partial^2 \theta}{\partial \phi^2} +$$

$$+\epsilon^2\frac{\partial^2 \theta}{\partial z^2} - \frac{3}{4}R_a(\theta^4 - 1), \qquad (2.5\text{a,b,c,d,e})$$

subject to the boundary conditions

$$\begin{aligned} u = 0 = v = w = \theta \quad &\text{on} \quad r = s(z), \\ u, v, w, \theta < \infty \quad &\text{on} \quad r = 0. \end{aligned} \qquad (2.6)$$

We have introduced the following non-dimensional quantities

$$r = \frac{r'}{a_0},\ z = \frac{\epsilon z'}{a_0}, \ldots (u, v, w) = \frac{(u', v', \epsilon w')}{\epsilon U_\infty},\ \theta = \frac{T'}{t_\infty},\ \nu = \frac{\mu}{\rho_\infty}, \qquad (2.7)$$

$$p = \frac{(p' - p_\infty)a_0}{\mu U_\infty},\ G_r = \frac{g\beta T_\infty a_0^2}{\nu U_\infty},\ R = \frac{U_\infty a_0}{\nu},\ P_r = \frac{\mu c_p}{k},\ R_a = \frac{16\sigma a_0 T_\infty^3}{3\alpha k},$$

subsequently $r = (3R_a)^{\frac{1}{2}} \cdot \frac{r}{2}$.

U_∞ is a typical axial velocity, R is the Reynolds number of flow, G_r is the free convection parameter (Grashof number), P_r is the Prandtl number, μ is the kinematic viscosity, g is gravity, R_a is the radiation parameter, θ is the temperature, and a_0 is a characteristic radius. Also

$$\nabla^2 = \frac{\partial}{\partial r^2} + \frac{1}{r}\frac{\partial}{\partial r} + \frac{1}{r^2}\frac{\partial^2}{\partial \phi^2}.$$

Combining (2.5b,c) we get

$$R\epsilon^2\left[\frac{1}{r}\frac{\partial}{\partial r}\left(r\left[u\frac{\partial v}{\partial r}+\frac{v}{r}\frac{\partial v}{\partial \phi}+\frac{uv}{r}+w\frac{\partial u}{\partial z}\right]\right)-\frac{1}{r}\frac{\partial}{\partial \phi}\left(u\frac{\partial u}{\partial r}+\frac{v}{r}\frac{\partial u}{\partial \phi}+\frac{u^2}{r}+w\frac{\partial u}{\partial z}\right]\right)=$$
$$=\nabla^2\left[\frac{1}{2}\frac{\partial}{\partial r}(rv)-\frac{1}{r}\frac{\partial u}{\partial \phi}\right]+G_r\left(\frac{\partial \theta}{\partial r}\sin\phi+\frac{1}{r}\frac{\partial \theta}{\partial \phi}\cos\phi\right). \tag{2.8}$$

Equation (2.8) will be useful in subsequent analysis.

The mathematical statement of the problem simply put is a solution of Eqs (2.5a,d,e) and (2.8) subject to (2.6).

3. Leading approximations and solutions

The problem formulated in the previous Section is non-linear and coupled and not readily amenable to closed form analytical treatment. We therefore adopt an asymptotic analysis similar to that in Bestman [4] by expanding the velocity components and temperature in the form

$$u = u^{(0)} + \epsilon u^{(1)} + \ldots\ldots \text{etc.}, \tag{3.1a}$$

while the pressure is expanded as

$$p = \frac{1}{\epsilon}p^{(0)} + p^{(1)} + \ldots\ldots . \tag{3.1b}$$

Substituting (3.1) into Eqs (2.5a,d,e) and (2.8) we find that for the leading approximation

$$\frac{1}{r}\frac{\partial}{\partial r}(ru^{(0)})+\frac{1}{r}\frac{\partial v^{(0)}}{\partial \phi}=0,$$

$$-\frac{\partial p^{(0)}}{\partial z}+\frac{1}{r}\frac{\partial}{\partial r}\left(r\frac{\partial w^{(0)}}{\partial r}\right)=0,$$

$$\frac{\partial^2\theta^{(0)}}{\partial r^2}+\frac{1}{r}\frac{\partial \theta^0}{\partial r}-\frac{3}{4}R_a(\theta^{(0)4}-1)=0,$$

$$\nabla^2\left\{\frac{1}{r}\frac{\partial}{\partial r}(rv^{(0)})-\frac{1}{r}\frac{\partial u^{(0)}}{\partial \phi}\right\}+G_r\frac{\partial \theta^{(0)}}{\partial r}\sin\phi=0. \tag{3.2a,b,c,d}$$

The method of solution of (3.2) has been described elsewhere. See for instance Ogulu [5]. The results are

$$w^{(0)} = \frac{K}{4}(r^2-s^2),$$

$$V^{(0)} = -B(z)-\frac{3}{8}A(z)r^2+G_r\left\{\frac{5a_2r^4}{96}+\frac{7a_4r^6}{288}\right\},$$

$$U^{(0)} = B(z) + \frac{A(z)r^2}{8} - G_r\left\{\frac{a_2 r^4}{96} + \frac{a_4 r^6}{288}\right\},$$

$$\theta^{(0)} = a(z) + \left(\frac{a^4}{4} - \frac{1}{4}\right) r^2 + \left(\frac{a^7}{16} - \frac{a^3}{16}\right) r^4 + \dots, \tag{3.3a,b,c,d}$$

where a is the real positive root of the quartic equation

$$\theta_w = a(z) + \frac{3}{4}\left(\frac{a^4}{4} - \frac{1}{4}\right) R_a s^2 + O(R_a^2) \tag{3.4}$$

obtained on imposition of the boundary condition on (3.3). In our solutions, since R_a is small we have neglected terms containing squares or products of R_a. Subscript w indicates conditions at the wall. $A(z)$ and $B(z)$ are arbitrary functions of z given by

$$A(z) = G_r R_a^2 \left\{\frac{a_2 s^4}{512 R_a} + \frac{3a_4 s^4}{64}\right\}$$

and

$$B(z) = -3G_r R_a^3 \left\{\frac{a_2 s^4}{512 R_a} + \frac{a_4 s^4}{1024}\right\}.$$

Also K is the constant pressure at the left ventricle of the heart in a healthy person.

4. Higher approximations

The governing equations for the next approximation are

$$\frac{1}{r}\frac{\partial}{\partial r}(ru^{(1)}) + \frac{1}{r}\frac{\partial v^{(1)}}{\partial \phi} + \frac{\partial w}{\partial z} = 0,$$

$$R\left(u^{(0)}\frac{\partial w^{(0)}}{\partial r} + w^{(0)}\frac{\partial w^{(0)}}{\partial z}\right) = -\frac{dp^{(1)}}{dz} + \frac{1}{r}\left(r\frac{\partial w^{(1)}}{\partial r} + \frac{1}{r^2}\frac{\partial^2 w^{(1)}}{\partial \phi^2}\right),$$

$$R\left\{\frac{1}{r}\frac{\partial}{\partial r}\left[r\left(u^{(0)}\frac{\partial v^{(0)}}{\partial r} + \frac{v^{(0)}}{r}\frac{\partial v^{(0)}}{\partial \phi} + \frac{u^{(0)}v^{(0)}}{r} + w^{(0)}\frac{\partial u^{(0)}}{\partial z}\right)\right] -\right.$$

$$\left. -\frac{1}{r}\frac{\partial}{\partial \phi}\left(u^{(0)}\frac{\partial u^{(0)}}{\partial r} + \frac{v^{(0)}}{r}\frac{\partial u^{(0)}}{\partial \phi} + \frac{u^{(0)^2}}{r} + w^{(0)}\frac{\partial u^{(0)}}{\partial z}\right)\right\} =$$

$$= \nabla^2\left\{\frac{1}{r}\frac{\partial}{\partial r}(rv^{(1)}) - \frac{1}{r}\frac{\partial u^{(1)}}{\partial \phi}\right\} + G_r\left\{\left(\frac{\partial \theta^{(1)}}{\partial r}\sin\phi + \frac{1}{r}\frac{\partial \theta^{(1)}}{\partial \phi}\cos\phi\right)\right\},$$

$$R.P_r\left\{u^{(0)}\frac{\partial \theta^{(0)}}{\partial r} + w^{(0)}\frac{\partial \theta^{(0)}}{\partial z}\right\} = \frac{\partial^2 \theta^{(1)}}{\partial r^2} + \frac{1}{r}\frac{\partial \theta^{(1)}}{\partial r} + \frac{1}{r^2}\frac{\partial^2 \theta^{(1)}}{\partial \phi^2}$$

$$- 4.R_a \theta^{(0)3}\theta^{(1)}. \tag{4.1a,b,c,d}$$

The boundary conditions are

$$u^{(1)} = .v^{(1)} = 0. = w^{(1)} = \theta^{(1)} \quad \text{on} \quad r = s(z). \tag{4.2}$$

We seek a separable solution for $\Theta^{(1)}$ of the sort

$$\theta^{(1)} = \Theta_1^{(1)}(r,z) + \Theta_2^{(1)}(r,z)\cos\phi \tag{4.3}$$

then substituting for $u^{(0)}$, $w^{(0)}$ and $\theta^{(0)}$,in (4.1d) coupled with (4.3), we obtain equations for $\Theta_1^{(1)}$ and $\Theta_2^{(1)}$ from which on rejection of unbounded functions we can deduce that

$$\Theta_1^{(1)} = R.P_r\left\{H(z)I_0(\alpha r) - \frac{da}{dz}\frac{K}{4}\left(\frac{r^2}{\alpha}+\frac{s^2}{\alpha}\right) + \frac{da_2}{dz}R_a\frac{K}{4}\left(\frac{r^4}{\alpha}+\frac{s^2r^2}{\alpha}\right)\right\}$$

and

$$\Theta_2^{(1)} = D(z)I_1(\alpha r) + \alpha_1 r + f(r), \tag{4.4a,b}$$

where $H(z)$ and $D(z)$ are arbitrary functions, $I_n(\alpha r)$ is Bessel function of order n and $\alpha = 2R_a^{\frac{1}{2}}a^{\frac{2}{3}}.K_n$ will be used to denote Bessel function of the second kind subsequently. Also

$$a_2 = \frac{a^4}{4} - \frac{1}{4}$$

and

$$\alpha_1 = 2RP_rR_aa_2B(z),$$

and the constants $H(z)$ and $D(z)$ are obtained on imposition of the boundary condition $\Theta_1^{(1)} = 0$ on $r = s(z)$. They are

$$H(z) = \frac{1}{I_0(\alpha s)}\left\{\frac{da}{dz}\frac{k}{4}\frac{s^4}{\alpha}\left(1+\frac{1}{\alpha}\right) - \frac{da_2}{dz}R_a\frac{K}{2}\frac{s^2}{\alpha}\right\}$$

and

$$D(z) = -\frac{\alpha_1 s}{I_1(\alpha s)} - \frac{f(s)}{I_1(\alpha s)}.$$

The other functions and constants are as defined in Ogulu [5].

To obtain the axial velocity we write (4.1b) as

$$R\left(u^{(0)}\frac{\partial w^{(0)}}{\partial r} + w^{(0)}\frac{\partial w^{(0)}}{\partial z}\right) + \frac{dp^{(1)}}{dz} = \frac{1}{r}\frac{\partial}{\partial r}\left(r\frac{\partial w^{(1)}}{\partial r}\right) + \frac{1}{r^2}\frac{\partial^2 w^{(1)}}{\partial\phi^2}. \tag{4.5}$$

We seek a separable solution for $w^{(1)}$, of the sort

$$w^{(1)} = w_1^{(1)}(r,z) + w_2^{(1)}\cos\phi. \tag{4.6}$$

We put

$$u^{(0)} = U^{(0)} \cos\phi. \tag{4.7}$$

Substitute (4.6) and (4.7) in (4.5) and after some algebra we obtain

$$w_1^{(1)} = RK^2(4s^3 s_z r^2 - s s_z r^4 - 3s^5 s_z) + \frac{p_z^{(1)}}{4}(r^2 - s^2)$$

and

$$w_2^{(1)} = E(z)r + \frac{p_z^{(1)} r^2}{3} + \frac{KR}{4}\left(\frac{B(z)r^3}{8} + \frac{A(z)R_a r^4}{160} - G_r\left\{\frac{3.a_2 R_a^2 r^6}{8960} + \frac{a_4 R_a^3 r^8}{43008}\right\}\right), \tag{4.8a,b}$$

where $E(z)$ is an arbitrary function given by

$$E(z) = -\frac{p(1)_z s}{3} - \frac{KR}{4}\left(\frac{B(z)s^2}{8} + \frac{A(z)R_a s^3}{160} - G_r\left\{\frac{3.a_2 R_a^2 s^5}{8960} + \frac{a_4 R_a^3 s^7}{43008}\right\}\right)$$

and

$$s_z = \frac{ds}{dz} \quad \text{and} \quad p_z^{(1)} = \frac{dp^{(1)}}{dz}.$$

We continue the solution of Eq. (4.1). We seek separable solutions for $\theta^{(1)}$, $u^{(1)}$, $v^{(1)}$ and $w^{(1)}$, of the sort

$$\theta^{(1)} = \Theta_1^{(1)}(r,z) + \Theta_2^{(1)}(r,z)\cos\phi,$$

$$u^{(1)} = U_0^{(1)}(r,z) + U_1^{(1)}(r,z)\cos\phi + U_2^{(1)}(r,z)\cos 2\phi,$$

$$v^{(1)} = V_1^{(1)}(r,z)\sin\phi + V_2^{(1)}(r,z)\sin 2\phi,$$

$$w^{(1)} = w_1^{(1)} + w_2^{(1)}\cos\phi. \tag{4.9a,b,c,d}$$

Substituting (4.9b,d) in (4.1a) we obtain

$$\frac{1}{r}\frac{\partial}{\partial r}(rU_0^{(1)}) = -\frac{\partial w_1^{(1)}}{\partial z},$$

from which we can deduce that

$$U_0^{(1)} = \frac{R.K^2}{128}\{r^3(s^3 s_{zz} + 3s^2 s_z^2) - \frac{3}{2}r(5s^4 s_z^2 + s^5 s_{zz}) - \\ - \frac{r^5}{6}(s_z^2 + s s_z)\} + \frac{p_{zz}^{(1)}}{4}\left(\frac{s^2 r}{2} - \frac{r^3}{4}\right) - \frac{p_z^{(1)}}{4} s s_z r. \tag{4.10}$$

The boundary condition on $U_1^{(0)}$ gives

$$p_{zz}^{(1)}s^3 + 4p_z^{(1)}s^2 s_z + \frac{RK^2}{24}(2s^6 s_{zz} + 14s^5 s_z^2) = 0,$$

which is reminiscent of Reynold's equation in lubrication theory. We integrate the Reynold's equation to obtain

$$p_z^{(1)} = -\frac{RK^2 s^4}{12}$$

and

$$p_{zz}^{(1)} = -\frac{RK^2 s^3 s_z}{3}.$$

As observed in Bestman [1], to terms of order ϵ, the free convection currents have no effect on the pressure distribution.

We continue the solution of Eq. (4.1). Assume $G_r \gg R$ then (4.1c) becomes

$$\nabla^2\left\{\frac{1}{r}\frac{\partial}{\partial r}(rV^{(1)}) - \frac{1}{r}\frac{\partial w^{(1)}}{\partial \phi}\right\} + G_r\left\{\frac{\partial \theta^1}{\partial r}\sin\phi + \frac{1}{r}\frac{\partial \theta^{(1)}}{\partial \phi}\right\}\cos\phi = 0. \qquad (4.11)$$

We substitute (4.9) in (4.1a) and (4.11) to obtain, respectively,

$$\frac{1}{r}\frac{\partial}{\partial r}(rU_1^{(1)} + \frac{1}{r}V_1^{(1)}) = -\frac{\partial w^{(1)}}{\partial z}$$

and

$$\frac{1}{r}\frac{\partial}{\partial r}(rV_1^{(1)}) + \frac{1}{r}U_1^{(1)} = T(z)r -$$
$$G_r RP_r\left\{H(z)\frac{I_1(\alpha r)}{\alpha} - \frac{da}{dz}\frac{Kr^3}{16} + \frac{1}{2}\frac{da_2}{dz}R_a\frac{K}{\alpha}\left(\frac{r^5}{12} + \frac{s^2 r^3}{8}\right)\right\}. \qquad (4.12a,b)$$

We proceed to solve (4.12a,b) simultaneously. The results are

$$U_1^{(1)} = X(z) - \frac{T(z)}{8}r^2 + \frac{p_{zz}^{(1)}s^2 r}{6} + \frac{p_z^{(1)}}{3}ss_z r + \frac{RK^2}{64}\{5s^4 s_z^2 r + s^5 s_{zz} r +$$

$$+\frac{s_z^2 r^5}{35} + \frac{ss_{zz}r^5}{35}\} - G_r.R.P_r\left\{\frac{H(z)I_1(\alpha r)}{\alpha^2 r} - \frac{1}{384}\frac{da}{dz}Kr^4 + \frac{1}{2}\frac{da_2}{dz}\frac{R_a}{\alpha}K\left(\frac{r^6}{576} + \frac{s^2 r^4}{192}\right)\right\}$$

and

$$V_1^{(1)} = -X(z) + \frac{3}{8}T(z)r^2 - \frac{1}{6}p_z^{(1)}s_{zz}r - \frac{p_{zz}^{(1)}}{12}(s^2 r - 3r^3) -$$

$$-\frac{RK^2}{128}\{4r^3s^3s_{zz}+12r^3s^2s_z^2-3s^5s_{zz}r+5s^4s_z^2r+20s_{zz}r-\frac{5}{7}s_z^2-$$

$$-\frac{5}{7}ss_{zz}r^5\}+G_rRP_r\left\{\frac{H(z)}{\alpha}(I_0(\alpha r)+I_2(\alpha r))-\right. \tag{4.13a,b}$$

$$\left.-\frac{1}{75}\left(\frac{da}{dz}Kr^4+\frac{1}{2}\frac{da}{dz}R_a\frac{K}{\alpha}\left(\frac{7}{576}r^6+\frac{5}{192}s^2r^4\right)\right)\right\}.$$

On application of the no-slip boundary condition we obtain the constants $T(z)$ and $X(z)$ as

$$T(z)=\frac{2}{3}p_{zz}^{(1)}s^4-\frac{10}{3}p_z^{(1)}s_z+\frac{RK^2}{16}\left\{s^4s_{zz}+\frac{3714}{35}s^3s_z^2+20\frac{s_{zz}}{s}-4G_rRP_r\cdot\right.$$

$$\left.\cdot\left\{\frac{H(z)}{\alpha s^2}(I_0(\alpha s)+I_2(\alpha s)-\frac{H(z)I_1(\alpha s)}{\alpha^2s^3}-\frac{1}{224}\frac{da_2}{dz}R_a\frac{K}{\alpha}s^4-\frac{307}{29128}\frac{da}{dz}ks^2\right\}\right\},$$

$$X(z)=-\frac{17}{12}p_z^{(1)}s^2s_z-p_{zz}^{(1)}\left(\frac{s^3}{3}-\frac{s^6}{4}\right)+\frac{RK^2}{128}(40s^2+208.3s^5s_z^2+0.9s^6s_{zz})-$$

$$-G_rP_rR\left\{\frac{1}{2}\frac{H(z)}{\alpha}(I_0(\alpha r)+I_2(\alpha r))+\frac{3}{2}\frac{H(z)}{\alpha^2s}I_1(\alpha s)-\right.$$

$$\left.-\frac{161}{28224}\frac{da_2}{dz}R_a\frac{K}{\alpha}s^6-\frac{12661}{4441712}\frac{da}{dz}Ks^4\right\},$$

where $p_{zz}^{(1)}=\frac{d^2p^{(1)}}{dz^2}$.

Next we substitute Eq. (4.9) in (4.11a) and (4.11) to obtain

$$\frac{1}{r}\frac{\partial}{\partial r}(rU_2^{(1)})+\frac{2}{r}V_2^{(1)}=0$$

and

$$\nabla^2\left\{\frac{1}{r}\frac{\partial}{\partial r}(rV_2^{(1)})+\frac{2}{r}U_2^{(1)}\right\}=-G_r\left\{\frac{\partial\Theta_2^{(1)}}{\partial r}-\frac{1}{r}\Theta_2^{(1)}\right\}, \tag{4.14a,b}$$

where

$$\nabla^2=\left(\frac{\partial^2}{\partial r^2}+\frac{1}{r}\frac{\partial}{\partial r}-\frac{4}{r^2}\right)\sin 2\phi.$$

After some algebra Eq. (4.14b) becomes

$$\frac{1}{r}\frac{\partial}{\partial r}(rV_2^{(1)})+\frac{2U_2^{(1)}}{r}=A(z)r^2+C(r,z). \tag{4.15}$$

We now solve Eqs (4.14a) and (4.15) simultaneously. The results are

$$U_2^{(1)}=B(z)r+\frac{2}{15}A(z)r^3+Y(r,z)$$

and

$$V_2^{(1)}=-B(z)r-\frac{4}{15}A(z)r^3+H,$$

where $H=-\frac{1}{2}\frac{dY}{dr}$ and $Y(r,z)=-\frac{2}{r}\int C(r,z)dr$. The higher approximate solutions are now complete.

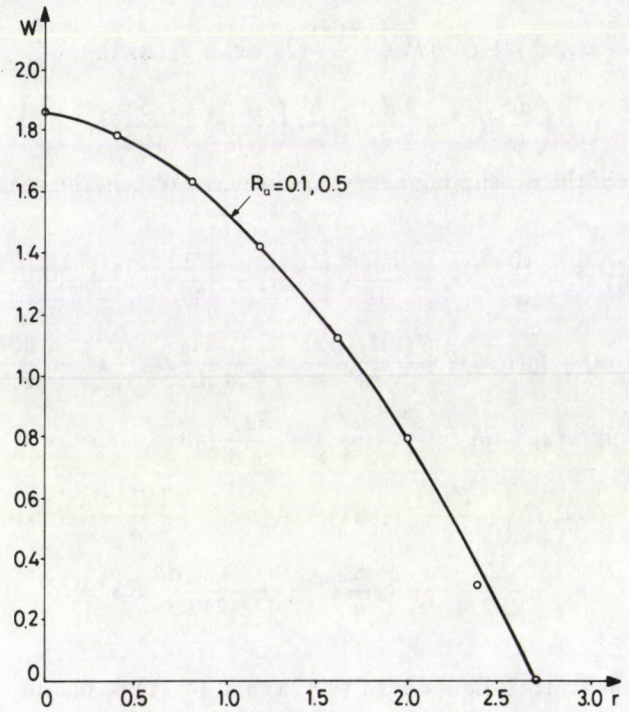

Fig. 1. Velocity profiles for flow in a tube of slowly varying radius. $R_a = 0.1, 0.5$; $z = 1$

5. Discussion of results

We have formulated and solved approximately expressions for the velocity components, pressure and temperature for flow in a heated tube of slowly varying section. From the viewpoint of deep heat muscle treatment, physiotherapy, we are interested mainly in the temperature distribution and the axial velocity profile because the axial velocity component is responsible for convection of nutrients to various parts of the body.

The expansions for the temperature and velocity are given as

$$\theta = \theta^{(0)}(r, z) + \epsilon\theta^{(1)}(r, \phi, z) \dots$$

and

$$w = w^{(0)}(r, z) + \epsilon w^{(1)}(r, \phi, z) + \dots .$$

ϵ is a small parameter, for simplicity, in this analysis we take $\epsilon = 0.001$. For the

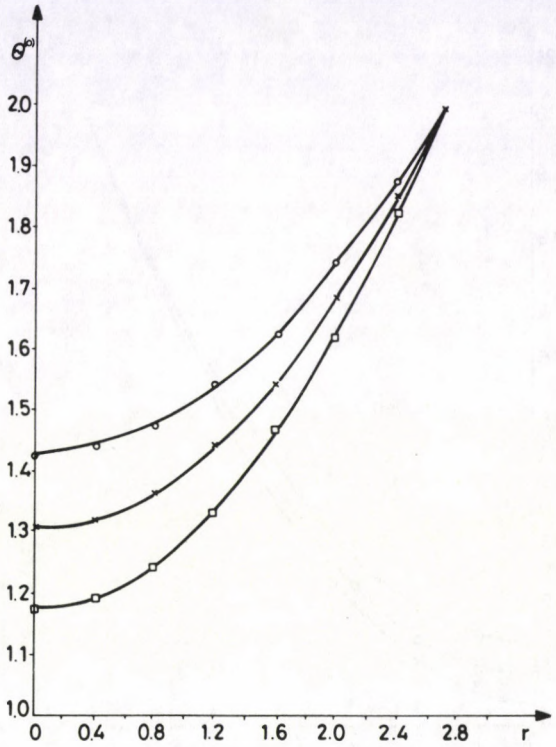

Fig. 2. Temperature distribution for flow in a tube of slowly varying radius. $R_a = 0.1, 0.2, 0.5$; $z = 1$; $\theta_w = 2$

higher approximate solution for the temperature and velocity, we have

$$\theta^{(1)} = \Theta_1^{(1)}(r, z) + \Theta_1^{(1)}(r, z).\cos\phi$$

and

$$w^{(1)} = w_1^{(1)}(r, z) + w_2^{(1)}(r, z).\cos\phi.$$

In the discussion of the velocity and temperature distributions and in Figs 1, 2 and 3 the value of ϕ is taken as zero. Other values of ϕ show insignificant change in the presentation. Without loss of generality we take $\theta = \theta^{(0)}$ only. For the velocity we consider only the first two terms of the expansion.

We solve the quartic equation (3.4) for 'a' for different values of the radiation parameter, R_a, to obtain the temperature distribution. For the axial velocity we take typical values of the various parameters in the equations for $w^{(0)}$ and $w^{(1)}$ for blood. The constant pressure in the left ventricle of the heart, K, we take as -1,

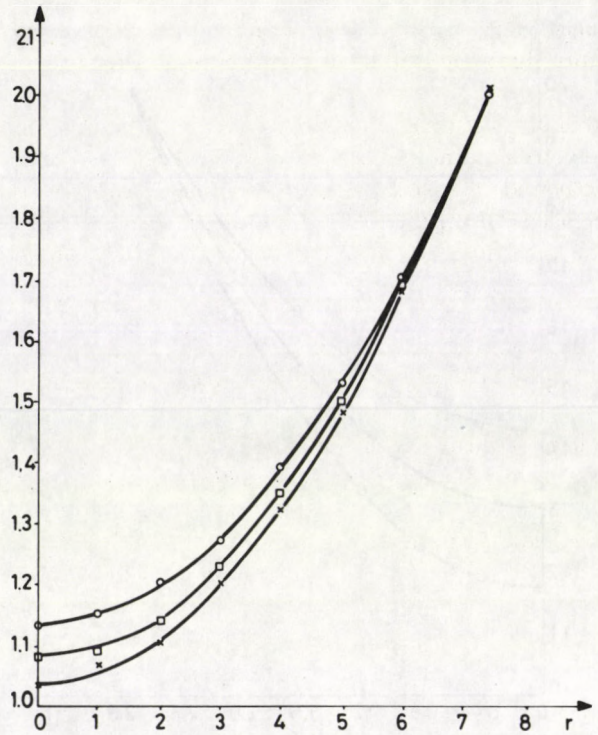

Fig. 3. Temperature distribution for flow in a tube of slowly varying radius. $R_a = 0.1, 0.2, 0.5$; $z = 2$

Reynolds number for blood as 40, Grashof number as 0.5 and Prandtl number as 25. These values are actually given in the literature, see for instance, Bestman [2].

Numerical discussion shall be considered only for a locally dilating tube of the form

$$s = e^z,$$

where $z = 0$ is taken as the inlet of the aorta.

Figures 2 and 3 show the temperature distribution for three different values of the radiation parameter at $z = 1, 2$. There is symmetry along the axis of the tube, that is at $r = 0$. A close look at Figs 2 and 3 suggests that the temperature decreases away from the walls of the blood vessel. This is not surprising since in addition to the heat source, extra heating results from friction between the blood vessel and the blood. This arises as a result of the increased blood flow. This increased blood flow is the reason why physicians use a hot water bottle in areas of suspected thrombus formation because increased blood flow is associated with increased supply of oxygen, nutrients and leucocytes which aid recovery. A well

oxygenated muscle heals a lot faster than a poorly oxygenated one. Leucocytes are the body scavengers, they eat up bacteria and germs which is why a good supply of them means a torn ligament will heal much more quickly for a patient undergoing physiotherapy.

Heat is actually a stimulus and the human body will react to any external stimulus. The external stimulus in this case is applied so that the body defense mechanism is activated in a positive manner. Blood supply to the diseased part of the body is increased during physiotherapy as shown in Fig. 1. Also from Fig. 1, it is obvious that once flow is set, further increase in the radiation parameter does not result in increased blood velocity.

As we all know, platelets aid blood clotting so an increase in blood velocity means more platelets would be available so that blood clots easily in cuts. If a boxer has a cut in the ring or a footballer has a knock in the field of play, the first line of treatment is the use of an ice pack. This is heat treatment except the heat in this case is negative heat (cold). This brings about the constriction of the blood vessels and the reduction of blood supply to the affected part, and of course, of oedema.

Hours later after the onset of oedema the second line of treatment follows; this time positive heat is applied to increase the blood supply to the affected area with the resultant increase in oxygen and nutrient supply.

Acknowledgements

One of the authors (A. O.) is grateful to the University of Science and Technology, Port Harcourt, for the financial support which made his trips to the International Centre for Theoretical Physics possible. He would also like to thank Professor Abdus Salam, the International Atomic Energy Agency and UNESCO for hospitality at the International Centre for Theoretical Physics, Trieste.

References

1. A. R. Bestman, J. Austral. Math. Soc., *B25*, 244, 1983.
2. A. R. Bestman, J. Austral. Math. Soc., *B*, 179, 1988.
3. P. Cheng, AIAA, *2*, 1662, 1964.
4. A. R. Bestman, Peristaltic pumping in a heated tube at low Reynolds number, in Proc. 16th Midwestern Fluid Mechanics Conference, 10, 1979.
5. A. Ogulu, Ph. D. Thesis. Rivers State University of Science and Technology, Port-Harcourt, Nigeria, 1991.

Nomenclature

T'	dimensional temperature
r'	dimensional radial coordinate
z'	dimensional axial coordinate
u', v', w'	dimensional velocity components

ϵ	a small parameter
s	an arbitrary function
ρ	fluid density
μ	kinematic viscosity
k	thermal conductivity
β	coefficient of volume expansion
c_p	specific heat at constant pressure
∞	denotes reference condition
α	absorption coefficient
σ	Stefan–Boltzmann constant
r	radial coordinate
z	axial coordinate
ϕ	azimuthal coordinate
u, v, w	velocity components
R_a	radiation parameter
P_r	Prandtl number
R	Reynolds number
G_r	Grashof number
p	pressure
U_∞	typical axial velocity
a_0	characteristic radius
$u^{(0)}, v^{(0)}, w^{(0)}$	leading component of the velocity vector
$p^{(0)}$	leading component of the pressure
$p_z^{(1)}$	perturbed pressure gradient
K	applied pressure gradient
I_n	Bessel function of the 1st kind of order n
k_n	Bessel function of the 2nd kind of order n

Acta Physica Hungarica 73 (1), pp. 17–27 (1993)

DEEP HEAT MUSCLE TREATMENT A MATHEMATICAL MODEL – II

A. OGULU*

International Centre for Theoretical Physics
Trieste, Italy

and

A. R. BESTMAN**

Mathematics Department, University of Port Harcourt
Port Harcourt, Nigeria

(Received 10 September 1992)

The effect of viscosity variation on the flow of blood during deep heat muscle treatment is studied. Two methods: an asymptotic series expansion technique and a perturbation technique are employed to obtain the temperature distribution. The results are compared with the problem of Part I. A novel development in this part of the study is the combined asymptotic patching and matching technique.

1. Introduction

In the first Part of the study we looked at the differential approximation for radiation with radiative heat transfer as applied to a fluid with constant viscosity and thermal conductivity. Some workers in this field (Pedley [1]) feel that the velocity profiles in large arteries are approximately flat, suggesting that the effect of viscosity is confined to thin boundary layers on the walls of the blood vessel.

Whole blood cannot be regarded as a homogeneous fluid in the smallest blood vessels because the diameters and spacing of red cells are comparable with capillary diameters, and some workers (Rowan [2]) feel that the viscosity of blood varies considerably. In this Part of our study therefore we want to look at the effect variation in viscosity would have on the velocity and temperature profiles.

The approach used in this Part of the study is again the differential approximation for radiation with radiative heat transfer with the viscosity and thermal conductivity assumed to vary with temperature. Also account is taken of conductive as well as convective heat transfer. The governing equations are presented in Section 2. Since these equations are non-linear asymptotic solutions are developed for them in Section 3. Section 4 is devoted to the qualitative discussion of the results.

*Permanent address: Department of Physics, R/S University of Science and Technology, Port Harcourt, Nigeria.

**Regretfully, Professor A. R. Bestman passed away before the publication of this report.

2. Formulation of the problem

The problem is formulated and non-dimensionalised as in Ogulu and Bestman [3] except that here the viscosity is varied with the temperature; so the non-dimensional equations of continuity, momentum and energy, in cylindrical polar coordinates (r, ϕ, z) with velocity components (u, v, w), Byron et al [4] which we propose here are:

$$\frac{1}{r}\frac{\partial}{\partial r}(ru) + \frac{1}{r}\frac{\partial v}{\partial \phi} + \epsilon\frac{\partial w}{\partial z} = 0,$$

$$R\epsilon^2\left(u\frac{\partial u}{\partial r} + \frac{v}{r}\frac{\partial u}{\partial \phi} - \frac{v^2}{r} + w\frac{\partial u}{\partial z}\right) = -\frac{\partial p}{\partial r} - \epsilon\left[\frac{1}{r}\frac{\partial}{\partial r}\left(2r\theta\frac{\partial u}{\partial r}\right) -\right.$$

$$\left. -\frac{1}{r}\frac{\partial}{\partial \phi}\left(\theta\left[r\frac{\partial}{\partial r}\left(\frac{v}{r}\right) + \frac{1}{r}\frac{\partial u}{\partial \phi}\right]\right) + \frac{1}{r}\theta\left[2\left(\frac{1}{r}\frac{\partial v}{\partial \phi} + \frac{u}{r}\right)\right] - \epsilon\frac{\partial}{\partial r}\left(\theta\left[\frac{\partial w}{\partial r} + \epsilon\frac{\partial u}{\partial z}\right]\right) + \right.$$

$$+\epsilon G_r(\theta - 1)\cos\phi,$$

$$R\epsilon^2\left(u\frac{\partial v}{\partial r} + \frac{v}{r}\frac{\partial v}{\partial \phi} - \frac{uv}{r} + w\frac{\partial v}{\partial z}\right) = -\frac{1}{r}\frac{\partial p}{\partial \phi} - \epsilon\left[\frac{1}{r^2}\frac{\partial}{\partial r}\left(r^2\theta\left[r\frac{\partial}{\partial r}\left(\frac{v}{r}\right) + \frac{1}{r}\frac{\partial u}{\partial \phi}\right]\right) -\right.$$

$$\left. -\frac{\partial}{\partial \phi}\left(2\theta\left[\frac{1}{r}\frac{\partial v}{\partial \phi} + \frac{u}{r}\right]\right) - \epsilon\frac{\partial}{\partial z}\left(\theta\left[\frac{\partial v}{\partial z} + \frac{1}{r}\frac{\partial w}{\partial r}\right]\right)\right] - \epsilon G_r(\theta - 1)\sin\phi,$$

$$R\epsilon\left(u\frac{\partial w}{\partial r} + \frac{v}{r}\frac{\partial w}{\partial \phi}\frac{v}{r}\frac{\partial w}{\partial z}\right) = -\epsilon^2\frac{\partial}{\partial z}\left(2\theta\frac{\partial w}{\partial z}\right) - \epsilon\frac{\partial p}{\partial z} + \frac{1}{r}\frac{\partial}{\partial r}\left(r\theta\left[\frac{\partial w}{\partial r} + \epsilon^2\frac{\partial u}{\partial z}\right]\right) +$$

$$+\frac{1}{r}\frac{\partial}{\partial \phi}\left(\theta\left[\epsilon^2\frac{\partial v}{\partial z} + \frac{1}{r}\frac{\partial w}{\partial \phi}\right]\right), \qquad \text{(2.1a,b,c,d,e)}$$

$$RP_r\epsilon\left(u\frac{\partial \theta}{\partial r} + \frac{v}{r}\frac{\partial \theta}{\partial \phi} + w\frac{\partial \theta}{\partial z}\right) = \frac{1}{r}\frac{\partial}{\partial r}\left(r\theta\frac{\partial \theta}{\partial r}\right) + \frac{1}{r^2}\frac{\partial}{\partial \phi}\left(\theta\frac{\partial \theta}{\partial \phi}\right) +$$

$$+\epsilon^2\frac{\partial}{\partial z}\left(\theta\frac{\partial \theta}{\partial z}\right) - \frac{3}{4}R_a(\theta^4 - 1).$$

We found it useful in the analysis to eliminate the pressure gradient between (2.1b and c) and the result is

$$R\epsilon\left[\frac{\partial}{\partial r}\left(r\left[u\frac{\partial v}{\partial r} = \frac{v}{r}\frac{\partial v}{\partial \phi} - \frac{uv}{r} + w\frac{\partial v}{\partial z}\right]\right) - \frac{\partial}{\partial \phi}\left(u\frac{\partial u}{\partial r} + \frac{v}{r}\frac{\partial u}{\partial \phi} - \frac{v^2}{r} + w\frac{\partial u}{\partial z}\right)\right] =$$

$$= -\frac{\partial}{\partial \phi}\left[r\left(\frac{1}{r^2}\frac{\partial}{\partial r}\left(r^2\theta\left[r\frac{\partial}{\partial r}\left(\frac{v}{r}\right) + \frac{1}{r}\frac{\partial u}{\partial \phi}\right]\right) - \frac{\partial}{\partial \phi}\left(2\theta\left[\frac{1}{r}\frac{\partial v}{\partial \phi} + \frac{u}{r}\right]\right) -\right.\right.$$

$$\left.\left. -\epsilon\frac{\partial}{\partial z}\left(\theta\left[\frac{\partial v}{\partial z} + \frac{1}{r}\frac{\partial w}{\partial \phi}\right]\right)\right)\right] + \frac{\partial}{\partial \phi}\left[\frac{1}{r}\frac{\partial}{\partial r}\left(2r\theta\frac{\partial u}{\partial r}\right) - \frac{1}{r}\frac{\partial}{\partial \phi}\left(\theta\left[r\frac{\partial}{\partial r}\left(\frac{v}{r}\right) +\right.\right.\right.$$

$$+\frac{1}{r}\frac{\partial u}{\partial \phi}\Big]\Big) + \frac{1}{r}\theta\left(\frac{1}{r}\theta\left[2\left(\frac{1}{r}\frac{\partial v}{\partial \phi}+\frac{u}{r}\right)\right] - \epsilon\frac{\partial}{\partial z}\left(\theta\left[\frac{\partial w}{\partial r}+\epsilon\frac{\partial u}{\partial z}\right]\right)\right] -$$

$$-G_r\left[\frac{\partial}{\partial r}(r[\theta-1]\sin\phi)+\frac{\partial}{\partial \phi}([\theta-1]\cos\phi)\right]. \tag{2.2}$$

All the various quantities in (2.1) and (2.2) either shown or unmentioned, have been defined in Ogulu [5].

The problem has now been put in mathematical terms. The boundary conditions are

$$u = v = 0 = w \quad \text{on} \quad r = s(z),$$

$$\theta = \theta_w \quad \text{on} \quad r = s(z). \tag{2.3a,b}$$

3. Basic approximate solutions

The inherent non-linearity of Eqs (2.1) and (2.2) makes solutions difficult to obtain in a closed form. Solutions are therefore obtained by series asymptotic expansions.

For the velocity components we write

$$u = u^{(0)}(r,\phi,z) + \epsilon u^{(1)} + \ldots \text{etc.}$$

For the temperature and pressure we write

$$\theta = \theta^{(0)}(r,z) + \epsilon\theta^{(1)}(r,\phi,z) + \ldots,$$

$$p = \frac{1}{\epsilon}p^{(0)}(z) + p^{(1)}(r,\phi,z) + \ldots, \tag{3.1}$$

where ϵ is a very small parameter. Substituting (3.1a,b,c,d,e) in (2.1a,d,e) and (2.2); and collecting terms without ϵ we obtain these basic approximations

$$\frac{1}{r}\frac{\partial}{\partial r}(ru^{(0)}) + \frac{1}{r}\frac{\partial v^{(0)}}{\partial \phi} = 0, \tag{3.2a}$$

$$-\frac{1}{r}\frac{\partial}{\partial r}\left(r\theta^{(0)}\left[\frac{\partial w^{(0)}}{\partial r}\right]\right) = -\frac{\partial p^{(0)}}{\partial z}, \tag{3.2b}$$

$$\frac{1}{r}\frac{\partial}{\partial r}\left(r\theta^{(0)}\frac{\partial \theta}{\partial r}\right) - \frac{3}{4}R_a(\theta^{(0)4}-1) = 0, \tag{3.2c}$$

$$\frac{\partial}{\partial \phi}\left[\frac{1}{r}\frac{\partial}{\partial r}\left(2r\theta^{(0)}\frac{\partial u^{(0)}}{\partial r}\right) - \frac{1}{r}\frac{\partial}{\partial \phi}\left(\left[\theta^{(0)}\left[r\frac{\partial}{\partial r}\left(\frac{v^{(0)}}{r}\right)+\frac{1}{r}\frac{\partial u^{(0)}}{\partial \phi}\right]\right)+\right. \tag{3.2d}$$

$$\left.+\frac{1}{r}\theta^{(0)}\left[2\left(\frac{1}{r}\frac{\partial v^{(0)}}{\partial \phi}+\frac{u^{(0)}}{r}\right)\right] - \frac{1}{r}\frac{\partial}{\partial \phi}\left(\theta^{(0)}\left[r\frac{\partial}{\partial r}\left(\frac{v^{(0)}}{r}\right)+\frac{1}{r}\frac{\partial u^{(0)}}{\partial \phi}\right]\right) -$$

$$-r\frac{\partial}{\partial\phi}\left(2\theta^{(0)}\left[\frac{1}{r}\frac{\partial v^{(0)}}{\partial\phi}+\frac{u^{(0)}}{r}\right]\right)\Bigg]-G_r r\frac{\partial\theta^{(0)}}{\partial r}\sin\phi=0.$$

Let $\frac{dp^{(0)}}{dr}$ be the externally applied pressure gradient, then the elementary solution of Eq. (3.2b) subject to the boundary condition $w^{(0)}=0$ on $r=s(z)$, is

$$w^{(0)}=\frac{K}{2}\left[\int_0^r\frac{\zeta}{\theta^{(0)}(\zeta)}d\zeta-\int_0^{s(z)}\frac{\zeta}{\theta^{(0)}(\zeta)}d\zeta\right]. \tag{3.3}$$

The basic approximate solution for the temperature is obtained from (3.2c) employing both the series expansion method as in [3] and a perturbation method. For the series expansion the solution is

$$\theta^{(0)}=[a(z)+(a(z)^4-1)\frac{9}{36}R_a r^2]^{\frac{1}{2}}. \tag{3.4}$$

$a(z)$ is defined in [3].

For the perturbation method we first linearize (3.2c) to obtain

$$\frac{\partial^2\psi_n}{\partial\zeta^2}+\frac{1}{\zeta}\frac{\partial\psi_n}{\partial\zeta}-\psi_n^n=C, \tag{3.4a}$$

from which we now get

$$\theta^{(0)}=[\theta_w^2+\frac{9}{16}R_a(r^2-s^2)]^{\frac{1}{2}}, \tag{3.5}$$

when $n=0$, $C=0$ and

$$\theta^{(0)}=\frac{\theta_w}{I_0^{\frac{1}{2}}(\frac{3}{2}R_a^{1/2}s)}I_0^{\frac{1}{2}}\left(\frac{3}{2}R_a^{\frac{1}{2}}s\right), \tag{3.6}$$

when $n=1$; $C=0$. See Ogulu [5] for the method of solution. $I_n(x)$ is a modified Bessel function of the first kind of order n; θ_w is the temperature at the wall of the blood vessel.

A plot of $\theta^{(0)}$ against r based on Eqs (3.5) and (3.6), (Figs 1 and 2) show that there is no difference between ψ_0 and ψ_1 so we can confidently perturb ψ_2 as $\psi_1+\varphi$.

To obtain the small correction φ, we write

$$\psi_2=\varphi+\psi_1. \tag{3.7}$$

On substitution of (3.4a) in (3.7) we can show that

$$\frac{\partial\varphi}{\partial\zeta^2}+\frac{1}{\zeta}\frac{\partial\varphi}{\partial\zeta}-2\psi_1\varphi=\psi_1^2-\psi_1. \tag{3.8}$$

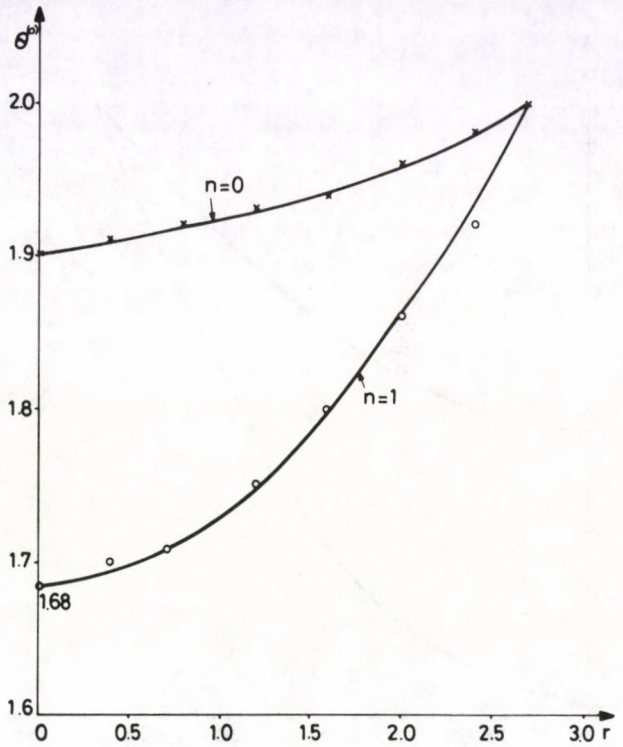

Fig. 1. Temperature distribution based on Eqs (3.5) and (3.6). $R_a = 0.1$; $\theta_w = 2$; $z = 0$; $n = 0$ and $n = 1$

$I_0(0)$ is one (1), so $\psi_1 = A(z) + 1$ hence when ζ is small we deduce that

$$\frac{\partial^2 \varphi}{\partial \zeta^2} + \frac{1}{\zeta}\frac{\partial \varphi}{\partial \zeta} - 2\varphi(B(z)+1) = B(z)I_0(\zeta)[B(z)+1], \tag{3.9}$$

where $B(z)$ is an arbitrary function of z. Consequently

$$\varphi = A(z)I_0(\alpha\zeta) + \frac{\alpha}{1-\alpha^2} \cdot B(z)I_0(\zeta)[B(z)+1]. \tag{3.10}$$

$A(z)$ is an arbitrary function of z and $\alpha = [2(B(z)+1)]^{\frac{1}{2}}$.

For large ζ we use the transformation in Abramowitz and Stegun [6] to reduce the differential equation, whence we have

$$0.5\frac{\partial^2}{\partial \zeta^2} - \phi_1 \Phi = 0.5[A(z)I_0(\zeta) + 1]]. \tag{3.11}$$

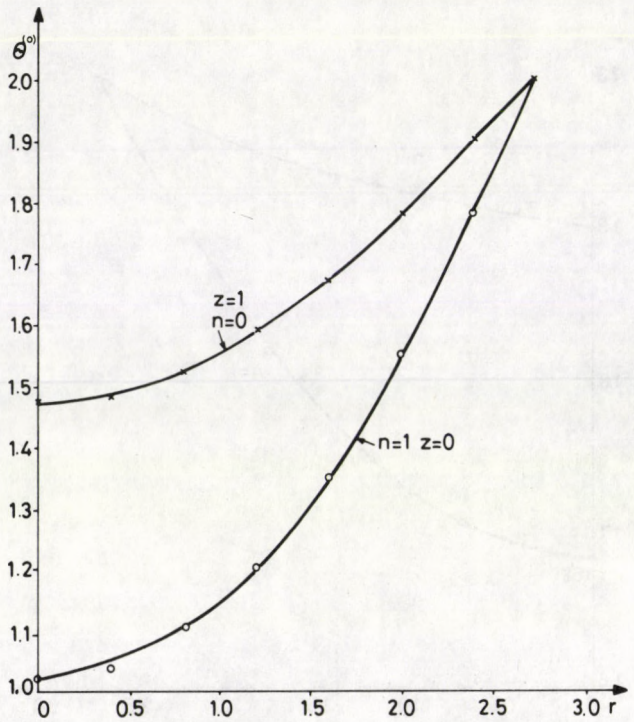

Fig. 2. Temperature distribution based on Eqs (3.5) and (3.6). $R_a = 0.5$; $\theta_w = 2$; $z = 0$

An appeal to the WKB approximation, Bestman [7] would give the solution of (3.11). We introduce the Green's function $G(\zeta, \zeta^*)$ such that

$$0.5\frac{\partial^2 G}{\partial \zeta^2}(\zeta^*, \zeta^*) - R(x)G(\zeta^*, \zeta^*) = -\delta(\zeta - \zeta^*),$$

$$G(\zeta, \zeta^*) = 0 = G(\zeta^*, \zeta_{II}).$$

$\delta(x)$ is Dirac delta function.

In the determination of the Green's function $G(\zeta^*, \zeta^*)$ we retain only the eikonal and transport terms; thus

$$G_1(\zeta^*, \zeta^*) = C_1(\zeta^*)Q^{\frac{-1}{4}} + C_2(\zeta^*)Q^{\frac{-1}{4}},$$

$$G_{II}(\zeta^*, \zeta^*)2C_4(\zeta^*)\exp\left[-\frac{1}{(0.5)^{\frac{1}{2}}}\int_{\zeta^*}^{\zeta_{II}} dtQ^{\frac{1}{2}}(t)\right]\sin h\left(\frac{1}{0.5}\right)^{\frac{1}{2}}\int_{\zeta}^{\zeta} dtQ^{\frac{1}{2}}(t)).$$

The constants C_1 and C_2 follow from the matching conditions

$$G_{\mathrm{I}}(\zeta^*,\zeta^*) = G_{\mathrm{II}}(\zeta^*,\zeta^*)$$

and

$$\frac{\partial G_{\mathrm{I}}}{\partial\zeta}(\zeta^*,\zeta^*) - \frac{\partial G_{\mathrm{II}}}{\partial\zeta}(\zeta^*,\zeta^*) = -\frac{1}{0.5},$$

while C_3 is obtained in terms of C_4 from the boundary condition $\zeta = \zeta_{\mathrm{II}}$. Hence

$$C_1(\zeta) = C_4(\zeta)\exp\left[-\frac{1}{(0.5)^{\frac{1}{2}}}\int_{\zeta}^{\zeta} dtQ^{\frac{1}{2}}(t)\right]\left[\sin h\left(\frac{1}{(0.5)^{\frac{1}{2}}}\int_{\zeta}^{\zeta} dtQ^{\frac{1}{2}}(t)\right) -\right.$$

$$-\frac{(0.5)^{\frac{1}{2}}}{2}Q^{\frac{-3}{2}}(\zeta^*)\sin h\left(\frac{1}{(0.5)^{\frac{1}{2}}}\int_{\zeta^*}^{\zeta_{\mathrm{II}}} dtQ^{\frac{1}{2}}(t)\right) + 2\cos h\left(\frac{1}{(0.5)^{\frac{1}{2}}}\int_{\zeta}^{\zeta} dtQ^{\frac{1}{2}}(t)\right)\Bigg] -$$

$$-\frac{(0.5)^{\frac{1}{2}}}{2}Q^{-\frac{1}{2}}(\zeta)\sin h\left(\frac{1}{(0.5)^{\frac{1}{2}}}\int_{\zeta}^{\zeta} dtQ^{\frac{1}{2}}(t)\right)(0.5)^{\frac{1}{2}}Q^{\frac{-1}{4}}(\zeta^*)+$$

$$+\frac{(0.5)^{\frac{1}{2}}}{2}Q^{\frac{-3}{2}}(\zeta^*)\exp\left[-\frac{1}{(0.5)^{\frac{1}{2}}}\int_{\zeta^*}^{\zeta_{\mathrm{II}}} dtQ^{\frac{1}{2}}(t)\right], \tag{3.12}$$

$$C_2(\zeta) = C_4(\zeta)\exp\left[-\frac{1}{(0.5)^{\frac{1}{2}}}\int_{\zeta^*}^{\zeta_{\mathrm{II}}} dtQ^{\frac{1}{2}}(t)\right]\left[\sin h\left(\frac{1}{(0.5)^{\frac{1}{2}}}\int_{\zeta^*}^{\zeta_{\mathrm{II}}} dtQ^{\frac{1}{2}}(t)\right)\right] =$$

$$= \frac{(0.5)^{\frac{1}{2}}}{4}Q^{-\frac{3}{2}}(\zeta^*)\sin h\left(\frac{1}{(0.5)^{\frac{1}{2}}}\int_{\zeta^*}^{\zeta_{\mathrm{II}}} dt\,Q^{\frac{1}{2}}(t)\right) - 2\cos h\left(\frac{1}{(0.5)^{\frac{1}{2}}}\int_{\zeta^*}^{\zeta_{\mathrm{II}}} dt\,Q^{\frac{1}{2}}(t)\right) -$$

$$-\frac{(0.5)^{\frac{1}{2}}}{4}Q^{-\frac{3}{2}}(\zeta^*)\Bigg] + \frac{(0.5)^{\frac{1}{2}}}{2}\sin h\left(\frac{1}{(0.5)^{\frac{1}{2}}}\int_{\zeta^*}^{\zeta_{\mathrm{II}}} dt\,Q^{\frac{1}{2}}(t)\right) + (0.5)^{\frac{1}{2}}Q^{-\frac{1}{4}}(\zeta^*), \tag{3.13}$$

$$C_3(\zeta^*) = -C_4(\zeta^*)\frac{\exp[-\frac{1}{(0.5)^{\frac{1}{2}}}\int_{\zeta^*}^{\zeta_{\mathrm{II}}} dt\,Q^{\frac{1}{2}}(t)]}{\exp[\frac{1}{(0.5)^{\frac{1}{2}}}\int_{\zeta^*}^{\zeta_{\mathrm{II}}} dt\,Q^{\frac{1}{2}}(t)]}. \tag{3.14}$$

We have two solutions for our small correction φ, one when ζ is small and the other when ζ is large. The two solutions have to be patched.

For ζ small we have

$$\varphi = A(z)I_0[2B(z)+1.\zeta] + \frac{\sqrt{2}.B[B(z)+1]^{\frac{1}{2}}}{1-2(B(z)+1)}I_0(\zeta). \tag{3.15}$$

For large ζ we have

$$\varphi = \int_{\zeta}^{\zeta^*} G_{\mathrm{I}}(\zeta, \zeta^*)(0.5)^{\frac{1}{2}}[B(z).I_0(\zeta^*)[B(z)+1]\zeta^{*\frac{1}{2}}]d\zeta^* +$$

$$+ \int_{\zeta^*}^{\zeta_{\mathrm{II}}} G_{\mathrm{II}}(\zeta^*, \zeta_{\mathrm{II}})(0.5)^{\frac{1}{2}}[B(z).I_0(\zeta^*)[B(z)+1]\zeta^* \frac{1}{2}]d\zeta^*. \tag{3.16}$$

Abramowitz and Stegun [6] give the series expansion for I_0 as

$$I_0(\zeta) = 1 + \frac{1}{4}\zeta^2 + \ldots,$$

hence the patching condition is

$$\zeta \gg 2\sqrt{\frac{(1+B(z))}{B(z)}}.$$

Finally, for the u and v components of the velocity we put

$$u^{(0)} = U^{(0)}(r)\cos\phi$$

and

$$v^{(0)} = V^{(0)}(r)\sin\phi$$

in our leading equations (3.2a,d); the result is a fourth order linear differential equation. An appeal to Newton–Ralphson algorithm readily gives the solution to these equations.

4. Discussion of results

In Part I we looked at the differential approximation for radiation with radiative heat transfer for a fluid with constant viscosity. In this Part we are considering a fluid with variable viscosity. In essence we want to look at the effect of variation of viscosity on the velocity and temperature profiles. Here the viscosity is assumed to vary with temperature. Since this is purely for comparison we have only considered the basic approximate solutions for the pressure, velocity and temperature. This would be enough to give a clue as to any difference between the assumption that the viscosity of blood varies as the temperature is varied; and the assumption that the viscosity of blood is constant during deep heat muscle treatment.

Figures 1 and 2 show the temperature profiles for the cases when $n = 0, 1$ based on Eqs (3.5) and (3.6) which compare favourably well with the temperature profile for the constant viscosity fluid. (See Ogulu and Bestman [3].) Both these

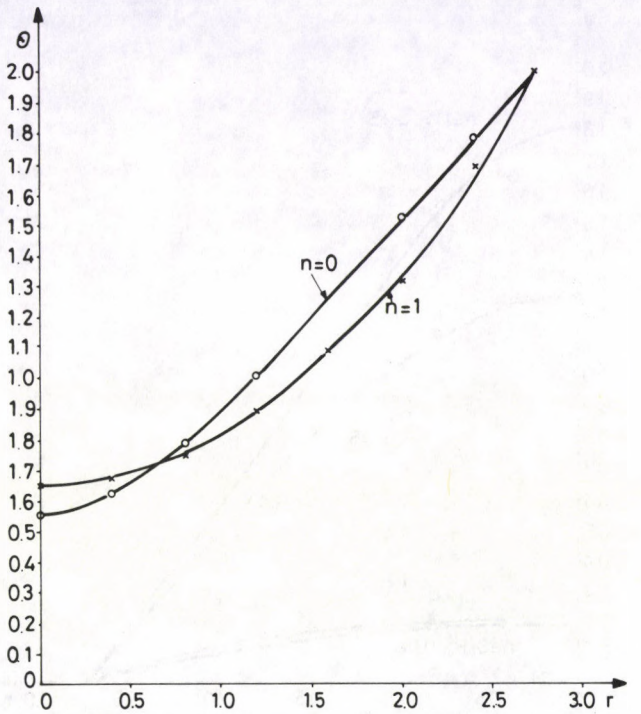

Fig. 3. Temperature distribution based on Eqs (3.5) and (3.6). $R_a = 1$; $\theta_w = 2$; $z = 1$; $n = 0$ and $n = 1$

profiles are of the same order of magnitude which means the variation in the viscosity has not affected the temperature distribution. This is in agreement with the conclusion of Pedley [1].

If one accepts the fact that for a constant viscosity fluid once the flow is set further increase in the radiation parameter is not accompanied by subsequent increase in the velocity then the agreement between the two cases becomes even more remarkable as depicted in Fig. 4.

In whole of this analysis we assume that the radiation parameter R_a is small; but as can be seen from Fig. 3, the analysis is valid even for radiation parameters as large as one (1). This shows that our perturbation of the temperature is quite accurate.

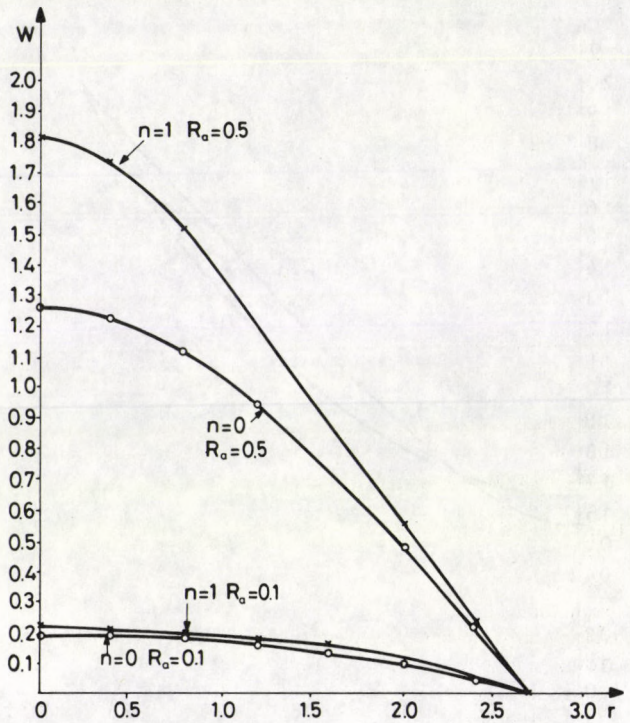

Fig. 4. Velocity distribution for flow with variable viscosity based on Eq. (3.3) for $n = 1$; $R_a = 0.5$; $z = 1$ and $n = 1$; $R_a = 0.1$; $z = 1$

Acknowledgements

One of the authors (A. O.) is grateful to the University of Science and Technology, Port Harcourt, for the financial support which made his trips to the International Centre for Theoretical Physics possible. He would also like to thank Professor Abdus Salam, the International Atomic Energy Agency and UNESCO for hospitality at the International Centre for Theoretical Physics, Trieste.

References

1. J. T. Pedley, Fluid Dynamics of Large Blood Vessels. Cambridge University Press, Cambridge, 1980.
2. J. O. Rowan, Physics and Circulation. Medical Physics Handbook 9. Adam Hilger Ltd, Bristol, 1981.
3. A. Ogulu and A. R. Bestman, Acta Phys. Hung., *73*, 3, 1993.

4. B. R. Byron, W. E. Stewart and E. N. Lightfoot, Transport Phenomenon. Wiley International Edition, New York, 1960.
5. A. Ogulu, Ph. D. Thesis. Rivers State University of Science and Technology, Port-Harcourt, Nigeria, 1991.
6. M. Abramowitz and I. A. Stegun, A Handbook of Mathematical Functions. Dover Publications Inc., New York.
7. A. R. Bestman, Il Nuovo Cimento, *11c*, No 3, 1988.

Nomenclature

ϵ	a small parameter
s	an arbitrary function
r	radial coordinate
z	axial coordinate
ϕ	azimuthal coordinate
u, v, w	velocity components
R_a	radiation parameter
P_r	Prandtl number
R	Reynolds number
G_r	Grashof number
p	pressure
a_0	characteristic radius
$u^{(0)}, v^{(0)}, w^{(0)}$	leading component of the velocity vector
$p^{(0)}$	leading component of the pressure
$p_z^{(1)}$	perturbed pressure gradient
K	applied pressure gradient
I_n	Bessel function of the 1st kind of order n
k_n	Bessel function of the 2nd kind of order n
φ	small correction
θ_w	wall temperature
$G_{\mathrm{I}}, G_{\mathrm{II}}$	Green's function
C_1, C_2, C_3, C_4	constants
δ	Dirac delta function

Acta Physica Hungarica 73 (1), pp. 29–34 (1993)

ELECTRICAL AND OPTICAL PROPERTIES OF POLYCRYSTALLINE Ag-DOPED CdS THIN FILMS

M. A. KHALID and H. A. JASSEM

Department of Physics, College of Science
University of Basrah, Basrah, Iraq

(Received in revised form 1 December 1992)

CdS and CdS:Ag thin films were prepared using the spray pyrolysis technique. The prepared films were deposited on glass substrate kept at a temperature of (420±10) °C. The optical and electrical properties have been studied for CdS and CdS:Ag (0.1 – 2.5) wt%.

The energy gaps were obtained as a function of doping concentration, which were found to vary from (2.4 ± 0.01) to (2.21 ± 0.01) eV in the doping concentration range (0–2.5) wt%. The electric conductivity was obtained from the I–V characteristics which was measured along the plane of film using the gap method. The effect of dopant concentration on electric conductivity is discussed.

All the measurements were carried out at room temperature.

Introduction

CdS has a direct band gap of 2.4 eV at room temperature (Gupta and Agnihotri [1]) and it is a suitable material for application to windows of P-Si/n-CdS type heterojunction solar cells (Couzza et al [2]), photoconductor devices (Amalnerkar et al [3]) as well as in photovoltaic devices (Mitchell et al [4]). Studies have been made on CdS thin films prepared by various methods such as sputtering (Yang and Im [5]), sintering (Gupta et al [6]), chemical vapour deposition (Partain et al [7]) evaporation (Norian and Edington [8]) and spray pyrolysis method (Kim and Park [9]). Various dopants have been tried according to the films applications (Nakayama [10], Shinkalgar and Pawar [11], Lokhande and Pawar [12], Kim and Park [9]). However, as far as the authors know no work has been published to date on the optical and electrical properties of sprayed CdS:Ag.

In the present study, CdS and Ag-doped CdS films were prepared by the spray pyrolysis method which is known to be a simple and low-cost process. The optical absorption and electric conductivity have been studied and discussed.

Experimental details

The cadmium sulphide films were prepared by pyrolytic decomposition of $CdCl_2$ and thiourea. Solution of CdS with (0.5) M concentration has been prepared by dissolving (1.023) gm of $CdCl_2$ and (0.5271) gm of $(NH_2)_2CdS$ of the compound

in (100) ml deionized water of each. The ratio of Cd:S in the sprayed solution was 1:1.

Silver-doped films were prepared by adding different weight percentage (0.1 – 2.5) wt% of Ag by dissolving a proper amount of AgCl in deionized water and added to the solution. The obtained solution is immediately sprayed with the help of a double nozzle sprayer onto (420±10) °C heated substrate of glass slides. The sprayer set-up and experimental details of preparation have been described elsewhere (Raza et al [13], Agnihotri et al [14]). The thickness of the prepared samples was in the range of (0.21 – 0.65) μm. The films were clear, yellow in colour and transparent. For optical absorptance measurements, a Pye-Unicam SP-800 UV/VIS double beam spectrophotometer covering the range from (200–900) μm was used.

The electric conductivity was obtained from the I–V characteristic which was measured along the plane of the film using the gap method (Chen–Chwe et al [15], Slawh [16]). Each sample had Coplanar Aluminium stripe contacts, with a gap of 2 mm and a length of 10 mm.

All I–V measurements for coplanar dark conductivity for CdS and CdS:Ag were carried out at room temperature.

Analysis of results and discussion

The optical absorption data were analysed in terms of the theory of Bardeen et al [17] which gives for a direct transition:

$$\alpha = B(h\nu - E_g)^{\frac{1}{2}}/h\nu,$$

where α is the absorption coefficient, E_g the direct band gap, $h\nu$ is the photon energy and B is constant depending on the probability of transition (Neumann et al [18]).

The plot of $(\alpha h\nu)^2$ versus $h\nu$ is shown in Figs 1a, 1b for CdS and CdS:Ag for different doping concentrations. Extrapolation of the straight line to $(\alpha h\nu)^2 = 0$ gives the direct allowed band gap E_g.

Figure 2 shows the obtained energy gap from Figs 1a, 1b as a function of doping concentration. It can be seen that as doping concentration increased, the energy gap decreased. The reduction in the values of energy gap may be related to the increase in the donor levels which make the semiconductors in the degenerate state (Sze [19]). The effect may cause the conduction band to extend into the gap (tail) which reduces the forbidden energy gap. This result agrees with that reported by Slawh et al [20] for CdS:In films. The energy gap of CdS thin film agree with that reported by Agnihotri and Gupta [21].

The electric conductivity of CdS and CdS:Ag thin films has been investigated using the gap method. Table I presents the electric conductivity as a function of Ag wt%.

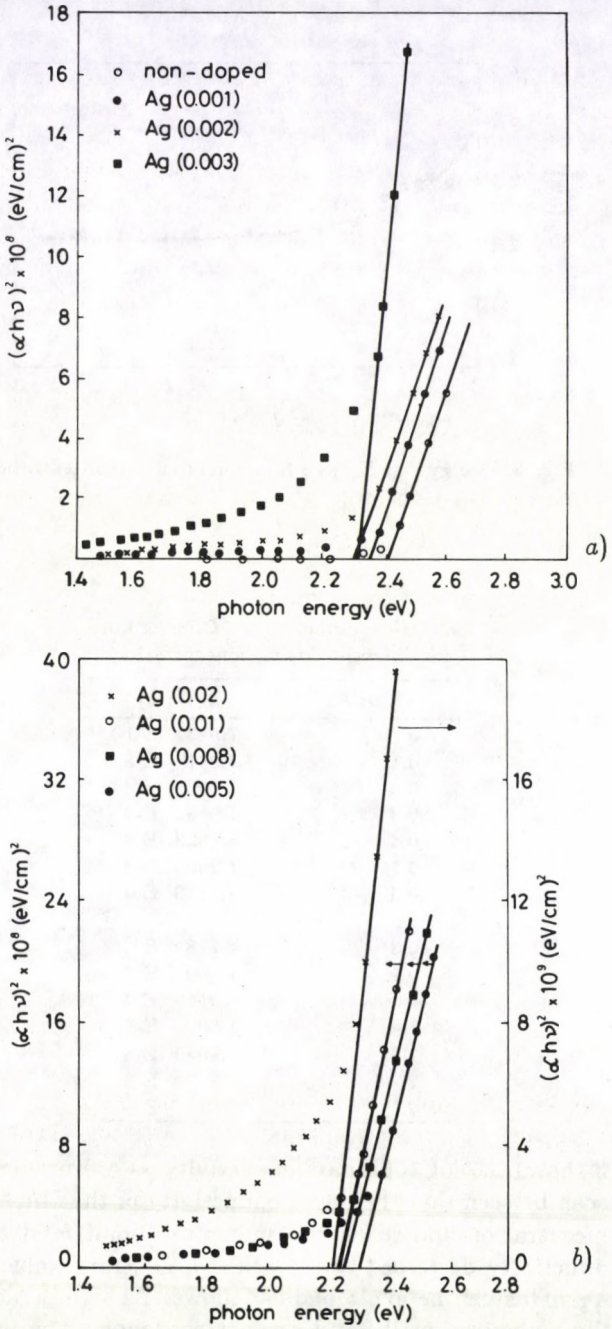

Figs 1a,1b. $(\alpha h\nu)^2$ vs photon energy for CdS and CdS:Ag for different silver concentrations

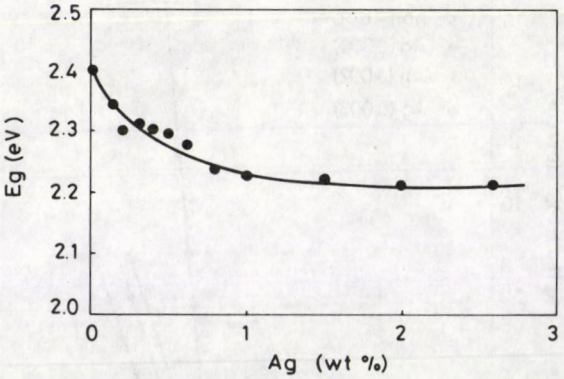

Fig. 2. Energy gap E_g as a function of silver concentration

Table I
Electric conductivity of CdS:Ag film for different doping concentrations

Ag wt%	$\sigma(\Omega\text{cm})^{-1}$
0	7.943 E-10
0.1	7.941 E-8
0.2	1 E-4
0.3	1.995 E-4
0.4	3.1623 E-3
0.5	1.259 E-2
0.6	2.5119 E-4
0.8	1.778 E-6
0.9	1.000 E-6
1	5.0119 E-7
1.4	1.00 E-7
1.7	1.9953 E-8
2	1.259 E-8
2.5	1.5849 E-8

Figure 3 shows the log coplanar conductivity as a function of Ag-doped concentration. It can be seen that the dark conductivity of the film first increased with Ag doping concentration and reached a maximum point for 0.5 wt% Ag. Afterwards the conductivity decreased and reached a constant value for doping larger than 2 wt% Ag. This can be explained as follows: Ag can be doped into Cd sites of CdS thin film substitutionally and can act as donor. The increase of the carrier density of a film at a rather low concentration stage less than 0.5 wt% may though be due to this effect. Similar observations have been reported for CdS:In by Mizuhashi [29], Suzuki et al [23] and Hayashi et al [24]). After that, as the doping

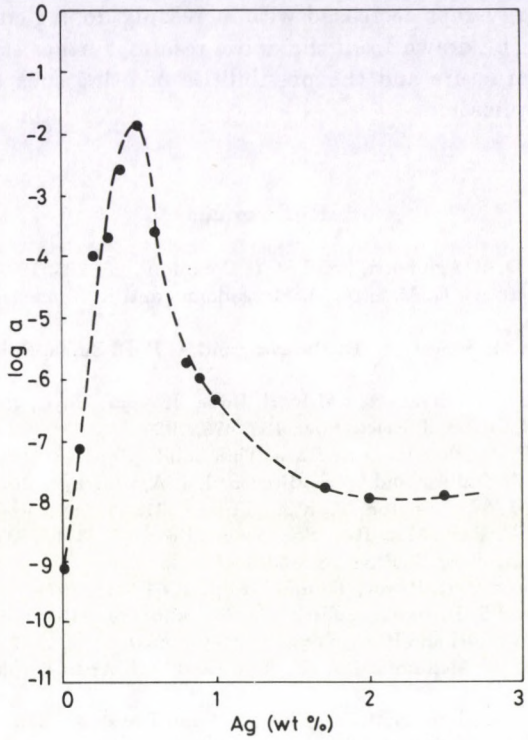

Fig. 3. Plot of log coplanar conductivity (σ) vs Ag wt% doping concentration

increases there is a possibility that Ag^{+1} would go to the interstitial position rather the vacancy position of Cd^{2+} and probably this may be the reason why conductivity decreases for doping larger than 0.5 wt% Ag. The interstitial Ag ions act as recombination centres decreasing the number of charge carriers and the conductivity as well. Similar results have been reported for CdS-doped Al (Lokhande and Pawar [12]) and $Cd_{0.75}Zn_{0.25}S$ doped Sn (Oda [25]). For a high doping stage greater than 2 wt% Ag, conductivity seems rather constant and goes into compensated stage.

Conclusion

The spray pyrolysis technique can be used to deposit pure and Ag-doped n-type thin films (0.21 μm – 0.65 μm thick) with large range conductivities (10^{-10} – 10^{-12} $\Omega^{-1}cm^{-1}$); 0.5 wt% Ag doping gives the highest conductivity. From these results we conclude that the Ag atoms were doped substitutionally at low level of concentration into the CdS and act as donor centres while doped interstitially at high concentration and act as compensation acceptor centres.

The energy gaps were calculated as a function of doping concentration. It was found that the energy gaps decreased with increasing doping concentration. Before any conclusion can be drawn from the above results, further studies are needed to identify the film structure and the possibilities of using such technique and such films in devices applications.

References

1. B. K. Gupta and O. P. Agnihotri, Solid State Commun., *23*, 295, 1977.
2. C. Couzza, M. Garozzo, G. Maletta, D. Margadonna and R. Tomaciello, Appl. Phys. Lett., *37*, 569, 1980.
3. D. P. Amalnerkar, M. S. Setty, N. R. Pavaskar and A. P. B. Sinha, Bull. Mater. Sci., *2*, 1251, 1980.
4. K. W. Mitchell, A. L. Fahrenbuch and R. H. Bube, J. Appl. Phys., *48*, 4365, 1977.
5. H. G. Yang and H. B. Im, J. Elect. Soc., *133*, 479, 1986.
6. B. K. Gupta, O. P. Agnihotri and A. Raza, Thin Solid Films, *48*, 153, 1978.
7. L. D. Partain, G. J. Sullivan and C. E. Birchenall, J. Appl. Phys., *50*, 551, 1979.
8. K. H. Norian and J. W. Edington, Thin Solid Films, *75*, 35, 1981.
9. Y. T. Kim and S. C. Park, Mat. Res. Soc. Symp. Proc., *77*, 311, 1987.
10. N. Nakayama, Japn. J. Appl. Phys., *8*, 450, 1969.
11. A. G. Shinkalgar and S. H. Pawar, Thin Solid Films, *61*, 313, 1979.
12. C. D. Lokhande and S. H. Pawar, Solid State Commun., *44*, 1137, 1982.
13. R. Raza, O. P. Agnihotri and P. K. Kupta, J. Phys., *B10*, 1871, 1977.
14. O. P. Agnihotri, M. T. Mohammed, A. K. Abass and K. I. Arshak, Solid State Commun., *43*, 195, 1983.
15. Chen-Chwe, R. S. Feigelson and R. H. Bude, J. Appl. Phys., *43*, 386, 1972.
16. G. G. Slawh, M. Sc. Thesis, Basrah University, 1990.
17. J. Bardeen, F. J. Slatt and L. J. Hail, Photoconductivity Conference 1954, Wiley, New York, p. 146, 1956.
18. H. Neumann, B. Perit, N. A. K. Abdul-Hussein and R. D. Tomlinson, Crys. Res. Technol., *17*, 469, 1982.
19. S. M. Sze, Phys. of Semiconductor Devices, Wiley, New York, p. 21, 1969.
20. G. G. Slawh, M. A. Khalid and W. Z. Manookian, J. of Math. and Phys., (Iraq), *12*, 355, 1991.
21. O. P. Agnihotri and B. K. Gupta, Japn. J. Appl. Phys., *18*, 317, 1979.
22. M. Mizuhashi, Thin Solid Films, *70*, 91, 1980.
23. T. Suzuki, Y. Ema and T. Hayashi, Japn. J. Appl. Phys., *26*, 2009, 1987.
24. T. Hayashi, T. Nishikura, T. Suzuki and Y. Ema, Japn. J. Appl. Phys., *64*, 3542, 1988.
25. S. M. Oda, M. Sc. Thesis, Basrah University, 1990.

Acta Physica Hungarica 73 (1), pp. 35–44 (1993)

EFFECT OF EQUATORIAL ELECTROJET ON ELECTRON CONTENT VARIATIONS AT TWO LONGITUDINALLY SEPARATED LOW LATITUDE STATIONS

P. K. BHUYAN

Department of Physics, Dibrugarh University
Dibrugarh-786004, Assam, India

(Received in revised form 8 December 1992)

Total ionospheric electron content (IEC) obtained simultaneously at two low latitude stations, Udaipur (22.6 °N, 69.6 °E, dip latitude 14.4 °N) and Gauhati (23.8 °N, 83.6 °E, dip latitude 14.2 °N) during solar minimum has been analyzed to investigate the effect of equatorial electrojet and spatial separation. Results show that the mean peak levels of ionization in winter and summer are about equal at Gauhati whereas at Udaipur winter IEC is less than that obtained in summer. The difference in solstitial behaviour was brought about by reduction in the winter level of ionization at Udaipur compared to that at Gauhati. Diurnal and seasonal variations of IEC at these two locations under the influence of strong equatorial electrojet (EEJ) were found to be dissimilar as a result of which difference between the two sets of data increases. Latitudinal variation of IEC as derived from observations along a chain of stations centered around 71 °E meridian in the Indian low latitude region shows that the position of the crest of the anomaly varies with season but not with the strength of EEJ. IEC for Gauhati does not correspond to the anomaly level along 71 °E indicating a longitudinal variation within the Indian zone.

1. Introduction

The ATS-6 campaign in India (September 1975 to August 1976) provided a unique opportunity for intercomparison of ionospheric electron content (IEC) obtained at a group of stations located across the Indian low latitude region. Study of correlation of ionospheric parameters is important from the viewpoint of predictions in space-time configurations where observational facilities do not exist. Klobuchar and Johanson [1], Kane [2], Soicher et al [3], Bhuyan et al [4] and Bhuyan and Tyagi [5] had investigated various aspects of variability in electron content for low and midlatitudes. Klobuchar and Johanson [1] and Bhuyan and Tyagi [5] had observed that the correlation of mean daytime IEC decreases with increasing longitudinal and/or latitudinal separation between observing stations. Kane [2] showed that at American midlatitudes, the difference between IEC measured at two locations only 400 km apart could be as high as 50 %. Neutral winds play a major role in IEC variability at midlatitudes, on the other hand, at low latitudes, variations in the equatorial electrojet (EEJ) strength mainly influences the day to day variability (Rama Rao et al [6]; Dabas et al [7]). The location of observing stations with respect to the geomagnetic equator and their longitudinal separation was also

Table I
Co-ordinates of the observing stations

Station	Geographic		Subionospheric at 420 km		
	Lat °N	Long °E	Lat °N	Long °E	Dip Lat °N
Udaipur	27.4	75.3	22.6	69.6	14.4
Gauhati	26.1	91.5	23.8	83.6	14.2

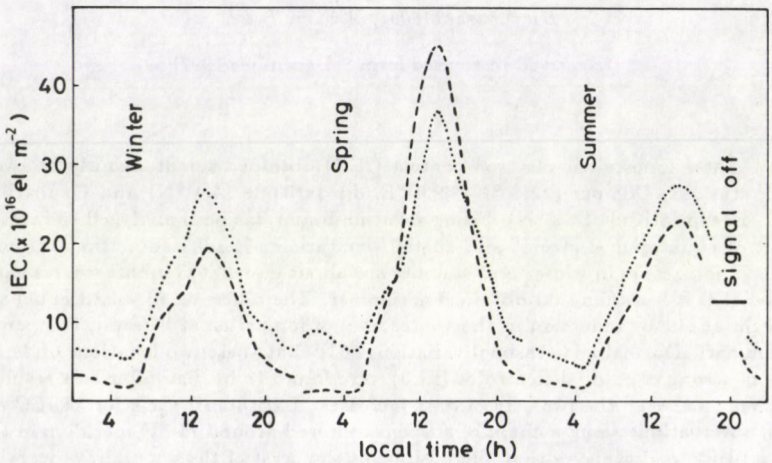

Fig. 1. Mean diurnal variation of IEC at the two stations, Udaipur (broken curve) and Gauhati (dotted curve) for the period October 1975 to July 1976

found to contribute to difference in magnitude of observed IEC near the crest of the anomaly in the Indian zone (Bhuyan et al [4]). The aim of this paper was to investigate the effects of longitudinal separation and EEJ, if any, on the diurnal and seasonal variations of IEC obtained simultaneously at Udaipur (lat. 22.6 °N, long. 69.6 °E) and Gauhati (lat. 23.8 °N, long. 83.6 °E) situated near the northern crest of the equatorial anomaly.

2. Data

Simultaneous IEC data used in this analysis for the period November 1975 to July 1976 were obtained by monitoring the Faraday rotation angle of 140 MHz beacon transmissions from ATS-6 positioned over the Indian Ocean (35 °E) during its phase–II campaign. The co-ordinates and other relevant details of the observing stations are given in Table I.

3. Results

3.1. Comparison of seasonal variation

Scrutiny of individual daily plots of IEC for Gauhati and Udaipur revealed that the diurnal variation is quite similar on some days whereas on some other days, IEC at the two stations register dissimilar variations. The day-to-day variability was found to be random and sometimes very high at both locations. Hourly average IEC for the three seasons viz. winter (Dec./Jan.), spring (Apr.) and summer (June/July) for the two locations plotted against local time was shown in Fig. 1. It may be seen that a semiannual variation in IEC_{max} with peak in equinox and troughs in the solstices is evident both at Gauhati and Udaipur. However, the summer and winter peak levels are different in each case. At Udaipur, winter IEC_{max} (19.5×10^{16} el.m^{-2}) is considerably less than that in summer (23.2×10^{16} el.m^{-2}) whereas at Gauhati, winter and summer levels are about equal (26.9×10^{16} el.m^{-2} and 27.2×10^{16} el.m^{-2}, respectively). Observed variation of the individual as well as average IEC were further confirmed by obtaining the relative electron content ($IEC-IEC_{min}$) at each data point, which neutralizes the effect of any probable error in the base level ionization. The mean daily range of IEC (IEC_{max}–IEC_{min}) obtained for winter and summer at Udaipur and Gauhati are 17.9×10^{16} el.m^{-2}, 21.5×10^{16} el.m^{-2} and 21.5×10^{16} el.m^{-2}, 22.7×10^{16} el.m^{-2}, respectively. We may see that the summer daily range is about equal but in winter, at Udaipur, the daily range falls to a level below that of summer. Therefore, the difference in the solstitial behaviour of electron content was caused by reduction in the winter level at Udaipur. Around 75 °E meridian, observations during the AST-6 period had revealed that the winter anomaly (i.e. winter electron content being higher than summer electron content) was present only at locations confined within the equatorward trough region of the equatorial anomaly (Bhuyan [8]). At locations outside the anomaly region, summer IEC was higher compared to that in winter, transition between these two different seasonal variation patterns occurring around Ahmedabad (dip lat. 13 °N) where IEC was comparable in both the solstices. Klobuchar et al [9] had shown that in the Indian zone, during solar minimum, the crest of the anomaly normally centres around Ahmedabad with latitudinal shifts depending on season. The subionospheric points of Udaipur and Gauhati are thus generally located northward of the crest of the anomaly and it is reasonable to expect similar seasonal variation at these two places. Contrarily, while IEC at Udaipur show normal seasonal variation expected at a location outside the crest of the anomaly, IEC at Gauhati exhibit seasonal variation observed in the transition region. Bhuyan et al [4] had reported earlier that a small difference in latitude coupled with the difference in longitude of two subionospheric intersections plays a critical role in determining the magnitude of IEC measured in the vicinity of the equatorial anomaly crest in the Indian zone. The difference in relative position of the two subionospheric points (for Udaipur and Gauhati) vis-a-vis the geomagnetic equator and their longitudinal separation seems to have affected the seasonal variation of IEC at these two locations.

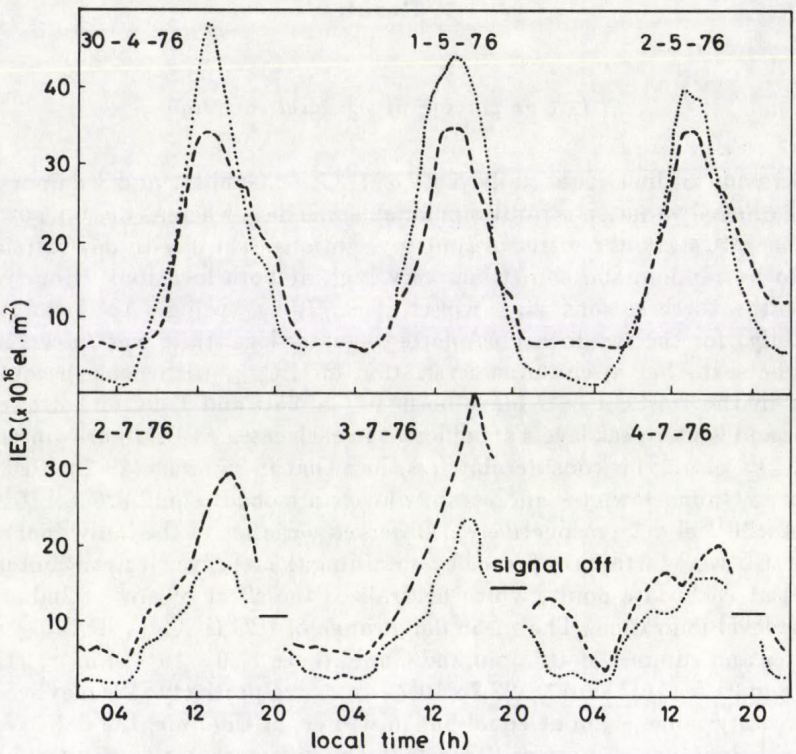

Fig. 2. Diurnal variation of IEC for three consecutive strong (top) and normal (bottom) EEJ days at Udaipur (dotted) and Gauhati (broken)

3.2. Effect of equatorial electrojet (EEJ)

The short as well as longterm variability of IEC in and around the northern equatorial anomaly region in India was found to be mainly controlled by the variations in equatorial electrojet strength. Dabas et al [7], Rama Rao et al [6] made a quantitative study of the electrojet control over the equatorial anomaly in IEC using data from a chain of six Indian stations ranging from the dip equator to 40 °N dip during the low activity period of 1975–76, utilizing the same data base. They found that the position of the crest of the anomaly depends strongly upon the integrated electrojet strength. During strong EEJ days, the crest of the anomaly was found to form beyond 40 °N dip, i.e. the northernmost station of the latitudinal chain, while on days of no electrojet or counter electrojet, no anomaly was found. Since both the stations are located near the crest of the anomaly at approximately equal distances away from the geomagnetic equator, effect of EEJ on IEC measured both at Gauhati and Udaipur could be expected to be similar provided longitudinal separation between the two stations is not taken into consideration. Variations in the

EEJ current at the equator can be obtained by taking the difference in the deviation ΔH of the H field at an equatorial station to that at a station situated well outside the equatorial electrojet region according to Rush and Richmond [10] and Chandra and Rastogi [11]. For the present analysis, EEJ strength had been calculated as ΔH_{T-A} following Chandra and Rastogi [11] where T represents Trivandrum (mag. lat. 0.3 °N) and A is for Alibag (mag. lat. 9.5 °N). EEJ strength calculated as above was found by Dabas et al [7] to be well correlated with the day-to-day variability in electron content in the Indian zone during the low solar activity period of 1975–76. In Fig. 2, diurnal variation of IEC at Gauhati and at Udaipur are plotted for two periods of three consecutive days during which EEJ was strong (top) and normal (bottom). EEJ was considered strong for the day in which the maximum value of ΔH_{T-A} exceeded 50 nT and normal when $\Delta H_{T-A} < 40$ nT. The peak level of IEC at Udaipur gradually decreases from 47.9×10^{16} el.m^{-2} on day 1 to 44.0×10^{16} el.m^{-2} on day 2 and to 39.8×10^{16} el.m^{-2} on day 3 during strong EEJ. During the same period, IEC at Gauhati remained at the peak level of 34.1×10^{16} el.m^{-2} on all three days. On the other hand, when EEJ activity was normal, IEC at both stations rise and fall in unison from one day to the next. The day-to-day variations were further confirmed by obtaining similar curves for relative IEC. The period chosen for Fig. 2 was at random and many such periods in which IEC at the two locations vary independently could be found.

3.3. Comparison of IEC

The relative variation of IEC measured at one station with respect to that obtained at another can be studied by plotting data of one station against those of the other station. If the IEC measured over a length of time matches well then a simple relationship of the type $y = mx$, where m is unity, should be expected. However, since Fig. 1 indicates that the diurnal curves averaged over the seasons for Udaipur and Gauhati do not match well, we could look for a systematic deviation of one set from the other which is related to some geophysical factors like season or magnetic activity. Bhuyan and Tyagi [12] investigated IEC correlation at three low latitude stations in the Indian and East Asian longitude sectors during solar minimum and studied the relative deviation of IEC during quiet (QQ) and disturbed (DD) days and in different seasons of the year. They observed that the deviation of IEC was influenced by season but not by magnetic activity. In Fig. 3, the monthly mean relative IEC grouped into winter (Nov., Dec., Jan., Feb.), spring (March, Apr.) and summer (May, June, July) at Gauhati is plotted for all local times against the corresponding values similarly obtained at Udaipur. The Figure indicates that IEC at Udaipur and Gauhati match each other only in summer. In winter, IEC measured at Gauhati is higher while in spring, Udaipur values are much higher compared to those correspondingly obtained at Gauhati. There had, therefore, been systematic seasonal deviation of IEC observed at the two stations with respect to each other.

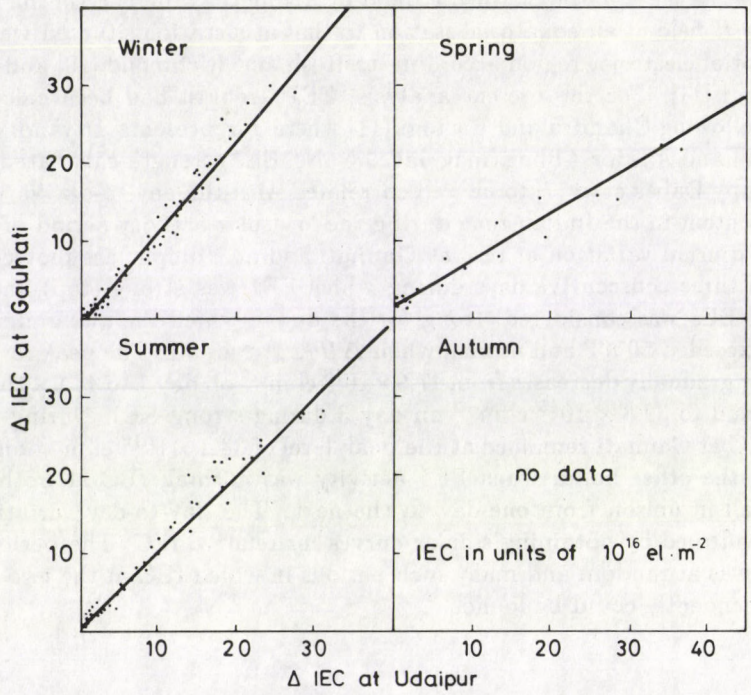

Fig. 3. Monthly mean relative IEC ($IEC-IEC_{min}$) at Gauhati plotted against corresponding values of Udaipur for all local times

3.4. Effect of EEJ on relative deviation

During days of strong EEJ, day-to-day variability at Udaipur and Gauhati was found to be different (Section 3.2) whereas similar variation had been noticed during days of normal EEJ. To check any possible effect of EEJ strength, relative IEC at Gauhati is plotted against those of Udaipur for strong electrojet days in winter and summer in Fig. 4. Sufficient number of simultaneous data for strong EEJ could not be found in spring. It may be seen from the Figure that during strong EEJ, difference between the two sets of data increases with increase in electron content in winter. In summer, too, IEC at Udaipur increases relative to the corresponding values at Gauhati. The discrepancy further increases for higher values of IEC, i.e. during daytime maximum hours giving the curve a rather skewed shape.

Figure 5 further stresses the influence of EEJ on relative variation of IEC at Udaipur and Gauhati. The data are for normal EEJ days. It can be seen that IEC at two locations are about equal in summer at all local times when in winter, IEC at Gauhati is marginally higher than the corresponding values at Udaipur. Comparison of Figs 3,4 and 5 shows that the average relative behaviour is influenced by strong EEJ activity. Superimposition of Figs 3 and 5 indicates that the separation of strong

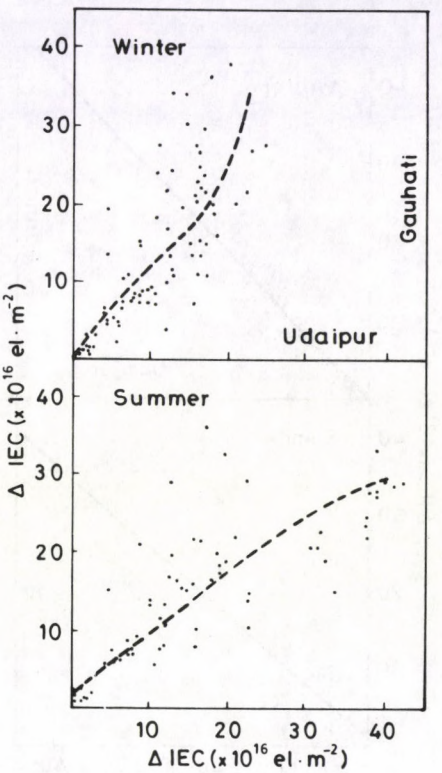

Fig. 4. Relative IEC of Gauhati at all local times plotted against those of Udaipur for strong EEJ days

EEJ days from the monthly average leads to indentical values of IEC at the two stations in both winter and summer. For higher values of ΔIEC ($> 20 \times 10^{16}$ el.m^{-2} in winter and $> 25 \times 10^{16}$ el.m^{-2} in summer), the monthly mean data points lie entirely on the Gauhati and Udaipur side, respectively, of the regression lines (Fig. 3). Since the discrepancy between the two sets of data under the influence of strong EEJ increases for higher values of IEC (Fig. 4), it may be concluded that the average behaviour of IEC is influenced by EEJ activity and the electrojet effects are discernible in high daytime values of IEC.

4. Discussion

Changes in the electric current system in the atmosphere are known to induce variations in the horizontal component (H) of the earth's magnetic field on the surface of the earth. The relatively strong belt of current along the magnetic

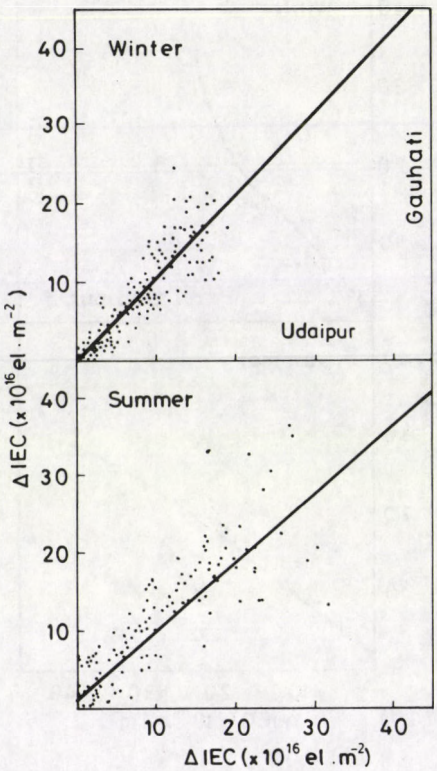

Fig. 5 Same as in Fig. 4 for normal EEJ days

equator at E region heights, termed as the equatorial electrojet, in association with the magnetic field gives rise to an $E \times B$ vertical drift of ionization at the equator (Balsely and Woodman [13]). Ionization at the equator is lifted vertically upward by the electrodynamic drift during the electrojet (normally during daytime) to higher altitudes which later diffuse along geomagnetic field lines to higher latitudes giving rise to the phenomenon known as the 'Appleton' or equatorial anomaly (Martyn [14]). Variations in the $E \times B$ upward drift velocity will result in lifting up of the ionization to varying altitudes and thereby producing the peak of the anomaly at different latitudes. Rama Rao et al [6] had found that during a strong electrojet day, the crest of the anomaly tends to form northward of the normal latitudinal position. However, seasonal variations in the position of the crest of the anomaly with respect to the equator had also been observed during this period. In winter, the crest of the anomaly shifts equatorward relative to its position in summer, while in equinox, it moves further north beyond average location in summer. In Fig. 6, IEC–IEC_{min} at 1400 h local time along the latitudinal chain centering around 71 °E meridian has

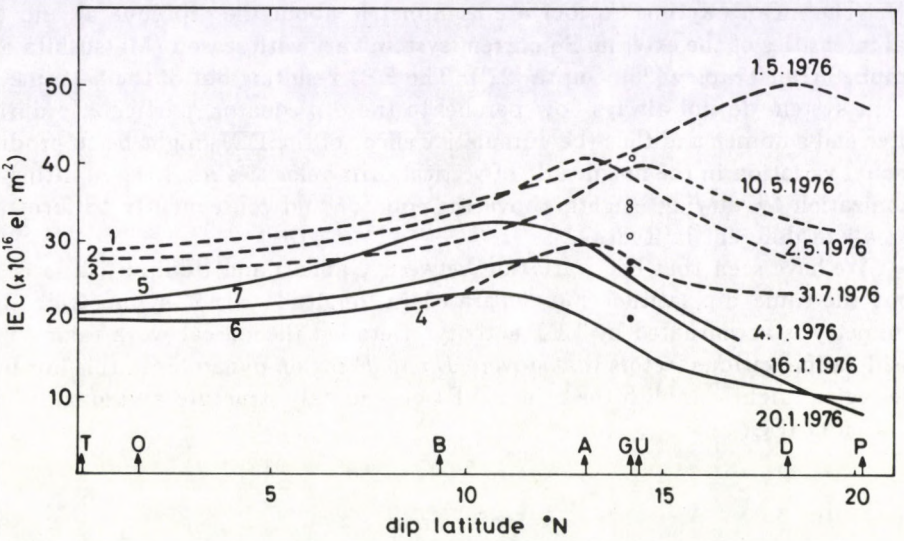

Fig. 6. Latitudinal variation of ΔIEC at 1400 h L.T. for selected days of strong electrojet. Solid lines represent winter and broken lines represent summer days. Dots and circles are corresponding values for Gauhati in winter and summer, respectively

been shown for some strong EEJ days to illustrate the shifting of the anomaly crest with respect to the equator. The curves were drawn through points corresponding to the stations Trivandrum (7.9 °N, 73.3 °E; dip lat. 0.1 °N) Ootacumund (11.0 °N, 73.5 °E; dip lat. 1.6 °N), Bombay (17.8 °N, 69.8 °E; dip lat. 9.3 °N), Ahmedabad (21.5 °N, 69.4 °E; dip lat. 13.1 °N), Udaipur, Delhi (26.2 °N, 72.2 °E; dip lat. 18.3 °N), and Patiala (28.3 °N, 72.1 °E; dip lat. 20.2 °N). Circles and dots are the corresponding data points for Gauhati. It could be seen from the Figure that the anomaly peaks near Bombay in winter and around Udaipur in summer with a tendency to move further north in an early summer day. Relative IEC for Gauhati does not correspond to the anomaly level as deduced from observations along the chain of stations around 71 °E on any day of strong EEJ. IEC at Gauhati is higher than the corresponding values at Udaipur in winter and lower in summer. Longitudinal separation of Gauhati (by 12°) from the other stations seems to have contributed to the observed mismatch in IEC behaviour.

The structure of the equatorial anomaly in IEC was shown to correspond to electrojet strength (Iyer et al [15]; Singh et al [16]) while Jain et al [17] had shown that at low latitudes, stormtime changes in IEC were controlled to a large extent by changes in electrojet strength. Figure 6 shows that the equatorial anomaly which is well developed under the strong EEJ peaks at different latitudes in different seasons. Thus the position of the crest of the anomaly appears to be influenced by season rather than by EEJ activity. It would be worthwhile to look for a mechanism coupled to the EEJ and responsible for this spatial shift in the anomaly peak with

season. The EEJ and Sq current systems are coupled interactive systems (Forbes [18]). The mean daytime Sq foci are asymmetric about the dip equator and the total intensities of the external Sq current system vary with season (Matsushita and Campbell [19]; Trapley [20], Gupta [21]). The EEJ resulting out of the asymmetric current system do not always flow parallel to the dip equator, particularly during winter and summer and thus the cumulative effect of the EEJ might be to produce seasonal variation in the magnitude of vertical drift velocities resulting in lifting up of ionization to varying heights above the equator and consequently to form the anomaly at different latitudes.

We have seen that IEC variation between Gauhati and Udaipur, situated at about the same dip latitude but separated in longitude is not symmetric. The asymmetry is accentuated by EEJ activity. Detailed theoretical work taking into consideration various factors that govern E and F region dynamics in this low latitude region might establish the role of EEJ on anomaly structure and longitudinal variation in IEC.

References

1. J. A. Klobuchar and J. M. Johanson, Report AFGL-TR-77-0185, Air Force Geophysics Laboratory, Bedford, Mass., U.S.A, 1977.
2. R. P. Kane, Ann. Geophys., *38*, 145, 1982.
3. H. Soicher, J. A. Klobuchar and P. H. Doherty, Proc. COSPAR/URSI Symposium on Beacon Satellite Studies of the Earth's Environment, ed. T. R. Tyagi, New Delhi, 409, 1983.
4. P. K. Bhuyan, L. Singh and T. R. Tyagi, Indian J. Radio Space Phys., *13*, 185, 1984.
5. P. K. Bhuyan and T. R. Tyagi, Indian J. Phys., *64B*, 419, 1990.
6. P. V. S. Rama Rao, A. Dasgupta, J. A. Klobuchar and R. G. Rastogi, Proc. COSPAR/URSI Symposium on Beacon Satellite Studies of the Earth's Environment, ed. T. R. Tyagi, New Delhi, 393, 1983.
7. R. S. Dabas, P. K. Bhuyan, T. R. Tyagi, R. K. Bhardwaj and J. B. Lal, Radio Sci., *19*, 749, 1984.
8. P. K. Bhuyan, Current Sci., *62*, 631, 1992.
9. J. A. Klobuchar, K. N. Lyer, M. O. Vats and R. G. Rastogi, Indian J. Radio Space Phys., *6*, 159, 1977.
10. C. M. Rush and A. D. Richmond, J. Atmos. Terr. Phys., *35*, 1171, 1973.
11. H. Chandra and R. G. Rastogi, Indian J. Radio Space Phys., *3*, 332, 1974.
12. P. K. Bhuyan and T. R. Tyagi, Proc. International Beacon Satellite Symposium, Tucuman, Argentina, 139, 1990.
13. B. B. Balsely and R. F. Woodman, J. Atmos. Terr. Phys., *31*, 365, 1969.
14. D. F. Martyn, Proc. Royal Soc., London, *A189*, 241, 1947.
15. K. N. Iyer, M. R. Deshpande and R. G. Rastogi, Indian Acad. Sci., *84A*, 129, 1976.
16. M. Singh, H. S. Grum and A. R. Jain, Indian J. Radio Space Phys., *8*, 44, 1979.
17. A. R. Jain, M. R. Deshpande, G. Sethia, R. G. Rastogi, M. Singh, H. S. Gurm, A. V. Janve and R. K. Rai, Indian J. Radio Space Phys., *7*, 254, 1978.
18. J. M. Forbes, Rev. Geophys. Space. Phys., *19*, 469, 1981.
19. S. Matsushita and W. H. Campbell, Physics of Geomagnetic Phenomena, Academic Press, New York, 1967.
20. J. D. Trapley, J. Atmos. Terr. Phys., *35*, 1063, 1973.
21. J. C. Gupta, Pure Apl. Geophys., *110*, 2076, 1973.

Acta Physica Hungarica 73 (1), pp. 45–49 (1993)

BULK VISCOSITY AS A SOURCE OF INFLATIONARY COSMOLOGY

C. WOLF

Department of Physics, North Adams State College
N. Adams, MA (01247) USA

(Received 9 December 1992)

By considering a homogeneous and isotropic universe with matter admitting a bulk viscosity coefficient depending on the energy density, curvature squared and the energy density times the curvature squared we study the spectrum of allowed inflationary cosmologies when all these effects are present simultaneously. We also demonstrate that when the equation of state for matter violates the dominant energy condition inflation is never possible unless the bulk viscosity coefficient admits negative contributions from the above mentioned effects.

1. Introduction

Inflationary cosmology originally developed as a scheme to resolve the flatness, horizon and monopole abundance problems of conventional big bang cosmology [1]. Old inflation [1], new inflation [2], chaotic inflation [3] and extended inflation [4] all address the same problems with extended inflation offering us the best theory for how the universe inflates in the beginning to resolve the flatness and horizon problems and then slows down in its expansion rate so as to allow the true vacuum to percolate. In extended inflation a Brans–Dicke type scalar is used as a catalyst to provide the initially fast rate of inflation and the later slowing down of the scale factor expansion [5]. Even if a scalar potential is not present to provide the driving force for the above mechanisms of inflation there exist other dynamical schemes that can lead to inflationary like cosmologies, namely bulk viscosity driven inflation [6] and higher curvature driven inflation [7]. Such mechanisms are important for they suggest that inflation might not be a generic result of a theory with a scalar field displaced from the minimum of the potential but rather a general feature of early universe cosmology independent of the initial conditions. This is the spirit behind the "cosmic no-hair theorem" [8,9,10] along with the conjecture that inflation might be an "attractor in initial condition space" [11]. Actually, if quantum gravity ultimately determines the initial conditions for conventional cosmology then it might be of interest to study those cosmological scenarios wherein quantum effects are already imbedded in the cosmology being studied. One example of this is curvature dependent bulk viscosity where the effect of pair creation in a background gravitational field generates an effective curvature dependent bulk viscosity coefficient [12,13]. Actually energy dependent bulk viscosity has been studied as a

means of representing particle creation in the early universe as well as describing dissipative processes related to primordial entropy generation [14]. Bulk viscosity can also represent in a phenomenological manner the conversion of massive string modes into massless modes if strings are the fundamental constituents of the early universe [15].

In a previous note we have studied the influence of energy dependent, curvature dependent and energy dependent times curvature dependent bulk viscosity on inflation and calculated the rate of inflation in each case generated around the Planck era [16]. In this note we extend the analysis and study the rate of inflation when all three of these forms of bulk viscosity are simultaneously present. We also demonstrate that if the equation of state of matter violates the dominant energy condition that inflation is never possible in the presence of the above forms of bulk viscosity unless one or more of the contributions to the bulk viscosity coefficient are negative. Since the inflationary solutions derived in this note add to the already present large list of inflationary cosmologies, it gives us further reason to believe in the "cosmic no-hair theorem" and the belief that inflation might ultimately be a result of quantum effects generated around the Planck era.

2. Bulk viscosity and inflation

We begin our analysis by writing the homogeneous, isotropic metric as

$$(dS)^2 = dt^2 - R^2\left(\frac{dr^2}{1-Kr^2} + r^2 d\theta^2 + r^2\sin^2\theta(d\phi)^2\right), \quad (K = 0, \pm 1), \tag{2.1}$$

the Ricci components are

$$R_{00} = \frac{3\ddot{R}}{R},$$
$$R_{ij} = \left(\frac{\ddot{R}}{R} + 2\left(\frac{\dot{R}}{R}\right)^2 + \frac{2K}{R^2}\right) g_{ij}. \tag{2.2}$$

For the matter, we have [17]

$$T_{\mu\nu} = (\overline{P} + \epsilon)U_\mu U_\nu - g_{\mu\nu}\overline{P}, \tag{2.3}$$

where

$$\overline{P} = P - \xi U^a_{;a} = P - 3\xi\left(\frac{\dot{R}}{R}\right).$$

($U^0 = 1$, $U^i = 0$), ξ = bulk viscosity coefficient.

We next assume an equation of state of the form $P = \alpha\epsilon$ (α = constant).

For the bulk viscosity coefficient we add together the constituent effects referred to in [16] and write

$$\xi = C_1(\epsilon) + C_2(R_S)^2 + C_3(\epsilon)(R_S)^2. \tag{2.4}$$

Here $R_S = R_{\mu\nu}g^{\mu\nu}$, C_1, C_2, C_3 are constant.

For a flat universe $K = 0$, we have

$$R_S = R_{\mu\nu}g^{\mu\nu} = 6\frac{\ddot{R}}{R} + 6\left(\frac{\dot{R}}{R}\right)^2. \tag{2.5}$$

Using Eqs (2.2), (2.3), (2.4) and (2.5) the Einstein equations read

$$\left(\text{here} \quad T_{00} = \epsilon,\ T_{ij} = -\overline{P}g_{ij} = -\left(P - 3\xi\frac{\dot{R}}{R}\right)g_{ij},\ T = \epsilon - 3\overline{P}\right),$$

$$3\frac{\ddot{R}}{R} = -k\left[\epsilon - \frac{1}{2}\left(\epsilon - 3\alpha\epsilon + 9(C_1\epsilon + C_2(R_S)^2 + C_3\epsilon(R_S)^2)\frac{\dot{R}}{R}\right)\right], \tag{2.6}$$

$$\left(k = \frac{8\pi G}{C^4},\ C = 1\right),$$

$$\frac{\ddot{R}}{R} + 2\left(\frac{\dot{R}}{R}\right)^2 = -k\begin{bmatrix} -\alpha\epsilon + 3(C_1\epsilon + C_2(R_S)^2 + C_3(\epsilon)(R_S)^2)\dfrac{\dot{R}}{R} \\ -\frac{1}{2}\left(\epsilon - 3\alpha\epsilon + 9(C_1\epsilon + C_2(R_S)^2 + C_3\epsilon(R_S)^2)\dfrac{\dot{R}}{R}\right) \end{bmatrix}. \tag{2.7}$$

Solving for $k\epsilon$ in Eq. (2.6) and Eq. (2.7) and equating them we have

$$\frac{3\frac{\ddot{R}}{R} - \frac{9}{2}k\frac{\dot{R}}{R}(C_2(R_S)^2)}{\frac{1}{2} + \frac{3\alpha}{2} - \frac{9C_1\dot{R}}{2R} - \frac{9}{2}C_3(R_S)^2\frac{\dot{R}}{R}} = \frac{\frac{\ddot{R}}{R} + 2\left(\frac{\dot{R}}{R}\right)^2 - \frac{3}{2}kC_2(R_S)^2\frac{\dot{R}}{R}}{\frac{\alpha}{2} - \frac{1}{2} - \frac{3}{2}C_1\frac{\dot{R}}{R} - \frac{3}{2}C_3\frac{\dot{R}}{R}(R_S)^2}. \tag{2.8}$$

We now insert the inflationary solution $R - R_0\theta^{\beta+}$ into Eq. (2.8) giving

$$\beta^5(9C_3(144) + \beta^3(432kC_2) + \beta(9C_1) + (-3\alpha - 3) = 0. \tag{2.9}$$

We now study the following cases for Eq. (2.9).

Case I

If $C_3 = 0$ and $\alpha > -1$ (equation of state obeying dominant energy condition $P + \epsilon \geq 0$), $C_1, C_2 > 0$ then Eq. (2.9) has one positive root which is the inflationary solution, the value of β is for $\alpha = 1/3$,

$$\beta = \sqrt[3]{\frac{2}{432kC_2} + \frac{1}{18}\sqrt{81\left(\frac{4}{432kC_2}\right)^2 + 12\left(\frac{18C_1}{864C_2k}\right)^3}} + \sqrt[3]{\frac{2}{432kC_2} - \frac{1}{18}\sqrt{81\left(\frac{4}{432kC_2}\right)^2 + 12\left(\frac{18C_1}{864C_2k}\right)^3}}.$$

Case II

If $\alpha < -1$ (violation of the dominant energy condition) and C_3, C_2, $C_1 > 0$ then Eq. (2.9) has no positive roots and inflation does not occur.

Case III

$C_3, C_2, C_1 > 0$ and $\alpha > -1$ then Eq. (2.9) has one positive root and inflation again occurs, the root must be found by numerical analysis of Eq. (2.9).

Case IV

Even if $\alpha < -1$ and $C_3 < 0$, and $C_1, C_2 > 0$ then Eq. (2.9) has one positive root and inflation occurs, inflation will also occur if $\alpha < -1$ and $C_1 < 0$; $C_2, C_3 > 0$ or $C_2 < 0$; $C_1, C_3 > 0$ or $C_1 > 0$; $C_2, C_3 < 0$ or $C_2 > 0$; $C_1, C_3 < 0$ or $C_3 > 0$; $C_2, C_1 < 0$; or $C_1, C_2, C_3 < 0$ in which case Eq.(2.9) has at least one positive root. The roots would have to be found by analysis of Eq. (2.9).

3. Conclusion

The fact that inflation always occurs for the bulk viscosity coefficient having the general form in Eq. (2.4) providing the equation of state obeys the dominant energy condition ($P + \epsilon \geq 0$) suggests that cosmologies admitting bulk viscosity generate part of the solution space included in the general "no-hair theorem" for inflation. It is also of interest that even if the dominant energy condition is violated that inflation still occurs providing the coefficients (C_1, C_2, C_3) fulfill the inequalities in Case IV. The fact that multiple positive roots may occur suggests that the form of bulk viscosity studied above may generate a cosmology admitting double inflation.

Lastly it would be of interest to ask if the coefficients (C_1, C_2, C_3) could be calculated from a quantum gravitational model to ascertain their positive or negative nature. As in the case of "induced gravity" [18] the sign of the coefficients C_1, C_2, C_3 may depend on the heavy fields that induce them. It is intriguing that the flavor attached to inflationary cosmology has changed over the past ten years from a theory which sought to solve the flatness and horizon problems of the universe so that of searching for a cosmic no-hair theorem ultimately related to the quantum gravitational state of the universe around the Planck era. Classical cosmologies with their matter content, their homogeneity and isotropy or lack of it, may all be late time solutions to a quantum cosmology with very specific characteristics generating random initial conditions at the classical boundary. These initial conditions might show up in a way not expected in classical cosmology and general features, such as bulk viscosity or other dissipative processes might include the spectrum of uncertainty given to us from the Planck era. The fact that the general form of bulk viscosity studied in this note generates a wide solution space for inflation suggests that this way of thinking might be generic and correct.

Acknowledgement

I should like to thank the physics departments of Williams College and Harvard University for the use of their facilities.

References

1. A. Guth, Phys. Rev. *D23*, 347, 1981.
2. P. J. Steinhardt and M. S. Turner, Phys. Rev. *D29*, 2162, 1984.
3. A. D. Linde, Phys. Lett., *B129*, 177, 1983.
4. E. W. Kolb, D. S. Salopek and M. S. Turner, Phys.. Rev., *D42*, 3925, 1990.
5. C. Brans and R. H. Dicke, Phys. Rev., *124*, 925, 1961.
6. T. A. Verwimp and D. K. Callebaut, Proc. of 26th Liège Int. Astrophysics Colloquium (The Univ. of Liège, Belgium) July 1–4, 1986.
7. W. M. Swen, Proc. of 26th Liège Int Astrophysics Colloquium (The Univ. of Liège, Belgium) July 1–4, 1986.
8. F. Hoyle and J. V. Narlikar, Proc. of Roy. Soc., *A273*, 1, 1963.
9. G. W. Gibbons and S. W. Hawking, Phys. Rev., *D15*, 2783, 1977.
10. S. W. Hawking and I. Moss, Phys. Lett., *B110*, 35, 1977.
11. D. G. Goldswirth, Phys. Lett., *B243*, 41, 1990.
12. V. Z. Gurovich and A. Starobinsky, Sov. Phys. (J.E.T.P.), *50*(5), 844, 1979.
13. C. Wolf, Phys. Lett., *A127*, 129, 1988.
14. J. A. S. Lima and A. S. M. Germano, Phys. Lett., *A170*, 373, 1992.
15. C. Wolf, Hadronic J., *10*, 59, 1987.
16. C. Wolf, submitted to Pramana, 1992.
17. C. Wolf, Astron. Nachr., *309*, (3), 177, 1988.
18. S. Adler, Rev. of Mod. Phys., *54*, (No. 3), 729, 1981.

Acta Physica Hungarica 73 (1), pp. 51-58 (1993)

A SUPERSPACE ORIGIN FOR AN EXTENDED GAUGE MODEL

C. M. DORIA, R. M. DORIA* and F. A. B. RABELO DE CARVALHO**

University of Warwick, Mathematics Institute
CV7 4A2 Coventry, England
** Universidade Federal do Rio de Janeiro*
Ilha do Foundão, Rio de Janeiro, Brasil
*** Universidade Católica de Petrópolis (UCP)*
25600 Petrópolis, RJ, Brasil

(Received 12 January 1993)

Supersymmetry provides an example of Gauge Theories where the presence of more than one gauge potential in the same group naturally emerges. Particularly, we study the Abelian case in three dimensions. A dynamics accounting for the presence of only two potential fields in a single group is obtained via a soft-breaking of supersymmetry.

1. Introduction

Symmetry environment should not be restricted to the simple fusion between Group Theory and Quantum Theory. The existence of a symmetry can be developed in a space larger than the limit where the number of potential fields rotating under the same group equals the number of generators of the group. This context motivates us to make the statement that a gauge group also rules a Gauge Theory where N-families of potential fields are transforming as

$$\begin{aligned} A_\mu &\to U A_\mu U^{-1} + \frac{i}{g}\partial_\mu U \cdot U^{-1}, \\ B_\mu &\to U B_\mu U^{-1} + \frac{i}{g}\partial_\mu U \cdot U^{-1}, \\ &\vdots \qquad\qquad \vdots \\ N_\mu &\to U N_\mu U^{-1} + \frac{i}{g}\partial_\mu U \cdot U^{-1}. \end{aligned} \tag{1}$$

However, such an affirmation (1) cannot be tested experimentally. This is so because a field cannot be directly measured. Therefore, it is not possible to think of experimental models that would distinguish the fields A_μ, B_μ, etc.

Considering such a limitation that field theory offers for laboratory to test (1), we move to the theoretical approach in order to get some reasons to justify the opinion (1). Gradually, different insights have been developed to identify these

potential fields as independent fields [1]. This discussion could be advocated by classifying the arguments in two differents aspects: global and local. A global point of view means that the existence of distinguished fields in (1) is originated from the proper Gauge Theory Structure. A local aspect means to show evidences for (1) through the study of a specific Lagrangian.

A first, and perhaps the most natural argument against (1) is that it would contain a hidden transformation which correlates the potential fields. Thus, as a first global argument to advocate the defense, we would recall the existence of a geometrical motivation, based on the Kaluza–Klein approach. This means that a global justification for (1) can be originated in terms of the spontaneous compactification of a higher-dimensional theory of coupled Yang–Mills gravity with non-trivial torsion [1]. As a local defense, we would argue by determining the propagators of the theory and their respective poles, or by specifying the number of degrees of freedom and the quantum numbers of the different potentials. For that, it becomes necessary to choose a specific Lagrangian and then, calculate such entities. As an example, consider the following Lagrangian

$$L_G = G_{\mu\nu}G^{\mu\nu} + m^2(A_\mu - B_\mu)^2,$$

where

$$G_{\mu\nu} = \partial_\mu A_\nu - \partial_\nu B_\mu + g[B_\mu, A_\nu]. \tag{2}$$

Practical calculations show the presence of a spectrum with two different quanta in (2). In parallel, the accusation of a hidden symmetry between A_μ and B_μ fields can be shown to be a source for breaking gauge invariance.

The motivation of this work is to develop another general argument to assume that (1) contains fields with different quantum numbers [2]. The proposal is that supersymmetry already contains informations for the inclusion of more than one potential field in a single simple group. Thus, in order to develop such a global thesis for (1), this work will be organized as follows. In Section 2, it will be stressed that the superspace formulation of an Abelian theory naturally induces the presence of more than one potential field in the same group. However, in Section 3, it will be shown that under requirement of certain constraints, the theory exhibits the existence of only one potential field. Finally, in Section 4, we shall discuss the possibility of formulating a dynamics for the second potential field but which avoids other models with undesirable spins.

2. A supersymmetric spectrum for QED in three dimensions

Consider the following superspace action

$$S = \int d^3x d^2\theta (D^\alpha \phi^*)(D_\alpha \phi), \tag{3}$$

where ϕ is a complex scalar superfield and D_α the covariant derivative,

$$D_\alpha \equiv \partial_\alpha + i\theta^\beta \partial_{\alpha\beta}. \tag{4}$$

For (1) to be rendered covariant under the internal symmetry U (1),

$$\phi'(x;\theta) = e^{iq\Lambda(x;\theta)}\phi(x;\theta), \tag{5}$$

the concept of gauge covariant derivative is required. However, for the supersymmetric extension, it emerges the possibility of generating two types of covariant derivatives

$$\nabla_\alpha \equiv D_\alpha + iqg\Gamma_\alpha \tag{6}$$

and

$$\nabla_{\alpha\beta} \equiv \partial_{\alpha\beta} + iqg\Delta_{\alpha\beta}. \tag{7}$$

(6) and (7) satisfy the Bianchi identities

$$[\nabla_{A'}[\nabla_{B'}\nabla_C\}] + [\nabla_{B'}[\nabla_{C'}\nabla_A\}] + [\nabla_{C'}[\nabla_{A'}\nabla_B\}] = 0. \tag{8}$$

The notation is $\nabla_A \equiv (\nabla_\alpha; \nabla_{\alpha\beta})$, where $\alpha(= 1, 2)$ denotes the spinor index and the pair $\alpha\beta$ the space-time index. Consequently, these two species of derivatives, ∇_α and $\nabla_{\alpha\beta}$, that the superspace presents, generate two superfields Γ_α and $\Delta_{\alpha\beta}$.

Our purpose is to characterize the spectrum developed through the superfields obtained from (6), (7) and (8). The gauge invariance requirement also yields the following transformations

$$\Gamma'_\alpha = \Gamma_\alpha - \frac{1}{g} D_\alpha \Lambda, \tag{9}$$

$$\Lambda'_{\alpha\beta} = \Delta_{\alpha\beta} - \frac{1}{g}\partial_{\alpha\beta}\Lambda, \tag{10}$$

where $\Lambda \equiv \Lambda(x, \theta)$ is a real scalar superfield.

For the real spinorial superfield $\Gamma_\alpha(x;\theta)$ one gets

$$\Gamma(x;\theta) = \{X_\alpha(x), M(x); A_{\alpha\beta}(x), \lambda_\alpha(x)\}. \tag{11}$$

Adopting the component fields of the gauge parameter superfield as

$$\Lambda(x;\theta) = \{B(x), \eta_\alpha(x), G(x)\} \tag{12}$$

it yields,

$$X'_\alpha = X_\alpha - \frac{1}{g}\eta_\alpha, \tag{13}$$

$$A'_{\alpha\beta} = A_{\alpha\beta} + \frac{1}{g}\partial_{\alpha\beta}B, \tag{14}$$

$$M' = M - \frac{1}{2g}G, \tag{15}$$

$$\lambda'_\alpha = \lambda_\alpha. \tag{16}$$

Notice that the components $X_\alpha(x)$ and $M(x)$ are pure gauge modes, and so, the parameters $\eta_\alpha(x)$ and $G(x)$ can be chosen in such a way that X_α and M be eliminated. This means that (11) carries only an $U(1)$-gauge field, $A_{\alpha\beta}(x)$, and its supersymmetric partner, $\lambda_\alpha(x)$.

Similarly, the superfield $\Delta_{\alpha\beta}$ contains the following components,

$$\Delta_{\alpha\beta}(x;\theta) = \{v_{\alpha\beta}(x), \psi_{(\gamma,\alpha\beta)}(x), \zeta_\alpha(x), u_{\alpha\beta}(x)\} \tag{17}$$

transforming under $U(1)$ according to:

$$V'_{\alpha\beta} = V_{\alpha\beta} - \frac{1}{g}\partial_{\alpha\beta}B, \tag{18}$$

$$\psi'_{(\gamma,\alpha\beta)} = \psi_{(\gamma,\alpha\beta)} - \frac{1}{g}\partial_{(\alpha\beta}\eta_{\gamma)}, \tag{19}$$

$$\zeta'_\alpha = \zeta_\alpha + \frac{1}{g}\partial^\lambda_\alpha\eta_\lambda, \tag{20}$$

$$u'_{\alpha\beta} = u_{\alpha\beta} - \frac{1}{g}\partial_{\alpha\beta}G, \tag{21}$$

where $V_{\alpha\beta}(x)$ is a vector field; $\psi_{(\gamma,\alpha\beta)}(x)$ is a Rarita–Schwinger field in three dimensions (spin 3/2); $\zeta_\alpha(x)$ is a fermion field (spin 1/2); and $u_{\alpha\beta}$ is also a vector field but with a different dimension from $v_{\alpha\beta}(x)$. Thus $\Delta_{\alpha\beta}(x;\theta)$ carries six bosonic and six fermionic off-shell degrees of freedom.

Thus, (11) and (17) put in evidence the presence of more than one vector field in the same group, as a natural consequence of supersymmetry. There is an abundance of spinors, vectors, and so on, as members of a same multiplet. However, our interest here is to demonstrate just the presence of more than one potential field transforming under the same group. Comparing (14) and (18), we observe that the vector fields $A_{\alpha\beta}(x)$ and $v_{\alpha\beta}(x)$ materialize our search for. They are fields with the same dimension and transforming with the same term $\partial_{\alpha\beta}B(x)$. This means that the supersymmetric version of QED in three dimensions, with (11) and (17), exhibits the presence of two potential fields in the same group. Nevertheless, we should still study about the possibilities that theory offers for controlling the $\Gamma_\alpha(x;\theta)$ and $\Lambda_{\alpha\beta}(x;\theta)$ component fields.

3. An imposed super – QED$_3$

Supersymmetry is a typical example of a gauge theory where the presence of more fields in the same group proliferates. (11) and (17) contain fermions and

bosons transforming under the same $U(1)$ group. Therefore, this Section is devoted to the study of how to control such a proliferation. In order to restrict the degrees of freedom that the theory offers, we should take into account the constraints. Thus they should be understood consistently through the Bianchi identities. The simple supersymmetry algebra in flat superspace is realized by

$$\{D_\alpha, D_\beta\} = -2^i \partial_{\alpha\beta}. \tag{22}$$

Notice the connection between the supersymmetry and the space-time derivatives. The extension of (22) in terms of the gauge-covariant derivative algebra is

$$[\nabla_A, \nabla_B] = T^C_{AB} \nabla_C + F_{AB}, \tag{23}$$

where T^C_{AB} denotes the torsion components and F_{AB} the field-strength superfields. Substituting (22) into (23) one gets a non-trivial torsion for the flat superspace

$$T^{\gamma,\delta}_{\alpha\beta} = -2i\delta^\gamma_{(\alpha}\delta^\delta_{\beta)}, \tag{24}$$

all the other torsion components being zero. However, such results are not necessarily the same for a $U(1)$-covariant theory. A procedure is to carry (24) as a constraint. This means that it works at a boundary condition between the geometry generated from the usual and by the covariant derivatives.

A second constraint which can be imposed is

$$F_{(\alpha\beta)} = 0. \tag{25}$$

(25) in (23) gives

$$\Delta_{\alpha\beta} = \frac{i}{2}(D_\alpha \Gamma_\beta + D_\beta \Gamma_\alpha). \tag{26}$$

(26) shows that the connections Γ_α and $\Delta_{\alpha\beta}$ are not independent. Their component fields are the same. This means that, under certain circumstances, the additional degrees of freedom introduced by $\Delta_{\alpha\beta}$ can be eliminated. However, relation (25) is not enough to complete the work. This is so because (23) still contains field strengths, $F_{\alpha,\beta\gamma}$ and $F_{\alpha\beta,\gamma\delta}$ that must be proved to be dependent on Γ_α.

Informations about the field-strength superfields $F_{\alpha,\beta\gamma}$ and $F_{\alpha\beta,\gamma\delta}$ can be obtained from the Bianchi identities. Although these identities are only algebraic relations, they become useful to establish relations amongst the fundamental superfields in theory. Thus, considering the impositions over torsion (24) and over superfield field strength (25) one gets from (8) the information that the superfield $F_{\alpha,\beta\gamma}$ is such that its completely symmetric part is zero

$$F_{(\alpha,\beta\gamma)} = 0. \tag{27}$$

Then, decomposing the tensor $F_{\alpha,\beta\gamma}$ into its irreducible representations

$$F_{\alpha,\beta\gamma} = F_{(\alpha,\beta\gamma)} + \frac{2}{3}F_{[\alpha,\beta]\gamma} + \frac{2}{3}F_{[\alpha,\gamma]\beta} \tag{28}$$

and defining

$$W_\alpha = F^\beta, \beta\alpha \tag{29}$$

gives

$$F_{\alpha,\beta\gamma} = \frac{1}{2}C_{\alpha\beta}W_\gamma + \frac{1}{3}C_{\alpha\gamma}W_\beta. \tag{30}$$

Substituting (26) in (23) and comparing with (30) one gets

$$W_\gamma = -gD^\beta D_\gamma \Gamma_\beta + \frac{g}{2}(D_\gamma D_\beta \Gamma^\beta - D^2\Gamma_\gamma). \tag{31}$$

Similarly, we obtain

$$F_{\alpha\beta,\gamma\delta} = \partial_{\alpha\beta}\Delta_{\gamma\delta} - \partial_{\gamma\delta}\Delta_{\alpha\beta}. \tag{32}$$

Thus (26), (31), (30) and (12) show that $\Gamma_\alpha(x;\theta)$ is the only basic superfield that theory with constraints (24) and (25) is envolving.

4. A special dynamics

The presence of several fields in a single supersymmetry multiplet creates the discussion on whether supersymmetry does not contain circumstances to be conveniently chosen in order to propitiate more than one kind of dynamics. In order to organize such a situation where just some intended fields propagate, we submit the following action

$$S_{\text{total}} = S_I + S_{II}, \tag{33}$$

where

$$S_I = S_{\text{Gauge}} + S_{\text{g.f.}} + S_{\text{int}} + S_{\text{mass}}, \tag{34}$$

$$S_{II} = S_{\text{broken}} + S_{\text{int/broken}}, \tag{35}$$

with

$$S_{\text{Gauge}} = \int d^3x d^2\theta (D^k D^\alpha \Gamma_k)(D^\lambda D_\alpha \Gamma_\lambda), \tag{36}$$

$$S_{\text{g.f.}} = \frac{1}{2\alpha}\int d^3x d^2\theta (D^\alpha \Gamma_\alpha) D^2 (D^\beta \Gamma_\beta), \tag{37}$$

$$S_{\text{int}} = \int d^3x d^2\theta (\nabla_\alpha \phi) * (\nabla^\alpha \phi), \tag{38}$$

$$S_{\text{mass}} = \int d^3x d^2\theta m\phi * \phi, \tag{39}$$

$$S_{\text{broken}} = \frac{1}{4}\int d^3x d^2\theta\, \theta^2 (\partial_k^\alpha \Delta^{k\beta} + \partial_k^\beta \Delta^{k\alpha}) \cdot (\partial_\alpha^\lambda \Delta_{\lambda\beta} + \partial_\beta^\lambda \Delta_{\lambda\alpha}), \tag{40}$$

$$S_{\text{int/broken}} = \frac{1}{4}\int d^3x d^2\theta\, \theta^2 (\nabla_{\alpha\beta}\phi) * (\nabla^{\alpha\beta}\phi). \tag{41}$$

Then, we have to analyse what the corresponding spectroscopy for (33) is offering. Note that from (36) there appears a propagation for the photon and photino, the gauge fixing term (37) also receives contribution from the pure gauge modes, but (34) does not produce any information for the thesis of this work. Observe that (33) contains an abundance of fields transforming in the same $U(1)$ group. However, the thesis here is that gauge invariance allows the existence of a dynamics with more than one potential field in the same group. Thus the task is to break supersymmetry as in (35), in such a way to eliminate the matter-fields $\psi_{(\alpha\beta\gamma)}(x)$, $\zeta_\alpha(x)$ and the vector field $u_{\alpha\beta}(x)$, but without losing gauge invariance. This attempt is organized through (40). There, only $v_{\alpha\beta}(x)$ field propagates. Including (41), a scalar electrodynamics for this second potential field is generated.

5. Conclusion

The supersymmetrization process, when carried out in superspace naturally requires the presence of more than one potential field in the same group. These fields originate from the covariantization process of the supersymmetric derivatives D_α and $\partial_{\alpha\beta}$. This process introduces the presence of two super-connection terms. By examining their respective components fields, one finds two gauge-potential fields that are independent, but transforming under the same group.

However, usually, the presence of these potential fields is bypassed by introducing suitable constraints in order to relate the fields that originally emerged independently in the theory. Thus, the thesis that a gauge group supports the transformation of more than one potential field can be advocated. This means that, through the relaxation of certain constraints usually imposed on the field-strength superfields, the proof of the existence of a superspace geometry with more than one connection appears.

Finally, through the decoupling of undesirable matter fields inside of the superfield $\Delta_{\alpha\beta}(x;\theta)$, the process is concluded. Thus, arguments based on supersymmetry for characterizing the existence of a global assumption for justifying the presence of more than one potential field in the same group are thought to be completed. The study was performed in three dimensions just for the sake of simplicity. It could as well be carried out in four dimensions with the same conclusions: supersymmetry, unless certain constraints are enforced, naturally leads to gauge theories where at least two gauge potentials appear transforming under the same group.

Acknowledgements

The authors would like to express their gratitude to the Brazilian Council for Scientific and Technological Development (CNPq) for their fellowships. They are also very grateful to the Coca-Cola of Brazil, through Sônia Barreto, and to Johnson & Higgins Corretores de Seguros, through Dr. Michael Wyles, for the invaluable financial help.

References

1. For a Kaluza–Klein origin see: R. M. Doria and C. Pombo, Il Nuovo Cim., *96*, B2, 1986; C. M. Doria, R. M. Doria, J. A. Helayel-Neto, Rev. Bras. Fis., *17*, 3, 1987. For a supersymmetric origin see: N. Chair, J. A. Helayel-Neto and William Smith, Phys. Lett. *B233*, 173, 1989; C. A. S. Almeida, R. M. Doria, Rev. Bras. de Fis., *21*, No. 3, 1991; C. A. S. Almeida, R. M. Doria, A Less-Constrained (2,0) Super Yang-Mills Model: The Coupling to Non-linear σ Models, UCP preprint 90/4.
   For a σ model origin see: R. M. Doria, J. A. Helayel-Neto and S. Mokhtari, Europhys. Lett., *16(1)*, 1991.
2. R. M. Doria, F. A. B. Rabelo de Carvalho, Braz. J. Phys., *23*, No. 1; R. M. Doria, G. Olveira Neto, F. A. B. Rabelo de Carvalho, A Consistent Spectroscopical Analysis for an Extended Gauge Model, UCP preprint 90/9; R. M. Doria and J. A. Helayel-Neto, Tensors and Invariants in a Generalized Gauge Model, UCP preprint 91/7.
3. S. J. Gates Jr., M. T. Grisaru, S. Rocek and W. Siegel, in Superspace, Chap. 1, Benjamin-Cummings Publ., Mass., 1983.

Acta Physica Hungarica 73 (1), pp. 59-66 (1993)

THERMOSOLUTAL CONVECTION IN A ROTATING FLUID IN HYDROMAGNETICS IN POROUS MEDIUM

R. C. SHARMA and V. K. BHARDWAJ

Department of Mathematics, Himachal Pradesh University
Shimla-171005, India

(Received 26 January 1993)

Thermosolutal instability of an electrically conducting fluid in porous medium in presence of a uniform rotation and a uniform magnetic field, simultaneously, has been considered. The stable solute gradient and rotation postpone the onset of instability. For a non-rotating system, the medium permeability and magnetic field have destabilizing and stabilizing effects, respectively. However, in the presence of rotation, when the magnetic field has a stabilizing/destabilizing effect, the medium permeability has a destabilizing/stabilizing effect under certain condition. The rotation, magnetic field and stable solute gradient introduce oscillatory modes in the system which were non-existent in their absence.

1. Introduction

A detailed account of the thermal convection in a horizontal layer of fluid heated from below, in the absence and presence of rotation and magnetic field, has been given in a treatise by Chandrasekhar [1]. Veronis [9] has investigated the problem of thermohaline convection in a layer of fluid heated from below and subjected to a stable salinity gradient. Thermosolutal convection problems arise in oceanography, limnology and engineering, e.g. ponds built to trap solar heat (Tabor and Matz [8]) and some Antarctic lakes (Shirtcliffe [5]). The physics is quite similar in the stellar case in that helium acts like salt in raising the density and in diffusing more slowly than heat.

The medium has been considered to be non-porous in all the above studies. Lapwood [2] has studied the stability of convective flow in hydrodynamics in a porous medium using Rayleigh's procedure. Wooding [10] has considered the Rayleigh instability of a thermal boundary layer in flow through porous medium. The gross effect, when the fluid slowly percolates through the pores of the homogeneous and isotropic porous medium, is represented by Darcy's law. As a result, the usual viscous term in the equation of motion is replaced by the resistance term $-(\frac{\mu}{k_1})\mathbf{q}$ where μ, k_1 and $\mathbf{q}$ stand for the fluid viscosity, medium permeability and the filter (Darcian) velocity, respectively.

The problem of thermosolutal convection in fluids in a porous medium is of importance in ground water hydrology, soil sciences, geophysics and astrophysics. The physical properties of comets, meteorites and interplanetary dust strongly suggest

the importance of porosity in the astrophysical context (McDonnel [4]). The effect of a magnetic field on the stability of such a flow is of interest in geophysics, e.g. in the study of the Earth's core where the Earth's mantle, which consists of conducting fluid, behaves like a porous medium which can become convectively unstable as a result of differential diffusion. Another application of the results of flow through a porous medium in the presence of a magnetic field is in the study of the stability of a convective flow in the geothermal region. It has been remarked by Stommel and Fedorov [7] and Linden [3] that the length scales characteristic of double-diffusive convective layers in the ocean may be sufficiently large that the Earth's rotation might be important in their formation. Also, the rotation of the Earth distorts the boundaries of a hexagonal convection cell in a fluid through a porous medium and the distortion plays an important role in the extraction of energy in the geothermal regions.

Keeping in mind the importance in ground water hydrology, soil sciences, geophysics and astrophysics, the thermosolutal convection in a porous medium in the presence of uniform rotation and uniform magnetic field, simultaneously, has been considered in the present paper.

2. Perturbation equations

Here we consider a layer of electrically conducting fluid of thickness d in porous medium acted on by a uniform magnetic field $\mathbf{H}(0, 0, H)$, uniform rotation $\Omega(0, 0, \Omega)$ and gravity force $\mathbf{g}(0, 0, -g)$. This layer is heated and soluted from below such that a uniform temperature gradient $\beta \left(= \left|\frac{dT}{dz}\right|\right)$ and a uniform solute concentration gradient $\beta' \left(= \left|\frac{dC}{dz}\right|\right)$ are maintained.

Let δp, $\delta\rho$, θ, γ, $\mathbf{q}(u, v, w)$ and $\mathbf{h}(h_x, h_y, h_z)$ denote, respectively, the perturbations in pressure p, density ρ, temperature T, solute concentration C, velocity $(0, 0, 0)$ and magnetic field $\mathbf{H}$. Then the linearized hydromagnetic perturbation equations appropriate to the problems are

$$\frac{1}{\epsilon}\frac{\partial \mathbf{q}}{\partial t} = -\frac{1}{\rho_0}\nabla\delta p + \mathbf{g}\frac{\delta\rho}{\rho_0} - \frac{\nu}{k_1}\mathbf{q} + \frac{1}{4\pi\rho_0}(\nabla \times \mathbf{h}) \times \mathbf{H} + \frac{2}{\epsilon}(\mathbf{q} \times \Omega), \tag{1}$$

$$\nabla \cdot \mathbf{q} = 0, \tag{2}$$

$$\nabla \cdot \mathbf{h} = 0, \tag{3}$$

$$\epsilon\frac{\partial \mathbf{h}}{\partial t} = (\mathbf{H} \cdot \nabla)\mathbf{q} + \epsilon\eta\nabla^2\mathbf{h}, \tag{4}$$

$$E\frac{\partial \theta}{\partial t} = \beta w + \kappa\nabla^2\theta, \tag{5}$$

$$E'\frac{\partial \gamma}{\partial t} = \beta' w + \kappa'\nabla^2\gamma, \tag{6}$$

where $E = \epsilon + (1-\epsilon)\frac{\rho_s c_s}{\rho c}$. Here, ρ, c and ρ_s, c_s stand for density and specific heat of fluid and solid (porous matrix) material, respectively. ϵ, k_1, η, $\mathrm{g}(0,0,-g)$, ν, κ and κ' denote the medium porosity, medium permeability, resistivity, gravitational acceleration, kinematic viscosity, thermal diffusivity and the solute diffusivity, respectively. E' is a solute parameter analogous to E. The equation of state is

$$\rho = \rho_0[1 - \alpha(T - T_0) + \alpha'(C - C_0)], \tag{7}$$

where the suffix zero refers to values at the reference level $z = 0$ and α, α' stand for thermal coefficient of expansion and an analogous solvent coefficient α'. The change in density $\delta\rho$ caused by the perturbations θ and γ in temperature and concentration is given by

$$\delta\rho = -\rho_0(\alpha\theta - \alpha'\gamma). \tag{8}$$

The steady-state solution is

$$\mathbf{q} = (0,0,0), \quad T = T_0 - \beta z, \quad C = C_0 - \beta' z, \quad \rho = \rho_0[1 + \alpha\beta z - \alpha'\beta' z]. \tag{9}$$

Equations (1)–(6) and (8) give

$$\left(\frac{1}{\epsilon}\frac{\partial}{\partial t} + \frac{\nu}{k_1}\right)\nabla^2 w - g\left(\frac{\partial^2}{\partial x^2} + \frac{\partial^2}{\partial y^2}\right)(\alpha\theta - \alpha'\gamma) - \frac{H}{4\pi\rho_0}\nabla^2\frac{\partial h_z}{\partial z} + \frac{2\Omega}{\epsilon}\frac{\partial\zeta}{\partial z} = 0, \tag{10}$$

$$\left(\frac{1}{\epsilon}\frac{\partial}{\partial t} + \frac{\nu}{k_1}\right)\zeta = \frac{H}{4\pi\rho_0}\frac{\partial\xi}{\partial z} + \frac{2\Omega}{\epsilon}\frac{\partial w}{\partial z}, \tag{11}$$

$$\epsilon\left(\frac{\partial}{\partial t} - \eta\nabla^2\right)h_z = H\frac{\partial w}{\partial z}, \tag{12}$$

$$\epsilon\left(\frac{\partial}{\partial t} - \eta\nabla^2\right)\xi = H\frac{\partial\zeta}{\partial z}, \tag{13}$$

$$\left(E\frac{\partial}{\partial t} - \kappa\nabla^2\right)\theta = \beta w, \tag{14}$$

$$\left(E'\frac{\partial}{\partial t} - \kappa'\nabla^2\right)\gamma = \beta' w. \tag{15}$$

Let us consider the case of fluid layer in which both the boundaries are free, the most appropriate case for stellar atmospheres (Spiegel [6]), and the adjoining medium is electrically nonconducting. The boundaries are assumed to be perfect conductors of both heat and solute concentration. The boundary conditions appropriate to the problem are

$$w = \frac{\partial^2 w}{\partial z^2} = \theta = \gamma = \frac{\partial h_z}{\partial z} = 0 \quad \text{at} \quad z = 0 \quad \text{and} \quad z = d. \tag{16}$$

3. Dispersion relation

Let us analyze the disturbances into normal modes, assuming that the perturbation quantities are of the form

$$[w, \theta, \gamma, h_z, \zeta, \xi] = [W(z), \Theta(z), \Gamma(z), K(z), Z(z), X(z)] \cdot \exp(ik_x x + ik_y y + nt), \quad (17)$$

where k_x, k_y are the wave numbers along the x and y directions, respectively, $k = (k_x^2 + k_y^2)^{1/2}$ is the resultant wave number and n is, in general, a complex constant.

Expressing the coordinates x, y, z in the new unit of length d and putting $a = kd$, $\sigma = nd^2/\nu$ and $D = \frac{d}{dz}$, Eqs (10)–(15), with the help of expression (17), in nondimensional form become

$$\left(\frac{\sigma}{\epsilon} + \frac{1}{p_l}\right)(D^2 - a^2)W = -\frac{gd^2a^2}{\nu}(\alpha\theta - \alpha'\gamma) + \frac{Hd}{4\pi\rho_0\nu}(D^2 - a^2)DK - \frac{2\Omega d^3}{\epsilon\nu}DZ, \quad (18)$$

$$\left(\frac{\sigma}{\epsilon} + \frac{1}{p_l}\right)Z = \frac{2\Omega d}{\epsilon\nu}DW + \frac{Hd}{4\pi\rho_0\nu}DX, \quad (19)$$

$$(D^2 - a^2 - Ep_1\sigma)\Theta = -\left(\frac{\beta d^2}{\kappa}\right)W, \quad (20)$$

$$(D^2 - a^2 - E'q\sigma)\Gamma = -\left(\frac{\beta' d^2}{\kappa'}\right)W, \quad (21)$$

$$(D^2 - a^2 - p_2\sigma)K = -\left(\frac{Hd}{\epsilon\eta}\right)DW, \quad (22)$$

$$(D^2 - a^2 - p_2\sigma)X = -\left(\frac{Hd}{\epsilon\eta}\right)DZ. \quad (23)$$

Here $p_l = \frac{k_1}{d^2}$ is the dimensionless medium permeability, $p_1 = \frac{\nu}{\kappa}$ is the Prandtl number, $p_2 = \frac{\nu}{\eta}$ is the magnetic Prandtl number and $q = \frac{\nu}{\kappa'}$ is the Schmidt number. The boundary conditions (16) transform to

$$W = D^2W = \Theta = \Gamma = DK = 0 \quad \text{at} \quad z = 0 \quad \text{and} \quad z = 1. \quad (24)$$

Using the boundary conditions (24), it can be shown that all the even order derivatives of W must vanish for $z = 0$ and 1. Eliminating Θ, Γ, K, X and Z from Eqs (18)–(23) and using the proper solution

$$W = W_0 \sin \pi z,$$

W_0 being constant, we obtain the dispersion relation

$$R_1 = \frac{(1+x)(1+x+iEp_1\sigma_1)\left\{\left(\frac{i\sigma_1}{\epsilon}+\frac{1}{p}\right)(1+x+ip_2\sigma_1)+Q_1\right\}}{x(1+x+ip_2\sigma_1)} + S_1\frac{(1+x+iEp_1\sigma_1)}{(1+x+iE'q\sigma_1)} + \frac{T_{A_1}(1+x+ip_2\sigma_1)(1+x+iEp_1\sigma_1)}{x\left\{\left(\frac{i\sigma_1}{\epsilon}+\frac{1}{p}\right)(1+x+ip_2\sigma_1)+Q_1\right\}}, \tag{25}$$

where

$$x = \frac{a^2}{\pi^2}, \quad p = \pi^2 p_l, \quad R_1 = \frac{g\alpha\beta d^4}{\nu\kappa\pi^4}, \quad S_1 = \frac{g\alpha'\beta' d^4}{\nu\kappa'\pi^4},$$

$$Q_1 = \frac{H^2 d^2}{4\pi\rho_0\nu\eta\epsilon\pi^2}, \quad T_{A_1} = \frac{4\Omega^2 d^4}{\nu^2\epsilon^2\pi^4} \quad \text{and} \quad i\sigma_1 = \frac{\sigma}{\pi^2}.$$

4. The stationary convection

For the stationary convection, $\sigma = 0$ and Eq. (25) reduces to

$$R_1 = \left(\frac{1+x}{x}\right)\left[\frac{1+x}{p}+Q_1\right] + S_1 + T_{A_1}\frac{p(1+x)^2}{x\{1+x+pQ_1\}}. \tag{26}$$

Equation (26) yields

$$\frac{dR_1}{dS_1} = +1, \tag{27}$$

$$\frac{dR_1}{dT_{A_1}} = \frac{p(1+x)^2}{x(1+x+pQ_1)}, \tag{28}$$

which imply that the stable solute gradient and the rotation have stabilizing effects on the thermosolutal convection in porous medium. Equation (26) also gives

$$\frac{dR_1}{dQ_1} = \frac{(1+x)}{x(1+x+pQ_1)^2}[(1+x+pQ_1)^2 - p^2T_{A_1}(1+x)] \tag{29}$$

and

$$\frac{dR_1}{dp} = -\frac{(1+x)^2}{xp^2(1+x+pQ_1)^2}\left[(1+x+pQ_1)^2 - p^2T_{A_1}(1+x)\right]. \tag{30}$$

It is clear from Eq. (29) that in the absence of rotation ($T_{A_1} = 0$)

$$\frac{dR_1}{dQ_1} = \frac{1+x}{x}, \tag{31}$$

which means that the magnetic field has stabilizing effect for non-rotating system. The magnetic field has still a stabilizing effect if

$$p^2T_{A_1}(1+x) < (1+x+pQ_1)^2. \tag{32}$$

However, the magnetic field has a destabilizing effect if

$$p^2 T_{A_1}(1+x) > (1+x+pQ_1)^2. \tag{33}$$

It is evident from Eq. (30) that in the absence of rotation ($T_{A_1} = 0$),

$$\frac{dR_1}{dp} = -\frac{(1+x)^2}{xp^2}, \tag{34}$$

which means that the medium permeability has still a destabilizing effect if

$$p^2 T_{A_1}(1+x) < (1+x+pQ_1)^2. \tag{35}$$

But if

$$p^2 T_{A_1}(1+x) > (1+x+pQ_1)^2, \tag{36}$$

the medium permeability has a stabilizing effect on thermosolutal convection in porous medium.

5. The oscillatory modes

Here we examine the possibility of oscillatory modes, if any, coming into play due to the presence of rotation, magnetic field on the thermosolutal convection in porous medium. Multiplying Eq. (18) by W^*, the complex conjugate of W, integrating over the range of z and making use of (19)–(23) together with the boundary conditions (24), we obtain

$$\begin{aligned}&\left(\frac{\sigma}{\epsilon}+\frac{1}{p_l}\right) I_1 + \frac{g\alpha'\kappa' a^2}{\nu\beta'}(I_4 + E'q\sigma^* I_5) + \frac{\epsilon\eta}{4\pi\rho_0\nu}(I_6 + p_2\sigma^* I_7)\\ &+ d^2\left(\frac{\sigma^*}{\epsilon}+\frac{1}{p_l}\right) I_8 + \frac{\epsilon\eta d^2}{4\pi\rho_0\nu}(I_9 + p_2\sigma I_{10}) = \frac{g\alpha\kappa a^2}{\nu\beta}(I_2 + Ep_1\sigma^* I_3),\end{aligned} \tag{37}$$

where

$$I_1 = \int_0^1 (|DW|^2 + a^2|W|^2)dz,$$

$$I_2 = \int_0^1 (|D\Theta|^2 + a^2|\Theta|^2)dz,$$

$$I_3 = \int_0^1 |\Theta|^2 dz,$$

$$I_4 = \int_0^1 (|D\Gamma|^2 + a^2|\Gamma|^2) dz,$$

$$I_5 = \int_0^1 |\Gamma|^2 dz,$$

$$I_6 = \int_0^1 (|D^2K|^2 + 2a^2|DK|^2 + a^4|K|^2) dz,$$

$$I_7 = \int_0^1 (|DK|^2 + a^2|K|^2) dz,$$

$$I_8 = \int_0^1 |Z|^2 dz,$$

$$I_9 = \int_0^1 (|DX|^2 + a^2|X|^2) dz,$$

$$I_{10} = \int_0^1 |X|^2 dz, \tag{38}$$

which are all positive definite. Substituting $\sigma = \sigma_r + i\sigma_i$ and then equating real and imaginary parts of Eq. (37), we obtain

$$\sigma_r \left[\frac{I_1}{\epsilon} + \frac{g\alpha'\kappa' a^2}{\nu\beta'} E' q I_5 + \frac{\epsilon\eta}{4\pi\rho_0\nu} p_2 I_7 + \frac{d^2}{\epsilon} I_8 + \frac{\epsilon\eta d^2}{4\pi\rho_0\nu} p_2 I_{10} - \frac{g\alpha\kappa a^2}{\nu\beta} E p_1 I_3 \right]$$
$$= -\left[\frac{I_1}{p_l} + \frac{g\alpha'\kappa' a^2}{\nu\beta'} I_4 + \frac{\epsilon\eta}{4\pi\rho_0\nu} I_6 + \frac{d^2}{p_l} I_8 + \frac{\epsilon\eta d^2}{4\pi\rho_0\nu} I_9 - \frac{g\alpha\kappa a^2}{\nu\beta} I_2 \right] \tag{39}$$

and

$$\sigma_i \left[\frac{I_1}{\epsilon} - \frac{g\alpha'\kappa' a^2}{\nu\beta'} E' q I_5 - \frac{\epsilon\eta}{4\pi\rho_0\nu} p_2 I_7 - \frac{d^2}{\epsilon} I_8 + \frac{\epsilon\eta d^2}{4\pi\rho_0\nu} p_2 I_{10} + \frac{g\alpha\kappa a^2}{\nu\beta} E p_1 I_3 \right] = 0. \tag{40}$$

Equation (39) simply tells us that σ_r may be positive or negative which means that there may be stability or instability in the presence of rotation and magnetic field on thermosolutal convection in porous medium.

Equation (40) means that the modes may be non-oscillatory or oscillatory. In the absence of stable solute gradient, rotation and magnetic field, Eq. (40) reduces to

$$\sigma_i \left[\frac{I_1}{\epsilon} + \frac{g\alpha\kappa a^2}{\nu\beta} E p_1 I_3 \right] = 0, \tag{41}$$

and so $\sigma_i = 0$ which means that oscillatory modes are not allowed and the principle of exchange of stabilities is satisfied for thermosolutal convection in porous medium in the absence of stable solute gradient, magnetic field and rotation. The presence of each brings oscillatory modes in the system which were non-existent in their absence.

References

1. S. Chandrasekhar, Hydrodynamic and Hydromagnetic Stability, Dover Publication, New York, 1981.
2. E. R. Lapwood, Proc. Camb. Phil. Soc., *44*, 508, 1948.
3. P. F. Linden, Geophys. Fluid Dynamics, *6*, 1, 1974.
4. J. A. M. McDonnel, Cosmic Dust, John Wiley & Sons, Toronto, 1978, p. 330.
5. T. G. L. Shirtcliffe, J. Geophys. Res., *69*, 5257, 1964.
6. E. A. Spiegel, Astrophys. J., *141*, 1068, 1965.
7. H. Stommel and K. N. Fedorov, Tellus, *19*, 306, 1967.
8. H. Tabor and R. Matz, Solar Energy, *9*, 177, 1965.
9. G. Veronis, J. Marine Res., *23*, 1, 1965.
10. R. A. Wooding, J. Fluid Mech., *9*, 183, 1960.

Acta Physica Hungarica 73 (1), pp. 67-73 (1993)

ANALYTICAL SOLUTIONS TO CLASSES OF TRIGONOMETRIC AND HYPERBOLIC POTENTIALS WITH THE JACOBI POLYNOMIALS

Z. YALÇIN,[1] M. SIMSEK and S. SIMSEK*

Department of Physics, Faculty of Arts and Sciences, Gazi University
06500 Ankara, Turkey
**Department of Physics, Faculty of Education, Gazi University*
06500 Ankara, Turkey

(Received 9 February 1993)

We have presented a new class of analytical solvable trigonometric and hyperbolic type potentials, related to the Jacobi Polynomials, using the previously unconsidered equations. It should be remarked that several quasi-exactly solvable potentials having restricted parameters have similar energy eigenvalue expressions.

1. Introduction

It is well known that the Schrödinger wave equation is only solvable for a limited number of potential energy functions. The supersymmetric WKB method (SWKB) is one of the useful techniques to calculate the exact energy spectra of the exactly solvable potentials. In fact, the general proof that the supersymmetric WKB method always yields exact energy spectrum for shape-invariant potentials is as valid for a spherically symmetric shape-invariant potential in the radial wave equation as it is for a shape-invariant potential in one dimension [1]. The supersymmetric approach involves a pair of one-dimensional supersymmetric partner potentials of the form $V_{\pm}(x) = W^2(x) \pm W'(x)$. In this formalism, if the ground state wavefunction is known, by using the logarithmic derivative of the wave function, one can formally treat supersymmetric potential $W(x)$, and then the partner potentials, $V_{\pm}(x)$, of the system [1].

Recently, Lévai [2,3] has suggested a simple method, based on the supersymmetric quantum mechanics and shape invariance, for generating exactly solvable problems of non-relativistic quantum mechanics. He applied the method to the Jacobi, generalized Laguerre and Hermite polynomials [2]. Then, by using this method, a number of new solvable potentials have been reported [2–6].

In this letter we want to apply the method to the new type trigonometric and hyperbolic potentials, which are related to the Jacobi Polynomials. It should also be remarked that some of our results are quasi-exact, because there are restrictions between the potential parameters. By quasi-exact in this work we mean non-exact or not all the spectra of the given potential.

[1]Permanent address: Department of Physics, Faculty of Arts and Sciences, Yüzüncü Yil University Van, Turkey

2. Lévai method

The single dimensional Schrödinger equation or radial Schrödinger equation was related to the hypergeometric equations, which involve orthogonal polynomials. The Schrödinger equation can be transformed into various linear homogeneous second-order differential equations. Any function $F(g(x))$ satisfies the second-order differential equation

$$\frac{d^2F(g)}{dx^2} + Q(g)\frac{dF(g)}{dg} + R(g)F(g) = 0. \tag{1}$$

In this case, once choosing $Q(g(x))$ and $R(g(x))$, Eq. (1) is reduced to a special case of hypergeometric equations [2].

The Schrödinger equation in one dimension

$$\frac{d^2\Psi(x)}{dx^2} + [E' - V'(x)]\Psi(x) = 0, \tag{2}$$

where $V'(x) = \frac{2\mu}{\hbar^2}V(x)$, and $E' = \frac{2\mu}{\hbar^2}E$. Lévai has determined the relations between the Schrödinger equation and the hypergeometric equation given in Eq. (1). He considered the solution of the Schrödinger equation as in the form

$$\Psi(x) = f(x)F(g(x)), \tag{3}$$

where $f(x)$ is given by

$$f(x) \simeq (g')^{-1/2} \exp\left[\int^g Q(g)dg\right] \tag{4}$$

and $E - V(x)$ is given like

$$E' - V'(x) = R(g(x))(g')^2 - (f''/f). \tag{5}$$

Substituting $f(x)$ in the Eq. (5), expressed explicitly in the form of Eq. (4), one can also easily construct $E - V(x)$ in terms of $g(x)$, $Q(g(x))$ and $R(g(x))$:

$$E' - V'(x) = \frac{g'''}{2g'} - \frac{3}{4}\left(\frac{g''}{g'}\right)^2 + (g')^2\left[R(g) - \frac{1}{2}\frac{dQ(g)}{dg} - \frac{1}{4}Q^2(g)\right], \tag{6}$$

where $g(x)$ is a function corresponding to the argument of the hypergeometric function. The purpose of this approach is to find the fraction of the right-hand side of Eq. (6) corresponding to the potential and energy. The form of $Q(g(x))$ and $R(g(x))$ is well defined for any solution $F(g(x))$ of a hypergeometric equation [7]. It was soon noticed that as applications of this method, a number of solvable potentials have been reported by using Jacobi polynomials. Lévai [2,3] used the 1.

type hypergeometric equation, its solutions are the Jacobi polynomials (Eq. 26.6.1. in [7]). Then, Williams [5] followed this approach by using the 3. type hypergeometric equation (Eq. 22.6.3. in [7]). More recently, we have studied the method as another application [6] by using Eq. (22.6.4) in [7], i.e., we considered the 4. type hypergeometric equation in [7].

Firstly, Lévai considered the differential equations

$$\frac{(g')^2}{(1-g^2)} = C, \quad \frac{(g')^2}{(1-g^2)^2} = C \quad \text{and} \quad \frac{(g')^2 g}{(1-g^2)^2} = C \tag{7}$$

to find $g(x)$. Then, Williams applied the method by considering the equations

$$\frac{(g')^2}{(1-g)^2} = C \quad \text{and} \quad \frac{(g')^2}{(1+g)^2} = C. \tag{8}$$

Thereafter, following these studies, we performed [6] equations

$$(g')^2 = C \quad \text{and} \quad \frac{(g')^2}{\cos^2(\frac{g}{2})} = C. \tag{9}$$

It should be noted that the first equation in the Eq. (9) was also considered by Lévai [2] before, but he studied the Laguerre polynomials to solve the 1. type hypergeometric equation for the Coulomb potential.

Moreover, Lévai classified the potentials (related to the Jacobi polynomials) as PI, PII and PIII types in the previous studies [2–4].

3. Trigonometric and hyperbolic type potentials

We will now reconsider Eq. 22.6.3 for $\alpha = \beta = 1$,

$$\frac{d^2F(g)}{dx^2} + \left[\frac{n(n+3)+2}{1-g^2}\right] F(g) = 0 \tag{10}$$

and Eq. 22.6.4 for $\alpha = \beta = 1/2$ in [7],

$$\frac{d^2F(g)}{dx^2} + (n+1)^2 F(g) = 0. \tag{11}$$

So, we have rewritten Eq. (6) taking into consideration Eqs (10–11) as

$$E' - V'(x) = \frac{g'''}{2g'} - \frac{3}{4}\left(\frac{g''}{g'}\right)^2 + (n(n+3)+2)\frac{(g')^2}{1-g^2} \tag{12}$$

and

$$E' - V'(x) = \frac{g'''}{2g'} - \frac{3}{4}\left(\frac{g''}{g'}\right)^2 + (n+1)^2(g')^2. \tag{13}$$

It is to be noted that Eqs (12) and (13) are the special case of Eq. (11) for $\alpha = \beta = 1$ in [4] and for $\alpha = \beta = 1/2$ Eq. (11) in [6], respectively. The corresponding wave functions in Jacobi polynomials

$$F(g) = (1-g)(1+g)P_n^{1,1}(g) \tag{14}$$

and

$$F(g) = \left(\sin(\frac{g}{2})\right)\left(\cos(\frac{g}{2})\right) P_n^{1/2,1/2}(\cos g) \tag{15}$$

which both satisfy Eq. (1) separately.

In order to have the potential and energy on the left-hand side of Eqs (12–13), we can get different kinds of $g(x)$ functions. Here we consider two types of differential equations to find $g(x)$

$$\frac{g'''}{2g'} = C_1 \tag{16}$$

and

$$\frac{g'''}{2g'} = C_2 + h(x), \tag{17}$$

where C_i are definite constants. Thus, there are many possibilities for $g(x)$ satisfying Eqs (16–17). For the moment, let us now go back to relations (12–13) to see what really happens if we take a specific $g(x)$ and then determine E_n, $V(x)$ and $\Psi(x)$. However, as can be seen from the Table, we choose eight different g to calculate the energy spectra of the potentials.

4. Conclusion

We have shown that the previously unconsidered Eqs (16–17) give a few practicable reparametrized potentials. As remarked in the Table PIII and PIV are not related to the classifications of Lévai, they indicate the potentials which are produced by Eq. (10) and Eq. (11), respectively. Table I includes a number of family of exactly and quasi-exactly solvable potentials corresponding to special values of the parameters involved in Jacobi polynomials. An interesting property of many of these potentials is that although the corresponding wave functions are expressed in different terms of the Jacobi polynomials, they give the same or similar energy eigenvalue expressions.

On the other hand, some energies are independent of at least one of the potential parameters. Also, there are restrictions between the potential parameters which are indicated in Table I. Despite these negative results, we may compare their energy spectra with the Coulomb problem (by choosing $\pm 2B^2 = Z_1 Z_2$ or $\frac{1}{2} Z_1 Z_2$). That is to say analytically solvable periodical and hyperbolic types of potentials have been suggested to the interested applied physicists.

Table I

Parametric potentials (related to the Jacobi polynomials $P_n^{\alpha\beta}(x)$) with their properties including energy eigenvalues and eigenfunctions ($\hbar = 2\mu = 1$). The range of trigonometric and hyperbolic type potentials are $0 < x < \pi a/2$ and $-\infty < x < \infty$, respectively

Diff. Eq.	$g(x)$	$V(x)$	E_n	$f(x)F(g(x))$
$\frac{g'''}{g'} = C_1$ (PIV)	$\cos(ax)$	$\frac{3}{4}a^2\cot^2(ax) - [B\sin(ax)]^2$ $B = (n+1)a$	$-\frac{1}{2}a^2$ or $\frac{-1}{2}[\frac{B}{n+1}]^2$	$(-a\sin(ax))^{\frac{-1}{2}}\cos(\frac{g}{2})\sin(\frac{g}{2})P_n^{\frac{1}{2}\frac{1}{2}}(\cos(g))$
(PIII)		$\frac{3}{4}a^2\cot^2(ax)$	$a^2[n(n+3)+3/2]$	$[-a\sin(ax)]^{\frac{-1}{2}}(1-g)(1+g)P_n^{1,1}(g)$
$\frac{g'''}{g'} = C_1$ (PIV)	$\cosh(ax)$	$\frac{3}{4}a^2\coth^2(ax) - [B\sinh(ax)]^2$ $B = (n+1)a$	$\frac{1}{2}a^2$ or $\frac{1}{2}[\frac{B}{n+1}]^2$	$(a\sinh(ax))^{\frac{-1}{2}}\cos(\frac{g}{2})\sin(\frac{g}{2})P_n^{\frac{1}{2}\frac{1}{2}}(\cos(g))$
(PIII)		$\frac{3}{4}a^2\coth^2(ax)$	$a^2[n(n+3)+5/2]$	$[a\sinh(ax)]^{\frac{-1}{2}}(1-g)(1+g)P_n^{1,1}(g)$
$\frac{g'''}{g'} = C_1$ (PIV)	$\sin(ax)$	$\frac{3}{4}a^2\tan^2(ax) - [B\cos(ax)]^2$ $B = (n+1)a$	$-\frac{1}{2}a^2$ or $\frac{-1}{2}[\frac{B}{n+1}]^2$	$(a\cos(ax))^{\frac{-1}{2}}\cos(\frac{g}{2})\sin(\frac{g}{2})P_n^{\frac{1}{2}\frac{1}{2}}(\cos(g))$
(PIII)		$\frac{3}{4}a^2\tan^2(ax)$	$a^2[n(n+3)+3/2]$	$[a\cos(ax)]^{\frac{-1}{2}}(1-g)(1+g)P_n^{1,1}(g)$
$\frac{g'''}{g'} = C_1$ (PIV)	$i\sinh(ax)$	$\frac{3}{4}a^2\tanh^2(ax) - [B\cosh(ax)]^2$ $B = (n+1)a$	$\frac{1}{2}a^2$ or $\frac{1}{2}[\frac{B}{n+1}]^2$	$(ia\cosh(ax))^{\frac{-1}{2}}\cos(\frac{g}{2})\sin(\frac{g}{2})P_n^{\frac{1}{2}\frac{1}{2}}(\cos(g))$
(PIII)		$\frac{3}{4}a^2\tanh^2(ax)$	$-a^2[n(n+3)+3/2]$	$[ia\cos(ax)]^{\frac{-1}{2}}(1-g)(1+g)P_n^{1,1}(g)$

Table I (continued)

Diff. Eq.	$g(x)$	$V(x)$	E_n	$f(x)F(g(x))$
$\frac{g'''}{g'} = C_1$	$\sinh(ax)$	$\frac{3}{4}a^2\tanh^2(ax) - [B\cosh(ax)]^2$	$\frac{1}{2}a^2$ or $\frac{1}{2}[\frac{B}{n+1}]^2$	$(a\cosh(ax))^{\frac{-1}{2}}\cos(\frac{g}{2})\sin(\frac{g}{2})P_n^{\frac{1}{2}\frac{1}{2}}(\cos(g))$
(PIV)		$B = (n+1)a$		
(PIII)		$\frac{3}{4}a^2\tanh^2(ax) - A\frac{1+\sinh^2(ax)}{1-\sinh^2(ax)}$	$\frac{A}{2[n(n+3)+3/2]}$	$[a\cos(ax)]^{\frac{-1}{2}}(1-g)(1+g)P_n^{1,1}(g)$
		$A = a^2[n(n+3)+2]$		
$\frac{g'''}{g'} = C_2 + h(x)$	$\tanh(ax)$	$-[B\,\mathrm{sech}^2(ax)]^2$	$-a^2$ or $-[\frac{B}{n+1}]^2$	$(a\,\mathrm{sech}^2(ax)^{\frac{-1}{2}}\cos(\frac{g}{2})\sin(\frac{g}{2})P_n^{\frac{1}{2}\frac{1}{2}}(\cos(g))$
(PIV)		$B = (n+1)a$		
(PIII)		$-A\,\mathrm{sech}^2(ax)$	$-\frac{A}{n(n+3)+2}$	$[a\,\mathrm{sech}^2(ax)]^{\frac{-1}{2}}(1-g)(1+g)P_n^{1,1}(g)$
		$A = a^2[n(n+3)+2]$		
$\frac{g'''}{g'} = C_2 + h(x)$	$\coth(ax)$	$-[B\,\mathrm{cosech}^2(ax)]^2$	$-a^2$ or $-[\frac{B}{n+1}]^2$	$(-a\,\mathrm{cosech}^2(ax))^{\frac{-1}{2}}\cos(\frac{g}{2})\sin(\frac{g}{2})P_n^{\frac{1}{2}\frac{1}{2}}(\cos(g))$
(PIV)		$B = (n+1)a$		
(PIII)		$-A\,\mathrm{cosech}^2(ax)$	$-\frac{A}{n(n+3)+2}$	$[-a\,\mathrm{cosech}^2(ax)]^{\frac{-1}{2}}(1-g)(1+g)P_n^{1,1}(g)$
		$A = a^2[n(n+3)+2]$		
$\frac{g'''}{g'} = C_2 + h(x)$	$-i\cot(ax)$	$[B\,\mathrm{cosec}^2(ax)]^2$	a^2 or $[\frac{B}{n+1}]^2$	$(ia\,\mathrm{cosec}^2(ax))^{\frac{-1}{2}}\cos(\frac{g}{2})\sin(\frac{g}{2})P_n^{\frac{1}{2}\frac{1}{2}}(\cos(g))$
(PIV)		$B = (n+1)a$		
(PIII)		$A\,\mathrm{cosec}^2(ax)$	$-\frac{A}{n(n+3)+2}$	$[ia\,\mathrm{cosec}^2(ax)]^{\frac{-1}{2}}(1-g)(1+g)P_n^{1,1}(g)$
		$A = a^2[n(n+3)+2]$		

References

1. E. Witten, Nucl. Phys., B, *185*, 513, 1981; F. Cooper and B. Freedman, Ann. Phys. NY, *146*, 262, 1983; J. W. Dabrowska, A. Khare and U. P. Sukhatme, J. Phys. A.: Math. Gen., *21*, L195, 1988; E. Kasap, B. Gonul and M. Simsek, Chem. Phys. Lett., *172*, 499, 1990; D. T. Barclay and C. J. Maxwell, Phys. Lett. A, *157*, 357, 1991 and references therein.
2. G. Lévai, J. Phys. A.: Math. Gen., *22*, 689, 1989.
3. G. Lévai, J. Phys. A.: Math. Gen., *24*, 131, 1991.
4. G. Lévai, J. Phys. A.: Math. Gen., *25*, L521, 1992.
5. B. W. Williams, J. Phys. A.: Math. Gen., *24*, L667, 1991.
6. M. Simsek and Z. Yalçin, Another class of solvable potentials related to the Jacobi Polynomials (submitted).
7. M. Abramowitz and I. A. Stegun, Handbook of Mathematical Functions, Dover, New York, 1970.

Acta Physica Hungarica 73 (1), pp. 75-85 (1993)

BEHAVIOUR OF CHARACTERISTIC WAVE FRONTS IN A SIMPLE DISSOCIATING GAS

T. NAGY

Department of Physics, Miskolc University
3515 Miskolc-Egyetemváros, Hungary

(Received 3 March 1993)

After surveying the main features of a simple dissociating gas, the propagation speed of characteristic wave fronts through such a medium is determined. Then the growth equations of the plane, cylindrical and spherical waves are obtained under the assumption that they penetrate into a uniform region at rest. It is discussed on what conditions a weak discontinuity damps out, forms a focus and terminates into a shock, respectively.

1. Introduction

Thomas [1], using the theory of singular surfaces proposed and developed by himself [2], has investigated the propagation of weak discontinuities in an ideal gas, which is uniform and at rest before the arrival of the wave front. He has derived the growth equation of the waves and shown that a discontinuity in the gradient of any field variable can become infinite in a finite time, i.e. a shock can arise. By the same method Kaul [3] has studied the propagation of weak waves in ideal gases considering the entropy and the sound speed as dependent variables instead of pressure and density.

Since the high-temperature real gas effects (vibrational excitation, dissociation, electronic excitation, ionization etc.) may affect significantly the behaviour of weak discontinuities, it has become necessary to include into the gasdynamic weak wave theory these effects. The behaviour of weak waves in dissociating gases has been studied by a number of authors. Shankar [4] has extended the analysis of Thomas to a Lighthill–Freeman type [5,6] ideal dissociating gas. This work was reconsidered by Shankar and Jain [7], who, following Elcrat [8], have studied the non-uniform propagation of weak discontinuities in an unsteady flow of a dissociating gas. Ram and Gaur [9] have obtained growth equations for weak waves propagating through a uniform region of a Lighthill–Clarke [5,10] dissociating gas. Rai and Gaur [11] have further generalized and developed this work and given a more satisfactory and detailed analysis of weak discontinuities in a dissociating gas. In these studies the assumption of Lighthill's ideal dissociating gas is used, i.e. to count just one-half of the total vibrational energy excited. Although in certain temperature range this assumption is quite reasonable, unfortunately for low dissociation the ideal dissociating gas model is unsuitable. Namely, in the fully molecular limit (as the degree of dissociation tends to zero at low temperatures) the Lighthill

gas becomes a perfect gas with constant specific heats, but with a ratio of specific heats $\gamma = 4/3$. This incorrect representation is an obvious result of the approximation to the vibrational energy. Hence it would be more realistic and valuable to treat the dissociating diatomic gas by a more accurate model.

In the present paper, using the method of characteristics, we discuss the propagation of plane, cylindrical and spherical weak waves into a static and uniform region of a simple dissociating gas [12]. In a simple dissociating gas the translational, rotational, and vibrational energies are assumed at equilibrium, vibrational energies being those pertaining to the simple harmonic oscillator model.

2. Basic equations

In this Section we survey the main features of such a dissociating gas which obeys the model proposed by Li [12] and for which the reaction rate equation introduced by Clarke [10] is valid. The gas under consideration is assumed to be a pure homonuclear diatomic gas such as oxygen and nitrogen. The temperature range is such that vibrational excitation and dissociation may occur but electronic excitation and ionization are negligible. (For oxygen and nitrogen this means temperatures up to 7000 K.) We note that at temperatures where the dissociation is important, the radiation heat loss from the gas may not be negligibly small. However, in order to simplify the problem, we exclude such an effect. The partially dissociated gas is assumed to consist of a mixture of atoms A and molecules A_2, which take part in the simple reversible reaction

$$A_2 + M \underset{k_r}{\overset{k_f}{\rightleftharpoons}} A + A + M.$$

Here the third body M can be either A_2 or A and k_f and k_r are the reaction rate coefficients for the forward and reverse reactions. k_f and k_r are traditionally assumed to be functions of temperature alone, further they have different values depending on whether M is a molecule or an atom. Following Clarke, we consider both species to be equally effective. It is assumed that each gas species is thermally perfect during the dissociation and the atomic and molecular partition functions (treating the molecule as a rigid rotator and simple harmonic oscillator) can be factorized. The local rotational temperature of the molecules and the translational temperature of both components are assumed to be identical and equal to the local static temperature of the gas.

With these assumptions, neglecting the molecular transport effects leading to viscosity, diffusion and heat conduction, the set of differential equations governing the one-dimensional unsteady flow of a dissociating gas can be written [5,10,12] in the form

$$\rho_t + u\rho_x + \rho u_x + \nu\frac{\rho u}{x} = 0, \tag{1}$$

$$\rho u_t + \rho u u_x + p_x = 0, \tag{2}$$

$$\rho h_t + \rho u h_x - p_t - u p_x = 0, \tag{3}$$

$$q_t + u q_x = W, \quad W = \frac{K(1-q) - q^2}{\tau}, \tag{4}$$

$$p = (1+q)RT\rho, \tag{5}$$

$$h = \left\{ \frac{7}{2} + \frac{3}{2}q + (1-q)e_v + \frac{T_d}{T}q \right\} RT, \quad e_v = \frac{T_v/T}{\exp(T_v/T) - 1}, \tag{6}$$

where p, ρ, T, h and u denote the gas pressure, density, temperature, specific enthalpy and velocity, respectively; R is the gas constant for A_2, q is the degree of dissociation, $\tau = \{4\rho^2 k_r(1+q)/m^2\}^{-1}$ is the forward-reaction time, m is the molecular weight of A_2, $K = (\rho_d/\rho)\exp(-T_d/T)$ is the equilibrium constant, $\rho_d = C(T/T_v)^{1/2}\{1 - \exp(-T_v/T)\}$ is the characteristic density of dissociation (C is a constant), T_d and T_v are the characteristic temperatures for dissociation and vibration; t is the time and x is the single spatial coordinate being either axial in flows with planar geometry or radial in cylindrically and spherically symmetric flows. The letter subscripts denote partial differentiation unless stated otherwise and the parameter ν takes the values 0, 1 and 2 for planar, cylindrical and spherical symmetry, respectively. The above equations describe a hypothetical gas which exhibits, during dissociation, the main features of a real dissociating gas such as oxygen or nitrogen. (For oxygen, $C = 265000$ kg/m^3, $T_v = 2230$ K and $T_d = 59000$ K. For nitrogen, $C = 214000$ kg/m^3, $T_v = 3340$ K and $T_d = 113000$ K.) Combining Eqs (1), (3), (4), (5) and (6) we get

$$p_t + u p_x + \rho a^2 \left(u_x + \nu \frac{u}{x} \right) + DWp = 0, \tag{7}$$

where

$$a = \left(\gamma \frac{p}{\rho} \right)^{1/2}$$

is the frozen sound speed,

$$\gamma = \frac{7 + 3q + 2(1-q)e_v^2 \exp(V)}{5 + q + 2(1-q)e_v^2 \exp(V)}$$

is the ratio of frozen specific heats ($V = T_v/T$) and

$$D = 2\frac{T_d/T - 2/(1+q) - e_v - (1-q)e_v^2 \exp(V)/(1+q)}{5 + q + 2(1-q)e_v^2 \exp(V)}.$$

Since $T_d/T > 8$, $0 < e_v < 1$ and $0 < e_v^2 \exp(V) < 1$, it follows at once that $D > 0$.

Using matrix notation, Eqs (1), (2), (4) and (7) can be written in the form

$$\mathbf{U}_t + \mathbf{A}\mathbf{U}_x + \mathbf{B} = 0, \tag{8}$$

in which $\mathbf{U}$ is a column vector with four components (ρ, u, q, p), $\mathbf{0}$ is a null vector and the matrices $\mathbf{A}$ and $\mathbf{B}$ can be read off by inspection of Eqs (1), (2), (4) and (7). This system is hyperbolic and may describe both propagation of wave and discontinuity in space-time. A function $\mathbf{U}(x,t)$ satisfying (8) everywhere except at a characteristic curve $\Sigma(t)$, where $\mathbf{U}$ is continuous, but $\mathbf{U}_t$ and $\mathbf{U}_x$ may suffer finite jumps, is said to be a weak wave or a weak discontinuity. Denoting the jump of $\mathbf{U}$ across Σ by $[\mathbf{U}]$, we have

$$\frac{\delta}{\delta t}[\mathbf{U}] = [\mathbf{U}_t] + \frac{d\Sigma}{dt}[\mathbf{U}_x], \tag{9}$$

where $\delta/\delta t$ denotes time derivative as observed from the wave front. Taking jump in (8), using (9) and applying the condition of continuity $[\mathbf{U}] = \mathbf{0}$, we obtain

$$\left(\mathbf{A} - \frac{d\Sigma}{dt}\mathbf{I}\right)[\mathbf{U}_x] = \mathbf{0}, \tag{10}$$

where $\mathbf{I}$ is the unit matrix. Consequently, if there occurs finite discontinuity in the derivatives $\mathbf{U}_x$ across Σ, the characteristic speed of propagation is an eigenvalue of $\mathbf{A}$. It follows immediately that there are four families of characteristic curves:

$$\frac{dx}{dt} = u \pm a, \quad \frac{dx}{dt} = u, \quad \frac{dx}{dt} = u. \tag{11}$$

Two of these characteristics represent waves propagating in the $\pm x$ direction with the frozen sound speed, the remaining two form a set of double characteristics representing the particle path.

3. Derivation of the growth equation

In studying a wave phenomenon governed by hyperbolic equations, it is usually more natural and convenient to use the characteristics of the governing system as the reference frame. Thus we introduce two characteristic variables α and β as follows:

(i) α is a wave tag so that α is constant along an outgoing characteristic $dx/dt = u + a$. If an outgoing wave is generated at time $\bar{t}$, it will be labelled by $\alpha = \bar{t}$.

(ii) β is a particle tag so that β is constant along a particle path $dx/dt = u$. If the characteristic wave front traverses a fluid particle at time t^*, its path will be labelled by $\beta = t^*$.

It is now clear that for each pair of values (α, β) there is a corresponding pair (x,t) so that $x = x(\alpha,\beta), t = t(\alpha,\beta)$. In view of this transformation, we get the following relations:

$$x_\alpha = u t_\alpha, \tag{12}$$

$$x_\beta = (u + a)t_\beta, \tag{13}$$

$$\mathbf{U}_t = \frac{\mathbf{U}_\beta x_\alpha - \mathbf{U}_\alpha x_\beta}{J}, \tag{14}$$

$$\mathbf{U}_x = \frac{\mathbf{U}_\alpha t_\beta - \mathbf{U}_\beta t_\alpha}{J}, \tag{15}$$

where

$$J = \frac{\partial(x,t)}{\partial(\alpha,\beta)} = -at_\alpha t_\beta. \tag{16}$$

The transformation from the space-time (x,t) plane to the plane of characteristic parameters (α,β) will be one to one if the Jacobian J does not vanish anywhere. Since doubling or overlapping of fluid particles is prohibited by physical considerations, $t_\beta \neq 0$. Consequently, $J = 0$ if and only if $t_\alpha = 0$, when two adjoining characteristics merge into a shock wave.

Transforming (8) into the characteristic coordinate system (α,β), we get

$$(a\rho_\alpha - \rho u_\alpha)t_\beta + \rho u_\beta t_\alpha + \nu\frac{\rho u a t_\alpha t_\beta}{x} = 0, \tag{17}$$

$$(\rho a u_\alpha - p_\alpha)t_\beta + p_\beta t_\alpha = 0, \tag{18}$$

$$q_\alpha - Wt_\alpha = 0, \tag{19}$$

$$(ap_\alpha - \rho a^2 u_\alpha)t_\beta + \rho a^2 u_\beta t_\alpha + \nu\frac{\rho a^2 u a t_\alpha t_\beta}{x} + DWpat_\alpha t_\beta = 0. \tag{20}$$

The combination of (18) and (20) yields

$$ap_\beta t_\alpha + \rho a^2 u_\beta t_\alpha + \nu\frac{\rho a^2 u a t_\alpha t_\beta}{x} + DWpat_\alpha t_\beta = 0. \tag{21}$$

Since the wave front is a characteristic surface, the primitive field variables are continuous across it. Thus the boundary conditions are

$$[\rho] = 0, \quad [u] = 0, \quad [q] = 0, \quad [p] = 0, \quad t = \beta \quad \text{at} \quad \alpha = 0. \tag{22}$$

The unperturbed flow ahead of the wave is assumed to be uniform and at rest, so the above conditions demand that

$$\rho_\beta = 0, \quad u_\beta = 0, \quad q_\beta = 0, \quad p_\beta = 0, \quad t_\beta = 1 \quad \text{at} \quad \alpha = 0. \tag{23}$$

The evaluation of Eqs (12)–(13) and (17)–(20) at the wave front yields

$$x_\alpha = 0, \quad x_\beta = a, \tag{24}$$

$$\rho_\alpha = \frac{\rho}{a}u_\alpha, \quad q_\alpha = 0, \quad p_\alpha = \rho a u_\alpha \tag{25}$$

at $\alpha = 0$.

To compute $\lambda = [u_x]$ at the wave front, which is the wave amplitude, we invoke (15), (16) and (23) which give

$$\lambda = -\frac{u_\alpha}{at_\alpha} \quad \text{at} \quad \alpha = 0. \tag{26}$$

Differentiating (13) and (21) with respect to α, (12) and the last equation of (25) with respect to β and using (22), (23), (25), we find that at the wave front $\alpha = 0$

$$u_{\alpha\beta} = -\left(\omega + \frac{\nu a}{2x}\right) u_\alpha, \tag{27}$$

$$t_{\alpha\beta} = -\frac{\psi}{a} u_\alpha, \tag{28}$$

where

$$\omega = \frac{Dq^2}{2\tau\gamma}\left\{(\gamma - 1)\left(\frac{1}{2} + \frac{T_d}{T} - e_v\right) - 1\right\}$$

and

$$\psi = \frac{\gamma + 1}{2} - \frac{4(1+q)^2(1-q)e_v^2 \exp(V)\{V + 2e_v \exp(V) - 2\}}{\{5 + q + 2(1-q)e_v^2 \exp(V)\}^2\{7 + 3q + 2(1-q)e_v^2 \exp(V)\}}.$$

Since $\gamma > 9/7$, $e_v^2 \exp(V)\{V + 2e_v \exp(V) - 2\} < 4$, it follows that $\omega > 0$ and $\psi > 0$.

Integrating (27) with respect to β on the line of constant $\alpha(= 0)$, we obtain

$$u_\alpha = u_{\alpha 0}(x/x_0)^{-\nu/2} \exp(-\omega t), \tag{29}$$

where $u_{\alpha 0}$ and x_0 are the values of u_α and x at $t = 0$, respectively. Making use of (29) in (28) and integrating with respect to β, we get

$$t_\alpha = t_{\alpha 0} - (\psi/a)u_{\alpha 0} \int_0^t (x/x_0)^{-\nu/2} \exp(-\omega \hat{t}) d\hat{t}, \tag{30}$$

where $t_{\alpha 0}$ is the value of t_α at $t = 0$. Using (29) and (30) in (26) and keeping in mind that $x = x_0 + at$, we finally obtain

$$\lambda(t) = \frac{\lambda_0 F(t)}{1 + \lambda_0 \psi I(t)}, \tag{31}$$

where

$$F(t) = (1 + at/x_0)^{-\nu/2} \exp(-\omega t), \quad I(t) = \int_0^t F(\hat{t}) d\hat{t}$$

and $\lambda_0 (\neq 0)$ is the value of $\lambda(t)$ at $t = 0$. When the initial amplitude is positive, we speak of an expansion wave, in the case of a negative initial value the wave is a compressive one. Equation (31) gives the variation of the wave amplitude with time. Further we study this result in detail to explore the possibilities of the shock formation.

5. Behaviour at the wave front

Plane waves ($\nu = 0$)

For a plane wave (31) reduces to

$$\lambda(t) = \frac{\lambda_0 \exp(-\omega t)}{1 + (\lambda_0/\lambda_c)\{1 - \exp(-\omega t)\}}, \tag{32}$$

where $\lambda_c = \omega/\psi$. It is apparent form (32) that if $\lambda_0 > 0$ (i.e. for an expansion wave front) $\lambda(t)$ is continuous and monotonically decreasing over $[0, \infty)$, and $\lambda \to 0$ as $t \to \infty$. This means that all expansion waves decay continuously and damp out ultimately. If $\lambda_0 < 0$ (compressive wave front), the behaviour of $\lambda(t)$ depends on the relative magnitudes of $|\lambda_0|$ and λ_c. Hence we call the quantity λ_c the critical initial amplitude.

(i) If $|\lambda_0| > \lambda_c$, there exists a finite critical time $t_c > 0$, given by

$$t_c = \frac{1}{\omega} \log \frac{1}{1 - \omega/|\lambda_0|}, \tag{33}$$

such that $\lambda(t)$ is continuous and finite on $[0, t_c)$, but $|\lambda| \to \infty$ as $t \to t_c$. Thus the weak discontinuity grows without bound and steepens into a shock wave after the finite time t_c.

(ii) If $|\lambda_0| < \lambda_c$, $|\lambda(t)|$ is finite, continuous, monotonically decreasing and tends to zero as $t \to \infty$, i.e. such a compressive wave decays and flattens out ultimately.

(iii) When $|\lambda_0| = \lambda_c$, the wave propagates with the initial discontinuity without any growth or decay.

These results differ from the well-known property of hydrodynamical flows that all compressive disturbances terminate into shocks. The dissociation has a stabilizing effect on the tendency of the wave surface to grow into a shock, in the sense that in certain cases it disallows the shock wave formation.

Diverging cylindrical waves ($\nu = 1$, $x_0 = R_0 > 0$)

If the diverging wave surface at $t = 0$ is a cylinder of radius R_0, at any later time it is a cylinder of radius $R = R_0 + at$. For this case the wave amplitude, the critical value of the initial discontinuity and the time taken for the shock formation are given by the following expressions:

$$\lambda(t) = \frac{\lambda_0 (1 + at/R_0)^{-1/2} \exp(-\omega t)}{1 + \frac{\lambda_0}{\lambda_c}\left\{1 - \frac{\operatorname{erfc}(\phi + \omega t)^{1/2}}{\operatorname{erfc}(\phi^{1/2})}\right\}}, \tag{34}$$

$$\lambda_c = \frac{\omega}{\psi} \frac{\exp(-\phi)}{\pi^{1/2}\phi^{1/2}\mathrm{erfc}(\phi^{1/2})}, \tag{35}$$

$$\mathrm{erfc}(\phi + \omega t_c)^{1/2} = (1 - \lambda_c/|\lambda_0|)\mathrm{erfc}(\phi^{1/2}), \tag{36}$$

where $\mathrm{erfc}(x) = (2/\sqrt{\pi}) \int_x^\infty \exp(-t^2)dt$ is the complementary error function, $\phi = \omega R_0/a$. The evolutionary behaviour of diverging cylindrical waves is quite similar to that of plane waves with the difference that for $|\lambda_0| = \lambda_c$ the amplitude of a compressive wave is not constant but it varies with t as

$$\lambda(t) = -\frac{\omega}{\psi} \frac{\exp(-\phi - \omega t)}{\pi^{1/2}(\phi + \omega t)^{1/2}\mathrm{erfc}(\phi + \omega t)^{1/2}}.$$

By applying L'Hospital's rule it turns out that in this case $|\lambda| \to \omega/\psi$ as $t \to \infty$, i.e. the wave takes a stable form ultimately. Since $\mathrm{erfc}(x) < \exp(-x^2)/(x\pi^{1/2})$, λ_c is greater for a diverging cylindrical wave than for a plane one. In other words, the geometrical spreading helps to attenuate the wave amplitude. It is easy to verify that

$$\frac{\partial \lambda_c}{\partial R_0} < 0, \quad \frac{\partial t_c}{\partial R_0} < 0,$$

which imply that the initial curvature has a stabilizing influence.

Converging cylindrical waves ($\nu = 1$, $x_0 = -R_0 < 0$)

If at $t = 0$ the converging wave front is a cylinder of radius R_0, then at a later time $t \leq t^* = R_0/a$ it is a cylinder of radius $R = R_0 - at$. (At t^* the curvature of the wave surface becomes infinite, which indicates the formation of a focus.) For such a wave

$$\lambda(t) = \frac{\lambda_0(1 - at/R_0)^{-1/2}\exp(-\omega t)}{1 + \frac{\lambda_0}{\lambda_c^*}\left\{1 - \exp(-\omega t)\frac{\mathrm{daw}(\phi - \omega t)^{1/2}}{\mathrm{daw}(\phi^{1/2})}\right\}}, \tag{37}$$

$$\lambda_c^* = \frac{\omega}{\psi} \frac{1}{2\phi^{1/2}\mathrm{daw}(\phi^{1/2})}, \tag{38}$$

where $\mathrm{daw}(x) = \int_0^x \exp(t^2 - x^2)dt$ is Dawson's integral. If $\lambda_0 > 0$, $\lambda(t)$ is positive, finite and continuous on $[0, t^*)$, further $\lambda \to \infty$ as $t \to t^*$. The numerator of (37) becomes unbounded at t^*, whereas the denominator remains positive and finite. Therefore we conclude that all expansion waves form a focus at a finite time t^*. When $\lambda_0 < 0$, there are again three possibilities as in the case of diverging compressive waves.

(i) If $|\lambda_0| > \lambda_c^*$, there exists a finite critical time $t_c^* < t^*$ defined by the equation

$$\exp(-\omega t_c^*)\mathrm{daw}(\phi - \omega t_c^*)^{1/2} = (1 - \lambda_c^*/|\lambda_0|)\mathrm{daw}(\phi^{1/2}) \tag{39}$$

such that $\lambda(t)$ is finite and continuous over $[0, t_c^*)$, and $|\lambda| \to \infty$ as $t \to t_c^*$. Thus in this case a shock forms before a focus can.

(ii) If $|\lambda_0| < \lambda_c^*$, the denominator in (37) converges to a finite negative limit, whereas the numerator tends to infinity as $t \to t^*$. So $\lambda(t)$ is finite and continuous over $[0, t^*)$, and $|\lambda| \to \infty$ as $t \to t^*$. This situation corresponds to the formation of a focus within a finite time t^*.

(iii) If $|\lambda_0| = \lambda_c^*$, the numerator of $\lambda(t)$ tends to infinity and the denominator approaches to zero as $t \to t^*$. Hence $\lambda(t)$ is finite and continuous over $[0, t^*)$ and $|\lambda| \to \infty$ as $t \to t^*$. This case corresponds to the simultaneous formation of a shock due to steepening and a focus due to curvature effects.

The function $x\,\mathrm{daw}(x)$ is zero at $x = 0$, in the beginning it grows (at $x_1 \approx 0.924$ it is equal to $1/2$), presents a maximum at $x_2 \approx 1.502$ and then declines slowly, approaching to $1/2$ asymptotically. Therefore λ_c^* is less than, equal to, or greater than λ_c for a plane wave according as $\phi^{1/2}$ is greater than, equal to, or less than x_1. It can be proved that

$$\frac{\partial t_c^*}{\partial R_0} > 0, \quad \frac{\partial \lambda_c^*}{\partial R_0} \lessgtr 0 \quad \text{when} \quad \phi^{1/2} \lessgtr x_2.$$

We see that, in contrast to the diverging waves, the shock formation time decreases with increasing curvature. λ_c^* depends on R_0 in an interesting way.

Diverging spherical waves ($\nu = 2,\ x_0 = R_0$)

If the diverging wave front at $t = 0$ is a sphere of radius R_0, at any later time it is a sphere of radius $R = R_0 + at$. For this case the wave amplitude, the critical value of the initial discontinuity and the time taken for the shock formation are given by the following expressions:

$$\lambda(t) = \frac{\lambda_0(1 + at/R_0)^{-1} \exp(-\omega t)}{1 + \frac{\lambda_0}{\lambda_c}\left\{1 - \frac{\mathrm{E}_1(\phi+\omega t)}{\mathrm{E}_1(\phi)}\right\}}, \tag{40}$$

$$\lambda_c = \frac{\omega}{\psi} \frac{\exp(-\phi)}{\phi \mathrm{E}_1(\phi)}, \tag{41}$$

$$\mathrm{E}_1(\phi + \omega t_c) = (1 - \lambda_c/|\lambda_0|\mathrm{E}_1(\phi), \tag{42}$$

where $\mathrm{E}_1(x) = \int_x^\infty t^{-1} \exp(-t) dt$ is the first Schlömilch function. The evolutionary behaviour of diverging spherical waves is quite similar to that of diverging cylindrical waves with the remark that for $|\lambda_0| = \lambda_c$ the amplitude of a compressive wave is of the form

$$\lambda(t) = -\frac{\omega}{\psi} \frac{\exp(-\phi - \omega t)}{(\phi + \omega t)\mathrm{E}_1(\phi + \omega t)}.$$

By applying L'Hospital's rule it turns out that in this case $|\lambda| \to \omega/\psi$ as $t \to \infty$, quite like to the diverging cylindrical waves. From the inequality $\mathrm{E}_1 < \exp(-x)/x$,

it follows that λ_c is greater for a diverging spherical wave than for a plane one. It is a simple matter to show that

$$\frac{\partial \lambda_c}{\partial R_0} < 0, \quad \frac{\partial t_c}{\partial R_0} < 0,$$

just like for diverging cylindrical waves.

Converging spherical waves ($\nu = 2$, $x_0 = -R_0 < 0$)

If at $t = 0$ the converging wave front is a sphere of radius R_0, then at a later time $t \leq t^* = R_0/a$ it is a sphere of radius $R = R_0 - at$. (Obviously, at t^* a focus forms.) For such a wave (31) assumes the form

$$\lambda(t) = \frac{\lambda_0 (1 - at/R_0)^{-1} \exp(-\omega t)}{1 + \frac{\lambda_0}{\Lambda} \left\{ 1 - \frac{\mathrm{Ei}(\phi - \omega t)}{\mathrm{Ei}(\phi)} \right\}}, \tag{43}$$

where

$$\Lambda = \frac{\omega}{\psi} \frac{\exp(\phi)}{\phi \mathrm{Ei}(\phi)},$$

and $\mathrm{Ei}(x) = \int_{-\infty}^{x} t^{-1} \exp(t) dt$ is the exponential integral function.

Since $\mathrm{Ei}(x) \to -\infty$ as $x \to 0$, for $\lambda_0 > 0$ both the numerator and the denominator of (43) become unbounded at t^*. Applying L'Hospital's rule, we get $\lambda(t) \to \infty$ as $t \to t^*$, which means that all expansive waves form a focus at t^*. If $\lambda_0 < 0$, then there exists a finite time $t_c^* < t^*$ given by

$$\mathrm{Ei}(\phi - \omega t_c^*) = (1 - \Lambda/|\lambda_0|)\mathrm{Ei}(\phi), \tag{44}$$

such that $\lambda(t)$ is continuous and finite on $[0, t_c^*)$, but $|\lambda| \to \infty$ as $t \to t_c^*$, because the denominator of (43) vanishes whereas the numerator remains finite. This means that all spherically converging compressive waves, no matter how weak initially, steepen up into shock waves before the formation of the focus. This is in contrast to the corresponding case of converging cylindrical waves. It can be shown that

$$\frac{\partial t_c^*}{\partial R_0} > 0,$$

like the converging cylindrical waves.

Acknowledgement

This work was supported by the Hungarian Scientific Research Fund under Contract No. OTKA-2350.

References

1. T. Y. Thomas, J. Math. Mech., *6*, 455, 1957.
2. T. Y. Thomas, J. Math. Mech., *6*, 311, 1957.
3. C. N. Kaul, J. Math. Mech., *10*, 393, 1961.
4. R. Shankar, Int. J. Eng. Sci., *9*, 1157, 1971.
5. M. J. Lighthill, J. Fluid Mech., *2*, 1, 1957.
6. N. C. Freeman, J. Fluid Mech., *4*, 407, 1958.
7. R. Shankar and S. K. Jain, Acta Phys. Hung., *45*, 113, 1978.
8. A. R. Elcrat, Int. J. Eng. Sci., *15*, 29, 1977.
9. R. Ram and M. Gaur, Acta Phys. Hung., *40*, 85, 1976.
10. J. F. Clarke, J. Fluid Mech., *7*, 577, 1960.
11. A. Rai and M. Gaur, Can. J. Phys., *66*, 334, 1988.
12. T. Y. Li, ARS J., *31*, 170, 1961.

Acta Physica Hungarica 73 (1), pp. 87-93 (1993)

THE CORIOLIS FORCE EFFECT ON THE LEVEL STRUCTURE OF ODD-MASS Re ISOTOPES

S. U. EL-KAMEESY

Physics Department, Faculty of Science, Ain Shams University
Cairo, Egypt

(Received in revised form 9 March 1993)

A study of the Coriolis force effect on the last odd particle in odd-Re isotopes is undertaken based on the cranking model and Nilsson model including pairing force. Accordingly, the level structure of the ground state bands of odd-mass Re isotopes is discussed and satisfactory results are obtained by that model as compared with the experimental results. Furthermore, determination of the deformation parameter δ of each nucleus is undertaken by different methods and it is found that δ decreases substantially with the addition of each neutron pair.

1. Introduction

The experimental investigation of transitional nuclei, where the nuclear shape changes considerably with nucleon number, remains a fertile testing ground as theoretical nuclear models become more refined. One of such series of nuclei is the odd-proton $^{181-187}$Re isotopes. It is of interest to map the systematic changes in energy level structure with deformation in these nuclei. The level schemes of odd-Re isotopes have been investigated using a variety of experimental techniques [1–6]. The results of these experiments have been interpreted successfully for the most part in terms of the Nilsson model [7], although there remain some aspects of the level structure that need explanation. Perhaps one of the most striking anomalies in this region is the Coriolis force effect on the last odd particle. This effect was studied previously by many authors [8,9] and they have shown that the systematic largeness of the moment of inertia of odd-A nuclei as compared with those of the ground state bands of neighbouring even nuclei is due to that effect. The correction to the moment of inertia from the last odd particle comes from the second order of the Coriolis force. Numerical calculations of this effect were performed previously [10] and generally satisfactory results were obtained for most of odd-A nuclei. But there are still discrepancies between experimental and theoretical calculations in the region of odd-Re isotopes. Accordingly, it was thought worthwhile to reinvestigate the odd-Re isotopes to extend our knowledge of their level structure via the study of the Coriolis force effect.

2. The Coriolis force and Coriolis force anti-pairing (CAP) effects on the last odd particle

In most of the treatments concerning the CAP effect the quasi-particle method has been employed [11–13]. The essential approximation in this method is to replace the pairing interaction in the original Hamiltonian by a pairing potential, whose strength is given by the gap parameter, Δ_C ($\tau = p$ for proton and $\tau = n$ for neutron). The CAP effect is described in terms of the decrease of this gap parameter with increasing frequency of the rotation, Ω, or equivalently, the total angular momentum of the system, I.

Taking into account only the lowest order effects of the Coriolis force the total energy in the laboratory system can be written as

$$E_0(\Omega) = E_0'(\Omega) + \Omega\langle\hat{J}_x\rangle, \tag{1}$$

where $E_0'(\Omega)$ is the corresponding total energy in the rotating system and is given by

$$E_0'(\Omega) = E_0(\Delta_\tau) - \frac{1}{2}\Omega^2\psi_0, \tag{2a}$$

$$E_0(\Delta_\tau) = 2\sum_i(\epsilon_i - \lambda)\nu_1^2 - \sum_\tau \Delta_\tau 2u_i\nu_i + \sum_\tau \frac{\Delta_\tau^2}{G_\tau}, \tag{2b}$$

$$\langle\hat{J}_x\rangle = \Omega\psi_0 = \sqrt{I(I+1)}. \tag{2c}$$

The first and the second terms in Eq. (2b) describe the single particle and the pairing energy, respectively. The symbols u_i and ν_i are the usual occupation parameters [10], i.e.

$$u_i^2 = \frac{1}{2}\left(1 + \frac{\epsilon_i - \lambda}{E_i}\right), \tag{3a}$$

$$\nu_i^2 = \frac{1}{2}\left(1 - \frac{\epsilon_i - \lambda}{E_i}\right), \tag{3b}$$

where $E_i = \sqrt{(\epsilon_i - \lambda)^2 + \Delta^2}$. Also, G_τ in the third term is the strength parameter of the original pairing force. Also, ψ_0 is the moment of inertia and is given by the well-known formula

$$\psi_0 = 2\sum_{i,j}\frac{J_{ij}^2}{E_i + E_j}(u_i\nu_j - u_j\nu_i)^2, \tag{4}$$

where J_{ij} is the matrix element of the single-particle angular momentum $\hat{J}_x$,

$$J_{ij} = \langle i|\hat{J}_x|j\rangle. \tag{5}$$

Inserting Eq. (2a) into (1) and replacing Ω by I with the help of Eq. (2c), the total energy $E_0(\Omega)$ is expressed as a function of the angular momentum,

$$E_0(I) = E_0(\Delta_\tau) + \frac{1}{2\psi_0(\Delta_\tau)}I(I+1). \tag{6}$$

Following the minimization condition:

$$\frac{\partial E_0(I)}{\partial \Delta_\tau} = 0, \tag{7}$$

which leads to the gap equation [12]

$$\frac{2}{G_\tau} = \sum_i \frac{1}{E_i(\Delta_\tau)} + \frac{I(I+1)}{\psi_0^2(\Delta_\tau)} \frac{\partial \psi_0(\Delta_\tau)}{\partial \Delta_\tau}. \tag{8}$$

Using this equation and solving Δ_τ up to the lowest order in $I(I+1)$, one obtains

$$\Delta_\tau = \Delta_\tau^{(0)} + \frac{1}{2C_\tau \psi_0^2(\delta_\tau^{(0)})} \left[\frac{\partial \psi_0}{\partial \Delta_\tau}\right] I(I+1), \tag{9a}$$

$$C_\tau = \sum_i \frac{(\Delta_\tau^{(0)})^2}{E_i^3}. \tag{9b}$$

where $\Delta_\tau^{(0)}$ is the energy gap for $I = 0$.

Inserting Eq. (9a) into (6), one finally obtains up to the second order in $I(I+1)$,

$$E_0(I) = E_0(\Delta_\tau^{(0)}) + \frac{1}{2\psi_0(\Delta_\tau^{(0)})} I(I+1) + B_\Delta I^2(I+1)^2, \tag{10}$$

where the B-parameter is expressed as

$$B_\Delta = \sum_\tau (-1) \frac{1}{8\psi_0^4(\Delta_\tau^{(0)})} \frac{1}{C_\tau} \left(\frac{\partial \psi_0}{\partial \Delta_\tau}\right)^2. \tag{11}$$

The contribution to the energy from the last odd particle is just the quasiparticle energy, $\zeta_i(\Omega)$. Thus, the total energy of a band associated with a quasiparticle state i is given by

$$E_i(\Omega) = E_0(\Omega) + \zeta_i(\Omega). \tag{12}$$

In order to estimate the contribution to the B-parameter from the last odd particle, it is sufficient to retain terms only up to the third or fourth order in J_i and ζ_i, respectively. Proceeding further and according to the treatment given in [10], one can easily obtain

$$E_i(I, K_i) = E_0(\Delta_\tau^{(0)}) + E_i(\Delta_\tau^{(0)}) + \frac{1}{2\psi_i(\Delta_\tau^{(0)})} [I(I+1) - K_i^2] + B[I(I+1) - K_i^2]^2. \tag{13}$$

K_i is the projection of the angular momentum I in the symmetry axis and ψ_i is the total moment of inertia, including the contributions from both the even core and the last odd particle,

$$\psi_i = \psi_0 + \delta\psi_i,$$

Table I
The mean deformation parameters for odd-mass Re isotopes

Isotope	δ (nuclear orientation)	δ (Coulomb excitation)	δ (theoretical)
^{181}Re	–	0.19	0.212
^{183}Re	0.2075(8)	0.19	0.2116
^{185}Re	0.194(3)	0.19	0.1973
^{187}Re	0.181(4)	0.19	0.1838

where the correction to the moment of inertia is: $\delta\psi_i = -2\zeta_i^{(2)}$.

The centrifugal B-parameter is given as a sum of the contributions representing the CAP and Coriolis force effect on the last odd particle,

$$B = B_\Delta + B_C, \tag{14a}$$

$$B_\Delta = \sum_\tau \frac{(-1)}{8C_\tau \psi_i^4} \left(\frac{\partial \psi_i}{\partial \Delta_\tau}\right)^2, \tag{14b}$$

$$B = \frac{1}{\psi_i^4}\zeta_i^{(4)}. \tag{14c}$$

3. Method of calculation

According to the treatment given before, calculations of the B-parameter for one-quasiparticle bands of odd-Re isotopes were undertaken.

By fitting the calculated energy gap to even-odd mass differences, the values for $G_p = \frac{24}{A}$ and $G_n = \frac{18}{A}$ have been suggested [14].

The deformation parameter δ is taken from the information obtained from the nuclear orientation technique [6]. In the frame of the rotational model the spectroscopic quadrupole moment Q is connected with the intrinsic quadrupole moment Q_0 via the Bohr–Mottelson relation

$$Q = Q_0 \frac{3K^2 - J(J+1)}{(J+1)(2J+3)}. \tag{15}$$

Thus the configuration $J^\pi K$ has to be known for the determination of Q_0 from the measured Q. Accordingly the ground state deformation δ for the odd-A Re isotopes is estimated and tabulated in Table I.

Further calculations of the deformation parameter were undertaken both from Coulomb excitation experimental data and theoretical consideration [15] and the results obtained are given in Table I. However, a readjustment of the parameter δ was undertaken within the obtained results so as to reproduce the observed level order and the moment of inertia as well as possible. Also, from Table I it is seen that the mean deformation parameter of odd-A Re isotope decreases by the increasing mass number A.

4. Results and discussion

Numerical calculations of the A- and B-parameter for one-quasiparticle ground state bands of odd-A Re nuclei were undertaken following the prescription given above. The (obtained) results are presented in Table II.

The experimental values of the A- and B-parameters were determined by applying the rotational formula

$$E(I,K) = E_K + AI(I+1) + BI^2(I+1)^2 + (-1)^{I+1}\frac{(I+K)!}{(I-K)!}(A_1 + B_1 I(I+1) + \ldots). \tag{16}$$

E_K is the band head energy, A_1 and B_1 are parameters representing higher order terms arising from the Coriolis interaction and depending on K which is the projection of the angular momentum. The results obtained for A- and B-parameters are included in Table II.

Table II
Experimental and calculated A- and B-parameters

Isotope	A_{exp}	B_{exp}	A	B	B_Δ	B_c
^{181}Re	17.1	−0.020	14.1	−0.022	−0.0244	0.0024
^{183}Re	16.46	−0.022	15.6	−0.0240	−0.0263	0.0023
^{185}Re	18.2	−0.027	19.5	−0.030	−0.0332	0.0032
^{187}Re	19.9	−0.028	21.0	−0.026	−0.031	0.0050

From these data one can clearly see a characteristic orbital dependence of the B-parameter similar to that known for the A-parameter. Actually, the parameters A and B are correlated. Furthermore, our calculated results are in agreement with those obtained from experiments. In our study, the contribution from B_Δ is found to be larger than that from B_c and accordingly the B-parameter remains negative like those of the ground state bands of even–even nuclei.

The CAP effect could be obtained by means of the derivative of the moment of inertia with respect to the energy gap [10].

The strength of Coriolis coupling could be viewed by drawing a relation; $\frac{E_I - E_{I-1}}{2I}$ vs $(2I)^2$ as shown in Fig. 1. From this Figure it is obvious that clear oscillations are obtained in the case of ^{187}Re ground state band which supports the large calculated value of B_c compared to those of the rest of Re-isotopes.

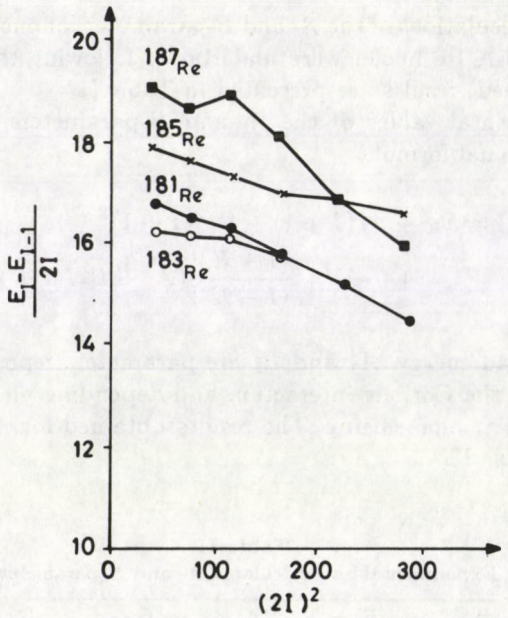

Fig. 1. Coupling effects in the odd-mass Re isotopes yrast bands

5. Conclusions

The rotational parameters A and B of the ground state bands of odd-A isotopes were evaluated by means of the cranking model and the Nilsson model. The results of our calculations agree quite well with A and B-parameters derived from experimental data. The positiveness of B-parameters in most bands of odd-A nuclei is not found in our study concerning odd-A Re isotopes. This may arise from the large negative value of the CAP force effect on the last odd particle which is positive.

The oscillations obtained in Fig. 1 in the case of ^{187}Re show that the Coriolis coupling is strong compared with those of ^{181,183,185}Re isotopes.

References

1. A. N. Herman, E. A. Heighway and J. D. MacArther, Can. J. Phys., *48*, 1040, 1970.
2. V. Barbec, L. Maly and M. Vebecky, Izv. Akad. Nauk. SSSR, Ser. Fiz., *35*, 1562, 1971.
3. M. T. Lu and W. P. Alford, Phys. Rev., *C3*, 1243, 1971.
4. J. K. Tuli, Nucl. Data Sheets, 36, 45, 1982; C. M. Lederer and V. S. Shirley, Table of Isotopes, 7th ed. 1978.

5. D. S. Brenner and R. A. Meyer, Phys. Rev., *C13*, 3, 1288, 1976.
6. H. Ernst, E. Hagn and E. Zech, Phys. Rev., *C23*, 4, 1739, 1981.
7. K. S. Krane and W. A. Steyert, Phys. Rev., *C7*, 1555, 1973.
8. A. Bohr and B. R. Mottelson, Nuclear Structure, W. A. Benjamin, New York, 1975.
9. B. R. Mottelson and S. G. Nilsson, Mat. Fys. Skr. Dan Vid. Selsk., *1*, 8, 1959.
10. Ikuko Hamamoto and Takeshi Udgawa, Nucl. Phys., *A126*, 241, 1969.
11. E. U. Marshalek, Phys. Rev., *139*, B770, 1965; Phys. Rev., *158*, 993, 1967.
12. K. Y. Chan and J. G. Valatin, Nucl. Phys., *82*, 222, 1966.
13. D. R. Bes, S. Landowne and M. A. J. Mariscotti, Phys. Rev., *166*, 1045, 1968.
14. S. G. Nilsson and O. Prior, Mat. Fis. Medd. Dan. Vid. Selsk., *32*, 16, 1961.
15. C. Ekstrom, H. Rubinstein and P. Moller, Phys. Ser., *14*, 199, 1976.

Acta Physica Hungarica 73 (1), pp. 95–117 (1993)

SURVEY ARTICLE

STATISTICAL STUDIES OF LEVEL CORRELATIONS AND CHAOTIC PHENOMENA IN SPECTROSCOPY

L. NEMES

Research Laboratory for Inorganic Chemistry
Hungarian Academy of Sciences
1502 Budapest, Hungary

(Received 2 April 1993)

This review covers some modern applications of statistical methods in the analysis of complicated molecular spectra, obtained usually with laser excitation. Among the available fluctuation measures, special emphasis is given to the nearest neighbour separation and spectral rigidity measures, and attention is called to the power spectrum (or statistical Fourier-transform) method.

From the high-resolution spectroscopic techniques used to obtain spectra of highly vibrationally excited molecules, the stimulated emission pumping (SEP) scheme is very successful in simplifying the high excitation regions. Examples of SEP applications are given, especially to acetylene, in greater details. Finally the role of molecular rotation in molecular dynamical and statistical studies is stressed.

1. Introduction

In recent years there is an increased interest in the interpretation of complex molecular spectra obtained usually with laser excitation. With high energy excitation it is possible to reach large values of vibrational quantum numbers. Traditional spectroscopy deals with spectra wherein each transition can be assigned to valid quantum numbers and thus can be analyzed in a conventional fashion. With the coming of lasers and their applications in laser-induced processes it became evident that the common methods of spectroscopic analysis are not always easily applicable at high vibrational excitation where the energy level density is extremely large. On the other hand, e.g. chemical applications of lasers demand an understanding of this energy region.

In this review we shall cover some relatively recent techniques that allow us to gain at least a partial explanation of complex spectra. Such studies inevitably lead to basic questions concerning regularity in molecular spectra and involve problems about ergodic or chaotic behaviour in quantum systems. We shall shortly summarize recent views on quantum ergodicity in molecular spectra. The relevance to laser-excited molecular processes shall occasionally be emphasized as it is this aspect that provides the most important impetus for such studies.

2. A short historical overview

As we shall see the analytical approach to high energy density regions is mostly statistical in nature. It is through a statistical study of energy level systems or even actual spectral features from which we hope to extract information on regularity and dynamical behaviour. Such studies were pioneered by Wigner in nuclear physics [118,119,120,121] who proposed a form for the distribution of first neighbour spacings in highly excited nuclear spectra.

This statistical approach is closely linked to the theory of random matrices (Bohigas and Giannoni [17], Brody et al [20], Carmeli [23], Mehta [84], Porter [102] because — as Wigner pointed out — the statistical properties of spectra of complicated Hamiltonians are similar to those of random Hamiltonians. The applications of random matrix statistics to atomic spectra have emerged in the last twenty years (Camarda and Georgopulos [22], Rosenzweig and Porter [107]) with a rapid expansion to molecular spectroscopy (for NO_2: Haller, Koppel and Cederbaum [56,57], Hardwick [59], Lehmann and Coy [75,76], Smalley et al [108], Zimmerman, Koppel and Cederbaum [117] — for acetylene: Abramson et al [1,2,3], Engel and Levine [37], Farantos [39], Holme and Levine [63,64,65], McIlroy and Nesbitt [86], Pique et al [94,95,97], Sumpter and Thompson [109], Sundberg et al [110], — for Ar_3: Leitner, Berry and Whitnell [77] — for formaldehyde: Miller et al [87], Polik et al [99,100].

Following the simple applications of first neighbour spacing statistics, more advanced statistical tools have been worked out. Thus the spectral rigidity measure (Δ_3) was introduced by Dyson and Mehta [32], and Bohigas and Giannoni [16] to test long-range correlations among levels, the so-called F-statistics (Dyson [33]) to find levels in sequences to be eliminated from the analysis, and several other correlation and fluctuation measures (Brody et al [20]).

For modern polyatomic applications not only the various spacing distributions and the Δ_3-statistics became widely used, but additional fluctuation measures have been developed for spectral line strength (Alhassid, Levine [4], Brickman, Engel and Levine [19], Coy, Hernandez and Lehmann [27], Heller, Sundberg [61], Kommandeur et al [73], Porter, Thomas [101]), and for fluorescent lifetimes (Engel et al [35]). In this review we shall deal only with energy level statistics, occasionally mentioning spectral line strength distributions.

An additional technique for testing long-range order or correlatedness in optical spectra is the statistical Fourier-transform of energy level sequences or experimental frequency spectra (Jost, Lombardi [69]), Leviandier, Lombardi, Jost, Pique [78], Levine, Kinsey [79], Lombardi, Labastie, Bordas, Broyer [81], Lorquet, Engel, Levine [82], Pique, Joyeux, Manners, Sitja [98], Remacle, Levine [106]). This method provides information on the time-scale of various processes leading to the experimental spectra. Ergodic behaviour in spectra may also be quantified by the fractal dimension of the trajectories in phase space (Grassberger and Procaccia [47]), and by Kolmogorov entropy (Pesin [93]). Excellent examples for this approach are in the recent literature (Beck, Leitner, Berry [9], Berry [14]).

3. Regularity, ergodicity and chaos in spectroscopy

One of the interesting questions of contemporary physics is whether chaotic phenomena in classical dynamics appear in some form in the quantum mechanical description. The literature on this subject is very extensive (e.g., Berry [10,11,12,13], Casati et al [24], Heller [62], Tabor [112]).

It is characteristic of classically chaotic dynamics that it grows from the non-linearity in the governing system of dynamical equations. Chaos means the irregular and unpredictable evolution of a non-linear system in time. Quantum systems are not chaotic in the way classical systems are. The Schroedinger equation that is the basis of the wave mechanical description is a linear equation in the sense that if two different wavefunctions satisfy it then also does any linear combination of those functions. Thus a linear superposition is maintained indefinitely and the solutions are periodic and quasi-periodic. In contrast to classical dynamics, molecular systems do not have well-defined trajectories in phase space on time scales long relative to the excitation time of internal motions. Due to the Heisenberg uncertainty relationship it is not possible to prepare an individual spectroscopic state in which the position and momentum coordinates of the nuclei and electrons are sharply defined; they have a finite distribution instead. While in classical chaos particle trajectories have an infinitely complicated substructure (Gutzwiller [55]), in the quantum mechanical description these trajectories are blurred.

There are several terms that are frequently used in the discussion of the dynamical behaviour; regularity, ergodicity and chaoticity. In addition one encounters frequently the qualification: "stochastic". It is not attempted here to separate clearly the meaning of these terms (in relation to spectroscopic behaviour) but a few words are appropriate.

A stochastic process is one that is a function of a random variable (in addition of being a function of time), and the random element is usually some external influence on the system. The irregular behaviour of a classical system, modelling a quantum system like molecules, is not a result of some random external influence but is due to the intrinsic properties of the system itself. Therefore, strictly speaking molecular systems cannot properly be regarded as stochastic. Still this term is very widely used.

Ergodic behaviour is defined in statistical mechanics. When we have a classical system where the trajectory of motion in phase space samples uniformly the latter, the time average of a given quantity equals its phase (ensemble) average.

Bohr's correspondence principle requires that in a high excitation state, like nearly dissociated or nearly ionized molecular states, where the energy density is very great, the molecular quantum system should correlate with the classical description. Therefore one would expect some manifestation of classically chaotic behaviour in a quantum system, or quantum phenomenon, like molecular spectra. This manifestation is found in the statistical properties of molecular energy levels and in transitions among them. Ergodicity or regular behaviour, and chaotic limits shall in the following be studied from a statistical viewpoint. Regular spectroscopic behaviour may be related to the regularity of the underlying classical motion,

whereas irregular (or chaotic) behaviour of the corresponding classical system manifests itself in a very different statistical behaviour in spectroscopy. The transition between regular and irregular (chaotic) classical systems is provided by the KAM theorem (Kolmogorov–Arnold–Moser) (Arnold [15], Kolmogorov [72], Moser [88]). It is possible to study the statistical properties of energy levels in the semiclassical limit; $\hbar \to 0$, as was shown by Berry [11,12] using Gutzwiller's method (Gutzwiller [48,49,50,51,52], see also: Balian and Bloch [7]). In this way classical periodic orbits may be related to semiclassical energy levels. In the semiclassical description quantization is provided by the Einstein–Brillouin–Keller (EBK) quantization (based on Einstein's paper in 1917; [34]). This corresponds to 'old quantum theory' which was superseded by wave mechanics, but for the study of molecular chaos in the semiclassical limit has been rediscovered and widely used (see: Tabor [112], Section 6, pp. 228-279). In terms of EBK quantization rules a regular spectrum corresponds to regions of integrable (regular) motion that can be quantized according to these rules, whereas irregular (chaotic) spectra cannot be so quantized. As we shall see, one may model certain spectroscopic observations on this semiclassical approach that provides insight into spectral statistical characteristics.

4. The mathematical apparatus of statistical spectroscopy

Before applying most of the statistical probes to molecular energy levels or actual molecular spectra a procedure is needed to place those sequences on the same footing. For this purpose one has to separate the average density of levels from fluctuations about that average (Brody et al [20], Bohigas and Giannoni [17], Haller, Koppel and Cederbaum [56]). This is because we want to reduce different energy level systems to the same basis that then allows a comparison of the statistical behaviour of highly excited nuclear levels to those of molecular excitations. This is achieved by a suitable mapping of the original energy level system: $E \to \tilde{E}$. Taking $N(E)$ as the cumulative density of the energy levels it is seen to fluctuate about a smooth average: $N_{\text{av}}(E)$:

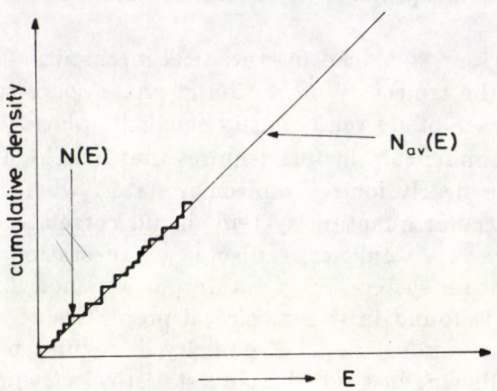

Fig. 1. Cumulative energy level distribution

Now if

$$\tilde{E}_i = N_{\mathrm{av}}(E_i); \quad i = 1, 2, 3, \ldots$$

$$N_{\mathrm{av}}(E) = \int_0^E \varrho_{\mathrm{av}}(E')dE' = \int_0^{\tilde{E}} \varrho_{\mathrm{av}}(\tilde{E}')d\tilde{E} = \tilde{E} = \hat{N}_{\mathrm{av}}(\tilde{E}). \tag{1}$$

The new energy level sequence $\tilde{E}_i$ has a constant density; $\varrho_{\mathrm{av}}(\tilde{E}) = 1$, and it may be split up to a secular part (showing a smooth change with energy, that is universal) and a fluctuation part (that is specific to the system):

$$\hat{N}(\tilde{E}) = \hat{N}_{\mathrm{av}}(\tilde{E}) + \hat{N}_{\mathrm{fl}}(\tilde{E}) = \tilde{E} + \hat{N}_{\mathrm{fl}}(\tilde{E}). \tag{2}$$

We shall be concerned only about the fluctuation part $N_{\mathrm{fl}}(\tilde{E})$. This carries the statistical information on the energy level system. Taking into account the fact that energies (eigenvalues) are not continuous functions, Eq. (1) can be rewritten:

$$N_{\mathrm{av}}(E) = \sum_{i=1}^{n} \Theta(E - E_i), \tag{3}$$

where $\Theta(E)$ is the Heaviside step function, and $\tilde{E}$ can be given as:

$$\tilde{E} = b_1^{-1}[N_{\mathrm{av}}(E) - b_0], \tag{4}$$

so that:

$$\hat{N}_{\mathrm{av}}(\tilde{E}) = b_0 + b_1\tilde{E}. \tag{5}$$

This procedure is called "unfolding" ("deconvolution" or "mapping") and might be a sensitive function of the choice for $N_{\mathrm{av}}(E)$, i.e. of the way we approximate the average behaviour of the energy level system. There are various possibilities for this, one of these is the use of a polynomial expansion:

$$N_{\mathrm{av}}(E) = \sum_{k=1}^{m} a_k E^k. \tag{6}$$

Alternatively, one may use a cubic spline function smoothing (Press et al [103], Chapter 3), or apply a moving average (Wong, French [122], Venkataraman [115]):

$$\tilde{E}_{i+1} = \tilde{E}_i + (2k+1)(E_{i+1} - E_i)/(E_{j_2+1} - E_{j_1}), \tag{7}$$

where i runs over the energy levels, and $j_1 = \max(1, i-k)$ and $j_2 = \min(n-1, i+k)$, n is the total number of energy levels and k is the number of consecutive spacings between the energy levels over which averaging is done.

All these unfolding methods produce level sequences of nearly unit local mean spacing (density). The fluctuation properties of spectra may either be stationary (invariant to translation along the energy axis), or not stationary. In the latter case one is interested in asymptotic properties of energy level sequences.

4.1. Fluctuation measures

With respect to the statistical nature of $\hat{N}_{\text{fl}}(\tilde{E})$ in Eq. (2) there are two extreme cases, the case of a complete lack of correlation among energy levels, and the case of very strong correlations. There are a number of mathematical techniques to test such correlations. Historically the first of these was suggested by Wigner (Wigner [118,119]) that relates to the distribution of spacings among adjacent levels: $P(S)$ (S stands for first neighbour spacing between unfolded energies: $\tilde{E}$). This method relies on the absence or presence of repulsion between levels.[1]

For a completely random energy level sequence, the probability of a spacing is independent of the magnitude of the spacing and one has a Poissonian distribution law: (using first neighbour spacings (S) in terms of local spacing units. The local spacing unit is 1 for an unfolded energy level sequence):

$$P(S) = \exp(-S). \tag{8}$$

On the other hand when there is (linear) level repulsion, the probability of a spacing is proportional to the spacing magnitude:

$$P(S) = (\pi/2)S\exp(-\pi S^2/4). \tag{9}$$

There is an important difference between the Poisson (Eq. (8)) and Wigner (Eq. (9)) distributions; for a random energy level sequence the most probable spacing is zero (level clustering), whereas for the Wigner (strongly correlated) distribution zero spacing has zero probability (level repulsion).

In order to model strong correlations among energy levels, which is the case for highly excited nuclear spectra, Wigner proposed random matrix theory (Wigner [118,119], Brody et al [20]). Random matrix theory is reminiscent of statistical mechanics in the sense that it deals with ensemble averages over stochastic quantities. These ensembles are formed of matrices possessing random structure. Depending on the way such a random matrix is defined there are three types of matrix ensembles: the Gaussian orthogonal ensembles (GOE), the Gaussian unitary ensembles (GUE), and the symplectic ones. If the physical system is invariant under time-reversal and under rotations the matrices are real symmetric with random elements having independent Gaussian distributions. The ensemble must be invariant to orthogonal transformations and consists of matrices of identical dimension. The GOE model

[1]Repulsion between energy levels may be understood in terms of avoided crossings, or the "non-crossing rule" (Neumann and Wigner [89], Berry [11]). This rule applies only when we select energy levels possessing the same symmetry. In the case of vibronic energy levels this involves the same electronic state and vibrational quantum numbers (or combinations of vibrational quantum numbers that correspond to the same symmetry of the product of vibrational wavefunctions), the same total angular momentum quantum number (usually J) and the same parity (behaviour towards space inversion). In addition there is a need to study as complete as possible level systems in the given symmetry, so that no (or a minimal number of) energy levels should be missing, and no spurious levels should occur. All the following statistical measures presuppose this kind of symmetry selection, the use of so-called "pure sequences".

represents the strongest possible level correlations and it is frequently feasible to give analytical formulae for this limit of the various fluctuation measures. The GUE limit corresponds to systems for which the Hamiltonian does not possess time reversal and rotation symmetry, such matrices have complex Hermitian structure. Finally the symplectic ensembles correspond to systems that are time-reversal invariant but not invariant under rotations, and if the system has half-odd-integer total angular momentum the matrices of the ensemble are quaternion real. The importance of GUE and symplectic ensembles is little in the field of molecular spectroscopy.

Random matrices also show ergodic property so that their ensemble averages are equal to spectral averages of a member (Pandey [91]). As a consequence when we choose one member of the ensemble it will be representative of the whole ensemble. This ergodicity property shall be utilized in the application of the various fluctuation measures.

We can now return to the discussion of the fluctuation measures with these two limits in mind; the completely random Poissonian sequences and the strongly correlated GOE limit.

The spacing distribution discussed previously does not include information on spacing correlations. This is obtained for two adjacent nearest-neighbour spacings, as a spectral average, by:

$$c = \sum_i (S_i - 1)(S_{i+1} - 1) / \sum_i (S_i + 1)^2. \tag{10}$$

For the Poissonian case $c = 0$, while in the GOE limit the first-order spacings are anticorrelated: $c = -0.271$ (Brody et al [20], Garrison [43]).

Another very useful statistics is the spectral rigidity; $\Delta_3(L)$ (Bohigas, Giannoni [16], Dyson, Mehta [32], French et al [41,42]). Spectral rigidity measures the least-squares deviation of the cumulative energy density $\hat{N}(\tilde{E})$ in Eq. (2) from the best straight line fitting it:

$$\Delta_3(\alpha; L) = (1/L) \min_{A,B} \int_{\alpha}^{\alpha+L} [\hat{N}(\tilde{E}) - A\tilde{E} - B]^2 d\tilde{E}, \tag{11}$$

where $\hat{N}(\tilde{E})$ is the number of levels below $\tilde{E}$, A and B are constants of the fitting, L measures the length of the level sequence, and α is the beginning of the L interval. The value actually used in the analysis is the spectral average:

$$\langle \Delta_3(\alpha, L) \rangle = \overline{\Delta}_3(L). \tag{12}$$

For analytical purposes sums are used instead of the integral in Eq. (12), such formulae are found in Bohigas and Giannoni [16] and Feingold and Fishman [40]. Spacing distributions and the $\Delta_3(L)$ statistics are independent fluctuation measures and are complementary information; spacing distribution measures short range correlations, while $\Delta_3(L)$ characterizes long-range ones. For a Poissonian level $\overline{\Delta}_3(L) = L/15$, whereas for a GOE sequence:

$$\overline{\Delta}_3(L) = (1/\pi^2)(\ln L - 0.0687). \tag{13}$$

The meaning of these two limiting expressions is that for a random set of levels the variance of deviations from the mean behaviour is proportional to the number of levels, whereas for the strongly correlated case the increase is only logarithmical. It is quite possible to find cases where spacing distributions indicate strong correlations, while spectral rigidity is low. It is often found that for actual level systems (theoretically computed or experimentally determined) the increase of $\overline{\Delta}_3(L)$ with L is slower than indicated by the GOE limit in Eq. (13), and saturation is observed (see e.g. Zimmermann et al [116]). It is possible to relate $\overline{\Delta}_3(L)$ to the sum over classical periodic orbits and find the general criterion for the saturation of spectral rigidity. This occurs when $L \gg L_{\max}$, where $L_{\max}$ is given by semiclassical considerations (Berry [12]) as

$$L_{\max} = h\langle d\rangle / T_{\min} \simeq \hbar^{-(N-1)}, \tag{14}$$

where $\langle d\rangle$ is the mean level spacing: $\langle d\rangle^{-1} \simeq \hbar^N$, and N is the number of freedoms in the semiclassical system. $T_{\min}$ in Eq. (14) is the period of the shortest classical closed orbit.

In addition to these two most important statistical measures, there are a number of others. One of these is the "number statistic"; $n(L)$, which is a discrete variable counting the number of levels contained in the interval L. Provided the spectral sequence is unfolded, the average of $n(L)$ is L. The useful measures derived from this quantity are its higher moments, its variance $\sum^2(L)$, its skewness $\gamma_1(L)$ and its excess $\gamma_2(L)$ (Pandey [90]).

All of these (and previous fluctuation measures) are derivable from the level correlation functions. The k-level correlation function is defined as (Bohigas–Giannoni [17]):

$$\tilde{R}(E_1, \ldots, E_k) = (N!/(N-k)!) \int \cdots \int P_N(E_1, \ldots, E_N) dE_{k+1} \ldots dE_N, \tag{15}$$

where P_N is the joint probability density of the energy level E_i:

$$P_N(E_1, E_2, \ldots, E_N) = C_N \exp(-(1/4\sigma^2) \sum_i E_i^2) \prod |E_i - E_j|, \tag{16}$$

where C_N is a normalization constant, and σ^2 is the variance of the eigenvalue E_i.

In Eq. (16) $P_N(E_1 \ldots E_N)\, dE_1 \ldots dE_N$ gives the probability of having one level at E_1, another at $E_2 \ldots$ and another at E_N within the intervals $\{E_j, E_j + dE_j\}$.

When we unfold the energies $E_i \to \tilde{E}_i$ (see earlier) a new set of k-level correlation functions is obtained:

$$R_k(\tilde{E}_1, \tilde{E}_2 \ldots \tilde{E}_N) = \lim_{N \to \infty} \frac{\tilde{R}_k(E_1, \ldots, E_k)}{\tilde{R}_1(E_1) \ldots \tilde{R}_1(E_k)}. \tag{17}$$

The functions R_k characterize the fluctuation properties of levels completely.

Of central importance are the k-level cluster functions

$$Y_k(\tilde{E}_i \dots \tilde{E}_k) = \sum_G (-1)^{k-m}(m-1)! \prod_{j=1}^{m} R_{G_j} \quad (\tilde{E}_t, \text{ with } t \text{ in } G_j), \tag{18}$$

where G stands for division of the indices $1, 2 \dots k$ into subgroups $[G_1, G_2, \dots, G_m]$. The most significant of the cluster functions is the two-level one: $k = 2$, when there are two subgroups: $m = 1$ [(1,2)] and $m = 2$ [(1),(2)]:

$$Y_2(\tilde{E}_1, \tilde{E}_2) = -R_2(\tilde{E}_1, \tilde{E}_2) + R_1(\tilde{E}_1)R_1(\tilde{E}_2). \tag{19}$$

Another possibility is to use the probability that in a sequence of unfolded levels $\{\tilde{E}_i\}$ of mean spacing unity, a length L contains exactly k levels. This is given by

$$E(k;L) = \lim_{N\to\infty} (N!/(N-k)!) \int \cdots \int_{\text{in}} d\tilde{E}_i \dots d\tilde{E}_k \int \cdots \int_{\text{out}} d\tilde{E}_{k+1} \dots d\tilde{E}_N P_N(E_1 \dots E_N), \tag{20}$$

where the first group of integrals is performed on the variables inside the interval $[\alpha, \alpha + L]$ and the other group is an outside integral. The probability $E(k;L]$ in Eq. (20) is simply related to various fluctuation measures, e.g. the nearest neighbour spacing distribution $p(\tilde{E})$ in Eq. (8):

$$p(\tilde{E}) \equiv p(0, \tilde{E}) = (d^2/d\tilde{E}^2)E(0, \tilde{E}). \tag{21}$$

Practically it is better to use integrated quantities:

$$y_k(L) = \int_0^L \cdots \int_0^L Y_k(\tilde{E}_1 \dots \tilde{E}_k) d\tilde{E}_1 \dots d\tilde{E}_k. \tag{22}$$

Using y_k quantities the various number statistics can be easily given as, e.g. the average number of levels in an interval L:

$$\overline{n(L)} = y_1(L) = L. \tag{23}$$

The variance of this number is:

$$\Sigma^2(L) = \overline{(n(L) - L)^2} = y_1(L) - y_2(L). \tag{24}$$

Particularly important are the quantities related to the two-level cluster function $Y_2(\tilde{E}_1, \tilde{E}_2)$ in Eq. (19) which will be called two-point measures. E.g.:

$$1 - Y_2(\tilde{E}) = \sum_{k=0}^{\infty} p(k, \tilde{E}), \tag{25}$$

so that all orders of spacing distributions are two-point measures. Using $Y_2(\tilde{E})$ we may write the variance of the number statistic $\sum^2(L)$ as

$$\sum^2(L) = L - \int_0^L (L-r)Y_2(r)dr \tag{26}$$

and establish a relationship between $\overline{\Delta}_3(L)$ and $\sum^2(L)$:

$$\overline{\Delta}_3(L) = (2/L^4)\int_0^L (L^3 - 2L^2r + r^3)\sum^2(r)dr. \tag{27}$$

For a Poissonian spectrum of energy levels the relationships for the various fluctuation measures are simple: For spacing distributions:

$$p(k, L) = (L^k/k!)\exp(-L). \tag{28}$$

For k-level cluster functions:

$$Y_1(\tilde{E}) = 1; \quad Y_k(\tilde{E}_1, \tilde{E}_k) = 0; \quad k \geq 2 \tag{29}$$

and also:

$$\sum^2(L) = L \quad \text{and} \quad \overline{\Delta}_3(L) = L/15. \tag{30}$$

In the GOE limit these formulae are considerably more complicated. Analytical forms for the different cluster functions (Eq. (18)) were derived on the basis of Mehta's work [83]. Mehta and Pandey [85] gave relationships among functions related to spacing distributions, on the one hand, and the k-level correlation and cluster functions, on the other.

The two-level cluster function $Y_2(r)$ is given for the limiting cases of small and large r values:

$$Y_2(r)_{r\to 0} \to 1 - (1/6)\pi^2 r + (1/60)\pi^4 r^3 + \ldots \tag{31a}$$

and

$$Y_2(r)_{r\to\infty} \to (1/\pi^2 r^2) - (1 + \cos^2 \pi r)/\pi^4 r^4 + \ldots . \tag{31b}$$

The quantity $1 - Y_2(r)$ is 1 for the Poissonian case (see Eq. (29)), while it increases from zero asymptotically to unity for the GOE limit.

The $\overline{\Delta}_3(L)$ formula was already given in Eq. (13) while

$$\sum^2(L) = (1/\pi^2)\ln L + 0.44 \tag{32}$$

for the GOE case.

4.2. The power spectrum statistics

In addition to the above statistical tests in recent years another important fluctuation measure has been added to the arsenal; the statistical Fourier-transform (FT) technique. In their first paper on this topic Leviandier et al [78] introduced this robust method to detect long-range correlations in optical spectra. The method consists simply of taking the Fourier-transform of a set of energy levels, or directly spectroscopic data. There have been a number of theoretical papers describing the properties of this method (Coy and Lehmann [26]; Coy, Hernandez and Lehmann [27], Jost and Lombardi [69], Levine and Kinsey [79], Lombardi, Labastie, Bordas and Broyer [81]; Pique, Chen, Field and Kinsey [94,95], Pique, Joyeux, Manners and Sitja [98]; Remacle and Levine [106]).

The Fourier-transform of energy levels or spectral lines is denoted in many different ways, let us adopt here $C(t)$, where t refers to time, and the abscissa may be given in dimensionless (t/ϱ) units (ϱ is energy density measured per frequency interval). The quantity examined is the square modulus of the Fourier-transform $|C(t)|^2$, or as it is usually denoted in signal processing: the power spectrum. This has to be spectrally or ensemble averaged prior to use. The power spectrum contains two main components, a fast and a slow component. The fast component, whose amplitude is proportional to the square of the number of lines or energy levels, is the Fourier-transform of the overall spectral envelope, whereas the more significant slow component is the Fourier-transform of the shape of the spectral lines, and its amplitude is proportional to N only:

$$\langle |C(t)|^2 \rangle = N^2 A_E^2(t) \langle y \rangle^2 \langle L(t,\Gamma) \rangle^2 + N \langle y^2 \rangle \langle L^2(t,\Gamma) \rangle \cdot \\ \cdot [1 - G(t) b_2(t)] \otimes A_E^2(t), \tag{33}$$

where $\otimes$ denotes the convolution operation (see: Pique et al [94]), and N is the number of lines in the spectrum, $A_E(t)$ is the Fourier-transform of the spectral envelope, $L(t,\Gamma)$ is the FT of the normalized line-shape of individual lines (of width Γ), y is the integrated line intensity, and the angle bracket $\langle , \rangle$ denotes averaging over all spectral features. The quantity $G(t)$ is related to the distribution of line intensity y and line width Γ in the spectrum. For a Lorentzian line shape $G(t=0) = \langle y \rangle^2 \langle \Gamma \rangle^2 / \langle y^2 \rangle \langle \Gamma^2 \rangle$.

When there are correlations in the spectrum (or within a set of energy levels) a "correlation hole" appears between the fast and the slow components of the power spectrum. The fast component that depends on level density and not level spacing, is not important for the study of level statistics. In the case of a theoretical spectrum of unfolded energy levels represented by sticks of equal amplitude, the fast component reduces to a very narrow channel. It is the slow component of the square modulus that is proportional to $1 - b_2(t)$, where $b_2(t)$, the two-level form factor is the Fourier-transform of the two-point correlation function $Y_2(E)$ in Eq. (25):

$$b_2(t) = \int_{-\infty}^{+\infty} Y_2(r) \exp(2\pi i t r) dr. \tag{34}$$

When correlations exist among levels or spectral features ($Y_2 \neq 0$), the amplitude of the slow component is multiplied by $1 - b_2(t)$, and since the latter difference is zero for the GOE limiting case for $t/\varrho = 0$, and rises approximately to unity for $t > \varrho$ (average level density), a correlation hole is displayed. The correlation hole is "filled" for an uneven distribution of line intensities, as $G(t) < 1$ for such a case, and this reduces the observability of the hole. Extensive noise of the spectrum leads also to the filling of the correlation hole.

An enormous advantage of the power spectrum method is that the correlation hole persists (but becomes narrower) when several pure sequences are superimposed, as it happens in transforming actual spectral details. So the technique is capable of detecting correlations in any mixture of levels or different stretches of spectra.

All this is true only for spectral or ensemble averages, or smoothed FT spectra. Individual level sequences or single lengths of spectra lead to total modulation, "speckle noise" is observed. This is analogous to diffraction of laser light from a rough surface. In the modulation there is a lot of information on the spectral fine structure, that is, however, not needed for correlation analysis.

Through the two-level cluster function $Y_2(\tilde{E}_1, \tilde{E}_2)$ in Eq. (19) the power spectrum is related to the spectral rigidity statistics (Lombardi et al [81]):

$$\Delta_3(r) = \int [1 - b_2(t)] K(r,t) dt, \tag{35}$$

where $K(r,t)$ is a kernel function:

$$K(r,t) = (1/(2\pi t)^2)[1 - F(y)^2 - 3F'(y)^2], \tag{36}$$

where, in turn

$$F(y) = (\sin(y)/y); \quad y = \pi r t.$$

Equations (35) and (36) can be derived from Eqs (27) and (33) by inverting the order of integrations. It is then also seen that $|C(t)|^2$, $\Delta_3(r)$ and $\Sigma^2(r)$ are all closely related and therefore all convey information on second order correlations between the location of two levels. The disadvantage of the power spectrum, viz. that it is very noisy, as opposed to the relatively smooth behaviour of the spectral rigidity $\Delta_3(r)$ and $\sum^2(r)$ statistics, may be turned into an advantage, since one is then free to handle this noisy appearance by any noise reducing method chosen at will.[2]

Depending on the nature of the quantum system to which the statistical Fourier-transform method is applied we have four well defined examples (see Lombardi et al [81]), these are shown in Fig. 2 containing sketches of smoothed power spectra.

[2]The author is grateful to Professor Rémi Jost, CNRS Service National des Champs Intenses, Grenoble, France, for pointing out this property.

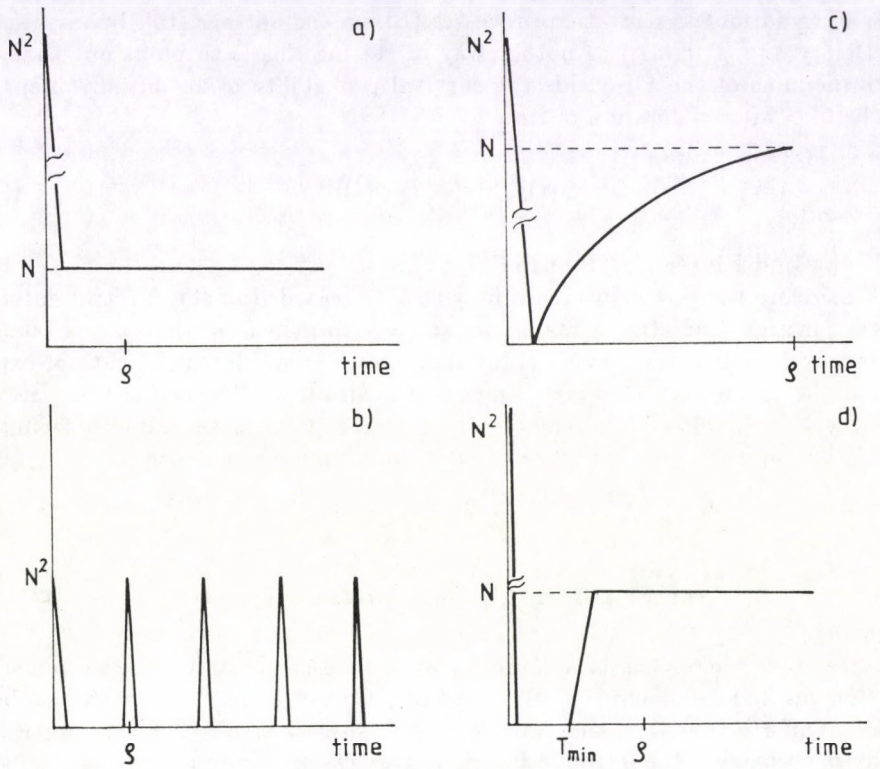

Fig. 2. Power spectral behaviour

Cases a, b, c and d correspond to a Poissonian (random) spectrum, a GOE spectrum, the harmonic oscillator and finally a set of uncoupled anharmonic oscillators. To understand the four typical forms in Fig. 2 we can apply the simple recipe in Lombardi et al [81] (based on Balian and Bloch [7,8], Berry [12]; Gutzwiller [48,49,50,51,53,54]).

An understanding of the behaviour of $|C(t)|^2$ may be obtained by a thought experiment. Let us start classical orbits from a phase space point (p, q) for the problem. At every time such an orbit closes upon itself (returns to (p, q)) enter a peak into the power spectrum. Then the harmonic oscillator yields regular peaks separated by the oscillator period T, whereas a set of anharmonic oscillators shows up a flat hole, as nothing is found in the spectrum prior to the closing of the shortest orbit ($T_{\min}$). In strongly correlated systems the number of closed orbits decreases with time and that gives rise to the correlation hole.

Before leaving the subject of the power spectrum fluctuation measure, it is very important to point out another approach or philosophy of power spectra. The calculation of the constant amplitude stick spectrum of energy levels is equivalent to the estimation of the time evolution of a molecular wavefunction. There is therefore a strong connection between the theory of statistical Fourier-transformation and the

theory of radiationless relaxation processes (Bixon and Jortner [15], Lahmani et al [74], Delory and Tric [31]). Another way of stating this is to point out that the square modulus of the FT yields the survival probability of an initially prepared state $|\psi(0)>$ after a duration of time t;

$$|C(t)|^2 = |\langle\psi(0)|\psi(t)\rangle|^2 \tag{37}$$

(see Levine and Kinsey [79], Pique et al [94]).

Therefore the power spectrum may also be regarded as the spectral autocorrelation function (see also: a maximum entropy formalism of the autocorrelation function by Remacle and Levine [106], and the relationship to the rate of exploration of the phase space (Lorquet, Engel and Levine [82]). The connection between mode selective chemistry — a centrally important aspect of laser-induced chemistry — and the application of the power spectrum method described above was given by Levine and Jortner [80].

5. Examples from high-resolution spectroscopy

In spite of the obvious lack of molecular spectroscopic analyses about ten years ago (Bohigas and Giannoni [17], Brody et al [20]), in recent times there has been a surge of efforts to extend such analyses to high-resolution molecular spectra, as already mentioned in the Introduction. The greatest problem in applying the usual fluctuation measures to molecular spectra is the extraction of a statistically significant sample size of line or level sequences of definite symmetry and good quantum numbers from the very complicated structure of highly excited molecular spectra. It is characteristic of such studies that when complete ro-vibronic (electronic excited state) or ro-vibrational (electronic ground state) analyses are available usually only levels with $J = 0$ (no rotation) are included. This is meant to simplify the construction of symmetry-wise pure sets, and to reduce the number of features to a manageable size. However, when high vibrational excitation occurs assignment of the spectral features is frequently not possible, and, of course, this is exactly why one would like to use the statistical method described here.

In such cases special experimental techniques are sought that lead to spectral simplification, or the power spectrum method is used that, as pointed out before, is comparatively insensitive to symmetry mixtures and spectroscopic resolution. In the following a number of recent examples shall be quoted. Special attention is devoted to the SEP (stimulated emission pumping) method developed in 1981 and applied since then.

In their seminal paper Leviandier et al [78] applied the newly proposed method to the highly excited acetylene (C_2H_2) vibrational levels, and to singlet–triplet anticrossing (ac) spectra of methyl-glyoxal. Acetylene vibrational spectra were obtained by the SEP method (to be described later). This was the first example of using the Fourier-transform method to a highly excited vibrational spectrum (at about

27900 cm^{-1}) and it gave an independent proof (relative to earlier statistical examinations) of strong correlations. The ac spectra of methyl-glyoxal were only taken at a vibrational excitation level of 3000 cm^{-1} and couplings in those spectra were known to be very small.

Jost and Lombardi [69] used the optical-microwave double resonance data of Lehmann and Coy [75] to show the lack of level correlations in those spectra, and the SEP spectra of acetylene, taken by Abramson et al [2], to demonstrate strong correlations objectively (objectivity being provided by the independent power spectrum method). Their own singlet–triplet anticrossing spectra of methyl-glyoxal (CH_3–CO–CHO) displayed strong correlations in the T_1 electronic state. One of their main conclusions was that only two-step, state-to-state processes, such as optical–optical or microwave–optical double resonance, or the optical anticrossing technique can provide spectra with sufficient spectral purity for statistical correlation studies. Molecular beam techniques may also help reducing spectral congestion prior to such an analysis.

Among molecular studies one of the most interesting cases is that of nitrogen dioxide (NO_2). This molecule has a very complicated vibronic spectrum between 12000 and 25000 cm^{-1} (Hsu et al [66]). In this spectral region there are four electronic states potentially interacting with one another (Jackels and Davidson [67,68]; Gillispie and Khan [44,45]). The assignment and interpretation of the observed spectra have not yet been achieved. The molecule has been the subject of many statistical approaches (Haller, Koppel and Cederbaum [56,57]; Hardwick [59]; Lehmann and Coy [75,76]; Persch et al [92]; Smalley et al [108]; Zimmermann, Koppel and Cederbaum [116,117]). Hardwick conjectured in 1985 [59] that all selection rules based upon the rotational quantum numbers are broken, and the spectrum is an ideal example of total ergodicity. Lehmann and Coy [76], however, found in their microwave–optical double resonance experiments that although the intensity distribution of the spectral lines indicate perfect ergodicity (Heller's F parameter approaches 1/3, see: Heller [60]), the first neighbour separations and the Δ_3 spectral rigidity tests show regular classical dynamics (Poissonian behaviour). Their study involved not only vibronic band origins ($J = 0$) but rotational branches of known J value as well. A similar study by Jost and Lombardi [69], using the power spectrum method indicated no correlation hole in the NO_2 spectra. So, in spite of the fact that many more rotational transitions were found than expected with strict rotational selection rules, the statistical behaviour of levels did not display classical chaoticity signs.

Many such problems may be approached, as we have already noted, by stimulated emission pumping, and before looking at further examples a short characterization of the SEP method is given.

6. Experimental studies of level correlations by SEP spectroscopy

There are several methods in spectroscopy to access high vibrational levels with great specificity and resolution. One of these is direct overtone pumping and

another important tool is stimulated emission pumping.

Direct overtone pumping utilizes lasers of appropriate fundamental frequency or harmonics. An early example of this method was reported by Swofford et al [111]. A modern laser system for this purpose is the Ti^{3+}: sapphire laser that allows one to excite the range between 700 and 1100 nm (9000 and 15000 cm^{-1}, resp.). Coy et al [28] reported the use of this laser in double resonance studies on ammonia. The measurement of overtones at high energy requires very sensitive modulation detection techniques, such as optoacoustic spectroscopy, as overtone intensities are usually very low.

In 1981 Kittrell et al [70] devised a double resonance method to obtain simplified spectra of highly excited vibrational states (between about 8000 and 30000 cm^{-1}). The technique is capable of accessing specific vibrationally excited levels of the electronic ground state. Figure 3 is a simple sketch of this folded variant of optical–optical double resonance (OODR).

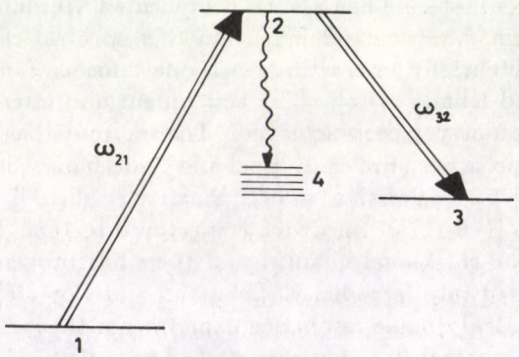

Fig. 3. The scheme for the SEP experiment ω_{21}: pumping; ω_{32}: dumping; → 4 fluorescence

A laser is used to pump population from level 1 (of the electronic ground state) to level 2 (of an excited electronic state), and a second laser is used to force population from level 2 into a high excited vibrational state in the ground electronic state (3). Both lasers are narrow bandwidth tunable pulsed lasers in the visible range that are frequency multiplied when necessary. The process may be monitored by using fluorescence (spontaneous side fluorescence or induced one by a third laser) to the ground state (indicated by levels 4 in Fig. 3) so the obvious requirement is that there should be an observable fluorescence from level 2. The two lasers involved in the experiment may be time shifted and used in antipropagating arrangement so that Doppler broadening can also be eliminated resulting in highly resolved spectra.

The selection of levels involved is controlled by Franck–Condon factors between the two electronic states so an additional requirement for good SEP spectra

is that the two potential surfaces should be sufficiently different. This is automatically satisfied when electronic excitation results in major changes in geometry. The method was originally applied to the $B \leftarrow X$ system of iodine (I_2).

Other versions of the SEP experiment are also known with different detection methods, such as polarization-labelling (Brand et al [18]). For a review see: Hamilton et al [58].

The SEP method has been used extensively on the acetylene (C_2H_2) molecule, and many statistical tests were performed (Abramson et al [1,2,3]; Engel and Levine [37]; Farantos [39]; Holme and Levine [63,64,65]; Pique et al [94,95,96]; Sumpter and Thompson [109]; Sundberg et al [110]).

Acetylene has vibronic transitions $\tilde{A}(^1A_u) \leftarrow \tilde{X}(^1\Sigma_g^+)$ that were sampled both at about 9550 cm^{-1} above the vibrationless level of the $S_0(\tilde{X}\ ^1\Sigma_g^+)$ state and about 28000 cm^{-1} above the vibrational origin. In the high energy region very unusual spectral features were observed; "clumps" of lines, with a clump width of about 1.5 cm^{-1}, containing, in high resolution, about 70 individual components. An analysis of these features showed that they all belong to the same J quantum number, and vibrational angular momentum quantum number $l = 0$ (σ_g^+). All clumps have very similar structure. The intensity distribution within and among the clumps showed a convincingly ergodic behaviour. As all other quantum numbers cease to be "good" at this high level of excitation, symmetry is completely defined by J, l and parity so that appropriate statistical tests could be made.

Pique et al [95], used the FT technique to detect strong correlations among 1500 cm^{-1} long pure vibrational sequences in the SEP spectrum around 26500 cm^{-1}. In another work on the same SEP spectra of acetylene Sundberg et al [110] carried out both intensity distribution studies and applied static fluctuation measures (such as $P(S)$ and $\Delta_3(L)$). All these measures suggested a near GOE behaviour for highly vibrationally excited $\tilde{X}$ levels, in accordance with the results of Abramson et al [3].

Pique et al [94] reported a more detailed analysis of the 26000 cm^{-1} range SEP spectra. The smoothed power spectra had time dependent features corresponding to the correlation hole, the recovery time from it, and recurrences. The width of the spectral clumps and that of their fine structure lines define two time scales (t_ϱ = 20 ps and 267 ps, resp.) that could be related to the recovery time from the correlation hole (t_{corr}) (3 ps for a single spectral stretch, 45 ps for a spectral average). For a GOE-like spectrum the theoretical expectation is that $t_{corr} = t_\varrho$, whereas for the HCCH spectra $t_{corr} \simeq t_\varrho/6$ from which the conclusion was drawn that several symmetry species or good quantum numbers exist even in this high excitation regime. However, about 1400 cm^{-1} higher (at 27900 cm^{-1}, see: Abramson et al [3]) the power spectra suggest fully chaotic dynamics. The works of Pique et al [94,95] showed that the power spectrum provides more dynamical characterization of the statistical behaviour than the single number fluctuation measures (e.g. spacing and spectral rigidity).

One more study on acetylene should be mentioned (Chen et al [25]) via the SEP technique in the 11400–15700 cm^{-1} range above zero-point level. These spectra were rotationally resolved and allowed the examination of the coupling

of rotation and vibration. There are five vibrational normal modes for acetylene ($\nu_1, \nu_2(\Sigma_g^+), \nu_3(\Sigma_u^+), \nu_4(\pi_g), \nu_5(\pi_u)$). The $\tilde{A} \leftarrow \tilde{X}$ electronic excitation involves a large change of geometry (the CCH bond angle changes from 180° in the $\tilde{X}$ state to 120° in the $\tilde{A}$ state, and the C–C bond length increases from 0.1208 nm to 0.138 nm) so the strongest vibrational progressions are those of ν_4 (trans-bending mode) and its combination with the C–C stretch (ν_2) mode. Reduced term value plots showed a significant difference between $l = 0$ and $l = 2$ levels. (The l quantum number measures vibrational angular momentum from the two degenerate modes: $l = |l_4 \pm l_5|$). It was found that while the $l = 0$ levels were unperturbed, the $l = 2$ levels are strongly affected by vibration–rotation interactions.

In spite of these strong perturbations the two-point correlation statistics did not exhibit level repulsion, the fluctuation measures were all close to Poissonian behaviour. The authors drew the conclusion that the separation of vibrational and rotational degrees of freedom persists even at this high excitation regime.

The SEP technique has become quite widespread in the study of near dissociation vibrational behaviour, that is so important for chemistry, and has enabled a number of very interesting molecular dynamic studies. Another well studied example is that of formaldehyde (CH_2O), from the George Harrison Spectroscopy Laboratory at the Massachusetts Institute of Technology, Cambridge, USA.

In a series of papers (Dai et al [29,30]; Reisner et al [104,105]; Vaccaro et al [114]) very careful and extensive vibrational–rotational analyses were reported for the range 4500–9300 cm^{-1}. In formaldehyde there are strong Coriolis and Fermi perturbations that increase in strength with rising vibrational energy and level density. The SEP technique allowed a major simplification of the emission spectra and by its use it has become possible to state that molecular rotation is important in intramolecular vibrational dynamics. The interactions destroy the goodness of vibrational and K rotational quantum numbers, leading to an increase of vibrational density over the usual anharmonic level counts (for such estimates see e.g. Toselli et al [113]). Such studies (Dai el al [30]) have, however, led to a surprising conclusion, viz., that the increasing complexity of the spectrum with increasing J value (angular momentum) results in diminishing chaotic behaviour. This is an explicable but intriguing finding.

Among SEP studies on more exotic molecules the case of the Na trimer (Na_3) (Broyer et al [21]) may be mentioned. A theoretical discussion of the SEP spectrum was given by Gomez Llorente et al [46] who concluded that the SEP spectra may be fully interpreted, regarding vibrational dynamics, using a classical Hamiltonian.

7. Conclusion and outlook

This overview paper strived to summarize, perhaps in a rather selective and superficial way, the modern use of statistical methods in the analysis of molecular spectra. Contrary to the original pessimistic predictions in one of the fundamental works in this field, in the review by Brody et al [20]: *"Parenthetically it should be*

clear that, because of the limited amount of information contained in the fluctuations, highly detailed level-to-level calculations, as often carried out especially for nuclei, should in many cases not be worth the great labor involved in making them" (see: p. 469 in [20]), the past ten or so years have displayed steadily growing activity in statistical spectroscopy. (To be correct it should be mentioned that Brody et al modified their previous conclusion for cases of interesting symmetry effects!) One of the most promising mathematical techniques appears to be the power spectrum method, already casting contemporary studies into a framework much more interesting for the chemist who aspires to selective laser chemistry and therefore appreciates the connection between the methods of static spectroscopy and dynamical phenomena on the picosecond time scale extractable from the former via Fourier-transformation. Let us quote here R. D. Levine in "Mode Selective Chemistry" ([80]): *"The exploration of phase correlation can be conveniently discussed in terms of time correlation functions. The simplest is the autocorrelation function of the initially excited region., This can be obtained from the experimental spectrum by taking its Fourier-transform. Dynamical computations can, of course, directly yield the correlation functions. Obtaining the information from experiment is however of obvious interest"* (p. 549 in [80]).

There is a close link between studies of classical chaos on simple systems relevant to molecular spectroscopy, and the type of statistical studies reviewed here. One aspect is especially interesting and could perhaps contribute to further developments: the role of molecular rotation. Although it is not simple to extract molecular levels of known rotational (and overall) symmetry from spectroscopy, the interest in such aspects is obvious. Most of the attention so far has been centered on vibrational behaviour with rotations eliminated. We know notwithstanding that molecular rotation has a very important effect, some of its recognitions stemming already from its contributions to classical chaos (Fahrer and Schlier [38]). An even more significant aspect is the involvement of rotational dynamics in intramolecular energy redistribution (Knight [71]). Intramolecular state mixing is decisively important for the unravelling of intramolecular photochemical and photophysical processes and it has become evident that it is not enough to consider solely the vibrational Hamiltonian in accounting for time-averaged and time-resolved spectroscopic experiments. Intramolecular energy flow is central to the understanding of the breaking of molecular bonds, so it is central in efforts to understand chemical processes both on the traditional level and induced with the help of lasers.

The field of statistical spectroscopy is undergoing maturation but perhaps it has not yet won the battle among spectroscopists who still believe in completely assignable spectra, and any failure in obtaining such a full analysis is thought to be curable by more exacting studies. It is the hope of the present author that with an increase of statistical activity on difficult assignment cases molecular spectroscopy will benefit from such approaches.

Acknowledgements

The author would like to acknowledge the support of the Hungarian National Research Fund (contract numbers: OTKA 1233/1987, and OTKA O-SI/3079) provided by the funding organization to develop laser spectroscopic and laser-chemical research activity at the Research Laboratory for Inorganic Chemistry, Hungarian Academy of Sciences.

He is also grateful to Professor Eli Pollak at the Weizmann Institute of Science, Chemical Physics Department, Rehovoth, Israel, for an invitation to a short term research stay, and to Professor Rémi Jost, Service National des Champs Intenses (C.N.R.S.), Grenoble, France, for extensive correspondence on the statistical Fourier spectroscopic method.

References

1. E. Abramson, C. Kittrel, J. L. Kinsey and R. W. Field, J. Chem. Phys., *76*, 2293, 1982.
2. E. Abramson, R. W. Field, D. Imre, K. K. Innes and J. L. Kinsey, J. Chem. Phys., *80*, 2298, 1984.
3. E. Abramson, R. W. Field, D. Imre, K. K. Innes and J. L. Kinsey, J. Chem. Phys., *83*, 453, 1985.
4. Y. Alhassid and R. D. Levine, Phys. Rev., *A40*, 5277, 1989.
5. U. I. Arnold, Russ. Math. Survey, *18*, 85, 1963.
6. R. Balian, Nuovo Cim., *57*, 183, 1968.
7. R. Balian and C. Bloch, Ann. Phys., (N.Y.) *69*, 76, 1972.
8. R. Balian and C. Bloch, Ann. Phys., (N.Y.) *85*, 514, 1974.
9. T. L. Beck, D. M. Leitner and R. S. Berry, J. Chem. Phys., *89*, 1681, 1988.
10. M. V. Berry, in: Chaotic Behaviour of Deterministic Systems (Les Houches Lectures No. 36) (eds G. Iooss, R. H. G. Helleman and R. Stora), North Holland, Amsterdam, 1983, pp. 171–271.
11. M. V. Berry, in: Deterministic Chaos (ed. H. G. Schuster), Physik Verlag, Weinheim, 1984, p. 123.
12. M. V. Berry, Proc. Roy. Soc. London, Ser. *A400*, 229, 1985; *A413*, 183, 1987.
13. M. V. Berry, in: Quantum Chaos and Statistical Nuclear Physics (eds T. H. Seligman and H. Nishioka), Springer Lecture Notes in Physics, No. 263, 1986, pp. 1–17.
14. R. S. Berry, Z. Phys. D-Atoms, Molecules and Clusters, *12*, 161, 1989.
15. M. Bixon and J. Jortner, J. Chem. Phys., *50*, 3284, 1969.
16. O. Bohigas and M. J. Giannoni, Ann. Phys., (N.Y.) *89*, 393, 1975.
17. O. Bohigas and M. J. Giannoni, in: Mathematical and Computational Methods in Nuclear Physics (eds J. S. Dehesa, J. M. Gomez and A. Polls), Lecture Notes in Physics, Vol. 209, Springer, New York, 1984.
18. J. C. D. Brand, K. J. Cross and R. J. Hayward, Can. J. Phys., *57*, 1455, 1979.
19. J. Brickmann, Y. M. Engel and R. D. Levine, Chem. Phys. Lett., *137*, 441, 1987.
20. T. A. Brody, J. Flores, J. B. French, P. A. Mello, A. Pandey and S. S. M. Wong, Rev. Mod. Phys., *53*, 385, 1981.
21. M. Broyer, G. Delacretaz, G. O. Ni, R. L. Whetten, J. P. Wolf and L. Woste, J. Chem. Phys., *90*, 4620, 1989; Phys. Res. Lett., *62*, 2100, 1989.
22. H. S. Camarda and P. D. Georgopulos, Phys. Rev. Lett., *50*, 492, 1983.
23. M. Carmeli, Statistical Theory and Random Matrices, Marcel Dekker, New York, 1983.
24. G. Casati, B. N. Chirikov, J. Ford, F. M. Izraelev, in: Stochastic Behaviour in Classical and Quantum Hamiltonian Systems (eds G. Casati, J. Ford), Springer Lecture Notes in Physics, No. 93, 1979, pp. 334–352.
25. Y. Chen, S. Halle, D. M. Jonas, J. L. Kinsey and R. W. Field, J. Opt. Soc. Amer, *B7*, 1805, 1990.

26. S. L. Coy and K. K. Lehmann, Phys. Rev., *A36*, 404, 1987.
27. S. L. Coy, R. Hernandez and K. K. Lehmann, Phys. Rev., *A40*, 5933, 1989.
28. S. L. Coy, B. Abel, J. J. Klassen and J. I. Steinfeld, Lecture presented at the Conference on Molecular Energy Transfer, Nijmegen, The Netherlands, 1991.
29. H. -L. Dai, C. L. Korpa, J. L. Kinsey and R. W. Field, J. Chem. Phys., *82*, 1688, 1985.
30. H. -L. Dai, R. W. Field and J. L. Kinsey, J. Chem. Phys., *82*, 2161, 1985.
31. J. M. Delory and C. Tric, Chem. Phys., *3*, 54, 1974.
32. F. J. Dyson and M. L. Mehta, J. Math. Phys., *4*, 701, 1963.
33. F. J. Dyson, J. Math. Phys., *13*, 90, 1972.
34. A. Einstein, Verh. Deutsch. Phys. Ges., *19*, 82, 1917, English version: On the Quantization Condition of Sommerfeld and Epstein, JILA Report No. 116, University of Colorado, Boulder, Colorado, 1980.
35. Y. M. Engel, R. D. Levine, J. W. Thoman, Jr., J. I. Steinfeld and R. I. McKay, J. Chem. Phys., *86*, 6561, 1987.
36. Y. M. Engel and R. D. Levine, J. Chem. Phys., *89*, 4633, 1988.
37. Y. M. Engel and R. D. Levine, Chem. Phys. Lett., *164*, 270, 1989.
38. N. Fahrer and C. Schlier, J. Chem. Phys., *97*, 7008, 1992.
39. S. C. Farantos, J. Chem. Phys., *85*, 641, 1986.
40. M. Feingold and S. Fishman, Physica, *25D*, 181, 1987.
41. J. B. French, P. A. Mello and A. Pandey, Phys. Lett., *B80*, 17, 1978.
42. J. B. French, P. A. Mello and A. Pandey, Ann. Phys., (N.Y.) *113*, 277, 1978.
43. J. D. Garrison, Ann. Phys., (N.Y.) *30*, 269, 1964.
44. G. D. Gillispie, A. U. Khan, A. C. Wahl, R. P. Hosteny and M. Krauss, J. Chem. Phys., *63*, 3425, 1975.
45. G. D. Gillispie and A. U. Khan, J. Chem. Phys., *65*, 1624, 1976.
46. J. M. Gomez Llorente and H. S. Taylor, J. Chem. Phys., *91*, 953, 1989.
47. P. Grassberger and I. Procaccia, Phys. Rev. Lett., *50*, 346, 1983; Physica, *D9*, 189, 1983; Phys. Rev., *A28*, 2591, 1983.
48. M. C. Gutzwiller, J. Math. Phys., *8*, 1979, 1967.
49. M. C. Gutzwiller, J. Math. Phys., *10*, 1004, 1969.
50. M. C. Gutzwiller, J. Math. Phys., *11*, 1791, 1970.
51. M. C. Gutzwiller, J. Math. Phys., *12*, 343, 1971.
52. M. C. Gutzwiller, in: Path Integrals and their Applications in Quantum, Statistical and Solid-State Physics (eds G. J. Papadopoulos, J. T. Devreese). Plenum Press, New York, 1978, pp. 163–200.
53. M. C. Gutzwiller, Phys. Rev. Lett., *45*, 150, 1980.
54. M. C. Gutzwiller, Physica, *D7*, 341, 1983.
55. M. C. Gutzwiller, Mild Chaos, in: Chaotic Behaviour in Quantum Sytems (ed. G. Casati). Plenum Press, New York, 1985.
56. E. Haller, H. Koppel and L. S. Cederbaum, Chem. Phys. Lett., *101*, 215, 1983.
57. E. Haller, H. Koppel and L. S. Cederbaum, J. Mol. Spectr., *111*, 377, 1985.
58. C. E. Hamilton, J. L. Kinsey and R. W. Field, Annu. Revs. Phys. Chem., *37*, 493, 1986.
59. J. L. Hardwick, J. Mol. Spectr., *109*, 85, 1985.
60. E. J. Heller, Farad. Discuss. Chem. Soc., *75*, 141, 1983.
61. E. J. Heller and R. L. Sundberg, in: Chaotic Behaviour in Quantum Systems (ed. G. Casati). Plenum Press, New York, 1985.
62. E. J. Heller, in: Quantum Chaos and Statistical Nuclear Physics (eds T. H. Seligman and H. Nishioka), Springer Lecture Notes in Physics, No. 263, 1986, pp. 162–181.
63. T. A. Holme and R. D. Levine, J. Chem. Phys., *89*, 3379, 1988.
64. T. A. Holme and R. D. Levine, Chem. Phys. Lett., *150*, 393, 1988.
65. T. A. Holme and R. D. Levine, Chem. Phys., *131*, 169, 1989.
66. D. K. Hsu, D. L. Monts and R. N. Zare, Spectral Atlas of Nitrogen Dioxide. Academic Press, New York, 1978.
67. C. F. Jackels and E. R. Davidson, J. Chem. Phys., *64*, 2908, 1976.

68. C. F. Jackels and E. R. Davidson, J. Chem. Phys., *65*, 2941, 1976.
69. R. Jost and M. Lombardi, in: Quantum Chaos and Statistical Nuclear Physics (eds T. H. Seligman and H. Nishioka) Lecture Notes in Physics, Vol. 263, Springer, New York, 1986, p. 72.
70. C. Kittrell, E. Abramson, J. L. Kinsey, S. A. McDonald, D. E. Reisner and R. W. Field, J. Chem. Phys., *75*, 2056, 1981.
71. A. E. W. Knight, in: Excited States. Vol. 7, Academic Press, New York, 1988.
72. A. N. Kolmogorov, Dokl. Akad. Nauk. SSSR, *98*, 525, 1954; English version: Proceedings of the 1954 Internatl. Congress of Mathematics, North-Holland, Amsterdam, 1957.
73. J. Kommandeur, W.L. Meerts, Y.M. Engel and R.D. Levine, J. Chem. Phys., *88*, 6810, 1988.
74. F. Lahmani, A. Tramer and C. Tric, J. Chem. Phys., *60*, 443, 1974.
75. K. K. Lehmann and S. L. Coy, J. Chem. Phys., *83*, 3290, 1985.
76. K. K. Lehmann and S. L. Coy, Ber. Bunsenges. Phys. Chem., *92*, 306, 1988.
77. D. M. Leitner, R. S. Berry and R. M. Whitnell, J. Chem. Phys., *91*, 3470, 1989.
78. L. Leviandier, M. Lombardi, R. Jost and J. P. Pique, Phys. Rev. Lett., *56*, 2449, 1986.
79. R. D. Levine and J. L. Kinsey, Proc. Natl. Acad. Sci. USA, *88*, 11133, 1991.
80. R. D. Levine and J. Jortner, in: Mode Selective Chemistry (eds J. Jortner et al), Kluwer Academic Publ., Dordrecht, Netherlands, 1991.
81. M. Lombardi, P. Labastie, M. C. Bordas and M. Broyer, J. Chem. Phys., *89*, 3479, 1988.
82. J. C. Lorquet, Y. M. Engel and R. D. Levine, Chem. Phys. Lett., *175*, 461, 1990.
83. M. L. Mehta, Nucl. Phys., *18*, 395, 1960.
84. M. L. Mehta, Random Matrices and the Statistical Theory of Energy Levels. Academic Press, New York, 1967.
85. M. L. Mehta and A. Pandey, J. Phys., *A16*, L601, 1983.
86. A. McIlroy and D. J. Nesbitt, J. Chem. Phys., *92*, 2229, 1990.
87. W. H. Miller, R. Hernandez, C. B. Moore and W. F. Polik, J. Chem. Phys., *93*, 5657, 1991.
88. J. Moser, Nachr. Akad. Wiss. Goettingen Math. Phys., *K1*, 1, 1962.
89. J. von Neumann and E. P. Wigner, Phys. Zeitschr., *30*, 467, 1929.
90. A. Pandey, Doctoral Dissertation, University of Rochester, 1978, unpublished.
91. A. Pandey, Ann. Phys., (N.Y.) *119*, 170, 1979.
92. G. Persch, E. Mehdizadeh, W. Demtroder, Th. Zimmermann, H. Koppel and L. S. Cederbaum, Ber. Bunsenges. Phys. Chem., *92*, 312, 1988.
93. Y. B. Pesin, Russ. Math. Survey, *32*, 55, 1977.
94. J. P. Pique, Y. Chen, R. W. Field and J. L. Kinsey, Phys. Rev. Lett., *58*, 475, 1987.
95. J. P. Pique, Y. Chen, R. W. Field and J. L. Kinsey, J. Phys. Colloque, C7, Suppl. No. 12, *48*, C7-655, 1987.
96. J. P. Pique, Y. M. Engel, R. D. Levine, Y. Chen, R. W. Field and J. L. Kinsey, J. Chem. Phys., *88*, 5972, 1988.
97. J. P. Pique, M. Lombardi, Y. Chen, R. W. Field and J. L. Kinsey, Ber. Bunsenges. Phys. Chem., *92*, 422, 1988.
98. J. P. Pique, M. Joyeux, J. Manners and G. Sitja, J. Chem. Phys., *95*, 8744, 1991.
99. W. F. Polik, D. R. Guyer and C. B. Moore; J. Chem. Phys., *92*, 3453, 1990.
100. W. F. Polik, D. R. Guyer, W. H. Miller and C. B. Moore, J. Chem., Phys., *92*, 3471, 1990.
101. C. E. Porter and R. G. Thomas, Phys. Rev., *104*, 483, 1956.
102. C. E. Porter (ed.), Statistical Theories of Spectra: Fluctuations, Academic Press, New York, 1965.
103. W. H. Press, B. P. Flannery, S. A. Teukolsky and W. T. Vettering, Numerical Recipes, the Art of Scientific Computing. Cambridge University Press, Cambridge, 1989.
104. D. E. Reisner, P. H. Vaccaro, C. Kittrel, R. W. Field, J. L. Kinsey and H. -L. Dai, J. Chem. Phys., *77*, 573, 1982.
105. D. E. Reisner, R. W. Field, J. L. Kinsey and H. -L. Dai, J. Chem. Phys., *80*, 5968, 1984.
106. F. Remacle and R. D. Levine, Chem. Phys. Lett., *181*, 307, 1991.
107. N. Rosenzweig and C. E. Porter, Phys. Rev., *120*, 1698, 1960.
108. R. E. Smalley, L. Wharton and D. H. Levy, J. Chem. Phys., *63*, 4977, 1975.

109. B. G. Sumpter and D. L. Thompson, J. Chem. Phys., *82*, 4557, 1985; ibid. *86*, 2805, 1987.
110. R. L. Sundberg, E. Abramson, J. L. Kinsey and R. W. Field, J. Chem. Phys., *83*, 466, 1985.
111. R. L. Swofford, M. E. Long and A. C. Albrecht, J. Chem. Phys., *65*, 179, 1976.
112. M. Tabor, Chaos and Integrability in Non-linear Dynamics. John Wiley, New York, 1989, Chapter 6.
113. B. M. Toselli and J. R. Barker, Chem. Phys. Lett., *159*, 499, 1989.
114. P. H. Vaccaro, J. L. Kinsey, R. W. Field and H. -L. Dai, J. Chem. Phys., *78*, 3659, 1983.
115. R. Venkataraman, J. Phys., *B15*, 4293, 1982.
116. Th. Zimmermann, H. -D. Meyer, H. Koppel and L. S. Cederbaum, Phys. Rev, *A33*, 4334, 1986.
117. Th. Zimmermann, H. Koppel and L. S. Cederbaum, J. Chem. Phys., *91*, 3934, 1989.
118. E. P. Wigner, Ann. Math., *53*, 36, 1951.
119. E. P. Wigner, Contribution to Conference on Neutron Physics by Time-of-Flight, Oak Ridge National Laboratory Report, No. 2309, 1956, p. 59.
120. E. P. Wigner, Canadian Mathematical Congress Proceedings, University of Toronto Press, Toronto, Canada, 1957, p. 174, reprinted in Porter [102]; p. 188.
121. E. P. Wigner, SIAM Rev., *9*, 1, 1957.
122. S. S. M. Wong and J. B. French, Nucl. Phys., *A198*, 188, 1972.

Acta Physica Hungarica 73 (1), p. 119 (1993)

CORRIGENDA

EQUATION FOR CATHODIC GLOW SHEATH

S. HOLLÓ and B. NYÍRI

Light Source Development Department TUNGSRAM Ltd
1340 Budapest, Hungary

(Acta Phys. Hung., 72, 1, pp. 71–88, 1992)

Figure 11 on page 85 should be replaced by

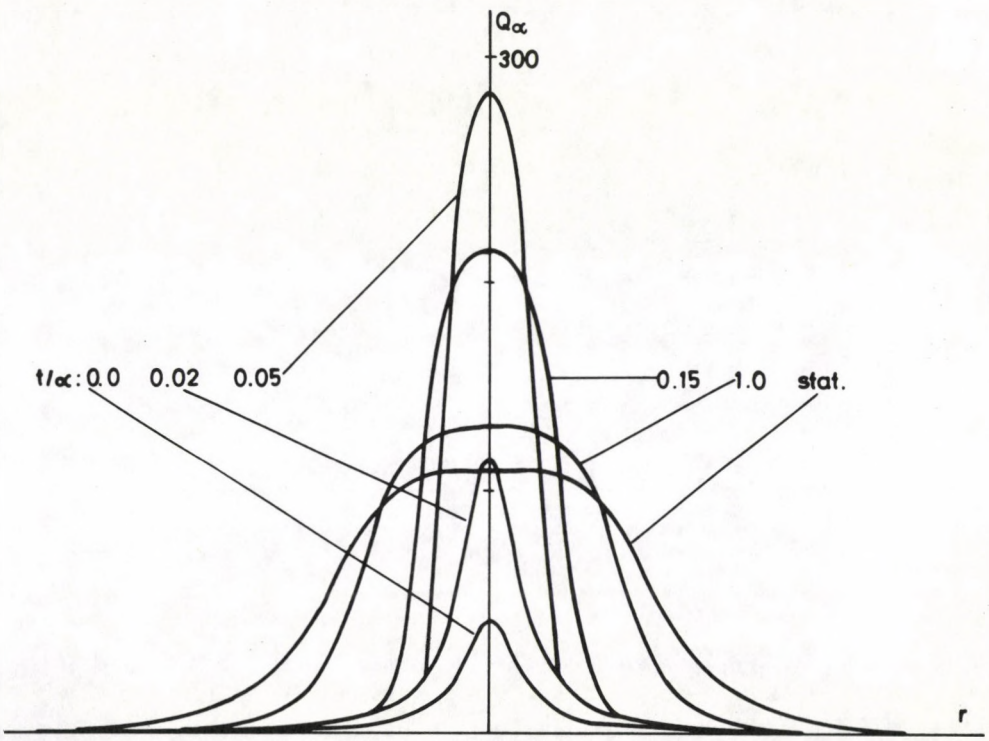

Fig. 11. Charge distributions during the transient shown in Fig. 10 taken at times 0, 0.02, 0.05, 0.15, 1.0, and infinity

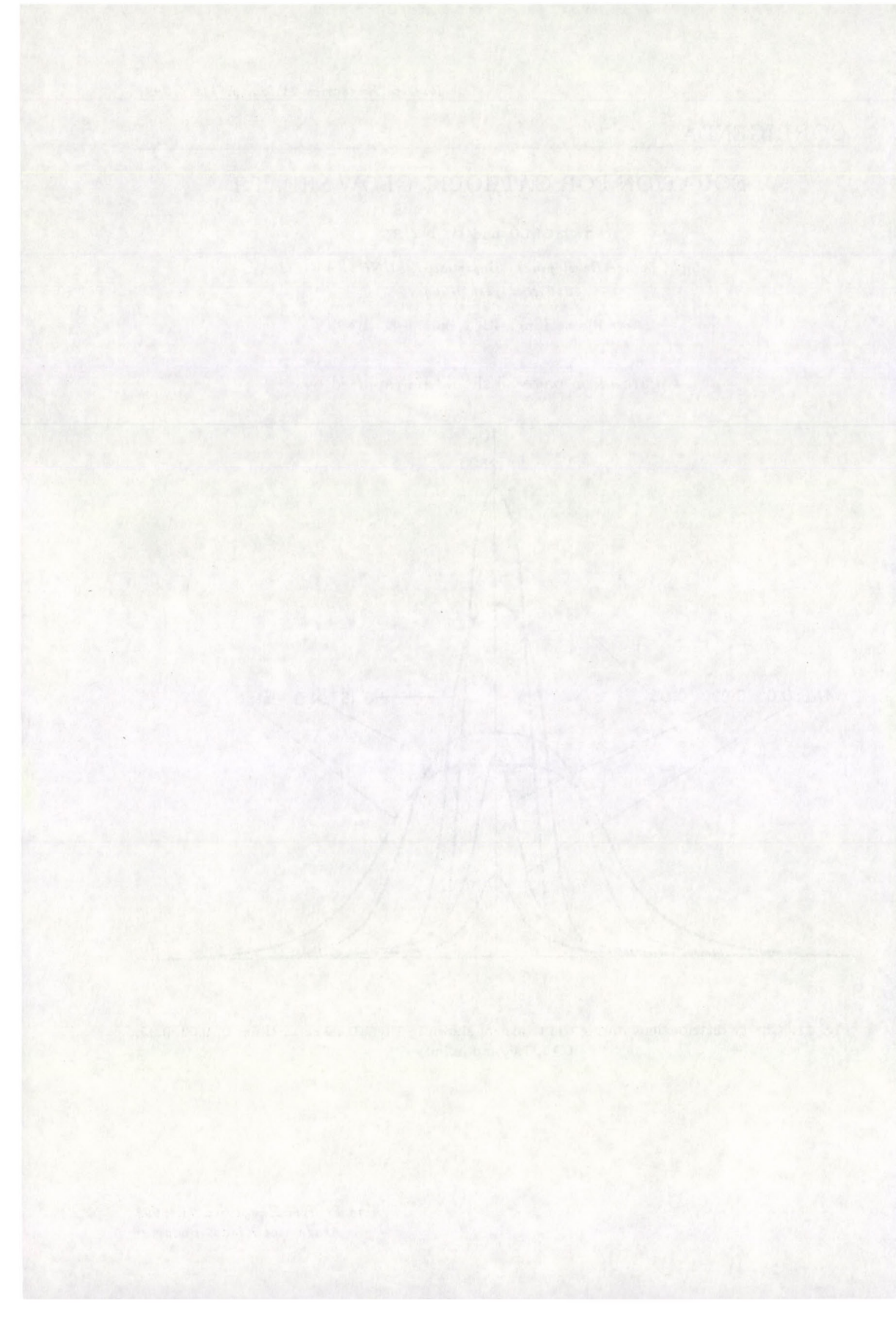

Acta Physica Hungarica 73 (1), p. 121 (1993)

AMENDMENT

to

the Contents of Volume 72 of
Acta Physica Hungarica

The following amendment is to be inserted after the Section "OPTICS AND ELECTRODYNAMICS" in the Contents of (the preceding) Volume 72 of Acta Physica Hungarica:

– –

FLUIDS, PLASMAS AND ELECTRIC DISCHARGES

– –

Acta Physica Hungarica 73, 1993
Akadémiai Kiadó, Budapest

Physics

Spacetime without Reference Frames

by
T. MATOLCSI

In the concept of this book spacetime is the fundamental notion; the points of spacetime are structured with the assumption of absolute time and absolute velocity of light resulting in the non-relativistic and special relativistic case, respectively. This gives the possibility of developing both the non-relativistic and the special relativistic chapters along the same notions: world line, observer, splitting of spacetime to space and time, reference frames, splitting of classical fields to spacelike and timelike components, the symmetry groups of spacetime (the Galilean and the Poincaré group).
The book contains lots of examples with detailed calculations through which the reader can clearly understand the connection between the traditional way of thinking and the new way of handling the problems presented in the book; the well-known special relativistic paradoxes are treated in detail. In the general relativistic case, only the basic thoughts are expressed.
The mathematics involved is rather simple and it is summarized in the second part of the book.

This book is an enlarged and revised version of "A concept of Mathematical Physics — Models for Space-Time" by T. Matolcsi

In English. 1992. Approx. 400 pages. Numerous figures. 17 x 25 cm. Hardbound.
Approx. $ 50.00

Akadémiai Kiadó, Budapest

Manuscript received by Akadémiai Kiadó:
7 April 1993
Manuscript received by TYPOTEX Ltd for TEX typesetting:
30 April 1993
Date of publication: 10 August 1993
PRINTED IN HUNGARY
Akadémiai Kiadó és Nyomda Vállalat
Budapest

NOTES TO CONTRIBUTORS

I. PAPERS will be considered for publication in Acta Physica Hungarica only if they have not previously been published or submitted for publication elsewhere. They may be written in English, French, German or Russian.

Papers should be submitted to

Prof. I. Kovács, Editor
Department of Atomic Physics, Technical University
1521 Budapest, Budafoki út 8, Hungary

Papers may be either articles with abstracts or short communications. Both should be as concise as possible, articles in general not exceeding 25 typed pages, short communications 8 typed pages.

II. MANUSCRIPTS

1. Papers should be submitted in three copies.
2. The text of papers must be of high stylistic standard, requiring minor corrections only.
3. Manuscripts should be typed in double spacing on good quality paper, with generous margins.
4. The name of the author(s) and of the institutes where the work was carried out should appear on the first page of the manuscript.
5. Particular care should be taken with mathematical expressions. The following should be clearly distinguished, e.g. by underlining in different colours: special founts (italics, script, bold type, Greek, Gothic, etc.); capital and small letters; subscripts and superscripts, e.g. x^2, x_3; small *l* and l; zero and capital O; in expressions written by hand: *e* and *l*, *n* and *u*, *v* and v, etc.

A List of Symbols on a separate sheet should be attached to each paper.

6. References should be numbered serially and listed at the end of the paper in the following form: J. Ise and W. D. Fretter, Phys. Rev., *76*, 933, 1949.

For books, please give the initials and family name of the author(s), title, name of publisher, place and year of publication, e.g.: J. C. Slater, Quantum Theory of Atomic Structures, I. McGraw-Hill Book Company, Inc., New York, 1960.

References should be given in the text in the following forms: Heisenberg [5] or [5].

7. Captions to illustrations should be listed on a separate sheet, not inserted in the text.
8. In papers submitted to Acta Physica all measures should be expressed in SI units.

III. ILLUSTRATIONS AND TABLES

1. Each paper should be accompanied by three sets of illustrations, one of which must be ready for the blockmaker. The other sets attached to the copies of the manuscript may be rough drawings in pencil or photocopies.
2. Illustrations must not be inserted in the text.
3. All illustrations should be identified in blue pencil by the author's name, abbreviated title of the paper and figure number.
4. Tables should be typed on separate pages and have captions describing their content. Clear wording of column heads is advisable. Tables should be numbered in Roman numerals (I, II, III, etc.).

IV. RETURN OF MATERIAL

Owing to high postage costs, the Editorial Office cannot undertake to return *all* material not accepted for any reason for publication. Of papers to be revised (for not being in conformity with the above Notes or other reasons) only *one* copy will be returned. Material rejected for lack of space or on account of the Referees' opinion will not be returned to authors outside Europe.

Acta Physica Hungarica

VOLUME 73, NUMBERS 2–4, 1993

Akadémiai Kiadó, Budapest
ACTA PHYS. HUNG. APAHAQ 73 (2–4) 123–346 (1993) HU ISSN 0231–4428

ACTA PHYSICA HUNGARICA

A JOURNAL OF THE HUNGARIAN ACADEMY OF SCIENCES

EDITED BY
I. KOVÁCS

Acta Physica **publishes original papers on subjects in physics. Papers are accepted in English, French, German and Russian.**

Acta Physica is published in one volume per year (4 issues) by

AKADÉMIAI KIADÓ
Publishing House of the Hungarian Academy of Sciences
H–1117 Budapest, Prielle Kornélia u. 19–35.

Subscription information

Orders should be addressed to

AKADÉMIAI KIADÓ
H–1519 Budapest, P.O. Box 245

Subscription price for Volume 73 (1993) in 4 issues US$ 84, including normal postage, airmail delivery US$ 20.00.

Acta Physica Hungarica is abstracted/indexed in Chemical Abstracts, Mathematical Reviews, Science Abstracts, Physics Briefs, Risk Abstracts, Engineering Information, Inc. EI Page One Database

CONTENTS

CONDENSED MATTER

ASTROPHYSICS

Manuscript received by Akadémiai Kiadó:
21 September 1993
Manuscript received by TYPOTEX Ltd for TEX typesetting:
7 October 1993
Date of publication: 20 December 1993
PRINTED IN HUNGARY
Akadémiai Kiadó és Nyomda Vállalat
Budapest

Acta Physica Hungarica 73 (2-4), pp. 123-128 (1993)

ON THE MODIFICATION OF EINSTEIN–MAXWELL FIELD EQUATIONS

J. N. S. KASHYAP

Unit of Fundamental Researches, Amara Khaira Chak, Kandava Varanasi, (U. P.) India

(Received in revised form 20 October 1992)

Here the Einstein–Maxwell equations in general relativity are modified in the light of the Maxwell macroscopic theory which deals with electromagnetic behaviour of ponderable matter and an axially symmetric solution of physical interest is obtained.

1. Introduction

Before 1905, gravitation and electromagnetism were thought of as independent of each other. But with the construction of the Einstein–Maxwell field equations based on Lorentz electron theory the philosophy behind gravitation has changed. Now the gravitational force may also be interpreted as a force produced by the interaction of magnetic field and electric current [1]. On macroscopic ground the Einstein–Maxwell field equations have a somewhat unsatisfactory status. It is hence interesting to find a modified set of field equations. In the present paper, our attempt is to modify the Einstein–Maxwell field equations with the help of the Maxwell macroscopic theory for ponderable matter and to show how gravitation is interrelated with electromagnetism.

2. Field equations

Connecting the electric field strength E, electric displacement D, magnetic field strength H and magnetic induction B with the density of charge ϱ and conduction current J the Maxwell field equations for ponderable matter can be written in the usual vector language as:

$$\begin{aligned} \mathrm{div} D &= \varrho, \\ \mathrm{div} B &= 0, \\ \mathrm{curl}\, E &= -\frac{1}{c}\frac{\partial B}{\partial t}, \\ \mathrm{curl}\, H &= \frac{1}{c}\left(\frac{\partial D}{\partial t} + J\right), \end{aligned} \tag{1}$$

where

$$B = \mu H, \quad D = \epsilon E. \tag{2}$$

Here the dielectric constant ϵ and magnetic permeability μ are regarded as functions of the position and time. In 4-dimensional language the field equations (1) can be expressed as

$$F_{\lambda\mu,\nu} + F_{\mu\nu,\lambda} + F_{\nu\lambda,\mu} = 0 \tag{3}$$

and

$$\frac{\partial}{\partial x^\nu}\left(\sqrt{-g}H^{\mu\nu}\right) = J^\nu. \tag{4}$$

Here the antisymmetric electromagnetic tensors $F_{\lambda\mu}$ and $H_{\lambda\mu}$ are defined in the usual sense as

$$F_{\lambda\mu} = \begin{matrix} 0 & B_z & -B_y & E_x \\ -B_z & 0 & B_x & E_y \\ B_y & -B_x & 0 & E_z \\ -E_x & -E_y & -E_z & 0 \end{matrix} \tag{5}$$

and

$$H_{\lambda\mu} = \begin{matrix} 0 & H_z & -H_y & D_x \\ -H_z & 0 & H_x & D_y \\ H_y & -H_x & 0 & D_z \\ -D_x & -D_y & -D_z & 0 \end{matrix} \tag{6}$$

For gravitational consideration we can take [2]

$$\epsilon = \mu = \phi. \tag{7}$$

Following the method due to Tolman [3] in the field equations (1) and regarding the integration as taken over a definite fixed volume in space we obtain

$$\int \Phi\left(D \cdot \frac{\partial D}{\partial t} + B \cdot \frac{\partial B}{\partial t} + D \cdot J\right) dv = -c \int [D \times B]_n d\sigma \tag{8}$$

and

$$\int \left\{ D\varrho + \frac{\Phi}{c}\left[J \times B + \frac{\partial}{\partial t}(D \times B)\right]\right\} dv = \int [D\mathrm{div}D + (\mathrm{curl}B) \times B + (\mathrm{curl}D) \times D] dv \tag{9}$$

in the usual notations, provided

$$\eta^{ikl} u_i (\Phi_k X_l - \Phi_l X_k) = 0. \tag{10}$$

Here η^{ikl} is a tensor density antisymmetric in all the suffixes, U_i represents a unit vector in the x^i-direction and $X = (X_1, X_2, X_3)$ stands for H or E. In the case of free space, where we take $\epsilon = \mu = 1$, the condition (10) is identically satisfied and (8) and (9) reduce to

$$\int \left(E \cdot \frac{\partial E}{\partial t} + H \cdot \frac{\partial H}{\partial t} + E \cdot J\right) dv = -c \int [E \times H]_n d\sigma \tag{11}$$

and

$$\int \left[\left(\varrho E + \frac{J \times H}{c} \right) + \frac{1}{c} \frac{\partial}{\partial t} (E \times H) \right] dv = - \int \frac{\partial p_{ij}}{\partial x^j} dv, \tag{12}$$

where p_{ij} are electromagnetic stresses defined as

$$\begin{aligned} p_{ii} &= -\frac{1}{2}(E_i^2 - E_j^2 - E_k^2 + H_i^2 - H_j^2 - H_k^2), \\ p_{ij} &= -(E_i E_j + H_i H_j). \end{aligned} \tag{13}$$

Equation (11) gives the rate of flow of electromagnetic energy across the boundary of the fixed volume of space and (12) shows how the rate of change in the total momentum inside the boundary is related with the electromagnetic stresses at its surface. The electromagnetic energy momentum tensor in free space is given as

$$E_\lambda^\sigma = -F^{\sigma\alpha} F_{\lambda\alpha} + \frac{1}{4} \delta_\lambda^\sigma F^{\alpha\beta} F_{\alpha\beta}. \tag{14}$$

Here $F_{\lambda\mu}$ is defined in terms of 4-potential vector A_λ as

$$F_{\lambda\mu} = A_{\lambda,\mu} - A_{\mu,\lambda}. \tag{15}$$

Consequently, by virtue of (8) and (9) the electromagnetic energy momentum tensor K_λ^σ in space filled with matter is related to E_λ^σ as follows:

$$K_\lambda^\sigma = \Phi^2 E_\lambda^\sigma. \tag{16}$$

Therefore, the Einstein–Maxwell field equations may be modified from the principle of stationary action

$$\delta \int \sqrt{-g} (R + k\Phi F_{\lambda\mu} H^{\lambda\mu} + l\Phi_\lambda \Phi^\lambda) d^4x \tag{17}$$

as follows:

$$R_{\lambda\mu} - \frac{1}{2} R g_{\lambda\mu} = 2k K_{\lambda\mu} - l(\Phi_\lambda \Phi_\mu - \frac{1}{2} g_{\lambda\mu} \Phi_\alpha \Phi^\alpha) \tag{18a}$$

and

$$\Box \Phi = \frac{k}{l} F_{\lambda\mu} H^{\lambda\mu}. \tag{18b}$$

Here, k and l are arbitrary constants and the covariant d'Alembertian $\Box$ is defined to be a covariant divergence of Φ^α, where covariant $\Phi_\alpha = \frac{\partial \Phi}{\partial x^\alpha}$.

3. An axially symmetric solution

In cylindrical polar coordinates (ϱ, φ, z, t) we take the axially symmetric metric [4]:

$$ds^2 = -e^{2(\alpha-\beta)}(d\varrho^2 + dz^2) - \varrho^2 e^{-2\beta} d\varphi^2 + e^{2\beta} dt^2, \tag{19}$$

where α and β are functions of ϱ and z only. If we define the electromagnetic 4-potential vector A_λ as

$$A_\lambda = (0, \epsilon, 0, \xi), \tag{20}$$

then from (15), the only non-vanishing components of $F_{\lambda\mu}$ are

$$F_{12} = -\epsilon_1, \quad F_{23} = \epsilon_3, \quad F_{14} = -\xi_1, \quad F_{34} = -\xi_3. \tag{21}$$

Throughout this section the lower suffixes 1 and 3 after a function indicate partial differentiation with respect to ϱ and z, respectively. Now for the metric (19) the field equations (18) with the help of (14), (16) and (21) can be recast in the form as follows:

$$\beta_1^2 - \beta_3^2 - \frac{\alpha_1}{\varrho} = k\Phi^2 \left[\frac{\epsilon_1^2 - \epsilon_3^2}{\varrho^2 e^{-2\beta}} - \frac{\xi_1^2 - \xi_3^2}{e^2\beta}\right] - \frac{l}{2}(\Phi_1^2 - \Phi_3^2), \tag{22}$$

$$\alpha_{11} + \alpha_{33} + \beta_1^2 + \beta_3^2 = -k\Phi^2 \left[\frac{\epsilon_1^2 + \epsilon_3^2}{\varrho^2 e^{-2\beta}} + \frac{\xi_1^2 + \xi_3^2}{e^2\beta}\right] - \frac{l}{2}(\Phi_1^2 + \Phi_3^2), \tag{23}$$

$$\alpha_{11} + \alpha_{33} + \beta_1^2 + \beta_3^2 - 2\nabla\beta = k\Phi^2 \left[\frac{\epsilon_1^2 + \epsilon_3^2}{\varrho^2 e^{-2\beta}} + \frac{\xi_1^2 + \xi_3^2}{e^2\beta}\right] - \frac{l}{2}(\Phi_1^2 + \Phi_3^2), \tag{24}$$

$$\frac{\alpha_3}{\varrho} = 2\left\{\beta_1\beta_3 - k\Phi^2 \left[\frac{\epsilon_1\epsilon_3}{\varrho^2 e^{-2\beta}} - \frac{\xi_1\xi_3}{e^2\beta}\right] + \frac{l}{2}(\Phi_1\Phi_3\right\}, \tag{25}$$

$$\epsilon_1\xi_1 + \epsilon_3\xi_3 = 0, \tag{26}$$

$$\nabla\Phi = -\frac{k}{l}\Phi\left(\frac{\epsilon_1^2 + \epsilon_3^2}{\varrho^2 e^{-2\beta}} - \frac{\xi_1^2 + \xi_3^2}{e^2\beta}\right), \tag{27}$$

where

$$\nabla \equiv \frac{\partial^2}{\partial\varrho^2} + \frac{\partial^2}{\partial z^2} + \frac{1}{\varrho}\frac{\partial}{\partial\varrho}. \tag{28}$$

Also, from (10) and (21) we have

$$\epsilon_1\Phi_1 + \epsilon_3\Phi_3 = 0, \tag{29}$$

$$\xi_1\Phi_3 - \xi_3\Phi_1 = 0. \tag{30}$$

By virtue of (29) and (30) the Eq. (26) is identically satisfied. If we take

$$\nabla\Phi = 0, \tag{31}$$

then, from Eq. (27) we have

$$\frac{\epsilon_1^2+\epsilon_3^2}{\varrho^2 e^{-2\beta}} = \frac{\xi_1^2+\xi_3^2}{e^{2\beta}}. \tag{32}$$

From (31) we get

$$\Phi = 1 + m/r, \tag{33}$$

where m is an arbitrary constant and $r = (\varrho^2 + z^2)^{1/2}$. Making use of (33) in (29) and (30) we get

$$\rho\epsilon_1 + z\epsilon_3 = 0, \tag{34}$$

$$z\xi_1 - \rho\xi_3 = 0. \tag{35}$$

From (23), (24) and (32) we further have

$$\nabla\beta = -2k\Phi^2 \left(\frac{\xi_1^2+\xi_3^2}{e^{2\beta}}\right). \tag{36}$$

From (36) we obtain

$$\xi_1^2 + \xi_3^2 = \frac{e^2 r^2}{(m+k)^6}, \tag{37}$$

provided

$$\beta = -\log(1 + m/r) \tag{38}$$

and

$$k = -\frac{m^2}{2e^2}, \tag{39}$$

e being another arbitrary constant. From (35) and (37) we get

$$\xi_1 = \frac{e\rho}{(m+r)^3}, \quad \xi_3 = \frac{ez}{(m+r)^3}. \tag{40}$$

Now, from (32), (34) and (37) we obtain

$$\epsilon_1 = -\frac{e\rho z}{r^2(m+r)}, \quad \epsilon_3 = \frac{e\rho^2}{r^2(m+r)}. \tag{41}$$

By making use of the values of Φ, β, ξ_1, ξ_3, ϵ_1 and ϵ_3 from (33), (38), (40) and (41) in (22), (23) and (25) we get

$$\alpha_1 = \frac{lm^2}{2}\frac{\rho(\rho^2 - z^2)}{r^6}, \tag{42}$$

$$\alpha_{11} + \alpha_{33} = -\frac{lm^2}{2r^4}, \tag{43}$$

$$\alpha_3 = lm^2 \frac{\rho^2 z}{r^6}. \tag{44}$$

The equation (42) or (44), after integration gives

$$\alpha = -\frac{m^2\rho^2}{2r^4}, \tag{45}$$

provided $l = 2$. For the value of α so obtained Eq. (43) is identically satisfied. Therefore, making use of (38) and (45) in (19) we obtain

$$ds^2 = -\left(1+\frac{m}{r}\right)^2 \exp\left(-\frac{m^2\rho^2}{r^4}\right)(d\rho^2+dz^2) - \rho^2\left(1+\frac{m}{r}\right)^2 d\Phi^2 + \left(1+\frac{m}{r}\right)^{-2} dt^2.$$

This solution is an analogue of the Synge solution [4]. It is also worth noting that the difficulty, which comes in solving the Einstein–Maxwell field equations due to their non-linearity [5], is expected to be removed here.

Acknowledgement

The author wishes to express his sincere thanks to the Referee for his useful suggestions.

References

1. J. N. S. Kashyap, Jour. Math. Phys. Sci., *23*(3), 275, 1989.
2. R. H. Dicke, Rev. Mod. Phys., *29*(3), 363, 1957.
3. R. C. Tolman, Relativity, Thermodynamics and Cosmology, Oxford University Press, Oxford, 1934.
4. J. L. Synge, Relativity — The General Theory, North Holland Publishing Co. Amsterdam, pp. 312–316, 1960.
5. J. N. S. Kashyap, Acta Phys. Hung., *45*(4), 293, 1978.

Acta Physica Hungarica 73 (2–4), pp. 129-135 (1993)

THEORETICAL STUDIES OF THE OPTIMUM DESIGN CONSIDERATIONS IN RING DYE LASER

H. EL-KASHEF

Physics Department, Faculty of Science, Tanta University
Tanta, Egypt

(Received in revised form 12 January 1993)

The theoretical studies of the optimum geometrical design considerations in the ring resonator of the dye laser are studied. The position of the minimum waists and the range of stabilisation parameters using the optical matrices are calculated. The design considerations of the high passive stability, and low optical losses are discussed. Additionally, a single-mode, broad-band and low-loss ring laser resonator of length 600 mm, using a minimum number of optical elements is reported.

Introduction

The resonator is one of three important parts of laser construction beside the active medium and the pumping light source. Fundamentally, a ring laser resonator consists of three mirrors at least, where a coherent light wave is produced. This produced light will be amplified in laser material (active medium) by the induced emission. The optical components contained in the resonator and its geometrical design decide the qualitative and quantitative characteristics of the produced laser beam.

Continuous wave (cw) dye lasers [1,2], have mostly been evolved directly from earlier laboratory research instruments, their designs tend to remain complicated, and they can be difficult and tedious to operate. On the other hand, different designs of resonators are used [3–5]. Some of the most common shortcomings include the use of elaborate mechanical resonator structures that require exacting initial alignment and continuing realignments, complicated intracavity beam paths, which are often folded into several dimensions. In addition, these lasers [1–5] use very long four or five mirrors resonator. Introducing the elements of single mode selection (birefringent filter, thin and thick etalon), unidirectional device, scanning and astigmatism compensation elements, leads to very high losses, high costs and good passive stability cannot be achieved.

In this paper these common shortcomings are eliminated, and new features are added. Many original ideas are conceived and tested. Theoretical calculations are carried out for optimum design considerations, such as the correct waist size, enough place for the resonator internal elements, low optical losses, small circumference, freedom from astigmatism, broad-band, high passive stability and simple adjustment. All these advantages are assembled in a new design of ring dye laser cavity.

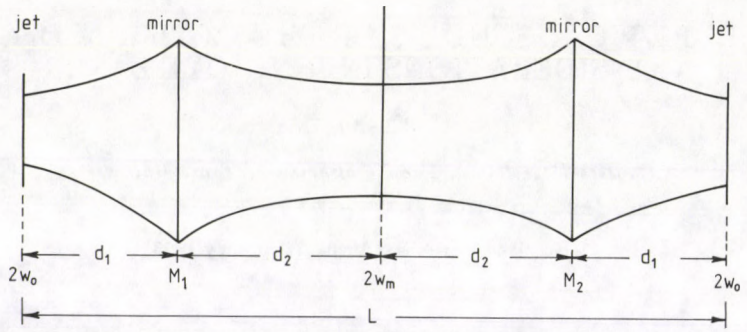

Fig. 1. The numerical values of the resonator: $w_0 = 15.4\ \mu$m, $w_m = 218.5\ \mu$m, $d_1 = 26.25$ mm and $d_2 = 27.5$ mm (The plane mirrors have no effect on the beam parameters)

Theoretical

The mathematical calculations which describe the laser beam in the simple resonator structure using optical matrices were studied [6]. We extend the calculations for more complicated active resonator structures.

The propagation of Gaussian beam is defined using the complex parameter q as follows [7]:

$$\frac{1}{q} = \frac{1}{R} - \frac{i\lambda}{\pi w^2}, \tag{1}$$

where w is a measure for the beam cross-section (beam waist), and R is a measure for the beam divergence (radius of the wavefront). The ring resonator is a periodic sequence of optical systems. The elements of ABCD matrix of this system can be used to calculate the mode parameters of the resonator. One uses the ABCD law [7] and postulates self-consistency by putting $q_1 = q_2 = q$. One has

$$q_1 = q_2 = q = \frac{Aq + B}{Cq + D}.$$

The roots of the resulting quadratic equation are:

$$\frac{1}{q} = \frac{D - A}{2B} \pm \frac{i}{2B}\sqrt{4 - (A + D)^2}, \tag{2}$$

which yields stable periodic sequences when the trace $(A + D)$ obeys the inequality:

$$(A + D)^2 \leq 4, \quad -2 \leq A + D \leq 2. \tag{3}$$

As shown in Fig. 1, the resonator is divided at the middle of the jet (the jet represents only an optical pathlength in condensed medium) into two symmetrical parts. It could be considered as the sum of two distances in air, one with optical pathlength $2d_1$ between the spherical mirrors. The rest of the pathlength is $2d_2$. This means that $2d_1 + 2d_2 = L$, where L is the circumference. The spherical mirror will act as a lens of focal length $f = R/2$. From the condition of symmetry the minimum of beam expansion is w_0 in the middle of the jet (see Fig. 1) and oppositely to w_m in the resonator. The total matrix of the resonator at the selected position in the jet is:

$$M = \begin{pmatrix} A & B \\ C & D \end{pmatrix}, \tag{4}$$

where

$$A = D = 2\left(1 - \frac{d_1}{f}\right) \cdot \left(1 - \frac{d_2}{f}\right) - 1,$$

$$B = -2f\left(1 - \frac{d_1}{f}\right)^2 \cdot \left(1 - \frac{d_2}{f}\right) - 2f\left(1 - \frac{d_1}{f}\right),$$

$$C = -\frac{2}{f}\left(1 - \frac{d_2}{f}\right).$$

The stability criterion of Eq. (3) gives the condition for d_1:

$$d_{\min} \leq d_1 \leq d_{\max} \tag{5}$$

where $d_{\min} = f$, $d_{\max} = \frac{f d_2}{d_2 - f}$. For d_1 inside the stability range, one can calculate the size of the beam in the jet by comparing Eqs (1), (2):

$$\frac{1}{q} = \frac{1}{R} - \frac{i\lambda}{\pi w_0^2} = \frac{D - A}{2B} \pm \frac{i}{2B}\sqrt{4 - (A + D)^2}. \tag{6}$$

Since $A = D$ and q is imaginary, this means $1/R = 0$. By exact observation one can put the matrix as a function of d_1, $d_{\max}$ and $d_{\min}$:

$$M = \begin{pmatrix} A & B \\ C & D \end{pmatrix}, \tag{7}$$

$$A = D = \frac{(d_1 - d_{\min}) - (d_{\max} - d_1)}{(d_{\max} - d_{\min})},$$

$$B = -2\frac{(d_{\max} - d_1) \cdot (d_1 - d_{\min})}{(d_{\max} - d_{\min})},$$

$$C = -2\frac{1}{(d_{\max} - d_{\min})},$$

$$d_{\max} - d_{\min} = \frac{f^2}{d_2 - f},$$

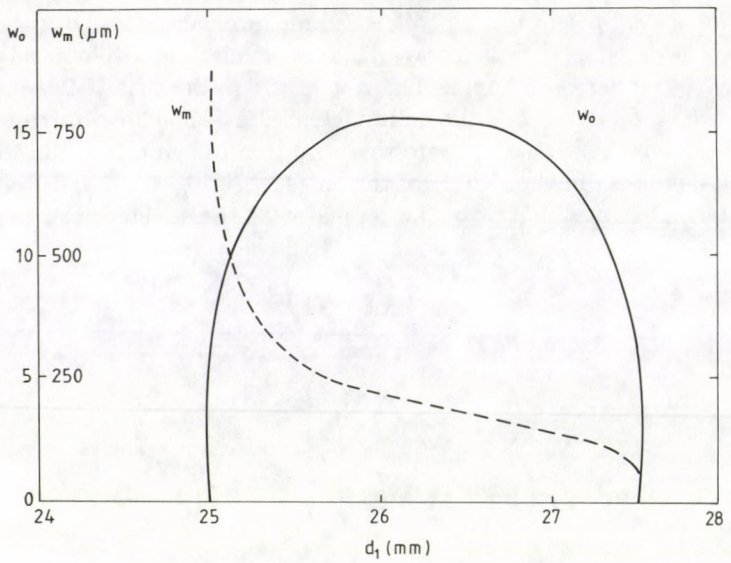

Fig. 2. The values of the beam waist w_0, w_m in μm as a function of the mirror separations ($f = d_{\min} = 25$ mm, $d_{\max} = 27.5$ mm, and $\lambda = 600$ nm)

then the beam radius in the jet:

$$w_0^4 = \frac{\lambda^2}{\pi^2}(d_1 - d_{\min})(d_{\max} - d_1). \tag{8}$$

The calculation of the beam parameter q_m at a position opposite to the jet in the resonator is similarly carried out, where $d_1 \cdot d_2$ will be changed, and still $A = D$. This gives the waist at this position:

$$w_m^4 = \frac{\lambda^2}{\pi^2}(d_2 - \overline{d_{\min}}) \cdot (\overline{d_{\max}} - d_2), \tag{9}$$

with

$$\overline{d_{\min}} = f = d_{\min}, \quad \overline{d_{\max}} = \frac{d_2 f}{d_2 - f},$$

therefore and dependent on d_1, $d_{\min}$ and $d_{\max}$,

$$w_m^4 = \frac{\lambda^2}{\pi^2} \frac{d_{\min}^4}{(d_{\max} - d_{\min})^2} \frac{d_{\max} - d_1}{(d_1 - d_{\min})}. \tag{10}$$

Figure 2 represents the dependence of waist size on d_1($f = 25$ mm, $d_{\min} = 25$ mm, $d_{\max} = 27.5$ and $L = 600$ mm) in the middle of the stability range, i.e. for

$$d_1 = \frac{d_{\max} + d_{\min}}{2},$$

or

$$d_{\max} - d_1 = d_1 - d_{\min},$$

then

$$w_m^2 = \frac{\lambda}{\pi} \frac{d_{\min}^2}{(d_{\max} - d_{\min})}, \tag{11}$$

when $d \gg f$, then in the first approximation:

$$d_{\max} - d_{\min} = \frac{f^2}{d_2 - f} \approx \frac{f^2}{d_2} \tag{12}$$

and

$$d_{\max} - d_{\min} \approx 2f + \frac{f^2}{d_2}, \tag{13}$$

then for w_m:

$$w_m^2 \approx \frac{\lambda}{\pi} \cdot d_2, \tag{14}$$

and for w_0:

$$w_0^2 \approx \frac{\lambda}{\pi} \frac{f^2}{2d_2}. \tag{15}$$

The arrangement of Fig. 1 as treated previously is a simplified model which can be applied for all resonators. It consists of two spherical mirrors (one minimum waist) and any suggested numbers of plane mirrors. This is accepted for most commercial lasers and many lasers developed in the institutes of research, for example [1–5].

Experimental results and discussion

As a result of the previous calculations and experimental studies the optimum geometrical construction of the ring cavity leads to a new design shown in Fig. 3.

The developed cavity is compact in size ($L = 600$ mm). This leads to an easy selection of the single mode operation, where the laser modes are separated by a distance $c/L = 500$ MHz, c being the velocity of light. The other developed lasers [1–5] have long resonators of more than 1250 mm. This cavity consists of a minimum number of frequency selective elements necessary for obtaining highly efficient single mode operation:

(i) The cavity is used in addition to the Lyot filter (three quartz crystal plates of thickness ratio 1:4:16), a new development of Mach–Zehnder Interferometer

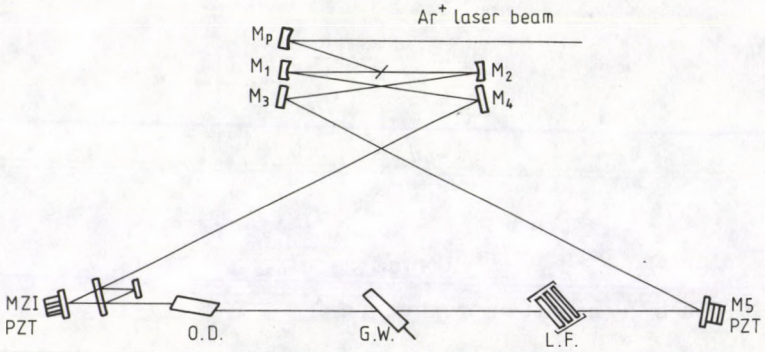

Fig. 3. The new design of ring resonator. M_p: pumping mirror, M_1–M_2: spherical mirrors. M_3–M_5: plane mirrors O.D.: optical diode, L.F.: Lyot filter, G.W.: glass wedge, MZI: Mach–Zehnder Interferometer (two plane mirrors and 50 % beam splitter)

(MZI) with a free spectral range = 42.5 GHz for single mode selection and tuning [8]. This MZI is placed in the corner of the cavity instead of one mirror. The incident angle of the laser beam on MZI is 15°, which makes it broad-band etalon. The experimental results showed that it caused losses of less than 0.5 %. The references lasers [1–5] used two etalons, thin and PZT driven thick etalon for laser frequency selection and tuning, which leads to high losses and complicated alignment.

(ii) The incident angle on the spherical mirrors is about 3.5°. This is carried out by using two plane mirrors M3, M4 beside the spherical mirrors, which eliminates the astigmatism with more than 95 % without inserting astigmatism compensation rhombs of certain length inside the cavity as in the other lasers [1–5].

(iii) In this cavity a glass wedge of thickness 4.5 mm and wedge angle of 0.5° is used to extend the scanning range of the cavity up to 50 GHz. This wedge is placed on a micrometer displacement table. The other lasers [1–5] used dual galvo plates with a scan range of about 30 GHz.

(iv) This cavity used a new development of optical diode for achieving one directional beam independent of wavelength [9]. It caused losses of 0.24 % at λ = 589.3 nm. The others [1–5] consist of two or more separated optical parts for this aim which add more complications in the adjustment and also high losses.

(v) This cavity used a plane mirror PZT translator for laser frequency tuning while the others used a spherical PZT mirror translator, which makes disturbance by cavity scanning.

(vi) In this cavity the beam displacement due to the insertion of optical elements are self compensated, where the beam displacement caused by the optical diode is fully compensated by that caused by the Lyot filter and glass wedge. This

leads to only 0.054 mm beam displacement when all the elements responsible for single mode selection are introduced to the cavity.

(vii) The cavity is symmetric in construction and consists of an even number of resonator mirrors which leads to a small deviation angle on all mirrors and accordingly high reflectivity and broad band.

(viii) The laser resonator and the single mode elements are built on a granite stone plate (100 × 28 cm), used efficiently for acoustic isolation between the components.

Conclusion

The calculated optimum design considerations lead to the optimum selection of the optical elements and their separations. The new cavity construction eliminates many highly expensive optical elements which cause high losses and many adjustment complications. This eliminates many holders and reduces accordingly mechanical and acoustic vibrations to a minimum. Simple efficient single mode operation is obtained using Lyot filter and MZI. Among others the characteristics of the cavity are: compactness in size, freedom from astigmatism and high passive stability.

References

1. T. F. Johnston, Jr, R. H. Brady and W. Proffitt, Appl. Opt., *214*, (13), 2307, 1982.
2. D. M. Kane and M. H. Dunn, Opt. Commun., *48*, (5), 295, 1984.
3. J. C. Bergquist and Lee Burkins, Opt. Commun., *50*, (6), 379, 1984.
4. C. R. Pollock, J. Kasper, G. K. Ernst, W. E. Ernst, S. Blit and F. K. Tittel, Appl. Opt., *18*, (12), 1907, 1979.
5. H. W. Schroder, L. Stein, D. Frolich, B. Fugger and H. Welling, Appl. Phys., *14*, 377, 1977.
6. H. Kogelnik and T. Li, IEEE, *54*, (10), 1312, 1966.
7. A. E. Siegman, An Introduction to Lasers and Masers, McGraw Hill Book Comp., New York, 1971.
8. H. El-Kashef and G. E. Hassan, J. Mod. Opt., *39*, (1), 43, 1992.
9. H. El-Kashef and G. E. Hassan, Delta Journal of Science *16*, (2), 50, 1992.

Acta Physica Hungarica 73 (2–4), pp. 137-151 (1993)

UNIFIED DESCRIPTION OF THE EQUILIBRIUM OF UNIFORMLY, SLOWLY ROTATING POLYTROPES

J. P. SHARMA and R. B. YADAV*

Department of Applied Sciences, M. M. M. Engineering College
Gorakhpur (U.P.), India

(Received 20 April 1993)

Using an approximation technique, we have considered a unified description of the equilibrium structure of slowly rotating polytropes of index 1 in Newtonian theory governed by the equation of state P = constant ρ^{γ}. Approximate analytical solutions to the equilibrium equations have been presented in different phase planes. Graphical material shows a comparative study of the runs of U_Θ with V_Θ (Fig. 1), U_P with V_P (Fig. 2), U_ρ with V_ρ (Fig. 3) and Θ with ξ_Θ (Fig. 4) between rotating (angular velocity $W = 0.05$ and 0.15) and non-rotating ($W = 0$) configurations. Transformations connecting solutions in these phase planes have been obtained. Other physical properties of the configurations are described in terms of the solutions of the structure equation.

1. Introduction

The importance of the effects of rotation on a self-gravitating body obeying a polytropic equation of state of the form $P = K\rho^{1+\frac{1}{n}}$ (K and n are the two disposable constants) is well known, as for example, rotation brings about changes in physical structure and the shape of the body. Considerable amount of work has been done by several eminent authors in Newtonian theory (for example, Jeans [1, 2]; Chandrasekhar [3]; Chandrasekhar et al [4]; Roberts [5]; James [6]; Monaghan et al [7]; Cunningham [8]; Carl J. Hansen et al [9]; Sharma et al [10]) as well as in general relativity theory (GRT) (for example, Hartle [11]; Hartle et al [12]; Hartle [13, 14]; Hartle et al [15, 16]) to study the structure and stability of various forms (for example, ellipsoidal, spheroidal, cylindrical and rings) that a self-gravitating body may take due to rotation. In case of slow or rapid rotation most of the authors have experienced considerable difficulties in solving the structure equations by known numerical methods (variational or perturbation analysis, R.K. method, etc.) until quite recently (Sharma [17]) the rotational problem of highly rotating polytropes has been tackled by Pade' (2,2) approximation technique, as also used elsewhere (Sharma [18, 19]). In this method, we do not require to perform numerical integrations of the structure equations, instead, as given below, solutions are obtained in simple and compact form from which the desired parameters can be obtained directly. And further, computer programs are, however, not necessarily

* Working as a Research Assistant supported by a grant from CST (U.P.), Lucknow, India.

required, that is, calculations can be carried out even with the aid of an electronic pocket calculator. It seems, therefore, worth while to employ the present technique for solving the rotational, polytropic problem which may assist in eliminating the lengthy and cumbersome process of numerical integrations. The present technique would also be equally helpful for solving rapidly rotating polytropic problems.

In contrast to the previous works, we will present in Section 2 the structure equations in generalized form from which spheroidal, cylindrical and plane-symmetric cases can be easily obtained. Approximate analytical solutions for $\gamma = 2$ in (ξ_Θ, Θ), (V_Θ, U_Θ), (V_P, U_P) and (V_ρ, U_ρ) planes are given in Section 3. Section 4 presents the transformations connecting the solutions in these phase planes. Figures 1 to 4 represent a comparative study of the characteristic features of spheroidal, cylindrical, and plane-symmetric configurations rotating with small velocities $W = 0.05$ and 0.15. To test the reasonableness of our analytical technique, this is compared with its non-rotating counter part ($W = 0$ (solid curves)). Integral properties of the polytropes, and the physical significance of V_Θ, U_Θ, V_P, U_P and V_ρ, U_ρ variables is given in Section 5.

2. Generalized, polytropic structure equations

(i) Structure equation in (ξ_Θ, Θ) *phase plane*

The fundamental equations governing the structure of a polytropic configuration of index n rotating with angular velocity Ω can be expressed as

$$\frac{P}{\rho} = \nabla\phi + \frac{1}{2}\Omega^2\chi^2, \quad \chi^2 = x^2 + y^2, \tag{1}$$

$$P = K\rho^{1+\frac{1}{n}}, \tag{2}$$

$$\nabla^2\phi = -4\pi G\rho, \tag{3}$$

where P is the pressure, ρ the density, ϕ the gravitational potential, $\overline{\chi}$ the vectorial distance from the axis of rotation, K a constant, and G the gravitational constant (6.67×10^{-8} dynes cm^2/gm^2). If we introduce r as the distance from the centre of the polytrope, and define the dimensionless variables Θ, and ξ_Θ by the relation

$$\rho \equiv \rho_c\Theta^n;\ r \equiv \alpha_\Theta\xi_\Theta = \left[\frac{(n+1)K}{4\pi G}\rho_c^{\frac{1}{n}-1}\right]^{\frac{1}{2}}\xi_\Theta,\ W = \frac{\Omega^2}{2\pi G\rho_c}, \tag{4}$$

where ρ_c is the central density, then Eqs (1), (2) and (3) give

$$\frac{1}{\xi_0^N}\frac{d}{d\xi_\Theta}\left(\xi_\Theta^N\frac{d\Theta}{d\xi_\Theta}\right) = -\Theta^n + W, \quad \left(W = \frac{\Omega^2}{2\pi G\rho_c}\right), \tag{5}$$

which satisfies the boundary conditions

$$\Theta = 1, \quad \frac{d\Theta}{d\xi_\Theta} = 0 \quad \text{at} \quad \xi_\Theta = 0. \tag{6}$$

Equation (5) would describe a broad spectrum of polytropic configurations: $N = 2, 1$ and 0 represent, respectively, spheroidal, cylindrical, and plane-symmetric shapes. For non-zero values of W, it does not seem possible to obtain exact solutions of Eq. (5) and, as mentioned in the introductory part, one may then take resort to the numerical methods. Using Pade' (2,2) approximation technique, we present here approximate analytical solutions of this equation for small values of $W = 0.05$ and 0.15.

(ii) Arrangement of the solutions in (V_Θ, U_Θ) phase plane

As in non-rotating case [18], we shall discuss here briefly the arrangement of the solutions in the (V_Θ, U_Θ) plane. Consider the following two functions U_Θ and V_Θ defined as

$$U_\Theta = -\frac{\xi_\Theta(\Theta^n - W)}{\Theta'}, \quad V_\Theta = -\frac{\xi_\Theta \Theta'}{\Theta}, \tag{7}$$

where we have used dash ($'$) to denote differentiation with respect to ξ. The first order differential equation between V_Θ and U_Θ, equivalent to Eq. (5), can be obtained as follows:

Differentiating the first equation in (7) with respect to ξ_Θ, and making use of Eq. (5), we obtain

$$\frac{1}{U_\Theta}\frac{dU_\Theta}{d\xi_\Theta} = \frac{1}{\xi_\Theta}[(1+N) - U_\Theta - nfV_\Theta]; \quad f = \Theta^n/\Theta^n - W. \tag{8}$$

Similarly, from the second equation in (7), we have

$$\frac{1}{V_\Theta}\frac{dV_\Theta}{d\xi_\Theta} = \frac{1}{\xi_\Theta}[(1-N) + U_\Theta + V_\Theta]. \tag{9}$$

Combining Eqs (8) and (9), we have

$$\frac{V_\Theta}{U_\Theta}\frac{dU_\Theta}{dV_\Theta} = -\left[\frac{U_\Theta + nfV_\Theta - (1+N)}{U_\Theta + V_\Theta + (1-N)}\right]. \tag{10}$$

Non-rotating case ([20]) can be obtained by putting $W = 0$. Unlike the non-rotating case, it is not possible to express the derivative $\frac{dU_\Theta}{dV_\Theta}$ (or dV_Θ/dU_Θ) solely in terms of U_Θ and V_Θ. We may find that $U_\Theta \to 1 + N$, $V_\Theta \to 0$ as $\xi_\Theta \to 0$.

(iii) Discussion in (V_P, U_P) plane

Equations (1), (2) and (3) enable us to write the generalized equation in (ξ_P, P) plane in the form

$$\frac{1}{\xi_P^N}\frac{d}{d\xi_P}\left(\xi_P^N P^{-\frac{n}{n+1}}\frac{dP}{d\xi_P}\right) = -P^{\frac{n}{n+1}} + \sigma W, \tag{11}$$

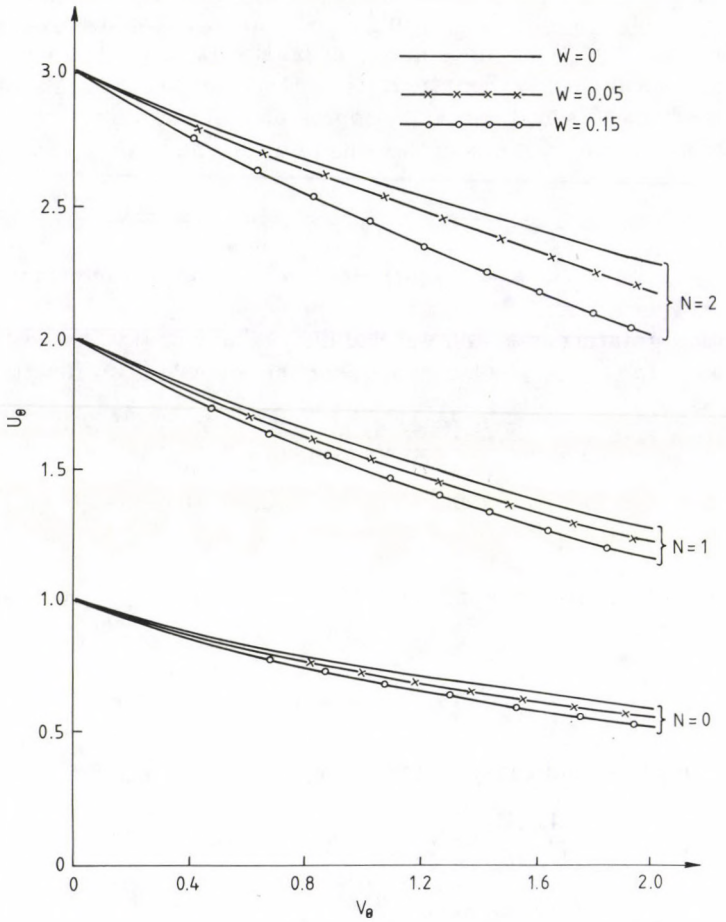

Fig. 1. Runs of U_Θ with V_Θ for slowly rotating $N = 0, 1$ and 2 configurations of polytropic index 1. Solid curves (–) represent non-rotating configurations

where

$$r \equiv \alpha_P \xi_P \equiv \frac{K^{\frac{n}{n+1}}}{2\sqrt{\pi G}} \xi_P;\ \rho = \rho_c \Theta^n;\ \sigma = \rho_c K^{\frac{n}{n+1}}. \tag{12}$$

Let the variables U_P and V_P be defined by

$$U_P = -\frac{\xi_P \left(P^{\frac{2n}{n+1}} - \sigma P^{\frac{n}{n+1}} W \right)}{P'}, \quad V_P = -\frac{\xi_P P'}{P}. \tag{13}$$

Proceeding as above in para (ii), we obtain the generalized first-order differential

equation between V_P and U_P in the form

$$\frac{V_P}{U_P}\frac{dU_P}{dV_P} = -\frac{U_P + f_1 V_P - (1+N)}{U_P + \delta V_P + (1-N)}, \tag{14}$$

$$\delta = \frac{1}{n+1}, \quad f_1 = \left(\frac{n}{n+1}\right)\left(\frac{P^{\frac{n}{n+1}}}{P^{\frac{n}{n+1}} - \sigma W}\right).$$

We may find that $U_P \to (1+N)$, $V_P \to 0$ as $\xi_P \to 0$.

(iv) Discussion in (V_ρ, U_ρ) plane

As in the preceding sections (ii) and (iii), making use of Eqs (1), (2) and (3), the generalized equation in (ξ_ρ, ρ) plane can be expressed as

$$\frac{1}{\xi_\rho^N}\frac{d}{d\xi_\rho}\left(\xi_\rho^N \rho^{\frac{1}{n}-1}\frac{d\rho}{d\xi_\rho}\right) = -\rho + \rho_c W, \tag{15}$$

where

$$r \equiv \alpha_\rho \xi_\rho \equiv \left[\frac{K(n+1)}{4\pi n G}\right]^{\frac{1}{2}} \xi_\rho. \tag{16}$$

Assume that

$$U_\rho = -\frac{\xi_\rho(\rho^{2-\frac{1}{n}} - \rho_c \rho^{1-\frac{1}{n}} W)}{\rho'}, \quad V_\rho = -\frac{\xi_\rho \rho'}{\rho}, \tag{17}$$

then, after differentiations of U_ρ and V_ρ with respect to ξ_ρ, and making certain simplifications, we obtain the following first-order differential equation, equivalent to (5), in the form

$$\frac{V_\rho}{U_\rho}\frac{dU_\rho}{dV_\rho} = -\frac{U_\rho + f_2 V_\rho - (1+N)}{U_\rho + \beta V_\rho + (1-N)}, \tag{18}$$

$$f_2 = \rho/\rho - \rho_c W; \quad \beta = \frac{1}{n}.$$

Near the origin $(\xi_\rho \to 0)$ $U_\rho \to 1+N$, $V_\rho \to 0$.

(v) First-order differential equations in (Z_Θ, y_Θ), (Z_P, y_P) and (Z_ρ, y_ρ) planes

We define the new variables z_Θ and y_Θ by

$$z_\Theta = \log\{n(\Theta^n - W)\} + 2\log\xi_\Theta, \; y_\Theta = \frac{dz_\Theta}{dt_\Theta}, \; \xi_\Theta = e^{-t_\Theta}. \tag{19}$$

Then, after some simplifications, Eq. (5) reduces to the first-order differential equation

$$\left[y_\Theta \frac{dy_\Theta}{dz_\Theta} + (1-N)y_\Theta + 2(1-N) - f_3(\Theta, y_\Theta)\right] f_4(\Theta) + e^{z_\Theta} = 0, \tag{20}$$

where

$$f_3(\Theta, y_\Theta) = \left[\frac{(1-\frac{1}{n})(\Theta^n - W)}{\Theta^n} - 1\right](y_\Theta + 2)^2; \; f_4(\Theta) = \frac{\Theta^n - W}{\Theta^{n-1}}.$$

We may find that $f_3(\Theta, y_\Theta) \to 0$, $f_4(\Theta) \to 1$ (near the origin) as $n \to \infty$ and $W = 0$. This leads to give our previous result [17] for the isothermal spheroidal configuration. If we further define

$$(i) \quad Z_P = \xi_P^{-m} P; \quad \xi_P = e^{-t_P}, \quad m = -2,$$

$$(ii) \quad y_P = \frac{dZ_P}{dt_P} = -\xi_P^{-m+1} \frac{dP}{d\xi_P} + mZ_P, \tag{21}$$

and

$$Z_\rho = \xi_\rho^{-m} \rho; \quad \xi_\rho = e^{-t_\rho}, \quad m = -2,$$

$$y_\rho = \frac{dZ_\rho}{dt_\rho} = -\xi_\rho^{-m+1} \frac{d\rho}{\xi_\rho} + mZ_\rho, \tag{22}$$

then Eqs (11) and (15) reduce to the first-order differential equations

$$y_P \frac{dy_P}{dz_P} + (1-m)y_P + (m-1)Wz_P - \frac{n}{n+1} z_P^{-1} y_P^2 + W\left(1 - \frac{n}{n+1}\right)(Wz_P - 2y_P)$$
$$+ f_5(\xi_P, z_P) - \sigma w f_6(\xi_P, z_P) = 0, \tag{23}$$

where

$$f_5(\xi_P, z_P) = \xi_P^{\frac{2-W}{n+1}} Z^{\frac{2n}{n+1}}; \quad f_6(\xi_P, Z_P) = \xi_P^{\frac{W_n}{n+1}} Z_P^{\frac{n}{n+1}}$$

and

$$y_\rho \frac{dy_\rho}{dZ_\rho} + (1-m)y_\rho + (m-1)WZ_\rho + W^2 Z_\rho + \tag{24}$$
$$- f_7(\xi_\rho, Z_\rho)(W^2 Z_\rho^2 + y_\rho^2 - 2WZ_\rho y_\rho) - 2Wy_\rho + Z_\rho f_8(\xi_\rho, Z_\rho) = 0,$$

where

$$f_7(\xi_\rho, Z_\rho) = \frac{(1-\frac{1}{n})}{Z_\rho + \rho_c w \xi_\rho^W},$$

$$f_8(\xi_\rho, Z_\rho) = \xi_\rho^2 (\xi^W Z_\rho + \rho_c w)^{1-\frac{1}{n}}.$$

We note, for $n \to \infty$ and $W \to 0$ we revert to our previous results for static, isothermal, spherical configuration ($N = 2$) [17].

3. Solutions for $\gamma = 2$

(i) Approximate analytical solutions of Eq. (10)

We assume a series expansion of the form

$$U_\Theta = (1+N) + a_\Theta V_\Theta + b_\Theta V_\Theta^2 + c_\Theta V_\Theta^3 + d_\Theta V_\Theta^4 + \ldots \tag{25}$$

which satisfies the initial conditions $U_\Theta \to (1+N)$, $V_\Theta \to 0$ as $\xi_\Theta \to 0$ (Section 2 (ii)). By the usual procedure, we determine the coefficients a_Θ, b_Θ, c_Θ, d_Θ, ..., successively with the help of Eq. (10). Finally, we obtain the desired solution in the form of rational function (Pade' (2,2) approximant):

$$U_\Theta(2,2) = (1+N)\frac{1 + A_\Theta V_\Theta + B_\Theta V_\Theta^2}{1 + C_\Theta V_\Theta + D_\Theta V_\Theta^2}, \tag{26}$$

where

$$A_\Theta = \frac{1}{(1+N)} a_\Theta + C_\Theta, \quad B_\Theta = \frac{1}{(1+N)}(b_\Theta + a_\Theta C_\Theta) + D_\Theta,$$
$$C_\Theta = \frac{a_\Theta d_\Theta - b_\Theta c_\Theta}{\Delta_\Theta}, \quad D_\Theta = \frac{c_\Theta^2 - b_\Theta d_\Theta}{\Delta_\Theta},$$
$$\Delta_\Theta = b_\Theta^2 - a_\Theta c_\Theta.$$

Note the physical significance of variables (V_Θ, U_Θ) as given in Section 3 (i). Figure 1 provides a comparative study of the variation of physical variable U_Θ with V_Θ for $N = 2, 1$ and 0 configurations rotating with small angular velocity $W = 0.05$ and 0.15. U_Θ is a monotonic decreasing function of V_Θ, and it decreases somewhat faster for $N = 2$ configuration than for $N = 1$ and $N = 0$ configurations. The value of U_Θ decreases as the angular velocity W increases, and it has larger values for $N = 2$ configuration than for $N = 1$ and $N = 0$ configurations. Static $N = 2, 1$ and 0 configurations as shown by solid curves (–) have somewhat larger values of U_Θ than their rotating counterparts.

(ii) Approximate analytical solutions of Eqs (5), (14) and (18)

Corresponding to Eqs (5) (14) and (18), we assume the following series expansions

$$\Theta = 1 + a_\Theta^* \xi_\Theta^2 + b_\Theta^* \xi_\Theta^4 + c_\Theta^* \xi_\Theta^6 + d_\Theta^* \xi_\Theta^8 + \ldots \ (\xi_\Theta \to 0), \tag{27}$$

$$U_P = (1+N) + a_P V_P + b_P V_P^2 + c_P V_P^3 + d_P V_P^4 + \ldots \ (\xi_P \to 0) \tag{28}$$

and

$$U_\rho = (1+N) + a_\rho V_\rho + b_\rho V_\rho^2 + c_\rho V_\rho^3 + d_\rho V_\rho^4 + \ldots \ (\xi_\rho \to 0), \tag{29}$$

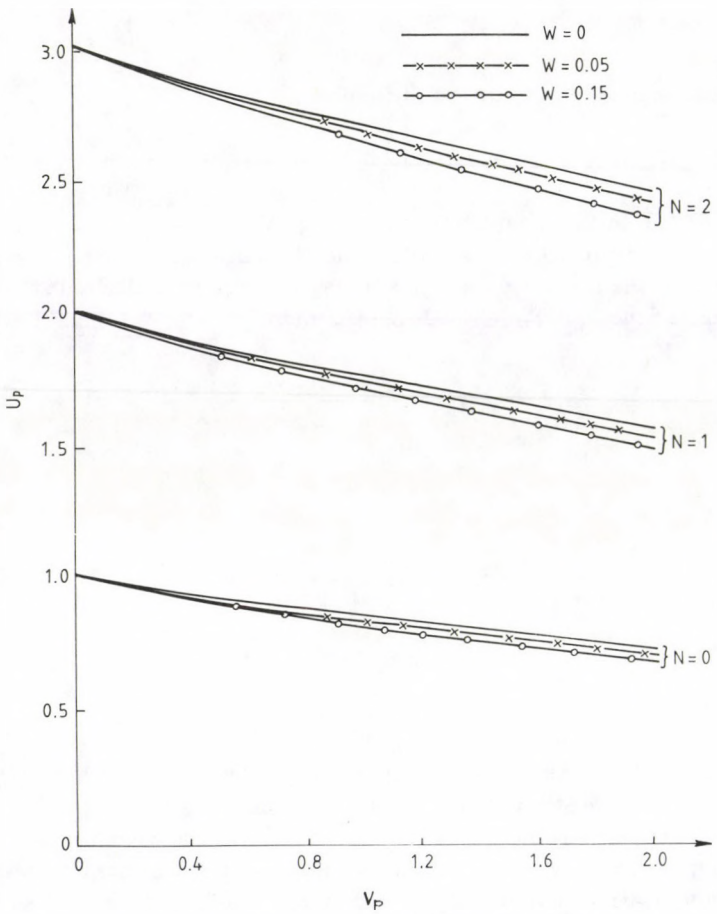

Fig. 2. Runs of U_P with V_P for slowly rotating $N = 0, 1$ and 2 configurations of polytropic index 1. Solid curves (–) represent non-rotating configurations

which satisfy the initial conditions: $\Theta \to 1$, $\xi_\Theta \to 0$; $U_P \to (1+N)$, $V_P \to 0$; and $U_\rho \to (1+N)$, $V_\rho \to 0$, respectively. Values of the coefficients a^*_Θ, b^*_Θ, c^*_Θ, d^*_Θ; a_P, b_P, c_P, d_P; a_ρ, b_ρ, c_ρ, d_ρ are determined in a similar way as mentioned in Section 3. Approximate analytical solutions of Eqs (5), (14) and (18) are then given by

$$\Theta(2,2) = \frac{1 + A^*_\Theta \xi^2_\Theta + B^*_\Theta \xi^4_\Theta}{1 + C^*_\Theta \xi^2_\Theta + D^*_\Theta \xi^4_\Theta}, \tag{30}$$

$$U_P(2,2) = (1+N)\frac{1 + A_P V_P + B_P V_P^2}{1 + C_P V_P + D_P V_P^2}, \tag{31}$$

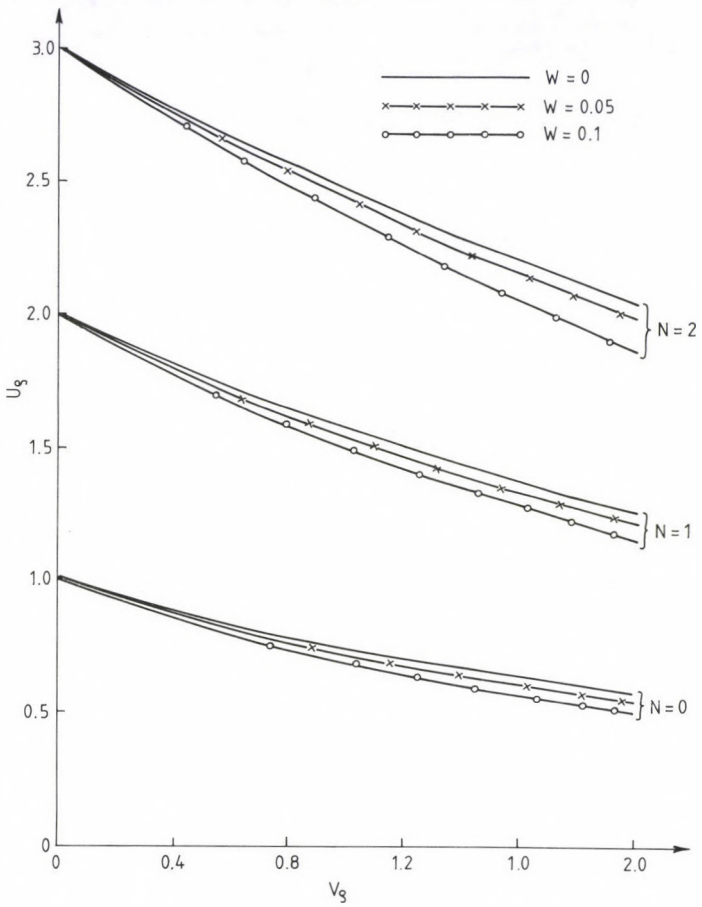

Fig. 3. Runs of U_ρ with V_ρ for slowly rotating $N = 0, 1$ and 2 configurations of polytropic index 1. Solid curves (–) represent non-rotating configurations

$$U_\rho(2,2) = (1+N)\frac{1 + A_\rho V_\rho + B_\rho V_\rho^2}{1 + C_\rho V_\rho + D_\rho V_\rho^2}. \tag{32}$$

Results of our calculations are displayed diagrammatically (Figs 2, 3, and 4) for two chosen values of angular velocity $W = 0.05$ and 0.15. For comparison, the non-rotating case ($W = 0$) is shown by solid curve (–). (V_P, U_P) curves in Fig. 2 show decreasing trends similar to Fig. 1. Values of U_P are somewhat higher than those of U_Θ. Other behaviours of (V_P, U_P) curves are similar to (V_Θ, U_Θ) curves (Fig. 1).

Decreasing trends in (V_ρ, U_ρ) curves for $N = 2, 1$ and 0 configurations have

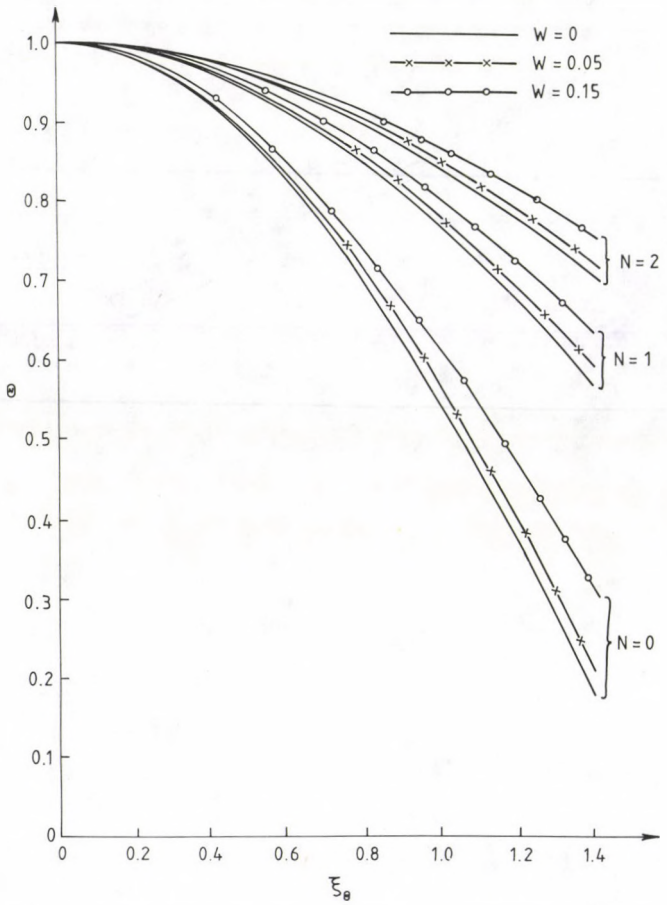

Fig. 4. Solution curves for slowly rotating $N = 0, 1$ and 2 configurations of polytropic index 1. Solid curves (–) represent non-rotating configurations

been noted as in Figs 1 and 2. Values of U_ρ are found to be smaller than those of U_P (Fig. 2) and U_Θ (Fig. 1). Other characteristic features of (V_ρ, U_ρ) curves are similar to (V_P, U_P) and (V_Θ, U_Θ) curves.

Figure 4 represents solution curves (ξ_Θ, Θ) for $N = 2, 1$ and 0 configurations. Figure 4 clearly indicates that the value of Θ increases as W increases, and possesses higher values for $N = 2$ configuration than for $N = 1$ and 0 configurations. Θ monotonically decreases as ξ increases, but it falls off more rapidly for $N = 0$ configuration than for $N = 1$ and $N = 2$ configurations.

Values of the coefficients A_P, B_P, C_P D_P; A_ρ, B_ρ, C_ρ, D_ρ; and A^*_Θ, B^*_Θ, C^*_Θ, D^*_Θ are given in Appendix A.

4. Transformations connecting the solutions in different phase planes

Dividing the first equation in (7) by the first equation in (13) and using the Eqs (2), (4) and (12), we find

$$U_\Theta = U_P. \tag{33}$$

From equations (4), (7) and (17) we have

$$U_\Theta = U_\rho. \tag{34}$$

Combining Eqs (33) and (34), we get

$$U_P = U_\rho. \tag{35}$$

Similarly, from the set of equations (2), (4), (7), (12), (13) and (4), (7), (16), (17) we derive that

$$V_\Theta = \frac{1}{n+1} V_P = \delta V_P; \quad \delta = (1/(n+1)), \tag{36}$$

and

$$V_\Theta = \beta V_\rho. \tag{37}$$

Hence, from the foregoing equations, we have

$$V_P = \gamma V_\rho; \quad \gamma = \beta/\delta. \tag{38}$$

Using equations (4), (12), (16), (19), (21) and (22), one may obtain the transformations connecting the solutions in (z_Θ, y_Θ), (z_P, y_P), and (z_ρ, y_ρ) planes.

5. Integral properties of the configurations and physical significance of (U_Θ, V_Θ), (U_P, V_P) and (U_ρ, V_ρ) variables

(a) Integral properties

Some of the important integral properties associated with the description of spheroidal, cylindrical, and plane-symmetric configurations are as follows:

1. Spheroidal configuration:

$$\text{Mass, } M = \int_v \rho \, dv, \tag{39}$$

which, with the help of Eq. (4), can be expressed as

$$M = 4\pi\alpha_\Theta^3 \rho_c \int_0^{\xi_\Theta} \xi_\Theta^2 \Theta^n d\xi_\Theta = 4\pi\alpha_\Theta^3 \rho_c |\xi_\Theta^2 \Theta'|. \tag{40}$$

$$\text{Internal energy, } U = \frac{1}{\gamma - 1} \int_v P dv. \tag{41}$$

Using Eqs (2) and (4) in Eq. (41), we obtain, after some simplifications,

$$U = \frac{4(n+1)\pi\alpha_\Theta^3 K \rho_c^{1+\frac{1}{n}}}{9(\gamma - 1)} \left[2\xi_{\Theta_1}^3 \Theta'^2(\xi_{\Theta 1}) - \int_0^{\xi_{\Theta_1}} \xi_{\Theta 1}^3 \Theta' \Theta'' d\xi \right]. \tag{42}$$

$$\text{Moment of inertia, } I = \int_v \rho dv \chi^2 = 4\pi\alpha_\Theta^3 \rho_c \chi^2 |\xi_\Theta^2 \Theta'(\xi_\Theta)|. \tag{43}$$

2. Cylindrical configuration:

$$\text{Mass, } M = \int_v \rho \, dv = 2\pi\alpha_\Theta^2 \rho_c |\xi_{\Theta 1} \Theta'|. \tag{44}$$

$$\text{Internal energy, } U = \frac{1}{\gamma - 1} \int_v P dv = \frac{(n+1)\pi K \alpha_\Theta^2 \rho_c^{1+\frac{1}{n}}}{2(\gamma - 1)} |\xi_{\Theta 1} \Theta'| 2. \tag{45}$$

$$\text{Moment of inertia, } I = \int_v \rho dv \chi^2 = 2\pi\alpha_\Theta^2 \rho_c \chi^2 |\xi_\Theta \Theta'|. \tag{46}$$

3. Plane-symmetric configuration:

$$\text{Mass, } M = \int_v \rho \, dv = 2\rho_c \alpha_\Theta |\Theta'|. \tag{47}$$

$$\text{Internal energy, } U = \frac{1}{\gamma - 1} \int_v P dv = \frac{2(n+1)\alpha_\Theta K \rho_c^{1+\frac{1}{n}}}{\gamma - 1} \int_0^{\xi_{\Theta 1}} \xi_\Theta \Theta' d(\Theta'). \tag{48}$$

$$\text{Moment of inertia, } I = 2 \int_v \rho dv \chi^2 = 2\rho_c \alpha_\Theta \chi^2 |\Theta'|. \tag{49}$$

In above expressions $\xi_{\Theta 1}$ denotes the value of ξ_Θ for which Θ vanishes.

(b) Physical significance of (V_Θ, U_Θ), (V_P, U_P) and (V_ρ, U_ρ) variables

The following expressions describe the physical significance of (V_Θ, U_Θ), (V_P, U_P) and (V_ρ, U_ρ) variables for spheroidal, cylindrical and plane-symmetric configurations:

1. Spheroidal configuration:

$$U_\Theta = -\frac{\xi_\Theta(\Theta^n - W)}{\Theta'} = \frac{3}{\overline{\rho}(\xi_\Theta)}\{\rho(\xi_\Theta) - \rho_c W\},$$

$$V_\Theta = -\frac{\xi_\Theta \Theta'}{\Theta} = \frac{1}{4\pi\alpha_\Theta^3 \rho^{1-\frac{1}{n}} \rho^{\frac{1}{n}}} \left\{\frac{M(\xi_\Theta)}{\xi_\Theta}\right\};$$

$$U_P = -\frac{\xi_P(P^{\frac{2n}{n+1}} - \sigma P^{\frac{n}{n+1}} W)}{P'} = \frac{3}{(n+1)\rho_c^{\frac{1}{n}-1} K^{\frac{1-n}{1+n}}} \left\{\frac{\rho(\xi_P) - \rho_c W}{\overline{\rho}(\xi_P)}\right\},$$

$$V_P = -\frac{\xi_P P'}{P} = \frac{(n+1)}{4\pi\alpha_P^3 \rho_c^{1-\frac{1}{n}} \rho^{\frac{1}{n}}} \left\{\frac{M(\xi_P)}{\xi_P}\right\};$$

$$U_\rho = -\frac{\xi_\rho(\rho^{2-\frac{1}{n}} - \rho_c \rho^{1-\frac{1}{n}} W)}{\rho'} = \frac{3}{n\rho^{\frac{1}{n}-1} \rho^{\frac{1}{n}}} \left\{\frac{\rho(\xi_\rho) - \rho_c W}{\overline{\rho}(\xi_\rho)}\right\},$$

$$V_\rho = -\frac{\xi_\rho \rho'}{\rho} = \frac{n}{4\pi\alpha_\rho^3 \rho_c^{1-\frac{1}{n}} \rho^{\frac{1}{n}}} \left\{\frac{M(\xi_\rho)}{\xi_\rho}\right\}.$$

2. Cylindrical configuration:

$$U_\Theta = -\frac{\xi_\Theta(\Theta^n - W)}{\Theta'} = \frac{2\{\rho(\xi_\Theta) - \rho_c W\}}{\overline{\rho}(\xi_\Theta)},$$

$$V_\Theta = -\frac{\xi_\Theta \Theta'}{\Theta} = \frac{1}{2\pi\alpha_\Theta^2 \rho_c^{1-\frac{1}{n}} \rho^{\frac{1}{n}}} M(\xi_\Theta);$$

$$U_P = -\frac{\xi_P\left(P^{\frac{2n}{n+1}} - \rho_c P^{\frac{n}{n+1}} K^{\frac{n}{n+1}} W\right)}{P'} = \frac{2}{(n+1)\rho_c^{1-\frac{1}{n}} K^{\frac{1-n}{1+n}}} \frac{\{\rho(\xi_P) - \rho_c W\}}{\overline{\rho}(\xi_P)},$$

$$V_P = -\frac{\xi_P P'}{P} = \frac{(n+1)}{2\pi\alpha_P^2 \rho_c^{1-\frac{1}{n}} \rho^{\frac{1}{n}}} M(\xi_P);$$

$$U_\rho = -\frac{\xi_\rho\left\{\rho^{2-\frac{1}{n}} - \rho_c \rho^{1-\frac{1}{n}} W\right\}}{\rho'} = \frac{2\{\rho(\xi_\rho) - \rho_c W\}}{n\rho_c^{\frac{1}{n}-1} - \overline{\rho}(\xi_\rho)},$$

$$V_\rho = -\frac{\xi_\rho \rho'}{\rho} = \frac{nM(\xi_\rho)}{2\pi\alpha_\rho^2 \rho_c^{1-\frac{1}{n}} \rho^{\frac{1}{n}}}.$$

3. Plane-symmetric configurations:

$$U_\Theta = -\frac{\xi_\Theta(\Theta^n - W)}{\Theta'} = \frac{1}{\overline{\rho}(\xi_\Theta)}\{\overline{\rho}(\xi_\Theta) - \rho_c W\},$$

$$V_\Theta = -\frac{\xi_\Theta \Theta'}{\Theta} = \frac{1}{2\alpha_\Theta \rho_c^{1-\frac{1}{n}} \rho^{\frac{1}{n}}} \left\{ \frac{M(\xi_\Theta)}{\xi_\Theta^{-1}} \right\};$$

$$U_P = -\frac{\xi_P (P^{\frac{2n}{n+1}} - \rho_c P^{\frac{n}{n+1}} K^{\frac{n}{n+1}} W)}{P'} = \frac{3}{(n+1)\rho_c^{\frac{1}{n}-1} K^{\frac{1-n}{1+n}}} \left\{ \frac{\rho(\xi_P) - \rho_c W}{\overline{\rho}(\xi_P)} \right\},$$

$$V_P = -\frac{\xi_P P'}{P} = \frac{(n+1)}{2\alpha_P \rho_c^{1-\frac{1}{n}} \rho^{\frac{1}{n}}} \left\{ \frac{M(\xi_P)}{\xi_P^{-1}} \right\};$$

$$U_\rho = -\frac{\xi_\rho (\rho^{2-\frac{1}{n}} - \rho_c \rho^{1-\frac{1}{n}} W)}{\rho'} = \frac{1}{n\rho_c^{\frac{1}{n}-1}} \left\{ \frac{\rho(\xi_\rho) - \rho_c W}{\overline{\rho}(\xi_\rho)} \right\},$$

$$V_\rho = -\frac{\xi_\rho \rho'}{\rho} = \frac{n}{2\alpha \rho_c^{1-\frac{1}{n}} \rho^{\frac{1}{n}}} \left\{ \frac{M(\xi_\rho)}{\xi_\rho^{-1}} \right\}.$$

Appendix A

From Eqs (27) and (30), the values of the coefficients A^*_Θ, B^*_Θ, C^*_Θ, D^*_Θ are found to be

$$\begin{aligned} &A^*_\Theta = a^*_\Theta + C^*_\Theta, \quad B^*_\Theta = b^*_\Theta + a^*_\Theta C^*_\Theta + D^*_\Theta, \\ &C^*_\Theta = (b^*_\Theta c^*_\Theta - a^*_\Theta d^*_\Theta)/\Delta_\Theta, \quad D^*_\Theta = (b^*_\Theta d^*_\Theta - c^{*2}_\Theta)/\Delta_\Theta; \\ &\Delta_\Theta = a^*_\Theta c^*_\Theta - b^{*2}_\Theta. \end{aligned} \tag{A1}$$

Similarly, from the set of equations (28), (31) and (29), (32), the values of the coefficients A_P, B_P, C_P, D_P; A_ρ, B_ρ, C_ρ, D_ρ are determined as

$$\begin{aligned} &A_P = (1+N)^{-1} a_P + C_P, \quad B_P = (1+N)^{-1}(b_P + a_P C_P) + D_P, \\ &C_P = \frac{a_P d_P - b_P c_P}{\Delta_P}, \quad D_P = \frac{c_P^2 - b_P d_P}{\Delta_P}, \\ &\Delta_P = b_P^2 - a_P c_P. \end{aligned} \tag{A2}$$

$$\begin{aligned} &A_\rho = (1+N)^{-1} a_\rho + C_\rho, \quad B_\rho = (1+N)^{-1}(b_\rho + a_\rho C_\rho) + D_\rho, \\ &C_\rho = \frac{(a_\rho d_\rho - b_\rho c_\rho)}{\Delta_\rho}, \quad D_\rho = \frac{(c_\rho^2 - b_\rho d_\rho)}{\Delta_\rho}, \\ &\Delta_\rho = b_\rho^2 - a_\rho c_\rho. \end{aligned} \tag{A3}$$

Acknowledgements

R. B. Yadav acknowledges useful discussions with Dr. J. P. Sharma under whose valuable guidance the present work has been completed. He is also thankful to C. S. T., U. P., Lucknow for providing financial assistance to the Research Project under which the work has been done.

References

1. J. H. Jeans, Phil. Trans. R. Soc., London, *213A*, 457, 1914.
2. J. H. Jeans, Astronomy and Cosmology (2nd ed.), Cambridge University Press, Cambridge, 1928.
3. S. Chandrasekhar, M. N., *93*, 390, 1933.
4. S. Chandrasekhar and N. R. Lebovitz, Ap. J., *136*, 1082, 1962.
5. P. H. Roberts, Ap. J., *138*, 809, 1963.
6. R. James, Ap. J. *140*, 552, 1964.
7. J. J. Monaghan and Ian W. Roxburgh, M. N. R. A. S., *131*, 1965.
8. C. T. Cunningham, Ap. J., *211*, 568, 1977.
9. Carl J. Hansen, L. Morris, Aizenman Randy and R. Rose, Ap. J., *207*, 736, 1976.
10. J. P. Sharma and R. B. Yadav, Jour. P. A. S., *1*, 95, 1990.
11. J. B. Hartle, Ap. J. *150*, 1005, 1967.
12. J. B. Hartle and K. S. Thorne, Ap. J., *153*, 807, 1968.
13. J. B. Hartle, Ap. J., *158*, 719, 1969.
14. J. B. Hartle, Ap. J., *161*, 111, 1970.
15. J. B. Hartle, K. S. Thorne and S. M. Chitre, Ap. J., *176*, 177, 1972.
16. J. B. Hartle and J. L. Friedman, Ap. J., *196*, 653, 1975.
17. J. P. Sharma and R. B. Yadav, Acta Phys. Hung., *72*(1), 55, 1992.
18. J. P. Sharma, D. Sc. Thesis, A Study of Some Problems of Stellar and Planetary Structures, University of Gorakhpur, Gorakhpur (U. P.), India, 1981.
19. J. P. Sharma, Ap. J., *329*, 232, 1988.
20. S. Chandrasekhar, An Introduction to the Study of Stellar Structure, Chicago University Press, Chicago, 1939.

Acta Physica Hungarica 73 (2-4), pp. 153-163 (1993)

LARMOR RADIUS EFFECT ON RAYLEIGH–TAYLOR INSTABILITY OF A PARTIALLY IONIZED PLASMA IN COMPOSITE MEDIUM

K. PRAKASH and S. MANCHANDA

Department of Mathematics, D. C. C., Himachal Pradesh University
Summer Hill, Shimla-171005, India

(Received 23 April 1993)

The simultaneous effects of finite ion Larmor radius (FLR) and collisions with neutral atoms are investigated on the stability of an infinitely conducting plasma of variable density in the presence of a horizontal magnetic field. The perturbations propagating along the ambient magnetic field are considered. It is established that, real part of n is negative, where n is the growth rate of disturbance, so that instability does not arise in the form of increasing amplitude, i.e. overstability. A variational principle is used to obtain an approximate solution of the problem. Further the case of two semi-infinitely extending plasmas of constant densities separated by a horizontal interface is considered. It is found that the system is stable (for some wave numbers) for potentially stable configuration and unstable (for other wave numbers) for potentially unstable configuration even if there are collisions with dust particles. Also criteria determining stability and instability are independent of FLR effects.

1. Introduction

A detailed treatment of Rayleigh–Taylor instability, together with the possible extensions in various domains of interest has been given by Chandrasekhar [1]. The finite ion Larmor radius (FLR) has individually been shown to have a stabilizing influence on thermal instability, thermosolutal instability and gravitational instability by several authors [2–8]. Melchior and Popowich [9] have considered the FLR effect on Kelvin–Helmholtz instability in a fully ionized plasma while that on Rayleigh–Taylor instability has been studied by Singh and Hans [10].

Quite often the plasma is not fully ionized and is, instead, partially ionized. A partially ionized plasma represents a state which often exists in the universe and there are several situations when the interaction between the ionized and neutral gas components becomes important in cosmic physics. Strömgren [11] has reported that ionized hydrogen is limited to certain rather sharply bounded regions in space surrounding, for example, O-type stars and clusters of such stars and that the gas outside these regions is essentially non-ionized. A stabilizing effect of collisionals on Rayleigh–Taylor configuration has been shown by Hans [12] and Bhatia [13]. But the collisional effects are found to be destabilizing for a sufficiently large collisional frequency on Kelvin–Helmholtz configuration by Rao and Kalra [14] and Hans [12].

In the present paper we study the simultaneous effects of ion Larmor radius and collisions with neutral atoms on the stability of well known Rayleigh–Taylor

configuration in hydromagnetics (Chandrasekhar [1]). We regard the medium as being a mixture of an infinitely conducting component and a neutral component interacting through mutual collisions. We make the assumptions that the individual components, by themselves, behave like continuum plasmas and that the effects on the neutral component resulting from magnetic field, pressure and gravity are negligible. The case of a uniform horizontal field and longitudinal perturbations is considered. Next, a variational principle is developed to obtain the approximate solutions.

2. Perturbation equations

The model we consider consists of two inviscid, homogeneous, semi-infinitely extending plasmas separated by a plane interface at $z = 0$, each region being permeated with a neutral component of the same density. Initially the configuration is at rest. We give a small disturbance to the system. The linearized perturbation equations for the mixture of the hydromagnetic plasma and a neutral gas moving together in a uniform horizontal magnetic field $\mathbf{H}(H, 0, 0)$ and downward gravitational field $\mathbf{g}(0, 0, -g)$ are

$$\rho \frac{\partial \mathbf{q}}{\partial t} = -\nabla \delta \overleftrightarrow{P} + \frac{1}{4\pi}(\nabla \times \mathbf{h}) \times \mathbf{H} + \mathbf{g}(\delta\rho) + \rho_d \nu_c (\mathbf{q}_d - \mathbf{q}), \tag{2.1}$$

$$\frac{\partial \mathbf{q}_d}{\partial t} = -\nu_c (\mathbf{q}_d - \mathbf{q}), \tag{2.2}$$

$$\frac{\partial}{\partial t}(\delta\rho) = (\mathbf{q} \cdot \nabla)\rho, \tag{2.3}$$

$$\frac{\partial \mathbf{h}}{\partial t} = (\mathbf{H} \cdot \nabla)\mathbf{q}, \tag{2.4}$$

$$\nabla \cdot \mathbf{q} = 0 \quad \text{and} \quad \nabla \cdot \mathbf{h} = 0, \tag{2.5}$$

where ρ and ρ_d are the unperturbed densities for the hydromagnetic and the neutral component, respectively. ν_c denotes the collisional frequency between the two components and $\overleftrightarrow{P}$ denotes the plasma pressure rendered tensorial due to finite ion Larmor radius effect. Here $\delta\rho$, $\delta\overleftrightarrow{P}$, $\mathbf{q}(u, v, w)$, $\mathbf{q}_d(l, r, s)$, $\mathbf{h}(h_x, h_y, h_z)$ denote, respectively, the perturbations in density ρ, stress tensor $\overleftrightarrow{P}$, hydromagnetic plasma velocity (initially zero), neutral component velocity (initially zero) and magnetic field $\mathbf{H}$. Magnetic permeability of the medium is assumed to be unity.

For the magnetic field along x-axis, $\delta\overleftrightarrow{P}$ taking into account the FLR effects has the following components:

$$P_{xx} = p, \quad P_{xy} = P_{yx} = -2\rho\nu \left(\frac{\partial w}{\partial x} + \frac{\partial u}{\partial z} \right),$$

$$
\begin{aligned}
P_{xz} &= P_{zx} = 2\rho\nu\left(\frac{\partial u}{\partial y} + \frac{\partial v}{\partial x}\right), \\
P_{yz} &= P_{zy} = \rho\nu\left(\frac{\partial v}{\partial y} - \frac{\partial w}{\partial z}\right), \\
P_{yy} &= p - \rho\nu\left(\frac{\partial v}{\partial z} + \frac{\partial w}{\partial y}\right), \\
P_{zz} &= p + \rho\nu\left(\frac{\partial v}{\partial z} + \frac{\partial w}{\partial y}\right),
\end{aligned}
\tag{2.6}
$$

where p is the scalar part of the pressure and $\rho\nu = \frac{NT}{4\omega_H}$; ω_H is the ion-gyration frequency, while N and T denote, respectively, the number density and temperature of ions and K^* is the Boltzmann constant.

Analyzing the disturbances in terms of longitudinal modes, we seek the solutions of Eqs (2.1)–(2.5) in which $x - t$ dependence is given by

$$\exp(iKx + nt), \tag{2.7}$$

where k denotes the wave number of disturbance and n is the growth rate of disturbance.

Eliminating $\mathbf{q}_d$ between Eqs (2.1) and (2.2), and using (2.6) and (2.7), Eqs (2.1)–(2.5) can be written as

$$\left[n\rho + \frac{\rho_d\nu_c}{n+\nu_c}\right] u = -ik\delta p - 2ik\nu D(\rho v), \tag{2.8}$$

$$\left[n\rho + \frac{\rho_d\nu_c}{n+\nu_c}\right] v = -2\rho\nu(D^2 + k^2)w + \nu D(\rho Dw) + \frac{ikHh_y}{4\pi}, \tag{2.9}$$

$$
\begin{aligned}
\left[n\rho + \frac{\rho_d\nu_c}{n+\nu_c}\right] w = &-D(\delta p) + 2\rho\nu k^2 v - \nu D(\rho Dv) + \\
&+ \frac{gw}{n}(DP) + \frac{H}{4\pi}(ikh_z - Dh_x),
\end{aligned}
\tag{2.10}
$$

$$\eta\delta\rho = -w(D\rho), \tag{2.11}$$

$$n\mathbf{h} = ikH\mathbf{q}, \tag{2.12}$$

$$iku + Dw = 0 \tag{2.13}$$

and

$$ikh_x + Dh_z = 0, \tag{2.14}$$

where

$$D = \frac{d}{dz}.$$

If we eliminate δp from Eqs (2.8) and (2.10) and use Eqs (2.11)–(2.14), we obtain the following pair of equations in w and v

$$n^2(\rho k^2 w - D(\rho Dw)) - gk^2(D\rho)w - \frac{H^2k^2}{4\pi}(D^2 - k^2)w - \tag{2.15}$$
$$- \nu n k^2[2(D^2 + k^2)(\rho v) - D(\rho Dv)] + \frac{\nu_c}{n + \nu_c} n^2[\rho_d k^2 w - D(\rho_d Dw)] = 0$$

and

$$\left[n\rho + \frac{\rho_d \nu_c}{n + \nu_c} n + \frac{H^2k^2}{4\pi n}\right] v = -\nu \left[2\rho(D^2 + k^2)w - D(\rho Dw)\right] . \tag{2.16}$$

3. Boundary conditions

On a boundary, vertical motion is not possible, thus

$$w = 0, \tag{3.1}$$

on a boundary free or rigid.

If the plasma is bounded by two rigid boundaries which are both ideally conducting, no disturbance within it can change the electromagnetic quantities outside. This merely leads to the boundary condition (3.1). A boundary condition on v can be prescribed by preluding the presence of surface charge or surface current at the rigid boundaries which are perfectly conducting. Thus we choose

$$v = 0, \tag{3.2}$$

at a surface bounded by an ideal conduction.

If the plasma is confined between two free boundaries, the tangential stresses $P_{xz} = 2\rho\nu ikv + \frac{ikH^2w}{4\pi n}$ and $P_{yz} = -\rho\nu Dw$ vanish. Hence

$$v = Dw = 0, \tag{3.3}$$

at a free boundary. Should there be discontinuities in the density as in the case of two superposed layers of different densities, we require the continuity of the vertical component of velocity, tagential stresses and pressure at interface. Thus

$$w, \quad \rho Dw, \quad \rho v, \quad \rho_d Dw, \quad \rho_d v \tag{3.4}$$

and the total pressure must be continuous as at the interface.

4. A variational principle

We shall show that the Eqs (2.15) and (2.16) subject to the foregoing boundary conditions are characterized by a variational principle.

Let n_i and n_j denote the two characteristic values, and let the solutions belonging to these characteristic values be distinguished by the subscripts i and j. Multiplying Eq. (2.15) for i by w_j and integrating with respect to z over the whole vertical extent of the plasma (denoted by $\int_L$), we obtain with the help of Eq. (2.16) and boundary conditions,

$$n_i^2 \int_L \rho \left(w_i w_j + \frac{1}{k^2} Dw_i Dw_j \right) dz + \frac{\nu_c}{n_i + \nu_c} n_i^2 \int_L \rho_d \left(w_i w_j + \frac{1}{k^2} Dw_i Dw_j \right) dz -$$
$$- g \int_L (D\rho) w_i w_j dz + \frac{H^2 k^2}{4\pi} \int_L \left(w_i w_j + \frac{1}{k^2} Dw_i Dw_j \right) dz + n_i n_j \int_L \rho v_i v_j dz +$$
$$+ \frac{\nu_c n_i n_j}{n_j + \nu_c} \int_L \rho_d v_i v_j dz + \frac{H^2 k^2 n_i}{4\pi n_j} \int_L v_i v_j dz = 0. \tag{4.1}$$

Taking $i = j$ and suppressing the subscripts, we obtain the following variational formulation of the problem

$$n^2[I_1 + I_4 + I_6 + I_7] - gI_2 + I_3 + I_5 = 0, \tag{4.2}$$

where

$$I_1 = \int_L \rho \left[w^2 + \frac{1}{k^2} (dw)^2 \right] dz, \tag{4.3}$$

$$I_2 = \int_L (D\rho) w^2 dz, \tag{4.4}$$

$$I_3 = \frac{H^2 k^2}{4\pi} \int_L \left[w^2 + \frac{1}{k^2} (dw)^2 \right] dz, \tag{4.5}$$

$$I_4 = \int_L \rho v^2 dz, \tag{4.6}$$

$$I_5 = \frac{H^2 k^2}{4\pi} \int_L v^2 dz, \tag{4.7}$$

$$I_6 = \frac{\nu_c}{n + \nu_c} \int_L \rho_d \left[w^2 + \frac{1}{k^2} (Dw)^2 \right] dz, \tag{4.8}$$

$$I_7 = \frac{\nu_c}{n + \nu_c} \int_L \rho_d v^2 dz. \tag{4.9}$$

Consider a change δn^2 on n^2 of an arbitrary variation δw and δv in w and v, respectively to satisfy the boundary conditions (3.1) and (3.2) of the eigen-value problem, we have to the first order, from (4.2)

$$\delta n^2 (I_1 + I_4 + I_6 + I_7) + n^2 (\delta I_1 + \delta I_4 + \delta I_6 + \delta I_7) - g\delta I_2 + \delta I_3 + \delta I_5 = 0, \tag{4.10}$$

where δI_s ($s = 1$ to 7) are the corresponding variations in I_s ($s = 1$ to 7). After one or more integrations by parts, we find that these latter variations are given by

$$\frac{1}{2}\delta I_1 = \int_L \left[\rho w - \frac{1}{k^2} D(\rho Dw)\right] \delta w dz, \tag{4.11}$$

$$\frac{1}{2}\delta I_2 = \int_L (D\rho) w \delta w dz, \tag{4.12}$$

$$\frac{1}{2}\delta I_3 = \frac{H^2 k^2}{4\pi} \int_L \left(w - \frac{1}{k^2} D^2 w\right) \delta w dz, \tag{4.13}$$

$$\frac{1}{2}\delta I_4 = \int_L \rho v \delta v dz, \tag{4.14}$$

$$\frac{1}{2}\delta I_5 = \frac{H^2 k^2}{4\pi} \int_L v \delta v dz, \tag{4.15}$$

$$\frac{1}{2}\delta I_6 = \frac{\nu_c}{n + \nu_c} \int_L \left[\rho_d w - \frac{1}{k^2} D(\rho_d Dw)\right] \delta w dz \tag{4.16}$$

and

$$\frac{1}{2}\delta I_7 = \frac{\nu_c}{n + \nu_c} \int_L \rho_d \delta v dz. \tag{4.17}$$

Furthermore, δw and δv are connected by the relation

$$\delta n \left[\rho - \frac{H^2 k^2}{4\pi n^2} + \frac{\rho_d \nu_c^2}{(n + \nu_c)^2}\right] v + n \left[\rho + \frac{H^2 k^2}{4\pi n^2} + \frac{\rho_d \nu_c}{n + \nu_c}\right] \delta v =$$
$$= -\nu \left[2\rho(D^2 + k^2)\delta w - D(\rho D w)\right]. \tag{4.18}$$

If we substitute for I_s and δI_s ($s = 1$ to 7) in Eq. (4.10) and make use of Eq. (4.18), we obtain after some further integrations by parts,

$$\delta n^2 \left[I_1 + \frac{1}{n^2} I_5 + I_6\right] + \frac{2}{k^2} \int_L \left[n^2 \{\rho k^2 w - D(\rho D w)\} - g k^2 (D\rho) w + \right.$$
$$\frac{\nu_c}{n + \nu_c} n^2 \{\rho_d k^2 w - D(\rho_d D w)\} - \frac{H^2 k^2}{4\pi} (D^2 - k^2) w -$$
$$\left. - \nu k^2 n \{2(D^2 + k^2)(\rho v) - D(\rho D v)\}\right] \delta w dz = 0. \tag{4.19}$$

We observe that the quantity occurring as a factor of δw under the integral sign vanishes if and only if Eq. (2.15) is satisfied. Thus a necessary and sufficient condition for δn^2 to be zero to the first order for all small arbitrary variations δw and δv (connected by Eq. (4.18)) in w and v which is compatible with the boundary conditions is that w and v should be the solutions of the eigenvalue problem governed by Eqs (2.15) and (2.16). A variational procedure of solving for the characteristic values is, therefore, possible.

5. An important property of n

From Eq. (4.1), we have

$$n_i \int_L \rho \left(w_i w_j + \frac{1}{k^2} Dw_i Dw_j \right) dz - \frac{g}{n_i} \int_L (D\rho) w_i w_j dz + \\ + \frac{H^2 k^2}{4\pi n_i} \int_L \left(w_i w_j + \frac{1}{k^2} Dw_i Dw_j \right) dz + n_j \int_L \rho v_i v_j dz + \frac{H^2 k^2}{4\pi n_j} \int_L v_i v_j dz + \\ + \frac{\nu_c n_i}{n_i + \nu_c} \int_L \rho_d \left(w_i w_j + \frac{1}{k^2} Dw_i Dw_j \right) dz + \frac{\nu_c n_j}{n_j + \nu_c} \int_L \rho_d v_i v_j dz = 0. \tag{5.1}$$

Interchanging i and j and noting that the above integrals are symmetric in i and j, we obtain

$$n_j \int_L \rho \left(w_i w_j + \frac{1}{k^2} Dw_i Dw_j \right) dz - \frac{g}{n_j} \int_L (D\rho) w_i w_j dz + \\ + \frac{H^2 k^2}{4\pi n_j} \int_L \left(w_i w_j + \frac{1}{k^2} Dw_i Dw_j \right) dz + n_i \int_L \rho v_i v_j dz + \frac{H^2 k^2}{4\pi n_i} \int_L v_i v_j dz + \\ + \frac{\nu_c n_j}{n_j + \nu_c} \int_L \rho_d \left(w_i w_j + \frac{1}{k^2} Dw_i Dw_j \right) dz + \frac{\nu_c n_i}{n_i + \nu_c} \int_L \rho_d v_i v_j dz = 0. \tag{5.2}$$

Let us consider two solutions characterized by n and n^*, the complex conjugate of n. We expect that the corresponding solutions will also be the complex conjugates of each other. Hence if $n_i = n$, $n_i = n^*$, then $w_i = w$, $w_j = w^*$, $v_i = v$ and $v_j = v^*$.

Then, from (5.1) and (5.2) by addition and subtraction, we have

$$\mathrm{Re}(n) \left[\overline{I}_1 + \overline{I}_5 - \frac{g}{|n|^2} \overline{I}_2 + \frac{H^2 k^2}{4\pi |n|^2} \overline{I}_3 + \frac{H^2 k^2}{4\pi |n|^2} \overline{I}_4 + \frac{\nu_c^2 (\overline{I}_6 + \overline{I}_7)}{|n|^2 + 2\nu_c R_e(n) + \nu_c^2} \right] = \\ = \frac{-\nu_c |n|^2 (\overline{I}_6 + \overline{I}_7)}{|n|^2 + 2\nu_c R_e(n) + \nu_c^2}, \tag{5.3}$$

and

$$\mathrm{Im}(n) \left[\overline{I}_1 - \overline{I}_5 + \frac{g}{|n|^2} \overline{I}_2 - \frac{H^2 k^2}{4\pi |n|^2} (\overline{I}_3 - \overline{I}_4) + \frac{\nu_c^2 (\overline{I}_6 - \overline{I}_7)}{|n|^2 + 2\nu_c R_e(n) + \nu_c^2} \right] = 0, \tag{5.4}$$

where

$$\begin{aligned}
\overline{I}_1 &= \int_L \rho[|w|^2 + \frac{1}{k^2}|Dw|^2]dz, \\
\overline{I}_2 &= \int_L (D\rho)|w|^2 dz, \\
\overline{I}_3 &= \int_L [|w|^2 + \frac{1}{k^2}|Dw|^2]dz, \\
\overline{I}_4 &= \int_L |v|^2 dz, \\
\overline{I}_5 &= \int_L \rho|v|^2 dz, \\
\overline{I}_6 &= \int_L \rho_d[|w|^2 + \frac{1}{k^2}|Dw|^2]dz, \\
\overline{I}_7 &= \int_L \rho|v|^2 dz.
\end{aligned} \tag{5.5}$$

Integrals $\overline{I}_s$ ($s = 1$ to 7) are all positive.

If n is complex, $\mathrm{Im}(n) \neq 0$, hence (5.4) gives

$$\overline{I}_1 - \overline{I}_5 + \frac{g}{|n|^2}\overline{I}_2 - \frac{H^2k^2}{4\pi|n|^2}(\overline{I}_3 - \overline{I}_4) + \frac{\nu_c^2(\overline{I}_6 - \overline{I}_7)}{|n|^2 + 2\nu_c R_e(n) + \nu_c^2} = 0, \tag{5.6}$$

so that (5.3) gives

$$\begin{aligned}
2\mathrm{Re}(n)\left[\overline{I}_1 + \frac{H^2k^2}{4\pi|n|^2}\overline{I}_4 + \frac{\nu_c^2\overline{I}_6}{|n|^2 + 2\nu_c R_e(n) + \nu_c^2}\right] = \\
= -\frac{\nu_c|n|^2(\overline{I}_6 + \overline{I}_7)}{|n|^2 + 2\nu_c R_e(n) + \nu_c^2}.
\end{aligned} \tag{5.7}$$

From Eq. (5.7) it follows that $\mathrm{Re}(n)$ is negative, which implies that if oscillatory modes exist they should be stable, thus ruling out possibility of overstability.

6. Two semi-infinitely extending plasmas of constant densities separated by a horizontal plane

We consider the case when two semi-infinitely extending plasma layers of constant densities ρ_1 and ρ_2, and dust particle densities ρ_{d_1} and ρ_{d_2} are separated by a horizontal boundary at $z = 0$. The subscripts 1 and 2 distinguish the lower and upper plasma layers, respectively.

We choose the following trial function for $w(z)$,

$$w(z) = \begin{cases} Ae^{+kz} & z < 0; \\ Ae^{-kz} & z > 0, \end{cases} \tag{6.1}$$

which is consistent with the boundary conditions (3.1)–(3.3). Here the same constant A has been chosen to ensure the continuity of w at $z = 0$.

The value of v in the two regions can be calculated from Eq. (2.16) and noting that ρ is constant, we have

$$v(z) = \begin{cases} Z_1 e^{+kz} & z < 0; \\ Z_2 e^{-kz} & z > 0, \end{cases} \tag{6.2}$$

where

$$Z_{1,2} = \frac{-3\nu k^2 nA}{n^2\left[1 + \frac{\alpha_0\nu_c}{n+\nu_c}\right] + k^2 V_{1,2}^2}, \tag{6.3}$$

$$V_1^2 = \frac{H^2}{4\pi\rho_1} \quad \text{and} \quad V_2^2 = \frac{H^2}{4\pi\rho_2}. \tag{6.4}$$

We assume that $\frac{\rho_{d_1}}{\rho_1} = \frac{\rho_{d_2}}{\rho_2} = \alpha_0$ as the simplifying assumption does not obscure any of the essential features of the problem.

To evaluate the integrals I_s ($s = 1$ to 7) in Eq. (4.2), we divide the region of integration into three parts (i) $-\infty < z < -\epsilon$ (ii) $\epsilon < z < \infty$ (iii) $-\epsilon < z < \epsilon$ and then pass it over to the limit $\epsilon \to 0$. On substituting their values in Eq. (4.2), we obtain the following dispersion relation between h and k,

$$n^2 - gk(\alpha_2 - \alpha_1) + k^2 V_A^2 + \frac{\alpha_0\nu_c}{n+\nu_c} n^2(\alpha_1 + \alpha_2) + \frac{g}{2}\nu^2 k^4 n^2 \left\{ \frac{\alpha_1}{n^2\left[1 + \frac{\alpha_0\nu_c}{n+\nu_c}\right] + k^2 V_1^2} + \frac{\alpha_2}{n^2\left[1 + \frac{\alpha_0\nu_c}{n+\nu_c}\right] + k^2 V_2^2} \right\} = 0, \tag{6.5}$$

where

$$V_A = \left\{ \frac{H^2}{2\pi(\rho_1 + \rho_2)} \right\}^{1/2} \tag{6.6}$$

can be termed as mean Alfvén velocity and

$$\alpha_{1,2} = \frac{\rho_{1,2}}{\rho_1 + \rho_2}. \tag{6.7}$$

Letting $n = \frac{g}{V_A} n^*$, $k = \frac{g}{V_A^2} k^*$ and omitting the asterisks for simplicity, so that the Eq. (6.5) takes the following dimensionless form

$$A_9 n^9 + A_8 n^8 + A_7 n^7 + A_6 n^6 + A_5 n^5 + A_4 n^4 + A_3 n^3 + A_2 n^2 + A_1 n + A_0 = 0, \tag{6.8}$$

where

$$A_9 = 4, \quad A_8 = 12A,$$

$$A_7 = 4A^2 + \frac{2k^2 B}{\alpha_1 + \alpha_2} + 4\left\{k^2 - k(\alpha_2 - \alpha_1)\right\} + 2Lk^4 B,$$

$$A_6 = 2k^2B\left\{\frac{1}{\alpha_1\alpha_2} + Lk^2\right\}(A+\nu_c') + 4A^3 + \frac{2k^2AB}{\alpha_1\alpha_2} + \\ + (8A+4\nu_c')\{k^2 - k(\alpha_2-\alpha_1)\},$$

$$A_5 = \frac{2ABk^2}{\alpha_1\alpha_2}(A+2\nu_c') + \frac{k^4}{\alpha_1\alpha_2} + 2Lk^4(k^2+B\nu_c'^2) + \\ + (4A^2 + \frac{2k^2B}{\alpha_1\alpha_2} + 8A\nu_c')\left\{k^2 - k(\alpha_2-\alpha_1)\right\},$$

$$A_4 = \frac{k^4}{\alpha_1\alpha_2}(A+2\nu_c') + 2Ak^2\nu_c'\left(\frac{AB}{\alpha_1\alpha_2} + Lk^2\nu_c'B + 3Lk^4\right) + \\ + \left\{\frac{2Bk^2}{\alpha_1\alpha_2}(A+2\nu_c') + 4A^2\nu_c'\right\}\left\{k^2 - k(\alpha_2-\alpha_1)\right\},$$

$$A_3 = \frac{k^4\nu_c'}{\alpha_1\alpha_2}(1+2A) + 6Lk^6\nu_c'^2 + \left\{\frac{2Bk^2\nu_c'}{\alpha_1\alpha_2}(2A+\nu_c') + \frac{k^4}{\alpha_1\alpha_2}\right\} \times \\ \times \left\{k^2 - k(\alpha_2-\alpha_1)\right\},$$

$$A_2 = \frac{k^4\nu_c'A}{\alpha_1\alpha_2} + 2Lk^6\nu_c'^3 + \frac{k^4\nu_c'}{\alpha_1\alpha_2}(3+2AB\nu_c')\left\{k^2 - k(\alpha_2-\alpha_1)\right\},$$

$$A_1 = \frac{k^4\nu_c'}{\alpha_1\alpha_2}(1+2\nu_c')\{k^2 - k(\alpha_2-\alpha_1)\},$$

$$A_0 = \frac{k^4\nu_c'^2}{\alpha_1\alpha_2}\left\{k^2 - k(\alpha_2-\alpha_1)\right\},$$

$$A = (1+\alpha_0)\nu_c', \quad B = \alpha_1+\alpha_2, \quad \nu_c' = \nu_c\frac{V_A}{g}, \tag{6.9}$$

and $L = \frac{g\nu^2g^2}{V_A^6}$ is a non-dimensional number measuring the relative importance of FLR effects and magnetic field.

For the potentially stable configuration ($\alpha_2 < \alpha_1$), all the coefficients of Eq. (6.8) are positive, if

$$k > k^*, \tag{6.10}$$

where

$$k^* = \alpha_2 - \alpha_1. \tag{6.11}$$

So no positive real root or complex root with negative real part exists. Therefore, the medium is stable even in the presence of collisions for disturbances of all wave numbers as it is if there are none.

For the potentially unstable configuration ($\alpha_2 > \alpha_1$), the absolute term in Eq. (6.8) is negative, if

$$0 < k < k^*. \tag{6.12}$$

Therefore (6.8) possesses at least one real root which is positive leading to an instability of the configuration even if there are collisions with dust particles.

Also we see that k^* is independent of L, a measure of FLR effect. Hence we conclude that for longitudinal perturbations, the stability criterion is independent of magnetic viscosity.

References

1. S. Chandrasekhar, Hydrodynamic and Hydromagnetic Stability, Dover Publication, New York, 1981.
2. M. N. Rosenbluth, N. Krall and N. Rostoker, Nucl. Fusion Suppl., *1*, 143, 1962.
3. J. D. Jukes, Phys. Fluids, *7*, 52, 1964.
4. K. V. Roberts and J. B. Taylor, Phys. Rev. Letters, *8*, 197, 1962.
5. R. C. Sharma and K. Prakash, Z. Naturforsch., *30A*, 461, 1975.
6. R. C. Sharma and N. Rani, Z. Naturforsch., *41A*, 724, 1986.
7. R. C. Sharma and K. N. Sharma, Phys. Fluids, *24*, 2242, 1981.
8. P. D. Ariel, Astrophys. Space Sci., *141*, 141, 1988.
9. H. Melchior and M. Popowich, Phys. Fluids, *11*, 581, 1968.
10. S. Singh and H. K. Hans, Nucl. Fusion, *6*, 6, 1966.
11. B. Strömgen, Astrophys. J., *89*, 526, 1939.
12. H. K. Hans, Nucl. Fusion, *8*, 89, 1968.
13. P. K. Bhatia, Nucl. Fusion, *10*, 383, 1970.
14. S. S. Rao and G. L. Kalra, Canad. J. Phys., *45*, 2779, 1967.

Acta Physica Hungarica 73 (2–4), pp. 165-173 (1993)

STATIC ANISOTROPIC FLUID SPHERES IN D SPACE–TIME DIMENSIONS

T. HARKO

Oncological Institute
3400 Cluj, Romania

(Received 4 May 1993)

Using the Einstein field equations in the presence of a cosmological constant, the equations which describe the hydrostatic equilibrium of a static anisotropic fluid sphere are obtained in D ($D \geq 4$) space–time dimensions. With suitable transformations, the equation of mass-continuity and of hydrostatic equilibrium are given in a non-dimensional form. The formalism thus developed is used to study homogeneous charged fluid spheres in higher dimensions and for these configurations a complete solution is obtained.

1. Introduction

The study of static anisotropic fluid spheres is important for relativistic astrophysics [1]. The starting point is represented by the Schwarzschild solution from which all problems involving spherical symmetry can be modelled. Charged spheres in the presence of matter have been studied by Bohra and Mehra [2] and Omote and Sato [3] with mass–charge and radius–charge relations emerging from the static solution. Several other anisotropic fluid sphere configurations have been analyzed using various Ansätze [4], [5].

Lately, there has been an increasing interest in the study of compact astrophysical objects in D space–time dimensions, prior to any compactification. So, Krori et al [6] have extended the interior Schwarzschild solution with vanishing normal pressure of Florides [7] to D space–time dimensions in the presence of a cosmological constant. Wolf has analyzed fluid spheres [8] and charged fluid spheres [9] in D space–time dimensions with the condition of vanishing normal pressure. The Oppenheimer–Volkoff equation has been generalized to D ($D \geq 4$) space–time dimensions in [10].

The purpose of the present paper is to obtain the equations which describe the hydrostatic equilibrium of an anisotropic, spherically symmetric, static fluid configuration, in D space–time dimensions, $D \geq 4$ and in the presence of a cosmological constant (generalized mass–continuity and Oppenheimer–Volkoff equations). The formalism thus developed is used to study the homogeneous charged fluid sphere in D ($D \geq 4$) space–time dimensions, with a particular choice of the proper charge density. Mass–charge and radius–charge relations are obtained, too.

The present paper is organized as follows. In Section 2, using the Einstein field equations we deduce the generalized mass-continuity and Oppenheimer–Volkoff

equations in D space–time dimensions. A non-dimensional form of these equations is obtained in Section 3.The components of the energy–momentum tensor of a charged fluid sphere are obtained in the new variable in Section 4. For this configuration, the hydrostatic equilibrium equations are solved in Section 5. The results are summarized in Section 6.

2. The generalized Oppenheimer–Volkoff equation

In D space–time dimensions the spherically symmetric metric takes the form:

$$ds^2 = e^{\nu}(dx^0)^2 - e^{\lambda}dr^2 - r^2 d\Theta_1^2 - r^2\sin^2\Theta_1 d\Theta_2^2 - r^2\sin^2\Theta_1\sin^2\Theta_2 d\Theta_3^2 - \ldots$$
$$- r^2\sin^2\Theta_1\ldots\sin^2\Theta_{D-3}d\varphi^2. \tag{2.1}$$

Here:

$$x^0 = ct, \quad x^1 = r, \quad x^2 = \Theta_1, \quad x^3 = \Theta_2, \ldots, x^{D-2} = \Theta_{D-3}, \ldots, x^{D-1} = \varphi.$$

(r is the radial coordinate in D space–time dimensions) with domain:

$$0 \leq r < \infty, \quad 0 \leq \Theta_i \leq \pi \ (i = 1, D-3), \quad 0 \leq \varphi \leq 2\pi.$$

The Einstein equations are:

$$R_i^k - \frac{1}{2}R\delta_i^k = \frac{8\pi G}{c^4}T_i^k + \frac{8\pi G\Lambda}{c^4}, \tag{2.2}$$

where the components of the energy–momentum tensor are:

$$T_0^0 = \rho c^2, \quad T_1^1 = -p_r, \quad T_2^2 = \cdots = T_{D-1}^{D-1} = -p_{\perp}, \tag{2.3}$$

where $p_r \neq p_{\perp}$. The case $p_r = p_{\perp}$ corresponds to the isotropic fluid sphere (p_r is normal pressure, $p_{\perp}$ is transversal pressure).

Using (2.1) the field equations become:

$$\frac{(D-2)\lambda' e^{-\lambda}}{2r} - \frac{(D-2)(D-3)(e^{-\lambda}-1)}{2r^2} = \frac{8\pi G\rho}{c^2} + \frac{8\pi G\Lambda}{c^4}, \tag{2.4a}$$

$$\frac{(D-2)\nu' e^{-\lambda}}{2r} + \frac{(D-2)(D-3)(e^{-\lambda}-1)}{2r^2} = \frac{8\pi G}{c^4}p_r - \frac{8\pi G\Lambda}{c^4}, \tag{2.4b}$$

$$e^{-\lambda}\left(\frac{\nu''}{2} + \frac{\nu'^2}{4} - \frac{\nu'\lambda'}{4} + \frac{(D-3)(\nu'-\lambda')}{4r}\right) + \frac{(D-3)(D-4)(e^{-\lambda}-1)}{2r^2} =$$
$$= \frac{8\pi G}{c^4}p_{\perp} - \frac{8\pi G\Lambda}{c^4}. \tag{2.4c}$$

From $T^k_{i;k} = 0$ it follows:

$$\nu' = -\frac{2p_r'}{\rho c^2 + p_r} + \frac{2(D-2)(p_\perp - p_r)}{(\rho c^2 + p_r)r}. \tag{2.5}$$

From Eq. (2.4a) we obtain immediately:

$$\frac{d(r^{D-3}e^{-\lambda})}{dr} = (D-3)r^{D-4} - \frac{8\pi G}{c^2}\frac{2}{D-2}\rho r^{D-2} - \frac{16\pi G\Lambda r^{D-2}}{(D-2)c^4} \tag{2.6}$$

or

$$e^{-\lambda} = 1 - \frac{8\pi G}{c^2}\frac{2}{D-2}\frac{1}{r^{D-3}}\int_0^r \rho r^{D-2}dr - \frac{16\pi G\Lambda r^2}{(D-1)(D-2)c^4}$$

and

$$e^{-\lambda} = 1 - \frac{2GF(D)M}{r^{D-3}} - \frac{16\pi G\Lambda r^2}{(D-1)(D-2)c^4}, \tag{2.7}$$

where:

$$F(D) = \frac{1}{(D-2)2^{D-5}}, \tag{2.8}$$

$$M(r) = \frac{1}{c^2}\int_0^r \pi 2^{D-2}\rho r^{D-2}dr. \tag{2.9}$$

Using (2.9) and (2.5) in Eq. (2.4b) we obtain the generalized Oppenheimer–Volkoff equation in D space–time dimensions, for an anisotropic spherically symmetric configuration:

$$\frac{dp_r}{dr} = -\frac{G(\rho c^2 + p_r)[(8\pi/(D-2)c^4)(p_r - 2\Lambda/(D-1))r^{D-1} + (D-3)F(D)M]}{r^{D-2}\left(1 - \frac{2GF(D)M}{r^{D-3}} - \frac{16\pi G\Lambda}{(D-1)(D-2)c^4}r^2\right)} + \\ + \frac{(D-2)(p_\perp - p_r)}{r}. \tag{2.10}$$

3. Non-dimensional form of the generalized Oppenheimer–Volkoff equation

To obtain the non-dimensional form of the generalized Oppenheimer–Volkoff equation (2.10) and of the mass–continuity equation:

$$\frac{dM}{dr} = \frac{1}{c^2}\pi 2^{D-2}\rho r^{D-2}, \tag{3.1}$$

we shall introduce Ureche's [11] non-dimensional independent variable η and the non-dimensional functions $\xi(\eta)$, $P_r(\eta)$, $P_\perp(\eta)$ and $m(\eta)$ by means of the transformations:

$$r = a\eta, \quad \rho = \rho_c\xi, \quad p_r = \rho_c c^2 P_r, \quad p_\perp = \rho_c c^2 P_\perp, \quad M = M^* m. \tag{3.2}$$

Here a is a scale factor (a characteristic length), ρ_c and M^* being a characteristic density and mass, respectively.

Using (3.2) in Eqs (3.1) and (2.10) we obtain:

$$\frac{dm}{d\eta} = \eta^{D-2}\xi, \tag{3.3a}$$

$$\frac{dP_r}{d\eta} = -\frac{(\xi + P_r)[(P_r - \mu)\eta^{D-1} + (D-3)m]}{\eta^{D-2}(1 - \frac{2m}{\eta^{D-3}} - \mu\eta^2)} + \\ + \frac{(D-2)(P_\perp - P_r)}{\eta}, \tag{3.3b}$$

where we have taken:

$$M^* = \frac{1}{c^2}\pi 2^{D-2}\rho_c a^{D-1}, \tag{3.4a}$$

$$a^2 = \frac{(D-2)c^2}{8\pi G\rho_c}, \tag{3.4b}$$

$$\mu = \frac{2\Lambda}{(D-1)\rho_c c^2}. \tag{3.4c}$$

Here we have a set of two equations in four variables m, ξ, P_r and $P_\perp$. For a general solution we must specify two physically reasonable functional relations among the four variables. Usually suitable forms of ξ and P_r are chosen.

The system (3.1)–(2.10) or (3.3a–b) must be integrated with some boundary conditions. These conditions depend on the concrete physical meaning of ρ, p_r and $p_\perp$ and they have to be specified in every situation.

4. Energy–momentum tensor of a charged fluid sphere

The Lagrangian of the electromagnetic field in D dimensions is given by [9], [12]:

$$L = -\frac{1}{K}F_{ik}F^{ik} - \frac{1}{c}j^i A_i, \tag{4.1}$$

where K is a constant which will be determined by normalization. Varying (4.1) with respect to A_i gives the Maxwell equations:

$$\frac{1}{(-g)^{1/2}}\frac{\partial}{\partial x^k}[(-g)^{1/2}F^{ik}] = -\frac{K}{4c}j^i. \tag{4.2}$$

The energy–momentum tensor of the electromagnetic fields from (4.1) is:

$$T_{ik} = -\frac{4}{K}F_{i1}F^{1k} + \frac{1}{K}F_{1m}F^{1m}g_{ik}. \tag{4.3}$$

The current density j^i has only one component for $r < R$ (R is radius of sphere)

$$j^0 = \rho_e \frac{dx^0}{ds} = \rho_e e^{-\frac{\nu}{2}}. \tag{4.4}$$

Here ρ_e is the proper charge density. We set $\rho_e = \rho_0 e^{-\frac{\lambda}{2}}$ and we shall suppose that ρ_0 is constant.

The electromagnetic field has only one non-zero component F^{01} and (4.2) gives:

$$F^{01} = -\frac{e^{-\frac{\nu}{2}-\frac{\lambda}{2}}}{r^{D-2}} Q(r), \tag{4.5}$$

where

$$Q(r) = \frac{K}{4} \int_0^r \rho_0 r^{D-2} dr = \frac{K\rho_0}{4(D-1)} r^{D-1}. \tag{4.6}$$

In order that Q represents the charge within the $(D-1)$ dimensional sphere we have [9]:

$$K = \frac{4\pi^{(D-1)}(D-1)}{((D-1)/2)!} \tag{4.7}$$

Using (4.3) and (4.5) we find for the components of the energy–momentum tensor of a massive charged fluid sphere:

$$T_0^0 = \rho c^2 = \rho_m c^2 + \frac{2}{K} \frac{Q^2}{r^{2(D-2)}}, \quad T_1^1 = -p_r = -p + \frac{2}{K} \frac{Q^2}{r^{2(D-2)}}, \tag{4.8a}$$

$$T_2^2 = \cdots = T_{D-1}^{D-1} = -p_\perp = -p - \frac{2}{K} \frac{Q^2}{r^{2(D-2)}}, \tag{4.8b}$$

where ρ_m is the mass density and p is the hydrostatic pressure.

We shall consider in the following only the case of the homogeneous fluid sphere, that is we shall suppose that ρ_m is constant.

We shall introduce now the transformations (3.2) in the form:

$$r = a\eta, \quad \rho = \rho_m \xi, \quad p = \rho_m c^2 P, \quad p_r = \rho_m c^2 P_r, \quad p_\perp = \rho_m c^2 P_\perp, \tag{4.9}$$

which give:

$$\xi = 1 + \frac{\alpha}{2(D-1)} \eta^2, \tag{4.10a}$$

$$P_r = P - \frac{\alpha}{2(D-1)} \eta^2, \tag{4.10b}$$

$$P_\perp = P + \frac{\alpha}{2(D-1)} \eta^2, \tag{4.10c}$$

where

$$\alpha = \frac{(D-2)}{(D-1)} \frac{K\rho_0^2}{32\pi G \rho_m^2}. \tag{4.11}$$

We suppose that we have an equation of state of the form:

$$p = p(\rho_m). \tag{4.12}$$

If P is a decreasing (non-increasing) function of η, then from transformations (4.9) it follows that $P \in [0, P_c]$, where P_c is the value of P at the centre of the sphere.

We can generalize the classical restriction for the upper limit of the general relativity in D space–time dimensions in the form:

$$p \leq \frac{\rho_m c^2}{D-1}, \tag{4.13}$$

which gives $P \in [0, 1/(D-1)]$.

If we use the restriction

$$p \leq \rho_m c^2, \tag{4.14}$$

then $P \in [0, 1]$.

So, we have expressed the components of the energy–momentum tensor of a homogeneous charged fluid sphere in D ($D \geq 4$) space–time dimensions in a non-dimensional form.

5. Homogeneous charged fluid sphere in D space–time dimensions

Using the expressions (4.10a–c) in (3.3a–b) we obtain the following equations which describe the hydrostatic equilibrium of a homogeneous charged fluid sphere in D space–time dimensions:

$$\frac{dm}{d\eta} = \eta^{D-2}\left[1 + \frac{\alpha}{2(D-1)}\eta^2\right], \tag{5.1a}$$

with solution:

$$m(\eta) = \frac{\eta^{D-1}}{D-1}\left[1 + \frac{\alpha}{2(D+1)}\eta^2\right], \tag{5.1b}$$

(where we have used the boundary condition $m(0) = 0$, too) and

$$\frac{dP}{d\eta} = -\frac{(1+P)[P - \mu + (D-3)/(D-1) - 2\alpha\eta^2/(D^2-1)]\eta}{1 - [2/(D-1) + \mu]\eta^2 - \alpha\eta^4/(D^2-1)} + \alpha\eta. \tag{5.2a}$$

The Oppenheimer–Volkoff equation (5.2a) must be integrated with the boundary conditions:

$$P(0) = P_c, \quad P(\eta_s) = 0, \tag{5.2b}$$

where P_c is the hydrostatic pressure and $\eta_s = R/a$ is the value of the non-dimensional parameter η at the centre and at the surface of the sphere, respectively.

In order to solve Eq. (5.2a) we shall introduce a new variable:

$$y = \frac{\eta^2}{2} + \frac{(D^2-1)\gamma}{4\alpha}, \quad y \in [y_c, y_s], \tag{5.3}$$

where $y_c = (D^2-1)\gamma/4\alpha$ and y_s are the values of y at the centre of the sphere and at the surface, respectively.

We denote, too:

$$\gamma = \frac{2}{D-1} + \mu, \quad \delta^2 = \frac{(\gamma + 1/y_c)y_c^2}{\gamma}, \quad P_0 = 1 + P. \tag{5.4}$$

So, Eq. (5.2a) becomes:

$$\frac{dP_0}{dy} = -\frac{P_0(P_0 - \gamma y/y_c)}{\gamma(\delta^2 - y^2)/y_c} + \alpha \tag{5.5}$$

with the boundary condition

$$P_0(y_c) = 1 + P_c. \tag{5.6}$$

This equation is a Riccati type equation. It has two particular solutions of the form:

$$P_{1,2} = \gamma\left[y \pm \frac{1}{2}(D^2-5)^{\frac{1}{2}}(\delta^2 - y^2)^{\frac{1}{2}}\right]/y_c. \tag{5.7}$$

By means of the transformation:

$$z = \frac{P_0 - P_1}{P_0 - P_2}, \tag{5.8}$$

we obtain the equation:

$$\frac{dz}{dy} + \frac{(D^2-5)^{\frac{1}{2}}}{(\delta^2 - y^2)^{\frac{1}{2}}} z = 0, \tag{5.9}$$

with solution

$$z = C\exp[-(D^2-5)^{\frac{1}{2}}\sin^{-1}(y/\delta)], \tag{5.10}$$

where C is a constant of integration.

From (5.10), (5.8) and (5.7), using the boundary condition (5.6) and denoting:

$$P_s = \frac{(P_c + 1 - \gamma) - \frac{1}{2}[\gamma(D^2-5)/y_c]^{\frac{1}{2}}}{(P_c + 1 - \gamma) + \frac{1}{2}[\gamma(D^2-5)/y_c]^{\frac{1}{2}}} \exp[(D^2-5)^{\frac{1}{2}}\sin^{-1}(y_c/\delta)], \tag{5.11}$$

we obtain the final form of the hydrostatic pressure P, in the y variable:

$$P(y) = \gamma y/y_c - \frac{\gamma(D^2-5)^{\frac{1}{2}}(\delta^2 - y^2)^{\frac{1}{2}}}{2y_c} \frac{P_s \exp[-(D^2-5)^{\frac{1}{2}}\sin^{-1}(y/\delta)] + 1}{P_s \exp[-(D^2-5)^{\frac{1}{2}}\sin^{-1}(y/\delta)] - 1} - 1. \tag{5.12}$$

The expressions given above (5.12) and (5.1b) represent the exact solution of the equations which describe the hydrostatic equilibrium of a charged, homogeneous fluid sphere in D space–time dimensions.

From (2.5b), a straightforward integration yields:

$$e^{\nu} = C_0 \left[P_s e^{-(D^2-5)^{\frac{1}{2}} \sin^{-1}(y/\delta)} - 1 \right]^2 e^{-(D^2-5)^{\frac{1}{2}} \sin^{-1}(y/\delta)}, \tag{5.13}$$

C_0 being an integration constant.

In the variable y, we have, too:

$$e^{\lambda} = \frac{y_c}{\gamma(\delta^2 - y^2)}, \tag{5.14}$$

while the proper charge density is given by:

$$\rho_e = \rho_0 \left(\frac{\gamma}{y_c} \right)^{\frac{1}{2}} \frac{1}{(\delta^2 - y^2)^{\frac{1}{2}}}. \tag{5.15}$$

For $r > R$ we have:

$$F^{01} = -\frac{Q}{r^{D-2}} \quad (Q = \text{const.}), \tag{5.16}$$

where Q is the charge included within radius R and, consequently:

$$T_0^0 = -\frac{Q^2}{r^{2(D-2)}} \tag{5.17}$$

(no matter present, only electromagnetic field).

The Einstein equation (2.4a) gives in this case ($\nu + \lambda = 0$):

$$e^{-\lambda} = 1 - \frac{2GMF(D)}{r^{D-3}} + \frac{32\pi G Q^2}{(D-2)(D-3)Kc^4 r^{2(D-3)}} - \frac{16\pi G \Lambda r^2}{(D-1)(D-2)c^4}, \tag{5.18}$$

which represents the D-dimensional Reissner–Nordström–de Sitter solution for a central charge Q.

From (4.6) we obtain the total charge of the sphere:

$$Q = \frac{K\rho_0 R^{D-1}}{4(D-1)}. \tag{5.19}$$

In the variables (4.9) we have (m_s is the total mass of the sphere):

$$e^{\nu} = e^{-\lambda} = 1 - \frac{2m_s}{\eta^{D-3}} + \frac{\alpha \eta_s^{2(D-1)}}{(D-1)(D-3)\eta^{2(D-3)}} - \mu\eta^2. \tag{5.20}$$

Matching (5.20) to (5.13) at $\eta = \eta_s$ will give the value of the constant of integration C_0 in (5.13).

Equations (5.1b), (5.12), (5.13) and (5.14) represent the complete exact interior solution for a homogeneous charged fluid sphere, in D ($D \geq 4$) space–time dimensions, in the presence of a cosmological constant. The normal and transversal pressure can be easily found from (4.10a and c).

6. Conclusions

From (5.12) and (5.13) it follows that $y < \delta$, for all y. Particularly, for $y = y_s$, we obtain:

$$\eta_s < (2y_c)^{\frac{1}{2}} \left[(1 + 1/\gamma y_c)^{\frac{1}{2}} - 1\right]^{\frac{1}{2}} = \eta_M. \tag{6.1}$$

So, η_M gives an upper limit of the radius of the charged fluid sphere. Similarly, from (5.1b) we obtain:

$$m_s < \frac{\eta_M^{D-1}}{2(D-1)} \left[1 + \frac{\alpha}{2(D+1)} \eta_M^2\right] = m_M, \tag{6.2}$$

m_M being the upper limit of the total mass of the sphere.

In the above analysis we obtained a complete solution for a homogeneous charged fluid sphere in D space–time dimensions, whose proper charge density is represented by $\rho_e = \rho_0 e^{-\lambda/2}$ ($\rho_0 = \text{const.}$). We have not discussed the stability of such a sphere but it would most likely be unstable since the electrostatic repulsion would tend to destabilize it.

An interesting question is the possibility of observing such objects in an astrophysical setting. The observation of γ-ray bursts prompted investigators to suggest that there might be a relation between the strong-coupling phase of QED and the γ-ray bursts observed. Certain anomalies in the spectrum are characteristic of emissions from a charged object in more than four space–time dimensions [13].

Other physical aspects concerning fluid spheres in D space–time dimensions will be postponed to a future paper.

References

1. R. L. Bowers and E. P. T. Liang, Astrophys. J., *188*, 657, 1974.
2. M. L. Bohra and A. L. Mehra, Gen. Rel. Grav., *2*, 205, 1971.
3. M. Omote and H. Sato, Gen. Rel. Grav., *5*, 387, 1974.
4. T. Singh, G. P. Singh and R. S. Srivastava, Int. J. Theor. Phys., *31*, 545, 1992.
5. G. Magli and J. Kijowski, Gen. Rel. Grav., *24*, 139, 1992.
6. K. D. Krori, P. Borgohain and K. Das, Gen. Rel. Grav., *21*, 1099, 1989.
7. P. S. Florides, Proc. R. Soc. London, *A337*, 529, 1974.
8. C. Wolf, Acta Phys. Hung., *70*, 288, 1991.
9. C. Wolf, Can. J. Phys., *70*, 249, 1992.
10. T. Harko, Acta Phys. Hung., *72*, 251, 1992.
11. V. Ureche, Rev. Roum. de Phys., *25*, 301, 1980.
12. L. Landau and L. Lifschitz, Théorie des champs, Mir, Moscou, 1970.
13. L. Sokolowski, M. Litterio and F. Occhionero, Int. Center for Theor. Phys., Miramare, Trieste, Preprint No. IC/89, 199, 1989.

Acta Physica Hungarica 73 (2–4), pp. 175-180 (1993)

PERCOLATION PHENOMENA AND SELF TEMPERATURE CONTROL HEATER FOR THE MIXED SYSTEM Cu–PEG

M. M. MOSAAD

Physics Department, Faculty of Education
Kafr El-Sheikh, Egypt

(Received 18 May 1993)

Mixed samples of Cu–PEG were prepared by milling the materials together and compressed in the form of discs of 1–1.5 mm, 12 mm diameter, and cylinders of 12 mm diameter and 2.5 cm height. The percolative model is studied for the samples in the form of discs, for both conductivity and dielectric constant. It is found that the percolative model is obeyed for both of them within the experimental limits. We also found that the exponent value in the case of conductivity depends strongly on the type of the conductive filler.

For samples with concentrations greater than f_c and in the form of cylinders, we study variation of temperature with time after applying V_{ac}. We found that these types of samples can be used as heaters which gives constant temperature without any control devices. These heaters cover the lower temperature region which is useful in biological and medical research.

Introduction

The electrical properties of conductor–insulator composite systems attracted the attention of many investigators as subject of both theoretical and experimental interests and because of the growing application of these materials in the industry [1–5].

It is well known that conducting particles dispersed in a non-conducting matrix with a suitable amount make the total system to be a conductor. Among these systems some have been reported to have a switching characteristic: namely, the electrical resistance for these shows an anomalous increase at a certain temperature [6–8].

Copper-polyethylene glycol (Cu–PEG) is a conductor–insulator composite consisting of Cu particles embedded in an insulating PEG matrix.

To the best of our knowledge, it is not clear if the percolation model is capable of describing the electrical properties of Cu–PEG mixtures. The present paper deals with the study of the variation of conductivity and the dielectric constant of Cu–PEG mixture with the percentage of copper. We also try to study the switching characteristics of Cu–PEG above the threshold percolation.

Experimental

Copper–PEG composites were made containing different percentages of Cu including (in weight) 1.25/2.50/3.75/5.00/6.25/7.50/8.75/10.00/11.25/12.00/17.00 /20.00/, milling the compound together. Then the samples were compressed in the form of discs 1.0–1.5 mm thick and 12 mm diameter at 0.4 GN/cm^2 at room temperature. All the samples were mixed separately. The last three percentages were used in the switching study in the form of cylinders with 12 mm diameter and 2.5 cm length. We made a hole in the sample's centre for a thermocouple to measure its temperature. The copper used was 98.5 % very fine powder, atomic weight 63.54, obtained from Prolabo, Paris, France. The size of the copper grains in our samples was much smaller than the resolution of our optical microscope at a magnification of 1000×. PEG used was from BDH laboratory reagents, with an average molecular weight 3300–4000.

The capacitance of the mixture was deduced by an auto compute RLC-bridge APLAB model H912, USA at a frequency of 1 KHz. The values of the dielectric constant were determined using standard geometrical techniques in which the capacitance is assumed to be given by the usual expression for parallel plate capacitor.

Electric conductivity was measured using a Kithley type 617 programmable electrometer. A sample holder with brass electrodes was especially designed to fit the present electrical measurements. Good contact was attained by painting both surfaces of the sample with air drying conducting silver paste type RC, made in UK.

Results and discussion

Kirkpatrick [9] was the first to demonstrate numerically that the conductivity σ of an insulator–conductor composite vanishes below the percolation threshold f_c and that σ follows a power law above f_c

$$\sigma = \sigma_0 (f - f_c)^t. \tag{1}$$

In Eq. (1) f is the probability of finding the conductive phase which experimentally usually sets equal the fraction of the conductive phase. σ_0 is a prefactor that depends on details of the transport process. t (> 0) is a critical exponent which is about 2.0 in the three dimensions [10] and which should be independent of the chemical nature and geometrical properties of the constituents.

Also, Efros and Shklovskii [11] established theoretically that the dielectric constant ε of a conductor insulator composite would diverge near the threshold. Specifically ε would follow the following power law below f_c

$$\varepsilon = \varepsilon_0 (f_c - f)^{-s},$$

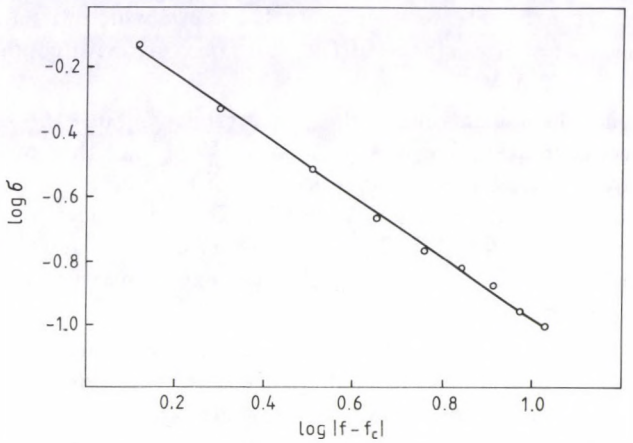

Fig. 1. D. C. conductivity versus $|f - f_c|$ in the log–log plot showing the relation $\sigma = \sigma_0 |f - f_c|^t$ with $t = 0.71 + 17$

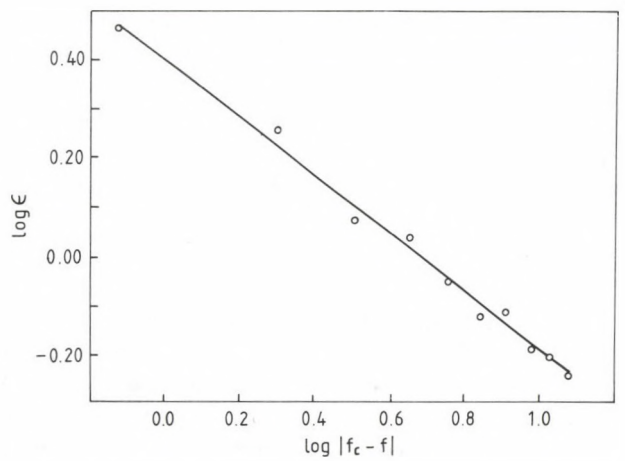

Fig. 2. Logarithmic plot of the dielectric constant as a function of $|f_c - f|$. The critical exponent s is $0.95 + 15$

where s (> 0) is another critical exponent, and is about 0.7 in three dimensions according to numerical simulation [12].

The percolation threshold (f_c) of the composite system described here lies

above 11.25 %. It is well known that f_c depends strongly on the shape of the conducting inclusion [13]. In this work we chose $f_c = 12$ % which was determined from the rapid decrease of the resistance of the same mixture with copper composition greater than f_0.

Figure 1 shows the logarithm of d.c. conductivity against the logarithm of the excess critical concentration ($\log|f - f_c|$) curve. We found that our data are very well described by the least square regression line of log conductivity on $\log|f - f_c|$. The experimental exponent value is 0.71 ± 0.17. This value does not agree with the theoretical expectation of 2.0 [14]. But our result agrees very well with our previous work on Cu–PVA [15]. Thus we can say that the exponent value depends strongly on the type of conductor filler.

Figure 2 shows a logarithmic plot of the measured dielectric constant as a function of $|f_c - f|$. We found that our data are very well described by the least squares regression line of log (dielectric constant) against $\log|f_c - f|$. The experimental exponent value agrees favourably with empirical values obtained from inorganic composites [16,17], and with our previous work [18]. It also agrees with the value obtained from computer simulations [12].

We can therefore state that the percolative model gives a suitable description of the dielectric constant and conductivity properties of the system studied within experimental limits.

Figure 3 illustrates the behaviour for three different samples (12 %, 17 %, 20 % Cu), each one supplied with three A. C. powers (i.e. we have nine conditions). The concentrations of the Cu and the applied voltage are indicated on each curve.

We notice that when the power is supplied to the sample, the temperature of the sample increases within a certain time and reaches a plateau which is maintained without any temperature control device. We can notice also that the plateau value depends strongly on the Cu percentage and the applied voltage.

Of course these samples can be used as heaters when we need a constant temperature, which is useful in biological and medical research. There are several characteristics for these heaters by Cu–PEG mixed system. Copper particles are easily dispersed in PEG matrices. As a consequence heaters with a required electric resistance can be easily made with an acceptable fluctuation of the resistance. These heaters cover the lower temperature region which is not obtained by barium titanate ceramics (70 °C). They could contribute to reducing energy consumption when they are used properly. The reason for saving energy could be that the unnecessary radiation loss, which is considered to be proportional to T^4, where T is the absolute temperature, is lower in the case of the heaters by Cu–PEG. The most important characteristic of these heaters is the steady state constant temperature which depends on the Cu concentration and the applied voltage. Therefore, it could be possible to make a heater which shows a desired steady state constant temperature.

The research to clarify the mechanism of conduction in these Cu–PEG systems relating this to the mechanism of anomalous increase in the electric resistance is now proceeding.

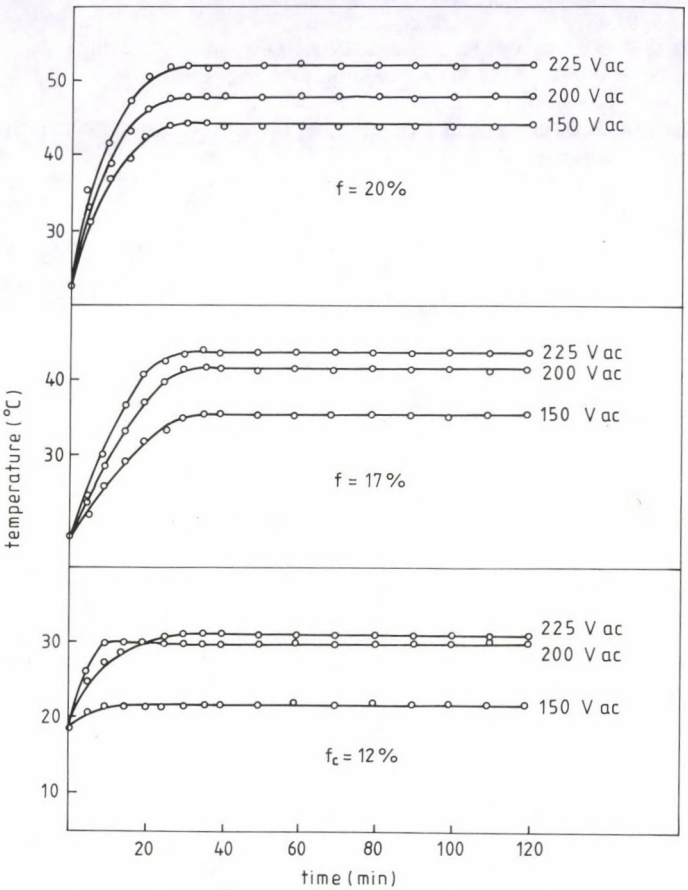

Fig. 3. Steady state constant temperature vs elapsed time after the supply of the power (150, 200, 225 V_{ac}) for the samples (Cu–PEG) with Cu concentration 12, 17, 20 %

References

1. R. Landauer, AIP Conf. Proc., *40*, 2, 1979.
2. C. Rajagopal, M. Satyam, J. Appl. Phys., *49*, 5536, 1978.
3. R. M. Simon, Polym. Plast. Technol. Eng., *17*, 1, 1981.
4. D. E. Davenport, Polym. Plast. Technol. Eng., *17*, 221, 1981.
5. K. T. Chung, A. Sabo, A. P. Pica, J. Appl. Phys., *53*, 6867, 1982.
6. K. Ohe, Y. Naota, Jpn. J. Appl. Phys., *10*, 99, 1971.
7. F. Bueche, J. Appl. Phys., *44*, 532, 1973.
8. F. Bueche, J. Polym. Sci., Polym. Phys., *11*, 1319, 1973.
9. S. Kirkpatrick, Rev. Mod. Phys., *45*, 574, 1973.
10. D. Stauffer, Introduction to Percolation Theory, Taylor and Francis, Philadelphia, 1985, p. 90.

11. A. L. Efros, B. I. Shklovskii, Phys. Stat. Sol., *B76*, 575, 1976.
12. J. P. Straley, Phys. Rev. B, *15*, 5733, 1977.
13. F. Carmona, P. Borreau and R. Conet, J. Phys. Lett., *41*, 534, 1980.
14. I. Balberg, S. Bozowski, Solid State Commun., *44*, 551, 1982.
15. M. M. Mosaad, Czech. J. Phys., *40*, 589, 1990.
16. D. M. Grannan, J. C. Graland and D. Btanner, Phys. Rev. Lett., *56*, 375, 1981.
17. C. S. Lobb, M. Tinkham, W. J. Skoopol, Solid State Commun., *27*, 1273, 1987.
18. M. M. Mosaad, J. Material Sci. Lett., *9*, 32, 1990.

Acta Physica Hungarica 73 (2–4), pp. 181-185 (1993)

INFLUENCE DES DEFAUTS THERMIQUES SUR LA DILATATION DES SOLIDES

Y. THOMAS

Institut de Recherches Scientifiques et Techniques
49045 Angers Cedex, France

(Reçu 8 juin 1993)

Une évaluation du rôle des vacances thermiques sur les diverses fonctions thermodynamiques d'un cristal est effectuée. Les cas d'une faible concentration des défauts dans des solides monoatomiques est illustré avec le cuivre et l'aluminium à l'aide des données expérimentales. Le coefficient de dilatation thermique apparaît comme le paramètre le plus sensible et le mieux adapté à l'étude des défauts thermiques dans les solides.

Relations théoriques

L'enthalpie libre d'un cristal réel à la pression P constante et à la température T peut être écrite [1]:

$$G_{(P,T)} = G_{0(P,T)} + \left[\sum_{i,j} n_j g_{ij}(P,T) - KT \ln D_{ij} \right],$$

où le premier terme représente la fonction de Gibbs du cristal supposé parfait (indice 0), n_j le nombre de défauts de type j, g_{ij} l'énergie due aux défauts des espèces i et j en interaction et D_{ij} le nombre des différentes manières de distribuer les n_j défauts supposés libres de migrer parmi les divers sites possibles (dont le nombre est influencé par les défauts en présence). Les termes g_{ij} et $\ln D_{ij}$ sont nuls pour $i \neq j$ si les interactions sont négligeables.

Si μ est le potentiel chimique, la condition d'équilibre des défauts de l'espèce j est:

$$\left(\frac{\partial G}{\partial n_j} \right)_{P,T} = \mu_j = 0.$$

La différentielle de G par rapport à P donne le volume:

$$V(P,T) = \left(\frac{\partial G}{\partial P} \right)_T = \left(\frac{\partial G_0}{\partial P} \right)_T + \sum_{i,j} \left[n_j \left(\frac{\partial g_{ij}}{\partial P} \right)_T + \left(\frac{\partial G}{\partial n_j} \right)_{P,T} \left(\frac{\partial n_j}{\partial P} \right)_T \right].$$

Le second terme du crochet est non nul dans le cas général d'une contrainte homogène et d'un cristal élastiquement anisotrope et doit être évalué selon chaque

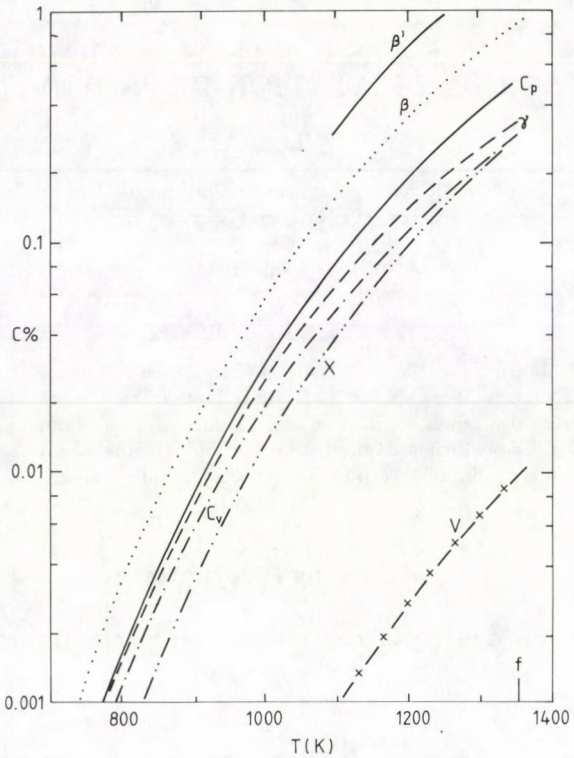

Courbes 1
Contributions relatives des vacances (C %) aux propriétés du cuivre en fonction de la température (T K). $h = 1170$ meV, $s = 1,5$ K, $x = 0,5v_a$, f: point de fusion.

cas, il est par contre nul à l'équilibre thermique ou si $(\partial n_j/\partial P)_T = 0$ pour des impuretés ou des dislocations statiques par exemple et on écrit alors:

$$V(P,T) = V_0(P,T) + \sum_{i,j} n_j \left(\frac{\partial g_{ij}}{\partial P}\right)_T \quad \text{où} \quad \left(\frac{\partial g_{ij}}{\partial P}\right)_T = x_{ij}$$

est le volume de formation de défaut j. L'enthalpie de défaut j peut s'écrire $h_{ij} = P \cdot x_{ij} + e_{ij}$ (énergie correspondante).

Le coefficient volumique β de dilatation thermique à P constant peut être déduit de:

$$V \cdot \beta = \left(\frac{\partial V(P,T)}{\partial T}\right)_P = V_0 \cdot \beta_0 + \sum_{ij} \left[n_j \left(\frac{\partial x_{ij}(P,T)}{\partial T}\right)_P + x_{ij} \left(\frac{\partial n_j}{\partial T}\right)_P \right],$$

ainsi que la compressibilité isotherme χ:

$$V \cdot \chi = \left(\frac{\partial V(P,T)}{\partial P}\right)_T = V_0 \cdot \chi_0 + \sum_{i,j}\left[n_j \left(\frac{\partial x_{ij}(P,T)}{\partial P}\right)_T + x_{ij}\left(\frac{\partial n_j}{\partial P}\right)_T\right]$$

afin de faire apparaître les contributions dues aux défauts (essentiellement des vacances).

Cas d'un cristal monoatomique

En présence de N atomes, on a $(N+n)$ sites possibles pour n vacances simples et $D = \frac{(N+n)!}{N!n!}$ avec une entropie de configuration $S = \ln D$.

A l'équilibre, en utilisant la formule de Stirling pour les grands nombres: $n = (N+n)e^{-g/KT} = (N+n)e^{(s-h)/KT}$ où s est l'entropie vibrationnelle de formation, h l'enthalpie de formation des vacances et g l'enthalpie libre relative aux vacances.

On en déduit:

$$V(P,T) = V_0(P,T) + n \cdot x(P,T),$$

$$V \cdot \beta = V_0 \cdot \beta_0 + n\left(\frac{\partial x(P,T)}{\partial T}\right)_P + x\left(\frac{\partial n}{\partial T}\right)_P.$$

Envisageons le cas fréquent d'une faible concentration de vacances: $(N+n) \gg n$ et $V_0 + nx \gg nx$, si V_a est le volume atomique [2]:

$$\beta = \beta_0 = \frac{n}{N \cdot v_a}\left[\left(\frac{\partial x(T,P)}{\partial T}\right)_P + \frac{x}{T}\left(\frac{h}{KT}\right)\right].$$

Il apparaît, par les défauts thermiques, deux contributions distinctes au coefficient β qui sont de même importance: $\left(\frac{\partial x}{\partial T}\right)_P \gg \frac{x}{T}$ car $\frac{h}{KT} \gg 1$ (ce n'est pas le cas si le terme x/T devient prépondérant).

Le volume $x = (\partial g/\partial P)_T$ de formation d'une vacance peut être divisé en deux contributions: la création d'un site et un terme de distorsion du réseau soit $x = v_a(1+d)$. On peut alors distinguer les coefficients: $\frac{1}{V}\left(\frac{\partial V}{\partial T}\right)_P$ pour un réseau réel et $\beta_0 + \frac{dnh}{NKT^2}$ pour le réseau correspondant supposé parfait. La différence $\beta' = nh/NT^2K$, où n'apparaît pas la dilatation d souvent inconnue, permet une évaluation directe du rôle des vacances.

La capacité thermique à pression constante est alors:

$$C_P = \left(\frac{\partial H}{\partial T}\right)_P = \frac{\partial}{\partial T}\left[-T^2\frac{\partial}{\partial T}\left(\frac{G}{T}\right)_P\right] \simeq C_{P_0} + n\left[\left(\frac{\partial h}{\partial T}\right)_P + \frac{h^2}{KT^2}\right]$$

ainsi que la compressibilité isotherme:

$$\chi \simeq \chi_0 + \frac{n}{Nv_a}\left[-\left(\frac{\partial x(T,P)}{\partial P}\right)_T + \frac{x^2}{KT}\right] \simeq \chi_0 + \frac{nx^2}{Nv_aKT}.$$

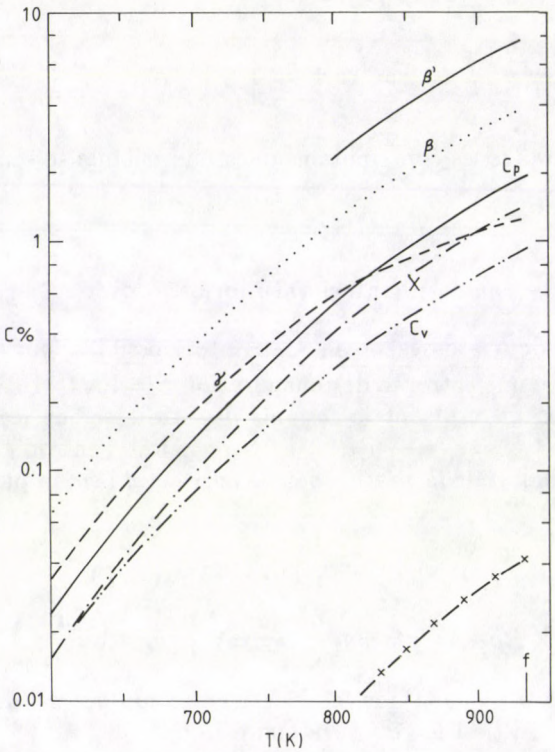

Courbes 2
Contributions relatives des vacances (C %) aux propriétés de l'aluminium en fonction de la température (T K). $h = 760$ meV, $s = 2,4$ K, $x = 0,5v_a$, f: point de fusion.

Notons que $x \simeq \frac{h}{T}\frac{\chi-\chi_0}{\beta-\beta_0}$ compte tenu de l'expression précédente de β. Ce volume croît à haute température par le phénomène d'auto-diffusion. Enfin [3], la relation $C_V = C_P - TV\beta^2/\chi$ permet de mettre en évidence la contribution des défauts à la capacité thermique à volume constant:

$$C_V \simeq C_{V_0} + \frac{n}{KT^2}\left(\frac{\chi_0 h - \beta_0 x T}{\chi_0}\right)\left(\frac{\chi h - \beta x T}{\chi}\right).$$

Cette contribution est positive car $\beta_0/\chi_0 \simeq \beta/\chi$ mais faible tant que $x \simeq h\chi/\beta T$. Les grandeurs x, h et s jouent un rôle analogue aux valeurs molaires partielles dans les solutions diluées si bien que, dans les expressions précédentes de C_P, C_V et χ, les termes $\left(\frac{\partial x}{\partial T}\right)_P$, $\left(\frac{\partial x}{\partial P}\right)_T$, $\left(\frac{\partial h}{\partial T}\right)_P$ et $\left(\frac{\partial s}{\partial T}\right)_P$ sont négligés.

Application au cuivre et à l'aluminium — conclusion

En adoptant $x = v_a/2$, à l'aide des données expérimentales pour le cuivre [4] et l'aluminium [5], les contributions relatives des vacances aux diverses propriétés thermodynamiques sont mises en évidence. Sur les courbes 1 et 2 on note, par exemple, C_P pour $(C_P - C_{P0})/C_{P0}$. Le paramètre de Grüneisen $\gamma = \beta V/\chi C_V$ est également représenté. Par manque de mesures très fiables, la résistivité électrique n'a pas été portée bien qu'elle semble également sensible à la présence de vacances [6].

Pour $x \in [hV_0\beta_0/C_{P0}, h\chi_0/\beta_0 T]$, avec les approximations signalées, la contribution au coefficient β apparaît comme la plus importante. La dilatation thermique est la propriété la plus sensible et donc la plus appropriée à l'étude des défauts du réseau cristallin (ceci reste vrai jusqu'à la valeur $x \approx v_a$).

Pour étendre ces résultats à divers défauts et structures, où faute d'approximations les expressions précédentes se compliquent, il sera sans doute nécessaire de relier les propriétés des défauts à celles des phonons pour expliciter la dilatation thermique vers les hautes températures [7].

References

1. R. E. Howard, A. B. Lidiard, Reports on Progress in Physics, *27*, 161, 1964.
2. J. T. Holder, A. V. Granato, Phys. Rev., *182*, 729, 1969.
3. Y. Thomas, Acta Phys. Hung., *48*, (4), 397, 1980.
4. R. O. Simmons, R. W. Baluffi, Phys. Rev., *129*, 1533, 1963;
   O. Vollmer, R. Kohlhaas, Z. angew. Phys., *25*, 365, 1968;
   C. R. Brooks et al, J. Chem. Phys. Solids, *29*, 565, 1968;
   Y. A. Chang, L. Himmel, J. Appl. Phys., *37*, 3567, 1966.
5. R. O. Simmons, R. W. Baluffi, Phys. Rev., *117*, 52, 1960;
   D. Gerlich, E. S. Fisher, J. Phys. Chem. Solids, *30*, 1197, 1969;
   C. R. Brooks, R. E. Bingham, J. Phys. Chem. Solids, *29*, 1553, 1968.
6. A. Ascoli, G. Guarini, G. T. Queirolo, Crystals Lattices Defects, *1*, 159, 1970.
7. V. Gallina, M. Omini, Phys. Stat. Sol., *7*, 771, 1964;
   J. Holder, A. V. Granato, J. Appl. Phys., *41*, 5152, 1970.

Acta Physica Hungarica 73 (2–4), pp. 187-196 (1993)

THREE BODY FORCES AND A NEW APPROACH TO THE LATTICE DYNAMICS OF SOME fcc METALS

M. K. MISHRA, PRADEEP GUPTA* and SMT. AMITA SHARMA**

Department of Physics, D. A. V. College
Kanpur, India
**Department of Physics, D. S. N. College*
Unnao, India
*** Department of Physics, R. B. S. College*
Agra, India

(Received 8 June 1993)

The results for the phonon dispersion curves along the major symmetry directions, second order elastic constants (SOEC) and zero point energy are obtained on the basis of modified scheme, centered around an empirical Morse potential for some fcc metals. This exponential potential is less parametric, which incorporates the exchange and correlation effects due to electrons in a simple and effective manner. These above computed results are compared with experimental findings with remarkable success.

1. Introduction

Recently much emphasis has been put on theoretical studies [1–9] of lattice dynamics based on Morse potential [10]. These studies explain excellently the elastic as well as the lattice dynamical behaviour of all types of cubic metals. With the volume forces recently Mohammad et al [1] have combined the central forces and arrived at a model explaining the phonon dispersion in cubic metals. It may be seen that the former forces, which are essentially of short range, may not be added to the latter ones, which are obviously of long range character. Singh and Rathore [2] have used the composite form of the cohesive energy as input data to explain the elastic and lattice dynamical behaviour of some cubic metals. This deficiency has been removed by Mishra [6] in his recent publication. Three body forces derived by Mishra et al [3–5] explain the lattice dynamical, elastic and thermophysical behaviour of metals in a broad manner. Mishra [6] used a modified Morse potential and applied it on fcc cobalt. Rathore et al [8] explained the lattice dynamics of some HCP metals successfully using the combined form of the empirical Morse potential. Theories given by Agrawal et al [7] and Aradhana and Rathore [9] added a new dimension to this type of study. But it is yet to know how they have developed a Modified Born–Mayer potential [1] then added to the Morse potential.

The present investigation, therefore, deals with the specific nature of the Generalised Morse potential which will be controlled by the factor P also in the

paired part of the potential and then this two body part has been added to the modified three body generalised part. We have found that the factor P is very important and may provide a correct scheme to predict the lattice dynamical and elastic behaviour and zero point energy of some fcc solids, i.e. Au, Ni, Pt and Pd. The subject matter of the present scheme uses a minimal number of parameters for expressing two and three body forces. The results obtained are excellent and surprising to report and very close to the experimental findings. This present scheme also incorporates the exchange and correlation effects due to electrons, which depend upon the variation of magnitude of P.

2. Theory

A. Two body part

Following Milstein [12] the attractive and the repulsive character of the two body potential are blended to form a generalised exponential pair potential which assumes the following forms for the atoms located at r.

$$\phi^x_{(r)} = D(P-1)^{-1}\left[\exp\{-P(r_0-r)\} - P\exp\{-\alpha(r_0-r)\}\right], \tag{2.1}$$

where D is the dissociation energy, α the parameter which measures the hardness of the potential, r_0 is the equilibrium distance and P is the exponent acquiring values within the different range.

The average interaction energy cohesive due to the potential may be expressed as

$$\phi^x_{(r_j)} = D\left\{2(P-1)\right\}^{-1}\sum_J \left[\exp\left\{-P(r_0-r_J)\alpha\right\} - P\exp\left\{-(r_0-r_J)\alpha\right\}\right]. \tag{2.2}$$

The quotient 2 in Eq. (2.2) takes care of the double counts. Putting

$$\beta = \exp(\alpha r_0), \tag{2.3}$$

we have a more compact form of the potential, i.e.

$$\phi^x_{(r_j)} = D\left\{2(P-1)\right\}^{-1}\sum_J \left\{\beta^P\exp(-P\alpha r_j) - \beta P\exp(-\alpha r_J)\right\}. \tag{2.4}$$

This distance r_J may be written as

$$r_J = (m_1^2+m_2^2+m_3^2)^{1/2}a = M_J a, \tag{2.5}$$

where (m_1, m_2, m_3) are integers denoting the co-ordinates of the J-th atom of the solids and a is the semi lattice constant. We have evaluated the present $\phi^x_{(r_j)}$ up to eight nearest neighbours (140 atoms) for fcc metals.

B. Three body part of the generalised and modified Morse potential

For the present purpose, the three body potential signifies an extra interaction energy affecting the pair owing to the presence of the third particle. In essence, it is a distance dependent three body potential, which arises due to the deformation of the electron shells caused by $(s-d)$ hybridisation. The short range three body exponential potential, capable of expressing the repulsive as well as attractive nature, coupling the atom (m,k) with its common nearest neighbours $(r_1 = r_2)$ may easily be written as

$$\phi^{y}_{(r_1,r_2)} = Q\{2(P-1)\}^{-1} \sum_{\substack{m'k' \\ m''k''}}^{1} \sum_{mk} [\beta^P \exp\{-\alpha P((r_1+r_2))\} - P\beta \exp\{-\alpha(r_1-r_2)\}], \tag{2.6}$$

where r_1 and r_2 are the separations of the atoms $(m'k')$ and $(m''k'')$ from the atom (mk). Q is the deformation parameter. Prime on the first summation denotes $m'k' \neq m''k''$.

C. The total potential

The total potential, responsible for the resultant interactions coupling the atoms of the crystalline solids may now be written as

$$\phi^{xy}_{(r_J,r_1,r_2)} = \phi^{x}_{(r_J)} + \phi^{y}_{(r_1,r_2)}. \tag{2.7}$$

3. Parameter evaluation

Singh and Rathore [2] have studied the lattice dynamics of some cubic metals based on the generalised Morse potential. According to this study, cohesive energy, lattice constant and compressibility are the input data for the empirical Morse potential. Compressibility and cohesive energy are, respectively, the sum of ionic interaction and interaction due to the electrons. Mishra and Rathore [3] have separated two and three body parts for compressibility. Mishra [6] has recently succeeded to elaborate the ionic behaviour and behaviour due to electrons on the most significant contribution to the binding energy, which arises from the interaction between the metal ions and the electrons, is not included in the potential [3], even though the potential is fitted to the total cohesive energy. In this note the following procedure has been adopted to separate the ionic interaction and the interaction due to electrons in terms of cohesive energy

$$\phi^{xy} = \phi^{x} + \phi^{y}, \tag{3.1}$$

Table I
The input data used

Metals	Two body bulk modulus $k^x(\times 10^{12}$ dyne/cm$^2)$	Ionic part of cohesive energy $\phi^x(\times 10^{12}$ erg)	Semi lattice constant (a) (nm)	P
Au	0.509	2.644	0.2040	3.15
Ni	1.571	3.125	0.1760	2.75
Pt	1.085	4.111	0.1960	2.75
Pd	0.887	2.738	0.945	2.75

Table II
The computed parameters

Metals	D ($\times 10^{12}$ erg)	α (nm^{-1})	r_0 (nm)	Cauchy's discrepancy ($\times 10^{12}$ dyne/cm^2)	Q ($\times 10^{-12}$ erg)
Au	6.536	0.1519	0.3133	1.223	1.245
Ni	0.413	0.1945	0.2589	0.265	3.698
Pt	0.470	0.1418	0.2971	1.742	18.434
Pd	0.345	0.1632	0.2889	1.043	15.616

Table III
Computed force constants ($\times 10^4$ dyne/cm)

Metals	α_1	β_1	α_2	β_2	β_3
Au	−0.128	3.183	0.034	−0.155	0.307
Ni	−0.272	3.576	0.089	−0.142	0.067
Pt	−0.326	2.978	0.041	−0.088	0.311
Pd	−0.216	1.864	0.039	−0.011	0.221

where ϕ^{xy} is the total cohesive energy, ϕ^x is the energy due to ions and ϕ^y the energy due to electrons.

Further

$$\phi^y = E_f + E_n + E_c, \tag{3.2}$$

where E_f (Fermi energy) $= -2.21/r^2$ Rydberg, E_n (exchange energy) $= -0.916/r$ Rydberg, E_c (correlation energy) $= [0.0622 \ln r - 0.096]$ Rydberg, while 1 Rydberg $= 21.79 \times 10^{-22}$ erg.

Hence the energy due to electrons

$$\phi^y = \left[\frac{2.21}{r^2} - \frac{0.916}{r} + (0.0622 \ln r - 0.096)\right] \text{Rydberg}. \tag{3.3}$$

Here r is the dimensionless quantity and may be varied like 2, 3, 4 or 5 while ln is the natural log.

The three parameters (D, α and r_0) depending upon the two body potential with an appropriate value of P, are evaluated by the procedure laid down by Girifalco and Weizer [13]. The deforming parameter Q is evaluated from the knowledge of measured Cauchy's discrepancy in the second order elastic constants.

4. Dynamical matrix

The elements of the diagonal and off-diagonal matrix may be given, after solving the usual secular determinant, as

$$\begin{aligned} D_{\alpha'\alpha'}(\mathbf{q}) =& 4(\beta_1 + 2\alpha_1) - 2(\beta_1 + \alpha_1)C_{\alpha'}(C_{\beta'} + C_{r'}) \\ & - 4\alpha_1 C\beta'(r' + 4\beta_2 S_{\alpha'} + 4\alpha_2(S^2_{\beta'} + S^2_{r'}), \qquad (4.1) \\ D_{\alpha'\beta'}(\mathbf{q}) =& 2(\beta_1 - \alpha_1)S_{\alpha'}S_{\beta'} + 4\beta_3[(C_{\alpha'} + C_{r'}) - 2], \qquad (4.2) \end{aligned}$$

where $C_{\alpha'} \cos(\frac{aq\alpha'}{2})$, $S_{\alpha'} = \sin(aq\alpha'/2)$.

Hence α_1, α_2 are the first and β_1, β_2 are the second derivatives of the potential $\phi^x_{(r_J)}$ while β_3 is the second derivative of $\phi^y_{(r_1,r_2)}$ (Table III).

5. Elastic constants

The second (SOEC) order elastic constant may be obtained as

$$C_{11} = m_1^4 \Omega^{-1} a^2 \sum_{m_1,m_2m_3} \frac{\partial^2 \phi^{(x)}_{(r_J)}}{\partial r^2} + m_1^2 m_1^2 \Omega^{-1} a^2 \sum_{m_1,m_2,m_3} \frac{\partial^2 \phi^y_{(r_1,r_2)}}{\partial r^2 \partial r_2}, \qquad (5.1)$$

where Ω is the atomic volume. The other constants like C_{12} and C_{14} are obtained by replacing m_1^4 with suitable combinations of m_1, m_2 and m_3.

6. Zero point energy

Zero point energy per mole has been computed using the method of Wallace [14], i.e.

$$E_0 = 0.5N \sum_{J,q} h\nu_{qJ} / \sum_q W_q, \qquad (6.1)$$

where N is the Avogadro number and W_q the statistical weight of an allowed wave vector in the irreducible part of the first Brillouin zone.

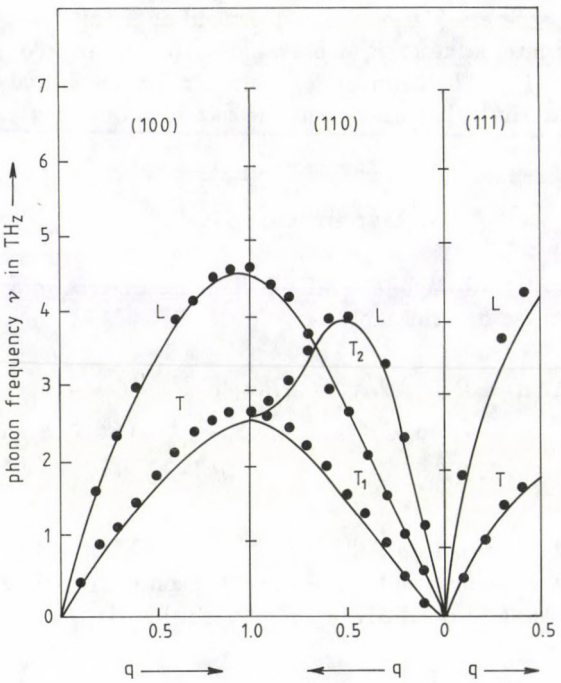

Fig. 1. Phonon dispersion relation for gold (P = 3.15) (—) present study; (• • •) experimental points

7. Discussion

The theoretical phonon dispersion relations for Au along the symmetry directions [100], [110] and [111] are shown in Fig. 1 along with the experimental points due to Lynn et al [15]. The comparison of theoretical results with the experimental ones reveals a good agreement, as is obvious from Fig. 1. Our theoretical results for phonon frequencies of Ni are shown in Fig. 2 along with experimental points due to Bergeneau et al [16]. The theoretical results compare well with the experiments for all the branches. The phonon dispersion curve of Pt is shown in Fig. 3. The agreement between calculated and observed values of Dutton et al [17] is found reasonably good for Pt in all branches. The experimental phonon frequencies in Pd were measured by Miller and Brochouse [18]. A study of Fig. 4 shows that the computed phonon dispersion relations in palladium have almost reproduced the experimental curves along all the symmetry directions.

Table IV predicts the second order elastic constants (SOEC) of all four fcc solids under study. Our results show a good agreement in SOEC of all the fcc

Table IV
The computed second order elastic constants ($\times 10^{12}$ dyne/cm^2)

Metals	C_{11}	C_{12}	C_{44}	Reference
Au	2.016	1.707	0.443	
	1.929*	1.638*	0.415*	[19]
Ni	2.512	1.586	1.331	
	2.500*	1.600*	1.185*	[20]
Pt	3.447	2.335	0.594	
	3.467*	2.507*	0.765*	[21]
Pd	2.194	1.636	0.594	
	2.271*	1.760*	0.717*	[22]

Table V
Computed values of zero-point energy (cal/mol)

Metals	Present work	Singh [23]	Domb and Salter [25]	Jain–Patel [24]
Au	415.0	423.0	458.0	406.6
Ni	860.0	864.4	876.0	–
Pt	572.0	525.6	580.0	–
Pd	665.0	621.0	685.0	–

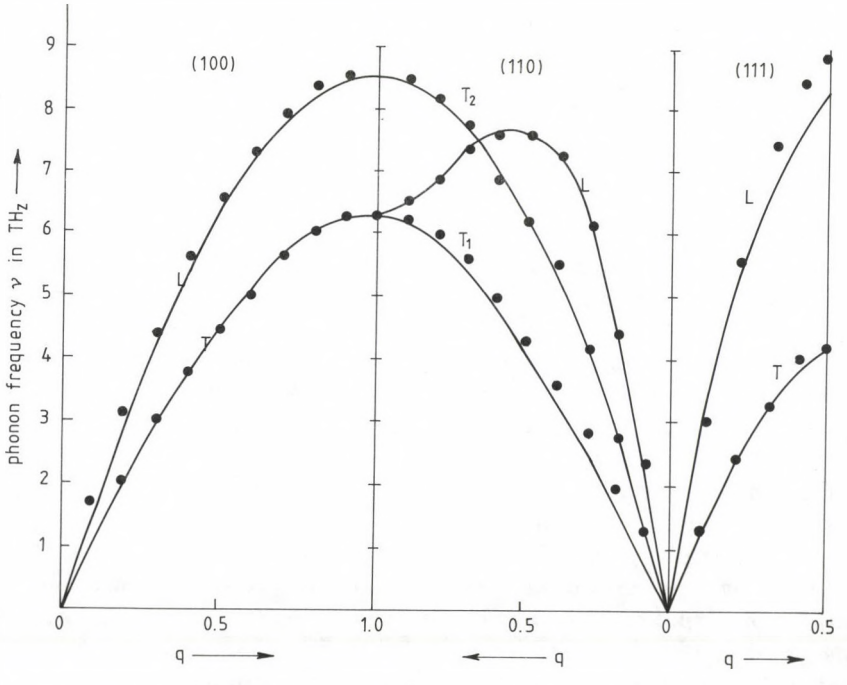

Fig. 2. Phonon dispersion relation for nickel ($P = 2.75$) (—) present study; (• • •) experimental points

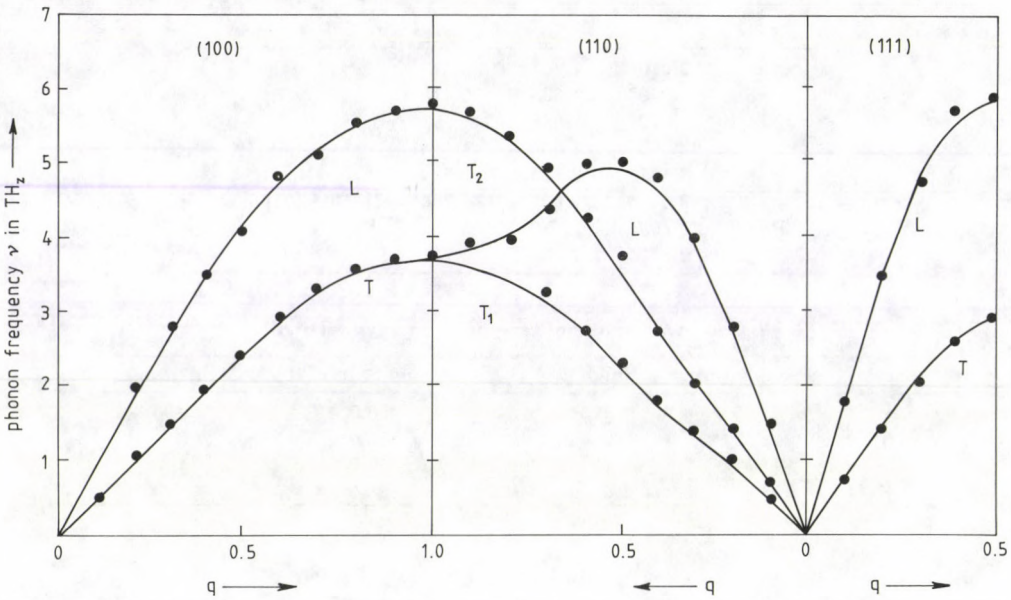

Fig. 3. Phonon dispersion relation for platinum ($P = 2.75$) (—) present study; (•••) experimental points

solids with corresponding experimental values reported therein. In order to make a further direct test of the model, we have also computed third order elastic constants (TOEC) and fourth order elastic constants (FOEC) for the same metals. These higher order elastic constants are not being reported here but can be had from the authors on request. The studies on higher order elastic constants are useful understanding the non linear strain–stress relationship, vibrational properties and anharmonic behaviour of the solids.

Our computed values of zero point energy (Table V) are compared with the calculations of Singh [23], Domb and Salter [25] and Jain and Patel [24]. Table V predicts the clear picture of our computed values with the other studies.

Finally, we have drawn the conclusion that the present investigation provides the satisfactory type of scheme which is centered around a more correct procedure of parameter evaluation. The used input parameters are purely ionic for the two body part while deforming parameter Q is explaining the three body part excellently.

One more interesting conclusion has also been drawn during the computation that the variation of the magnitude of P in this scheme gives very reasonable ionic as well as part due to electrons. If the value of magnitude of P is varied, the results are suddenly disturbed. The appropriation of the exponent (P) substantially includes the electronic exchange and correlation effects into the ionic couplings.

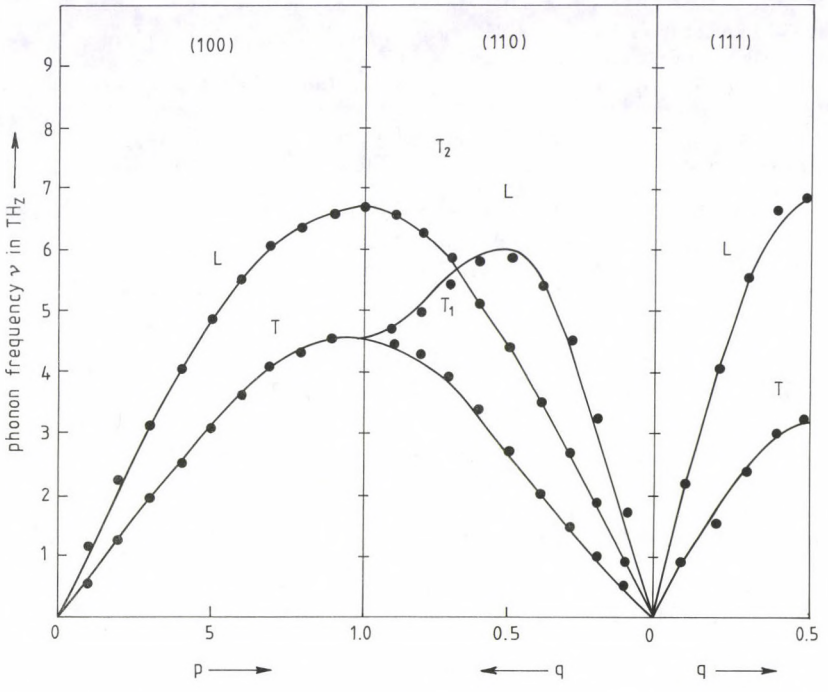

Fig. 4. Phonon dispersion curve for palladium ($P = 2.75$) (—) present study; (• • •) experimental points

The input data, computed parameters and computed force constants are given in Tables I, II and III, respectively.

Acknowledgement

Authors are very much thankful to Dr. K. Singh (Dept. of Physics, B.H.U., India) for providing computer facilities. We are highly obliged to Dr. R. P. S. Rathore (Dept. of Physics, R. B. S. College, Agra) for suggestions included herein.

References

1. K. Mohammad, M. M. Shukla, F. Milstein and J. L. Merz, Phys. Rev. (b), *29*, 3117, 1984; Solid State Commun., *48*, 147, 1983.
2. G. Singh and R. P. S. Rathore, Phys. Stat. Sol. (b), *135*, 513, 1986; Phys. Stat. Sol. (b), *136*, 57, 1986; Ind. J. Pure and Applied Phys., *24*, 303, 1986.

3. M. K. Mishra and R. P. S. Rathore, Acta Phys. Pol. (A), *75*, 525, 1989.
4. M. K. Mishra, A. K. Bajpai and S. K. Mishra, Ind. J. Pure and Applied Phys., *29*, 510, 1991.
5. M. K. Mishra, A. K. Bajpai and S. K. Mishra, Acta Phys. Hung., *71*, 67, 1991.
6. M. K. Mishra, Phys. Stat. Sol. (b), *162*, K-73, 1990.
7. R. M. Agrawal, Km Aradhana and R. P. S. Rathore, Ind. J. Pure and Applied Phys., *29*, 517, 1991.
8. R. P. S. Rathore, A. Singh and R. M. Agrawal, Phys. Stat. Sol. (b), *165*, 95, 1991.
9. Km. Aradhana and R. P. S. Rathore, Czech J. Phys., *B-40*, 686, 1990.
10. P. M. Morse, Phys. Rev., *34*, 57, 1929.
11. M. Born and J. E. Mayer, Z. Phys., *75*, 1, 1932.
12. F. Milstein, J. Appld Phys., *44*, 3825, 3832, 1973.
13. L. A. Girifalco and V. G. Weizer, Phys. Rev., *114*, 687, 1959.
14. D. C. Wallace, Thermodynamics of Crystals, John Wiley, N. Y., 1972.
15. J. W. Lyll, M. G. Smith and R. M. Nicklow, Phys. Rev., *8*, 3493, 1973.
16. R. L. Bergeneau, J. Cordes, G. Dolling and A. D. B. Woods, Phys. Rev., *136*, 1356, 1965.
17. D. H. Dutton, B. N. Brochouse and A. P. Miller, Can. J. Phys., *50*, 2915, 1972.
18. A. P. Miller and B. N. Brochouse, Can. J. Phys., *49*, 704, 1971.
19. Y. Hiki and A. V. Granto, Phys. Rev., *144*, 411, 1966.
20. J. Delaunay, Solid State Physics, eds F. Seitz and D. Turnbull, Academic Press, Inc. N. Y. 2, 249, 1956.
21. R. E. Macfarlane, J. A. Rayne and C. K. Jones, Phys. Lett. (A), *18*, 91, 1965.
22. G. A. Allers, J. R. Neighbours and H. Sato, Bull. Amer. Phys. Soc., *4*, 131, 1959.
23. M. Singh, Ind. J. Pure and Applied Phys., *22*, 741, 1984.
24. A. R. Jain and J. K. Patel, Solid State Commun., *56*, 635, 1985.
25. C. Domb and L. Salter, Phil. Mag. (GB), *43*, 1083, 1952.

Acta Physica Hungarica 73 (2–4), pp. 197-204 (1993)

ON THE VALIDITY OF THE MAXIMUM ENTROPY FORMALISM

E. S. FREIDKIN

Department of Physics, University of the Witwatersrand, WITS 2050 Johannesburg, Republic of South Africa[1]

(Received 15 June 1993)

A comparison is made between time development of the system, which follows from the exact solution of Grabert equation for fluctuation distribution function and that derived from the maximum entropy formalism. It is shown here that the maximum entropy formalism can describe the behaviour of the physical system for times sufficiently long only if the number of state variables under consideration is very large. Thus, the standard applications of the maximum entropy formalism with few state variables are erroneous.

1. Introduction

The maximum entropy formalism [1] starting with an information theoretic entropy analogue, which is the functional of the phase distribution, maximizes the entropy subject to the condition that the values of the energy and certain additional moments such as, for example, pressure and heat flux are specified. Lagrange multipliers are introduced and their subsequent evaluation enables to find the distribution function. Based on the information theory this approach asserts that the best phase space distribution consistent with a given value of energy and certain additional moments $\varepsilon_i(\mathbf{r})$ defined at all points in the system interior is given by:

$$\rho(x) = Z^{-1} \exp\{-\sum_{i=1}^{N} \lambda_i(\mathbf{r}) E_i(\mathbf{r}, x)\} d\mathbf{r}, \tag{1}$$

where Z is normalizing factor and the $\lambda_i(\mathbf{r})$ are chosen so that:

$$\varepsilon_i(\mathbf{r}) = E_i^{\text{averaged}}(\mathbf{r}, x) = \int \rho(x) E_i(\mathbf{r}, x) dx. \tag{2}$$

$E(\mathbf{r}, \mathbf{x}_i, \mathbf{p}_i)$ is thermodynamic variable at point $\mathbf{r}$ calculated as function of moments and coordinates of the particles. The maximum entropy so introduced:

$$S = -\int \rho(x) \ln \rho(x) dx \tag{3}$$

[1] Present address: Department of Physics and Astronomy, The State University of New Jersey-Rutgers, P. O. Box 849, Piscataway, New Jersey 08855-0849

has been extensively used and it was always taken for granted that the maximum entropy so defined can be used for the description of physical systems [2]. The possibility of defining Lagrange multipliers from (1,2) went without saying. In previous work [3] we proved that this assumption is wrong. Simultaneously with this assumption another has been made: that the maximum entropy, even defined when just a few moments, except of energy, are specified can serve for the description of physical systems for times sufficiently large ([2] and references therein). We will prove making use of fluctuation distribution function introduced in [4] that this assumption is erroneous. Consider the selected set $A_i(x)$ of dynamical functions of the phase distribution and the set of generalized velocities $\dot{A}_i(x)$, where $i\hat{L}$ is self-adjoint Liouville operator. Further on we will use the notation α for state variables and η for generalised velocities. The maximum entropy so defined also provides a distribution which is the average of the function:

$$\psi_a(x) = \delta(A(x) - \alpha)\delta(\dot{A}(x) - \eta), \tag{4}$$

$$a = (\alpha, \eta).$$

$\delta(A(x) - a)$ denotes a product of factors $\delta(A_i(x) - a_i)$ over the maximum entropy distribution

$$g(a) \equiv \int \rho(x)\psi_a(x)dx. \tag{5}$$

According to the information theory, $g(a)$ is the best fluctuation distribution consistent with the specified values of $A_i(x)$ and $\dot{A}_i(x)$. The time evolution of $g(a,t)$ is governed by the equation [5]:

$$\frac{\partial g}{\partial t} = -\sum_i \frac{\partial(\eta_i g)}{\partial \alpha_i} - \sum_i \frac{\partial(q_i g)}{\partial \eta_i} + \int\int d\alpha' d\eta' \int_0^t ds \sum_{ij} \frac{\partial D_{ij}(a, a', t-s)}{\partial \eta_i} \frac{\partial \left[\frac{g(a',s)}{p_\beta(a')}\right]}{\partial \eta'_j}. \tag{6}$$

Here:

$$\begin{aligned} p_\beta(a) &= \int \rho_\beta(x)\psi_a(x)dx, \\ v_a(a) &= p_\beta^{-1}(a) \int p_\beta(x)\dot{A}_i(x), \\ q_i(a) &= p_\beta^{-1}(a) \int \rho_\beta(x)(i\hat{L})^2 A_i(x)dx. \end{aligned} \tag{7}$$

The kernel $D(a, a', r)$ is defined as follows:

$$D_{ij}(a, a', r) = \int \rho_\beta(x)\psi_{a'}(x)[(i\hat{L})^2 A_j(x)](1 - \hat{P}) \exp[i\hat{L}(1 - \hat{P})\tau]\psi_a(x)(i\hat{L})^2 A_i(x), \tag{8}$$

$$\hat{P}X(\Gamma) = \int da \psi_a(\Gamma) \frac{Tr[\rho_\beta(x)\psi_a(x)X(x)]}{p_\beta(a)} \tag{9}$$

and $\hat{P}$ is the projection operator for the system in thermal contact with surroundings, defined in [4]. (See also [5], where the correct form for the integral term is (5) was derived. The equation holds provided the initial distribution satisfies:

$$Tr[\rho_\beta(x)\psi_a(x)F_{a'}(t)] = 0, \tag{10}$$

$$F_{a'} \equiv -\sum_i \frac{\partial[(1-\hat{P})\exp[i\hat{L}(1-\hat{P})t]\psi_{a'}(x)\hat{A}_i(x)]}{\partial\alpha_i'} - \sum_i \frac{\partial[(1-\hat{P})\exp[i\hat{L}(1-\hat{P})t]\psi_{a'}(x)(i\hat{L})\hat{A}_i(x)]}{\partial\eta_i'}. \tag{11}$$

This holds for maximum entropy distribution.

2. Solution of the equation for fluctuation distribution function

One can solve (5) using the Taylor expansion:

$$g(a,t) = \sum_{n=0}^{\infty} \frac{g^{(n)}(a)t^n}{n!}. \tag{12}$$

We readily establish the recurrence relation:

$$g^{(n+1)}(a) = -\sum_i \frac{\partial[\eta_i g^{(n)}(a)]}{\partial\alpha_i} - \sum_i \frac{\partial[q_i(a)g^{(n)}(a)]}{\partial\eta_i} + \sum_{m,k\geq 0}^{m+k+1=n} \sum_i \int A_i^k(a',a)g^{(m)}(a')da'. \tag{13}$$

$A_i^k(a,a')$ is defined from

$$-p_\beta(a')\frac{\partial D_{ij}(a,a',\tau)}{\partial\eta_j'} = \sum_{k=0}^{\infty} A_i^{(k)}(a',a)\frac{\tau^k}{k!}. \tag{14}$$

Now we are in a position to find the function $g(a,t)$ at an arbitrary time, provided we know the fluctuation distribution at time $t = 0$. Assume at time $t = 0$ the initial distribution corresponds to the maximum entropy distribution, namely is the best fluctuation distribution consistent with the specified values of α and η variables. We assume that the internal energy and heat flux per unit volume are the state variables of extended nonlinear thermodynamics. The assumption that

few variables are sufficient for the description of a physical system is common in nonlinear thermodynamics and maximum entropy formalism [4,6]. We will prove that the assumption is erroneous. In Section 3, making use of the solution of the Grabert equation, we will calculate the heat flux as function of t and the corresponding second moment of the heat flux. Making use of the result we will work out the expression for the corresponding maximum entropy distribution and fluctuation distribution. We can calculate from $g(a,t)$ as many moments, as we wish if they are included among the state variables on which $g(a,t)$ depends. In the next Section we calculate the second moment of the heat flux as it follows from the assumption that the system is described by the maximum entropy distribution and compare it with exact results.

3. Calculation of the moments of heat flux

The expression for the heat flux has the form:

$$Q_\alpha = \frac{1}{V}\sum_n \frac{p_{n\alpha}}{m}\left[\frac{p_n^2}{m} + \sum_{i\neq n} U(r_{in}) - h\right] - \frac{1}{2V}\sum_{n,\gamma,j} \frac{p_{n\gamma}U'(r_{n\gamma})}{r_{n\gamma}}(r_{n\gamma}-r_{j\gamma})(r_{n\alpha}-r_{j\alpha}). \tag{15}$$

See [7] α and γ label the components, $V(\mathbf{r})$ is the energy of the interaction between particles, V is the volume of the system, h is the enthalpy per particle

$$g^{(1)}(\mathbf{q}) = -\sum_{i=1}^{3} \frac{\partial[q_i(\mathbf{q})g^{(0)}(\mathbf{q})]}{\partial q_i}, \tag{16}$$

$$q_i(\mathbf{q}) = p_\beta^{-1}\int \rho_\beta(x)\psi_{\mathbf{q}}(x)(i\hat{L}Q_i(x))dx, \tag{17}$$

$q_i(\mathbf{q})$ equals zero as the integrand is an odd function of coordinates. Therefore:

$$g^{(1)}(\mathbf{q}) = 0. \tag{18}$$

For the second order term we obtain:

$$g^{(2)}(\mathbf{q}) = \sum_{i=1}^{3}\int A_i^{(0)}(\mathbf{x},\mathbf{q})g^{(0)}(\mathbf{x})d\mathbf{x} \tag{19}$$

and, after some transformations:

$$g^{(2)}(\mathbf{q}) = \sum_{i,j=1}^{3} \frac{\partial[Tr[\rho_\beta(x)\psi_{\mathbf{q}}(x)(i\hat{L}Q_i(x))(i\hat{L}Q_j(x))](\frac{\partial[\frac{g^{(0)}(\mathbf{q})}{p_\beta(\mathbf{q})}]}{\partial q_j})]}{\partial q_i}. \tag{20}$$

$Tr(\rho_\beta \psi_{\mathbf{q}}(i\hat{L}Q_i(x))(i\hat{L}Q_j(x))$ is calculated in fluctuation approximation.

$$Tr[\rho_\beta(x)\psi_{\mathbf{q}}(x)(i\hat{L}Q_i(x))(i\hat{L}Q_j(x))] = Tr[\rho_\beta(x)(i\hat{L}Q_i(x))(iLQ_j(x))]Tr[\rho_\beta(x)\psi_{\mathbf{q}}(x)]. \tag{21}$$

All integrals over momenta can be calculated exactly if one uses:

$$\overline{p_l^2(\mathbf{p}_{l'}\mathbf{A})^2} = A^2(mkT)^2(3+2\delta_{ll'}), \tag{22}$$

$$\overline{(\mathbf{p}_l\mathbf{A}_1)^2(\mathbf{p}_{l'}\mathbf{A}_2)^2} = (mkT)^2A_1^2A_2^2 + 2(mkT)^2(\mathbf{A}_1\mathbf{A}_2)^2\delta_{ll'}, \tag{23}$$

$$\overline{p_{n\alpha}p_{n'\alpha}p_{n\beta}p_{n'\beta}} = (mkT)^2(\delta_{nn'} + \delta_{\alpha\beta} + \delta_{nn'}\delta_{\alpha\beta}). \tag{24}$$

If we assume the gas density to be small and take into account only correlation functions of the second order after some lengthy calculation, we obtain:

$$\begin{aligned} Tr[(i\hat{L}Q_i(x))(i\hat{L}Q_j(x))] = \delta_{ij}\frac{\rho^2}{V}\int \exp(-\beta V(r))d\mathbf{r}\left[\frac{133}{30}\left(\frac{kT}{m}\right)^2[V'^2(r)]+\right. \\ \left.+\frac{11}{15}\left(\frac{kT}{m}\right)^2 rV'(r)V''(r)\right] + \delta_{ij}\frac{\rho^2}{V}\int \exp(-\beta V(r))d\mathbf{r}\left[\frac{1}{6}(kT/m)^2r^2[V''(r)]^2-\right. \\ \left.-\frac{1}{12m^2}[V(r)V'(r)]^2\right] - \delta_{ij}\frac{\rho^2}{V}\int \exp(-\beta V(r))d\mathbf{r}\frac{1}{12m^2}r^2[V'(r)]^2, \end{aligned} \tag{25}$$

$$Tr[\rho_\beta(x)\psi_{\mathbf{q}}(x)] = \left[\frac{3}{2\pi}\overline{q^2}^{-1}\right]^{3/2}\exp\left(-\frac{3}{2}\frac{\mathbf{q}^2}{\mathbf{q}^2}\right). \tag{26}$$

In (26)

$$\overline{q^2} = \frac{15}{2}\frac{\rho}{V}\frac{(kT)^3}{m} \tag{27}$$

and we take into account only leading over density terms. In order to proceed with further evaluation, we must do definite assumptions, concerning the potential and the initial form of fluctuation distribution.

4. The evaluation of time of the validity of maximum entropy formalism

We assume that initially the distribution $g(a,t)$ corresponded to the maximum entropy distribution with specified values of internal energy and heat flux $\mathbf{Q}$. The corresponding function is easily found. The density distribution is:

$$\rho_{\mathbf{Q}}(x) = Z^{-1}\exp[-\beta H - \overrightarrow{\gamma}(\mathbf{Q})\mathbf{Q}(x)], \tag{28}$$

$$Z = V^N(2\pi mkT)^{\frac{3N}{2}}. \tag{29}$$

The typical volume considered in nonequilibrium thermodynamics is of the order 10^{-18} m^3. The result is valid for $Q < 10^4$ W/m^2, which holds in all cases of interest.

$$\overrightarrow{\gamma}(\mathbf{Q}) = \gamma_0 \mathbf{Q}, \tag{30}$$

$$\gamma_0 = -\frac{4}{35}\frac{V}{\rho}\frac{m}{(kT)^3}.$$

From here we find:

$$g^{(0)}(\mathbf{q}) = \left[\frac{1}{5\pi}\frac{V}{\rho}\frac{m}{(kT)^3}\right]^{\frac{3}{2}} \exp\left(-\frac{mV}{5\rho(kT)^3}q^2\right) \exp(-\overrightarrow{\gamma}(\mathbf{Q})\mathbf{q}). \tag{31}$$

If we assume that from $t = 0$ and further on the system is described by the maximum entropy distribution, then in (28) we must substitute $\overrightarrow{\gamma}(\mathbf{Q})$ where $\overrightarrow{\gamma}(\mathbf{Q}) = \gamma_0 \mathbf{Q}(t)$ is calculated according to the formula:

$$\mathbf{Q}(t) = \mathbf{Q}(0) + \int d\mathbf{q}[g(\mathbf{q}, t) - g(\mathbf{q}, 0)]\mathbf{q}. \tag{32}$$

The distribution

$$g(\mathbf{q}, t) = \sum_{n=0}^{\infty} \frac{g^{(n)}(\mathbf{q})t^n}{n!} \tag{33}$$

enables us to calculate second moment.

$$\mathbf{Q}^2(t) = \mathbf{Q}^2(0) + \int d\mathbf{q}[g(\mathbf{q}, t) - g(\mathbf{q}, 0)]\mathbf{q}^2. \tag{34}$$

On the other hand, we can calculate the second moment of the heat flux, using the maximum entropy distribution

$$\mathbf{Q}^2(t) = \int d\mathbf{q} \left[\frac{1}{5\pi}\frac{V}{\rho}\frac{m}{(kT)^3}\right]^{\frac{3}{2}} \exp\left(-\frac{mV}{5\rho(kT)^3}q^2\right) \exp(-\overrightarrow{\gamma}(\mathbf{Q})\mathbf{q})\mathbf{q}^2. \tag{35}$$

Our aim is to compare these two results. Let us calculate the relative deviation of the second moment with respect to $t = 0$

$$\Delta(t) \equiv \frac{\mathbf{Q}^2(t) - \mathbf{Q}^2(0)}{\mathbf{Q}^2(0)}. \tag{36}$$

The quantity $\Delta(t)$ calculated exactly will be compared with that calculated according the maximum entropy formalism. We can proceed further to evaluate it if we make definite assumptions concerning the shape of the intermolecular potential $V(\mathbf{r})$. For the evaluation we suppose that the gas consists of molecules of Ne

at atmospheric pressure and room temperature interacting through the Sutherland potential:

$$V(r) = \infty \quad \text{for} \quad r < \sigma,$$
$$V(r) = -\varepsilon \left(\frac{\sigma}{r}\right)^6 \quad \text{for} \quad r > \sigma. \tag{37}$$

See [8]. We introduce the notation: $\Lambda_{\text{exact}}(t)$ for Λ calculated exactly and $\Lambda_{\text{m.e.f.}}(t)$ for Λ calculated according the maximum entropy formalism

$$\delta(t) \equiv \Lambda_{\text{exact}}(t) - \Lambda_{\text{m.e.f.}}(t). \tag{38}$$

In the expansion of $\delta(t)$ over powers of t we get the striking result. (The term, proportional to t, of course equals zero by the definition of the maximum entropy formalism). But even in the second order (!!!) over time the disagreement between maximum entropy approach and exact solution is notable

$$\delta(t) = 1053 \text{ m}^{-1} \varepsilon^4 \sigma (kT)^{-3} \rho t^2. \tag{39}$$

For the evaluation we take neon at room temperature:

$$\sigma = 0.233 \text{ nm}, \tag{40}$$
$$\frac{\varepsilon}{k} = 192 \text{ K},$$
$$\rho = 2.445 \times 10^{25} \text{ m}^{-3}$$

and get:

$$\delta(t) = \left(\frac{t}{\tau_0}\right)^2, \tag{41}$$
$$\tau_0 = 2.8 \times 10^{-12} \text{ s}.$$

Therefore, only for $t < \tau_0$ the assumption that the system can be described by maximum entropy distribution gives the results which coincide with the results of exact calculation!

5. Conclusions

We investigated the problem of the validity of the maximum entropy formalism. In particular, we presented the first evaluation of the time for which maximum entropy distribution is valid for the description of physical systems. One can get the same order of magnitude for other potentials of interaction between particles and for other moments specified. The maximum entropy formalism turns out to be valid (if one assumes that at some time the system was described in this way) only for a period of time of 10^{-2}(!!!) atomic collisions and further on strongly disagrees with the results of exact evaluation. Thus, it turns out to be completely insufficient. Of course, if the number of moments in question [9] tends to infinity, the maximum entropy formalism gives exact results but there is no practical point to use such approach.

Acknowledgement

The author is indebted to Professor R. E. Nettleton for helpful discussions.

References

1. E. T. Jaynes, Phys. Rev., *106*, 620, 1957; *108*, 171, 1957.
2. The Maximum Entropy Formalism. Eds. R. D. Levine and M. Tribus. The MIT Press, Cambridge, Massachusetts, 1978.
3. E. S. Freidkin and R. E. Nettleton, Il Nuovo Cimento, *105B*, 1389, 1990.
4. H. Grabert, Projection Operator Technique in Nonequilibrium Statistical Mechanics. Springer Verlag, Berlin, Heidelberg, New York, 1982.
5. R. E. Nettleton and E. S. Freidkin, Physica, *158A*, 672, 1989.
6. J. Casas Vazquez, D. Jou and G. Lebon, Recent Developments in Nonequilibrium Thermodynamics. Springer, Berlin, 1984.
7. P. Resibois and M. de Leener, Classical Kinetic Theory of Fluids, John Wiley & Sons, New York, London, Sydney, Toronto, 1977.
8. J. O. Hirschfelder, C. F. Curtiss, R. B. Bird, Molecular Theory of Gases and Liquids. John Wiley & Sons, New York, 1964.
9. H. Grad, Commun. Pure Appl. Math. *2*, 331, 1949.

Acta Physica Hungarica 73 (2-4), pp. 205-223 (1993)

Ω MATRIX OF GENERALIZED GAUGE MODELS

J. V. DOMINGOS, R. M. DORIA and R. PORTUGAL*

Universidade Católica de Petrópolis (UCP-ICEN)
Petrópolis, Brazil
**Centro Brasileiro de Pesquisas Físicas (CBPF-DCP)*
Rio de Janeiro, Brazil

(Received in revised form 2o July 1993)

In generalized gauge models a so-called Ω matrix is developed. It is a non-dynamical entity which correlates different field bases. In this paper such an Ω matrix is explicitly evaluated for the cases with two, three and four fields rotating under a single group. The corresponding propagator transformations between these field bases are also calculated. An interacting potential expression depending on primordial parameters is shown.

1. Introduction

The viewpoint of associating two or more independent gauge potentials to a single compact and simple gauge group has been shown to be supported by differential-geometric arguments. Indeed an analysis based on a Kaluza–Klein coupled matter–gravity theory [1] and a description of gauge potentials in terms of connection on principal fibre bundles [2] enforce the possibility of introducing independent potentials is association to a single group and, at same time, allow a geometrical interpretation for the extra gauge fields that are introduced. Another proof was also derived by relaxing supersymmetry constraints [3]. Thus these three different origins allow to be written a generalized gauge model based on the following transformations:

$$A_{\mu I}(x) \to A'_{\mu I}(x) = U A_{\mu I}(x) U^{-1} + U \partial_\mu U^{-1}, \tag{1.1}$$

where $I = 1, \ldots, N$. Equation (1.1) brings consequences on inducing the classical generation of non-linear σ-model [4].

This generalized model can also be developed with matter fields [5]. This means that distinct flavours can be understood as rotating under a same group

$$\Phi_a \to \Phi'_a = e^{i\alpha Q} \Phi_a, \tag{1.2}$$

where Φ_a is any matter field with $a = 1, \ldots, N$ and Q is a diagonal charge matrix with q_a eigenvalues.

A first consequence of these of generalized models is that the relationship between fields and quanta is no longer univoque. The situation appears where for

a given field basis one gets that a corresponding field will carry various quanta, a result which can be verified by calculating the poles of the corresponding propagator. However, we should observe that for spin-0 and spin-1/2 there is always a field basis which is completely diagonalized. However, for high order spin cases just one sector can be diagonalized. For instance, for Eq. (1.1) the longitudinal sector will preserve a non-diagonal kinetic term while the transverse sector is diagonalized.

The motivation here is a non-dynamical entity which such generalized gauge model develops. It was identified as Ω matrix and its origin comes from the possible field rotation that theory contains:

$$\varphi = \Omega\Phi, \tag{1.3}$$

where φ and Φ are associated to field reparametrizations.

The so-called Φ-basis is a column vector containing the fields in Eq. (1.2). They generate the following diagonal Lagrangian

$$\mathcal{L}[\Phi] = \Phi^{+}\Box\Phi - \Phi^{+}m^{2}\Phi. \tag{1.4}$$

In parallel, there is the considered φ-basis, which corresponding Lagrangian

$$\tilde{\mathcal{L}}[\varphi] = \varphi^{+}\Box K\varphi - \varphi^{+}M^{2}\varphi \tag{1.5}$$

is invariant under

$$\varphi_a(x) \to \varphi'_a(x) = (e^{i\alpha(x)\tilde{Q}})_{ab}\varphi_b(x), \tag{1.6}$$

where $\tilde{Q}$ is an N-dimensional charge matrix, not necessarily diagonal. Reality condition says that K and M are hermitean. Their matrix elements are built up in terms of the so-called primordial parameters. They represent elements in such generalized gauge theories which are revealed when one works with non-diagonal field basis as Eq. (1.5). Due to the fact that such coefficients contain the property of parametrizing the model in the sense that can take any value without violating gauge symmetry, they were entitled as primordial parameters.

As a first glimpse on Ω matrix existence at such generalized gauge model we can derive the following relationship between the above charge matrices:

$$\tilde{Q} = \Omega Q \Omega^{-1} \tag{1.7}$$

which shows the influence of such initial parameters.

Notice that the Ω matrix creates scalars and tensors and shows that symmetry can change its shape in the sense that depending on the field basis it will appear in different representations for a given symmetry. Nevertheless such field reparametrizations equally describe the N-involved quanta. This property of quanta invariance was proved in [5] where it is shown that quantum numbers as spin, mass, charges, discrete symmetries which define a quantum are independent of Ω transformations. Consequently, gauge theories involving various fields rotating under a same

single group offer a kind of field reference system which says that a given quantum physics can be described through different 'field coordinates' or field reparametrizations. Therefore such proposed Ω matrix, similarly to the Lorentz matrix and to the gauge-fixing approach, belongs to the family of observators.

The Ω matrix provokes a new kind of choice on the calculation process, and it develops a method for investigating the relationships inside of such generalized gauge models. The first effort of this work is to calculate Ω explicitly. For this, Section 2 is devoted to cases involving two, three, and four fields, Section 3, to studying propagators transforming under such Ω matrix. And finally, experimental parameters as masses, coupling constants and effective potentials are calculated in Section 4 in terms of such primordial parameters. Calculations were performed through the algebraic system Reduce [6] and Maple [7].

2. Ω matrix

The objective of this Section is to evaluate the Ω matrix explicitly. For this cases involving two, three and four fields rotating under a same group will be studied. Three calculation methods were developed.

The first one means to diagonalize step by step Eq. (1.5). For this, one introduces two unitary (orthogonal) matrices S and R, where S diagonalizes the kinetic matrix K and R the correspondent mass matrix obtained after S rotation. We call $\tilde{K}$ the the diagonalized K matrix. By the use of Eqs (1.3)–(1.5) it is quite straightforward to show that the expression of Ω matrix is given by [5]:

$$\Omega = S^t \tilde{K}^{-1/2} R^t, \tag{2.1}$$

where $K > 0$ means the Ω existence condition. However, in practice expression (2.1) is very hard for doing calculations even considering algebraic computer methods.

A second method for building up the Ω matrix can be developed by using the following relationship [8]:

$$\Omega\Omega^+ = K^{-1} \tag{2.2}$$

and

$$\Omega^{-1}(K^{-1}M^2)\Omega = m^2, \tag{2.3}$$

which can be obtained from Eqs (1.3)–(1.5). One can note from Eq. (2.2) that Ω is not hermitean. Equation (2.3) can also be used to calculate the physical masses, given by the diagonal m^2 matrix, in terms of the primordial parameters.

Suppose that (λ, ω) are the eigenvalues of $K^{-1}M^2$

$$(K^{-1}M^2)w = \lambda w. \tag{2.4}$$

Then if one defines v as:

$$v = \Omega^{-1} w, \tag{2.5}$$

it yields,

$$\Omega^{-1}(K^{-1}M^2)\Omega v = \lambda v. \tag{2.6}$$

From (2.3) one can see that the elements of the diagonal matrix m^2 are $(K^{-1}M^2)$ eigenvalues. Then from Eq. (2.6), one can choose a set of eigenvalues and eigenvectors $(\lambda_1, v_1); (\lambda_2, v_2); \ldots; (\lambda_N, v_N)$ such that:

$$v_1 = \begin{pmatrix} 1 \\ 0 \\ \vdots \\ 0 \end{pmatrix}; \quad v_2 = \begin{pmatrix} 0 \\ 1 \\ \vdots \\ 0 \end{pmatrix}; \quad \ldots; \quad v_n = \begin{pmatrix} 0 \\ 0 \\ \vdots \\ 1 \end{pmatrix} \tag{2.7}$$

are satisfying the orthonormality and completeness conditions.

Therefore the corresponding set for Eq. (2.4) is $(\lambda_1, w_1 = \Omega v_1); \ldots; (\lambda_N, w_N = \Omega v_N)$ where each w_i correspond to the $i^{\text{th}}\Omega$ column

$$w_a = \begin{pmatrix} \Omega_{1a} \\ \vdots \\ \Omega_{Na} \end{pmatrix} \tag{2.8}$$

and are satisfying the following relationship

$$\sum_a w_a w_a^+ = K^{-1}. \tag{2.9}$$

Once obtained w_a satisfying Eq. (2.9) one is able to read off the elements of Ω matrix.

This second method will be taken in order to evaluate the Ω matrix. The K and M matrix are preserved general, however, obeying the conditions of K and M being hermitean and $K > 0$. We will explicitly exhibit the Ω matrix now.

First, for the case involving two fields, $N = 2$, the initial matrices are

$$K = \begin{pmatrix} k_{11} k_{12} \\ k_{12}^* k_{22} \end{pmatrix}, \quad M^2 = \begin{pmatrix} m_{11} m_{12} \\ m_{12}^* m_{22} \end{pmatrix}. \tag{2.10}$$

In this case and in the following ones the diagonal elements of K and M^2 are real constants. The correspondent Ω matrix is:

$$\Omega = \begin{pmatrix} \underset{c_1}{\frac{-2c_1(k_{12}m_{22} - k_{22}m_{12})}{-\alpha + k_{11}m_{22} + k_{12}m_{12}^* - k_{12}^* m_{12} - k_{22}m_{11}}} & \underset{c_2}{\frac{-2c_2(k_{12}m_{22} - k_{22}m_{12})}{\alpha + k_{11}m_{22} + k_{12}m_{12}^* - k_{12}^* m_{12} - k_{22}m_{11}}} \end{pmatrix}, \tag{2.11}$$

where

$$|c_1|^2 = \frac{\alpha k_{11} - k_{11}^2 m_{22} + k_{11}k_{12}m_{12}^* + k_{11}k_{12}^* m_{12} + k_{11}k_{22}m_{11} - 2k_{12}k_{12}^* m_{11}}{2\alpha \det(K)}, \tag{2.12}$$

$$|c_2| = \frac{\alpha k_{11} + k_{11}^2 m_{22} - k_{11}k_{12}m_{12}^* - k_{11}k_{12}^* m_{12} - k_{11}k_{22}m_{11} + 2k_{12}k_{12}^* m_{11}}{2\alpha \det(K)}, \tag{2.13}$$

with

$$\begin{aligned}\alpha^2 = {} & k_{11}^2 m_{22}^2 - 2k_{11}k_{12}m_{12}^* m_{22} - 2k_{11}k_{12}^* m_{12}m_{22} - 2k_{11}k_{22}m_{11}m_{22} + \\ & 4k_{11}k_{22}m_{12}m_{12}^* + k_{12}^2 m_{12}^{*2} + 4k_{12}k_{12}^* m_{11}m_{22} - 2k_{12}k_{12}^* m_{12}m_{12}^* - \\ & 2k_{12}k_{22}m_{11}m_{12}^* + k_{12}^{*2}m_{12}^2 - 2k_{12}^* k_{22}m_{11}m_{12} + k_{22}^2 m_{11}^2.\end{aligned} \tag{2.14}$$

The physical masses are given by:

$$m^2 = \begin{pmatrix} \frac{k_{11}m_{22} - k_{12}m_{12}^* - k_{12}^* m_{12} + k_{22}m_{11} - \alpha}{2\det(K)} & 0 \\ 0 & \frac{k_{11}m_{22} - k_{12}m_{12}^* - k_{12}^* m_{12} + k_{22}m_{11} + \alpha}{2\det(K)} \end{pmatrix}. \tag{2.15}$$

For $N = 3$, considering that

$$K = \begin{pmatrix} k_{11} & k_{12} & k_{13} \\ k_{12}^* & k_{22} & k_{23} \\ k_{13}^* & k_{23}^* & k_{33} \end{pmatrix}, \quad M^2 = \begin{pmatrix} m_{11} & m_{12} & m_{13} \\ m_{12}^* & m_{22} & m_{23} \\ m_{13}^* & m_{23}^* & m_{33} \end{pmatrix}, \tag{2.16}$$

one gets

$$\Omega = \begin{pmatrix} \frac{c_1(n_1 r_1 + n_2)}{r_1^2 + d_1 r_1 + d_2} & \frac{c_2(n_1 r_2 + n_2)}{r_2^2 + d_1 r_2 + d_2} & \frac{c_3(n_1 r_3 + n_2)}{r_3^2 + d_1 r_3 + d_2} \\ \frac{c_1(n_3 r_1 + n_4)}{r_1^2 + d_1 r_1 + d_2} & \frac{c_2(n_3 r_2 + n_4)}{r_2^2 + d_1 r_2 + d_2} & \frac{c_3(n_3 r_3 + n_4)}{r_3^2 + d_1 r_3 + d_2} \\ c_1 & c_2 & c_3 \end{pmatrix}, \tag{2.17}$$

with

$$\begin{aligned}|c_1|^2 = {} & ((n_1 n_4 - n_2 n_3)(k_{11}k_{22} - k_{12}k_{12}^*) + (n_1 d_2 - n_1 r_2 r_3 - n_2 d_1 - n_2 r_2 - n_2 r_3) \\ & (k_{11}k_{23} - k_{13}k_{12}^*) - (d_1 n_4 - d_2 n_3 + n_3 r_2 r_3 + n_4 r_2 + n_4 r_3)(k_{12}k_{23} - k_{13}k_{22})) \\ & (r_2 + d_1 r_1 + d_2)/((n_1 n_4 - n_2 n_3)(r_1 - r_2)(r_1 - r_3)\det(K)).\end{aligned} \tag{2.18}$$

Coefficients $|c_2|$ and $|c_3|$ are obtained by substituting Eq. (2.18) as

$$|c_2|^2 = |c_1|^2\{r_1 \leftrightarrow r_2\}, \tag{2.19}$$

$$|c_3|^2 = |c_1|^2\{r_1 \leftrightarrow r_3\}.$$

Other coefficients in Eq. (2.17) are given by

$$\begin{aligned}n_1 = {} & (k_{12}k_{23}m_{33} - k_{12}k_{33}m_{23} - k_{13}k_{22}m_{33} + \\ & k_{13}k_{23}^* m_{23} + k_{22}k_{33}m_{13} - k_{23}k_{23}^* m_{13})/\det(K),\end{aligned} \tag{2.20}$$

$$n_2 = (k_{13}m_{22}m_{33} - k_{13}m_{23}m_{23}^* - k_{23}m_{12}m_{33} + k_{23}m_{13}m_{23}^* + k_{33}m_{12}m_{23} - k_{33}m_{13}m_{22})/\det(K), \tag{2.21}$$

$$n_3 = -(k_{11}k_{23}m_{33} - k_{11}k_{33}m_{23} - k_{13}k_{12}^*m_{33} + k_{13}k_{13}^*m_{23} + k_{12}^*k_{33}m_{13} - k_{23}k_{13}^*m_{13})/\det(K), \tag{2.22}$$

$$n_4 = -(k_{13}m_{12}^*m_{33} - k_{13}m_{23}m_{13}^* - k_{23}m_{11}m_{33} + k_{23}m_{13}m_{13}^* + k_{33}m_{11}m_{23} - k_{33}m_{13}m_{12}^*)/\det(K), \tag{2.23}$$

$$\begin{aligned} d_1 = (&k_{11}k_{23}m_{23}^* - k_{11}k_{33}m_{22} - k_{12}k_{23}m_{13}^* + k_{12}k_{33}m_{12}^* + \\ &- k_{13}k_{12}^*m_{23}^* + k_{13}k_{22}m_{13}^* + k_{13}k_{13}^*m_{22} - k_{13}k_{23}^*m_{12}^* + \\ &k_{12}^*k_{33}m_{12} - k_{22}k_{33}m_{11} - k_{23}k_{13}^*m_{12} + k_{23}k_{23}^*m_{11})/\det(K), \end{aligned} \tag{2.24}$$

$$d_2 = (k_{13}m_{12}^*m_{23}^* - k_{13}m_{22}m_{13}^* - k_{23}m_{11}m_{23}^* + k_{23}m_{12}m_{13}^* + k_{33}m_{11}m_{22} - k_{33}m_{12}m_{12}^*)/\det(K). \tag{2.25}$$

r_1, r_2, r_3 are roots of the equation

$$r^3 + ar^2 + br + c = 0 \tag{2.26}$$

for

$$\begin{aligned} a = (&-k_{11}k_{22}m_{33} + k_{11}k_{23}m_{23}^* + k_{11}k_{23}^*m_{23} - k_{11}k_{33}m_{22} + \\ &k_{12}k_{12}^*m_{33} - k_{12}k_{23}m_{13}^* - k_{12}k_{13}^*m_{23} + k_{12}k_{33}m_{12}^* + \\ &- k_{13}k_{12}^*m_{23}^* + k_{13}k_{22}m_{13}^* + k_{13}k_{13}^*m_{22} + \\ &- k_{13}k_{23}^*m_{12}^* - k_{12}^*k_{23}^*m_{13} + k_{12}^*k_{33}m_{12} + k_{22}k_{13}^*m_{13} + \\ &- k_{22}k_{33}m_{11} - k_{23}k_{13}^*m_{12} + k_{23}k_{23}^*m_{11})/\det(K), \end{aligned} \tag{2.27}$$

$$\begin{aligned} b = (&k_{11}m_{22}m_{33} - k_{11}m_{23}m_{23}^* - k_{12}m_{12}^*m_{33} + k_{12}m_{23}m_{13}^* + \\ &k_{13}m_{12}^*m_{23}^* - k_{13}m_{22}m_{13}^* - k_{12}m_{12}m_{33} + k_{12}^*m_{13}m_{23}^* + \\ &k_{22}m_{11}m_{33} - k_{22}m_{13}m_{13}^* - k_{23}m_{11}m_{23}^* + k_{23}m_{12}m_{13}^* + \\ &k_{13}^*m_{12}m_{23} - k_{13}^*m_{13}m_{22} - k_{23}^*m_{11}m_{23} + k_{23}^*m_{13}m_{12}^* + \\ &k_{33}m_{11}m_{22} - k_{33}m_{12}m_{12}^*)/\det(K), \end{aligned} \tag{2.28}$$

$$c = -\det(M^2)/\det(K). \tag{2.29}$$

This equation is the characteristic equation of $K^{-1}M^2$ matrix. Therefore r_1 r_2 and r_3 are the physical masses.

For $N = 4$,

$$K = \begin{pmatrix} k_{11} & k_{12} & k_{13} & k_{14} \\ k_{12}^* & k_{22} & k_{23} & k_{24} \\ k_{13}^* & k_{23}^* & k_{33} & k_{34} \\ k_{14}^* & k_{24}^* & k_{34}^* & k_{44} \end{pmatrix}, \quad M^2 = \begin{pmatrix} m_{11} & m_{12} & m_{13} & m_{14} \\ m_{12}^* & m_{22} & m_{23} & m_{24} \\ m_{13}^* & m_{23}^* & m_{33} & m_{34} \\ m_{14}^* & m_{24}^* & m_{34}^* & m_{44} \end{pmatrix}, \tag{2.30}$$

yielding,

$$\Omega = \begin{pmatrix} \frac{c_1(n_1r_1^2+n_2r_1+n_3)}{r_1^3+d_1r^2+d_2r_1+d_3} & \frac{c_2(n_1r_2^2+n_2r_2+n_3)}{r_2^3+d_1l_2^2+d_2r_2+d_3} & \frac{c_3(n_1r_3^2+n_2r_3+n_3)}{r_3^3+d_1r_3^2+d_2r_3+d_3} & \frac{c_4(n_1r_4^2+n_2r_4+n_3)}{r_4^3+d_1r_4^2+d_2r_4+d_3} \\ \frac{c_1(n_4r_1^2+n_5r_1+n_6)}{r_1^3+d_1r_1^2+d_2r_1+d_3} & \frac{c_2(n_4r_2^2+n_5r_2+n_6)}{r_2^3+d_1r_2^2+d_2r_2+d_3} & \frac{c_3(n_4r_3^2+n_5r_3+n_6)}{r_3^3+d_1r_3^2+d_2r_3+d_3} & \frac{c_4(n_4r_4^2+n_5r_4+n_6)}{r_4^3+d_1r_4^2+d_2r_4+d_3} \\ \frac{c_1(n_7r_1^2+n_8r_1+n_9)}{r_1^3+d_1r_1^2+d_2r_1+d_3} & \frac{c_2(n_7r_2^2+n_8r_2+n_9)}{r_2^3+d_1r_2^2+d_2r_2+d_3} & \frac{c_3(n_7r_3^2+n_8r_3+n_9)}{r_3^3+d_1r_3^2+d_2r_3+d_3} & \frac{c_4(n_7r_4^2+n_8r_4+n_9)}{r_4^3+d_1r_4^2+d_2r_4+d_3} \\ c_1 & c_2 & c_3 & c_4 \end{pmatrix}, \tag{2.31}$$

with

$$|c_1|^2 = (b_{44}(n_1n_5n_9 - n_1n_6n_8 - n_2n_4n_9 + n_2n_6n_7 + n_3n_4n_8 - n_3n_5n_7) +$$
$$b_{34}(-n_1n_5d_3 - n_1n_5r_2r_3r_4 + n_1n_6d_2 - n_1n_6r_2r_3 - n_1n_6r_2r_4 - n_1n_6r_3r_4 + n_2n_4d_3 +$$
$$n_2n_4r_2r_3r_4 - n_2n_6d_1 - n_2n_6r_2 - n_2n_6r_3 - n_2n_6r_4 - n_3n_4d_2 + n_3n_4r_2r_3 + n_3n_4r_2r_4 +$$
$$n_3n_4r_3r_4 + n_3n_5d_1 + n_3n_5r_2 + n_3n_5r_3 + n_3n_5r_4) + b_{24}(n_1n_8d_3 + n_1n_8r_2r_3r_4 -$$
$$n_1n_9d_2 + n_1n_9r_2r_3 + n_1n_9r_2r_4 + n_1n_9r_3r_4 - n_2n_7d_3 - n_2n_7r_2r_3r_4 + n_2n_9d_1 +$$
$$n_2n_9r_2 + n_2n_9r_3 + n_2n_9r_4 + n_3n_7d_2 - n_3n_7r_2r_3 - n_3n_7r_2r_4 - n_3n_7r_3r_4 -$$
$$n_3n_8d_1 - n_3n_8r_2 - n_3n_8r_3 - n_3n_8r_4) + b_{14}(-n_4n_8d_3 - n_4n_8r_2r_3r_4 + n_4n_9d_2 -$$
$$n_4n_9r_2r_3 - n_4n_9r_2r_4 - n_4n_9r_3r_4 + n_5n_7d_3 + n_5n_7r_2r_3r_4 - n_5n_9d_1 - n_5n_9r_2 -$$
$$n_5n_9r_3 - n_5n_9r_4 - n_6n_7d_2 + n_6n_7r_2r_3 + n_6n_7r_2r_4 + n_6n_7r_3r_4 + n_6n_8d_1 +$$
$$n_6n_8r_2 + n_6n_8r_3 + n_6n_8r_4))(r_1^3 + d_1r_1^2 + d_2r_1 + d_3)/((n_1n_5n_9 - n_1n_6n_8 -$$
$$n_2n_4n_9 + n_2n_6n_7 + n_3n_4n_8 - n_3n_5n_7)(r_1 - r_2)(r_1 - r_3)(r_1 - r_4))$$

and similarly to the previous case

$$|c_2|^2 = |c_1|^2\{r_1 \leftrightarrow r_2\}, \tag{2.32}$$

$$|c_3|^2 = |c_1|^2\{r_1 \leftrightarrow r_3\}, \tag{2.33}$$

$$|c_4|^2 = |c_1|^2\{r_1 \leftrightarrow r_4\}. \tag{2.34}$$

Other coefficients in Eq. (2.31) are expressed as

$$n_1 = a_{14}, \tag{2.35}$$

$$n_2 = a_{12}a_{24} + a_{13}a_{34} - a_{14}a_{22} - a_{14}a_{33}, \tag{2.36}$$

$$n_3 = a_{12}a_{23}a_{34} - a_{12}a_{24}a_{33} - a_{13}a_{22}a_{34} +$$
$$a_{13}a_{24}a_{32} + a_{14}a_{22}a_{33} - a_{14}a_{23}a_{32}, \tag{2.37}$$

$$n_4 = a_{24}, \tag{2.38}$$

$$n_5 = -(a_{11}a_{24} - a_{14}a_{21} - a_{23}a_{34} + a_{24}a_{33}), \tag{2.39}$$

$$n_6 = -(a_{11}a_{24}a_{34} - a_{11}a_{24}a_{33} - a_{13}a_{21}a_{34} + a_{13}a_{24}a_{31} + a_{14}a_{21}a_{23} - a_{14}a_{23}a_{31}), \tag{2.40}$$

$$n_7 = a_{34}, \tag{2.41}$$

$$n_8 = -(a_{11}a_{34} - a_{14}a_{31} + a_{22}a_{34} - a_{24}a_{32}), \tag{2.42}$$

$$n_9 = a_{11}a_{22}a_{34} - a_{11}a_{24}a_{32} - a_{12}a_{21}a_{34} + a_{12}a_{24}a_{31} + a_{14}a_{21}a_{32} - a_{14}a_{22}a_{31}, \tag{2.43}$$

$$d_1 = -(a_{11} + a_{22} + a_{33}), \tag{2.44}$$

$$d_2 = a_{11}a_{22} + a_{11}a_{33} - a_{12}a_{21} - a_{13}a_{31} + a_{22}a_{33} - a_{23}a_{32}, \tag{2.45}$$

$$d_3 = -(a_{11}a_{22}a_{33} - a_{11}a_{23}a_{32} - a_{12}a_{21}a_{33} + a_{12}a_{23}a_{31} + a_{13}a_{21}a_{32} - a_{13}a_{22}a_{31}. \tag{2.46}$$

r_1, r_2, r_3, r_4 are the corresponding physical masses for $N = 4$, which are roots of the equation

$$r^4 + ar^3 + br^2 + cr + d = 0,$$

with

$$\begin{aligned}
a &= -(a_{11} + a_{22} + a_{33} + a_{44}),\\
b &= a_{11}a_{22} + a_{11}a_{33} + a_{11}a_{44} - a_{12}a_{21} - a_{13}a_{31}\\
&\quad - a_{14}a_{41} + a_{22}a_{33} + a_{22}a_{44} - a_{23}a_{32} - a_{24}a_{42}\\
&\quad + a_{33}a_{44} - a_{34}a_{43},\\
c &= -(a_{11}a_{22}a_{33} + a_{11}a_{22}a_{44} - a_{11}a_{23}a_{32}\\
&\quad - a_{11}a_{24}a_{42} + a_{11}a_{33}a_{44} - a_{11}a_{34}a_{43}\\
&\quad - a_{12}a_{21}a_{33} - a_{12}a_{21}a_{44} + a_{12}a_{23}a_{31}\\
&\quad + a_{12}a_{24}a_{41} + a_{13}a_{21}a_{32} - a_{13}a_{22}a_{31}\\
&\quad - a_{13}a_{31}a_{44} + a_{13}a_{34}a_{41} + a_{14}a_{21}a_{42}\\
&\quad - a_{14}a_{22}a_{41} + a_{14}a_{31}a_{43} - a_{14}a_{33}a_{41}\\
&\quad + a_{22}a_{33}a_{44} - a_{22}a_{34}a_{43} - a_{23}a_{32}a_{44}\\
&\quad + a_{23}a_{34}a_{42} + a_{24}a_{32}a_{43} - a_{24}a_{33}a_{42}),\\
d &= \det(a_{ij}).
\end{aligned} \tag{2.47}$$

a_{ij} and b_{ij} were defined as

$$a_{ij} = ((1/K)M^2)_{ij}, \tag{2.48}$$

$$b_{ij} = (1/K)_{ij}. \tag{2.49}$$

Concluding this Section, one notices that the rotation matrix Ω depends on primordial parameters written in the kinetic and mass matrices. In order to organize such results depending on primordial parameters we prefer to present them in a form which includes normalization constants c_i, the physical masses r_i and the coefficients n_i and d_i. The structure of Eqs. (2.16) and (2.17) can be generalized for the cases $N > 4$. A third method means to derive the Ω matrix through propagators expressions.

3. Propagators

At quantum level, the basic entities are the propagators. From [5] one knows that propagators are not invariant under Ω although their poles are preserved. The corresponding transformation law is

$$\langle T\Phi\Phi\rangle = \Omega^{-1}\langle(\varphi\varphi)\rangle\Omega^{t-1}. \tag{3.1}$$

Propagators are better investigated in φ-basis. This is so because in such a field reference system the expressions are written in terms of such primordial parameters. Although physics does not depend on any field basis, symmetry is more explicitly expanded at φ-basis, and so, any entity calculated there will reflect symmetry presence in more detail.

For this work $N = 2, 3$ cases will be calculated. The general expression for propagators at φ-basis is

$$\frac{1}{i}\langle T\varphi\varphi\rangle_{ij}^{N\times N} = \frac{1}{Kk^2 - M^2}|_{ij} = \sum_{l=1}^{N}\frac{(c_l)_{ij}}{k^2 - r_l^2}, \tag{3.2}$$

where r_l^2 are eigenvalues of the $K^{-1}M^2$ matrix and $(c_l)_{ij}$ coefficients to be determined.

For $N = 2$,

$$\frac{1}{Kk^2 - M^2}|_{ij}^{2\times 2} = \frac{(c_1)_{ij}}{k^2 - r_1^2} + \frac{(c_2)_{ij}}{k^2 - r_2^2}. \tag{3.3}$$

Splitting up the expressions, one gets the following propagators:

$$\langle\varphi_1\varphi_1\rangle = \frac{(c_1)_{11}}{k^2 - r_1^2} + \frac{(c_2)_{11}}{k^2 - r_2^2},$$

with

$$(c_1)_{11} = \frac{-m_{22} + k_{22}r_1^2}{(r_1^2 - r_2^2)},$$

$$(c_2)_{11} = \frac{m_{22} - r_2^2 k_{22}}{(r_1^2 - r_2^2)}, \tag{3.4}$$

and

$$\langle \varphi_2 \varphi_2 \rangle = \frac{(c_1)_{22}}{k^2 - r_1^2} + \frac{(c_2)_{22}}{k^2 - r_2^2},$$

with

$$(c_1)_{22} = \frac{m_{11} - k_{11} r_1^2}{(r_1^2 - r_2^2)},$$

$$(c_2)_{22} = \frac{m_{11} - k_{11} r_2^2}{(r_1^2 - r_2^2)}, \tag{3.5}$$

and for the non-diagonal cases

$$\langle \varphi_1 \varphi_2 \rangle = \langle \varphi_2 \varphi_1 \rangle = \frac{(c_1)_{12}}{k^2 - r_1^2} + \frac{(c_2)_{12}}{k^2 - r_2^2},$$

with

$$(c_1)_{12} = \frac{m_{12} - k_{12} r_1^2}{(r_1^2 - r_2^2)},$$

$$(c_2)_{12} = \frac{m_{12} - r_2^2 k_{12}}{(r_1^2 - r_2^2)}. \tag{3.6}$$

Poles r_1^2 and r_2^2 are the diagonal elements of matrix m^2 given by (2.15).

Equations (3.1) and (3.2) also work as a method for calculating the Ω matrix. Notice that Eq. (2.11) can be derived through Eqs (3.3)–(3.6).

The case $N = 3$ is studied in Appendix A.

4. Masses, coupling constants and effective interparticle potentials

A further aspect from these gauge models adopting more than one field rotating under a same group is that physical masses and coupling constants appear depending on more initial coefficients. For instance, in the case with two fields and adopting that kinetic and mass matrices use real, one gets from (2.15) the following expression for the physical masses:

$$(m_{\text{phys}}^2)_{1,2} = \frac{k_{11} m_{22} + k_{22} m_{11} - 2 k_{12} m_{12} \pm \alpha}{2(k_{11} k_{22} - k_{11}^2)}, \tag{4.1}$$

where

$$\alpha^2 = k_{11}^2 m_{22}^2 + k_{22}^2 m_{22}^2 + 4 k_{11} k_{12} m_{12}^2 + 4 k_{12}^2 m_{11} m_{22} - 4 k_{12} k_{12} m_{11} m_{12}^2 - 2 k_{11} k_{12} m_{12} m_{22}.$$

The fundamental consequence of Eq. (4.1) is that such generalized gauge models develop at three level physical masses expressions depending on primordial parameters.

For investigating more systematically about such a mass dependence on initial parameters one should compare with loop corrections. For this, we are going to take three cases with $\lambda\Phi^4$ type of interactions. The simplest situation is

$$\mathcal{L} = \frac{1}{2}\partial_\mu\Phi\partial^\mu\Phi - \frac{1}{2}m^2\Phi^2 - \frac{1}{4!}\lambda\Phi^4. \tag{4.2}$$

Then, from tadpole graph one reads the following expression [9]

$$m^2_{\text{phys}} = m^2_R - m^2_R\frac{\lambda_R}{16\pi^2}\left(1-\gamma+\ln\frac{4\pi\mu^2}{m^2_R}\right). \tag{4.3}$$

A next step would be to include two interacting fields

$$\begin{aligned}\mathcal{L} = &\frac{1}{2}\partial_\mu\Phi_1\partial^\mu\Phi_1 + \frac{1}{2}\partial_\mu\Phi_2\partial^\mu\Phi_2 + \\ &- \frac{1}{2}m_1^2\Phi_1^2 - \frac{1}{2}m_2^2\Phi_2^2 - \frac{G_1}{4!}\Phi_1^4 + \\ &- \frac{G_2}{4!}\Phi_2^4 - \frac{G_3}{4}\Phi_1^2\Phi_2^2.\end{aligned} \tag{4.4}$$

At one-loop, it yields

$$\begin{aligned}(m^2_{\text{phys}})_{1,2} = &m^2_{1,2} + \frac{G_1}{(4\pi)^2}m^2_{2,1}\left(\gamma - 1 + \ln\frac{m^2_{1,2}}{4\pi\mu^2}\right) + \\ &+ \frac{2G_3}{(4\pi)^2}m^2_{2,1}\left(\gamma - 1 + \ln\frac{m^2_{2,1}}{4\pi\mu^2}\right).\end{aligned} \tag{4.5}$$

Finally, one should consider a non-diagonal case

$$\begin{aligned}\mathcal{L} = &\frac{1}{2}\partial_\mu\Phi_1\partial^\mu\Phi_1 + \frac{1}{2}\partial_\mu\Phi_2\partial^\mu\Phi_2 + \\ &- \frac{1}{2}m_1^2\Phi_1^2 - \frac{1}{2}m_2^2\Phi_2^2 - \frac{1}{4!}G_1\Phi_1^4 + \\ &- \frac{1}{4!}G_2\Phi_2^4 - \frac{1}{3!}G_3\Phi_1^3\Phi_2 + \\ &- \frac{1}{4}G_4\Phi_1^2\Phi_2^2 - \frac{1}{3!}G_5\Phi_1\Phi_2^3.\end{aligned} \tag{4.6}$$

Including the counterterms, the effective action corresponding to the quadratic part is

$$\begin{aligned}\Gamma^{(2)}_{\text{finite}} = &\frac{1}{2}[(p^2 - m_1^2) + a]\Phi_1^2 + \\ &+ \frac{1}{2}[(p^2 - m_2^2) + b]\Phi_2^2 + c\Phi_1\Phi_2,\end{aligned}$$

where

$$a = \frac{G_1 m_1^2}{16\pi^2}\left(\ln\frac{4\pi\mu^2}{m_1^2} + 1 - \gamma\right) + \frac{G_4 m_2^2}{16\pi^2}\left(\ln\frac{4\pi\mu^2}{m_2^2} + 1 - \gamma\right),$$
$$b = \frac{G_2 m_2^2}{16\pi^2}\left(\ln\frac{4\pi\mu^2}{m_1^2} + 1 - \gamma\right) + \frac{G_4 m_1^2}{16\pi^2}\left(\ln\frac{4\pi\mu^2}{m_1^2} + 1 - \gamma\right), \tag{4.7}$$
$$c = \frac{G_3 m_1^2}{32\pi^2}\left(\ln\frac{4\pi\mu^2}{m_1^2} + 1 - \gamma\right) + \frac{G_5 m_2^2}{32\pi^2}\left(\ln\frac{4\pi\mu^2}{m_2^2} + 1 - \gamma\right).$$

Thus the physical masses are eigenvalues of the mass matrix

$$m^2_{\text{phys}} = \begin{pmatrix} m_1^2 - a & c \\ c & m_2^2 - b \end{pmatrix}. \tag{4.8}$$

Expanding up to $\hbar$, one obtains

$$(m^2_{\text{phys}})_{1,2} = \frac{1}{2}(m_1^2 + m_2^2 - a - b) + \pm\left[|m_1^2 - m_2^2| - \frac{|m_1^2 - m_2^2|a}{m_1^2 - m_2^2} + \frac{|m_1^2 - m_2^2|b}{m_1^2 - m_2^2}\right]. \tag{4.9}$$

Now from Eqs (4.3), (4.5) and (4.9) one also observes the existence of mass formula depending on theory initial parameters. Nevertheless, these expressions carry a fundamental difference from Eq. (4.1). It is due to the fact that their mass dependence on primordial parameters only appears after loop corrections. Thus the singular aspect in Eq. (4.1) is that it contains the situation where at classical limit such dependence on the initial set of parameters appears. This means that a special feature from such generalized gauge models is that variables involved in the Newton's second law are expected to be expressed in terms of more primordial parameters.

In order to show that the Ω matrix presence in the model is a consistent method a next step is to understand that these mass corrections do not depend on any field basis. From [5] one has that under field reparametrizations the effective actions are related through the following relationship

$$\Gamma^{(n)}_{i_1,i_2,\ldots,i_n}[\Phi] = \tilde{\Gamma}^{(n)}_{j_1,j_2,\ldots,j_n}[\varphi] \quad \Omega_{j_1,i_1}\Omega_{j_2,i_2}\ldots\Omega_{j_n i_n}. \tag{4.10}$$

At Φ-basis, the effective action can be written as

$$\Gamma[\Phi] = \frac{1}{2}\Phi^t[(p^2 - m^2) - i\pi]\Phi + \text{interactions} \tag{4.11}$$

and at φ-basis, as

$$\tilde{\Gamma}[\varphi] = \frac{1}{2}\varphi^t[(Kp^2 - M^2) - i\Sigma]\varphi + \text{interactions}. \tag{4.12}$$

Then, from (4.10) one gets

$$\Sigma = \Omega^{-1^t} \pi \Omega^{-1}. \tag{4.13}$$

Substituting (1.3) in (4.10) it yields that the equation which determines the physical masses

$$m^2_{\text{phys}} = p^2 - i\pi \tag{4.14}$$

is an invariant under Ω. Consequently, one verifies that shifts on the poles will not depend on any field parametrization basis.

A third analysis in this Section is on the coupling constant. Substituting (1.3) in (4.2), one derives that

$$G_{ijkl} = \Omega_{im}\Omega_{jn}\Omega_{kr}\Omega_{ls}\lambda_{mnrs}. \tag{4.15}$$

Equation (4.15) reveals that any coupling constant will depend on more primitive parameters. As an example, let us study a case at $N = 2$. Substituting (2.11) in Eq. (4.15) one obtains

$$\begin{aligned} G_{1111} = & \frac{16c_1^4(k_{12}m_{22} - k_{22}m_{12})^4}{(k_{11}m_{22} - \alpha - k_{22}m_{11})^4}\lambda_{1111} + \\ & \frac{16c_2^4(k_{12}m_{22} - k_{22}m_{12})^4}{(\alpha + k_{11}m_{22} - k_{22}m_{11})^4}\lambda_{1111} + \\ & \frac{64c_2(k_{12}m_{22} - k_{22}m_{12})^4 c_1^3}{(\alpha + k_{11}m_{22} - k_{22}m_{11})(k_{11}m_{22} - \alpha - k_{22}m_{11})^3}\lambda_{1122} + \\ & \frac{96c_2^2(k_{12}m_{22} - k_{22}m_{12})^4 c_1^2}{(\alpha + k_{11}m_{22} - k_{22}m_{11})^2(k_{11}m_{22} - \alpha - k_{22}m_{11})^2}\lambda_{1222} + \\ & \frac{64c_2^3(k_{12}m_{22} - k_{22}m_{12})^4 c_1}{(\alpha + k_{11}m_{22} - k_{22}m_{11})^3(k_{11}m_{22} - \alpha - k_{22}m_{11})}\lambda_{2222}, \end{aligned} \tag{4.16}$$

where c_1, c_2 and α are given by Eqs (2.12), (2.13) and (2.14).

From the above results one should understand the consequences on the interacting potential. From [5] one knows that the effective interactions do not depend on Ω. Taking the static potential case and assuming, as example, an interaction which involves just Φ_1 field, one gets

$$V_{\text{int}}(1 \to 1) = \frac{G^2_{1111}}{4\pi}\frac{e^{-m_1 r}}{r}. \tag{4.17}$$

Concluding this Section we should analyse that the expressions derived for masses, coupling constants and effective potentials are carrying a new aspect. These physical entities become written in terms of more primitive parameters which are inscribed when one writes the model at φ-basis. Consequently, these primordial parameters written at Eq. (1.5), become the basic constituents for physics to be defined. For instance, depending on their values tachyons will appear in Eq. (4.1).

Nevertheless, the main consequence of these initial coefficients is on the redefinition of the interacting potential. It has usually been defined in terms of three parameters: coupling constant, mass and distance. Analysing Eq. (4.17), one notes that G_{1111}, m_{phys} are expliciting a dependence on a more primordial set of variables given by Eqs (4.9) and (4.16), and so, the intensity of a given interaction will no more depend just on three variables.

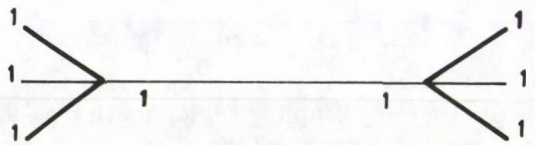

Fig. 1. An interparticle potential

5. Conclusion

Models involving the presence of more than one field in a same single group necessarily manipulate with field redefinitions. From this fact emerges a so-called Ω matrix. Therefore a first effort in this work was to calculate Ω explicitly. From Eqs (2.11), (2.17) and (2.31) one notices that Ω is adimensional and depends on free coefficients which can take any value without violating gauge symmetry. Although it was performed through a scalar case, the obtained expressions are generic. The results are the same for any generalized model involving fermions, vector bosons or tensors.

Ω matrix brings an elegant connection between the different field bases and divides the theoretical entities in scalars and tensors. For instance, Eqs (4.10) and (4.15) are expressing how the effective actions and coupling constants transform under Ω while the physical masses and the interaction potentials are scalars. Notice that this Ω matrix concentrates the information on primordial parameters that such generalized gauge models contain.

Finally, one should interpret on such primordial parameters. Three conditions in field theory are necessary for the classical limit to be reobtained. They are to consider a potential which is derived from the effective action

$$\Gamma = \sum_{n=0}^{\infty} \hbar^n \Gamma^{(n)} \tag{5.1}$$

without Planck corrections,

$$\Gamma^{(0)} = \int d^{\lambda}x\mathcal{L}^{\mathrm{cl}} \tag{5.2}$$

and on its non relativistic and static limits. After these requirements, the associated potential $V(x)$ means the potential energy from which Newton's law of motion states that

$$m\ddot{x} = F(x) = -\frac{\partial V}{\partial x}. \tag{5.3}$$

Now considering that Eq. (4.18) satisfies the above requirements, it works as an example, where generalized gauge models develop at three level a force strength expression depending on the distance and on such primordial parameters. Consequently, one derives that the velocity expression and the classical trajectory will appear depending not only on time, but also on primordial parameters written at initial Lagrangian, and that they are not necessarily associated to experimental values.

Acknowledgements

We are grateful to Marco Antonio Andrade, J. A. Helayel-Neto and Francis Wright for suggestions in the course of this work. Thanks are also due to FAPERJ, SHELL for the invaluable financial help. One of us (J. V. D.) would like to thank for the opportunity given by Dr. Michael Wyles through a scholarship.

Appendix A

Equation (1.3) preserves physics, however, propagators transform like Eq. (4.10). We present below the propagators at φ-basis, for $N = 3$:

$$\left.\frac{1}{Kk^2 - M^2}\right|_{ij}^{3\times 3} = \frac{(c_1)_{ij}}{k^2 - r_1^2} + \frac{(c_2)_{ij}}{k^2 - r_2^2} + \frac{(c_3)_{ij}}{k^2 - r_3^2}. \tag{A.1}$$

There is the following list of diagonal and non-diagonal propagators:

$$\langle\varphi_1\varphi_1\rangle = \frac{(c_1)_{11}}{k^2 - r_1^2} + \frac{(c_2)_{11}}{k^2 - r_2^2} + \frac{(c_3)_{11}}{k^2 - r_3^2},$$

with

$$(c_1)_{11} = -\frac{r_1 m_{22}k_{33} - k_{23}k_{23}^* r_1^4 + k_{22}k_{33}r_1^4 + r_1^2 m_{23}k_{23}^*}{(r_2^2 - r_1^2)(r_1^2 - r_3^2)} + \frac{m_{23}m_{23}^* + m_{22}m_{33} - r_1^2 k_{22}m_{33} + r_1^2 k_{23}m_{23}^*}{(r_2^2 - r_1^2)(r_1^2 - r_3^2)},$$

$$(c_2)_{11} = -\frac{r_2^2 k_{23} m_{23}^* - r_2^2 k_{22} m_{33} - r_2^2 m_{22} k_{33} + r_2^2 m_{23} k_{23}^*}{(r_2^4 - r_1^2 r_2^2 - r_2^2 r_3^2 + r_1^2 r_3^2)} + \frac{m_{22} m_{33} + r_2^4 k_{22} k_{33} - r_2^4 k_{23} k_{23}^* - m_{23} m_{23}^*}{(r_2^4 - r_1^2 r_2^2 - r_2^2 r_3^2 + r_1^2 r_3^2)(x - r_2^2)},$$

$$(c_3)_{11} = \frac{r_3^2 k_{22} m_{33} - r_3^4 k_{22} k_{33} + r_3^4 k_{23} k_{23}^* - r_3^2 k_{23} m_{23}^*}{(r_2^2 - r_3^2)(r_1^2 - r_3^2)} + \frac{r_3^2 m_{22} k_{33} - r_3^2 m_{23} k_{23}^* - m_{22} m_{33} + m_{23} m_{23}^*}{(r_2^2 - r_3^2)(r_1^2 - r_3^2)} \tag{A.2}$$

and

$$\langle \varphi_1 \varphi_2 \rangle = \langle \varphi_2 \varphi_1 \rangle = \frac{(c_1)_{12}}{k^2 - r_1^2} + \frac{(c_2)_{12}}{k^2 - r_2^2} + \frac{(c_3)_{12}}{k^2 - r_3^2},$$

with

$$(c_1)_{12} = \frac{r_2^4 k_{12} k_{33} - r_2^4 k_{13} k_{23}^* - m_{13} m_{23}^* - r_2^2 k_{12} m_{33}}{(r_2^2 - r_3^2)(r_2^2 - r_1^2)} + \frac{r_2^2 k_{13} m_{23}^* - r_2^2 m_{12} k_{33} + r_2^2 m_{13} k_{23}^* + m_{12} m_{33}}{(r_2^2 - r_3^2)(r_2^2 - r_1^2)},$$

$$(c_2)_{12} = -\frac{k_{12} k_{33} r_1^4 - m_{13} m_{23}^* - r_1^2 k_{12} m_{33} + m_{12} m_{33}}{(r_2^2 - r_1^2)(r_1^2 - r_3^2)} - \frac{k_{13} k_{23}^* r_1^4 + r_1^2 m_{13} k_{23}^* + r_1^2 k_{13} m_{23}^* - r_1^2 m_{12} k_{33}}{(r_2^2 - r_1^2)(r_1^2 - r_3^2)},$$

$$(c_3)_{12} = -\frac{r_3^2 k_{12} m_{33} - r_3^4 k_{12} k_{33} + r_3^4 k_{13} k_{23}^* - r_3^2 k_{13} m_{23}^*}{(r_3^4 - r_1^2 r_3^2 - r_2^2 r_3^2 + r_2^2 r_2^2)} + \frac{r_3^2 m_{12} k_{33} - r_3^2 m_{13} k_{23}^* - m_{12} m_{33} + m_{13} m_{23}^*}{(r_3^4 - r_1^2 r_3^2 - r_2^2 r_3^2 + r_2^2 r_2^2)} \tag{A.3}$$

and

$$\langle \varphi_1 \varphi_3 \rangle = \langle \varphi_3 \varphi_1 \rangle = \frac{(c_1)_{13}}{k^2 - r_1^2} + \frac{(c_2)_{13}}{k^2 - r_2^2} + \frac{(c_3)_{13}}{k^2 - r_3^2},$$

with

$$(c_1)_{13} = \frac{-m_{13} m_{22} - r_1^2 m_{22} - r_1^2 k_{12} m_{23} + r_1^2 k_{13} m_{22} - r_1^2 m_{12} k_{23}}{(r_2^2 - r_1^2)(r_1^2 - r_3^2)} + \frac{r_1^2 m_{13} k_{22} + r_1^4 k_{12} k_{23} - r_1^4 k_{13} k_{22} + m_{12} m_{23}}{(r_2^2 - r_1^2)(r_1^2 - r_3^2)},$$

$$(c_2)_{13} = -\frac{r_2^2 k_{13} m_{22} - r_2^2 k_{12} m_{23} - r_2^2 m_{12} k_{23} + r_2^2 m_{13} k_{22}}{(r_2^4 - r_1^2 r_2^2 - r_2^2 r_3^2 + r_1^2 r_3^2)} + \frac{r_2^4 k_{12} k_{23} - r_2^4 k_{13} k_{22} + m_{12} m_{23} - m_{13} m_{22}}{(r_2^4 - r_1^2 r_2^2 - r_2^2 r_3^2 + r_1^2 r_3^2)},$$

$$(c_3)_{13} = -\frac{r_3^2 k_{12} m_{23} - m_{23} - m_{13} m_{22} + r_3^2 k_{13} m_{22} + r_3^2 m_{13} k_{22}}{(r_2^2 - r_3^2)(r_1^2 - r_3^2)} - \frac{r_3^2 m_{12} k_{23} + m_{12} m_{23} - k_{13} k_{22} r_3^4 + k_{12} k_{23} r_3^4}{(r_2^2 - r_3^2)(r_1^2 - r_3^2)} \tag{A.4}$$

and

$$\langle \varphi_2 \varphi_2 \rangle = \frac{(c_1)_{22}}{k^2 - r_1^2} + \frac{(c_2)_{22}}{k^2 - r_2^2} + \frac{(c_3)_{22}}{k^2 - r_3^2},$$

with

$$(c_1)_{22} = \frac{k_{11} k_{33} r_1^4 + m_{11} m_{33} - m_{13} m_{13}^* + r_1^2 k_{13} m_{13}^*}{(r_2^2 - r_1^2)(r_1^2 - r_3^2)} - \frac{r_1^2 m_{11} k_{33} + r_1^2 m_{13} k_{13}^* - r_1^2 k_{11} m_{33} - k_{13} k_{13}^* r_1^4}{(r_2^2 - r_1^2)(r_1^2 - r_3^2)},$$

$$(c_2)_{22} = -\frac{r_2^2 m_{13} k_{13}^* - r_2^2 m_{11} k_{33} - r_2^2 k_{11} m_{33} - m_{13} m_{13}^*}{(r_2^2 - r_3^2)(r_2^2 - r_1^2)} - \frac{r_2^4 k_{13} k_{13}^* + r_2^4 k_{11} k_{33} + r_2^2 k_{13} m_{13}^* + m_{11} m_{33}}{(r_2^2 - r_3^2)(r_2^2 - r_1^2)},$$

$$(c_3)_{22} = \frac{r_3^2 k_{11} m_{33} - r_3^4 k_{11} k_{33} + r_3^4 k_{13} k_{13}^* - r_3^2 k_{13} m_{13}^*}{(r_3^4 - r_1^2 r_3^2 - r_2^2 r_3^2 + r_1^2 r_2^2)} + \frac{r_3^2 m_{11} k_{33} - r_3^2 m_{13} k_{13}^* - m_{11} m_{33} + m_{13} m_{13}^*}{(r_3^4 - r_1^2 r_3^2 - r_2^2 r_3^2 + r_1^2 r_2^2)} \tag{A.5}$$

and

$$\langle \varphi_2 \varphi_3 \rangle = \langle \varphi_3 \varphi_2 \rangle = \frac{(c_1)_{23}}{k^2 - r_1^2} + \frac{(c_2)_{23}}{k^2 - r_2^2} + \frac{(c_3)_{23}}{k^2 - r_3^2},$$

with

$$(c_1)_{23} = \frac{k_{13} k_{12}^* r_1^4 - m_{11} m_{23} - k_{11} k_{23} r_1^4 + m_{13} m_{12}^*}{(r_2^2 - r_1^2)(r_1^2 - r_3^2)} + \frac{r_1^2 k_{11} m_{23} - r_1^2 k_{13} m_{12}^* - r_1^2 m_{13} k_{12}^* + r_1^2 m_{11} k_{23}}{(r_2^2 - r_1^2)(r_1^2 - r_3^2)},$$

$$(c_2)_{23} = -\frac{m_{13}m_{12}^* + r_2^4 k_{13}k_{12}^* - m_{11}m_{23} - r_2^2 m_{13}k_{12}^*}{(r_2^2 - r_3^2)(r_2^2 - r_1^2)} + \frac{r_2^2 k_{11}m_{23} - r_2^2 k_{13}m_{12}^* + r_2^2 m_{11}k_{23} - r_2^4 k_{11}k_{23}}{(r_2^2 - r_3^2)(r_2^2 - r_1^2)},$$

$$(c_3)_{23} = \frac{r_3^4 k_{11}k_{23} - r_3^2 k_{11}m_{23} - r_3^4 k_{13}k_{12}^* + r_3^2 k_{13}m_{12}^*}{(r_3^4 - r_1^2 r_3^2 - r_2^2 r_3^2 + r_1^2 r_2^2)} + - \frac{r_3^2 m_{11}k_{23} + r_3^2 m_{13}k_{12}^* + m_{11}m_{23} - m_{13}m_{12}^*}{(r_3^4 - r_1^2 r_3^2 - r_2^2 r_3^2 + r_1^2 r_2^2)} \tag{A.6}$$

and finally,

$$\langle \varphi_3 \varphi_3 \rangle = \frac{(c_1)_{33}}{k^2 - r_1^2} + \frac{(c_2)_{33}}{k^2 - r_2^2} + \frac{(c_3)_{33}}{k^2 - r_3^2},$$

with

$$(c_1)_{33} = \frac{m_{12}m_{12}^* - m_{11}m_{22} + m_{22}r_2^2 k_{11} + r_2^4 k_{12}k_{12}^*}{(r_2^2 - r_3^2)(r_2^2 - r_1^2)} + - \frac{r_2^2 k_{12}m_{12}^* + r_2^2 k_{22}m_{11} - m_{12}r_2^2 k_{12}^* - r_2^4 k_{22}k_{11}}{(r_2^2 - r_3^2)(r_2^2 - r_1^2)},$$

$$(c_2)_{33} = -\frac{m_{12}m_{12}^* + k_{22}r_1^2 m_{11} - m_{11}m_{22} + m_{22}k_{11}r_1^2}{(r_2^2 - r_1^2)(r_1^2 - r_3^2)} + - \frac{k_{22}r_1^4 k_{11} - k_{12}r_1^2 m_{12}^* + k_{12}r_1^4 k_{12}^* - m_{12}k_{12}^* r_1^2}{(r_2^2 - r_1^2)(r_1^2 - r_3^2)},$$

$$(c_3)_{33} = \frac{r_3^2 k_{11}m_{22} - r_3^4 k_{11}k_{22} + r_3^4 k_{12}k_{12}^* - r_3^2 k_{12}m_{12}^*}{(r_3^2 - r_2^2)(r_3^2 - r_1^2)} + \frac{r_3^2 m_{11}k_{22} - r_3^2 m_{12}k_{12}^* - m_{11}m_{22} + m_{12}m_{12}^*}{(r_3^2 - r_2^2)(r_3^2 - r_1^2)}. \tag{A.7}$$

Physical masses r_1^2, r_2^2 and r_3^2 are roots of the cubic equations (2.26)–(2.29).

References

1. R. M. Doria and C. Pombo, Il Nuovo Cim., *96B*, 2, 1986; C. M. Doria, R. M. Doria, J. A. Helayel-Neto, Rev. Bras. Fís., *17*, 3, 1987.
2. C. M. Doria, R. M. Doria and J. A. Helayel-Neto, Comm. Theor. Phys., 1992.
3. N. Chair, J. A. Helayel-Neto and A. William Smith, Phys. Lett., *B 233*, 173, 1989; S. A. Dias, R. M. Doria, J. L. Matheus Valle, Rev. Bras. Fis., *21*, No. 1, 1991; C. M. Doria,

R. M. Doria, F. A. B. Rabelo de Carvalho, A Superspace Origin for an Extended Gauge Model, UCP preprint, 88/6; C. A. S. Almeida, R. M. Doria, Rev. Bras. Fis., *21*, No. 3, 1991; C. A. S. Almeida, R. M. Doria, A Less-Constrained (2,0) Super Yang–Mills Model: The Coupling to Non-linear σ-models, UCP preprint 90/4.

4. R. M. Doria, J. A. Helayel-Neto and S. Mokhtari, Europhys. Lett., *16*, (1), 1991.
5. R. M. Doria, F. A Rabelo de Carvalho, Braz. J. Phys., *23*, No 1; R. M. Doria, G. Oliveira Neto, F. A. B. Rabelo de Carvalho, A Consistent Spectroscopical Analysis for an Extended Gauge Model, UCP preprint 90/9; R. M. Doria and J. A. Helayel-Neto, Tensors and Invariants in a Generalized Gauge Model, UCP preprint 91/7.
6. Anthony C. Hearn, Reduce User's Manual Version 3.4, 1991.
7. A. Heck, Introduction to Maple, to be published.
8. M. A. Andrade, Master Thesis, CBPF, 1992.
9. J. Zinn-Justin, Quantum Field Theory and Critical Phenomena, Oxford Science Publications, Oxford, 1990.

Acta Physica Hungarica 73 (2-4), pp. 225-235 (1993)

THERMOSOLUTAL INSTABILITY OF AN OLDROYDIAN VISCOELASTIC FLUID IN POROUS MEDIUM

R. C. SHARMA and V. K. BHARDWAJ

Department of Mathematics, Himachal Pradesh University
Shimla 171005, India

(Received 20 July 1993)

The thermosolutal instability of an Oldroydian viscoelastic fluid in porous medium is considered. The effects of uniform rotation and uniform magnetic field, separately, have also been studied. The stable solute gradient, rotation and magnetic field are found to have stabilizing effects on the system. The medium permeability has destabilizing effect but in the presence of rotation it has both stabilizing and destabilizing effects depending on the rotation parameter. The magnetic field, rotation and stable solute gradient introduce oscillatory modes in the system which were non-existent in their absence.

1. Introduction

The thermal convection in a horizontal layer of a Newtonian viscous fluid has been discussed in detail by Chandrasekhar [4]. Bhatia and Steiner [2] have studied the thermal instability of a Maxwellian viscoelastic fluid in presence of rotation. The thermal instability of a Maxwellian viscoelastic fluid in hydromagnetics has also been considered by Bhatia and Steiner [3]. Veronis [13] has investigated the problem of thermohaline convection in a layer of Newtonian fluid heated from below and subjected to a stable salinity gradient. The medium has been considered to be non-porous in all the above studies.

There has been considerable interest in recent years in the study of the breakdown of the stability of a layer of fluid subject to a vertical temperature gradient in a porous medium and the possibility of convective flow. The stability of flow of a single-component fluid through a porous medium taking into account the Darcy resistance has been considered by Lapwood [7] and Wooding [14]. The Darcy's equation describes the incompressible flow of a Newtonian fluid of viscosity μ through a macroscopically homogeneous and isotropic porous medium of permeability k_1. If $\mathbf{q}$ is the filter velocity of the fluid, the resistance term $-(\frac{\mu}{k_1})\mathbf{q}$ replaces the usual viscous term in the equations of fluid motion. There is mounting evidence, both theoretical and experimental, which suggests that Darcy's equation sometimes provides an unsatisfactory description of the hydrodynamic conditions, particularly near boundaries of a porous medium. Beavers et al [1] have experimentally demonstrated the existence of shear within the porous medium near a surface where the porous medium is exposed to a freely-flowing fluid, thus forming

a zone of shear-induced fluid flow. The Darcy's equation, however, cannot predict the existence of such a boundary zone, as no macroscopic shear term is included in this equation (Joseph and Tao [6]). To be mathematically compatible with the Navier–Stokes equations and physically consistent with the above-mentioned experimentally observed boundary shear zone, Brinkman proposed the introduction of the term $(\frac{\mu}{\epsilon})\nabla^2\mathbf{q}$ in addition to $-(\frac{\mu}{k_1})\mathbf{q}$ in the equations of fluid motion. The elaborate statistical justification of the Brinkman equations has been presented by Saffman [10] and Lundgren [8].

Toms and Strawbridge [12] have demonstrated experimentally that a dilute solution of methyl methacrylate in n-butyl acetate agrees well with the theoretical model of Oldroydian viscoelastic fluid. The thermal instability in a rapidly rotating Oldroydian fluid has been considered by Eltayeb [5].

The present paper deals with the thermosolutal instability of an Oldroydian viscoelastic fluid in porous medium. The effects of uniform rotation and uniform magnetic field on the problem are also considered. The problem finds its relevance and usefulness in chemical technology and geophysics.

2. Perturbation equations

Consider an infinite horizontal layer of Oldroydian viscoelastic fluid of depth d in porous medium, heated and solute concentrated from below and acted on by gravity force $\mathbf{g}(0, 0, -g)$. The Oldroyd fluid is described by the constitutive relations (Oldroyd [9]):

$$\begin{gathered} T_{ij} = -p\delta_{ij} + \tau_{ij}, \\ \left(1 + \lambda\frac{\partial}{\partial t}\right)\tau_{ij} = 2\mu\left(1 + \lambda_0\frac{\partial}{\partial t}\right)e_{ij}, \\ e_{ij} = \frac{1}{2}\left(\frac{\partial q_i}{\partial x_j} + \frac{\partial q_j}{\partial x_i}\right), \end{gathered} \tag{1}$$

where T_{ij}, τ_{ij}, e_{ij}, p, q_i, x_i, μ, λ and λ_0 $(< \lambda)$ denote respectively the stress tensor, shear stress tensor, rate-of-strain tensor, scalar pressure, velocity, position vector, viscosity, stress relaxation time and strain retardation time. When a fluid permeates a porous material, the actual path of an individual particle of fluid cannot be followed analytically. The gross effect, as the fluid slowly percolates through the pores of the rock, is represented by the macroscopic Brinkman equation described above. Let $\delta\rho$, δp, $\mathbf{q}(u, v, w)$, Θ and γ denote respectively the perturbations in density ρ, pressure p, filter velocity (zero initially), temperature T and solute concentration C. Then the linearized thermosolutal perturbation equations through porous medium, following Boussinesq approximation, are

$$\begin{aligned} \frac{1}{\epsilon}\left(1 + \lambda\frac{\partial}{\partial t}\right)\frac{\partial\mathbf{q}}{\partial t} &= \left(1 + \lambda\frac{\partial}{\partial t}\right)\left[-\frac{1}{\rho_0}\nabla\delta p + \mathbf{g}\frac{\delta\rho}{\rho_0}\right] \\ &\quad + \frac{\nu}{\epsilon}\left(1 + \lambda_0\frac{\partial}{\partial t}\right)\left(\nabla^2 - \frac{\epsilon}{k_1}\right)\mathbf{q}, \end{aligned} \tag{2}$$

$$\nabla \cdot \mathbf{q} = 0, \tag{3}$$

$$\left(E\frac{\partial}{\partial t} - \kappa\nabla^2\right)\Theta = \beta w, \tag{4}$$

$$\left(E'\frac{\partial}{\partial t} - \kappa'\nabla^2\right)\gamma = \beta' w. \tag{5}$$

Here $\nu\ (= \mu/\rho_0)$, κ, κ', $\beta\ (= |\frac{dT}{dz}|)$ and $\beta'\ (= |\frac{dC}{dz}|)$ stand for the kinematic viscosity, the thermal diffusivity, the solute diffusivity, uniform temperature gradient and uniform solute concentration gradient, respectively. $E = \epsilon + (1-\epsilon)\frac{\rho_s c_s}{\rho_0 c_v}$ where ρ, c_v and ρ_s, c_s stand for density and specific heat of fluid and solid matrix, respectively. E' is an analogous solute constant.

The equation of state

$$\rho = \rho_0[1 - \alpha(T - T_0) + \alpha'(C - C_0)] \tag{6}$$

contains a thermal coefficient of expansion α and an analogous solvent coefficient α'. The suffix zero refers to values at the reference level $z = 0$. The change in density $\delta\rho$, caused by the perturbations Θ and γ in temperature and concentration, is given by

$$\delta\rho = -\rho_0(\alpha\Theta - \alpha'\gamma). \tag{7}$$

Eliminating δp between the three component equations of (2) and using (3), we obtain

$$\left(1 + \lambda\frac{\partial}{\partial t}\right)\left[\frac{1}{\epsilon}\nabla^2\frac{\partial w}{\partial t} - g\left(\frac{\partial^2}{\partial x^2} + \frac{\partial^2}{\partial y^2}\right)(\alpha\Theta - \alpha'\gamma)\right]$$
$$- \frac{\nu}{\epsilon}\left(1 + \lambda_0\frac{\partial}{\partial t}\right)\left(\nabla^2 - \frac{\epsilon}{k_1}\right)\nabla^2 w = 0. \tag{8}$$

Let us assume both the boundaries to be free. The case of two free boundaries is a little artifical except in stellar atmospheres (Spiegel [11]). However, this assumption allows us to obtain the analytical solution without affecting the essential features of the problem. The boundary conditions appropriate for the problem are (Chandrasekhar [4], Lapwood [7]):

$$w = \frac{\partial^2 w}{\partial z^2} = \Theta = 0 \quad \text{at} \quad z = 0 \quad \text{and} \quad z = d. \tag{9}$$

3. Dispersion relation and discussion

Analyzing the disturbances into normal modes, we assume that the perturbation quantities are of the form

$$[w, \Theta, \gamma] = [w(z), \Theta(z), \Gamma(z)]\exp(ik_x x + ik_y y + nt), \tag{10}$$

where k_x, k_y are wave numbers along x- and y- directions, respectively, k $(= \sqrt{k_x^2 + k_y^2})$ is the resultant wave number and n is, in general, a complex constant.

Assuming that x, y, z stand for the coordinates in the new unit of length d and letting $a = kd$, $\sigma = nd^2/\nu$, $F = \lambda\nu/d^2$, $F_0 = \lambda_0\nu/d^2$, $p_1 = \nu/\kappa$, $q = \nu/\kappa'$, $p_l = k_1/d^2$ and $D = \frac{d}{dz}$, Eqs (4), (5) and (8) using expression (10), in nondimensional form become

$$\left[(1+F\sigma)\frac{\sigma}{\epsilon} + \frac{1}{P_l}(1+F_0\sigma)\right](D^2-a^2)W + (1+F\sigma)\frac{gd^2a^2}{\nu}(\alpha\Theta - \alpha'\Gamma) - \frac{1}{\epsilon}(1+F_0\sigma)(D^2-a^2)^2W = 0, \tag{11}$$

$$(D^2 - a^2 - Ep_1\sigma)\Theta = -\left(\frac{\beta d^2}{\kappa}\right)W, \tag{12}$$

$$(D^2 - a^2 - E'q\sigma)\Gamma = -\left(\frac{\beta' d^2}{\kappa'}\right)W. \tag{13}$$

Operating Eq. (11) by $(D^2 - a^2 - Ep_1\sigma)(D^2 - a^2 - E'q\sigma)$ and using (12) and (13), thus eliminating Θ and Γ, we obtain

$$(D^2 - a^2 - Ep_1\sigma)(D^2 - a^2 - E'q\sigma)(D^2 - a^2)\left[\frac{\sigma}{\epsilon}(1+F\sigma) + \frac{1}{P_l}(1+F_0\sigma) - \frac{1}{\epsilon}(1+F_0\sigma)(D^2-a^2)\right]W$$
$$= (1+F\sigma)a^2[R(D^2 - a^2 - E'q\sigma) - S(D^2 - a^2 - Ep_1\sigma)]W, \tag{14}$$

where $R = \frac{g\alpha\beta d^4}{\nu\kappa}$ is the Rayleigh number and $S = g\alpha'\beta' d^4/\nu\kappa'$ is the analogous solute Rayleigh number.

The boundary conditions (9) transform to

$$W = D^2W = \Theta = \Gamma = 0 \quad \text{at} \quad z = 0 \quad \text{and} \quad 1. \tag{15}$$

Using the above boundary conditions, it can be shown that all the even order derivatives of W must vanish for $z = 0$ and 1 and hence the proper solution of Eq. (14) characterizing the lowest mode is

$$W = W_0 \sin \pi z, \tag{16}$$

where W_0 is a constant.

Substituting (16) in Eq. (14) and letting $R_1 = R/\pi^4$, $S_1 = S/\pi^4$, $i\sigma_1 = \sigma/\pi^2$, $x = a^2/\pi^2$ and $P = \pi^2 P_l$, we obtain the dispersion relation

$$R_1 = \frac{(1+x)(1+x+iEp_1\sigma_1)}{x(1+i\pi^2F\sigma_1)}\left[\frac{i\sigma_1}{\epsilon}(1+i\pi^2F\sigma_1) + (1+i\pi^2F_0\sigma_1)\left(\frac{1+x}{\epsilon} + \frac{1}{P}\right)\right] + S_1\frac{1+x+iEp_1\sigma_1}{1+x+iE'q\sigma_1}. \tag{17}$$

For the stationary convection, $\sigma = 0$ and Eq. (17) reduces to

$$R_1 = \frac{(1+x)^2}{x}\left(\frac{1+x}{\epsilon} + \frac{1}{P}\right) + S_1. \tag{18}$$

Thus for stationary convection, the stress relaxation time parameter F and the strain retardation time parameter F_0 vanish with σ and the Oldroydian fluid behaves like an ordinary Newtonian fluid. Equation (18) gives

$$\frac{dR_1}{dP} = -\frac{(1+x)^2}{xP^2}, \tag{19}$$

and

$$\frac{dR_1}{dS_1} = +1, \tag{20}$$

meaning thereby that medium permeability and stable solute gradient have destabilizing and stabilizing effects, respectively, on the thermosolutal convection for the stationary case.

4. Effect of rotation

Here the problem is considered to be the same as described in Section 2 except that the fluid is in a state of uniform rotation $\vec{\Omega}(0, 0, \Omega)$. The linearized perturbed equation of motion becomes

$$\frac{1}{\epsilon}\left(1 + \lambda\frac{\partial}{\partial t}\right)\frac{\partial \mathbf{q}}{\partial t} = \left(1 + \lambda\frac{\partial}{\partial t}\right)\left[-\frac{1}{\rho_0}\nabla\delta p - \mathbf{g}(\alpha\Theta - \alpha'\gamma) + 2(\mathbf{q} \times \vec{\Omega})\right] + \left(1 + \lambda_0\frac{\partial}{\partial t}\right)\left[\frac{\nu}{\epsilon}\nabla^2 - \frac{\nu}{k_1}\right]\mathbf{q}. \tag{21}$$

Equations (3)–(5) remain unaltered. Let $\zeta = \frac{\partial v}{\partial x} - \frac{\partial u}{\partial y}$ stand for the z-component of vorticity and express

$$\zeta = Z(z)\exp(ik_x x + ik_y y + nt). \tag{22}$$

Equations (3)–(5) and (21), using expressions (10) and (22), yield the dimensionless equations

$$(1 + F\sigma)\left[\sigma\epsilon(D^2 - a^2)W + \frac{gd^2a^2\epsilon}{\nu}(\alpha\Theta - \alpha'\Gamma) + \frac{2\Omega d^3}{\nu}DZ\right] = (1 + F^*\sigma)\left(D^2 - a^2 - \frac{\epsilon}{P_l}\right)(D^2 - a^2)W, \tag{23}$$

$$\left[(1 + F\sigma)\sigma\epsilon - (1 + F^*\sigma)\left(D^2 - a^2 - \frac{\epsilon}{P_l}\right)\right]Z = \frac{2\Omega d}{\nu}(1 + F\sigma)DW, \tag{24}$$

together with (12) and (13). The boundary conditions in addition to (15) are

$$DZ = 0 \quad \text{at} \quad z = 0 \quad \text{and} \quad 1. \tag{25}$$

Eliminating Θ, Γ and Z between Eqs (12), (13), (23) and (24) and using the proper solution (16), we obtain

$$R_1 = \frac{(1+x)(1+x+iEp_1\sigma_1)[i\epsilon\sigma_1(1+i\pi^2F\sigma_1)+(1+i\pi^2F_0\sigma_1)(1+x+\frac{\epsilon}{P})]}{x(1+i\pi^2F\sigma_1)} + S_1\frac{(1+x+iEp_1\sigma_1)}{(1+x+iE'q\sigma_1)} + T_{A_1}\frac{(1+x+iEp_1\sigma_1)(1+i\pi^2F\sigma_1)}{x[i\epsilon\sigma_1(1+i\pi^2F\sigma_1)+(1+i\pi^2F_0\sigma_1)(1+x+\frac{\epsilon}{P})]}, \tag{26}$$

where $T_{A_1} = \frac{T_A}{\pi^4}$.

4(a). The stationary convection

For the stationary convection, $\sigma = 0$ and Eq. (26) reduces to

$$R_1 = \frac{(1+x)^2}{x}(1+x+\frac{\epsilon}{P}) + S_1 + T_{A_1}\frac{(1+x)}{x}\frac{1}{(1+x+\frac{\epsilon}{P})}. \tag{27}$$

Equation (27) yields

$$\frac{dR_1}{dT_{A_1}} = \frac{(1+x)}{x(1+x+\epsilon/P)}, \tag{28}$$

$$\frac{dR_1}{dS_1} = +1, \tag{29}$$

which imply that the uniform rotation and stable solute gradient have stabilizing effects on the system. Equation (27) also gives

$$\frac{dR_1}{dP} = \left(\frac{1+x}{x}\right)\frac{\epsilon}{P^2}\left[\frac{T_{A_1}}{(1+x+\frac{\epsilon}{P})^2} - (1+x)\right]. \tag{30}$$

It is clear from Eq. (30) that the medium permeability has a destabilizing effect in the absence of rotation. It still has a destabilizing effect if

$$T_{A_1} < (1+x)\left(1+x+\frac{\epsilon}{P}\right)^2.$$

But the medium permeability has a stabilizing effect if

$$T_{A_1} > (1+x)\left(1+x+\frac{\epsilon}{P}\right)^2.$$

Thus the medium permeability has both stabilizing and destabilizing effects depending on the rotation parameter.

4(b). The oscillatory modes

Here we discuss the possibility of oscillatory modes, if any, coming into play due to the presence of rotation. Multiplying Eq. (23) by W^*, the complex conjugate of W, integrating over the range of z and making use of (12), (13) and (24) together with the boundary conditions (15) and (25), we obtain

$$\left[\sigma + \frac{(1+F_0\sigma)}{P_l(1+F\sigma)}\right] I_1 + \frac{g\alpha'\kappa' a^2}{\nu\beta'}(I_4 + E'q\sigma^* I_5)$$
$$+ d^2\left[\sigma^* + \frac{1}{P_l}(1+F_0\sigma^*)\right] I_6 + \frac{d^2}{\epsilon}(1+F_0\sigma^*)I_7$$
$$+ \frac{(1+F_0\sigma)}{\epsilon(1+F\sigma)} I_8 = \frac{g\alpha\kappa a^2}{\nu\beta}(I_2 + Ep_1\sigma^* I_3), \tag{31}$$

where

$$I_1 = \int_0^1 (|DW|^2 + a^2|W|^2)dz,$$
$$I_2 = \int_0^1 (|D\Theta|^2 + a^2|\Theta|^2)dz,$$
$$I_3 = \int_0^1 |\Theta|^2 dz,$$
$$I_4 = \int_0^1 (|D\Gamma|^2 + a^2|\Gamma|^2)dz,$$
$$I_5 = \int_0^1 |\Gamma|^2 dz,$$
$$I_6 = \int_0^1 |Z|^2 dz,$$
$$I_7 = \int_0^1 (|DZ|^2 + a^2|Z|^2)dz,$$
$$I_8 = \int_0^1 (|D^2W|^2 + 2a^2|DW|^2 + a^4|W|^2)dz \tag{32}$$

which are all positive definite. Putting $\sigma = \sigma_r + i\sigma_i$ in (31) and then equating real and imaginary parts, we obtain

$$\sigma_r\left[\left\{1 + \frac{(F+F_0+\sigma_r FF_0)}{(1+F\sigma_r)^2+F^2\sigma_i^2}\frac{1}{P_l}\right\} I_1 + \frac{g\alpha'\kappa' a^2}{\nu\beta'}E'qI_5 + d^2\left(1+\frac{F_0}{P_l}\right)I_6 + \right.$$
$$\left. + \frac{d^2F_0}{\epsilon}I_7 + \frac{(F+F_0+\sigma_r FF_0)}{(1+F\sigma_r)^2+F^2\sigma_i^2}\frac{I_8}{\epsilon} - \frac{g\alpha\kappa a^2}{\nu\beta}Ep_1 I_3\right]$$
$$= -\left[\frac{(1+FF_0+\sigma_i^2)}{(1+F\sigma_r)^2+F^2\sigma_i^2}\frac{I_1}{P_l} + \frac{g\alpha'\kappa' a^2}{\nu\beta'}I_4 + \frac{d^2}{P_l}I_6 + \right.$$
$$\left. + \frac{d^2}{\epsilon}I_7 + \frac{(1+FF_0\sigma_i^2)}{(1+F\sigma_r)^2+F^2\sigma_i^2}\frac{I_8}{\epsilon} - \frac{g\alpha\kappa a^2}{\nu\beta}I_2\right], \tag{33}$$

and

$$\sigma_i \left[I_1 - \frac{g\alpha'\kappa' a^2}{\nu\beta'} E' q I_5 - d^2 \left(1 + \frac{F_0}{P_l}\right) I_6 - \frac{F_0 d^2}{\epsilon} I_7 + \frac{g\alpha\kappa a^2}{\nu\beta} E p_1 I_3 \right] = 0. \quad (34)$$

It is clear from Eq. (33) that σ_r may be positive or negative implying thereby that there may be stability or instability in the presence of rotation, stable solute gradient, viscoelasticity and porosity on thermosolutal convection in an Oldroydian viscoelastic fluid in porous medium which is also true in their absence.

Equation (34) implies that $\sigma_i = 0$ or $\sigma_i \neq 0$ which means that the modes may be non-oscillatory or oscillatory. In the absence of stable solute gradient and rotation, Eq. (34) reduces to

$$\sigma_i \left[I_1 + \frac{g\alpha\kappa a^2}{\nu\beta} E p_1 I_3 \right] = 0,$$

which yields $\sigma_i = 0$ implying thereby that the oscillatory modes are not allowed and the principle of exchange of stabilities is satisfied for the porous medium in the absence of rotation and stable solute gradient.

The rotation and the stable solute gradient, thus, introduce oscillatory modes in the system which were non-existent in their absence.

5. Effect of magnetic field

Here the problem is considered to be the same as described in Section 2 except that the fluid is finitely (electrically) conducting and is acted on by a uniform magnetic field $\mathbf{H}(0, 0, H)$. The linearized perturbed equations are

$$\frac{1}{\epsilon}\left(1 + \lambda\frac{\partial}{\partial t}\right)\frac{\partial \mathbf{q}}{\partial t} = \left(1 + \lambda\frac{\partial}{\partial t}\right)\left[-\frac{1}{\rho_0}\nabla\delta p - \mathbf{g}(\alpha\Theta - \alpha'\gamma) + \right.$$
$$\left. + \frac{\mu_e}{4\pi\rho_0}(\nabla \times \mathbf{h}) \times \mathbf{H}\right] + \left(1 + \lambda_0\frac{\partial}{\partial t}\right)\left(\frac{\nu}{\epsilon}\nabla^2 - \frac{\nu}{k_1}\right)\mathbf{q}, \quad (35)$$

$$\nabla \cdot \mathbf{h} = 0, \quad (36)$$

$$\epsilon\frac{\partial \mathbf{h}}{\partial t} = (\mathbf{H} \cdot \nabla)\mathbf{q} + \epsilon\eta\nabla^2\mathbf{h}, \quad (37)$$

together with Eqs (3)–(5). μ_e, η and $\mathbf{h}(h_x, h_y, h_z)$ denote, respectively, the magnetic permeability, the resistivity and the perturbation in magnetic field $\mathbf{H}$. Substituting $p_2 = \frac{\nu}{\eta}$ and

$$h_z = K(z)\exp(ik_x x + ik_y y + nt), \quad (38)$$

Eqs (3)–(5) and (35)–(37), using expressions (10) and (38), yield the dimensionless equations

$$\left[(1+F\sigma)\sigma - \frac{1}{\epsilon}(1+F_0\sigma)\left(D^2 - a^2 - \frac{\epsilon}{P_l}\right)\right](D^2-a^2)W$$
$$+ (1+F\sigma)\left[\frac{gd^2a^2}{\nu}(\alpha\Theta - \alpha'\Gamma) - \frac{\mu_e H d}{4\pi\rho_0\nu}(D^2-a^2)DK\right] = 0, \tag{39}$$

$$(D^2 - a^2 - p_2\sigma)K = -\frac{Hd}{\epsilon\eta}DW, \tag{40}$$

together with (12) and (13). The boundary conditions in addition to (15) for free, electrically nonconducting boundaries are

$$DK = 0 \quad \text{at} \quad z = 0 \quad \text{and} \quad 1. \tag{41}$$

Eliminating Θ, Γ and K from Eqs (12), (13), (39) and (40) and using the proper solution (16), we obtain

$$R_1 = \frac{(1+x)(1+x+iEp_1\sigma_1)}{x(1+i\pi^2F\sigma_1)}\left[i\sigma_1\epsilon(1+i\pi^2F\sigma_1) + (1+i\pi^2F_0\sigma_1)\left(1+x+\frac{\epsilon}{P}\right)\right]$$
$$+ S_1\frac{(1+x+iEp_1\sigma_1)}{(1+x+iE'q\sigma_1)} + Q_1\left(\frac{1+x}{x}\right)\frac{(1+x+iEp_1\sigma_1)}{(1+x+ip_2\sigma_1)}, \tag{42}$$

where

$$Q_1 = \frac{\mu_e H^2 d^2}{4\pi\rho_0\nu\eta\pi^2}.$$

5(a). The stationary convection

For stationary convection ($\sigma = 0$), Eq. (42) reduces to

$$R_1 = \frac{(1+x)^2}{x}\left(1+x+\frac{\epsilon}{P}\right) + S_1 + Q_1\frac{(1+x)}{x}. \tag{43}$$

The Oldroydian viscoelastic fluid, thus, behaves like a Newtonian viscous fluid for the stationary convection. Equation (43) yields

$$\frac{dR_1}{dQ_1} = \frac{1+x}{x}, \tag{44}$$

$$\frac{dR_1}{dS_1} = +1, \tag{45}$$

$$\frac{dR_1}{dP} = -\frac{(1+x)^2}{x}\frac{\epsilon}{P^2}. \tag{46}$$

The magnetic field and stable solute gradient have stabilizing effects whereas the medium permeability has a destabilizing effect on the system.

5(b). The oscillatory modes

Here we examine the possibility of oscillatory modes. if any, coming into play due to the presence of magnetic field. Multiplying Eq. (39) by W^*, the complex conjugate of W, integrating over the range of z and making use of (12), (13) and (40) together with the boundary conditions (15) and (41), we obtain

$$\left[\sigma + \frac{(1+F_0\sigma)}{P_l(1+F\sigma)}\right] I_1 + \frac{g\alpha'\kappa' a^2}{\nu\beta'}(I_4 + E'q\sigma^* I_5) + \frac{(1+F_0\sigma)}{\epsilon(1+F\sigma)} I_8$$
$$+ \frac{\mu_e \eta\epsilon}{4\pi\rho_0\nu}(I_9 + p_2\sigma^* I_{10}) = \frac{g\alpha\kappa a^2}{\nu\beta}(I_2 + Ep_1\sigma^* I_3), \tag{47}$$

where $I_1 - I_5$ and I_8 are given by (32) and

$$I_9 = \int_0^1 (|D^2K|^2 + 2a^2|DK|^2 + a^4|K|^2)dz,$$

$$I_{10} = \int_0^1 (|DK|^2 + a^2|K|^2)dz, \tag{48}$$

which are all positive definite. Putting $\sigma = \sigma_r + i\sigma_i$ in Eq. (47) and then equating real and imaginary parts, we obtain

$$\sigma_r \left[I_1 + \frac{F + F_0 + \sigma_r F F_0}{(1+F\sigma_r)^2 + F^2\sigma_i^2}\left(\frac{I_1}{P_l} + \frac{I_8}{\epsilon}\right) + \frac{g\alpha'\kappa' a^2}{\nu\beta'} E'q I_5 + \frac{\mu_e\eta\epsilon}{4\pi\rho_0\nu} p_2 I_{10}\right.$$
$$\left. - \frac{g\alpha\kappa a^2}{\nu\beta} Ep_1 I_3\right] = -\left[\frac{(1+FF_0\sigma_i^2)}{(1+F\sigma_r)^2 + F^2\sigma_i^2}\left(\frac{I_1}{P_l} + \frac{I_8}{\epsilon}\right) + \right.$$
$$\left. + \frac{g\alpha'\kappa' a^2}{\nu\beta'} I_4 - \frac{g\alpha\kappa a^2}{\nu\beta} I_2 + \frac{\mu_e\eta\epsilon}{4\pi\rho_0\nu} I_9\right] \tag{49}$$

and

$$\sigma_i \left[I_1 - \frac{g\alpha'\kappa' a^2}{\nu\beta'} E'q I_5 - \frac{\mu_e\eta\epsilon}{4\pi\rho_0\nu} p_2 I_{10} + \frac{g\alpha\kappa a^2}{\nu\beta} Ep_1 I_3\right] = 0. \tag{50}$$

In the absence of stable solute gradient and magnetic field, Eq. (50) reduces to

$$\sigma_i \left[I_1 + \frac{g\alpha\kappa a^2}{\nu\beta} Ep_1 I_3\right] = 0,$$

which gives $\sigma_i = 0$ and hence the oscillatory modes are not allowed and the principle of exchange of stabilities is satisfied for the porous medium in the absence of stable solute gradient and magnetic field.

The stable solute gradient and magnetic field, thus, introduce oscillatory modes in the system which were non-existent in their absence.

References

1. G. S. Beavers, E. M. Sparrow and R. A. Magnuson, J. Basic Eng. Trans. ASME, *D92*, 843, 1970.
2. P. K. Bhatia and J. M. Steiner, Zeit. Angew. Math. Mech., *52*, 321, 1972.
3. P. K. Bhatia and J. M. Steiner, J. Math. Anal. Appl., *41*, 271, 1973.
4. S. Chandrasekhar, Hydrodynamic and Hydromagnetic Stability, Dover, New York, 1981.
5. I. A. Eltayeb, Zeit. Angew. Math. Mech., *55*, 599, 1975.
6. D. D. Joseph and L. N. Tao, Zeit. Angew. Math. Mech., *44*, 361, 1964.
7. E. R. Lapwood, Proc. Camb. Phil. Soc., *44*, 508, 1948.
8. T. S. Lundgren, J. Fluid Mech., *51*, 273, 1972.
9. J. G. Oldroyd, Proc. Roy. Soc. London, *A245*, 278, 1958.
10. P. G. Saffman, Stud. Appl. Math., *50*, 93, 1971.
11. E. A. Spiegel, Astrophys. J., *141*, 1068, 1965.
12. B. A. Toms and D. J. Strawbridge, Trans. Faraday Soc., *49*, 1225, 1953.
13. G. Veronis, J. Marine Res., *23*, 1, 1965.
14. R. A. Wooding, J. Fluid Mech., *9*, 183, 1960.

Acta Physica Hungarica 73 (2–4), pp. 237-241 (1993)

ELECTRON IMPACT DOUBLY DIFFERENTIAL K-SHELL IONIZATION CROSS-SECTION OF Ag

K. K. SUD

Department of Physics, Jai Narayan Vyas University
Jodhpur, 342001 India

(Received in revised form 27 July 1993)

Electron impact doubly differential K-shell ionization cross-section of Ag has been computed with incident electron energy 500 keV for different scattering angles by using the formalism of Sud and Moattar [10]. The results are compared with the available experimental data and good agreement is obtained in the higher scattered electron energy region.

1. Introduction

Theoretical investigations of electron impact doubly differential K-shell ionization cross-section, differential in energy and angle of one of the final state electrons, have been done by a number of workers [1–10]. We refer the readers to the work of Sud and Moattar [10] for the details of the available theoretical investigations [1–10] and, in particular, about the interaction Hamiltonian and the wave functions used for bound, incident and scattered electrons in them. Sud and Moattar [10] have obtained the expressions for the K-shell differential ionization cross-section by using Dirac plane waves for both incident and scattered electrons and the Darwin wave functions and relativistic Sommerfeld–Maue wave functions to represent the bound and continuum state, respectively. Sud and Moattar [10] have calculated the double differential K-shell ionization cross-sections and compared their results with the available experimental data of Quarles and Faulk [11] (for ^{29}C and ^{47}Ag by 300 keV incident electrons) and Komma and Nakel [12] (for ^{47}Ag and ^{79}Au by 300 keV electrons). A new result by Ruoff et al [13] for the electron impact ionization cross-sections for ^{47}Ag by 500 keV incident electrons at scattering angle 30° is now available. In the present investigation, we report the results of our computations of the double differential K-shell ionization cross-sections by using the theoretical formalism of Sud and Moattar [10] and compare it with the available experimental results of Ruoff et al [13].

2. Results and discussion

The explicit expression [10] for the double differential K-shell ionization cross-section, which includes the effect of the exchange of the spin of the atomic electron,

used in this work is given as

$$\frac{d^2\sigma}{dE_1 d\Omega_1} = \frac{4\alpha^2}{mc^2|\mathbf{k}_0|}\frac{|\mathbf{k}_1|}{[(\Delta E)^2/\hbar^2c^2-\mathbf{q}^2]^2}\frac{E_2}{mc^2}\frac{1}{(1+\frac{1}{4}z^2\alpha^2)(1+\frac{1}{4}\frac{\hbar^2\mathbf{k}_2^2}{m^2c^2})}$$
$$\times\frac{\exp\{-2(z/a_0|\mathbf{k}_2|)\tan^{-1}[(2|\mathbf{k}_2|z/a_0)/(\mathbf{q}^2-\mathbf{k}_2^2+z^2/a_0^2)]\}z^6}{[1-\exp(-2\pi z/a_0|\mathbf{k}_2|)]3a_0^6[(\mathbf{q}^2+\mathbf{k}_2^2+z^2/a_0^2)^2-4\mathbf{q}^2\mathbf{k}_2^2]^3}$$
$$\times\left(\left(-128\left[\frac{m^2c^2}{\hbar^2}+\frac{1}{2}\left(\frac{(\Delta E)^2}{\hbar^2c^2}-\mathbf{q}^2\right)\right]\right.\right.$$
$$\times\left\{\left(\mathbf{k}_2^2+\frac{z^2}{a_0^2}\right)\left[\left(\mathbf{q}^2+\mathbf{k}_2^2+\frac{z^2}{a_0^2}\right)^2-4\mathbf{q}^2\mathbf{k}_2^2\right]+q^4\left(3\mathbf{q}^2+\mathbf{k}^2+\frac{z^2}{a_0^2}\right)\right\}$$
$$\left[\frac{E_0(E_0-\Delta E)}{\hbar^2c^2}+\frac{1}{4}\left(\frac{(\Delta E)^2}{\hbar^2c^2}-\mathbf{q}^2\right)\right]\frac{[(\Delta E)^2/\hbar^2c^2-\mathbf{q}^2]}{\mathbf{q}^2}$$
$$\times\left[\left[\frac{m^2c^2}{\hbar^2}\frac{[(\Delta E)^2/\hbar^2c^2-\mathbf{q}^2]}{\mathbf{q}^2}\left\{512\mathbf{q}^2\left(3\mathbf{q}^2+\mathbf{k}_2^2+\frac{z^2}{a_0^2}\right)\right.\right.\right.$$
$$+256\frac{\hbar^2}{m^2c^2}\mathbf{q}^2\left[\left(2\mathbf{k}_2^2+\frac{z^2}{a_0^2}\right)\left(\mathbf{q}^2+\mathbf{k}^2+\frac{z^2}{a_0^2}\right)-4\mathbf{q}^2\mathbf{k}_2^2\right]$$
$$+8\frac{\hbar^4}{m^4c^4}\left[3\left(\mathbf{k}_2^2+\frac{z^2}{a_0^2}\right)\left(\mathbf{q}^2+\mathbf{k}^2+\frac{z^2}{a_0^2}\right)\left[\left(\mathbf{q}^2+\mathbf{k}_2^2+\frac{z^2}{a_0^2}\right)^2-4\mathbf{q}^2\mathbf{k}_2^2\right]\right.$$
$$\left.\left.-4\mathbf{q}^2\mathbf{k}_2^2\frac{z^2}{a_0^2}\left(3\mathbf{q}^2+\mathbf{k}_2^2+\frac{z^2}{a_0^2}\right)\right]\right\}-128\left\{\left(\mathbf{k}_2^2+\frac{z^2}{a_0^2}\right)\right.$$
$$\left.\left.\left.\left.\times\left[\left(\mathbf{q}^2+\mathbf{k}_2^2+\frac{z^2}{a_0^2}\right)^2-4\mathbf{q}^2\mathbf{k}_2^2\right]+\mathbf{q}^4\left(3\mathbf{q}^2+\mathbf{k}_2^2+\frac{z^2}{a_0^2}\right)\right\}\right]\right]\right)\right),$$

where in Eq. (1) $E_0(E_1)$ and $\hbar\mathbf{k}_0(\hbar\mathbf{k}_1)$ represent, respectively, the energy and momentum of the incident (scattered) electron and E_2, $\hbar\mathbf{k}_2$ is the energy and momentum of the ejected electron. The momentum transfer by the incident electron is given as

$$\mathbf{q}^2 = \mathbf{k}_0^2 - \mathbf{k}_1^2 - 2|\mathbf{k}_0||\mathbf{k}_1|\cos\Theta$$

and the energy transfer as $E = E_0 - E_1$.

We show in Fig. 1 differential cross-sections for ^{47}Ag as a function of scattering energy by electrons of incident energy 500 keV and at scattering angle 30° by using Eq. (1). The experimental data of Ruoff et al [13] is also presented in Fig. 1. It can be seen from Fig. 1 that the general trend in the variation of the differential K-shell ionization cross-section as a function of scattered energy in the higher scattered electron energy region agrees with the experimental data. In Fig. 2 we have shown the differential K-shell cross-section for ^{47}Ag by 500 keV electrons at different scattering angles (20°, 30°, 40°, 45° and 60°). It may be seen that the peak in the differential ionization cross-section vs scattered electron energy lies between the Moller energy E_M and E_{MB} (Moller energy + binding energy). The

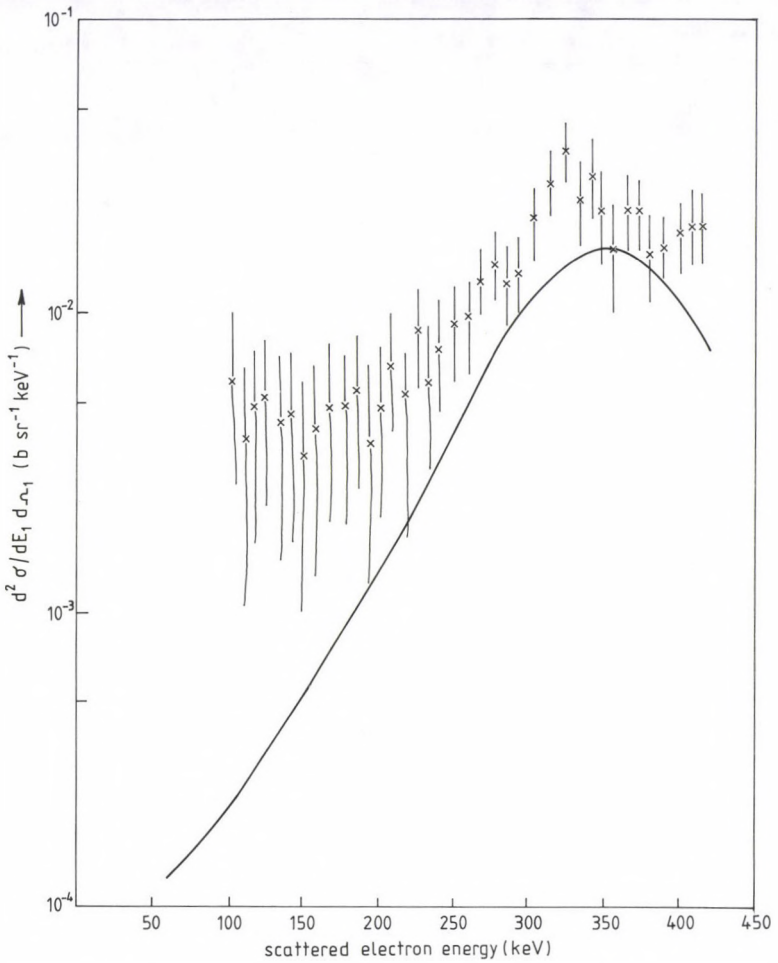

Fig. 1. The results of the present theoretical calculations of electron impact K-shell double differential ionization cross-section $d^2\sigma/dE_1\, d\Omega_1$, as a function of scattered electron energy by 500 keV electrons at scattering angle $\Theta = 30°$ and experimental data of Ruoff et al [13]

Moller energy is obtained from the kinematics of an electron scattering system and is given as:

$$E_{\mathrm{M}} = E_0 \cos^2 \Theta / [1 + E_0 \sin^2 \Theta / 2mc^2].$$

(E_0 is the incident electron energy, Θ is the scattering angle and m is the rest mass of the electron). We have shown E_{M} and E_{MB} by arrows in Fig . 2. It may be seen from Fig. 2 that the Moller peak in the differential K-shell ionization curves gets broader and shifts towards lower scattered electron energy for larger scattering

angles. This is as expected since the Moller energy decreases with the increase of scattering angle.

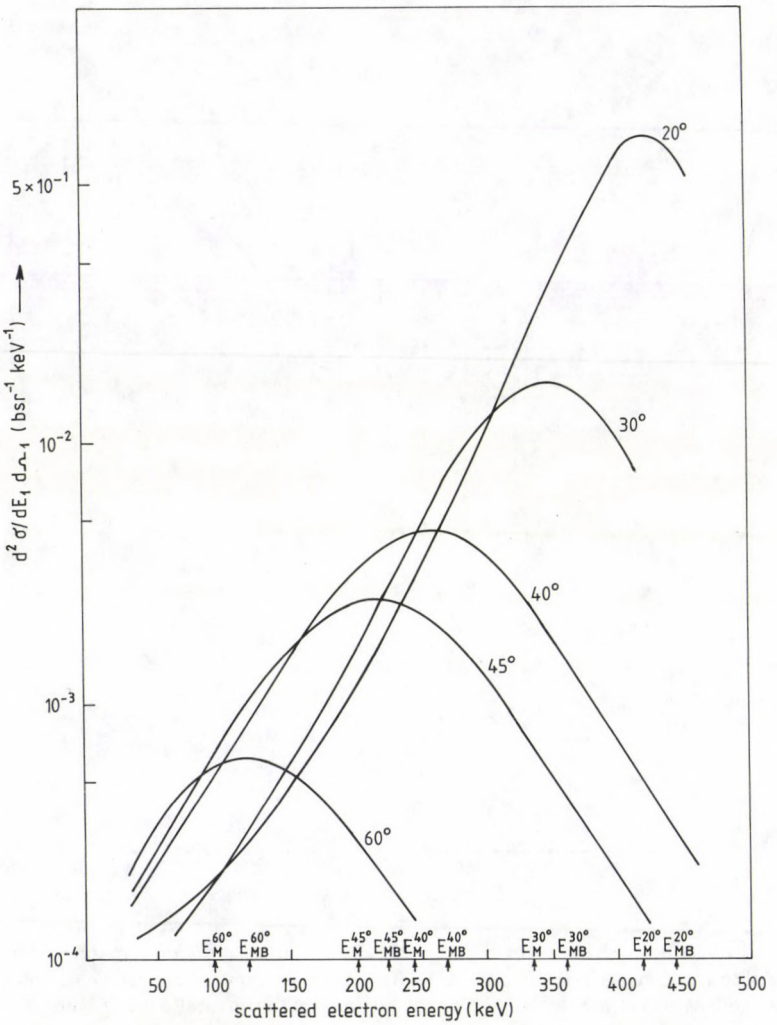

Fig. 2. The results of the present theoretical calculations of electron impact K-shell double differential ionization cross-section $d^2\sigma/dE_1\,d\Omega_1$, as a function of scattered electron energy by 500 keV electrons at different scattering angles. The scattering angle Θ, E_M (Moller energy), and E_{MB} (Moller energy + binding energy of K-shell) are indicated in the Figure

Finally, we conclude that the Sud and Moattar [10] theory correctly predicts the position and nature of variation of the peak in the doubly differential K-shell ionization cross-section vs the scattered electron energy curve. This investigation further suggests the necessity of higher incident energy electron impact differential

ionization cross-section measurements in the lower scattered electron energy region in Ag as well as in other targets, for the better understanding of the ionization process and for testing the theory.

References

1. G. W. Ford and C. J. Mullin, Phys. Rev., *110*, 520, 1958.
2. T. A. Weber, R. T. Deck and C. J. Mullin, Phys. Rev., *130*, 660, 1963.
3. A. K. Glasshold and G. Ialongo, Phys. Rev., *175*, 151, 1968; Phys. Rev., *186*, 266, 1969.
4. J. N. Das, Nuovo Cimento, *12B*, 197, 1972.
5. J. N. Das and A. N. Konar, J. Phys. B: At. Mol. Phys., *7*, 2417, 1974.
6. J. N. Das, J. Phys. B: At. Mol. Phys., *17*, 923, 1974.
7. B. L. Moiseiwitsch and P. H. Norrington, J. Phys. B: At. Mol. Phys., *12*, L283, 1979.
8. J. N. Das and S. Chakrobarty, Phys. Letter, *92A*, 127, 1982.
9. J. N. Das and S. Chakrobarty, Phys. Rev., *A32*, 176, 1985.
10. K. K. Sud and S. Moattar, J. Phys., *B23*, 2363, 1990.
11. C. A. Quarles and J. D. Faulk, Phys. Rev. Letter, *31*, 859, 1973.
12. M. Komma and W. Nakel, J. Phys., *B12*, L587, 1979.
13. H. Ruoff, E. Schule, J. Bonfert, H. Graf and W. Nakel, Rev. Sci. Instrument, *60*, 17, 1989.

Acta Physica Hungarica 73 (2–4), pp. 243–256 (1993)

TENSORS AND INVARIANTS IN A GENERALIZED SCALAR MODEL

R. M. DORIA* and J. A. HELAYËL-NETO* **

** Universidade Católica de Petrópolis (UCP-ICEN)*
Petrópolis, Brazil
*** Centro Brasileiro de Pesquisas Físicas (CBPF-DCP)*
Rio de Janeiro, Brazil

(Received 3 August 1993)

Gauge models involving several fields rotating under a single symmetry group develop the so-called Ω-matrix which is a consequence from field reparametrizations. It means a structure which belongs to the model scenario but without participating on the dynamics. Its main consequence is the advent of a kind of prescription where physical entities are divided between tensors and invariants. For instance, the renormalization group equation variables will not work as invariants under Ω; on the other hand, physical masses will.

1. Introduction

Field reparametrizations are currently performed in order to understand a number of points in field theory. For these rotations, Borcher's theorem has stipulated conditions for S-matrix invariance [1]. A consequence from these transformations is the appearance of scalars and tensors, for instance, the coupling constant becomes a tensorial entity under a field reparametrization. Therefore, when one studies a model which introduces different fields rotating under a same group [2], it will be natural to expect the development of new scalars and tensors under such fields redefinitions which obey [1]. In fact, these reparametrizations involving N fields develop an Ω-matrix [3]. It is an entity which does not belong to the dynamics of theory.

Thus, considering the scalar case, we have that the N-quanta developed by the model can be articulated under different field parametrizations. The diagonal basis-Φ is given by

$$\mathcal{L} = \Phi^{\dagger}\Box\Phi - \Phi^{\dagger}m^2\Phi, \tag{1.1}$$

while the non-diagonal basis-φ would be

$$\mathcal{L} = \varphi^{\dagger}K\Box\varphi - \varphi^{\dagger}M^2\varphi, \tag{1.2}$$

where K and M are Hermitean matrices. Equations (1.1) and (1.2) are invariant under the following global transformations

$$\Phi \rightarrow \Phi' = e^{i\alpha\tilde{Q}}\Phi, \tag{1.3}$$

$$\varphi \to \varphi' = e^{i\alpha Q}\varphi, \tag{1.4}$$

for $\tilde{Q}$ and Q being, respectively, diagonal and non-diagonal matrices. Comparing (1.1) and (1.2) we get the following relationships for Ω-matrix:

$$\Omega^{\dagger} K \Omega = 11,$$

$$\Omega^{\dagger} M^2 \Omega = m^2 \text{ (diagonal)} \tag{1.5}$$

with

$$\varphi = \Omega \Phi. \tag{1.6}$$

Being real scalars the Lagrangian and the action are invariant under (1.6)

$$\mathcal{L}[\varphi] = \mathcal{L}[\Omega\Phi] = \tilde{\mathcal{L}}[\Phi], \tag{1.7}$$

$$S[\varphi] = \tilde{S}[\Phi]. \tag{1.8}$$

Similarly, the Noether current

$$J^{\mu}[\varphi] = \tilde{J}^{\mu}[\Phi]. \tag{1.9}$$

Thus, a first clue for understanding such non-dynamical variable Ω would be to compare it with the Lorentz matrix Λ^{μ}_{ν}. Thus, while Lorentz transformations let the metric invariant

$$\Lambda^{t} \eta \Lambda = \eta, \tag{1.10}$$

one gets from (1.5) the similarity transformation

$$\Omega^{-1}(K^{-1}M^2)\Omega = m^2, \tag{1.11}$$

which says that poles are absolute variables.

Comparing (1.1) and (1.2), the following expression is derived

$$\Omega = S^{\dagger} \tilde{K}^{\frac{1}{2}} R^{\dagger}, \tag{1.12}$$

with

$$\tilde{K} = SRS^{t}, \tag{1.13}$$

where S and R are unitary matrices which diagonalize the kinetic and mass terms. From Eq. (1.12) we read the properties that Ω is not unitary (unless K is an indentity-multiple) and the condition for Ω invertibility is $\tilde{K}$ not to have zero eigenvalues. Equation (1.12) also informs that Ω does not make a group as the Lorentz matrix. It is because the closure property $\Omega\Omega' = \Omega''$ is not obtained.

Thus the appearance of these non-dynamical Ω transformations raises the necessity of exploring about the distinction between relative and absolute variables in a model which contains more than one field rotating under a same group. Fields will only work as coordinates now. Therefore, we need to systematize about the physical variables under Ω. For this, Section 2 studies at classical level and Section 3 at quantum level. Then, an example with $SO(N)$ symmetry is developed in Section 4.

2. Classical aspects

Although the set of Ω-matrices do not build up a group, they divide the physical entities into scalars and tensors. As studied before, Eq. (1.6) preserves the minimal action principle and the mass shell information [3]. It was also understood that Ω is a canonical transformation in the sense that it preserves the Hamilton's equation, commutation relations, charge algebra and Pauli–Jordan functions.

An interesting result obtained for being pointed out is that symmetry nature can change under Ω rotations. This means that symmetry can explit different representations under various field parametrizations. Substituting (1.6) in

$$\Phi \to \Phi' = U(w)\Phi, \tag{2.1}$$

one gets

$$\varphi \to \varphi' = T(w)\varphi, \tag{2.2}$$

where

$$T(w) = \Omega^{-1}U(w)\Omega. \tag{2.3}$$

Then, the following group algebra relationships

$$\begin{aligned} U(w) &= e^{iw^a G_a}, \quad UU^\dagger = 1, \\ [G_a, G_b] &= if_{abc}G_c, \\ \left[\tilde{Q}^a[\Phi], \Phi_i\right] &= t^a_{ij}\Phi_j, \\ \left[\tilde{Q}^a[\Phi], \tilde{Q}^b[\Phi]\right] &= if^{abc}Q_c[\Phi] \end{aligned} \tag{2.4}$$

will transform into

$$\begin{aligned} T(w) &= e^{iw^a H_a}, \quad TT^\dagger \neq 1, \\ H^a &= \Omega^{-1}G^a\Omega, \quad H^a \neq H^{a+}, \\ [H^a, H^b] &= if^{abc}H_c, \\ [Q^a[\varphi], \varphi] &= H^a_{ij}\varphi_j, \\ [Q^a[\varphi], Q^b[\varphi]] &= if^{abc}Q_c[\varphi]. \end{aligned} \tag{2.5}$$

Thus Eqs (2.4) and (2.5) are showing that a given symmetry will not depend on its shape for writing its physical meaning. However, different proofs still must be developed for this statement to be considered. For this we should first consider the mass invariance. The Φ-basis condition for mass preservation under (2.1) rotation is

$$[G_a, m^2] = 0. \tag{2.6}$$

Then, substituting (2.2) in (1.2) one gets that only under (2.6) is that such rotation will be preserved. This shows that the relevant aspects are on symmetry expressions as (2.6) and not on parametrizations basis.

A next classical step for showing that symmetry must not depend on field basis is to study local symmetries. It yields the following covariant derivative involving N potential fields:

$$\partial_\mu \Phi \to \mathcal{D}_\mu \Phi \equiv (\partial_\mu + i g_I V^a_{\mu I} G_a)\Phi, \tag{2.7}$$

with the notation

$$V_{\mu 1} \equiv \mathcal{D}_\mu, \quad V_{\mu i} \equiv X_{\mu i} \quad (i = 2, \ldots, N). \tag{2.8}$$

Thus

$$\mathcal{D}_\mu \Phi \to (\mathcal{D}_\mu \Phi)' = U(w)(\mathcal{D}_\mu \Phi) \tag{2.9}$$

and

$$\mathcal{D}'_\mu = U \mathcal{D}_\mu U^{-1}, \tag{2.10}$$

which yields

$$g\mathcal{D}'_\mu + g_i X'_{\mu i} = g U D_\mu U^{-1} + g_i U X^i_\mu U^{-1} - i U \partial_\mu U^{-1}. \tag{2.11}$$

Then we separate, by construction, Eq. (2.11) into non-homogeneous and homogeneous sectors,

$$D'_\mu = U D_\mu U^{-1} - \frac{i}{g} U \partial_\mu U^{-1}, \tag{2.12}$$

$$X'_{\mu i} = U X_{\mu i} U^{-1}. \tag{2.13}$$

Concluding, the Lagrangian for the matter sector in the Φ-basis is

$$\mathcal{L} = (\mathcal{D}_\mu \Phi)^\dagger (\mathcal{D}^\mu \Phi) - m^2 \Phi^\dagger \Phi. \tag{2.14}$$

We should now consider this local symmetry at φ-basis and verify its consistency. Working out the non-diagonal parametrization we get a covariant derivative $\nabla_\mu \varphi$ given by

$$\nabla_\mu = \Omega \mathcal{D}_\mu \Omega^{-1}, \tag{2.15}$$

$$\nabla_\mu \varphi = (\partial_\mu + i g_I V^a_{\mu I} H_a)\varphi, \tag{2.16}$$

$$\nabla_\mu \varphi = \Omega \mathcal{D}_\mu \Phi, \tag{2.17}$$

where we notice that the covariant derivative also transforms as a covariant object under a change of field basis.

Under gauge transformations this φ-covariant derivative transforms as

$$\nabla_\mu \xrightarrow{\text{gauge}} \nabla'_\mu = T(w) \nabla_\mu T(w)^{-1}, \tag{2.18}$$

$$\nabla_\mu \varphi \xrightarrow{\text{gauge}} (\nabla_\mu \varphi)' = T(w) \nabla_\mu \varphi, \tag{2.19}$$

which yields

$$i g_I V'_{\mu I} = i g_I T V_{\mu I} T^{-1} + T(\partial_\mu T^{-1}), \tag{2.20}$$

with the corresponding infinitesimal transformation

$$g_I \delta V^a_{\mu I} = -f^a_{bc} w^b V^c_{\mu I} - \partial_\mu w^a. \tag{2.21}$$

To systematize these gauge and field basis transformations, two basic consistency conditions must be verified. They are that the potential field transformations and the Lagrangian are invariants. Considering that structure functions f_{abc} and gauge parameter w are independent of rotations, one reads from Eq. (2.21)

$$\delta D_{\mu a} = -f_{abc} w^b D^c_\mu - \partial_\mu w^a, \tag{2.22}$$

$$\delta X^i_{\mu a} = -f_{abc} w^b X^{ci}_\mu, \tag{2.23}$$

with rewrites (2.10) and (2.11).

Substituting (1.6) in (2.14), we get the following expression for the Lagrangian at φ-reference system

$$\mathcal{L}[\varphi] = (\nabla_\mu \varphi)^\dagger K (\nabla^\mu \varphi) - \varphi^\dagger M^2 \varphi. \tag{2.24}$$

Then, by checking (2.2) and (2.19) in (2.24), it yields

$$\mathcal{L}'[\varphi'] = \mathcal{L}[\varphi]. \tag{2.25}$$

For the Abelian symmetry

$$\Phi \xrightarrow{U(1)} \Phi' = U(\alpha)\Phi, \tag{2.26}$$

where $U(\alpha) = e^{i\alpha Y}$, Y being a charge matrix $Y_{ij} = q_i \delta_{ij}$, similar results are obtained.

Another classical aspect to be considered under Ω rotations concerns the interactions. Considering the coupling of the free Lagrangian to external fields

$$S[\varphi] = \int d^4x \left(\frac{1}{2} \varphi^t \mathcal{P} \varphi + \frac{1}{2} \varphi^t J + \frac{1}{2} J^t \varphi \right) \tag{2.27}$$

it yields the following equation of motion

$$\mathcal{P}\varphi = -J, \tag{2.28}$$

with the solution

$$\varphi(x) = \varphi_0(x) - \int d^4y \mathcal{P}^{-1}(x;y) J(y). \tag{2.29}$$

Then the effective action corresponding to a current–current interaction result

$$S_{\text{eff}}[J_1; J_2] = -\int d^4x d^4y J_1^t(x)\mathcal{P}^{-1}(x;y)J_2(y). \tag{2.30}$$

Working out the effective action at Φ-basis we have

$$\tilde{S}_{\text{eff}}[\mathcal{J}_1; \mathcal{J}_2] = -\int d^4x d^4y \mathcal{J}_1^t(x)\sigma^{-1}(x,y)\mathcal{J}_2(y) \tag{2.31}$$

is written in terms of the operator σ and the sources $\mathcal{J}_1$ and $\mathcal{J}_2$. Substituting Eq. (1.6) in (2.27) one derives the following transformations laws

$$\begin{aligned} \Omega^t\mathcal{P}\Omega &= \sigma, \\ \Omega^t J_1 &= \mathcal{J}_1, \\ \Omega^t J_2 &= \mathcal{J}_2, \end{aligned} \tag{2.32}$$

which gives

$$\tilde{S}_{\text{eff}}[\mathcal{J}_1; \mathcal{J}_2] = S_{\text{eff}}[J_1; J_2]. \tag{2.33}$$

Now the question for physical interpretation will be to understand about which of the currents, $\mathcal{J}$ or J, describes the physical currents. For instance, a point-like charge which generates an electrical field should be written in terms of $\mathcal{J}$ or J? For analysing such argument let us consider as relevant the external currents coupled to the diagonal basis. Then, the following point-like charges electric potential will be associated

$$\mathcal{J}_\mu(x) = q\delta^3(\mathbf{x} - a). \tag{2.34}$$

Evaluating the case for static potentials one gets

$$\tilde{V}_{\text{int}}[\Phi] = \frac{\tilde{S}_{\text{eff}}}{\Delta t}[\Phi] = \frac{q_{1I}q_{2J}}{4\pi}\delta^{IJ}\frac{e^{-m_I|\mathbf{a}-\mathbf{b}|}}{|\mathbf{a}-\mathbf{b}|}, \tag{2.35}$$

where $\tilde{V}_{\text{int}}[\Phi]$ is a static potential describing the interaction between two static point-like charges localized in **a** and **b** points. Then from (2.33) we get the information that the above result is preserved in φ-basis:

$$\tilde{V}_{\text{int}}[\varphi] = \tilde{V}_{\text{int}}[\Phi]. \tag{2.36}$$

Concluding we would note that although the interaction between two static sources is independent from field parametrization the exchange of field quanta is more clear at diagonal basis. There it appears that just one pole m_I is the responsible for intermediate such interaction. This interpretation indicates that, at classical level, physics shows preference between such field bases.

3. Quantum aspects

The effective action is defined as

$$\tilde{\Gamma}[\Phi] = S_{\rm cl}[\Phi] + \Gamma_{\rm loop}[\Phi]; \tag{3.1}$$

it can also be written in the form:

$$\tilde{\Gamma}[\Phi] = \sum_{n=1}^{\infty} \frac{1}{n!} \int d^4x_1 \ldots d^4x_n \tilde{\Gamma}^{(n)}_{i_1 i_2 \ldots i_n}(x_1, x_2, \ldots, x_n)\Phi_{i_1}(x_1)\ldots\Phi_{i_n}(x_n). \tag{3.2}$$

Then, although the effective action must be preserved under a field basis change

$$\Gamma[\varphi] = \tilde{\Gamma}[\Phi] \tag{3.3}$$

one gets that its components will change. Substituting Eq. (1.6) in (3.2) we derive the following general expression

$$\tilde{\Gamma}^{(n)}_{i_1 i_2 \ldots i_n}[\Phi] = \Gamma^{(n)}_{j_1 j_2 \ldots j_n} \Omega_{j_1 i_1} \Omega_{j_2 i_2} \ldots \Omega_{j_n i_n}. \tag{3.4}$$

Consequently, the Feynman rules will change under a change of field basis. Propagators will transform as

$$\Delta_{ij} = \Omega_{im}\Omega_{jn}\tilde{\Delta}_{mn}, \tag{3.5}$$

while three and four vertices are

$$\Gamma^{(3)}_{ijk}(k;l;r)\delta^4(k+l+r) = \Omega^{-1}_{mi}\Omega^{-1}_{nj}\Omega^{-1}_{lk}\tilde{\Gamma}^{(3)}_{mnl}(k;l;r)\delta^4(k+l+r) \tag{3.6}$$

and

$$\Gamma^{(4)}_{ijkl}(k;l;q;r)\delta^4(k+l+q+r) = \Omega^{-1}_{mi}\Omega^{-1}_{nj}\Omega^{-1}_{pk}\Omega^{-1}_{lq}\tilde{\Gamma}^{(4)}_{mnpq}(k;l;q;r)\delta^4(k+l+q+r). \tag{3.7}$$

As a check, we can show that

$$\tilde{S}^{(2)}_{\rm cl}[\Phi] + \left(\tilde{\Gamma}^{(2)}_{\rm loop}\right)_{ij}\Phi^i\Phi^j = S^{(2)}_{\rm cl}[\varphi] + \left(\Gamma^{(2)}_{\rm loop}\right)_{mn}\varphi_m\varphi_n. \tag{3.8}$$

Given this dependence for the Feynman rules, it turns crucial to understand whether the poles are invariant under such field basis transformations. Considering the contribution to the effective action from the self-energy, we have

$$\tilde{\Gamma}[\Phi] = \frac{1}{2}\Phi^t[p^2 - m^2 - i\pi]\Phi + \text{interactions}, \tag{3.9}$$

where $(-i\pi)$ means the self-energy contribution from loop corrections. Similarly, for φ-basis, we get

$$\Gamma[\varphi] = \frac{1}{2}\varphi^t[Kp^2 - M^2 - i\Sigma]\varphi + \text{interactions}, \tag{3.10}$$

where $(-i\Sigma)$ is the corresponding quantum contribution to the effective action in the φ-basis. Then, from Eq. (3.14), it yields

$$\Gamma[\varphi] = \frac{1}{2}\varphi^t\Omega^{-1t}[(p^2 - m^2) - i\pi]\Omega^{-1}\varphi + \text{interactions}. \tag{3.11}$$

Thus Eqs (3.9) and (3.11) are showing that independently of field parametrizations the equation which determines the physical mass is given by

$$p^2 - m^2 - i\pi_{\text{free}}\,(p^2;\ \text{free coefficients}) = 0. \tag{3.12}$$

Another proof that the physical masses do not depend on field basis is to analyse the field propagators. From (3.4) their transformation law is

$$\langle T(\varphi\varphi)\rangle = \Omega\langle T\Phi\Phi\rangle\Omega^t. \tag{3.13}$$

Thus Eq. (3.13) shows a rotation which does not change the poles structure. More explicitly, we have

$$\langle T(\Phi(x)\Phi(y)\rangle = \frac{1}{\Box + m^2}\delta^4(x-y) = \Omega^{-1}\frac{1}{\Box + K^{-1}M^2}K^{-1}\Omega^{-1t}, \tag{3.14}$$

which shows that physical masses are $K^{-1}M^2$ matrix eigenvalues. Observe that this result was already predicted in Eq. (1.11).

The next analysis regards the wave-function, mass and coupling constant renormalizations for different field parametrizations. Defining $\tilde{K}^{(2)}$, and $K^{(2)}$ as the counterterms for the kinetic piece, and $\tilde{K}_m$, K_M those for the mass term, one writes

$$\tilde{\mathcal{L}}[\Phi] = -\frac{1}{2}\Phi_R^t\Box\Phi_R - \frac{1}{2}\Phi_R^t\tilde{K}^{(2)}\Box\Phi_R - \frac{1}{2}\Phi_R^t m_R^2\Phi_R - \frac{1}{2}\Phi_R^t\tilde{K}_m\Phi_R \tag{3.15}$$

and

$$\mathcal{L}[\varphi] = -\frac{1}{2}\varphi_R^t K\Box\varphi_R - \frac{1}{2}\varphi_R^t\Box K^{(2)}\varphi_R - \frac{1}{2}\varphi_R^t M^2\varphi_R - \frac{1}{2}\varphi_R^t K_M\varphi_R, \tag{3.16}$$

which yields the following wave-function renormalization:

$$\Phi_B = \tilde{Z}_\Phi^{\frac{1}{2}}\Phi_R, \tag{3.17}$$

where

$$\tilde{Z}_\Phi = 1 + \tilde{K}^{(2)}, \quad \tilde{Z}_\Phi = \tilde{Z}_\Phi^t \quad \text{(non-diagonal)}. \tag{3.18}$$

For the φ-basis,

$$\varphi_B = Z_\varphi^{\frac{1}{2}} \varphi_R, \tag{3.19}$$

$$Z_\varphi = 1 + K^{-1} K^{(2)} K^{\frac{1}{2}}, \tag{3.20}$$

$$Z_\varphi \neq Z_\varphi^t. \tag{3.21}$$

Notice that the K matrix is not renormalized.

Mass renormalizations in Φ and φ-basis are given respectively by

$$m_B^2 = m_R^2 + \delta\tilde{m}^2, \tag{3.22}$$

where

$$\delta\tilde{m}^2 = \tilde{K}_m - \frac{1}{2}\tilde{K}^{(2)} m_R^2 - \frac{1}{2} m_R^2 \tilde{K}^{(2)}, \tag{3.23}$$

$$\delta\tilde{m}^2 = (\delta\tilde{m}^2)^t \tag{3.24}$$

and

$$M_B^2 = M_R^2 + \delta M^2, \tag{3.25}$$

$$\begin{aligned} \delta M^2 = (\delta M^2)^t = & K_M - \frac{1}{2} M_R^2 K^{-1} K^{-\frac{1}{2}} K^{(2)} K^{\frac{1}{2}} + \\ & - \frac{1}{2} K^{\frac{1}{2}} K^{(2)} K^{-\frac{1}{2}} K^{-1} M_R^2. \end{aligned} \tag{3.26}$$

Observe that the non-renormalized K matrix interferes on mass parameters renormalization.

Considering the relationship

$$\varphi_R = \Omega \Phi_R, \tag{3.27}$$

where Ω is defined in terms of dimensionless parameters derived from the kinetic matrix K (non-renormalized) and from the mass matrix M at tree level (the renormalized mass without corrections in $\hbar$), one derives the following transformations between the field parametrizations

$$K^{(2)} = \Omega^{-1t} \tilde{K}^{(2)} \Omega^{-1}, \tag{3.28}$$

$$Z_\varphi = (K^{-1}\Omega) \tilde{Z}_\Phi \left(\tilde{K}^{-\frac{1}{2}} \Omega^{-1} \right) \tag{3.29}$$

and

$$\begin{aligned} \delta M^2 = & \Omega^{-1t} \tilde{K}_m \Omega^{-1} - \frac{1}{2} \Omega^{-1t} m_R^2 \Omega^t K^{-\frac{1}{2}} \Omega^{-1t} \tilde{K}^{(2)} \Omega^{-1} K^{\frac{1}{2}} + \\ & - \frac{1}{2} K^{\frac{1}{2}} \Omega^{-1t} \tilde{K}^{(2)} \Omega^{-1} K^{-\frac{1}{2}} \Omega m_R^2 \Omega^{-1}. \end{aligned} \tag{3.30}$$

The radiative corrections for the interaction terms are

$$\tilde{\mathcal{L}}_{\rm int}[\Phi] = -\frac{1}{4}\Lambda_{ijkl}\Phi_i\Phi_j\Phi_k\Phi_l - \frac{1}{4!}\tilde{K}^{(4)}_{ijkl}\Phi_i\Phi_j\Phi_k\Phi_l \tag{3.31}$$

or

$$\tilde{\mathcal{L}}_{\rm int}[\varphi] = -\frac{1}{4}\lambda_{ijkl}\varphi_i\varphi_j\varphi_k\varphi_l - \frac{1}{4!}K^{(4)}_{ijkl}\varphi_i\varphi_j\varphi_k\varphi_l \tag{3.32}$$

with

$$K^{(4)}_{ijkl} = \Omega^{-1}_{mi}\Omega^{-1}_{nj}\Omega^{-1}_{pk}\Omega^{-1}_{ql}\tilde{K}^{(4)}_{mnpq}. \tag{3.33}$$

Thus, from these different field channels for physics to be understood, an interesting question is about the renormalizability at Φ-basis. Being diagonal, it might not absorb the non-diagonal divergences. However, this non-renormalizability problem is just apparent. The physics equivalence between the different field bases allows to make this analysis in a chosen field basis-φ. Then, from such a boost, one gets diagonal and non-diagonal parameters which can absorb the wave functions and masses counterterms as Eqs (3.19) and (3.25) are demonstrating. Concluding, we note that, for this extended scalar model, while the mass spectrum is more evident at Φ-basis, the renormalizability turns clear at φ-basis.

A further step would be to understand the variations of the renormalization group equation under Ω. From Eqs (3.2) and (3.17) one derives the following relationship between bare and renormalized 1PI Green functions:

$$\begin{aligned}\tilde{\Gamma}^{(n)B}_{i_1i_2\ldots i_n}(p; m_B; G_B; \epsilon) &= \left(Z_\Phi^{-\frac{1}{2}}(G_B; \mu; \epsilon)\right)_{i_1j_1} \\ \ldots &\left(Z_\Phi^{-\frac{1}{2}}\right)_{i_nj_n}\tilde{\Gamma}^{(n)R}_{j_1j_2\ldots j_n}(p; m_R(\mu), G_R(\mu), \mu),\end{aligned} \tag{3.34}$$

where μ means the renormalization scale and ϵ the dimensional regularization parameter. Applying $\mu\frac{d}{d_\mu}$, it yields

$$\begin{aligned}&\left(Z_\Phi^{\frac{1}{2}}\right)_{k_1i_1}\left[\mu\frac{\partial}{\partial\mu}|_{G_B}\left(Z_\Phi^{-\frac{1}{2}}\right)_{i_1j_1}\right]\Gamma^{(n)R}_{j_1k_2\ldots k_n} + \ldots + \\ &+ \left(Z_\Phi^{\frac{1}{2}}\right)_{k_ni_n}\left[\mu\frac{\partial}{\partial\mu}|_{G_B}\left(Z_\Phi^{-\frac{1}{2}}\right)_{i_nj_n}\right]\Gamma^{(n)R}_{k_1k_2\ldots j_n} + \\ &+ \left[\mu\frac{\partial}{\partial\mu}|_{m_B,G_B} + \tilde{\gamma}^{(m)}_{k_l}\frac{\partial}{\partial m^R_{kl}} + \tilde{\beta}^{(G)}_{klmn}\frac{\partial}{\partial G^R_{klmn}}\right]\Gamma^{(n)R}_{k_1k_2\ldots k_n} = 0,\end{aligned} \tag{3.35}$$

where

$$\tilde{\gamma}^{(G)}_{ij} \equiv \mu\frac{\partial}{\partial\mu}m^R_{ij}|_{m_B.G_B}, \tag{3.36}$$

$$\tilde{\beta}^{(G)}_{ijkl} \equiv \mu\frac{\partial}{\partial\mu}G^R_{ijkl}|_{m_B,G_B}. \tag{3.37}$$

Similarly for φ-basis, one gets

$$\left(Z_{\varphi}^{\frac{1}{2}}\right)_{k_1 i_1}\left[\mu\frac{\partial}{\partial\mu}|_{\lambda_B}\left(Z_{\varphi}^{-\frac{1}{2}}\right)_{i_1 j_1}\right]\Gamma^{(n)R}_{j_1 k_2\ldots k_n}+\ldots+$$
$$+\left(Z_{\varphi}^{\frac{1}{2}}\right)_{k_n i_n}\left[\mu\frac{\partial}{\partial\mu}|_{\lambda_B}\left(Z_{\varphi}^{-\frac{1}{2}}\right)_{i_n j_n}\right]\Gamma^{(n)R}_{k_1 k_2\ldots j_n}+$$
$$+\left[\mu\frac{\partial}{\partial\mu}|_{M_B,\lambda_B}+\gamma^{(M)}_{k_l}\frac{\partial}{\partial m^R_{kl}}+\beta^{(\lambda)}_{klmn}\frac{\partial}{\partial G^R_{klmn}}\right]\Gamma^{(n)R}_{k_1 k_2\ldots k_n}=0, \tag{3.38}$$

where the coefficients are given by

$$\gamma^{(M)}_{ij}\equiv\mu\frac{\partial}{\partial\mu}|_{M_B,\lambda_B}M^R_{kl}$$

and

$$\beta^{(\lambda)}_{ijkl}\equiv\mu\frac{\partial}{\partial\mu}|_{M_B,\lambda_B}\lambda^R_{ijkl}, \tag{3.39}$$

with the renormalization coefficient $\tilde{Z}_{\Phi}$ and Z_{φ} defined through Eqs (3.18) and (3.20).

Consequently, the anomalous dimensions and the β functions will transform respectively as

$$\gamma^{(M)}=\Omega^{-1t}\tilde{\gamma}^{(m)}\Omega^{-1}, \tag{3.40}$$

$$\beta^{(\lambda)}_{ijkl}=\Omega^{-1}_{mi}\Omega^{-1}_{nj}\Omega^{-1}_{pk}\Omega^{-1}_{ql}\tilde{\beta}^{(G)}_{mnpq}. \tag{3.41}$$

Notice that, although the β- and γ-functions depend on the field parametrization basis, the physical information will be preserved. Equations (3.41) and (3.42) show that any zero on these functions will remain for any other field basis. Consequently, the information on finiteness structure is an invariant under such field reparametrizations.

As a last quantum aspect to be analysed here we would select the Slavnov–Taylor identity under Ω transformation. Considering that the classical symmetry holds for Γ, we have at Φ-basis:

$$\int d^4x\frac{\delta\tilde{\Gamma}}{\delta\Phi_i}\frac{\delta\tilde{\Gamma}}{\delta\mathcal{J}_i}=0 \tag{3.42}$$

an equation that has to be understood order by order in $\hbar$. Then, by substituting (16) and (2.32) in (2.41) one derives

$$\int d^4x\frac{\delta\Gamma}{\delta\varphi_i}\frac{\delta\Gamma}{\delta J_i}=0, \tag{3.43}$$

which shows that informations derived from S.T. identity will be preserved under field reparametrizations.

4. $SO(N)$ renormalization

Assuming mass degeneracy as dictated by $SO(N)$ symmetry,

$$\Phi' = S\Phi = e^{iw^a G_a}\Phi, \tag{4.1}$$

one gets that constraints between the counter terms $K^{(2)}$, $K^{(m)}$ and $K^{(4)}$ must be obtained through the Ward identity:

$$\int d^4x \frac{\delta\Gamma}{\delta\Phi_i}(G_a)_{ij}\Phi_j = 0, \tag{4.2}$$

which yields the following expressions

$$G_a\Gamma^{(1)} = 0, \tag{4.3}$$

$$S_{ik}S_{jl}\Gamma^{(2)}_{ij}(x;y) = \Gamma^{(2)}_{kl}(x;y), \tag{4.4}$$

$$S_{im}S_{jn}S_{kp}S_{lq}\Gamma^{(4)}_{mnpq} = \Gamma^{(4)}_{ijkl}. \tag{4.5}$$

Equations (4.4) and (4.5) indicate that $\Gamma^{(2)}$ and $\Gamma^{(4)}$ are invariant tensors under $SO(N)$ group.

Expressing the two- and four-point 1PI functions,

$$\Gamma^{(2)}_{ij} = (k^2 - m_R^2)\delta_{ij} + k^2K^{(2)}_{ij} - K^{(m)}_{ij}, \tag{4.6}$$

$$\Gamma^{(4)}_{ijkl} = \frac{1}{3}\lambda(\delta_{ij}\delta_{kl} + \delta_{ik}\delta_{jl} + \delta_{il}\delta_{jk}) + K^{(4)}_{ijkl}, \tag{4.7}$$

and considering that $K^{(2)}$ and $K^{(m)}$ are symmetric matrices while $SO(N)$ generators are antisymmetric, it yields by substituting (4.6) and (4.7) in (4.4) and (4.5), respectively,

$$\left[K^{(2)}, G_a\right] = 0, \tag{4.8}$$

$$\left[K^{(m)}, G_a\right] = 0 \tag{4.9}$$

and

$$G_{aim}K^{(4)}_{inpq} + G_{ain}K^{(4)}_{mipq} + G_{aip}K^{(4)}_{mniq} + G_{aiq}K^{(4)}_{mnpi} = 0. \tag{4.10}$$

Then, by virtue of the Schur's lemma

$$K^{(2)} = k^{(2)}11, \tag{4.11}$$

$$K^{(m)} = k^{(m)}11 \tag{4.12}$$

and

$$K^{(4)}_{ijkl} = k^{(4)} 11 \otimes 11. \tag{4.13}$$

Consequently, $SO(N)$ symmetry implies

$$\Phi_B = Z_\Phi^{\frac{1}{2}} \Phi_R,$$

where

$$Z_\Phi = (1 + k^{(2)})11, \tag{4.14}$$

$$m_B^2 = Z_\Phi^{-1} Z_m m_R^2,$$

where

$$Z_m = (1 + k^{(m)})11, \tag{4.15}$$

and

$$\lambda_B = Z_4 Z_\Phi^{-2} \lambda_R,$$

where

$$Z_4 = (1 + k^{(4)})11. \tag{4.16}$$

Equation (4.14) shows that the renormalization process with symmetry $SO(N)$ does not mix fields. From Eq. (4.15), we get that all masses renormalize equally in the sense that radiative corrections do not split the mass degeneracy dictated by $SO(N)$ symmetry. This argument can be verified by taking $k^2 = \mu^2$ as a zero in Eq. (4.4). It yields

$$\Gamma^{(2)}_{ij}(k^2 = \mu^2) = 0, \tag{4.17}$$

which says that all propagators have a same pole: $k^2 = \mu^2 = m_R^2 + (\delta m^2)_{\text{finite}}$. Therefore, since the symmetry is preserved the quadratic correction will preserve the mass degeneracy. Finally, from Eq. (4.16), we also observe that symmetry will protect that after renormalization no new vertex is created.

The important thing here to notice is that the same informations could be obtained through φ-basis as Section 3 shows. For instance, from Eq. (3.26), one gets

$$M_B^2 = M_R^2 + K^{(M)} - \frac{1}{2}(M_R^2)_{ik} K^{-1}_{kl} K^{(2)}_{lj} - \frac{1}{2} K^{(2)}_{ik} K^{-1}_{kl} (M_R^2). \tag{4.18}$$

Similarly for the coupling constants

$$\begin{aligned} \lambda^B_{mnpq} = \lambda^R_{mnpq} + K^{(4)}_{mnpq} - \frac{1}{2}\lambda^R_{mnpl} K^{-1}_{lr} K^{(2)}_{rq} + \\ - \frac{1}{2}\lambda^R_{mnlq} K^{-1}_{lr} K^{(2)}_{rp} - \frac{1}{2}\lambda^R_{mlpq} K^{-1}_{lr} K^{(2)}_{rn} - \frac{1}{2}\lambda^R_{lnpq} K^{-1}_{lr} K^{(2)}_{rm}. \end{aligned} \tag{4.19}$$

5. Conclusion

A clear consequence from assuming this generalized model (1.1) or (1.2) is the development of a Ω-matrix. These non-dynamical Ω transformations work on the ingredients of theory and split them into classes of invariants and tensors. This perspective brings a prescription that can be useful for understanding about the physicity of every variable building up the model. Symmetry representations, Feynman rules and the renormalization group equation contain such Ω dependence; while physical masses and the Slavnov–Taylor identity were shown to be invariants.

Another interesting consequence form Ω matrix relates the presence of diagonal and non-diagonal field basis. Although physics should not depend on them, some aspects are better seen depending on a given choice. Comparing to the case with spontaneous symmetry breaking one concludes that at Φ-basis the mass spectrum is more explicit (similarly to unitary gauge), but the renormalizability is not explicit. However, at φ-basis (analogous to renormalizable gauge), the renormalizability is evident.

Acknowledgements

Thanks to FAPERJ (Rio de Janeiro, Brazil), CNPq, and SHELL of Brazil for the invaluable financial help.

References

1. H. J. Borchers, Il Nuovo Cimento, *15*, 784, 1960; Comm. in Math. Phys., *1*, 281, 1985; H. J. Borchers and W. Zimmerman, Il Nuovo Cimento, *31*, 1047, 1964.
2. For a Kaluza–Klein origin see: R. M. Doria and C. Pombo, Il Nuovo Cim., *96B*, 2, 1986; C. M. Doria, R. M. Doria, J. A. Helayël-Neto, Rev. Bras. Fis., *17*, 3, 1987.
   For a supersymmetric origin see: N. Chair, J. A. Helayël-Neto and A. William Smith, Phys. Lett. B, *233*, 173, 1989; S. A. Dias, R. M. Doria, J. L Matheus Valle, Rev. Bras. Fis., *21*, 1, 1991; C. M. Doria, R. M. Doria, F. A. B. Rabelo de Carvalho, A superspace origin for an extended gauge model, UCP preprint 88/6; C. A. S. Almeida, R. M. Doria, Rev. Bras. Fis., *21*, 3, 1991; C. S. Almeida, R. M. Doria, A less-constrained (2,0) super Yang–Mills Model: The coupling to non-linear σ-models, UCP preprint 90/4.
   For a σ-model origin see: R. M. Doria, J. A. Helayël-Neto and S. Mokhtari, Europhys. Lett., *16*(1), 1991.
3. R. M. Doria, F. A. B. Rabelo de Carvalho, Braz. J. Phys. *23*, No 1; R. M. Doria, G. Oliveira Neto, F. A. B. Rabelo de Carvalho, A consistent spectroscopical analysis for an extended gauge model, UCP preprint 90/9.

Acta Physica Hungarica 73 (2-4), pp. 257-259 (1993)

RADIATIVE CORRECTIONS OF ORDER α TO SUPERALLOWED FERMI β-DECAYS

GÜNEŞ TANIR, BAŞAR ŞARER and DARIUSH AMIRHASHEMI

Gazi University, Faculty of Arts and Sciences
06500 Ankara, Turkey

(Received 24 August 1993)

The outer radiative corrections of order α to superallowed Fermi β-decays (^{14}O, ^{26m}Al, ^{34}Cl, ^{42}Sc, ^{46}V, ^{50}Mn and ^{54}Co) are calculated by applying an approximation to Fermi function. The results are compared to other studies.

Introduction

The calculation of the actual rate of β-decay has fundamental importance to find the precise values of vector coupling constant, half-lives, matrix elements, etc. A precise knowledge of the vector coupling constant for nuclear β-decay is necessary to test of Conserved Vector Current (CVC) theory. According to the CVC hypothesis all ft values for superallowed β-decay should be identical providing that small electromagnetic corrections are accounted for. One of the major uncertainties in the ft values of superallowed β-decay is the radiative correction. The f function should be modified by radiative corrections. Many authors [1,2,3] have worked on the corrections but discrepancies remained among their results. Radiative corrections arise from the interaction of the decaying nucleon and the emitted positron with the external electromagnetic field. These corrections are separated into: 1) "Outer" corrections of order α, $Z\alpha^2$, $Z^2\alpha^3$ ... and magnitude δ_1, δ_2, $\delta_3 \ldots \delta_R = \delta_1 + \delta_2 + \delta_3 + \ldots$ which are included in the experimental ft multiplying it by $(1 + \delta_R)$. δ_1 is given [3] by integrating a function $g(W, W_0)$ over the positron spectrum to the end point W_0:

$$\delta_1 = (\alpha/2\pi) g(W, W_0).$$

2) "Inner" corrections which are included in the primitive G_ν value: $G_\nu'^2 = G_\nu^2(1 + \Delta)$. Δ depends on the structure of decay, the details of strong interactions, and the applied model.

In this work, the outer radiative corrections are calculated by applying an approximation to Fermi function in the vector interaction of β-decay.

Details of calculations

The radiative correction of order α is given [4] by

$$\delta(Z,W_0)=\frac{\alpha}{2\pi}f^{-1}\int_1^{W_0}pW(W_0-W)^2F(Z,W)g(W,W_0)dW, \tag{1}$$

where $g(W,W_0)$ is a universal function and is given by the following expression:

$$\begin{aligned}g(W,W_0)&=3\ln M-3/4+4\left[\frac{\text{arctan}h\beta}{\beta}-1\right]\left[\frac{W_0-W}{3W}-3/2+\ln 2(W_0-W)\right]\\&+\frac{4}{\beta}L\left(\frac{2\beta}{1+\beta}\right)+\frac{1}{\beta}[\text{arctan}h\beta][2(1+\beta^2)\\&+\frac{(W_0-W)^2}{6W^2}-4\text{arctan}h\beta].\end{aligned} \tag{2}$$

The Fermi function for $Z\neq 0$ is:

$$F(Z,W_0)=2(1+\gamma)[\Gamma(2\gamma+1)]^{-2}(2pR)^{2(\gamma-1)}e^{\pi\alpha ZW/p}|\Gamma(\gamma+i\alpha ZW/p)|^2. \tag{3}$$

The calculation of the Fermi function using this expression is complex and boring. So many approximations are experimented and done. An approximation for the Fermi function in this work is considered:

$$F(Z,W_0)=1+\frac{\pi\alpha ZW}{p}, \tag{4}$$

where $p=\sqrt{W^2-1}$.

Results and discussion

Our results for δ_1 are listed in Table I. It can be seen that δ_1 decreases with increasing W_0 and the results are in agreement with others. The differences are mainly due to the contribution of the axial vector current. It has been assumed that radiative corrections of order α are dominant. However, it must be remembered that corrections of higher order (in particular of order $Z\alpha^2$) may be important.

Table I
Radiative correction for superallowed β-decay

Nucleus	Z	W_0	$\delta_1(Z,W_0)$ [3]	$\delta_1(Z,W_0)$ [5]	$\delta_1(Z,W_0)$ [6]	$\delta_1(Z,W_0)$
^{14}O	7	4.5392	1.29	1.19	1.29	1.30
^{26}Al	12	7.2827	1.11	1.01	1.11	1.13
^{34}Cl	16	9.7481	1.01	0.90	1.00	1.03
^{42}Sc	20	11.5743	0.94	0.84	0.94	0.97
^{46}V	22	12.7977	0.91	0.80	0.90	0.93
^{50}Mn	24	13.9357	0.88	0.77	0.87	0.90
^{54}Co	26	15.1301	0.86	0.74	0.84	0.87

References

1. A. Sirlin and R. Zucchini, Phys. Rev. Letters, *57*, No 16, 1994, 1986.
2. W. Jaus and G. Rasche, Phys. Rev. D, *35*, 3420, 1987.
3. D. H. Wilkinson, Nucl. Phys. A, *527*, 689c, 1991.
4. G. Kallen, Nucl. Phys., B*1*, 225, 1967; A. Sirlin, Phys. Rev., *164*, 1767, 1967.
5. A. Sirlin, Nucl. Phys., *B71*, 29, 1974.
6. N. Brene, M. Roos and A. Sirlin, Nucl. Phys., *B6*, 255, 1968.

Acta Physica Hungarica 73 (2–4), pp. 261–268 (1993)

COMPARISON OF TWO- AND ONE-COMPONENT PREEQUILIBRIUM EXCITON MODEL CALCULATIONS FOR SOME NEUTRON INDUCED REACTIONS

BAŞAR ŞARER and GÜNEŞ TANIR

Gazi University, Faculty of Arts and Sciences
06500 Ankara, Turkey

(Received in revised form 24 August 1993)

Two-component preequilibrium, used by Gupta, and analogously one-component exciton model descriptions are applied to neutron induced reactions such as ^{46}Ti(n,n′), ^{46}Ti(n,xp) and ^{27}Al(n,xp) at 14.6 MeV. This is the first complete calculation made by the two-component approach of Gupta. In order to obtain mean lives the time-integrated form of master equations is used.

Introduction

The basic feature of the exciton model is the time-dependent description of a nuclear reaction as a process in which the initial exciton state of the composite nucleus equilibrates through a series of successive states by energy conserving two-body residual interactions bringing about transitions between these states.

In the one-component formulation of the exciton model for preequilibrium nuclear reactions, neutron–proton distinguishability, suggested first by Cline and Blann [1], and then by several authors [2–7], is taken into account.

A two-component master equation approach for a nuclear system towards equilibrium is described by Gupta [5], two-components being the proton and neutron components, but to our knowledge no complete calculation has been done using this approach. In this study, two-component master equation approach for a nuclear system towards the equilibrium, as described by S. K. Gupta [5] and analogously one-component exciton model descriptions for ^{46}Ti(n,n′), ^{46}Ti(n,xp) and ^{27}Al(n,xp) neutron induced reactions, are applied and the results are compared to experiments.

Calculations and conclusions

In the two-component master equation approach for a nuclear system equilibrating towards the equilibrium has been suggested by Gupta [5], a state (n_π, n_ν) is described by (n, i), where $n_\pi = p_\pi + h_\pi$, $n_\nu = p_\nu + h_\nu$ and $i = h_\pi$. The

two-component master equation for the population $P(n,i,t)$ changing with time is written as

$$\begin{aligned}\frac{dP(n,i,t)}{dt} &= P(n-2,i-1,t)\lambda_+^{\pi}(n-2,i-1) + P(n-2,i,t)\lambda_+^{\nu}(n-2,i)\\ &+ P(n+2,i+1,t)\lambda_-^{\pi}(n+2,i+1) + P(n+2,i,t)\lambda_-^{\nu}(n+2,i)\\ &+ P(n,i-1,t)\lambda_0^{\nu\pi}(n,i-1) + P(n,i+1,t)\lambda_0^{\pi\nu}(n,i+1)\\ &- P(n,i,t)/\tau(n,i), \end{aligned} \tag{1}$$

where

$$\begin{aligned}\tau(n,i) = [&\lambda_+^{\pi}(n,i) + \lambda_+^{\nu}(n,i) + \lambda_-^{\pi}(n,i)\\ &+ \lambda_-^{\nu}(n,i) + \lambda_0^{\nu\pi}(n,i) + \lambda_0^{\pi\nu}(n,i) + L(n,i)]^{-1}. \end{aligned} \tag{2}$$

λ's are transition rates and $L(n,i)$ is the total emission probability from state (n,i). The maximum exciton number is given by $n = 2\sqrt{gE}$. The number of coupled equations in (1) grows quadratically with maximum exciton number, whereas in the one-component formulation the growth is linear. The number of two-component equations is $h_{\max}(h_{\max}+3)/2$, the number of equations for the one-component case is $h_{\max}$ only. Two-component transition rates are taken from [8]. It is true for the λ transition rates that

$$\lambda_+^{\nu}(n,i) = N\left(\frac{1}{2}gE\right)^2 \frac{n-\frac{1}{2}n_\gamma}{n(n+1)}, \tag{3}$$

$$\lambda_-^{\nu}(n,i) = Nh_\gamma p_\gamma (n - \frac{1}{2}n_\gamma - 1), \tag{4}$$

$$\lambda_0^{\gamma\gamma'}(h,i) = N\frac{1}{2}gE\frac{2p_\gamma h_{\gamma'}}{n}. \tag{5}$$

$\gamma = \pi$, $\gamma' = \nu$ or $\gamma = \nu$, $\gamma' = \pi$, $N = \frac{2\pi}{\hbar}|M|^2\frac{1}{2}g$, $\gamma = \pi$ or ν, $p_\pi = \pi_\alpha + i$, $p_\nu = n - \pi_\alpha - h - i$, $h_\nu = h - i$, where $|M|^2$ is the average squared two-body matrix element. Here, π_α is the number of protons in the projectile. In this paper, the squared matrix element for proton–proton, proton–neutron and neutron–neutron interactions has been taken to be equal. Here, $\frac{1}{2}g$ is the single particle level density both for protons and neutrons, that is single particle level density for proton and neutron can be given by $g_\pi = g_\nu = g/2 = \frac{1}{2}\frac{A}{13}$. The squared two-body matrix element has been assumed to be independent of the exciton type. The exciton energy and the (composite-nucleus) mass number dependence of $|M|^2$ is expected to be approximately [4]:

$$|M|^2 \simeq KA^{-3}E^{-1}, \tag{6}$$

where K is a free parameter. The density of the exciton states with energy E has been given by Ericson [9] as

$$\omega(n,i,E) = \frac{g^n E^{n-1}}{2^n(n-1)!p_\pi!h_\pi!p_\nu!h_\nu!}. \tag{7}$$

The differential particle emission rate from an (n,i) state is written as

$$W_\beta(n,i,\epsilon_\beta)d\epsilon = \frac{2s_\beta+1}{\pi^2\hbar^3}\mu_\beta\epsilon\sigma_\beta(\epsilon)d\epsilon\frac{\omega(p_\pi-\pi_\beta,h_\pi,p_\nu-\nu_\beta,h_\nu,U)}{w(p_\pi,h_\pi,p_\nu,h_\nu,E)}. \tag{8}$$

Here s_β, μ_β and ϵ are spin, reduced mass and energy of the emitted particle, respectively, σ_β is the absorption cross-section for the inverse reaction of ejectile. Inverse reaction cross-section has been calculated by the method given by Dostrovsky [10]. In (7) and (8) π_β and ν_β are the proton and neutron number of the emitted particle, U is the excitation energy of the residual nucleus.

The total emission rate in (2) is obtained by integrating over the outgoing particle energies and summing over all outgoing channels considered,

$$L(n,i) = \sum_\beta \int_0^{\epsilon\beta_{\max}} W_\beta(n,i,\epsilon_\beta)d\epsilon. \tag{9}$$

The spectrum for the emission of particle β is given by

$$\frac{d\sigma(\alpha,\beta)}{d\epsilon_\beta} = \sigma_\alpha \sum W_{\beta_\beta}(n,i,\epsilon)T(n,i). \tag{10}$$

Here, σ_α is the composite-nucleus formation cross-section by an incoming particle α, $T(n,i)$ is the time that the composite system spends in the (n,i) state, that is

$$T(n,i) = \int_0^\infty P(n,i,t)dt. \tag{11}$$

To obtain $T(n,i)$, we include the system (1) over the time variable and solved the system of linear algebraic equations:

$$\begin{aligned} -D(n,i) = P(n,i)|_0^\infty = {} & T(n-2,i-1)\lambda_+^\pi(n-2,i-1) + T(n-2,i)\lambda_+^\nu(n-2,i) \\ & + T(n+2,i+1)\lambda_-^\pi(n+2,i+1) + T(n+2,i)\lambda_-^\nu(n+2,i) \\ & + T(n,i-1)\lambda_0^{\nu\pi}(n,i-1) + (n,i+1)\lambda_0^{\pi\nu}(n,i+1) - \frac{T(n,i)}{\tau(n,i)}, \end{aligned} \tag{12}$$

where $D(n,i)$ is the initial population of the (n,i) state; at $t=0$ only $D(p_\alpha+2,0 \text{ or } 1) = P(p_\alpha+2,0 \text{ or } 1,0)$ is non-zero.

The time integrated one-component master equation is

$$-D(n) = \lambda_+(n-2)T(n-2) - \frac{T(n)}{\tau(n)} + \lambda_-(n+2)T(n+2), \tag{13}$$

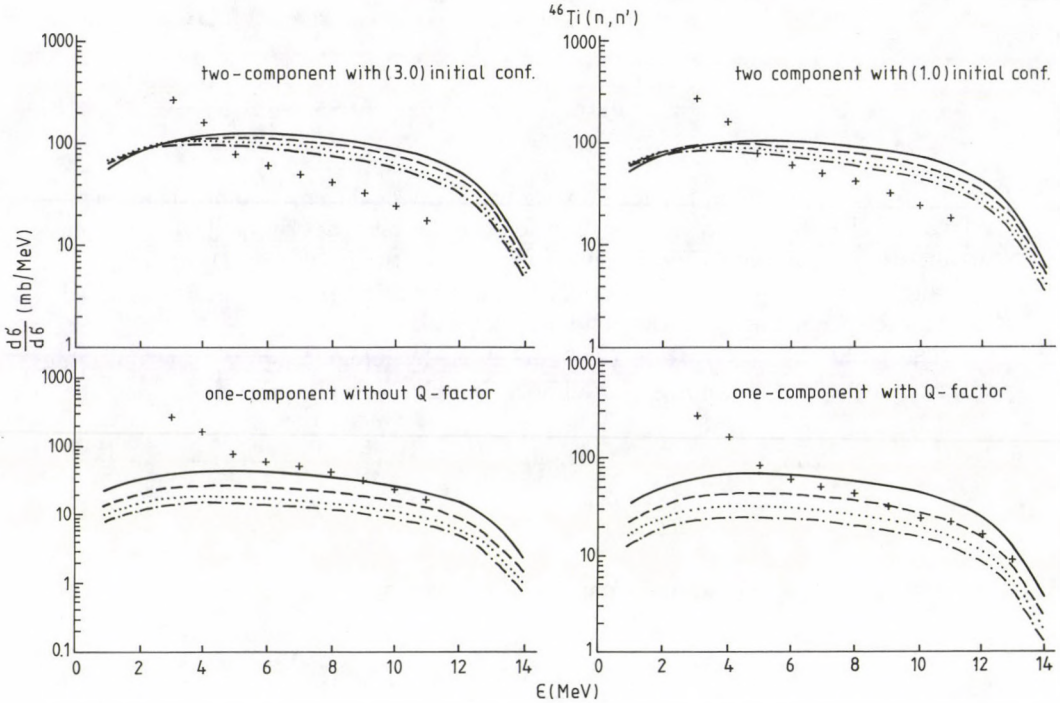

Fig. 1. Comparison of experimental and theoretical energy spectra of the ^{46}Ti(n,n′) reaction at 14.6 MeV, as described by the one- and two-component exciton models for various K values. The solid curves show $K = 100$ MeV^3, the dashed curves $K = 200$ MeV^3, the dotted curves $K = 300$ MeV^3, and the dashed–dotted curves $K = 400$ MeV^3. The plus signs represent the experimental data taken from [11]

where $\tau(n) = [\lambda_+(n) + \lambda_0(n) + \lambda_-(n) + L(n)]^{-1}$. To find the mean life $T(n, E)$, the system of linear algebraic equations (13) has been solved with the initial condition $D(n) = \delta_{nn_0}$. The transition rates are given by

$$\lambda_-(n) = \frac{2\pi}{\hbar}|M|^2 gph(n-2), \tag{14}$$

$$\lambda_0(n) = \frac{2\pi}{\hbar}|M|^2 g(gE)(n-1), \tag{15}$$

$$\lambda_-(n) = \frac{2\pi}{\hbar}|M|^2 \frac{g^3E^2}{(n+1)}. \tag{16}$$

The one component exciton state density is

$$\omega(p, h, E) = \frac{g^n E^{n-1}}{(n-1)!p!h!} \tag{17}$$

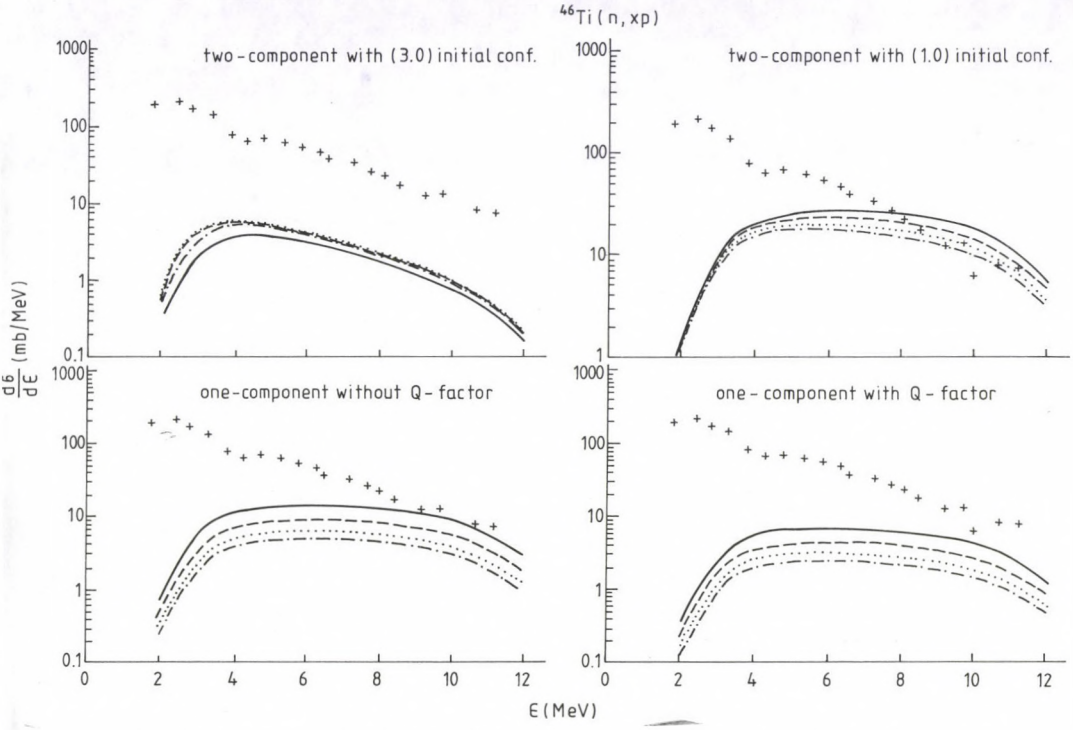

Fig. 2. The same as in Fig. 1, but for ^{46}Ti(n,xp) at 14.6 MeV. Experimental data are taken from [12]

and the one-component emission rate is given by

$$W_\beta(n,\epsilon_\beta) = \frac{2s_\beta+1}{\pi^2\hbar^3}\mu_\beta\epsilon_\beta\sigma_\beta(\epsilon_\beta)Q_\beta(p)\frac{\omega(p-p_\beta,h,U)}{\omega(p,h,E)}, \tag{18}$$

where p and h are the numbers of particles and holes, respectively and $Q_\beta(p)$ is the neutron–proton distinguishability factor for a neutron-induced reaction. This factor is to be chosen for neutron emission as $2-2z\frac{n-1}{n+1}$ and for proton emission as $2z\frac{n-1}{n+1}$. Here, $z = Z/A$ [5]. The spectrum for the emission of particle β is given as

$$\frac{d\sigma(\alpha,\beta)}{d\epsilon_\beta} = \sigma_\alpha \sum W_\beta(n,\epsilon_\beta)T(n,i), \tag{19}$$

where σ_α is the composite-nucleus formation cross-section by an incoming particle α, $T(n,i)$ is the time that the composite system spends in the state characterized by n,i state and is given as

$$T(n,i) = \int_0^\infty P(n,i,t)dt. \tag{20}$$

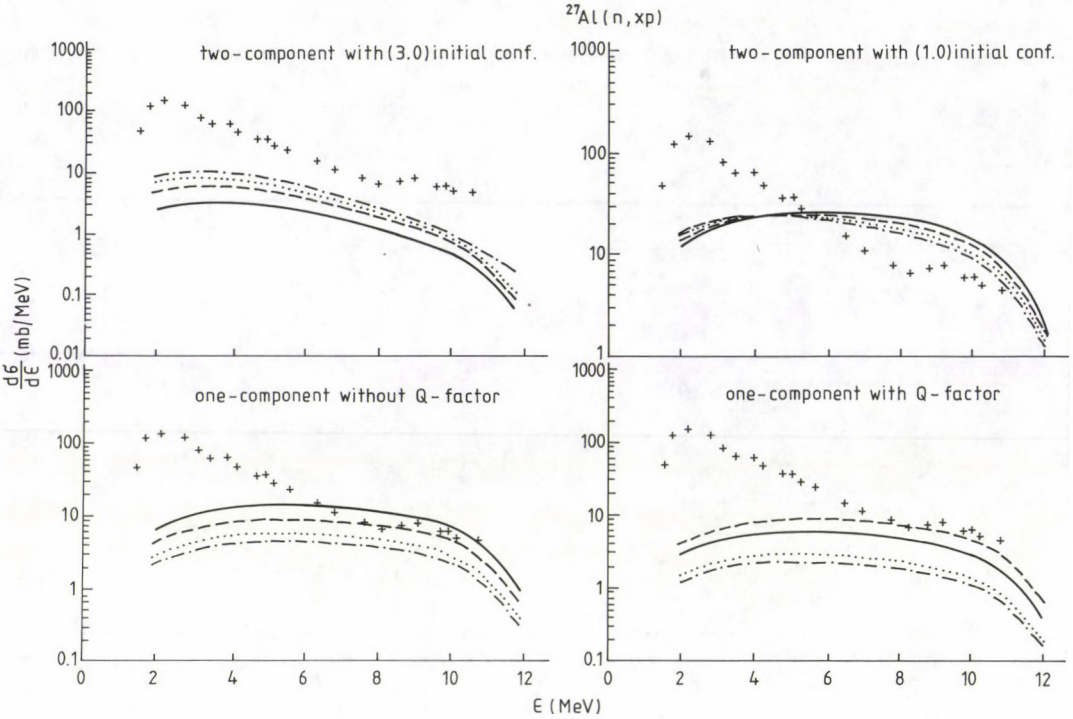

Fig. 3. The same as in Fig. 1, but for ^{27}Al(n,xp) at 14.6 MeV. Experimental data are taken from [12]

In this paper, only the emission of primary nucleons has been considered. Complex particles, gamma emissions and secondary particles have not been taken into account. In the course of calculations, level densities and transition rate formulae without corrections for the Pauli principle have been used.

In order to perform a detailed comparison, the free parameter K has been chosen to be 100, 200, 300 and 400 MeV^3, respectively and both the one- and two-component preequilibrium angle-integrated spectra have been calculated.

In the two-component preequilibrium calculations, for the initial exciton number both the $n = 1$ and $n = 3$ values are used. In the case for $n = 3$, there are two different configurations as $(n = 3, i = 0)$ and $(n = 3, i = 1)$. Only the $(n = 3, i = 0)$ configuration is used in the present calculations.

Figures 1–3 show a comparison between calculated and experimental angle-integrated spectra for each reaction. Results are presented from the calculations by the two- and one-component preequilibrium exciton models. The two-component results are compared to the analogous one-component exciton model calculations with and without the distinguishability factor Q [5].

In the ^{46}Ti + n at 14.6 MeV, the thresholds for secondary neutron and proton emission are about 5 MeV and 1 MeV, respectively. In the same entrance channel, the reaction threshold for $^2_1$H and $^3_1$H emission are about 6 MeV and 1 MeV, respec-

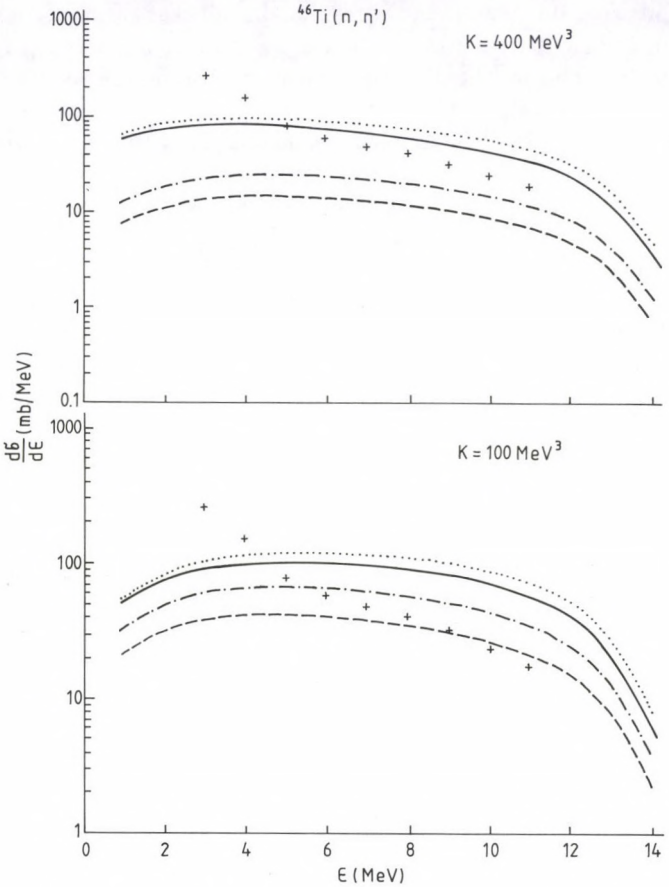

Fig. 4. Comparison between calculated and experimental energy spectra for the ^{46}Ti(n,n') reaction for $K = 100, 400$ MeV^3. The dotted curves show two-component results with (3,0) initial configuration, solid curves represent two-component calculations with (1,0) initial configuration and dashed curves represent one-component results without Q-factor while dashed–dotted curves correspond to the one-component calculations with Q-factor. The plus signs represent the experimental data [11]

tively. Therefore, neither primary deuteron and triton, nor secondary neutron and proton emissions can contribute to the whole process which is essentially governed by preequilibrium mechanism. Only $^4_2$He emission can contribute to the ^{46}Ti + n process.

In the reaction ^{27}Al + n at 14.6 MeV, both the emission of the primary $^3_1$H, the secondary neutron and proton are energetically forbidden. Only alpha and deuteron emissions can contribute to the angle-integrated cross-section.

For all the three reactions, the calculated results are, in general, in good agreement with the experimental data. In reaction ^{46}Ti(n,n') (Fig. 1), one-component calculations with and without a Q-factor, especially for $K = 200$ MeV^3, are in

good agreement with the experimental results. In the case of the Ti(n,xp) reaction, (Fig. 2), the best agreement is attained by the two-component description with (1,0) initial configuration and by the one-component exciton model with a Q-factor. On the other hand, the K values do not seem to affect the calculations. In the same reaction with $K = 100$ MeV^3 the one-component exciton model calculations with a Q-factor are better than the one-component calculations without a Q-factor.

In reaction ^{27}Al(n,xp) (Fig. 3) the one-component calculations, both with and without Q-factor are in better agreement with experiments than the two-component calculations. For each calculation, $K = 100$, 200 MeV^3 give better agreement with experimental results than higher K values do.

Figure 4 shows a comparison between the one- and two-component preequilibrium calculations as well as the experimental data for $K = 400$ MeV^3. Two-component results with initial configuration (1,0) show the best agreement with experimental data.

It is summarized here that the calculations have been performed with the following assumptions: (1) The squared matrix elements for proton–proton, proton–neutron and neutron–neutron interactions have been taken to be equal. (2) Single-particle level densities for neutron and proton have been taken to be equal. (3) Exciton state densities without corrections for the Pauli principle have been used. (4) Complex particles, gamma and secondary particle emissions are not taken into account. Despite the above approximations, the theoretical predictions are in good agreement with the experimental results.

References

1. C. K. Cline, M. Blann, Nucl. Phys., *A172*, 225, 1971.
2. C. K. Cline, Nucl. Phys., *A193*, 417, 1972.
3. M. Blann, Nucl. Phys., *A213*, 570, 1973.
4. C. Kalbach, Z. Phys., A-Atoms and Nuclei, *283*, 401, 1977.
5. S. K. Gupta, Z. Phys., A-Atoms and Nuclei, *303*, 329, 1981.
6. J. Dobes, E. Betak, Z. Phys., A-Atoms and Nuclei, *310*, 329, 1983.
7. C. Kalbach, Phys. Rev., *C33*, 818, 1986.
8. E. Běták, P. Obložinský, I. Ribanský, Nukleonika, *19*, 687, 1974.
9. T. Ericson, Adv. Phys., *9*, 425, 1960.
10. I. Dostrovsky, Z. Frenkel, Phys. Rev., *116*, 683, 1959.
11. D. Hermsdorf, A. Meister, S. Sassonoff, D. Seeliger, K. Seidel, F. Shahin, Zentralinstitut für Kernforschung, Rossendorf bei Dresden, Report ZfK-277, 1, 1974.
12. S. M. Grimes, R. C. Haight, J. D. Anderson, Nucl. Sci. Eng., *62*, 187, 1977.

Acta Physica Hungarica 73 (2–4), pp. 269–275 (1993)

COSMOLOGICAL TESTS FOR A TWO POTENTIAL THEORY OF ELECTROMAGNETISM

C. WOLF

Department of Physics, North Adams State College
North Adams, MA (01247), USA

(Received 24 August 1993)

By considering the propagative properties of the potentials in a two potential theory of electromagnetism we arrive at signatures characterisitc of a two photon theory when the two photons in the theory have a small rest mass and mix together in the Lagrangian.

1. Introduction

Classical electrodynamics and Quantum Electrodynamics have passed every conceivable test that experiment has confronted them with and the formal beauty and inner consistency of these theories represents a milestone in the history of theoretical physics. However, with the recent flurry of interest concerning a possible strong coupling phase of Q.E.D. motivated by the 1.8 MeV (e^+e^-) peaks generated in heavy ion collisions [1,2] questions regarding the validity of Q.E.D. as a strong coupling theory have surfaced. Along with these questions there has been a persistent interest from the theoretical community to understand magnetic charge and magnetic monopoles within the present structure of electrodynamics [3]. Dirac [4] originally proposed the idea of magnetic monopoles to arrive at an understanding of how electric charge was quantized in the world. His idea was, "if there is one unit of electric charge coupled to a magnetic monopole, quantization of electric charge results from the quantization of angular momentum for the electric charge,"

$$\frac{eg}{\hbar C} = \frac{n}{2}.$$

Schwinger [5] later discussed the interaction of two dyons (a dyon being a particle carrying electric and magnetic charge) and demonstrated that they obey the quantization condition

$$\frac{e_1 g_2 - e_2 g_1}{\hbar C} = \frac{n}{2} \quad (C = \text{speed of light}).$$

(e_1, g_1 = electric and magnetic charge of particle 1, e_2, g_2 = electric and magnetic charge of particle 2). With regard to interactions in the early universe, Witten [6] has shown that the electric charge of a dyon need not be quantized in the presence of CP violating interactions. Along the same line of reasoning Fischler and Preskill

[7] have demonstrated that monopoles can reduce the axion density to acceptable levels in the early universe with the monopole thus acquiring a non-integer electric charge. When magnetic charge is present in the theory, it is easy to demonstrate that a single vector potential does not exist for all points since

$$\frac{\partial}{\partial x^\nu}\left(\frac{\epsilon^{\mu\nu\alpha\beta}F_{\alpha\beta}}{2}\right) \neq 0. \tag{1.1}$$

If the right side of Eq. (1.1) is zero then the equation is the equivalent to the existence of a potential. To circumvent this problem, Cabibbo and Ferrari [8] long ago constructed a two potential theory of electromagnetism in the presence of magnetic charge. In a very interesting paper, Callegari et al [9] have discussed the structure of this theory when two photons are present (electric-like photons and magnetic-like photons) along with the effects that such a two potential theory would have on local electromagnetic phenomena. Their upper limits for the masses of the two photons are low but not completely ruled out by experiments. Along the same line of thought it was Vinciarelli [10] who emphasized that the dual symmetry of Maxwell's equation is unique to four-space time dimensions. This suggests that magnetic monopoles and dyons might be topological condensations arising from higher dimensional compactification. When the properties of the t'Hooft Polyakov monopole were studied for an SO_3 gauge Higgs system, it reinforced this idea with the topology of the gauge-Higgs fields being related to the magnetic charge of the field configuration [11]. Inspired by these theoretical considerations suggesting the existence of magnetic charge along with the desire to find a consistent formulation to describe electric and magnetic charge we study the propagative properties of photons in a two potential theory when mass terms are present for the photons and a mixing term is present in the Lagrangian.

We also arrive at the unique properties that would identify the presence of a two potential theory and suggest provisional ways of looking for these signatures in a cosmological setting.

2. Two potential theory of electromagnetism

We begin our analysis by writing the field tensor in a two potential theory of electromagnetism as

$$F_{\mu\nu} = \frac{\partial A_\mu}{\partial x^\nu} - \frac{\partial A_\nu}{\partial x^\mu} - \frac{\epsilon^{\alpha\beta}_{\mu\nu}}{2\sqrt{-g}}\left(\frac{\partial B_\alpha}{\partial x^\beta} - \frac{\partial B_\beta}{\partial x^\alpha}\right), \tag{2.1}$$

here A_μ is 4 vector potential, B_μ is 4 pseudo vector potential.

For the Lagrangian of electromagnetism with rest m_e for the electric like photon, and m_g for magnetic like photons we have

$$\begin{aligned}\mathcal{L} = &-\frac{1}{16\pi}F_{\mu\nu}F^{\mu\nu}\sqrt{-g} - J^\mu_e A_\mu\sqrt{-g} + J^\mu_g B_\mu\sqrt{-g} \\ &+ \frac{m_e^2C^2}{8\pi\hbar^2}A_\mu A^\mu\sqrt{-g} - \frac{m_g^2C^2}{8\pi\hbar^2}B_\mu B^\mu\sqrt{-g} + \frac{\alpha A_\mu B^\mu}{4\pi}\sqrt{-g},\end{aligned} \tag{2.2}$$

here J_e^μ is the electric current density, J_g^μ is the magnetic current density, α is a mixing constant.

Also the term $\alpha A_\mu B^\mu \sqrt{-g}$ destroys parity invariance since B_μ is a pseudo-vector.

We could retain parity invariance by introducing a constant static pseudo-scalar Φ_0 such that the mixing term reads

$$\alpha \Phi_0 A_\mu B^\mu \sqrt{-g}. \tag{2.3}$$

We, however, choose the original form in Eq. (2.2) to study wave propagation. Varying Eq. (2.2) with respect to A_μ gives

$$\frac{\partial}{\partial x^\nu}(\sqrt{-g}F^{\mu\nu}) + \frac{m_e^2 C^2}{\hbar^2} A^\mu = 4\pi\sqrt{-g} J_e^\mu - \alpha B^\mu. \tag{2.4}$$

Varying Eq. (2.2) with respect to B_μ gives

$$\frac{\partial}{\partial x^\nu}(\tilde{F}^{\mu\nu}) + \frac{m_g^2 C^2}{\hbar^2} B^\mu = 4\pi\sqrt{-g} J_M^\mu + \alpha A^\mu. \tag{2.5}$$

For the four vector potentials and pseudo-vector potential we have

$$A^\mu = (A_x, A_y, A_z, \Phi), \quad B^\mu = (B_x, B_y, B_z, \Psi),$$

The electric and magnetic fields are

$$\begin{aligned} E &= \overline{E}_x \hat{i} + \overline{E}_y \hat{j} + \overline{E}_z \hat{k}, \\ B &= \overline{B}_x \hat{i} + \overline{B}_y \hat{j} + \overline{B}_z \hat{k}. \end{aligned} \tag{2.6}$$

The field tensors now receive contributions from both the vector and pseudo-vector potential. Also if we consider an EM wave propagating in the x direction we have

$$A^\mu = (0, A_y, A_x, 0),$$

$$B^\mu = (0, B_y, B_z, 0).$$

Here the components of A^μ, B^μ depend only on x, t. The field tensor components are

$$\begin{aligned} F_{12} &= \overline{B}_z = \frac{\partial A_y}{\partial x} - \frac{1}{C}\frac{\partial B_z}{\partial t}, \\ F_{24} &= \overline{E}_y = -\frac{1}{C}\frac{\partial A_y}{\partial t} + \frac{\partial B_z}{\partial x}, \\ F_{13} &= \overline{B}_y = \frac{1}{C}\frac{\partial B_y}{\partial t} + \frac{\partial A_z}{\partial x}, \\ F_{34} &= \overline{E}_z = -\frac{1}{C}\frac{\partial A_z}{\partial t} - \frac{\partial B_y}{\partial x}. \end{aligned} \tag{2.7}$$

Eq. (2.4) now reads for $u = 2$

$$-\frac{\partial^2 A_y}{\partial x^2} + \frac{1}{C}\frac{\partial^2 B_z}{\partial t \partial x} + \frac{1}{C^2}\frac{\partial^2 A_y}{\partial t^2} - \frac{1}{C}\frac{\partial^2 B_z}{\partial t \partial x} + \frac{m_e^2 C^2}{\hbar^2} A_y = -\alpha B_y. \tag{2.8}$$

For $u = 3$ Eq. (2.4) reads

$$-\frac{\partial^2 A_z}{\partial x^2} - \frac{1}{C}\frac{\partial^2 B_y}{\partial t \partial x} + \frac{1}{C^2}\frac{\partial^2 A_z}{\partial t^2} + \frac{1}{C}\frac{\partial^2 B_y}{\partial t \partial x} + \frac{m_e^2 C^2}{\hbar^2} A_z = -\alpha B_z. \tag{2.9}$$

For $u = 2$ Eq. (2.5) reads

$$-\frac{1}{C}\frac{\partial^2 A_z}{\partial t \partial x} - \frac{\partial^2 B_y}{\partial x^2} + \frac{1}{C^2}\frac{\partial^2 B_y}{\partial t^2} + \frac{1}{C}\frac{\partial^2 A_z}{\partial t \partial x} + \frac{m_g^2 C^2}{\hbar^2} B_y = \alpha A_y. \tag{2.10}$$

For $u = 3$ Eq. (2.5) reads

$$\frac{1}{C}\frac{\partial^2 A_y}{\partial t \partial x} - \frac{\partial^2 B_z}{\partial x^2} - \frac{1}{C}\frac{\partial^2 A_y}{\partial t \partial x} + \frac{1}{C^2}\frac{\partial^2 B_z}{\partial t^2} + \frac{m_g^2 C^2 B_z}{\hbar^2} = \alpha A_z. \tag{2.11}$$

We now consider the following case for Eq. (2.8), Eq. (2.9), Eq. (2.10) and Eq. (2.11).

Case I

For a plane wave with zero mixing between the fields ($\alpha = 0$), $A_z = B_y = 0$, we have

$$\begin{aligned} A_y &= A_0 e^{i(k_1 x - \omega_1 t)}, \\ B_z &= B_0 e^{i(k_2 x - \omega_2 t)}, \end{aligned} \tag{2.12}$$

from Eq. (2.8) and Eq. (2.11)

$$\begin{aligned} \frac{\omega_1^2}{C^2} &= k_1^2 + \frac{m_e^2 C^2}{\hbar^2}, \\ \frac{\omega_2^2}{C^2} &= k_2^2 + \frac{m_g^2 C^2}{\hbar^2}. \end{aligned} \tag{2.13}$$

Here A_y and B_z propagate with different frequencies and wavelengths related by Eq. (2.13), though the potentials are monochromatic, from Eq. (2.7) the electric and magnetic fields $\overline{E}_y$, $\overline{B}_z$ are mixed states of two different frequencies and wavelengths. Thus plane waves with a slight frequency splitting given by Eq. (2.13) would be a signal for a two potential theory.

Case II

For non-polarized wave again from Eq. (2.8), Eq. (2.9), Eq. (2.10), Eq. (2.11) we would have ($\alpha = 0$)

$$\begin{aligned} A_y &= A_0 e^{i(k_1 x - \omega_1 t)}, \\ A_z &= \overline{A}_0 e^{i(k_1 x - \omega_1 t)}, \\ B_y &= B_0 e^{i(k_2 x - \omega_2 t)}, \\ B_z &= \overline{B}_0 e^{i(k_2 x - \omega_2 t)}, \end{aligned} \tag{2.14}$$

with the frequencies ω_1, ω_2 relating to k_1, k_2 by Eq. (2.13). The electric and magnetic fields given by Eq. (2.7) would again be a mixture of two different frequencies and wavelengths.

Case III

If $\alpha \neq 0$ (non zero mixing between A_μ, B_μ) we have upon substitution of

$$\begin{aligned} A_y &= A_0 e^{i(kx - \omega t)}, \\ A_z &= \overline{A}_0 e^{i(kx - \omega t)}, \\ B_y &= B_0 e^{i(kx - \omega t)}, \\ B_z &= \overline{B}_0 e^{i(kx - \omega t)} \end{aligned} \tag{2.15}$$

into Eq. (2.8), Eq. (2.9), Eq. (2.10) and Eq. (2.11)

$$\begin{aligned} A_0(k^2) - A_0\left(\frac{\omega^2}{C^2}\right) + \frac{m_e^2 C^2}{\hbar^2} A_0 &= -\alpha B_0, \\ \overline{A}_0(k^2) - \overline{A}_0\left(\frac{\omega^2}{C^2}\right) + \frac{m_e^2 C^2}{\hbar^2} \overline{A}_0 &= -\alpha \overline{B}_0, \\ B_0(k^2) - B_0\left(\frac{\omega^2}{C^2}\right) + \frac{m_g^2 C^2}{\hbar^2} B_0 &= +\alpha A_0, \\ \overline{B}_0(k^2) - \overline{B}_0\left(\frac{\omega^2}{C^2}\right) + \frac{m_g^2 C^2}{\hbar^2} \overline{B}_0 &= +\alpha \overline{A}_0. \end{aligned} \tag{2.16}$$

For small α the equations in Eq. (2.16) give for a consistent solution

$$\omega_+^2 \simeq k^2 C^2 + \frac{m_e^2 C^4}{\hbar^2} - \frac{\alpha^2 C^4}{\left(\frac{m_e^2 C^4}{\hbar^2} - \frac{m_g^2 C^4}{\hbar^2}\right)}, \qquad \omega_-^2 \simeq k^2 C^2 + \frac{m_g^2 C^4}{\hbar^2} + \frac{\alpha^2 C^4}{\left(\frac{m_e^2 C^4}{\hbar^2} - \frac{m_g^2 C^4}{\hbar^2}\right)}. \tag{2.17}$$

The two dispersion relations in Eq. (2.17) would go into Eq. (2.13) when A_z, B_y alone are present or A_y and B_z alone are present even in the presence of non-zero coupling. We see from the above analysis that the coupling between the two potentials can generate unpolarized waves which produce two monochromatic branches (ω_+, ω_-). The fields need not be a mixture of two frequencies although they could contain either of the two dispersive components in Eq. (2.17). The difference between the case of no-mixing between the fields ($\alpha = 0$) and mixing ($\alpha \neq 0$) is that with no mixing as in Case I and Case II both frequencies show up in the electric and magnetic field components while with mixing only one component need be present for unpolarized waves.

3. Conclusion

The analysis above has provided us with different signatures to look for in a cosmological setting, if $m_e \simeq 10^{-48}$ grams [9] we find that

$$\frac{m_e C}{\hbar^2} \simeq 3 \times 10^{-11} \text{ cm}^{-1}$$

and

$$\frac{m_e^2 C^4}{\hbar^2} \simeq 1.$$

We see from Eq. (2.17) that $\Delta\omega^2 \simeq 1 \text{ s}^{-2}$ which even for microwaves is an extremely small frequency shift. The way to look for the shift is to look for repetitive [12] signals of cosmological origin, for instance if the wave propagates over a distance of $10^6 P_c \simeq 10^{24}$ cm we might find a time delay between signals of ω_+, ω_- calculated as follows (neglecting α in Eq.(2.17))

$$t_+ = \frac{10^{24}}{V_+} = \frac{10^{24}}{C\sqrt{1 + \frac{m_g^2 C^2}{\hbar^2 k^2}}} = \frac{10^{24}}{C}\left(1 - \frac{10^{-21}}{2}\right),$$

$$t_- = \frac{10^{24}}{V_-} = \frac{10^{24}}{C\sqrt{1 + \frac{m_g^2 C^2}{\hbar^2 k^2}}} = \frac{10^{24}}{C}\left(1 - \frac{10^{-22}}{2}\right),$$

$$\Delta t = t_- - t_+ = \simeq \frac{10^{24}}{C}\left(\frac{10^{-21} - 10^{-22}}{2}\right) \simeq \frac{9}{2C} \times 10^2 \text{ s} \simeq 1.5 \times 10^{-8} \text{ s}.$$

Here we have assumed $k \approx 1$ (microwaves) and $m_g \simeq \frac{1}{\sqrt{10}} m_e$.

If we include the mixing term in Eq. (2.17) it would modify the calculation of t_+, t_-. If we increase the cosmological length scale we increase Δt. Thus any distinctive repetitive signals with very short time intervals between them might be signatures of the two potential theory. If such signals were found they would also

provide us with means to set limits on the two photon masses (m_e, m_g) and the mixing parameter α.

Two final points also have relevance, if there is evidence for a second potential, it would be interesting to ask how it would effect Aharonov–Bohm type experiments for electric and magnetically charged particles [13]. Certainly, the Lagrangian theory of particles with both potentials present would have to be constructed in order to ascertain the proper place of two potentials in a quantum formalism. Lastly, Field et al [14] have studied the rotation of the plane polarization of polarized light coming from cosmological sources when the Lagrangian of electrodynamics breaks both parity and Lorentz invariance. Within the context of the two potential theory here discussed, it would be of interest to ask how the parity violating term in Eq. (2.2) would effect the rotation of the plane of polarization of polarized light.

Acknowledgement

I'd like to thank the Physics Departments at Williams College and Harvard University for the use of their facilities.

References

1. D. G. Galdi, Comments on Nucl. Particle Physics *XIX*, (No. 3). 137, 1989.
2. R. Holdom, Phys. Lett. *213B*, 365, 1988.
3. R. Prasad and D. C. Joshi, Indian J. of Pure and Applied Phys., *28*, 31, 1990.
4. P. A. M. Dirac, Proc. Roy. Soc. A*133*, 60, 1931.
5. J. Schwinger, Phys. Rev., *144*, 1087, 1966.
6. E. Witten, Phys. Lett., *B86*, 287, 1979.
7. W. Fischler and J. Preskill, Phys. Lett., *B125*, 165, 1983.
8. C. Cabibbo and E. Ferrari, Il Nuovo Cimento, *23*, 1147, 1962.
9. G. Callegari, P. Fortini and D. Tartari, Acta Phys. Hung. *67*, 359, 1990.
10. P. Vinciarelli, Proc. of 1976 Int. School of Subnuclear Physics, Erice, Plenum Press, NY, 1978.
11. M. K. Prasad and C. M. Sommerfield, Phys. Rev. Lett., *35*, 760, 1975.
12. C. Wolf, Phys. Lett., *A145*, 413, 1990.
13. Y. Aharonov and D. Bohm, Phys. Rev., *115*, 485, 1959.
14. S. M. Carroll, G. B. Field and R. Jackiw, Phys. Rev., *D41*, 1231, 1990.

Acta Physica Hungarica 73 (2-4), pp. 277-289 (1993)

A VARIATIONAL APPROACH IN MAGNETOFLUID DYNAMICS

I. MERCHES*

Physics Department, University of Miami
Coral Gables, Florida 33124, USA

(Received 31 August 1993)

The definition of the electromagnetic field in terms of Hertz's potential makes it possible to give a variational formulation in the dynamics of ideal magnetofluids, both in non-relativistic and relativistic representations. The theory is applied in two cases: (i) Using Noether's theorem, the fundamental equations of conservation for our model of magnetofluid are obtained. (ii) By means of the four-dimensional generalization of Hertz's vector, a relativistically-covariant formulation of a constrained minimum energy problem in the case of force-free plasma configurations is given.

1. Introduction

The study of basic phenomena governing the behaviour of ideal megnetofluids by means of the variational formalism has been intensively performed soon after the moment when MHD became an independent field of research. The earliest papers (e.g. [1]–[5]) dealing with the variational derivation of fundamental equations of magnetofluid dynamics showed that the variational formalism is a very useful tool of investigation. Later, Dougherty [6], [7] extended this formalism in relativistic MHD, while Taylor [8], [9], Rund et al [10], and Wells [11], [12], [13] studied the minimum energy solutions for magnetofluids, in connection with their stability.

All aforementioned papers have a common point: the electromagnetic field $\mathbf{E}$, $\mathbf{B}$ is defined in terms of the usual set of potentials $\mathbf{A}$, ϕ, chosen as variational parameters. As we showed, the description of the electromagnetic field in terms of a special set of antipotentials $\mathbf{M}$, ψ makes it possible to give a variational formulation in both non-relativistic [14] and relativistic [15], [16] magnetofluid dynamics.

The purpose of the present paper is threefold: (i) To give a variational principle for ideal, non-relativistic magnetofluids, by means of Hertz's vector $\mathbf{Z}$. (ii) To extend this formalism, and give a relativistically-covariant formulation of the problem. (iii) To apply variational technique in two different problems: the cold plasma fundamental equations of conservation, and the stability of some force-free plasma configurations.

*On leave of absence from the Department of Theoretical Physics, AL. I. Cuza University, 6600 Iasi, Romania.

2. Preliminary

The *Hertz vector (potential)*, also called *polarization potential* [17], shows to be a useful instrument in electrodynamics, especially in the study of wave propagation and multipole radiation. It is a "superpotential", i.e. a potential for the usual potentials $\mathbf{A}$ and ϕ. To construct the Hertz vector, one starts from the equation of continuity

$$\rho^e_{,t} + j_{\alpha,\alpha} = 0. \tag{1}$$

Here ρ^e and $\mathbf{j}$ are the electric charge and current densities, respectively, the comma stands for partial derivative, while the Greek indices run from 1 to 3. In this formula and throughout the paper the Einstein's convention summation is used. Taking the Fourier transforms of ρ and $\mathbf{j}$

$$\rho^e(\mathbf{r},t) = (2\pi)^{-\frac{1}{2}} \int_{-\infty}^{+\infty} \rho^e(\mathbf{r},\omega) e^{i\omega t} d\omega,$$

$$\mathbf{j}(\mathbf{r},t) = (2\pi)^{-\frac{1}{2}} \int_{-\infty}^{+\infty} \mathbf{j}(\mathbf{r},\omega) e^{i\omega t} d\omega,$$

it follows from (1)

$$i\omega\rho^e(\mathbf{r},\omega) + \nabla\mathbf{j}(\mathbf{r},\omega) = 0. \tag{2}$$

The number of independent sources ρ^e, j_α can be reduced by one by introducing the vector function [17]

$$\mathbf{S}(\mathbf{r},t) = (2\pi)^{-\frac{1}{2}} \int_{-\infty}^{+\infty} \frac{1}{i\omega}\mathbf{j}(\mathbf{r},\omega) e^{i\omega t} d\omega, \tag{3}$$

which, in view of (1), yields

$$S_{\alpha,\alpha} = -\rho^e(\mathbf{r},t); \quad S_{\alpha,t} = j_\alpha(\mathbf{r},t). \tag{4a,b}$$

If the electromagnetic potentials are chosen as

$$A_\alpha = \epsilon_0\mu_0 Z_{\alpha,t}; \quad \phi = -Z_{\alpha,\alpha}, \tag{5a,b}$$

the Hertz vector $\mathbf{Z}(\mathbf{r},t)$ is then found as solution of the inhomogeneous wave equation

$$\Delta\mathbf{Z} - \epsilon_0\mu_0 \frac{\partial^2\mathbf{Z}}{\partial t^2} = -\frac{1}{\epsilon_0}\mathbf{S}. \tag{6}$$

Here and hereafter it is assumed that $\epsilon \simeq \epsilon_0$; $\mu \simeq \mu_0$. It is easy to show that (5a,b) satisfy the *Lorentz gauge condition*

$$A_{\alpha,\alpha} + \epsilon_0\mu_0\phi_{,t} = 0. \tag{7}$$

The electric field strength **E** and the magnetic induction **B**, in terms of **Z**, are then given by the relations:

$$E_\alpha = Z_{\beta,\beta\alpha} - \epsilon_0\mu_0 Z_{\alpha,tt}, \tag{8}$$

$$B_\alpha = \epsilon_0\mu_0\epsilon_{\alpha\beta\gamma}Z_{\gamma,\beta t}. \tag{9}$$

The importance of this representation is that the number of scalar functions defining the electromagnetic field reduces to three, $Z_\alpha(\alpha = 1, 2, 3)$, which is most useful, as we shall prove in the following.

3. A non-relativistic variational principle

Let our physical model be a charged, inviscid, compressible, one-component magnetofluid, undergoing isentropic motion in external electromagnetic field **E**, **B**. A suitable Lagrangian density

$$\mathcal{L} = \frac{1}{2}\epsilon_0 E_\gamma E_\gamma - \frac{1}{2\mu_0}B_\gamma B_\gamma + \frac{1}{2}\rho v_\gamma v_\gamma - \rho\epsilon + \rho(a_{,t} + v_\gamma a_{,\gamma})$$
$$- b\rho(s_{,t} + v_\gamma s_{,\gamma}) + \frac{e}{m}\rho(\epsilon_0\mu_0 v_\gamma Z_{\gamma,t} + Z_{\gamma,\gamma}). \tag{10}$$

Here s and ϵ are entropy and internal energy per unit mass, respectively, ρ the mass density, while $a(\mathbf{r}, t)$ and $b(\mathbf{r}, t)$ are two Lagrangian multipliers [19]. We also assume that the particle number density, n, is equal to the charge carrier number density: $\rho^e = en$, $\rho = mn$. The last term in (10) gives the interaction between hydrodynamics and electromagnetic fields.

If in the Euler–Lagrange equations

$$\frac{\partial\mathcal{L}}{\partial\varphi^{(s)}} - \frac{\partial}{\partial x_\alpha}\left(\frac{\partial\mathcal{L}}{\partial\varphi^{(s)}_{,a}}\right) - \frac{\partial}{\partial t}\left(\frac{\partial\mathcal{L}}{\partial\varphi^{(s)}_{,t}}\right) = 0 \tag{11}$$

we take as independent variational parameters $\varphi^{(s)}$: $Z_{\beta,\beta}$; $Z_{\beta,t}$; s; v_β, ρ, and use (8)–(10), we obtain:

$$(z_{\beta,\beta}) \qquad \epsilon_0 E_{\alpha,\alpha} - \rho^e = 0, \tag{12}$$

$$(Z_{\beta,t}) \qquad \mu_0^{-1}\varepsilon_{\alpha\beta\gamma}B_{\gamma,\beta} - \rho^e v_\alpha - \epsilon_0 E_{\alpha,t} = 0, \tag{13}$$

$$(s) \qquad b_{,t} + v_\alpha b_{\alpha,t} - T = 0, \tag{14}$$

$$(a) \qquad \rho_{,t} + (\rho v_\alpha)_{,\alpha} = 0, \tag{15}$$

$$v(\alpha) \qquad v_\alpha + a_{,\alpha} - bs_{,\alpha} + \epsilon_0\mu_0\frac{e}{m}Z_{\alpha,t} = 0, \tag{16}$$

$$(\rho) \qquad \frac{1}{2}v_\alpha v_\alpha - \frac{p}{\rho} + \alpha_{,t} + \frac{e}{m}(\epsilon_0\mu_0 v_\alpha Z_{\alpha,t} + Z_{\alpha,\alpha}) = 0, \tag{17}$$

i.e. Maxwell's source equations, the equation of continuity, a generalized Clebsch transformation, and a Bernoulli-type equation. In deriving equations (12)–(17) we have also used the fundamental thermodynamic equation for non-dissipating fluids (reversible processes):

$$Tds = d\epsilon - \rho^{-2} p \, d\rho. \tag{18}$$

Before going furher, we want to make some remarks on the constraints used to construct Lagrangian density (10). From the magnetohydrodynamic point of view, there are motions consistent with the dynamical equations which are not included in this principle. Indeed, if s is homogeneous in space, and $\mathbf{Z}$ does not explicitly depend on time, Eq. (16) leads to $\mathbf{v} = -\text{grad}a$, meaning that in this case the motion is restricted to irrotational flows. To remove this difficulty, Lin [20] introduced an additional vector constraint expressing the conservation of the identity of particles, in the form $\frac{d\mathbf{X}}{dt} = 0$. Later, Selinger and Whitham [21] showed that a single component of $\mathbf{X}$, i.e. a single equation of this type is enough to solve the problem. The specified component is one of the Lagrangian coordinates of the particle, even if the description of the motion is Eulerian. We wanted to emphasize this point in order to note that our description is not most general.

Next, we shall derive the equation of motion. To do this, we eliminate the Lagrangian multipliers a, b from (14)–(17). Multiplying (16) by v_α and introducing the result in (17), we obtain:

$$-\frac{1}{2} v_\alpha v_\alpha - \epsilon - \frac{p}{\rho} + a_{,t} + \frac{e}{m} Z_{\alpha,\alpha} + b v_{,\alpha} s_{,\alpha} = 0. \tag{19}$$

Taking the gradient of this equation and writing its x_α-component, we still have:

$$-v_\beta v_{\beta,\alpha} - \epsilon_{,\alpha} + \frac{1}{\rho} p_{,\alpha} + \frac{p}{\rho^2} \rho_{,\alpha} + a_{,\alpha t} + \frac{e}{m} Z_{\beta,\beta\alpha} + (b v_\beta s_{,\beta})_{,\alpha} = 0. \tag{20}$$

But

$$a_{,\alpha t} = -v_{\alpha,t} + (T - b_\beta b_\beta) s_{,\alpha} - b(v_\beta s_{,\beta})_{,\alpha} - \epsilon_0 \mu_0 \frac{e}{m} Z_{\alpha,tt},$$

and consequently:

$$-v_{\alpha,t} - \frac{1}{\rho} p_{,\alpha} + \frac{e}{m} E_\alpha - v_\beta v_{\beta,\alpha} - v_\beta b_{,\beta} s_{,\alpha}$$
$$-b(v_\beta s_{,\beta})_{,\alpha} + (b v_\beta s_{,\beta})_{,\alpha} + (T s_\alpha - \epsilon_{,\alpha} + \frac{p}{\rho^2} \rho_{,\alpha}) = 0. \tag{21}$$

In view of (18), the last bracket vanishes, while the sum of the last four terms gives:

$$\Gamma_\alpha = -b_\beta v_{\alpha,\beta} + \varepsilon_{\alpha\beta\gamma} v_\beta B_\gamma, \tag{22}$$

and Eq. (21) takes the final form

$$\frac{dv_\alpha}{dt} = -\frac{1}{\rho} p_{,\alpha} + \frac{e}{m} (E_\alpha + \varepsilon_{\alpha\beta\gamma} v_\beta B_\gamma),$$

which is the desired equation of motion.

4. A relativistically-covariant extension of the variational principle

In the relativistic approach to our formalism, we shall use so called "Galilean co-ordinates":

$$x^1 = x,\ x^2 = y,\ x^3 = z,\ x^4 = ct;\ g_{\alpha\beta} = \delta_{\alpha\beta},\ g_{44} = -1. \tag{23}$$

If the velocity four-vector u_i is defined by

$$u^\alpha = u_\alpha = \frac{\gamma}{c} v_\alpha; \quad u^4 = -u_4 = \gamma, \quad \gamma = \left(1 - \frac{v^2}{c^2}\right)^{-\frac{1}{2}}, \tag{24}$$

then we have:

$$u_i u^i = -1. \tag{25}$$

Here and hereafter, Latin indices run from 1 to 4.

First, we must transpose (5a,b) in Minkowski universe, i.e. we have to give a relativistically-covariant generalization of the Hertz potential. As one can see, only derivatives of $\mathbf{Z}$ appear in (5a,b). On the other hand, there is no time-component, so as to be associated with the space-components Z_α. Consequently, if we define the Hertz four-vector $Z^i(\mathbf{Z}, 0)$, then the four-potential can be written as:

$$A^i = \Phi^{ik}{}_{,k}, . \tag{26}$$

Here Φ_{ik} is an antisymmetric tensor, given by

$$\Phi^{ik} = \frac{1}{c}(Z^i u^k - Z^k u^i). \tag{27}$$

In the rest frame of reference ($u_\alpha = 0$, $u^4 = 1$), this formalism yields

$$A_\alpha = \Phi^{\alpha 4}{}_{,4} = \epsilon_0 \mu_0 Z_{\alpha,t}; \quad A^4 = \frac{1}{c}\phi = -\frac{1}{c} Z_{\alpha,\alpha},$$

in complete agreement with (5a,b). To make our result consistent with *any* inertial frame, we must consider the supplementary condition $\Phi_{\alpha\beta} = 0$. This condition is not at all artificial, but it follows from the definition of $\mathbf{Z}$: the second-order four-tensor Φ_{ik} has three independent components $\Phi_{\alpha 4}$.

To prove the consistency of this formalism, let us define the electromagnetic field tensor F_{ik} in terms of Φ_{ik}:

$$F^{jm} = \Phi^{mkj}{}_{,k} - \Phi^{jkm}{}_{,k} = g^{js}\Phi^{mk}{}_{,sk} - g^{ms}\Phi^{jk}{}_{,sk}. \tag{28}$$

As easy to verify, this leads to:

$$F^{\alpha\beta} = F_{\alpha\beta} = \epsilon_0 \mu_0 \varepsilon_{\alpha\beta\gamma} Z_{\gamma,\beta t} = \varepsilon_{\alpha\beta\gamma} B_\gamma,$$

$$F^{\alpha 4} = -F_{\alpha 4} = -\frac{1}{c} Z_{\beta,\beta\alpha} - \epsilon_0 m u_0 \frac{1}{c} Z_{\alpha,tt} = -\frac{1}{c} E_\alpha, \tag{29}$$

and similar formulas for the dual tensor $\hat{F}^{ik} = \frac{1}{2!}\epsilon^{iklmn} F_{lm}$:

$$\hat{F}_{\alpha\beta} = \frac{1}{c}\varepsilon_{\alpha\beta\gamma} E_\gamma; \qquad \hat{F}^{\alpha 4} = B_\alpha. \tag{30}$$

Next step is now to write the relativistically-covariant Lagrangian density. We shall write it as a combination of Lagrangian densities given by Halbwachs [22], Landau and Lifshitz [23], Herivel [19] and ourselves [15], in the form:

$$\mathcal{L} = -\frac{1}{4\mu_0}(\Phi^{ml}{}_{,l}^{\,j} - \Phi^{jb}{}_{,l}^{\,m})(\Phi_{ms}{}_{,j}^{\,s} - \Phi_{js}{}_{,m}^{\,s}) + ecn_0 u_j \Phi^{jk}{}_{,k}$$
$$- n_0 m_0(\epsilon + c^2) - \frac{1}{2}\lambda(u_j u^j + 1) + n_0 u^j a_{,j} - b n_0 u^j s_{,j}. \tag{31}$$

Here $n_0 m_0 = \rho_0$ and $e n_0 = \rho_0^e$ are the rest-frame mass and charge densities, respectively, while $\lambda(x^j)$, $a(x^j)$, and $b(x^j)$ are three Lagrangian multipliers. In the derivation (31), the following conditions of constraint have been used:

$$(n_0 u^j)_{,j} = 0, \tag{32}$$

$$u^j s_{,j} = 0, \tag{33}$$

i.e. equation of continuity and equation of conservation of entropy.

The Euler–Lagrange equations

$$\frac{\partial \mathcal{L}}{\partial \rho^{(s)}} - \frac{\partial}{\partial x^k}\left(\frac{\partial \mathcal{L}}{\partial \varphi_{,k}^{(s)}}\right) = 0 \qquad (s = \overline{1,l};\ k = \overline{1,4}) \tag{34}$$

give then:

$$(\Phi_{is}{}_{,k}^{\,s}) \qquad (\Phi^{km\,i}{}_{,m} - \Phi^{im\,k}{}_{,m})_{,k} = \mu_0 j^i, \tag{35}$$

$$(u^j) \qquad e n_0 c \Phi_{jk,}{}^{k} - \lambda u_j + n_0 a_{,j} - b n_0 s_{,j} = 0, \tag{36}$$

$$(n_0) \qquad e c u_j \Phi^{jk}{}_{,k} - m_0(\epsilon + c^2) + u^j a_{,j} - b u^j s_{,j} = 0, \tag{37}$$

$$(a) \qquad (n_0 u^j)_{,j} = 0, \tag{38}$$

$$(b) \qquad u^j s_{,j} = 0, \tag{39}$$

$$(s) \qquad u^j b_{,j} = 0, \tag{40}$$

i.e. Maxwell's source equations, a generalized Clebsch representation, a Bernoulli-type equation, the equation of continuity, and a vortex theorem for a and b. Equations (36) and (37) give $\lambda = -\rho_0(\epsilon + c^2)$, and Clebsch representation (36) takes the final form:

$$e c \Phi_{jk,}{}^{k} + m + o(\epsilon + c^2) u_j + a_{,j} - b s_{,j} = 0. \tag{41}$$

The equation of motion follows from (41) , by the help of (18), after some derivative and index manipulation:

$$\rho_0 \frac{d}{ds}[(\epsilon + c^2)u_i] = c(\Phi_{ks}{}^{s}{}_{,i} - \Phi_{is}{}^{s}{}_{,k})j^k - \rho_0 \frac{\partial \epsilon}{\partial x^i}. \tag{42}$$

Since ϵ is senseless in the case of one-particle system, in this particular situation Eq. (42) yields:

$$m_0 \frac{du^i}{ds} = e(\Phi_{ks}{}^{s}{}_{,i} - \Phi_{is}{}^{s}{}_{,k})u^k, \tag{43}$$

as expected.

5. Applications

(1). Using the representation of electromagnetic field in terms of Hertz's potential $\mathbf{Z}$, let us now derive the equations of transformation and conservation of the fundamental physical quantities, associated with our model: energy, momentum, and angular momentum. Following Noether's theorem, with each infinitesimal symmetry transformation one can associate a conservation differential equation. The general form of this equation is [4]

$$\frac{\partial}{\partial t}\int_V \gamma \, d\tau = -\oint_S \mathbf{G}.d\mathbf{S}, \tag{44}$$

with

$$\gamma = \left[\mathcal{L} - \frac{\partial \mathcal{L}}{\partial \varphi^{(s)}}\varphi^{(s)}_{,t}\right]\delta t - \frac{\partial \mathcal{L}}{\partial \varphi^{(s)}_{,t}}(\delta \mathbf{r}\cdot\nabla)\varphi^{(s)} + \frac{\partial \mathcal{L}}{\partial \varphi^{(s)}_{,t}}\delta\varphi^{(s)} + \delta\Omega_t, \tag{45}$$

$$\mathbf{G} = -\frac{\partial \mathcal{L}}{\partial(\nabla\varphi^{(s)})}\varphi^{(s)}_{,t}\delta t + \left[\mathcal{L}\delta\mathbf{r} - \frac{\partial \mathcal{L}}{\partial(\nabla\varphi^{(s)})}(\delta\mathbf{r}\cdot\nabla)\varphi^{(s)}\right] + \frac{\partial \mathcal{L}}{\partial(\nabla\varphi^{(s)})}\delta\varphi^{(s)} + \delta\vec{\Omega}. \tag{46}$$

We consider the following space-time infinitesimal symmetry transformations [24]:

(i) The Lagrangian density (10) is invariant with respect to the infinitesimal displacement of the time origin

$$r \to t' = t + \delta t; \quad \delta\mathbf{r} = 0; \quad \delta\varphi^{(s)} = 0. \tag{47}$$

Hence, in view of (10)–(17), after some vector algebra we obtain:

$$\gamma(t) = \left[-\frac{1}{2}\epsilon_0 E_\alpha E_\alpha - \frac{1}{2\mu_0}B_\alpha B_\alpha - \frac{1}{2}\rho v_\alpha v_\alpha - \rho\epsilon + \epsilon_0(E_\beta Z_{\alpha,\alpha})_{,\beta}\right]\delta t,$$

$$G^{(t)}_\alpha = \left[-\frac{1}{\mu_0}(\mathbf{E}\times\mathbf{B})_\alpha - \rho v_\alpha\left(\frac{1}{2}|\mathbf{v}|^2 + w\right) + \frac{1}{\mu_0}(\varepsilon_{\beta\alpha\gamma}B_\beta Z_{\theta,\theta})_{,\gamma} - \epsilon_0(E_\alpha Z_{\beta,\beta})_{,t}\right]\delta t.$$

Here $w = \epsilon + \frac{p}{\rho}$ is the specific enthalpy. Introducing these results into (44) and leaving out the constant δt, we arrive at

$$\frac{\partial}{\partial t}\int_V \left(\frac{1}{2}\rho|\mathbf{v}|^2 + \rho\epsilon + \frac{1}{2}\epsilon_0|\mathbf{E}|^2 + \frac{1}{2\mu_0}|\mathbf{B}|^2 d\right) d\tau$$

$$= -\oint_S \left[\rho\mathbf{v}\left(\frac{1}{2}|\mathbf{v}|^2 + w\right) + \frac{1}{\mu_0}(\mathbf{e}\times\mathbf{B})\right].d\mathbf{S}, \tag{48}$$

which is the energy conservation equation.

(ii) The Lagrangian density (10) is invariant with respect to the infinitesimal displacement of the origin of the reference frame

$$\mathbf{r} \to \mathbf{r}' = \mathbf{r} + \delta\mathbf{r}; \quad \delta t = 0; \quad \delta\varphi^{(s)} = 0. \tag{49}$$

Here $\delta\mathbf{r}$ is a constant vector, giving the direction and magnitude of translation. We find:

$$\gamma^{(r)} = [\epsilon_0(\mathbf{E}\times\mathbf{B})_{,\alpha} + \rho v_\alpha + \epsilon_0^2\mu_0(E_\beta Z_{\alpha,t})_{,\beta}\delta]x_\alpha,$$

$$G_\beta^{(r)} = [p\delta_{\alpha\beta} + \rho v_\alpha v_\beta + \left(\frac{1}{2}\epsilon_0|\mathbf{E}|^2 + \frac{1}{2\mu_0}|\mathbf{B}|^2\right)\delta_{\alpha\beta} - \epsilon_0 E_\alpha E_\beta - \frac{1}{\mu_0}B_\alpha B_\beta$$

$$-\epsilon_0^2\mu_0(E_\beta Z_{\alpha,t})_{,t} + \epsilon_0(\varepsilon_{\beta\gamma\theta}B_\theta Z_{\alpha,t})_{,\gamma}]\delta x_\alpha,$$

leading to the momentum conservation equation

$$\frac{\partial}{\partial t}\int_V [\rho v_\alpha + \epsilon_0(\mathbf{E}\times\mathbf{B})_\alpha]d\tau$$

$$= -\oint_S [\rho v_\alpha v_\beta + p\delta_{\alpha\beta} + \left(\frac{1}{2}\epsilon_0|\mathbf{E}|^2 + \frac{1}{2\mu_0}|\mathbf{B}|^2\right)\delta_{\alpha\beta} - \epsilon_0 E_\alpha E_\beta - \frac{1}{\mu_0}B_\alpha B_\beta]dS_\beta. \tag{50}$$

(iii) The Lagrangian density (10) is invariant with respect to an infinitesimal rotation of the axes, i.e.

$$\mathbf{r} \to \mathbf{r}' = \mathbf{r} + \mathbf{r}\times\delta\vec{\theta}; \quad \delta t = 0,$$

$$\mathbf{E}' = \mathbf{E} + \mathbf{E}\times\delta\vec{\theta}; \quad \mathbf{B}' = \mathbf{B} + \mathbf{B}\times\delta\vec{\theta},$$

$$\delta Z_{\alpha,t} = \varepsilon_{\alpha\beta\gamma}x_\beta\delta\theta_\gamma; \quad \delta Z_{\alpha,\alpha} = 0,$$

$$\delta v_\alpha = -\frac{e}{m}\epsilon_0\mu_0\delta Z_{\alpha,t},$$

leading to the equation of conservation of angular momentum:

$$\frac{\partial}{\partial t}\int_V \epsilon_{\alpha\beta\gamma}P_\alpha x_\beta d\tau = -\oint_S \varepsilon_{\alpha\beta\gamma}\pi_{\alpha\theta}x_\beta dS_\theta. \tag{51}$$

Here

$$p_\alpha = \rho v_\alpha + \epsilon_0 (\mathbf{E} \times \mathbf{B})_\alpha,$$

$$\pi_{\alpha\theta} = p\delta_{\alpha\theta} + \rho v_\alpha v_\theta + \left(\frac{1}{2}\epsilon_0 |\mathbf{E}|^2 + \frac{1}{2\mu_0}|\mathbf{B}|^2\right)\delta_{\alpha\theta} - \epsilon_0 E_\alpha E_\theta - \frac{1}{\mu_0} B_\alpha B_\theta.$$

To obtain these results, we used some vector and tensor calculus. The intermediate calculations are long, but not very interesting, and we leave to the reader a thorough proof of these equations.

(2). The study of plasma stability is closely related to the constraints on the system, i.e. the states of stable equilibrium *must* be consistent with the integrals of the equations of motion. In the earliest research on force-free magnetic fields and hydromagnetic stability, the nature of the stable solution was studied. It was shown (Chandrasekhar et al [25], Woltjer [26], [27], [28], Bernstein et al [29]) that, if the boundary conditions and the gauge are suitably chosen, then

$$I_1 = \int_V \mathbf{A}.\mathbf{B} d\tau; \quad I_2 = \int_V \mathbf{v}.\mathbf{B} d\tau \tag{52a,b}$$

are two integrals of motion. Here $\mathbf{v}$ is the magnetofluid velocity, and $\mathbf{A}$ the vector potential.

The research of constraint integrals (52a,b) was resumed a few years later by Calkin [4], Moffat [30], Wells [11], [12], [31], and closer to nowadays by Rund et al [10], in connection with the problem of the dynamic stability of closed plasma configurations. The constancy of (1a) was later investigated by Taylor, and again shown to be related to the generation of magnetic fields in toroidal plasma [8] and magnetic force-free equilibria [9]. The boundary conditions and the potential gauge which assure the time-constancy of the integrals (1a,b) may be stronger [28] or weaker [10], [30].

The purpose of this application is to give a relativistically-covariant formulation of a constrained minimum energy problem, namely the problem of minimizing the total energy of closed MHD system, subject to the constraints (1a,b), by means of the four-dimensional generalization of Hertz's vector. Using the theory of multiple integral isoperimetric problem [32], it was shown [10] that a necessary condition for an extreme value of the energy integral

$$J = \int_V \left[\frac{1}{2\mu_0}|\mathbf{B}|^2 + \frac{1}{2}\rho|\mathbf{v}|^2 + \nu U(\nu)\right] d\tau, \tag{53}$$

subject to constraints (1a,b), is:

$$E_Y(L) + \lambda_1 E_Y(Q_1) + \lambda_2 E_Y(Q_2) = 0. \tag{54}$$

In the last two formulas ν is the particle density, $Q_1 = \mathbf{a}.\mathbf{B}$, $Q_2 = \mathbf{v}.\mathbf{B}$, Y stands for dependent variables, while λ_1, λ_2 are two Lagrangian multipliers.

To apply this formalism in our case, we first observe that Q_1 and Q_2 may be regarded as the fourth-component of the four-vectors

$$R^m = \frac{1}{2}\varepsilon^{jmkl}(\Phi_{ls}{}^{,s}{}_{,k} - \Phi_{ks}{}^{,s}{}_{,l})\Phi_{ji}{}^{,i}, \tag{55}$$

$$S^m = \frac{1}{2}\varepsilon^{jmkl}(\Phi_{ls}{}^{,s}{}_{,k} - \Phi_{ks}{}^{,s}{}_{,l})u_j. \tag{56}$$

Therefore we have the following system:

$$E_Y + \lambda_m E_Y(R^m) + \mu_m E_Y(S^m) = 0, \tag{57}$$

where λ_m and μ_m are two four-vector Lagrangian multipliers. Assuming $\epsilon \ll c^2$, and using notations $\tilde{a} = \frac{a}{c^2}$; $\tilde{b} = \frac{b}{c^2}$, then performing the calculations in (57), after some tensor algebra and index manipulation we arrive at:

$$\frac{1}{2c}\left(2\lambda_m - \frac{\rho_0^e}{\rho_0}\right)\varepsilon^{jmkl}(\Phi_{ls}{}^{,s}{}_{,k} - \Phi_{ks}{}^{,s}{}_{,l}) + \mu_m\tilde{\omega}^{jm} = 0, \tag{58}$$

$$(\rho_0 u^j)_{,j} = 0, \tag{59}$$

$$[\rho_0 u^j + \frac{1}{2c}\mu_m\varepsilon^{jmkl}(\Phi_{ls}{}^{,s}{}_{,k} - \Phi_{ks}{}^{,s}{}_{,l})]s_{,j} = 0, \tag{60}$$

$$[\rho_0 u^j + \frac{1}{2c}\mu_m\varepsilon^{jmkl}(\Phi_{ls}{}^{,s}{}_{,k} - \Phi_{ks}{}^{,s}{}_{,l})]\tilde{b}_{,j} = 0, \tag{61}$$

where $\tilde{\omega}^{jm} = \frac{1}{2}\varepsilon^{jmkl}(u_{l,k} - u_{k,l})$. In view of (41), we still have:

$$m_0\tilde{\omega}^{jm} + \frac{e}{2c}\varepsilon^{jmkl}(\Phi_{ls}{}^{,s}{}_{,k} - \Phi_{ks}{}^{,s}{}_{,l}) = \tilde{C}_{jm}; \quad C_{jm} = \tilde{b}_j s_m - \tilde{b}, ms_j, \tag{62}$$

and Eq. (58) reads

$$\lambda_m\tilde{F}^{jm} + \mu_m\tilde{\omega}^{jm} + \eta_m\tilde{C}^{jm} = 0; \quad \eta_m = -\frac{\mu_m}{2m_0}. \tag{63}$$

Equation (63) shows that the four-tensors $\tilde{F}^{jm}$, $\tilde{\omega}^{jm}$, $\tilde{C}^{jm}$ are *linearly independent*. To realize the physical significance of this result, let us take $\lambda_m = (0,0,0,\lambda)$; $\mu_m = (0,0,0,\mu)$. Then the system (58)–(61) yields:

$$\begin{gathered}(2\lambda - \frac{e}{m}\mu)B_\alpha + \mu\varepsilon_{\alpha\beta\gamma}u_{\gamma,\beta} = 0,\\ (\rho_0 u_\alpha)_{,\alpha} = 0,\\ (\rho_0 u_\alpha + \mu B_\alpha)s_{,\alpha} = 0,\\ (\rho_0 u_\alpha + \mu B_\alpha)\tilde{b}_{,\alpha} = 0,\end{gathered} \tag{64}$$

which is precisely the conclusion drawn by Rund et al [10]; unless the flow is irrotational, the Euler–Lagrange equations of this isoperimetric problem imply that the four vectors fields $\mathbf{v}$, $\mathbf{B}$, $\nabla \times \mathbf{v}$, $\nabla \times \mathbf{B}$ are *collinear*.

6. Discussion

We first want to make some comments on the generalization of Hertz's potential in Minkowski's space, apart from the results previously obtained in this paper.

(a) It is obvious that the choice of three components of Hertz's vector, instead of the usual electromagnetic potentials, $\mathbf{A}$, ϕ yields a considerable simplification of any problem regarding determination of the electromagnetic field. This advantage becomes more important in case of complex applications.

(b) Since Φ^{ik} is antisymmetric, we have $\Phi^{km}{}_{,km} = 0$, and Eq. (35) simplifies to

$$\Phi^{im\,k}{}_{,mk} = \frac{\partial^2}{\partial x_k \partial x^k}\Phi^{im}{}_{,m} = -\mu_0 j^i, \tag{65}$$

where $\frac{\partial^2}{\partial x_k \partial x^k} = \Delta - \frac{1}{c^2}\frac{\partial}{\partial t^2}$ is the D'Alembert's operator. This is the relativistic form of the wave equation for $\Phi^{im}{}_{,m}$, i.e. for A^i. We conclude that Maxwell's source equations (35), written in terms of Hertz's potential, yield *straightforwardly* to the four-potential wave equation, without any auxiliary condition.

(c) As one knows, the Lorentz gauge condition for the four-potential A^i, which is $A^i_{,i} = 0$, must be *imposed* in order to get the inhomogeneous wave equation $\frac{\partial^2 A^i}{\partial x_k \partial x^k} = -\mu_0 j^i$, while using the Hertz four-vector we have $\Phi^{ik}{}_{,ik} = A^i_{,i} = 0$. In other words, the Lorentz condition is *contained* in the definition of the Hertz potential.

(d) As we showed [15], the electromagnetic field tensor F_{ik} can be written as

$$\tilde{F}_{ik} = M_{ik} + \tilde{P}_{ik}. \tag{66}$$

Here

$$M_{ik} = M_{k,i} - M_{i,k}; \quad M_\alpha = \mu_0 c M_{x^\alpha}, \quad M_4 = -M^4 = -\mu_0 \psi$$

is a four-dimensional curl of antipotential four-vector M_i,

$$\tilde{P}_{ik} = -\mu_0 \varepsilon_{iksm} P^s v^m; \quad P^s = (P^\alpha, 0); \quad v^m = (v^\alpha, 0)$$

is defined to give a four-dimensional generalization of Calkin's 'polarization' vector field $\mathbf{P}$, while the symbol "" stands for dual tensor. With these definitions, Maxwell's source equations take the form:

$$(F^{ik} - P^{ik})_{,k} = 0. \tag{67}$$

Let us now use the definition (28) of F^{ik} in terms of Φ^{ik} in (67). The result is:

$$\frac{\partial^2}{\partial x_k \partial x^k}\Phi^{is}{}_{,s} = -P^{is}{}_{,s}. \tag{68}$$

This shows that *the source of the tensor field Φ^{ik} is the polarization tensor P^{ik}*. In particular, for $i = \alpha$, *a solution* of (68) is $\frac{\partial^2}{\partial x_k \partial x^k}\mathbf{Z} = -\frac{1}{\epsilon_0}\mathbf{P}$, which emphasizes the physical significance of Hertz's vector.

7. Conclusion

The description of the electromagnetic field interacting with a charged fluid in terms of the Hertz potential proves to be useful in variational derivation of the fundamental system equations governing the behaviour of the chosen model. The advantage of the Hertz potential emerges from the fact that it reduces by one the number of field variables, which simplifies the calculation. The relativistically-covariant generalization of this formalism allows us to give a variational principle for ideal magnetofluids and make a straightforward connection with the tensor polarization properties of the medium. To give more motivation of the advantage of this representation, the Hertz vector has been used in the derivation of some fundamental equations of conservation in MHD. This method has been also applied in the study of equilibrium conditions of some force-free plasma configurations. All these results show that the use of Hertz's vector is advantageous not only in many classic problems of electrodynamics, but also in the theory of magnetofluids.

Acknowledgement

The author is indebted to Drs. D. R. Wells, C. Thio and G. Alexandrakis, for assistance and hospitality during his stay at the University of Miami, as a Fulbright scholar.

References

1. S. Katz, Phys. Fluids, *4*, 345, 1961.
2. C. H. Su, Phys. Fluids, *4*, 1376, 1961.
3. T. S. Lundgren, Phys. Fluids, *6*, 898, 1961.
4. M. G. Calkin, Can. J. Phys., *41*, 2241, 1963.
5. P. Penfield, Jr. and H. A. Haus, Phys. Fluids, *9*, 1195, 1966.
6. J. J. Dougherty, J. Plasma Phys., *4*, 761, 1970.
7. J. J. Dougherty, J. Plasma Phys., *11*, 331, 1974.
8. J. B. Taylor, Phys. Rev. Lett., *33*, 1139, 1974.
9. J. B. Taylor, Relaxation of Toroidal Discharges, Third Topical Conference on High-beta Plasmas, Culham Laboratory, 1975.
10. H. Rund, D. R. Wells and L. C. Hawkins, J. Plasma Phys., *20*, 329, 1978.
11. D. R. Wells, J. Plasma Phys., *4*, 645, 1970.
12. D. R. Wells, Pulsed High-beta Plasmas, ed. D. E. Evans, Pergamon Press, Oxford, 1976.
13. D. R. Wells, Laser and Particle Beams, *6*, 539, 1988.
14. I. Merches, Phys. Fluids, *12*, 2225, 1969.
15. I. Merches, J. Plasma Phys., *21*, 511, 1979.
16. I. Merches, J. Plasma Phys., *23*, 259, 1980.
17. R. H. Good, Jr. and T. J. Nelson, Classical Theory of Electric and Magnetic Fields, Academic, New York, 1971.
18. I. Merches, Acta Phys. Hung., *54*, 147, 1983.
19. J. W. Herivel, Proc. Camb. Phil. Soc., *51*, 334, 1955.
20. C. C. Lin, Liquid Helium, Proc. Int. School of Physics, Course XXI, New York, Academic, New York, 1963.
21. R. L. Selinger and G. B. Whitham, Proc. Roy. Soc. A, *305*, 1, 1968.

22. F. Halbwachs, Théorie Relativiste des Fluids a Spin, Gauthier-Villars, Paris, 1960.
23. L. D. Landau and E. M. Lifshitz, The Classical Theory of Fields, (3rd ed.), Pergamon Press, Oxford, 1971.
24. I. Merches and C. Baban, Ann. Sci. Univ. Iasi, 1993 (to be published).
25. S. Chandrasekhar and L. Woltjer, Proc. Nat. Acad. Sci. USA, *44*, 285, 1958.
26. L. Woltjer, Proc. Nat. Acad. Sci. USA, *44*, 489, 1958.
27. L. Woltjer, Proc. Nat. Acad. Sci. USA, *44*, 833, 1958.
28. L. Woltjer, Rev. Mod. Phys., *32*, 914, 1960.
29. I. B. Bernstein, E. A. Frieman, M. D. Kruskal and R. M. Kulsrud, Proc. Roy. Soc. A, *244*, 17, 1958.
30. H. K. Moffat, J. Fluid Mech., *35*, 117, 1969.
31. D. R. Wells and J.. Norwood, J. Plasma Phys., *3*, 21, 1969.
32. H. Rund, Utilitas Math., *1*, 157, 1972.

Acta Physica Hungarica 73 (2-4), pp. 291-310 (1993)

INFLUENCE OF WALL PROPERTIES ON HARTMANN FLOW AND HEAT TRANSFER IN A ROTATING SYSTEM

T. NAGY and Z. DEMENDY

Department of Physics, Miskolc University
3515 Miskolc-Egyetemváros, Hungary

(Received 20 September 1993)

The influence of rotation and physical properties of bounding walls on a generalized one-dimensional Hartmann flow (HF) and heat transfer is investigated. The channel rotates with a constant angular velocity about an axis perpendicular to the walls in a uniform transverse magnetic field. Exact solutions for the velocity, magnetic field, viscous stress, current density, temperature distribution, yield components, net electric current components, mean temperature as well as Nusselt numbers are derived. Effects of relevant parameters such as rotation parameter, Hartmann, Eckert and Prandtl numbers, wall conductivities, wall thicknesses are examined numerically and shown graphically.

1. Introduction

Theoretical study of magnetohydrodynamical (MHD) channel flows is of great interest due to its widespread applications in designing cooling systems with liquid metals, MHD generators, accelerators, pumps and flow meters. Hartmann [1] was the first to investigate the pressure driven flow of an electrically conducting, viscous and incompressible fluid between two infinite, parallel and non-conducting plates in the presence of a uniform transverse magnetic field. The effect of wall conductances has been studied by Chang and Yen [2]. The heat transfer aspect of the problem under different conditions has also been investigated. Alpher [3] was the first to assess the influence of wall properties on the heat transfer. Since he neglected the viscous dissipation and the heat generation within the walls, his analysis was incorrect to account for the wall influence. Yen [4] and Jagadeesan [5] studied the effect of viscous dissipation, Joule heating and unequal wall conductances on the temperature distribution. Snyder [6] extended these works including the heat generation within the walls and solved the model numerically. Javeri [7] developed further these results and investigated the simultaneous influence of viscous dissipation, Joule heating, unequal wall conductances and wall heat fluxes on the temperature field in the HF.

Study of interaction of Coriolis force with electromagnetic forces is important for some geophysical as well as astrophysical problems, therefore modelling of hydromagnetic flows in rotating channels has been vigorously pursued for the last two decades. In these studies, however, the walls have been taken as either non-conducting or perfectly conducting, or a combination of the two. Nanda and

Mohanty [8] considered the HF in a rotating channel with perfectly conducting walls. Datta and Jana [9] discussed the effect of rotation and Hall current on the HF using insulating walls. Jana, Datta and Mazumder [10] studied the MHD Couette flow in a rotating frame of reference when the fixed plate of the channel is perfectly conducting, the moving one is insulating. Raju and Rao [11] investigated this problem taking into account the Hall current but neglecting the induced magnetic field. Seth and Maiti [12] discussed the rotating hydromagnetic Couette flow between non-conducting plates where a biasing external electric field is applied. Unfortunately, for a number of physical situations the idealized wall conditions are inapplicable, particularly when we consider the heat transfer aspects of the problems. For example, the usual assumption of a wall which is a perfect insulator electrically and a perfect conductor thermally, cannot be valid because, according to the Wiedemann–Franz law, the ratio of heat and electric conductivities of metals is proportional to the absolute temperature and the proportionality factor is very small.

The purpose of this paper is to study in detail, under realistic wall conditions, the effect of rotation and external magnetic field on the hydromagnetic fields and heat transfer in a generalized HF. In the model the flow may be driven either by a pressure gradient or by motion of one of the walls. Exact solutions for the velocity, magnetic field, viscous stress, current density, temperature distribution, yield components, net electric current components, mean temperature as well as Nusselt numbers are derived. Effects of important parameters such as rotation parameter, Hartmann, Eckert and Prandtl numbers, wall conductivities, wall thicknesses are examined numerically and displayed in numerous figures.

2. Description of model

We consider a steady flow of an electrically and thermally conducting, viscous and incompressible fluid between two infinite parallel walls of given electrical and thermal conductivity. Let us denote with d, d_1 and d_2 the distance of plates, the thickness of lower and upper bounding walls respectively, as it is shown in Fig. 1. The lower wall rotates with a constant angular velocity Ω about the y-axis perpendicular to the walls. The x- and z-axes are fixed on the lower wall. The upper plate may move with a constant velocity $\mathbf{U} = (U_x, 0, U_z)$ with respect to the Cartesian (non-inertial) system of reference $\mathcal{K}(x, y, z)$. The unit vectors of $\mathcal{K}$ are $\mathbf{i}, \mathbf{j}$ and $\mathbf{k}$. Outside the channel (in vacuum) a uniform magnetic field $\mathbf{H}_o = (0, H_o, 0)$ is applied, but there is no external electric field. We assume all the material properties to be isotropic and constant, the magnetic permeability of plates and fluid is equal to the permeability μ of the vacuum.

The MHD equations governing the problem (balances of momenta and matter, Maxwell's equations and Ohm's law) in the frame of reference $\mathcal{K}(x, y, z)$ can be written in the form

$$\rho(\mathbf{V}\nabla)\mathbf{V} + 2\rho\Omega\mathbf{j} \times \mathbf{V} = -\nabla p^* + \rho\nu\nabla^2\mathbf{V} + \mu\mathbf{J} \times \mathbf{H}, \tag{1}$$

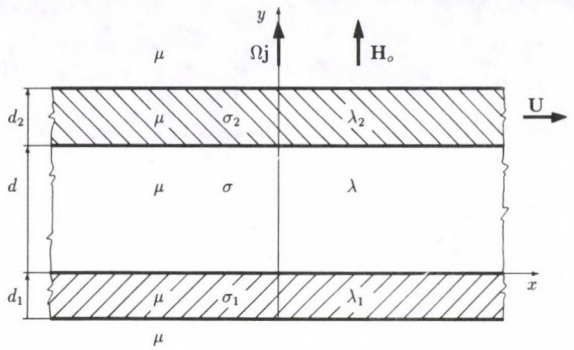

Fig. 1. Channel geometry and parameters

$$\nabla \mathbf{V} = 0, \tag{2}$$

$$\nabla \times \mathbf{H} = \mathbf{J}, \tag{3}$$

$$\nabla \times \mathbf{E} = 0, \tag{4}$$

$$\nabla \mathbf{H} = 0, \tag{5}$$

$$\mathbf{J} = \sigma(\mathbf{E} + \mu \mathbf{V} \times \mathbf{H}), \tag{6}$$

where $\mathbf{V}$ denotes the velocity; $\mathbf{H}$ the magnetic field; $\mathbf{E}$ the electric field; $\mathbf{J}$ the current density; ρ the mass density; ν the kinematic viscosity; σ the electric conductivity. The centrifugal term has been combined with the thermodynamic pressure p in the gyrostatic pressure $p^*=p-\rho\Omega^2(x^2+z^2)/2$. Eliminating $\mathbf{E}$ and $\mathbf{J}$ from (3)–(6), the induction equation is obtained

$$\nabla^2 \mathbf{H} + \mu\sigma \nabla \times (\mathbf{V} \times \mathbf{H}) = 0. \tag{7}$$

The first two equations, (1) and (2), have to be satisfied only in the fluid, the last five ones must be satisfied throughout all the space. In the following, the suffixes 1 and 2 refer to the values of corresponding quantities in the lower and upper plate, respectively.

Since the plates are infinite along x- and z-directions, all the physical quantities, excepting the pressure, depend only on y. From Eqs (2) and (5) it immediately follows that $V_y \equiv 0$ and $H_y \equiv H_o$, hence we can write

$$\mathbf{V} = (V_x, 0, V_z), \quad \mathbf{H} = (H_x, H_o, H_z), \quad \mathbf{E} = (E_x, E_y, E_z), \quad \mathbf{J} = (J_x, 0, J_z). \tag{8}$$

Equation (4) implies that E_x and E_z are constants. With the ansatz (8) Eqs (1) and (7) give

$$\rho\nu \frac{d^2 V_x}{dy^2} - 2\rho\Omega V_z + \mu H_o \frac{dH_x}{dy} - \frac{\partial p^*}{\partial x} = 0, \tag{9}$$

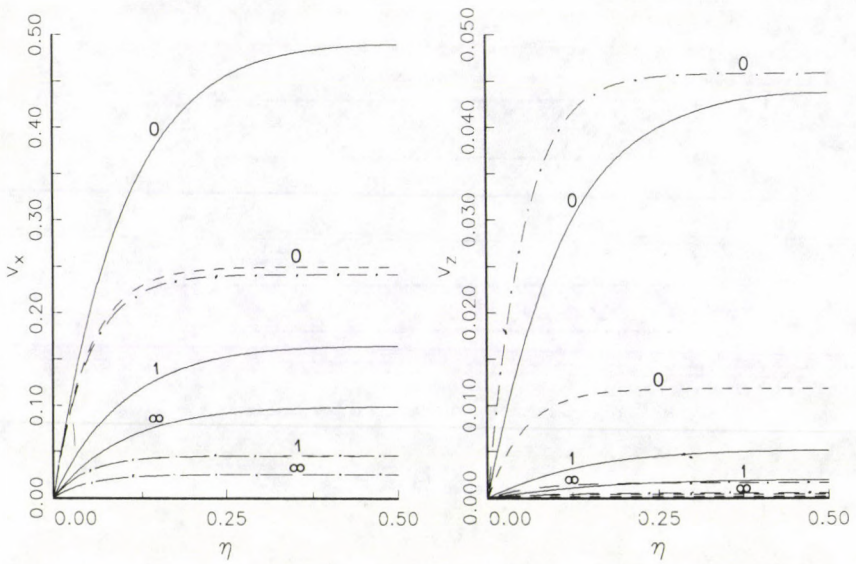

Fig. 2. Primary and secondary velocity profiles.——— $M^2 = 100$, $E^2 = 1$; - - - - $M^2 = 400$, $E^2 = 1$; -·-·-·- $M^2 = 400$, $E^2 = 4$

$$\frac{\partial}{\partial y}\left[p^* + \frac{\mu}{2}(H_x^2 + H_z^2)\right] = 0, \tag{10}$$

$$\rho\nu\frac{d^2V_z}{dy^2} + 2\rho\Omega V_x + \mu H_o\frac{dH_z}{dy} - \frac{\partial p^*}{\partial z} = 0, \tag{11}$$

$$\frac{d^2H_x}{dy^2} + \mu\sigma H_o\frac{dV_x}{dy} = 0, \tag{12}$$

$$\frac{d^2H_z}{dy^2} + \mu\sigma H_o\frac{dV_z}{dy} = 0. \tag{13}$$

Equation (10) indicates the magnetohydrodynamic pressure to be constant along the axis of rotation, moreover it follows from (9) and (11) that $\partial p^*/\partial x$ and $\partial p^*/\partial z$ are also constants. Without loss of generality we can stipulate that $\partial p^*/\partial z = 0$, i.e. the pressure gradient lies in the direction of the x-axis.

With the dimensionless variables

$$\eta = \frac{y}{d}, \quad v_x = \frac{V_x d}{\nu}, \quad v_z = \frac{V_z d}{\nu}, \quad h_x = \frac{H_x}{H_o\nu\mu\sigma}, \quad h_z = \frac{H_z}{H_o\nu\mu\sigma},$$

Eqs (9) and (11) can be rewritten as

$$v_x'' - 2E^2 v_z + M^2 h_x' + P = 0, \tag{14}$$

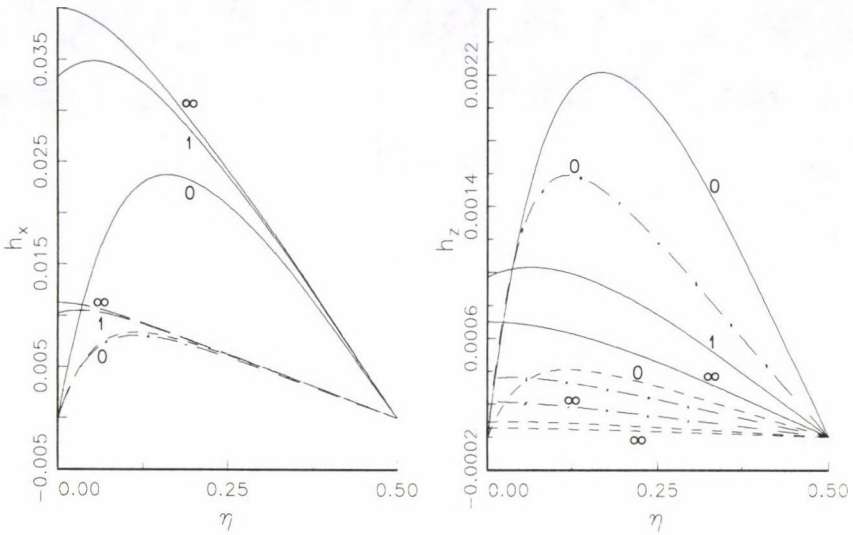

Fig. 3. Primary and secondary magnetic field profiles for $\phi_1 = \phi_2 (= \phi)$. ——— $M^2 = 100$, $E^2 = 1$; - - - - $M^2 = 400$, $E^2 = 1$; - · - · - · $M^2 = 400$, $E^2 = 4$

$$v_z'' + 2E^2 v_x + M^2 h_z' = 0, \tag{15}$$

Eqs (12) and (13) becomes

$$h_x'' + v_x' = 0, \tag{16}$$

$$h_z'' + v_z' = 0, \tag{17}$$

where $E^2 = \Omega d^2/\nu$ is the rotation parameter which is the reciprocal of the Ekman number, $M = \mu H_o d(\sigma/\rho\nu)^{1/2}$ is the Hartmann number, $P = -(d^3/\rho\nu^2)\partial p^*/\partial x$ is the dimensionless pressure gradient and the primes denote differentiation with respect to η.

Introducing complex variables for the velocity and the magnetic field

$$v(\eta) = v_x(\eta) + \imath v_z(\eta), \quad h(\eta) = h_x(\eta) + \imath h_z(\eta),$$

Eqs (14)–(17) reduce to the following simple forms

$$v'' + 2\imath E^2 v + M^2 h' + P = 0, \tag{18}$$

$$h'' + v' = 0. \tag{19}$$

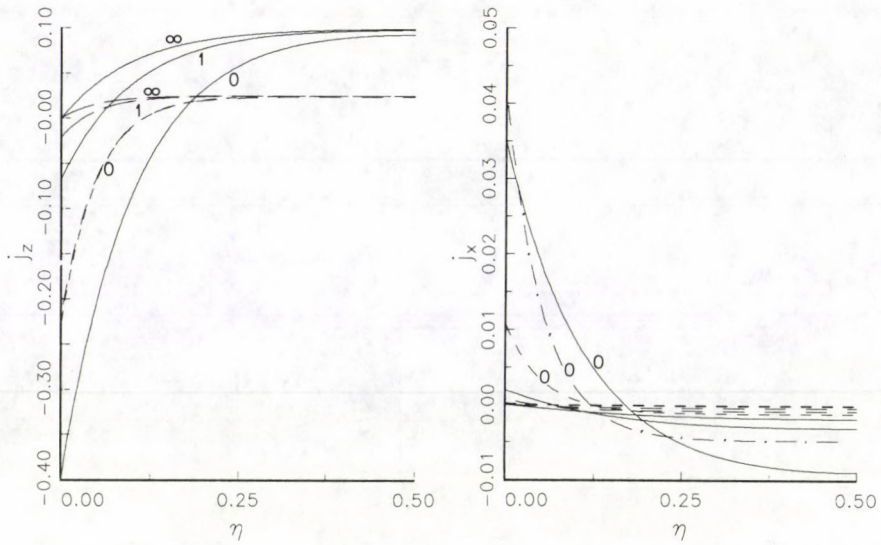

Fig. 4. Distribution of primary and secondary current densities. ——— $M^2 = 100$, $E^2 = 1$; - - - - $M^2 = 400$, $E^2 = 1$; -·-·-·- $M^2 = 400$, $E^2 = 4$

Let us now consider the boundary conditions (BC). As for the fluid, it does not slip along the walls, consequently

$$v(0) = 0, \quad v(1) = u, \tag{20}$$

where $u = u_x + \imath u_z$ with $u_x = U_x d/\nu$ and $u_z = U_z d/\nu$. The appropriate BC for the magnetic field can easily be deduced from the usual electromagnetic interface conditions. It follows from (3) and (6) that in the fluid

$$h' = \imath e - v, \tag{21}$$

while in the lower plate

$$h_1' = \imath e_1 s_1, \tag{22}$$

where $e = E_x d/\nu\mu H_o + \imath E_z d/\nu\mu H_o$ and $s_1 = \sigma_1/\sigma$ is the non-dimensional electric conductivity of the lower plate. Since the tangential component of the electric field is continuous at the boundaries, from (21) and (22) we get

$$h'(0) = h_1'/s_1. \tag{23}$$

The tangential component of the magnetic field has no jump either across the boundaries of the several regions, so $h_1(-\eta_1) = 0$ and $h_1(0) = h(0)$, where $\eta_1 = d_1/d$ is the

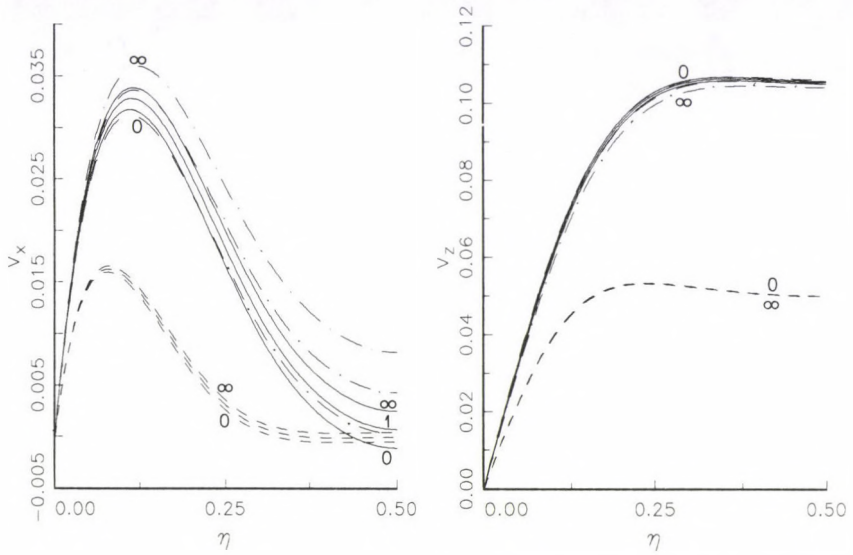

Fig. 5. Primary and secondary velocity profiles. ——— $M^2 = 4$, $E^2 = 50$; - - - - $M^2 = 4$, $E^2 = 100$; - · - · - · $M^2 = 9$, $E^2 = 50$

dimensionless thickness of the lower plate. Using these, (22) leads to the relation

$$h_1' = h(0)/\eta_1. \tag{24}$$

Inserting (24) into (23), we obtain the required magnetic BC at $\eta = 0$

$$h'(0) = h(0)/s_1\eta_1. \tag{25}$$

Finally, at the upper wall, in a similar way we find

$$h'(1) = -h(1)/s_2\eta_2, \tag{26}$$

where $s_2 = \sigma_2/\sigma$ and $\eta_2 = d_2/d$ are the non-dimensional electric conductivity and thickness of the upper wall. The BC are now complete.

To solve Eqs (18)–(19) at first we integrate (19) using the no-slip BC (20)

$$h' + v = h'(0), \tag{27}$$

then we substitute h' into (18). The result

$$v'' + (2\imath E^2 - M^2)v + P + M^2h'(0) = 0, \tag{28}$$

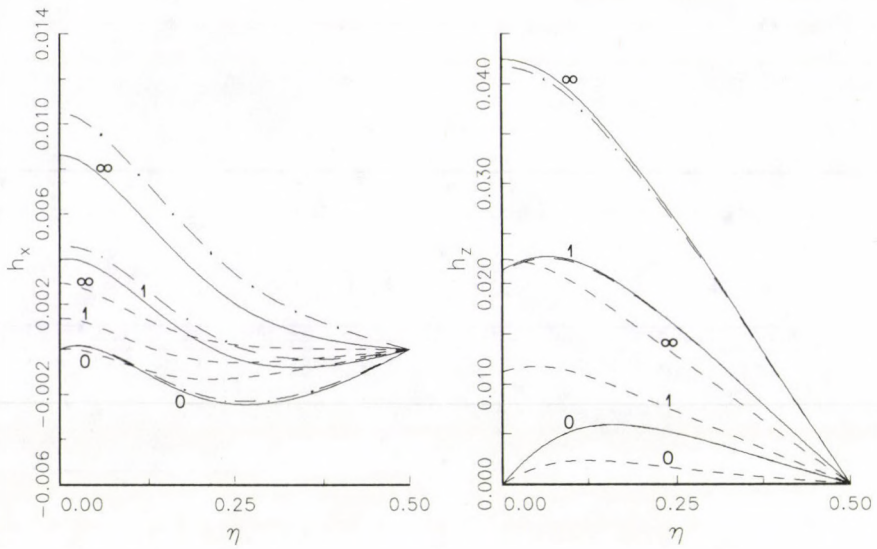

Fig. 6. Primary and secondary magnetic field profiles for $\phi_1 = \phi_2 (= \phi)$. ——— $M^2 = 4$, $E^2 = 50$; - - - - $M^2 = 4$, $E^2 = 100$; - · - · - · $M^2 = 9$, $E^2 = 50$

can easily be solved together with Eq. (27). The solutions satisfying the BC (20), (25) and (26) are

$$v(\eta) = \frac{\sinh k\eta}{\sinh k}(u + RQ) - R[\exp(-k\eta) - 1], \tag{29}$$

$$h(\eta) = h'(0)\eta - \frac{\cosh k\eta}{k \sinh k}(u + RQ) - R[\exp(-k\eta)/k + \eta] + K_o, \tag{30}$$

where $R = [P + M^2 h'(0)]/k^2$, $Q = \exp(-k) - 1$ and $k = \alpha - \imath\beta$ with

$$\alpha = \frac{1}{\sqrt{2}}(\sqrt{M^4 + 4E^4} + M^2)^{1/2}, \quad \beta = \frac{1}{\sqrt{2}}(\sqrt{M^4 + 4E^4} - M^2)^{1/2}.$$

The constant of integration K_o and the quantity $h'(0)$ are given as

$$K_o = u\Big(\frac{\coth k}{k} + \frac{1}{\phi_2}\Big) + RQ\Big(\frac{\coth k}{k} + \frac{1}{Q} + \frac{\exp(-k)}{kQ}\Big) - h'(0)\Big(1 + \frac{1}{\phi_2}\Big)$$

and

$$h'(0) = \frac{\phi_1\phi_2(uK_1 + PK_2)}{\phi_1 + \phi_2 + \phi_1\phi_2(1 - M^2K_2)}, \tag{31}$$

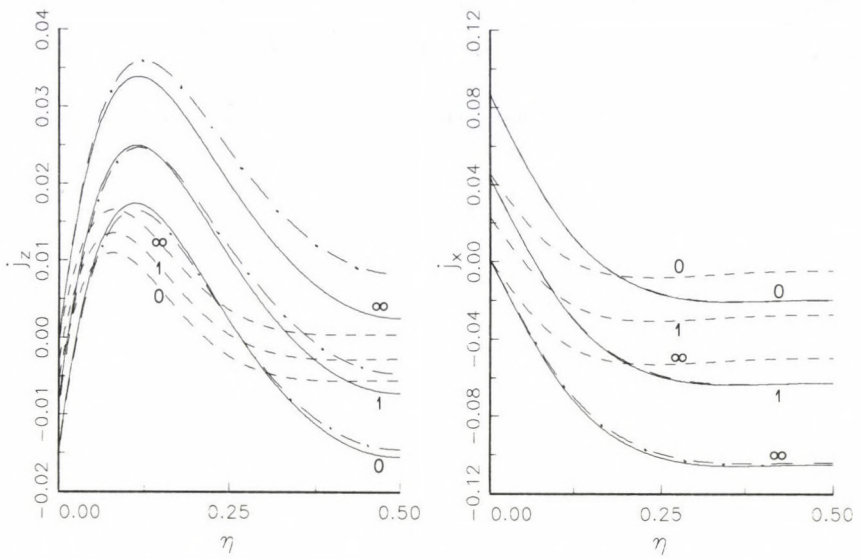

Fig. 7. Distribution of primary and secondary current densities. ——— $M^2 = 4$, $E^2 = 50$; - - - - $M^2 = 4$, $E^2 = 100$; - · - · - · $M^2 = 9$, $E^2 = 50$

where

$$K_1 = \frac{\cosh k - 1}{k \sinh k} + \frac{1}{\phi_2}, \quad K_2 = \frac{Q}{k^2}\left(\frac{\cosh k - 1}{k \sinh k} + \frac{1}{Q} + \frac{1}{k}\right).$$

$\phi_1 = s_1\eta_1$ and $\phi_2 = s_2\eta_2$ are the dimensionless electric conductances of the lower and upper wall of the channel.

For the sake of completeness, the non-dimensional viscous stress is given by

$$\tau_v(\eta) = |v'(\eta)|, \tag{32}$$

where

$$v'(\eta) = -Gk \cosh k\eta + Rk \exp(-k\eta). \tag{33}$$

The coefficient G is given as $G = -(u + RQ)/\sinh k$.

The components of the dimensionless current density $j_x = J_x d/H_o \nu\mu\sigma$ and $j_z = J_z d/H_o \nu\mu\sigma$ can be obtained from Eqs (3) and (27). It is easy to verify that

$$j = -\imath h' = \imath[v - h'(0)], \tag{34}$$

where

$$j(\eta) = j_x(\eta) + \imath j_z(\eta)$$

is the complex current density and

$$h'(\eta) = N + G\sinh k\eta + R\exp(-k\eta). \tag{35}$$

Here $N = h'(0) - R$. This means that the electric current distribution in the fluid differs from the velocity distribution only in an additive constant.

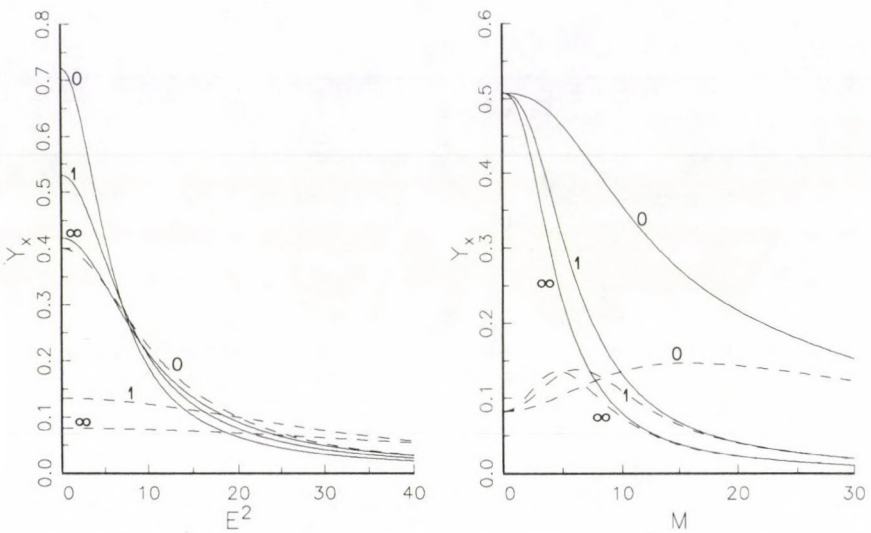

Fig. 8. Primary yield Y_x. LHS: ——— $M^2 = 10$, - - - - $M^2 = 100$; RHS: ——— $E^2 = 4$, - - - - $E^2 = 16$

From the practical point of view, some integral quantities such as yield or net electric current have extreme importance. The dimensionless yield of the flow is given by

$$Y = Y_x + \imath Y_z = \int_0^1 v(\eta)\,d\eta = \frac{\cosh k - 1}{k\sinh k}(u + RQ) + R(Q/k + 1), \tag{36}$$

the total electric current flowing through the fluid is simply related to $h(0)$, $h(1)$ and Y, $h'(0)$:

$$I = I_x + \imath I_z = \int_0^1 j(\eta)\,d\eta = \imath[h(0) - h(1)] = \imath[Y - h'(0)]. \tag{37}$$

3. Heat transfer

For the steady flow under consideration the internal energy balance has the form

$$\lambda\frac{d^2T}{dy^2}+\nu\rho\left[\left(\frac{dV_x}{dy}\right)^2+\left(\frac{dV_z}{dy}\right)^2\right]+\frac{1}{\sigma}\left[\left(\frac{dH_x}{dy}\right)^2+\left(\frac{dH_z}{dy}\right)^2\right]=0, \tag{38}$$

where T is the temperature, λ is the thermal conductivity. The second and the third term are the viscous and Joule dissipation, respectively. (38) holds both in the flow and in the walls, but in the latter case the second term vanishes, of course. Let the temperature of outer surfaces of the plates be a constant value T_o. Introducing the dimensionless temperature $\Theta = T/T_o$ and the thermal diffusivity of the fluid $\chi = \lambda/\rho c_p$, where c_p is the specific heat at constant pressure, Eq. (38) in the fluid reduces to

$$\Theta'' = F(\eta), \quad F(\eta) = -PrEc\,(|v'(\eta)|^2 + M^2\,|h'(\eta)|^2), \tag{39}$$

where $Pr = \nu/\chi$ is the Prandtl number, $Ec = \nu^2/d^2c_pT_o$ is the Eckert one. By using the formulae $h_1' = h(0)/\eta_1$ and $h_2' = -h(1)/\eta_2$, it is easy to show that within the walls the following equations are valid:

$$\Theta_1'' = F_1, \quad F_1 = -\frac{PrEcM^2}{l_1\eta_1\phi_1}\,|h(0)|^2, \tag{40}$$

$$\Theta_2'' = F_2, \quad F_2 = -\frac{PrEcM^2}{l_2\eta_2\phi_2}\,|h(1)|^2, \tag{41}$$

where $l_1 = \lambda_1/\lambda$ and $l_2 = \lambda_2/\lambda$ are the non-dimensional wall heat conductivities. Since both the temperature and the heat flux is continuous across the fluid-wall interfaces, the corresponding dimensionless boundary and matching conditions are

$$\Theta_1(-\eta_1) = 1, \quad \Theta_1(0) = \Theta(0), \quad \Theta_1'(0) = \Theta'(0)/l_1,$$

$$\Theta_2(1+\eta_2) = 1, \quad \Theta_2(1) = \Theta(1), \quad \Theta_2'(1) = \Theta'(1)/l_2.$$

Although the temperature distribution in the channel walls is a simple parabolic-function of η, the integration constants involve a complicated dependence on the geometry and material parameters of the model. With the functions

$$\bar{F}(\eta) = \int_0^\eta F(\eta')\,d\eta', \quad \bar{\bar{F}}(\eta) = \int_0^\eta \bar{F}(\eta')\,d\eta' \tag{42}$$

the solutions for the temperature can be written concisely. In the flow

$$\Theta = \bar{\bar{F}}(\eta) + C\eta + \bar{C}, \tag{43}$$

within the walls

$$\Theta_1 = F_1\eta^2/2 + C_1\eta + \bar{C}_1, \quad \Theta_2 = F_2\eta^2/2 + C_2\eta + \bar{C}_2. \tag{44}$$

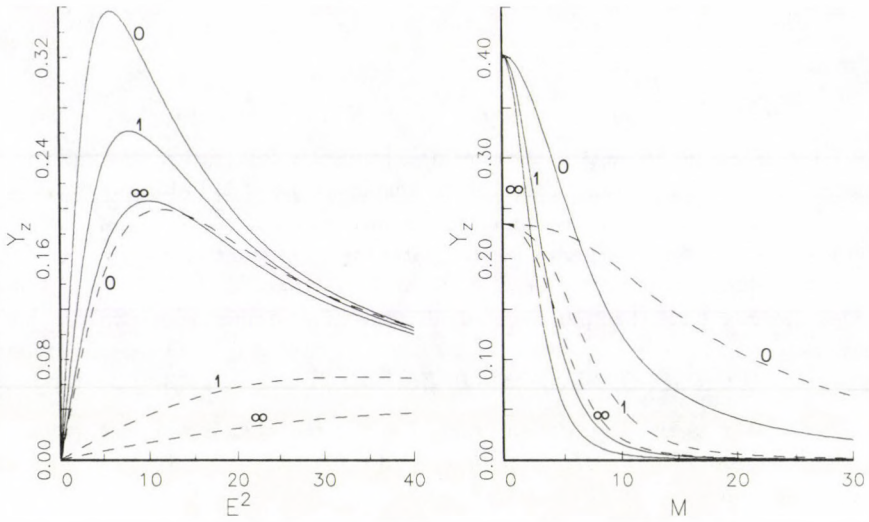

Fig. 9. Secondary yield Y_z. LHS: ——— $M^2 = 10$, - - - - $M^2 = 100$; RHS: ——— $E^2 = 4$, - - - - $E^2 = 16$

After some manipulations one finds

$$C = \frac{F_1\eta_1^2/2 - F_2\eta_2^2/2 - \bar{\bar{F}}(1) - \bar{F}(1)\eta_2/l_2}{1 + \eta_1/l_1 + \eta_2/l_2},$$

$$\bar{C} = 1 - F_1\eta_1^2/2 + C\eta_1/l_1,$$

$$C_1 = C/l_1, \quad C_2 = C/l_2 + \bar{F}(1)/l_2 - F_2,$$

$$\bar{C}_1 = \bar{C}, \quad \bar{C}_2 = C - C_2 + \bar{C} - F_2/2 + \bar{\bar{F}}(1).$$

The final step of the calculation is to give the functions $F(\eta)$, $\bar{F}(\eta)$ and $\bar{\bar{F}}(\eta)$ explicitly. Substituting Eqs (33) and (35) into (39), after a lengthy but straightforward algebra we get

$$F(\eta) = PrEc\,(a_1 + a_2\cos^2\beta\eta + a_3\sinh^2\alpha\eta + a_4\sin 2\beta\eta + a_5 e^{-2\alpha\eta} + a_6 e^{\alpha\eta}\cos\beta\eta + a_7 e^{\alpha\eta}\sin\beta\eta + a_8 e^{-\alpha\eta}\cos\beta\eta + a_9 e^{-\alpha\eta}\sin\beta\eta) \tag{45}$$

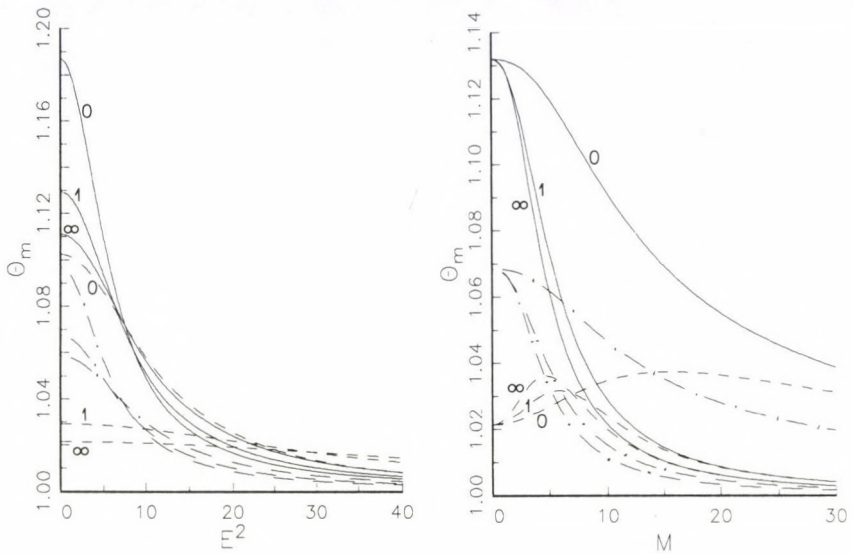

Fig. 10. Mean temperature Θ_m for $\eta_1 = \eta_2 = 0.25$, $\phi_1 = \phi_2 (= \phi)$, $l_1 = l_2 (= l)$ and $PrEc = 0.02$. LHS: ——— $M^2 = 10, l = 0.1$; - - - - $M^2 = 100, l = 0.1$; - · - · - · $M^2 = 10, l = 0.2$; RHS: ——— $E^2 = 4, l = 0.1$; - - - - $E^2 = 16, l = 0.1$; - · - · - · $E^2 = 4, l = 0.2$

with the coefficients

$$
\begin{aligned}
a_1 &= -M^2(N_s + G_s) + (M^2 - \gamma)(G_r R_r + G_i R_i), \\
a_2 &= (M^2 - \gamma)[G_s - 2(G_r R_r + G_i R_i)], \\
a_3 &= -(M^2 + \gamma) G_s, \\
a_4 &= (M^2 - \gamma)(G_r R_i - G_i R_r), \\
a_5 &= (M^2 + \gamma)(G_r R_r + G_i R_i - R_s), \\
a_6 &= -M^2(G_r N_r + G_i N_i), \\
a_7 &= -M^2(N_r G_i - N_i G_r), \\
a_8 &= M^2[N_r(G_r - 2R_r) + N_i(G_i - 2R_i)], \\
a_9 &= M^2[N_i(G_r - 2R_r) - N_r(G_i - 2R_i)],
\end{aligned}
$$

where $\gamma = \alpha^2 + \beta^2$, moreover the indices r, i and s refer to the real, imaginary part and square of absolute value of the actual quantity, respectively. Integrating $F(\eta)$, it is an easy task to find the functions

$$\bar{F}(\eta) = PrEc\,(b_1 + b_2\eta + b_3 \sinh 2\alpha\eta + b_4 \sin 2\beta\eta + b_5 \cos 2\beta\eta + b_6 e^{-2\alpha\eta} + b_7 e^{\alpha\eta} \cos\beta\eta + b_8 e^{\alpha\eta} \sin\beta\eta + b_9 e^{-\alpha\eta} \cos\beta\eta + b_{10} e^{-\alpha\eta} \sin\beta\eta) \tag{46}$$

with the coefficients

$$b_1 = (a_4/\beta + a_5/\alpha)/2 + [\alpha(a_8 - a_6) + \beta(a_7 + a_9)]/\gamma, \quad b_2 = a_1 + (a_2 - a_3)/2,$$

$$b_3 = a_3/4\alpha, \quad b_4 = a_2/4\beta, \quad b_5 = -a_4/2\beta, \quad b_6 = -a_5/2\alpha, \quad b_7 = (\alpha a_6 - \beta a_7)/\gamma,$$

$$b_8 = (\alpha a_7 + \beta a_6)/\gamma, \quad b_9 = -(\alpha a_8 + \beta a_9)/\gamma, \quad b_{10} = (-\alpha a_9 + \beta a_8)/\gamma,$$

and

$$\bar{\bar{F}}(\eta) = PrEc\,(c_1 + c_2\eta + c_3\eta^2 + c_4 \cosh 2\alpha\eta + c_5 \cos 2\beta\eta + c_6 \sin 2\beta\eta + c_7 e^{-2\alpha\eta} + c_8 e^{\alpha\eta} \cos\beta\eta + c_9 e^{\alpha\eta} \sin\beta\eta + c_{10} e^{-\alpha\eta} \cos\beta\eta + c_{11} e^{-\alpha\eta} \sin\beta\eta) \tag{47}$$

with the coefficients

$$c_1 = [b_4/\beta + (b_6 - b_3)/\alpha]/2 + [\alpha(b_9 - b_7) + \beta(b_8 + b_9)]/\gamma, \quad c_2 = b_1, \quad c_3 = b_2/2,$$

$$c_4 = b_3/2\alpha, \quad c_5 = -b_4/2\beta, \quad c_6 = b_5/2\beta, \quad c_7 = -b_6/2\alpha, \quad c_8 = (\alpha b_7 - \beta b_8)/\gamma,$$

$$c_9 = (\alpha b_8 + \beta b_7)/\gamma, \quad c_{10} = -(\alpha b_9 + \beta b_{10})/\gamma, \quad c_{11} = (-\alpha b_{10} + \beta b_9)/\gamma.$$

The determination of temperature distribution is now complete.

There are some additional parameters which are expedient to be defined. The dimensionless mean temperature Θ_m can be calculated by using the definition

$$\Theta_m = \int_0^1 \Theta(\eta)\, d\eta.$$

Substitution of (43) and evaluation of the integral leads to the result

$$\Theta_m = \bar{C} + C/2 + PrEc\,\Big(c_1 + c_2/2 + c_3/3 + c_4 \sinh 2\alpha/2\alpha + c_5 \sinh 2\beta/2\beta + c_6(1 - \cos 2\beta)/2\beta + c_7(1 - e^{-2\alpha})/2\alpha + \alpha(c_{10} - c_8)/\gamma + \beta(c_{11} + c_9)/\gamma + (e^{\alpha}/\gamma)[c_8(\alpha\cos\beta + \beta\sin\beta) + c_9(\alpha\sin\beta - \beta\cos\beta)] + (e^{-\alpha}/\gamma)[c_{10}(\beta\sin\beta - \alpha\cos\beta) - c_{11}(\alpha\sin\beta + \beta\cos\beta)]\Big). \tag{48}$$

The Nusselt number, which describes the heat transfer at the walls, is of engineering interest. The definition of the Nusselt number is based on the mean temperature:

$$Nu_1 = \Theta'(0)/[\Theta_m - \Theta(0)], \quad Nu_2 = \Theta'(1)/[\Theta_m - \Theta(1)].$$

In view (43), we get

$$Nu_1 = C/[\Theta_m - \bar{C}], \quad Nu_2 = [\bar{F}(1) + C]/[\Theta_m - \Theta(1)]. \tag{49}$$

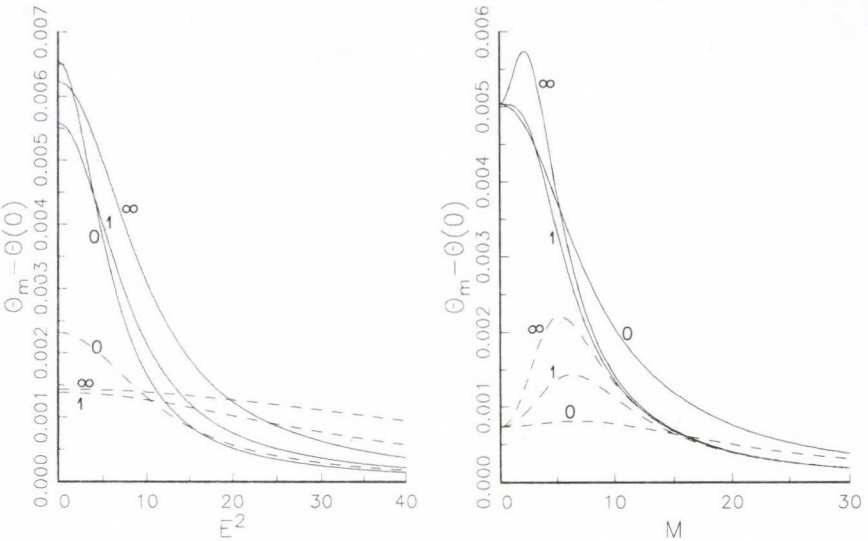

Fig. 11. $\Theta_m - \Theta(0)$ for $\eta_1 = \eta_2 = 0.25$, $\phi_1 = \phi_2 (= \phi)$, $l_1 = l_2 (= l)$ and $PrEc = 0.02$. LHS: ——— $M^2 = 10, l = 0.1$; - - - - $M^2 = 100, l = 0.1$; RHS: ——— $E^2 = 4, l = 0.1$; - - - - $E^2 = 16, l = 0.1$

4. Structure of the flow

Our purpose is to give a qualitative discussion for the effects of the rotation, magnetic field and wall properties. In the model we have altogether 11 dimensionless parameters, therefore a complete presentation of all the interesting quantities would enlarge the paper enormously. Consequently, we select some characteristic sets or extreme values of parameters. Although our analytical results are valid for the generalized HF (i.e. for the MHD Couette–Poiseuille flow), we analyse only the case of $u = 0$. In this subcase the velocity and current distributions in the fluid are symmetrical and (beside P, E and M) depend only on the sum of the wall electric conductances $\phi = \phi_1 + \phi_2$. Of course, the magnetic field and the current within the walls depend also on the individual values of ϕ_1 and ϕ_2. In this Section we consider the flow structure of this submodel in three particular cases of interest.

Case 1. $E^2 \ll 1$ and $M^2 \ll 1$. In this simplest case, in order to save place, the overall behaviour of fields is described without accompanying figures. If the system rotates slowly, the electric conductivity of the fluid is low and the applied magnetic field is weak, the magnitude of the secondary fields (SF) is much smaller than the magnitude of the corresponding primary fields (PF). (PF is defined by the dimensionless field components v_x, h_x and j_z, SF is defined by v_z, h_z and j_x.) The effect of external magnetic field on all the field variables is negligible. The PF is

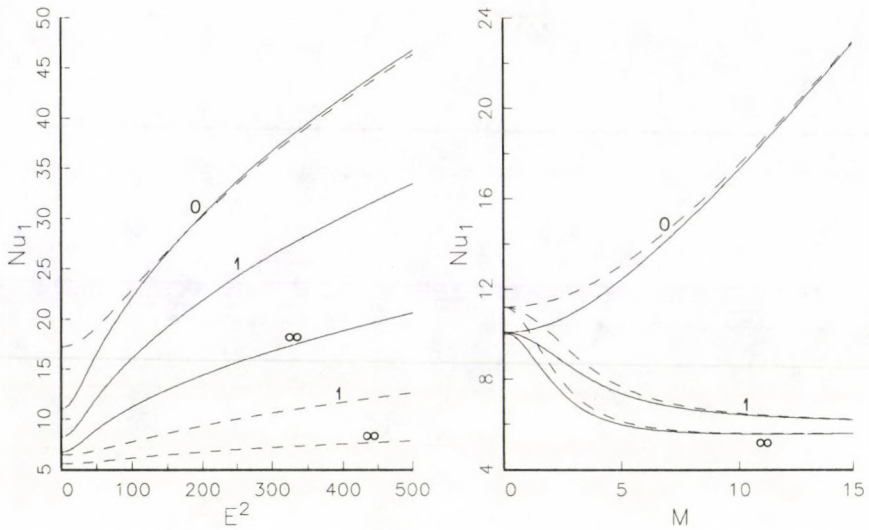

Fig. 12. Nusselt number Nu_1 for $\eta_1 = \eta_2 = 0.25$, $\phi_1 = \phi_2 (= \phi)$, $l_1 = l_2 (= l)$ and $PrEc = 0.02$. LHS: ——— $M^2 = 10$, $l = 0.1$; - - - - $M^2 = 100$, $l = 0.1$; RHS: ——— $E^2 = 4$, $l = 0.1$; - - - - $E^2 = 16$, $l = 0.1$

not affected by the rotation, while the magnitude of the SF increases linearly with E^2. This is quite natural: the SF is induced by the rotation.

The profiles of the primary and secondary velocity v_x and v_z are nearly parabolic having maxima at the middle of the channel. According to (34), the distribution of current density components j_z and j_x is also nearly parabolic. The velocity components are not affected by the wall properties, while the induced magnetic field and current density components depend strongly on the wall parameters. The magnitude of h_x and h_z grows as ϕ increases. When neither wall is a perfect conductor, j_z is (j_x) negative (positive) near to the walls and positive (negative) in the central region of the channel. j_z and $-j_x$ increase as ϕ increases. This is not surprising, because no accumulation of electric charge is possible in a steady flow, so the current has to form a closed loop. At insulated walls ($\phi = 0$) the current loop has to form inside the fluid, when at least one of the walls is perfectly conducting ($\phi = \infty$), the backward current can entirely pass through the wall. In a realistic case, when $\phi > 0$, a part of the backward current remains necessarily in the fluid.

Case 2. $M^2 \gg 1$ and $E^2 \sim O(1)$. It is seen from Figs 2–4 that when the applied magnetic field is strong and the rotation is slow, the magnitude of the SF is much less than the magnitude of the PF. Both the PF and the SF depend remarkably on the magnetic parameter M^2 and the wall parameter ϕ, whereas the

rotation has significant influence only on the SF. The magnitude of the SF shows a nearly linear growth with E^2. (We note that all the displayed figures have been made on taking $P = 10$. Each curve is labelled with the value of ϕ.)

Figure 2 shows clearly the characteristic effect of large Hartmann numbers on the velocity components. We observe that in any point both the primary and the secondary velocity decrease with an increase in M^2. From Figs 3 and 4 we see that the magnitudes of the induced magnetic field and current density components are also decreasing when M^2 increases. This is due to the overall retarding effect of the electromagnetic body force $\mu \mathbf{J} \times \mathbf{H}$. At high M^2 the velocity is nearly constant in the core of the flow and a boundary layer structure appears along the walls. Figures 3 and 4 show that the magnetic field and current density variations are also mostly confined to the layers contacting with the walls. As a result the flow can be divided into a boundary layer (BL) and a central core (CC) region. The BL may be identified as a modified Hartmann layer.

It is salient in Fig. 2 that the velocity components decrease remarkably as ϕ increases. In the CC h_x and j_z are unaffected by ϕ, while in the BL they increase with ϕ. Although h_z varies quasi linearly in the core, it depends on ϕ not only in the BL but also in the CC. With increasing wall conductivities $-j_x$ decreases in the CC and increases in the BL. In other words, decreasing ϕ makes the current induced in the core flowing back through the Hartmann layers and hence reduces the electromagnetic drag on the flow.

Case 3. $E^2 \gg 1$ and $M^2 \sim O(1)$. The numerical results for this case are presented in Figs 5–7. When the rotation is rapid and the magnetic field is not strong, the magnitude of the SF is larger than that of PF. It is surprising that both PF and SF weaken as the rotation accelerates. (We will explain this behaviour later.) We observe that the external magnetic field has an appreciable influence only on the PF.

Figure 5 shows that for large values of rotation parameter the velocity profiles are M-shaped having maxima near the walls. The slope of velocity profiles on the edges is determined by the parameter E according with the fact that the second derivatives of velocity in Eqs (14) and (15) are multiplied by $1/E^2$. This indicates the formation of a viscous BL.

The BL may be identified as a modified Ekman layer. The effects of the external magnetic field and the wall parameters on the velocity are negligible in the Ekman layers. In the CC there is no velocity component parallel with the pressure gradient (at least this component is very small), the transverse component is uniform. Thus in this region the fluid moves in the direction normal to the applied pressure gradient and the axis of rotation. (We note that in certain cases there exists a weak reverse flow in the direction of the pressure gradient.) The primary flow is more sensitive to the variation of magnetic field and wall properties than the secondary one, namely, v_x increases with M^2 and ϕ, further the influence of M^2 becomes stronger with growing ϕ. Near the limit $E^2 \to \infty$ the flow pattern is completely insensitive to the variation of magnetic field and wall properties because the Coriolis force dominates everywhere except in the BL.

The most rapid changes in the distribution of magnetic field and current

density are limited mostly to the BL contacting with the walls. In the CC region the magnetic field varies almost linearly, the current density is almost uniform, it can be noted that the influence of wall properties on these quantities is significant. The magnitude of h_x and h_z, further j_z and $-j_x$ increase with an increase in ϕ. Figure 7 reveals that in certain cases a reverse current arises not only in the vicinity of the walls but also in the core. As for the external magnetic field, it raises the magnitude of h_x and j_z.

The above results indicate that a suitable rotation can change the effect of the external magnetic field.

5. Behaviour of integral quantities

In this Section we examine the influence of various parameters on the yield, total electric current flowing through the fluid, mean temperature and Nusselt number.

Figure 8 shows the primary yield Y_x plotted against the rotation parameter E^2 and the Hartmann number M, respectively. From this figure it can be read off that accelerating rotation reduces the primary yield, i.e., as we have remarked earlier, the Coriolis force retards the primary flow. When the rotation is slow, M and ϕ diminish the value of Y_x, which is in agreement with the fact that the magnetic field usually exerts a retarding influence on the flow. However, for sufficiently large E^2 the primary yield increases in the beginning, attains a maximum and then decreases as M increases. Moreover, at low M the yield Y_x increases with raising ϕ, while for higher M the effect is just the opposite.

From Fig. 9 we see that the secondary yield Y_z first increases rapidly from the value zero, reaches a maximum and then decreases gradually as the rotation becomes stronger. The increasing magnetic field and wall conductances shift the maximum in the direction of larger rotation parameters. Since the secondary flow is driven by the rotation, at first sight this trend appears to be suprising. The explanation, however, is simple. Equations (14) and (15) show that the z-component of the Coriolis force (the driving force for the secondary flow) depends linearly on the primary velocity. Since initially v_x decreases slowly then rapidly with the rotation, the driving force increases in the beginning and reduces afterwards as E^2 grows. When the rotation is not too fast, Y_z decreases with increasing M and ϕ. Although the results are not presented here, further computations show that when E^2 is sufficiently large and ϕ is very small, Y_z at first increases slightly then decreases on intensifying the magnetic field.

Also it may be noted from Figs 8 and 9 that the relative importance of the secondary flow with respect to the primary one increases with strengthening rotation and decreases with intensifying magnetic field.

Notwithstanding that the yield Y and the current I are connected via the simple relation (37), the conclusions concerning the behaviour of yield cannot be * directly extended for the current since the quantity $h'(0)$ depends on all the input parameters. However, when $\phi = 0$, $I = \imath Y$, which suggests that the overall

behaviour of I and Y becomes similar at large values of ϕ. Needless to say, ϕ exerts completely different influences on these quantities.

To demonstrate the effect of various parameters on the thermal behaviour of the fluid, the dimensionless mean temperature Θ_m is investigated (Fig. 10) as a function of E^2 and M at symmetric material and geometrical properties of the walls. It is clear that Θ_m decreases with E^2 and $l(= l_1 = l_2)$. As for the Prandtl and Eckert numbers, it follows from Eqs (39)–(41) that the mean temperature increases with increasing values of dimensionless group $PrEc$.

Comparing Fig. 10 with Fig. 8, it is salient that the dependence of Θ_m and Y_x on the magnetic parameter is more or less similar. However, the maximum in Θ_m is not purely due to the enhanced viscous dissipation.

To explain this behaviour of Θ_m, at first let us consider Fig. 11 where $\Theta_m - \Theta(0)$ is plotted. We see that this quantity has also a maximum in the actual parameter range, further here the temperature difference increases remarkably with ϕ. The underlying physical mechanism in this parameter range is that the Joule dissipation attains a maximum, further for large ϕ the major part of the Joule heating is confined to the middle of the channel. This explains also the nature of the curves of Θ_m. We remark that Javeri [7] has discussed in detail the role of the different kinds of internal heat generation in the non-rotating HF.

Finally, to complete the survey on the heat transfer aspects of the problem, the Nusselt number Nu_1 is presented in Fig. 12 for symmetric walls. We observe that Nu_1 increases if the rotation parameter E^2 grows. In view Fig. 11, this means that the magnitude of heat flux decreases less quickly with E^2 than $\Theta_m - \Theta(0)$ does. It is interesting that for not too small values of ϕ the Nusselt number decreases then becomes a constant on increasing M gradually, while for very small ϕ it grows quasi linearly with M.

6. Remarks

(i) The analytic solution of temperature field and related quantities are very complicated, therefore it is advisable to check the validity of the final formulae. We have solved the whole problem numerically, too, using an infinite order Runge–Kutta method to find $v(\eta)$ and $h'(\eta)$. The $F(\eta)$, $\bar{F}(\eta)$, $\bar{\bar{F}}(\eta)$ and Θ_m quantities have been evaluated by an eight order Lagrange–Hermite integrator. The results of the two computations are in excellent agreement.

(ii) In the case of $u \neq 0$ the velocity and current density distributions also depend on the individual values of ϕ_1 and ϕ_2, therefore the problem becomes more complicated.

(iii) In an ionised gas where the density is low and/or the applied magnetic field is strong, the effect of Hall current becomes significant, therefore we have to use the generalized Ohm's law instead of (6). This problem requires further investigation.

Acknowledgement

This work was supported by the Hungarian Scientific Research Fund under Contract No. OTKA-2350.

References

1. J. Hartmann, Kgl. Danske Vidensk. Sels., Math.-Fys. Med., *15*, No. 6, 1937.
2. C. C. Chang and J. T. Yen, ZAMP, *13*, 266, 1962.
3. R. A. Alpher, Int. J. Heat Mass Transfer, *3*, 108, 1961.
4. J. T. Yen, J. Heat Transfer, *85*, 723, 1963.
5. K. Jagadeesan, AIAA J., *2*, 756, 1964.
6. W. T. Snyder, J. Heat Transfer, *86*, 552, 1964.
7. V. Javeri, Wärme- Stoffübertrag., *8*, 261, 1975.
8. R. S. Nanda and H. K. Mohanty, Appl. Sci. Res., *24*, 65, 1971.
9. N. Datta and R. N. Jana, J. Inst. Maths Applics, *19*, 217, 1977.
10. R. N. Jana, N. Datta and B. S. Mazumder, J. Phys. Soc. Jpn., *42*, 1034, 1977.
11. G. Krishnam Raju and V. V. Ramana Rao, Acta Phys. Hung., *44*, 363, 1978.
12. G. S. Seth and M. K. Maiti, Indian J. Pure Appl. Math., *13*, 931, 1982.

Acta Physica Hungarica 73 (2–4), pp. 311-343 (1993)

SURVEY ARTICLE

NOBLE GAS MIXTURE HOLLOW CATHODE LASERS

M. JÁNOSSY, L. CSILLAG, Z. DONKÓ and K. RÓZSA

Research Institute for Solid State Physics
of the Hungarian Academy of Sciences
1525 Budapest, Hungary

(Received 3 August 1993)

A review of noble gas mixture ion lasers operating cw in hollow cathode discharges is given. The basic properties of hollow cathode discharges and the main principles of tube construction are described. For the He–Kr, He–Ar and He–Ne–Xe systems laser transitions, excitation mechanisms, operation of the lasers and questions of lasers for practical use are discussed. The single frequency operation of the lasers and some problems connected to this are also dealt with.

1. Introduction

A large amount of research has been done in the field of gas lasers since the discovery of the first infrared He–Ne laser in 1961 [1]. This has led to the development of a large class of gas lasers for practical uses. The well-known He–Ne, He–Cd, Ar ion and CO_2 lasers operate in the positive column part of the discharge. The possibility of laser operation in the negative glow region has been the subject of detailed research since 1970 when Schuebel published basic results on hollow cathode discharge lasers [2,3]. In hollow cathode discharges the electron energy distribution is favourable due to the large number of high energy electrons present. This property offers a good possibility for excitation of high lying ionic levels, which are necessary to obtain laser operation in the visible and ultraviolet range of the spectrum. The hollow cathode discharge lasers operate at much higher pressures than the conventional positive column lasers which gives a good base to obtain single frequency operation [4].

Several types of hollow cathode lasers have been developed, which can be classified most simply by the way the active material is produced:

- noble gas–metal vapour lasers where the metal vapour is produced by heating. Typical representatives are the He–Cd [2], He–Zn [5], Ne–Tl [6] lasers.
- noble gas–metal vapour lasers where the metal vapour is produced by cathode sputtering. Typical lasers are He–Cu [7], Ne–Cu [8], He–Ag [9], He–Au [10], Ne–Al [11].
- noble gas mixture lasers, here the active medium is a mixture of He–Kr [12], He–Ar [13] and He–Ne–Xe [14].

In the case of metal vapour hollow cathode lasers a basic problem is the production of a uniform metal vapour density at the temperature needed to obtain the necessary vapour pressure. This basic problem of metal vapour lasers has not yet been solved in a satisfactory manner up to now. The production of metal vapour by cathode sputtering partly overcomes this problem. The metal vapour density obtained in this way is always below the optimum value, however [15], and it cannot be controlled independently from the discharge current. The cathode sputtering technique is particularly useful to produce laser action with metals where the necessary vapour pressure can be obtained only at high temperatures of 1100–1400 °C (Cu, Ag, Au, Al).

Noble gas mixture hollow cathode lasers operate at several ionic lines, mainly in the green–blue part of the spectrum. In these lasers the uniform density of the active medium in principle is reached and the laser tube can be operated at room temperatures. Both metal vapour lasers and noble gas mixture lasers have advantages and drawbacks. These questions are shortly dealt with in Part 3 and Part 4.

In this paper a review is given on noble gas mixture hollow cathode lasers, which is based mainly on work performed at the Gas Laser Laboratory of the Research Institute for Solid State Physics, Budapest. In Part 2 the basic properties of hollow cathode discharges are considered, which is followed in Part 3 by the discussion of construction problems related to the lasers. Laser transitions, excita-

tion mechanisms, operation conditions and some questions connected to a practical noble gas mixture laser are given in Part 4, in this Part explanations of some experimental observations are also presented. An important feature of the noble gas mixture lasers is the single frequency operation observed in case of TEM_{00} mode operation, phenomena and problems related to this are dealt with in Part 5.

2. Basic properties of hollow cathode discharges

Hollow cathode gas lasers operate in the *cold cathode abnormal glow* operation regime of electrical discharges. In *cold cathode* glow discharges electron emission from the cathode occurs due to the impact of positive ions, metastable atoms and ultraviolet photons onto the cathode surface. The electrons emitted from the cathode participate in collision processes where a sufficient number of charged and excited particles, as well as photons are created to maintain the discharge by liberating electrons from the cathode [16,17]. In the *abnormal glow* operation mode the whole cathode surface is covered by discharge and the discharge voltage increases with increasing current. (In normal glow regime the current density is quite low and constant, the discharge covers only a part of the cathode surface which increases with current.)

2.1. The spatial distribution of the discharge

The typical appearance of a glow discharge is shown in Fig. 1 for an ordinary plane cathode arrangement [16–18]. Only the cathode region of these discharges (consisting essentially of the cathode dark space and the negative glow) is used in hollow cathode lasers (see Fig. 2). In hollow cathode discharge geometries the negative glow (NG) region of the discharge is partly surrounded by the cathode surface, as it is shown schematically in Fig. 2. The cathode cavity is filled with the cathode dark space and the negative glow. There exists an optimal pressure where the self-maintenance mechanism of the discharge is the most efficient. This optimum can be observed as a voltage minimum when the pressure is changed at constant discharge current [17]. The radial intensity distribution of the emitted light also shows a characteristic behaviour as the gas pressure is changed [28]. Under optimal operating conditions the light intensity peaks in the central region of the cavity. With increasing pressure a relatively dark hole is formed in the middle of the discharge and at even higher pressure the negative glow tends to form a bright ring along the cathode surface. This effect is illustrated in Fig. 3. The radial distribution of the discharge is also influenced by the voltage and the current of the discharge. At high pressures where the middle of the cathode cavity is dark, by sufficiently increasing current it can be reached that the light intensity reaches its maximum in the axis of the discharge.

The cathode dark space (CDS) of abnormal glow discharges is characterized by large electric field (up to $10^3 - 10^4$ Vcm^{-1} at the cathode surface which decreases

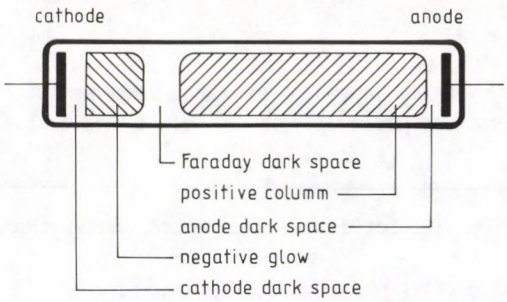

Fig. 1. Spatial distribution of a glow discharge (only the most important parts of the discharge are indicated)

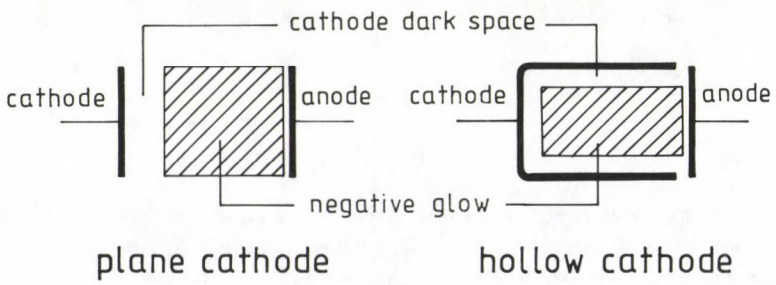

Fig. 2. A typical plane cathode and hollow cathode arrangement

to about zero at the CDS–NG boundary) and by a large electric field gradient. The typical voltage drop on the CDS is in the order of several hundred Volts. In the negative glow, however, the electric field is small. This region can be considered as created by the high energy electrons injected into it from the cathode dark space. These electrons dissipate most of their energy in the negative glow.

Because of the high electric field gradient in the CDS the electric field changes significantly along a mean free path of electrons. The motion of electrons therefore lacks *hydrodynamic equilibrium* and cannot be described with mobility data [19,20]. The negative glow is also a "non-hydrodynamic" region because of the injected high energy electrons.

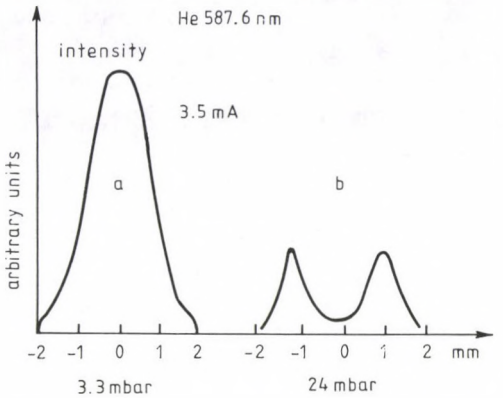

Fig. 3. Typical radial intensity of a spectral line in a cylindrical hollow cathode: (a) at "optimal" pressure and (b) "high" pressure

2.2. The hollow cathode effect

Typical voltage–current characteristics of a plane and a hollow cathode (HC) discharge are shown in Fig. 4. It can be seen in Fig. 4 that at a given discharge voltage the current (or current density) of the hollow cathode discharge is usually much greater. The increased current density of the HC can be explained in terms of the *hollow cathode effect*.

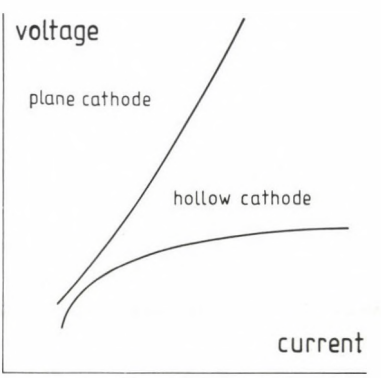

Fig. 4. Typical voltage–current characteristics of a plane cathode and hollow cathode discharge

The main reasons of the hollow cathode effect are summarized below [21].

- In plane cathode discharges the role of ultraviolet photons in the maintenance of the discharge is relatively unimportant [22]. In hollow cathode geometry photons and metastable atoms can reach the cathode with a higher probability and release more electrons than in an ordinary discharge. In HC discharges the importance of photoelectrons emitted by the cathode due to UV radiation from the discharge has been experimentally demonstrated [23,24].
- There may exist so-called "pendelelectrons" which oscillate in the potential well formed inside a hollow cathode and increase the ionisation and excitation rate [25,26]. The existence of oscillating electrons was proved experimentally [21] and is also supported by discharge modelling calculations [27].
- Non-linear processes (the rate of which depends non-linearly on the concentrations) may start to play an important role because of the increased concentration of excited and charged species in the negative glow.
- The fast electrons may also be focused by proper geometry.

2.3. The energy distribution of electrons

Hollow cathode discharges were found to be efficient sources for laser operation (see e.g. [28,29]). The electrons which acquire high energy in the cathode dark space and enter the negative glow can ionize the gas and excite high-lying electronic levels of atoms and ions efficiently. Metastable densities higher than in positive column discharges can be reached (a He 2^3S density of the order of $10^{13}/cm^3$ at discharge current densities around 100 mA/cm^2 [30]), which is important from the point of view of noble gas mixture lasers. The energy distribution of electrons entering the negative glow is therefore of practical importance. Because of the non-hydrodynamic nature of the cathode region the calculation of the electron energy distribution function (EEDF) is a laborious task. (The EEDF is usually obtained by solution of the Boltzmann equation or by Monte Carlo simulation [20].) The EEDF in the cathode region is very different from the EEDF in the positive column of glow discharges where it can be well approximated by a Maxwellian distribution (typically found in positive column discharge lasers e.g. He–Ne laser). Figure 5 shows the EEDF at the CDS–NG boundary calculated for a plane cathode discharge in He (at 300 volts discharge voltage and 5 mbar pressure) together with a Maxwellian EEDF with electron temperature corresponding to $kT_e = 5$ eV. The large extent of high energy electrons at the CDS–NG boundary can be clearly seen in Fig. 5.

Noble gas mixture lasers operate in a mixture of *buffer gas(es)* and a small amount of "active" gas which — from the point of view of the discharge — can be considered as an admixture. The small amounts of admixtures may have large effects on the parameters of the discharge as it was realized many decades ago [18,31]. The influence of admixtures on the operation of hollow cathode discharges is expected — at least qualitatively — to be the same as in the plane cathode case.

It was found that the admixtures quench the high energy tail of the EEDF [32]. This effect is demonstrated in Fig. 6, where the EEDF at the CDS–NG boundary

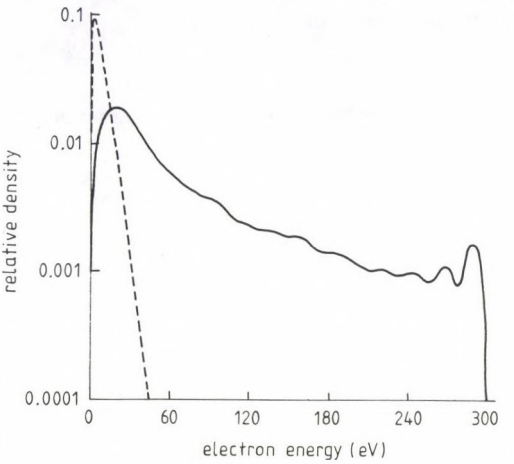

Fig. 5. The electron energy distribution function (EEDF) at the CDS–NG boundary at 300 V cathode fall (————) and a Maxwellian electron energy distribution of $kT_e = 5$ eV (- - - -)

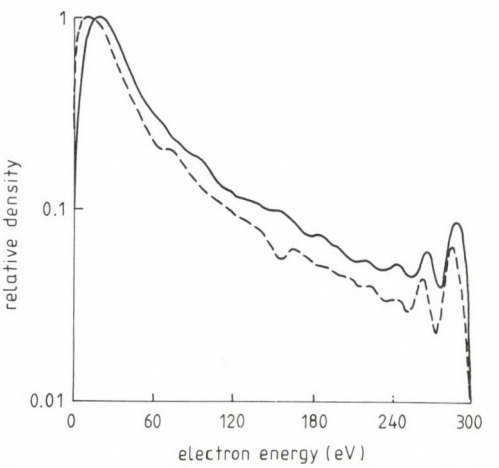

Fig. 6. The electron energy distribution function (EEDF) at the CDS–NG boundary at 300 V cathode fall in a pure He discharge (————) and in a mixture of He+0.8 % Kr (- - - -)

is plotted for a discharge in pure He and in the mixture of He and 0.8 % Kr. This is believed to be one of the causes of the decrease of laser power above a certain

pressure of the active gas. It was also found that the small admixtures play an important role in the maintenance of the discharge.

2.4. The effect of cathode sputtering

In hollow cathode lasers there also occurs the phenomenon of *cathode sputtering*. This process gives a possibility to utilize room temperature metal vapour laser operation. However, it is an undesired effect in noble gas mixture lasers. The sputtered cathode material may quench the energy of electrons and has a negative effect on laser performance. The cathode sputtering occurs due to the impact of heavy positive ions on the cathode surface. The sputtering yield depends on the type and energy of the ions [33]. The ion energy is influenced by the cathode fall voltage and the free path of ions which impact into the cathode.

The motion of positive ions in the cathode dark space is limited by *charge transfer processes*. Thus their free path depends on the charge transfer cross-sections and the concentration of the gas. In noble gas mixture lasers the large difference between the concentrations of the admixed gases may result in very different free paths for the different (buffer gas, active gas) ionic species. Consequently, the energy distribution of buffer and active gas ions may also be very different at the cathode surface. This is illustrated in Fig. 7, where the energy distribution of He^+ and Kr^+ ions is plotted for a plane cathode discharge. The Figure shows that krypton (being the active gas in a He–Kr^+ laser) is essential for laser operation but also causes undesired cathode sputtering.

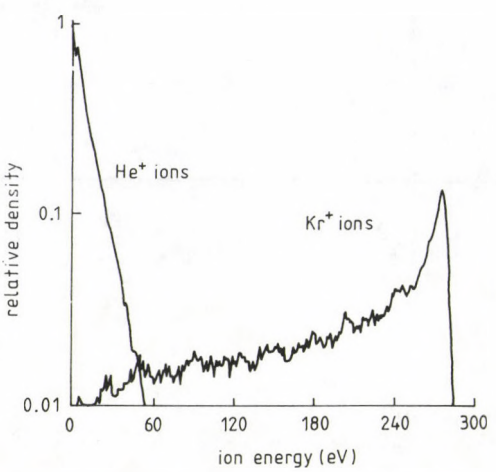

Fig. 7. Energy distribution of He^+ and Kr^+ ions on the cathode surface (in He+0.8 % Kr, cathode fall voltage: 300 V)

From the point of view of hollow cathode lasers both the voltage and the current density of the discharge play an important role in laser performance. The energy of electrons in the discharge is largely influenced by the cathode fall voltage. Therefore it is of importance to design hollow cathode geometries which result in higher operating voltage than the convential hollow cathode arrangements.

3. Construction principles of hollow cathode discharge tubes

There are several requirements to be satisfied by the design and construction of a hollow cathode laser tube. The discharge should only fill out the hollow cathode cavity, any other room occupied by the discharge decreases the excitation efficiency. The homogeneous discharge along the optical axis is also very useful. Since the large discharge plasma in one piece is a subject of instabilities and arcing, the plasma (especially in long tubes) has to be divided into several independent parts. These requirements are general for all of the different hollow cathode lasers. While at the cathode sputtered type of lasers there is a need for a high density of sputtered particles in the plasma, in the noble gas mixture lasers the density of sputtered metal should be kept as low as possible in order to avoid the effect of the metal vapour on the discharge. In the hollow cathode lasers the high energy of fast electrons is essential, which can be increased by different methods which increase the voltage of the discharge. The different excitation mechanisms, however, need different optimum electron energies. In the noble gas mixture lasers, where the excitation mechanism is energy transfer between metastable He atoms and noble gas ions, the too high electron energies may be disadvantageous, since they may decrease the metastable atom concentration. To satisfy all these requirements in one discharge arrangement is fairly difficult. Research on these problems is being carried out continuously. However, some guidelines and the review of some typical already existing laser constructions may help in understanding a large variety of discharge tubes, and could show some directions of the research in this field.

3.1. Stability of the discharge

The output power of the hollow cathode lasers often increases with increasing the current in a large range. However, above a certain current the discharge becomes unstable, contracts into a small volume and an arc discharge develops. This effect not only stops the laser oscillation, but may also damage the discharge tube. In our earlier investigations we have shown that, at a given construction, and gas quality and pressure, this arcing occurs around a certain current limit, the arcing threshold current. In a wide range this arcing does not depend on the current density on the cathode surface. A smaller volume of plasma, with higher current density is more stable against arcing [28]. Therefore in each construction it is advisable to avoid the large uninterrupted negative glow. The occurrence of arcing is strongly influenced in the case of an Al cathode by the oxide layer present on the surface [34].

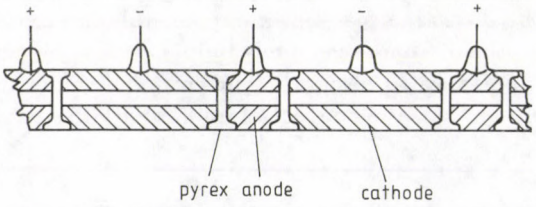

Fig. 8. Longitudinal discharge arrangement

3.2. Longitudinal and transversal discharge arrangements

The longitudinal discharge arrangements are usually the simplest ones, one example is shown in Fig. 8. The cathode is a cylindrical tube, and anodes are placed at the two ends of the cathode. The discharge is flowing along the tube from the anode into the cathode hollow. Such arrangements have several advantages. One is the simplicity of the tube. Simple discharge tubes can be built in this way and it can easily be arranged that the discharge should not flow outside the cathode cavity. One possibility for this is when the wall of the cathode tube is the wall of the discharge tube as well. Using such a construction the cooling of the cathode is easy, and the electrical connections need not to be introduced into the vacuum part of the discharge. A serious drawback of such arrangements is, however, that neither the current density, nor the electron energy distribution are constant along the tube. To flow the discharge deeper into the tube a certain voltage is necessary. This has to be compensated by the lower current density on the cathode surface. The density of the low energy electrons is increasing as we approach the end of the cathode, therefore no optimum conditions can be set along the cathode, and the output power from unit length is less than in the transversal arrangements [35]. Therefore short cathode lengths are preferred, however, then we lose the simplicity of the tube.

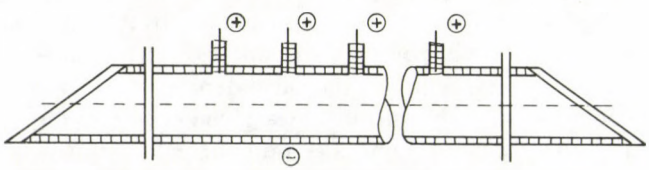

Fig. 9. "Flute type" discharge arrangement

In principle a "flute type" discharge tube (see Fig. 9) behaves similarly to the longitudinal arrangements [36]. Here a series of holes are drilled in the wall of the cylindrical hollow cathode. The anodes are placed into or above these holes and the discharge current flows through these holes between the anode and the cathode. However, this arrangement utilizes a large plasma in one piece which can be a source of different instabilities.

In the transversal arrangements the discharge is flowing across the tube and the homogeneous conditions of the discharge can be easily assured, especially in noble gas mixture discharges. In the following the main types of transversal arrangements are discussed.

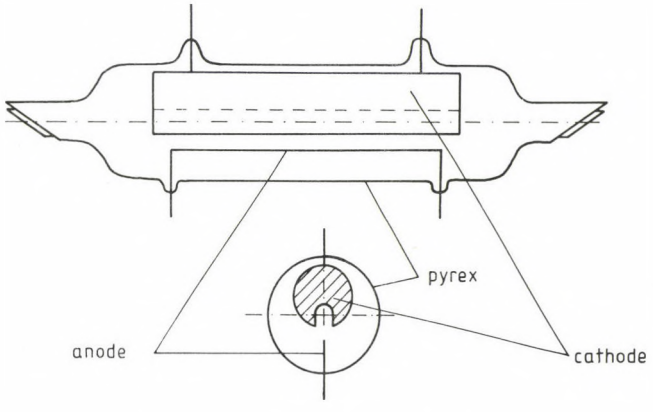

Fig. 10. Slotted hollow cathode arrangement

Slotted hollow cathode discharge tubes. The idea of the slotted hollow cathode [2] is demonstrated in Fig. 10, the cathode is here a rod placed into the vacuum envelope. A slot is cut along the cathode and the anode is placed opposite the slot. These constructions are simple, however, a considerable part of the current may flow outside the slot reducing the efficiency of such discharges, especially in the noble gas mixture lasers. On the other hand, the large cathode–anode distance has the advantage that the lifetime of the tube is long. The lifetime is usually limited by the short-circuit between the anode and the cathode due to the deposited sputtered cathode material.

Internal anode (low voltage) tubes. A more efficient use of the discharge current can be done if the anode is a rod and is placed into the cathode, along the cavity [37]. The cross-section of such an arrangement is illustrated in Fig. 11. Preferably the cavity has an elliptical cross-section and then the cross-section of the active volume is matching the laser beam profile.

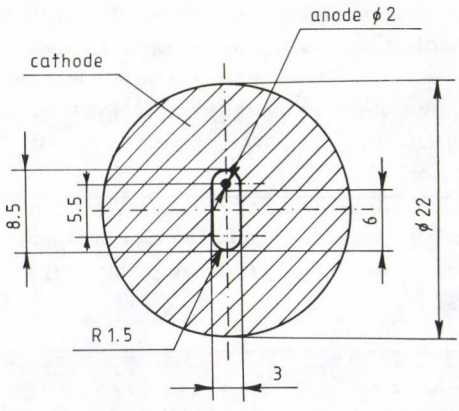

Fig. 11. Internal anode discharge tube arrangement with a single anode rod

3.3. Variable voltage discharge tubes

The conventional hollow cathode tubes have a flat voltage–current characteristic, the discharge voltage is about a few hundred volts. Modifying the discharge geometry, the efficiency of the discharge can be decreased by increasing the loss of the charges in the discharge. The increased voltage increases the density of the high energy part of the electron energy distribution and a more efficient excitation can be achieved. The threshold current of the lasers decreases while the efficiency and the output power increases [14].

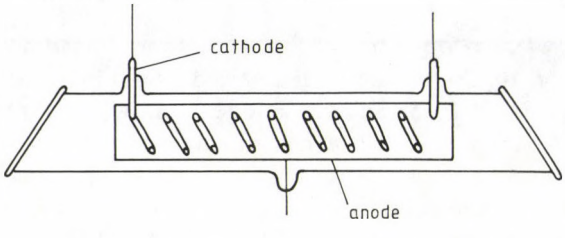

Fig. 12. Coil cathode discharge arrangement

One possibility to increase the voltage is to use a coil cathode introduced by Sabotinov and Grozeva [38]. This arrangement is illustrated in Fig. 12. The anode

is placed outside the cathode coil, and the discharge can flow into the middle of the coil between the windings. The voltage of the discharge can be tuned by changing the space between the windings. Part of the current can be lost by flowing between the threads and on the outer part of the cathode. This arrangement does not focus the fast electrons into the axis of the discharge. Therefore this discharge does not perform as well (especially at low currents) as the internal anode variable voltage discharges. On the other hand, the risk of short circuit is low as the anode can be placed relatively far from the coil cathode.

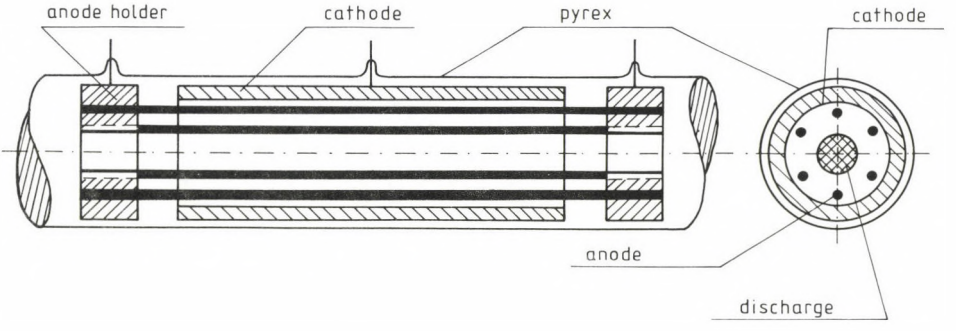

Fig. 13. Internal anode discharge arrangement with a series of anode rods

The voltage of the discharge can also be increased in different internal anode arrangements. If we place anode rods near the cathode surface into a cylindrical hollow cathode, as illustrated in Fig. 13, the voltage of the discharge can be set by the distance between the anode rods and by changing the number of the rods. This discharge has a large flexibility to increase different voltages. Low threshold current and high efficiency is characteristic of such discharges [14]. Since in the excitation mechanism of noble gas mixture lasers metastable He atoms are also involved a moderate increase of voltage gives the best efficiency [37]. Still better efficiency can be achieved in constructions where the anode rods are replaced by a thin wall (preferably stainless steel) tube, where the slots can be cut into the wall of the anode tube [39]. A cross-section of such a discharge is shown in Fig. 14. The sputtering of the cathode is disadvantageous since it not only unfavourably changes the electron energy distribution, but also limits the lifetime of the discharge tube due to the short-circuit caused by the deposited metal. This type of discharge combined with less sputtering cathode material (like graphite) may give the best performance to the noble gas mixture lasers. It is also clear that if the cathode sputters less, then more active gas (like Kr in He buffer) can be introduced into the discharge, which may provide a better lifetime, when the lifetime is determined by the clean-up of the active gas, and in high current discharges we may achieve better performances as well. These problems are the subject of present research.

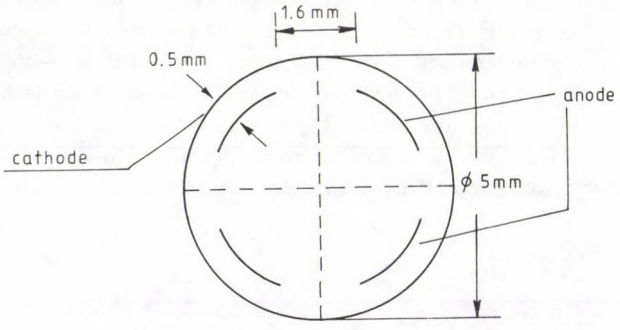

Fig. 14. Slotted internal anode discharge arrangement

4. Noble gas mixture lasers

4.1. History

The He–Kr ion laser operating cw in a hollow cathode discharge was discovered on the base of investigations where the characteristics of pulsed positive column 537.8 nm He–Cd^+ and 469.4 nm He–Kr^+ lasers were carefully compared [40]. It was found that the behaviour of the two pulsed laser systems is very similar. Since the green He–Cd laser was known to operate cw in a hollow cathode discharge the same was tried for He–Kr with the first experiment being immediately successful resulting in cw operation at 469.4 nm [12]. Later on using a high voltage hollow cathode tube cw laser operation was observed at other Kr II transitions too [41].

He–Ar mixture was also considered to be a candidate for cw operation at 476.5 nm in a hollow cathode discharge [42] but at first experiments failed to reach this. Rózsa obtained a gain factor [43] of 16 in a large cross-section (7 × 12 mm) transverse hollow cathode discharge tube, but was unable to reach oscillation [44]. The first successful oscillation in He–Ar at the 476.5 nm Ar II transition was obtained in a longitudinal type hollow cathode discharge [13]. The output power was found to be significantly lower than in He–Kr. Several new cw Ar II transitions were observed later in a high voltage hollow cathode tube [41].

The question of cw laser oscillation in a Ne–Xe mixture was puzzling first. The Ne–Xe laser operating at the 531.4 nm line of Xe II was observed to be stronger compared to He–Kr in pulsed positive column discharges [45]. In the cw hollow cathode discharge used for He–Kr [12] even the spontaneous 531.4 nm spectral line could not be observed. In the longitudinal discharge, where cw He–Ar oscillation was obtained, the 531.4 nm spontaneous line was clearly seen. No laser oscillation was observed, however, and measurements of the spontaneous intensity revealed

Table I

Gas mixture	Wavelength (nm)	Transition	Threshold current (A)
He–Kr	Kr II		
16 mbar He	A 651.0	$6s^4P_{5/2} - 5p^4S^0_{3/2}$	2.1
	B 512.6	$6s^4P_{3/2} - 5p^4D^0_{3/2}$	4.4
0.1 mbar Kr	B 469.4	$6s^4P_{5/2} - 5p^4D^0_{7/2}$	1.1
	B 458.3	$6s^4P_{3/2} - 5p^4D^0_{5/2}$	4.2
	B 438.7	$6s^4P_{5/2} - 5p^4P^0_{3/2}$	4.5
	B 431.8	$6s^4P_{5/2} - 5p^4P^0_{5/2}$	2

no maxima as a function of Ne and Xe pressure which phenomenon is usually characteristic for laser action. In the end in a high voltage hollow cathode discharge an accidental addition of He to Ne–Xe resulted in gain and then optimization of gas fill led to laser oscillation at 531.4 nm [14].

4.2 Laser transitions

He–Kr

Laser transitions of Kr II operating cw in hollow cathode discharges are summarized in Table I. Gas mixture, wavelengths, transition assignments and threshold currents are given in the Table. The data were obtained in a high voltage hollow cathode laser [41]. The active length of the discharge tube was 160 cm, it consisted of 16 segments each 10 cm long. The cathodes were made of pure Al, the inner diameter was 7 mm, the diameter of the volume left free by the six internal anodes was 3 mm. The reflection of laser mirrors used in this experiment was maximum for the wavelengths in question ($R > 99.5$ %), their radius of curvature was 3 m. Excitation of the discharge was by 12.5 Hz half wave rectified alternating current. In the Table the notation "A" denotes a laser transition not observed earlier at all, "B" denotes such ones which have been observed earlier only in pulsed positive column discharges [48]. It is noted that the transition at 431.8 nm was obtained first independently from us by Stefanova [46]. The strongest transition is at 469.4 nm with a threshold current of 1.1 A. Maximum output power obtained in this tube using a 2 % transmission mirror was 100 mW at 11 A.

He–Ar

Laser transitions of Ar II operating cw in hollow cathode discharges are given in Table II. Similarly to Table I gas mixture, wavelengths, transition assignments and threshold currents are contained in the Table. The data were obtained in the

Table II

Gas mixture	Wavelength (nm)	Transition	Threshold current (A)
He–Ar	Ar II		
15 mbar He	A 686.1	$4p^2P^0_{3/2} - 3d^2P_{3/2}$	2.3
0.9 mbar Ar	A 648.3	$4p^2S^0_{1/2} - 3d^2P_{3/2}$	2.5
	C 476.5	$4p^2P^0_{3/2} - 4s^2P_{1/2}$	2.2
	C 457.9	$4p^2S^0_{1/2} - 4s^2P_{1/2}$	4.2
	C 454.5	$4p^2P^0_{3/2} - 4s^2P_{3/2}$	3.5
Ar	Ar II		
1.1 mbar	476.5		6

same meaning as before, "C" denotes laser transitions which were observed for the first time in a hollow cathode discharge. The strongest transition is at 476.5 nm, the threshold current being 2.2 A. The maximum output power observed using a 2 % transmission output mirror was 21 mA at 10 A discharge current.

He–Ne–Xe

Laser transitions of Xe II operating cw in a hollow cathode discharge are summarized in Table III. Gas mixture, wavelengths, transition assignments and threshold currents are given in the Table. The data were obtained in a transverse hollow cathode discharge tube [47]. The tube was a slotted hollow cathode type with the bottom of the slot widened, the anode rod being placed into this part as it is shown in Fig. 15. The dimensions of the slot were 2×5 mm. The active length of the tube was 40 cm, it was built of 4 segments, each 10 cm long. Excitation was by 50 Hz repetition rate long pulses having a duration up to 0.5 ms. This type of excitation is considered to be cw since it is much longer than the time scale of collision processes leading to population inversion. In the Table the notation "B" denotes as previously laser transitions observed earlier only in pulsed positive column discharges [48]. The two transitions given in the lower part of the Table were observed cw first in a hollow cathode discharge by Solanki et al [49].

Bennett has made a critical evaluation of published laser transitions in that respect whether laser oscillation was really observed at these or not [50]. On the basis of data given by Solanki the 526.2 nm and 572.7 nm transitions are denoted as questionable. Experiments performed in [47] have shown unambiguously that there is laser oscillation at these transitions and the sufficient agreement of wavelength measurements with those of Solanki supports the correctness of the transition assignments of [49].

From Table III it can be seen that the optimum He and Ne pressures are significantly different for the two groups of laser lines (531.4 nm, 486.3 nm and 526.2 nm, 572.7 nm, respectively). Figures 16 and 17 show the dependence of the laser power on He and Ne pressure for the two groups of laser lines. The 531.4 nm transition was the strongest, at optimum gas fill 5 mW peak power was obtained at

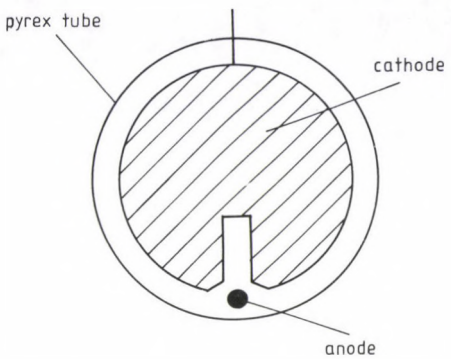

Fig. 15. Slotted hollow cathode discharge tube used for He–Ne–Xe laser

Table III

Gas mixture	Wavelength (nm)	Transition	Threshold current (A)
He–Ne–Xe	Xe II		
36 mbar He	B 531.4	$7s^4P_{5/2} - 6p^4D^0_{7/2}$	4
5 mbar Ne	B 486.3	$7s^4P_{5/2} - 6p^4P^0_{5/2}$	6.1
0.02 mbar Xe			
60 mbar He	526.2	$6p'^2D^0_{3/2} - 6s'^2D_{3/2}$	6.6
2.5 mbar Ne	572.7	$6p'^2D^0_{5/2} - 5d'^2F_{5/2}$	7.2
0.02 mbar Xe			

11 A. Weak laser oscillation was observed at 531.4 nm in 9 mbar Ne and optimum Xe, in He–Xe and He–Ar–Xe no laser action could be observed [14,47].

4.3. Excitation mechanisms

The excitation mechanisms for the laser systems are discussed in the following. Basically in all three types they are the same, some differences in details are discussed, however.

He–Kr laser

The high gas pressure (15–40 mbar) and the large mixture ratio (He/Kr~200/1) observed in the hollow cathode laser indicates that the excitation of the upper laser

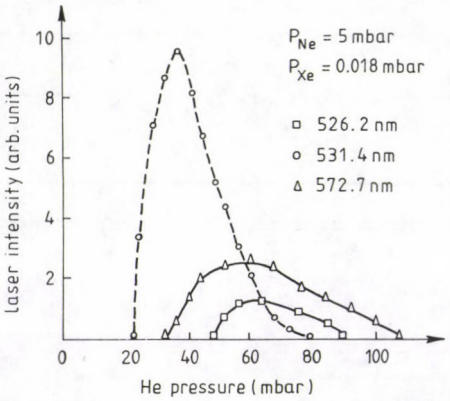

Fig. 16. Dependence of laser intensity on He pressure in case of different Xe II laser lines

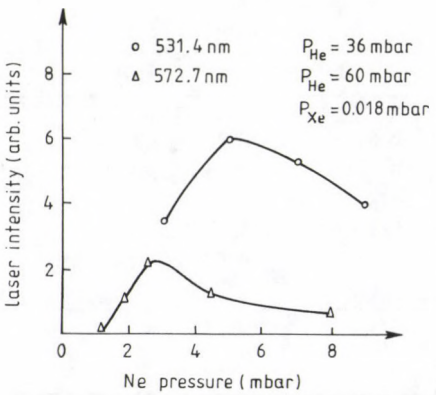

Fig. 17. Dependence of laser intensity on Ne pressure in case of different Xe II laser lines

level is similar to that in the pulsed positive column discharge [48] being a resonant collision of the second kind between He 2^3S metastables and ground state Kr ions

$$\mathrm{He}\,2^3\mathrm{S} + \mathrm{Kr}^+ \rightarrow \mathrm{He} + \mathrm{Kr}^{+*}. \qquad (1)$$

Several observations support this mechanism:

- in the hollow cathode discharge those laser transitions oscillate of which the upper level energy is near to that of the He 2^3S state.

- there is no laser oscillation at the transitions originating from lower energy levels, while there is laser oscillation at these transitions in pure Kr positive column discharges where they are excited by direct electron collisions.
- according to measurements in a hollow cathode discharge the intensity of the spontaneous 469.4 nm transition was found to be approximately 25 times stronger in He–Kr than in pure Kr [51].
- exciting the discharge by several hundred μs duration pulses after the 3 μs fall of the current pulse, the laser oscillates still for a time of the order of 20 μs in the afterglow.

The second kind collision process (1) occurs in principle with a high probability if the energy difference between the exciting He 2^3S level and the excited Kr ion level is small being the order of a few times kT (k is the Boltzmann constant, T is the gas temperature). In the case of (1) the energy difference is 0.35 eV, however, the He 2^3S energy is 19.82 eV, while that of the Kr ion level is 19.47 eV. The cross-section of the process according to [49] is large in spite of this, being in the order of 10^{-14} cm^2. The large energy difference is taken up by the colliding particles in the form of kinetic energy. The large cross-section can be explained by the Wigner spin conservation rule being fulfilled in (1) and this is more important than a near energy coincidence [52].

The lower laser level is populated mainly by direct electron collisions

$$\mathrm{e} + \mathrm{Kr} \rightarrow \mathrm{e} + \mathrm{Kr}^{+*} + \mathrm{e}.$$

The population of the lower level is usually not significant compared to that of the upper level. The lower level population will become noticeable only within special circumstances, which means excitation with square wave shaped high current pulses at low He pressures [53]. In this case at the fast 3 μs decay of the current pulse a peak appears in the laser pulse. This is explained by the fast depopulation of the electron collisionally excited lower level.

In the excitation of ground state Kr ions two processes can take part:

- Penning ionization by metastable He atoms

$$\mathrm{He}\,2^3\mathrm{S} + \mathrm{Kr} \rightarrow \mathrm{He} + \mathrm{Kr}^{+} + \mathrm{e} + \Delta E; \tag{2}$$

- Ionization by electron impact

$$\mathrm{e} + \mathrm{Kr} \rightarrow \mathrm{e} + \mathrm{Kr}^{+} + \mathrm{e}. \tag{3}$$

Calculations have been carried out to see what is the ratio of the excitation rate of processes (3) and (2) [54]. This ratio (R) of the excitation rates of electron impact ionization and Penning ionization has been determined in the case of a Maxwellian electron energy distribution valid in the positive column and using the electron energy distribution determined experimentally in the negative glow [55]. In the case of a Maxwellian distribution $R \sim 0.3$, while in case of the non-Maxwellian negative glow distribution $R \sim 120$ has been obtained. This result shows that in a

hollow cathode discharge electron impact is the dominant process for the production of Kr ions.

He–Ar laser

The high optimum gas pressure (15–40 mbar) and the large mixture ratio (He/Ar~30/1) indicates similarly to the He–Kr laser that the upper level is excited by the process

$$\mathrm{He}\, 2^3\mathrm{S} + \mathrm{Ar}^+ \rightarrow \mathrm{He} + \mathrm{Ar}^{+*}.$$

This process is supported by results of investigations performed on a laser excited by several hundred μs duration current pulses [53]. Here at the time of the fast 3 μs fall of the current pulse a peak appears in the laser pulse (Fig. 18). The laser operates in the afterglow for approximately 15 μs. The peak is interpreted as being caused by the increase of population inversion due to the difference in the slow decay of upper level population excited by long life He 2^3S atoms and the fast decay of the electron collisionally excited lower level.

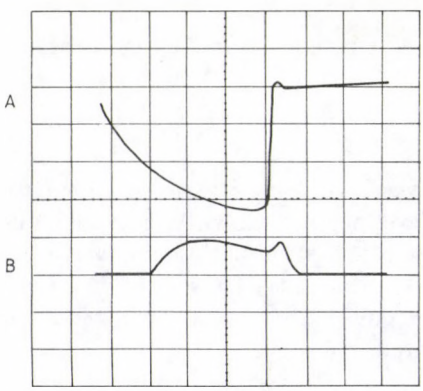

Fig. 18. Laser pulse (B) and current pulse (A, negative signal) at the 476.5 nm Ar II transition of the He–Ar laser. Current pulse 2A/division, time scale 50 μs/division. $P_{\mathrm{He}} = 32$ mbar, $P_{\mathrm{Ar}} = 0.6$ mbar

In the He–Ar system the energy difference between the He 2^3S (19.82 eV) and the upper laser level of the Ar ion (19.87 eV) is –0.05 eV. On the basis of this small energy difference it would be expected that the exciting process has a large cross-section. Investigations aiming on this show, however, that the cross-section is around 0.5×10^{-16} cm^2 [56], which is significantly smaller than in the case of He–Kr. In the He 2^3S–Ar ion collisions by the excitation of the $4p^2P^0_{3/2}$Ar ion level the Wigner spin conservation rule is not fulfilled. This shows again that for a large

collision cross-section spin conservation is more important than a near coincidence of energy. The smaller cross-section compared to He–Kr results that in He–Ar the upper level population is also lower which gives a lower output power. The ground state Ar ions are believed to be produced mainly in the same way as in He–Kr by electron impact [54]:

$$e + Ar \rightarrow e + Ar^+ + e.$$

He–Ne–Xe laser

In the He–Ne–Xe laser the relatively high Ne pressure (2–8 mbar) and the large Ne/Xe mixture ratio (Ne/Xe $\sim$ 250/1) makes it probable that the upper level is excited similarly as in pulsed positive column discharges [48] by collisions of the second kind

$$Ne\,1s_5 + Xe^+ \rightarrow Ne + Xe^{+*}.$$

This is supported by the observation that no laser oscillation was observed in He–Xe and He–Ar–Xe mixtures. The ground state Xe ions are produced mainly by electron impact [54].

Two questions arise in connection with the He–Ne–Xe laser

- what is the role of He in producing laser oscillation;
- what is the reason of the different optimum He and Ne pressures for the two groups of laser transitions.

He influences laser operation presumably in two ways. In a He–Ne mixture due to the resonant collisions of the second kind between He metastables and Ne atoms the density of Ne $1s_5$ metastables significantly increases. According to measurements of Solanki [49] a four times increase occurs in the Ne $1s_5$ density compared to that in pure Ne. Also it is important that in a given pressure He–Ne mixture a higher voltage is necessary to maintain the gas discharge than in pure Ne. As a consequence of the high voltage more high energy electrons are present in a He–Ne discharge, which increases the density of Xe ions.

The difference in optimum He and Ne pressures indicates a different excitation mechanism for the two groups of laser transitions. Measurements have shown that Ne is definitely necessary for laser oscillation. It has been considered to be likely that the two groups are excited by collisions of different Ne metastables ($1s_2$ and $1s_5$) with ground state Xe ions [47].

4.4. Laser output power and gas discharge parameters

The connection between laser output power and gas discharge parameters is quite complex. In the following some basic relations are dealt with. These are the dependence of output power on the partial pressure of the buffer and active gas, dependence of output power on discharge current, dependence of threshold current on gas pressure and the connection between optimum gas pressure and discharge

current. The relations are similar for all the three laser systems. Several investigations have been performed on the He–Kr laser [12, 37, 57, 58], results obtained at the 469.4 nm transition are presented. The laser operation parameters are strongly influenced by cathode geometry, so in each case the cathode arrangement used is specified. Excitation of the discharge was in most cases by 12.5 Hz repetition rate half wave rectified alternating current.

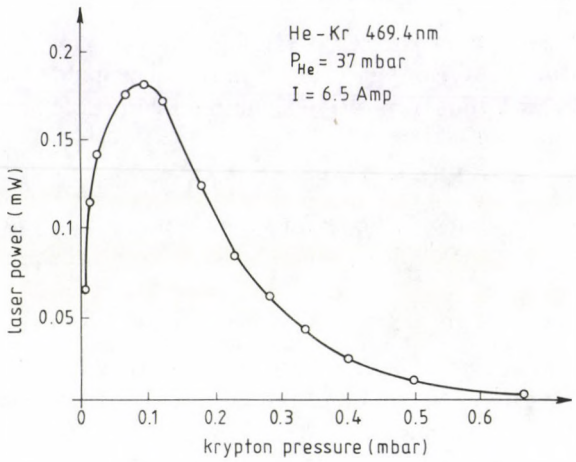

Fig. 19. Dependence of He–Kr laser power on Kr partial pressure

Figure 19 shows the dependence of laser power on Kr partial pressure obtained in a longitudinal hollow cathode arrangement [57]. As can be seen from the Figure laser power is very sensitive to the value of Kr partial pressure, the optimum being 0.1 mbar. Recent experiments in a graphite cathode high voltage discharge tube have resulted in an optimum of 0.3 mbar and laser oscillation occurred still at 0.9 mbar Kr partial pressure [59]. This observation is attributed to the presence of the high voltage, which allows a sufficient excitation of atomic species at such a high density of the active medium.

The dependence of threshold current on He pressure is shown in Fig. 20. The measurements were performed in a hollow cathode tube having three internal anodes [37]. It can be seen from the Figure that the threshold current is minimum around 14 mbar He pressure, it slightly increases below this but increases significantly at higher He pressures. The increase of the threshold current at low pressures is attributed to the presence of metal atoms resulting from cathode sputtering. The metal atoms due to their lower ionization potential reduce the density of high energy electrons and also that of He 2^3S atoms by Penning ionization. The increase of threshold current at high pressures is due to the change of the spatial distribution

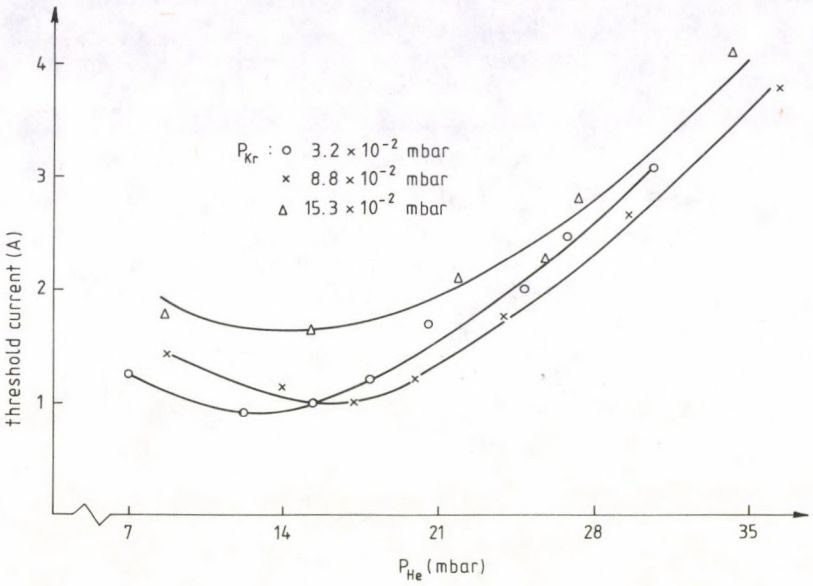

Fig. 20. Dependence of threshold current on He pressure for the 469.4 nm He–Kr laser

of the discharge [60]. At high pressures the discharge fills the whole cross-section of the tube only at higher discharge currents.

The dependence of laser power on discharge current measured at different He pressures is shown in Fig. 21. The results were obtained in the same internal anode tube as mentioned previously [37]. As can be seen from the Figure at low He pressures laser power saturates, while at higher pressures it strongly increases with increasing discharge current. The saturation is attributed to the presence of metal atoms resulting from cathode sputtering. As the He pressure is increased cathode sputtering is reduced but due to the change of the spatial distribution of the discharge the threshold current increases.

The optimum He and Kr partial pressures depend on the value of discharge current. Results measured in a d.c. excited transverse discharge hollow cathode laser [58] are presented in Fig. 22. As can be seen from the Figure increasing the discharge current optimum partial pressure values increase also. This relation can be explained on the basis of the change of the spatial distribution of the discharge [60].

The appearance of cathode sputtering and its influence on the 469.4 nm spontaneous line intensity is shown in Fig. 23. The measurement was made in a transverse slotted hollow cathode discharge excited by 0.5 ms duration square wave pulses [61]. As can be seen from the Figure the intensity of the 469.4 nm Kr II line

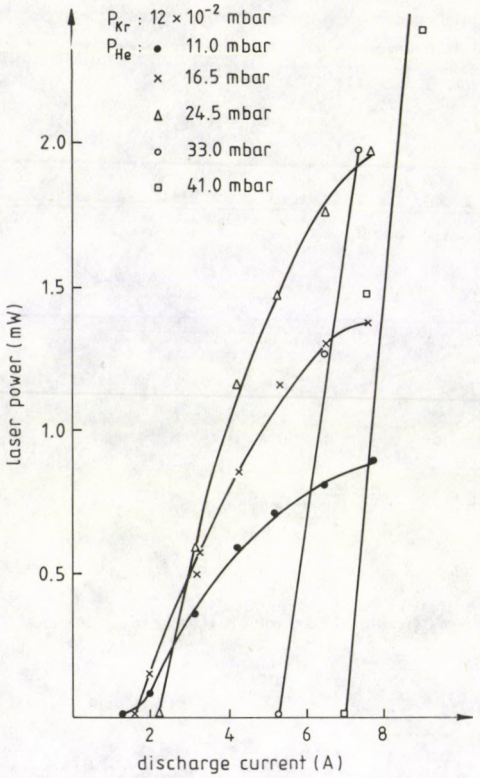

Fig. 21. Dependence of 469.4 nm He–Kr laser power on discharge current measured at different He pressures

tends to saturate in the current range where an abrupt increase of the intensity of the 396.1 nm Al I line occurs, the latter showing the appearance of a significant amount of Al vapour. It is emphasized that this occurs even at the high He pressure of 80 mbar where the data shown in Fig. 23 were obtained.

The gain and saturation parameter of the 469.4 nm He–Kr laser transition were measured as a function of discharge current in a six rod internal anode system [37]. These data were obtained from measuring output power as a function of loss produced by rotating a quartz window inside the laser resonator [72]. In this measurement a big advantage of the He–Kr laser system was that due to the large pressure broadening, the 469.4 nm transition has a homogeneous linewidth and oscillates only in a single axial mode. For measurement of the saturation parameter TEM_{00} mode operation was produced by inserting a diaphragm in the resonator. Excitation of the laser tube was quasi-cw with 100 μs halfwidth current pulses.

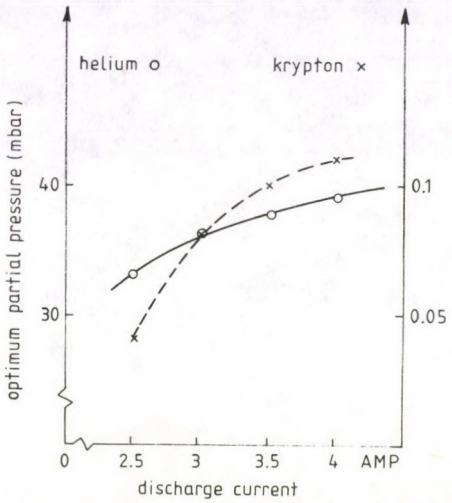

Fig. 22. Dependence of optimum He and Kr partial pressures on discharge current for the 469.4 nm He–Kr laser

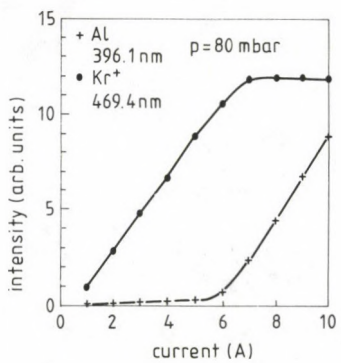

Fig. 23. Dependence of the spontaneous intensity of the 396.1 nm Al I and the 469.4 nm Kr II lines on discharge current at 80 mbar He and 0.2 mbar Kr pressure

The result of measurements are shown in Fig. 24 and Fig. 25. It can be seen from Fig. 24 that the saturation parameter increases with increasing discharge current and reaches a value of 150 W/cm^2 at 16 A peak current. Fig. 25 shows gain as a function of current, a value of 16%/m is measured at 16 A. Gain increases slower

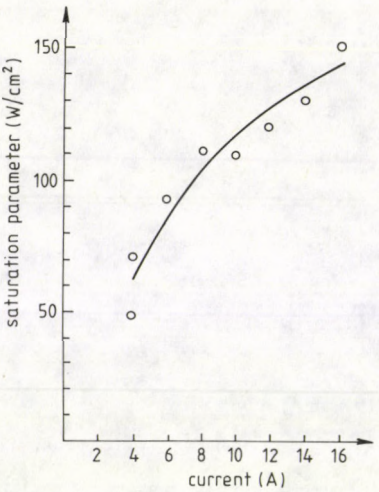

Fig. 24. Saturation parameter as a function of discharge current (He–Kr laser, 469.4 nm)

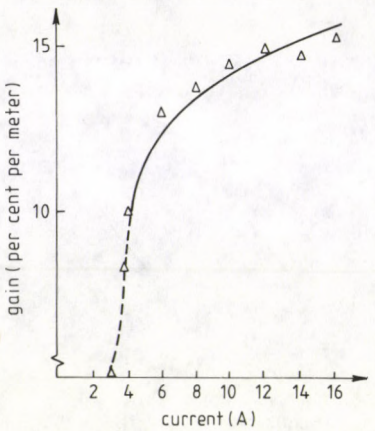

Fig. 25. Gain as a function of discharge current (He–Kr laser, 469.4 nm)

than linear with increasing discharge current, while the increase of output power is linear. Considering that output power is qualitatively proportional to the product of gain and saturation parameter, since the latter increases also slower than linear,

the product of them gives approximately a linear dependence.

4.5. Lasers for practical use

The cw noble gas mixture hollow cathode lasers have a perspective for practical applications. For this, however, a stable, long life laser is needed. Experiments have been carried out on the He–Kr laser to see possibilities and problems of constructions aimed on practical uses. A d.c. excited water cooled transverse discharge hollow cathode He–Kr laser was operated at 469.4 nm and 431.8 nm [58]. The active length of the laser was 40 cm. An output power of 5 mW could be obtained at the blue line and 0.4 mW at the violet line operating the discharge at 4 A current. The lifetime of the laser proved to be $\sim$ 100 hours, failure of the discharge tube being a short-circuit between the cathode and anode caused by the deposited metal arising from cathode sputtering [29,62].

Investigations have been made on a similar construction laser placed into a pyrex envelope and excited by 50 Hz repetition rate 0.4 ms duration current pulses [63]. Cataphoresis of Kr was found to affect seriously the pulse shape. A He–Kr mixture resulting in a near square wave laser output pulse was chosen for long time operation measurements. The pulse peak power was 20 mW, the average power 0.4 mW, respectively. The lifetime of the laser was 440 hours, tube failure being due to gas clean-up caused by cathode sputtering. As a practical application this laser was used in a single frequency operation mode to determine the resolving power and transmission function of a grating spectrograph [64].

The problem of a long life hollow cathode laser is not at all simple [29]. The efficiency of metal vapour lasers is higher than that of the noble gas mixture lasers, mainly due to the difference in excitation mechanisms. The metal vapour lasers are excited via a single step process [65], while the noble gas mixture lasers have a two step excitation mechanism. A disadvantage of metal vapours is the need of a high temperature to produce the metal vapour and it is difficult to reach a uniform vapour distribution. Noble gas mixture lasers can be operated at room temperatures, the active gas distribution is homogeneous. However, the amount of the active gas is limited and the laser is very sensitive to impurities. A practically unlimited amount of metal vapour can be produced by heating solid metal pieces and metal vapour lasers are much less sensitive to impurities due to these being absorbed in the deposited metal layers. The noble gas in metal vapour lasers is also absorbed here, however, which reduces the gas pressure. In cathode sputtering operated lasers gas clean-up and short-circuit between the electrodes, both caused by the sputtered metal are the main problems for a long life laser.

Our opinion is that both metal vapour and noble gas mixture systems are suitable for long life lasers intended for practical uses. However, in both cases a large amount of research and development work is still needed to reach this goal.

5. Single frequency operation

5.1. Basic considerations

It is well known that cw visible gas lasers operate usually in several axial modes simultaneously, the frequency difference of which being determined by the resonator length L ($\Delta\nu_{\text{mode}} = c/2L$), and the number of oscillating modes by the Doppler width of the gain curve, which amounts typically to 1–4 GHz. Doppler broadening is called inhomogeneous, because atoms with different velocities can interact with light waves of different frequencies. In a gas laser, however, the energy of radiation in one particular oscillating mode with a given frequency comes from a larger group of atoms having slightly different velocities, because their resonant frequencies are broadened due to the finite lifetimes of the participating energy levels. This broadening which is characterized by the radiative (natural) linewidth $\Delta\nu_n$ is called homogeneous. The homogeneous linewidth can be affected by other effects, e.g. by collisions with other atoms. This effect may be important at higher pressures. In most cases, for cw visible gas lasers, $\Delta\nu_n \ll \Delta\nu_D$ and also $\Delta\nu_n \leq \Delta\nu_{\text{mode}}$, resulting in multimode operation.

In many applications, however, single frequency operation is of great importance. For the selection of a single mode, there are several well-known methods from which the most common are the application of a short resonator length or the insertion of a frequency selective optical element like a Fabry–Perot etalon into the resonator. In the first case, however, the power available will be low, while in the second one there are extra costs and a significant part of the multimode power is lost.

A very attractive way to achieve single mode operation is the homogenisation of the gain curve by increasing the filling gas pressure. If the collision broadened natural linewidth $\Delta\nu_c$ is significantly larger than $\Delta\nu_{\text{mode}}$ and if it becomes comparable to $\Delta\nu_D$, then the mode with the highest gain will saturate the whole gain curve preventing the oscillation of all other modes. The main problem is here, however, that for most visible cw gas lasers, excited in the positive column of a discharge, the optimum gas pressure is much lower than that is needed for gain saturation, and therefore at the applied high pressure the output power again becomes too low.

This effect can be easily demonstrated with the red 632.8 nm He–Ne laser. A small standard He–Ne laser ($L \sim 40$ cm, $p \sim 4.5$ mbar, output power ~ 5 mW) oscillates commonly in three axial modes ($\Delta\nu_{\text{mode}} \approx 400$ MHz). Increasing the pressure to 9 mbar only one mode will oscillate, but the power drops below 2 mW.

5.2. Single mode hollow cathode lasers

The situation is much better in the case of hollow cathode excitation, because optimum gas pressures here proved to be significantly higher than those in positive column discharges. Therefore single frequency operation can be achieved at the

optimum laser conditions, even with large resonator lengths and without any optical mode selection technique. (The only problem, which can arise here is the transversal mode selection; the TEM_{00} mode can be selected either by applying an appropriate narrow bore cathode geometry or by inserting an additional diaphragm into the light path.)

The advantage of hollow cathode excitation in achieving single frequency operation without power loss was demonstrated for hollow cathode red He–Ne lasers by Cartaleva et al [66]. Pure single mode operation was achieved at $p_{He} = 9$ mbar, just at the optimum He pressure for the given cathode geometry.

As another example, the blue hollow cathode He–Kr laser can be mentioned. It was shown that this laser oscillated — above 20 mbar — always in a single axial mode [58]. With a tube of 40 cm active length at optimum conditions ($p_{He} \approx 40$ mbar, $I = 4.5$ A) 12 mW single frequency output could be achieved [67]. The linewidth was less than 10 MHz during the 10 ms measuring time. By changing the resonator length ($L = 1$ m) the single mode frequency could be tuned in a frequency range of 450 MHz which is three times larger than the axial mode separation ($\Delta\nu_{mode} \approx 144$ MHz). During the tuning, the laser power remained practically constant showing that the condition $\Delta\nu_c \gg \Delta\nu_{mode}$ is fulfilled indeed [67]. Similarly, single mode operation was also demonstrated in the hollow cathode $He–Ar^+$ $\lambda = 476.5$ nm laser [53].

5.3. Linewidth studies

To obtain a more clear picture on the processes involved and to obtain data on $\Delta\nu_c$ and $\Delta\nu_D$, linewidth measurements have been carried out [68,69] at several Kr^+ and Ar^+ lines, excited in a hollow cathode discharge using Fabry–Perot technique. The spontaneous lineshapes were measured under conditions similar to those used in cw hollow cathode lasers. From the experimental data first the collisional and Doppler linewidths ($\Delta\nu_c$ and $\Delta\nu_D$) were determined by deconvolution, and then from these linewidths collision broadening constants (α) and Doppler temperatures (T_D) were calculated.

Some of the results for two laser lines (Kr^+ 469.4 nm and Ar^+ 476.5 nm) and for two non-laser lines (Kr^+ 473.9 nm and Ar^+ 480.6 nm) are presented in Table IV. Zero pressure linewidth data ($\Delta\nu_0$) are taken from the literature and partly are calculated from level lifetimes. It has to be noted here that the upper levels of the two non-laser lines are supposed to be excited by electron impact, while the laser lines are excited mainly by second kind collisions of 2^3S He atoms with ground state ions.

From the results presented in Table IV, the following conclusions can be drawn:

1. In hollow cathode lasers, both laser transitions have large homogeneous linewidths compared to the typical axial mode separations and they are comparable to the Doppler linewidths. They differ, however, in their origin significantly. For Kr^+ 469.4 nm there is a small natural linewidth and a large pressure broadening

Table IV

Ion	Kr^+		Ar^+	
λ (nm)	469.4	473.9	476.5	480.6
$\Delta\nu_0$ (MHz)	43±3	200±50	500±50	23±6
$\Delta\nu_c$ (MHz)	560	500	620	170
$\Delta\nu_D$ (MHz)	1330	1160	1990	1980
α (MHz/mbar)	23	12	5	6
T_D (K)	710	545	780	785

Errors: $\Delta\nu_c$ and $\Delta\nu_D$: ±50 MHz;
α : ±1 MHz (Kr^+), ±3 MHz (Ar^+)

constant, while for Ar^+ 476.5 nm the situation is opposite: natural linewidth is larger, and pressure broadening is small.

2. The Doppler temperatures differ significantly for the two Kr^+ lines. This difference can be explained by the specific excitation mechanisms of the lines. According to (1) at the second kind collision excitation of the upper level of the Kr^+ 469.4 nm transition there is an excess energy ($\Delta E = 0.35$ eV), which has to be taken away by the colliding partners as kinetic energy. A simple calculation shows that this energy can cause a temperature rise of about 200 K for this group of Kr ions. The observed 160 K difference between the two T_D values is not far from this value. On the other side, at the excitation of the upper level of the Kr^+ 473.9 nm transition by electron impact no temperature change is expected. Thus the observed higher Doppler temperature for the Kr^+ 469.4 nm line gives a further support to the validity of the excitation mechanism for this laser transition. Furthermore, the Doppler temperature of the Kr^+ 473.9 nm line can be accepted as the average gas temperature. This assumption is supported by the fact that T_D deduced from the deconvolution of the He 501.6 nm line gave nearly the same value [T_D (He 501.6 nm) = (563 ± 50) K] [69].

3. The T_D values of the two argon lines are practically equal. According to the excitation mechanisms just this result was expected because at the excitation of the upper level of the Ar^+ 476.5 nm laser transition by second kind collisions with 2^3S He atoms a nearly exact energy resonance exists, $\Delta E = -0.05$ eV, therefore no temperature change should occur due to the collision process.

4. The T_D values of both Ar^+ lines are 260 K higher than the average gas temperature, as accepted before (Section 2). The origin of this excess Ar ion temperature is not clear. One possible explanation might be that in the production of ground state Ar ions not only high energy electrons, but also excited He_2^+ molecules take part. Namely it was shown that non-resonant charge transfer collisions between ground state Ar atoms and excited He_2^+ molecules, which are present in a large concentration in the high pressure hollow cathode discharge, have a large cross-section [70]. At this type of collision about 2.5–4.5 eV kinetic energy is taken away by the colliding partners [71], which could be responsible for the observed temperature rise of the Ar ions. Further studies are needed to support this assumption.

6. Summary

In this paper the properties of noble gas mixture hollow cathode lasers have been dealt with. The basic properties of hollow cathode discharges and construction principles for discharge tubes have been discussed. Laser transitions, excitation mechanisms, relations between laser output power and discharge parameters were described in detail. Some experiments aiming on the development of a practical He–Kr laser and the question of single mode operation have been also discussed.

Acknowledgement

Thanks are due to Mrs T. J. Forgács for help in preparing the manuscript. This work has been partly supported by the Hungarian Science Foundation OTKA, grants No. F-4475, T-4221, T-2935 and T-4227.

References

1. A. Javan, W. R. Bennett Jr. and D. R. Herriott, Physical Review Letters, *6*, 106, 1961.
2. W. K. Schuebel, Applied Physics Letters, *16*, 470, 1970.
3. W. K. Schuebel, IEEE Journal of Quantum Electronics, *QE-6*, 574, 1970.
4. T. Salamon, L. Csillag, M. Jánossy and K. Rózsa, Physics Letters, *45A*, 17, 1973.
5. J. A. Piper and P. Gill, Journal of Physics D. Applied Physics, *8*, 127, 1975.
6. M. G. Grozeva, N. V. Sabotinov and N. K. Vuchkov, Optics Communications, *29*, 339, 1979.
7. J. R. Mc Neil, G. J. Collins, K. B. Persson and D. L. Franzen, Applied Physics Letters, *27*, 595, 1975.
8. J. R. Mc Neil, G. J. Collins, K. B. Persson and D. L. Franzen, Applied Physics Letters, *28*, 207, 1976.
9. J. R. Mc Neil, W. L. Johnson, G. J. Collins and K. B. Persson, Applied Physics Letters, *29*, 172, 1976.
10. R. D. Reid, J. R. McNeil and G. J. Collins, Applied Physics Letters, *29*, 666, 1976.
11. D. C. Gerstenberger, R. D. Reid and G. J. Collins, Applied Physics Letters, *30*, 466, 1977.
12. M. Jánossy, L. Csillag, K. Rózsa and T. Salamon, Physics Letters, *45A*, 379, 1974.
13. M. Jánossy, L. Csillag and K. Rózsa, Physics Letters, *63A*, 84, 1977.
14. K. Rózsa, M. Jánossy, L. Csillag and J. Bergou, Optics Communications, *23*, 15, 1977.
15. F. J. de Hoog, J. R. Mc Neil, G. J. Collins and K. B. Persson, Journal of Applied Physics, *48*, 3701, 1977.
16. G. Francis, The Glow Discharge at Low Pressure, Handbuch der Physik, Vol XXII. p. 53, Springer, Berlin, 1956.
17. A. von Engel, Ionized Gases, Clarendon Press, Oxford, 1965.
18. G. F. Weston, Cold Cathode Glow Discharge Tubes, ILIFFE Books, London, 1968.
19. J. P. Boeuf and E. Marode, in Proceedings of the XVIth International Conference on Phenomena in Ionized Gases (ICPIG), Düsseldorf, Invited Papers, eds W. Bötticher, H. Wenk and E. Schulz-Gulde, p. 206, 1983.
20. L. C. Pitchford, J. P. Boeuf, P. Segur and E. Marode, Non-Equilibrium Electron Transport: A Brief Overview, in Nonequilibrium Effects in Ion and Electron Transport, ed. J. Gallagher, Plenum Press, New York, p. 1, 1990.
21. H. Helm, Z. Naturforschung, *27a*, 1812, 1972.
22. H. Helm, Beitr. Plasmaphysik, *18*, 233, 1979.

23. R. M. Chaudhri, M. M. Chaudhri and M. N. Chaudhri, in Proceedings of the XVIIIth International Conference on Phenomena in Ionized Gases Swansea, Contributed Papers, ed. W. T. Williams, p. 792, 1987.
24. R. M. Chaudhri, M. M. Chaudhri, F. Deba and M. N. Chaudhri, Int. J. Electronics, *62*, 679, 1987.
25. A. Güntherschulze, Z. Physik, *19*, 313, 1923.
26. H. Helm, F. Howorka and M. Pahl, Z. Naturforschung, *27a*, 1417, 1972.
27. Z. Donkó, Z. Naturforschung, *48a*, 457, 1993.
28. K. Rózsa, Z. Naturforschung, *35a*, 649, 1980.
29. K. Rózsa and M. Jánossy, in Proceedings of the XVIth International Conference on Phenomena in Ionized Gases (ICPIG), Düsseldorf, Invited Papers, eds W. Bötticher, H. Wenk and E. Schulz-Gulde, p. 150, 1983.
30. M. Stefanova, Thesis, p. 109, Sofia 1980 (in Bulgarian).
31. A. A. Kruithof and F. M. Penning, Physica, *4*, 430, 1937.
32. Z. Donkó and M. Jánossy, J. Phys. D: Appl. Phys., *25*, 1323, 1992.
33. R. Behrisch, Sputtering by Particle Bombardment, Springer, Berlin, 1981.
34. K. Rózsa, P. Apai, M. Jánossy, J. Bergou, K. Fujii, G. Rubin, M. B. Denton, H. Phillips and F. A. Hopf, Proceedings of XVII. ICPIG, Budapest, Vol. 2, p. 931, 1985.
35. J. Mizeraczyk, J. Wasilewski, J, Konieczka, W. Urbanik, M. Grozeva and J. Pavlik, Proceedings of the International Conference Lasers 81, New Orleans, p. 877, 1981.
36. K. Fujii, T. Takashi and Y. Asami, IEEE Journal of Quantum Electronics, *QE-11*, 111, 1975.
37. M. Jánossy, K. Rózsa, L. Csillag and Le Trong Muu, Acta Phys. Hung., *56*, 147, 1984.
38. M. Grozeva and N. Sabotinov, Optics Communications, *41*, 57, 1982.
39. Z. Zhang, N. D. Perry and R. C. Tobin, Journal of Applied Physics, *71*, 64, 1992.
40. M. Jánossy, Doctoral Thesis, p. 27, Budapest 1990 (in Hungarian).
41. M. Jánossy, K. Rózsa, L. Csillag and J. Bergou, Physics Letters, *68A*, 317, 1978.
42. M. Jánossy, L. Csillag K. Rózsa and T. Salamon, Physics Letters, *47A*, 411, 1974.
43. M. V. Pyatakhin, M. Jánossy, L. Csillag, A. N. Oraevsky and A. F. Suchkov, Kvantovaja Elektronika, *18*, 414, 1991.
44. K. Rózsa and M. Jánossy, unpublished.
45. L. Dana, private communication.
46. Y. Pacheva, M. Stefanova and P. Pramatarov, Optics Communications, *27*, 121, 1978.
47. M. Jánossy, P. Mezei and P. Horváth, Optics Communications, *65*, 287, 1988.
48. L. Dana and P. Laures, Proceedings of the IEEE, *53*, 78, 1965.
49. R. Solanski, E. L. Latush, D. C. Gerstenberger, W. R. Fairbank Jr. and G. J. Collins, Applied Physics Letters, *35*, 317, 1979.
50. W. R. Bennett, Atomic Gas Laser Transition Data, a Critical Evaluation, IFI/Plenum, New York, 1979.
51. K. Rózsa and M. Jánossy, unpublished.
52. C. S. Willett, Introduction to Gas Lasers: Population Inversion Mechanisms, Pergamon Press, Oxford, p. 35, 1974.
53. M. Jánossy, P. Mezei, P. Horváth and L. Csillag, Optics Communications, *68*, 58, 1988.
54. M. Jánossy and P. Tuovinen, Acta Phys. Hung., *46*, 167, 1979.
55. P. Gill and C. E. Webb, Journal of Physics D: Applied Physics, *10*, 299, 1977.
56. P. Mezei, M. Jánossy and M. Grindhammer, Proceedings of XVII. ICPIG Budapest, Vol. 2, p. 919, 1985.
57. M. Jánossy, K. Rózsa, L. Csillag and Le Trong Muu, Avtometria, *1*, 45, 1984.
58. M. Jánossy, K. Rózsa, P. Apai and L. Csillag, Optics Communications, *49*, 278, 1984.
59. M. Jánossy and P. Mezei, to be published.
60. P. Mezei, P. Apai, M. Jánossy and K. Rózsa, Optics Communications, *78*, 259, 1990.
61. Z. Donkó and M. Jánossy, Pure and Applied Optics, *1*, 127, 1992.
62. M. Jánossy, K. Rózsa, P. Apai and L. Csillag, Symposium Optika 84, G. Lupkovics, A. Podmaniczky, Co-Editors, Proceedings of SPIE 473, p. 198, 1984.

63. M. Jánossy, K. Rózsa, P. Apai, P. Mezei, P. Horváth, L. Csillag and N. Kroó, Applied Physics, *B49*, 343, 1989.
64. P. Apai, L. Csillag and M. Czétényi, Proceedings of Symposium Optika 88, Budapest, Vol. II, p. 425, 1988.
65. G. J. Collins, Journal of Applied Physics, *44*, 4633, 1973.
66. S. Cartaleva, V. Stefanov and L. Csillag, Zhurnal Prikladnoj Spektroskopii, *34*, 727, 1981.
67. L. Csillag, M. Jánossy, K. Rózsa and S. Cartaleva, Proceedings of the 1-st Symposium on Laser Spectroscopy, Pécs, Hungary, Vol. 1, p. 66, 1986.
68. L. Csillag, M. Jánossy and K. Rózsa, Applied Physics, *B52*, 90, 1991.
69. L. Csillag and M. Jánossy, Applied Physics, *B55*, 401, 1992.
70. M. Tsuji, M. Furusawa and Y. Nishimura, Chemical Physics Letters, *169*, 49, 1990.
71. J. J. Leventhal, J. D. Earl and H. H. Harris, Physical Review Letters, *35*, 719, 1975.
72. B. S. Patel, Sh. Charan, A. Mallik and P. Swarup, Journal of Physics D: Applied Physics, *7*, L40, 1974.

Acta Physica Hungarica 73 (2–4), pp. 345-346 (1993)

BOOK REVIEW

Nonlinear Superconductive Electronics and Josephson Devices
G. Costabile, S. Pagano, N. F. Pedersen and M. Russo (eds) Plenum Press, New York, 1991

The basic phenomenon of the Josephson's effect is represented by the tunneling of electronic pairs between two superconductors through a non-superconducting layer. On the one hand, this phenomenon has an extraordinary importance from the point of view of fundamental research and, on the other hand, it is very important from the point of view of the technical application and measuring technique. Both of these arguments were significantly increased after the appearance of high-temperature superconductors.

The book reviewed here is devoted to the main problems of the superconducting electronics based mostly on the Josephson effect. It consists of the lectures presented in the workshop held in Capri, September 3–7, 1990, under the auspices of the NATO and the CNR.

A very fast development in the field of superconducting electronics can be observed and even a number of commercial devices start to use superconducting components both in analog and digital circuits. The papers of this book cover many recent achievements concerning the theory and practice of Josephson's effect based fine, quick and low-power electronics.

Among them the impressive Japanese results in developing very fast superconducting circuitry (32 000 junction 4 bit Josephson's processor and progress on Josephson's computer) are reported in the article of S. Takada.

As the examples of analog application a new Josephson's voltage standard (a 14 000 junction 10 Volt chip) was presented by J. Niemeyer et al, while D. Andreone et al reported the biharmonic junction's drive and H. G. Meyer et al the external synchronization in Josephson's arrays, respectively. R. Blundell et al and D. Winkler et al were dealing with the great development of superconducting mixers based on superconductor–insulator–superconductor junctions, which are unique for highly sensitive millimeter-wave receivers having noise levels down to the quantum limit. The up-to-date problems of SQuID-s of extreme sensitivity and high-T_c SQuID-s in measuring technique were discussed in the papers of M. B. Ketchen, V. Fogliatti et al and G. J. Cui et al. Questions of the operation of superconducting electronics are covered in the papers of A. Barone et al (nuclear particle detection), J. B. Green (fast analog signal processing), Y. Zang (flux flow type Josephson's oscillator) and A. Andreone et al (thin film superconducting cavities).

Numerous papers of the book deal with different results of fundamental research of this field, e.g. noise in Josephson's junctions (J. B. Hansen), switching dynamics in the presence of quantum fluctuations (P. Silvestrini), ultra-small junctions (T. Claeson et al and S. A. Hattel et al) and quantum simulation of Josephson's junctions (A. Davidson et al).

A great part of articles in this book was devoted to the study of non-linear effects in Josephson's junctions. Among others, the interaction between solitons and electromagnetic field (G. Filatrella et al), microwave boundary coupling (M. Salerno et al), strongly coupled junctions in microstrip resonators (H. D. Jensen et al), Josephson's transmission lines coupling (M. Cirillo), phase locking in series arrays (W. Krech and H. G. Meyer), solitons in inhomogeneous long junctions (A. V. Ustionov), fluxon dynamics (T. Skiniotis et al), imaging of spatial structures (T. Doderer), critical current in long junctions (S. Pagano et al), magnetic tuning

(T. Holst and J. B. Hansen), turbulence and chaos in Josephson's junctions (L. E. Querrero and M. Octavio) and new solutions of sine-Gordon system were analyzed.

As far as the basic questions of high-T_c superconductors are concerned, some structural and intrinsic aspects of this subject have been investigated in this book, namely the vortex propagation in granular thin films (G. A. Ovsyannikov et al) and the non-linear properties of BCS gap equation and bifurcations (M. P. Soerensen).

Summarizing very briefly the subject presented indicates the statement that superconducting electronics has reached the level above the fundamental research to prepare the way for useful applications.

I. Kirschner

CONTENTS

Volume 73

FLUIDS, PLASMAS AND ELECTRIC DISCHARGES

CONDENSED MATTER

ASTROPHYSICS

INTERDISCIPLINARY

NOTES TO CONTRIBUTORS

I. PAPERS will be considered for publication in Acta Physica Hungarica only if they have not previously been published or submitted for publication elsewhere. They may be written in English, French, German or Russian.

Papers should be submitted to

Prof. I. Kovács, Editor
Department of Atomic Physics, Technical University
1521 Budapest, Budafoki út 8, Hungary

Papers may be either articles with abstracts or short communications. Both should be as concise as possible, articles in general not exceeding 25 typed pages, short communications 8 typed pages.

II. MANUSCRIPTS

1. Papers should be submitted in three copies.
2. The text of papers must be of high stylistic standard, requiring minor corrections only.
3. Manuscripts should be typed in double spacing on good quality paper, with generous margins.
4. The name of the author(s) and of the institutes where the work was carried out should appear on the first page of the manuscript.
5. Particular care should be taken with mathematical expressions. The following should be clearly distinguished, e.g. by underlining in different colours: special founts (italics, script, bold type, Greek, Gothic, etc.); capital and small letters; subscripts and superscripts, e.g. x^2, x_3; small *l* and l; zero and capital O; in expressions written by hand: *e* and *l*, *n* and *u*, *v* and v, etc.

A List of Symbols on a separate sheet should be attached to each paper.

6. References should be numbered serially and listed at the end of the paper in the following form: J. Ise and W. D. Fretter, Phys. Rev., *76,* 933, 1949.

For books, please give the initials and family name of the author(s), title, name of publisher, place and year of publication, e.g.: J. C. Slater, Quantum Theory of Atomic Structures, I. McGraw-Hill Book Company, Inc., New York, 1960.

References should be given in the text in the following forms: Heisenberg [5] or [5].

7. Captions to illustrations should be listed on a separate sheet, not inserted in the text.
8. In papers submitted to Acta Physica all measures should be expressed in SI units.

III. ILLUSTRATIONS AND TABLES

1. Each paper should be accompanied by three sets of illustrations, one of which must be ready for the blockmaker. The other sets attached to the copies of the manuscript may be rough drawings in pencil or photocopies.
2. Illustrations must not be inserted in the text.
3. All illustrations should be identified in blue pencil by the author's name, abbreviated title of the paper and figure number.
4. Tables should be typed on separate pages and have captions describing their content. Clear wording of column heads is advisable. Tables should be numbered in Roman numerals (I, II, III, etc.).

IV. RETURN OF MATERIAL

Owing to high postage costs, the Editorial Office cannot undertake to return *all* material not accepted for any reason for publication. Of papers to be revised (for not being in conformity with the above Notes or other reasons) only *one* copy will be returned. Material rejected for lack of space or on account of the Referees' opinion will not be returned to authors outside Europe.